



HAL
open science

Etude du remodelage du ventricule droit dans l'hypertension pulmonaire : du phénotypage approfondi à l'étude de la protéomique

Myriam Amsallem

► **To cite this version:**

Myriam Amsallem. Etude du remodelage du ventricule droit dans l'hypertension pulmonaire : du phénotypage approfondi à l'étude de la protéomique. Cardiologie et système cardiovasculaire. Université Paris-Saclay, 2019. Français. NNT : 2019SACLS003 . tel-02280123v1

HAL Id: tel-02280123

<https://theses.hal.science/tel-02280123v1>

Submitted on 6 Sep 2019 (v1), last revised 12 Sep 2019 (v2)

HAL is a multi-disciplinary open access archive for the deposit and dissemination of scientific research documents, whether they are published or not. The documents may come from teaching and research institutions in France or abroad, or from public or private research centers.

L'archive ouverte pluridisciplinaire **HAL**, est destinée au dépôt et à la diffusion de documents scientifiques de niveau recherche, publiés ou non, émanant des établissements d'enseignement et de recherche français ou étrangers, des laboratoires publics ou privés.

Right Ventricular Remodeling in Pulmonary Hypertension: from Deep Phenotyping to Proteomics Profiling

**Etude du Remodelage du Ventricle Droit dans
l'Hypertension Pulmonaire: du Phénotypage
approfondi à l'étude de la Protéomique**

Thèse de doctorat de l'Université Paris-Saclay
préparée à l'Université Paris Sud
Unité de Recherche et Innovation – INSERM U999
Hôpital Marie Lannelongue

École doctorale n°569 Innovation thérapeutique:
du fondamental à l'appliqué
Spécialité de doctorat: Physiologie, Physiopathologie

Thèse présentée et soutenue à L'Hôpital Marie Lannelongue (Le Plessis Robinson),
le 4 Janvier 2019, par

Dr. AMSALLEM Myriam

Composition du Jury :

Mr Le Pr Marc HUMBERT PU-PH, INSERM, Paris Sud	Président du Jury
Mme La Pr Marion DELCROIX PU-PH, KU Leuven - Belgium	Rapporteur
Mr Le Pr Alain COHEN-SOLAL PU-PH, INSERM, Paris Diderot	Rapporteur
Mr le Pr Olivier SANCHEZ PU-PH, INSERM, Paris Descartes	Examineur
Mr Le Pr Marc HUMBERT PU-PH, INSERM, Paris Sud	Examineur
Mr Le Pr Olaf MERCIER PU-PH, INSERM, Paris Sud	Directeur de thèse
Mr Le Pr Elie FADEL PU-PH, INSERM, Paris Sud	Co-Directeur de thèse

To my parents, Yaël and my family

ACKNOWLEDGEMENTS

I would like to express my gratitude to my PhD mentor **Professor Olaf MERCIER MD PhD**, Professor of Medicine and Director of the Research and Innovation Unit at Marie Lannelongue Hospital, for his excellent supervision, precious mentorship and outstanding support during my PhD years. I am very grateful to have been able to learn so much from you and complete all these exciting projects during my PhD.

I would like to deeply thank my PhD co-mentor **Professor Elie FADEL MD PhD**, Professor of Medicine, Director of the Department of Thoracic, Vascular Surgery and Heart-Lung Transplantation and Medical Director of Marie Lannelongue Hospital for his excellent mentorship, inspirational leadership and eternal support in all my projects. I would like to warmly thank you for having welcomed me a few years ago at Marie Lannelongue Hospital and made me feel like home, while provided me with the ideal conditions to conduct my research.

I would like to thank the President of the dissertation committee, **Professor Marc HUMBERT MD PhD**, Professor of Medicine and Director of the INSERM U999 research unit for doing me the honor of judging my thesis.

I would like to thank the two thesis examiners (“rapporteurs”), **Professor Marion DELCROIX MD PhD**, Professor of Medicine and Director of the Center for Pulmonary Vascular Disease (KU Leuven, Belgium) and **Professor Alain COHEN-SOLAL MD PhD**, Professor of Medicine and Director of the INSERM U942 unit at Lariboisiere Hospital (Paris Diderot VII) for doing me the great honor of judging my thesis, taking the time to review my work and provide precious feedback in their quality of international experts in the field.

I would like to also thank **Professor Olivier SANCHEZ MD PhD**, Professor of Medicine and member of the INSERM UMR1140 for his interest on my thesis and expertise in the field.

I could never thank enough my mentor **Professor Francois HADDAD MD**, Clinical Associate Professor of Medicine and Director of Stanford Cardiovascular Institute Biomarker and Phenotypic Core Laboratory (Stanford, CA, USA) for having taught me all I know about right heart failure, imaging and pulmonary hypertension during all these years, unrevealing the mysteries of the right ventricle. I am deeply grateful to have unexpectedly met you in room H2170 in 2014, and have become your mentoree since then. You are a true model for me, not only as a clinician, researcher, mentor but above all as a human being.

To all my friends and colleagues from Marie Lannelongue Hospital and the Research and Innovation and INSERM U999 units: I would like to thank you for having welcomed me in your exceptional family. I have learnt, progressed and grown so much during these years among your team.

A special thank you to Jennifer ARTHUR ATAAM PhD for being my friend and guide during this PhD, always available, motivated and ready to go on scientific adventures with me!

I would like to thank Julien GUIHAIRE MD PhD and David BOULATE MD PhD for the pleasure to work with them, their teaching and their support, Samantha GUIMARON MD

MS for her support and being such an amazing friend and colleague during our fun weekends reading MRIs and echos, Lilia LAMRANI MS for her kind and precious help with the projects, Fanny LOISEL PhD, Benoit DECANTE MS, Florence LECERF MS and Pierre MOLINIE for their help and support, and all the clinical team from the Cardiovascular and the Imaging Departments of Marie Lannelongue Hospital.

Finally, I would like to express my infinite gratitude to my family, who has supported me so much during these years of intense work.

To my parents, the words are missing to thank you for all your help, love and support since I started my studies, a “few” years ago... Thank you for your support even when I came to announce you that I wanted to complete a second “tesina”/thesis, thanks for being a true model for me, and always encourage me to do my best in everything, even miles away.

To Yaël, my love, thank you for your unconditional support, love and infinite patience during these years; you are my inspiration.

To David, Laura, Matan and Orel, my sunshines, for your support and love. Thank you to my little loves Matan and Orel for those precious breaks during my PhD: you are next in the doctoral lineage! To all my family, great-aunt Jeanine, uncles, cousins, but also those who left us too soon, with a particular thought for my grandfather Georges.

Finally, to all my (past and future) patients, hoping that conducting these studies will help to make me a better physician.

TABLE OF CONTENTS

ACKNOWLEDGEMENTS	3
TABLE OF CONTENTS	5
LIST OF PUBLICATIONS	8
LIST OF FIGURES	11
LIST OF TABLES	13
ABBREVIATIONS	14
INTRODUCTION	16
Part 1- PATHOPHYSIOLOGY of the CARDIOPULMONARY UNIT	18
1.1 Physiology of the Pulmonary Circulation	19
1.1.a Main definitions	19
1.1.b The inverse resistance-capacitance relationship.....	21
1.1.c The mean and systolic pulmonary arterial pressure collinearity.....	23
1.1.d Transpulmonary-pressure gradient versus diastolic pulmonary gradient.....	23
1.1.e Rediscovering the pressure-cardiac output, a window to exercise-induced PH.....	25
1.2 The Right Ventricle	26
1.2.a Embryology and anatomy of the right heart.....	26
1.2.b Right heart versus left heart.....	27
1.3 Pulmonary Hypertension	28
1.3.a Definitions	28
1.3.b Classification of pulmonary hypertension.....	29
1.4 Right heart adaptation to pressure overload	31
1.4.a Right ventricular-pulmonary arterial coupling	31
1.4.b Right heart adaptation to pressure overload.....	32
1.4.c Right ventricular adaptation to PH: beyond increased afterload?	33
1.4.d Molecular changes underlying right heart adaptation to PH	34
1.4.d.i Metabolic changes and the role of the mitochondria.....	36
1.4.d.ii Myocardial ischemia.....	36
1.4.d.iii Immunity and proteomic biomarkers.....	38

Part 2- RIGHT HEART IMAGING	47
2.1 Echocardiography	47
2.1.a Principles and advantages	47
2.1.b Latest developments.....	53
2.1.b.i Right ventricular deformation imaging.....	53
2.1.b.ii Three-dimensional echocardiography.....	55
2.1.c Limitations and unmet needs.....	56
2.1.c.i Controversy of estimating pulmonary arterial pressure by echocardiography.....	56
2.1.c.ii Need for standardization of 2D echocardiography.....	58
2.1.c.iii Non-invasive assessment of right heart adaptation to load.....	60
2.2 Cardiac Magnetic Resonance	62
2.2.a Principles and advantages.....	62
2.2.b Latest developments.....	64
2.2.b.i Extracellular matrix – Fibrosis.....	64
2.2.b.ii 4D MRI blood flow.....	68
2.2.c Limitations and unmet needs.....	69
2.2.c.i Reversibility of DCE after PH surgery	69
2.2.c.ii Validation of MRI 4D flow in PH.....	70
2.3 Multimodality of Right Heart Phenotyping	71
 HYPOTHESIS and OBJECTIVES	 74
 MATERIAL and METHODS	 78
1. Study cohorts	79
1.1 Ethical and regulatory aspects.....	79
1.2 Diagnosis of pulmonary hypertension and classification.....	79
1.3 Demographics, functional status and pulmonary functional testing.....	80
2. Right heart assessment	81
2.1 Hemodynamics using right heart catheterization.....	81
2.2 Resting trans-thoracic echocardiography.....	81
3. Circulating biomarkers	83

3.1 Enzyme-Linked ImmunoSorbent Assay (ELISA)	83
3.1.a Principles	83
3.1.b Advantages	84
3.1.c Limitations	84
3.2 Multiplex Arrays (Luminex®).....	84
3.2.a Principles.....	84
3.2.b Advantages.....	85
3.2.c Limitations.....	85
RESULTS	86
Chapter 1- ACCURACY of ECHOCARDIOGRAPHY for PH DETECTION	87
Study 1: Addressing the controversy of estimating pulmonary arterial pressure by echocardiography.....	87
Chapter 2- RIGHT HEART NON-INVASIVE IMAGING, LOAD ADAPTATION and RISK PREDICTION in PH	99
Study 1: Right Heart End-Systolic Remodeling Index Strongly Predicts Outcomes in Pulmonary Arterial Hypertension: Comparison With Validated Models	99
Study 2: Load Adaptability in Patients With Pulmonary Arterial Hypertension.....	124
Study 3: Non-invasive Right Ventricular Load Adaptability in Patients with Scleroderma-Associated Pulmonary Arterial Hypertension.....	135
Chapter 3- RIGHT HEART REMODELING and IMMUNITY	148
Study 1: Preoperative C-Reactive Protein Predicts Early Postoperative Outcomes After Pulmonary Endarterectomy in Patients with Chronic ThromboEmbolic Pulmonary Hypertension	148
Study 2: Proteomics of Right Heart Failure in Patients with Pulmonary Arterial Hypertension	181
DISCUSSION	211
CONCLUSION and PERSPECTIVES	218
REFERENCES	223
SUPPLEMENTARY MATERIALS	248
FRENCH SUMMARY	326

LIST OF PUBLICATIONS

- **PUBLICATIONS of the THESIS**

1- **M. Amsallem**, J.M. Sternbach, S. Adigopula, Y. Kobayashi, T.A. Vu, R. Zamanian, D. Liang, G. Dhillon, I. Schnittger, M.V. McConnell, F. Haddad, “Addressing the Controversy of Estimating Pulmonary Arterial Pressure by Echocardiography.” *Journal of the American Society of Echocardiography* (2016) ;29:93-102. doi:10.1016/j.echo.2015.11.001.

2- **M. Amsallem**, A.J. Sweatt, M. Aymami, T. Kuznetsova, M. Selej, H. Lu, O. Mercier, E. Fadel, I. Schnittger, M.V. McConnell, M. Rabinovitch, R.T. Zamanian, F. Haddad, “Right Heart End-Systolic Remodeling Index Strongly Predicts Outcomes in Pulmonary Arterial Hypertension: Comparison With Validated Models.” *Circulation: Cardiovascular Imaging* (2017) ;10(6).pii:e005771. doi:10.1161/CIRCIMAGING.116.005771.

3- **M. Amsallem**, D. Boulate, M. Aymami, J. Guihaire, M. Selej, J. Huo, A.Y. Denault, M.V. McConnell, I. Schnittger, E. Fadel, O. Mercier, R.T. Zamanian, F. Haddad, “Load Adaptability in Patients With Pulmonary Arterial Hypertension.” *American Journal of Cardiology* (2017) ;120:874-882. doi:10.1016/j.amjcard.2017.05.053.

4- **M. Amsallem**, S. French, N. Ouazani, S. Li, K. Kudelko, R.T. Zamanian, F. Haddad, L. Chung, “Non-Invasive Right Ventricular Load Adaptability Indices in Patients with Scleroderma-Associated Pulmonary Arterial Hypertension” *Pulmonary Circulation* (2018) ;8:2045894018788268. doi:10.1177/2045894018788268.

- **OTHER PUBLICATIONS**

5- **M. Amsallem**, T. Kuznetsova, K. Hanneman, A. Denault, F. Haddad, “Right Heart Imaging in Patients with Heart Failure: a Tale of Two Ventricles.” *Current Opinion in Cardiology* (2016) ;31:469-82. doi:10.1097/HCO.0000000000000315.

- 6- **M. Amsallem**, D. Boulate, Z. Kooreman, R.T. Zamanian, G. Fadel, I. Schnittger, E. Fadel, M.V. McConnell, G. Dhillon, O. Mercier, F. Haddad, “Investigating the Value of Right Heart Echocardiographic Metrics for Detection of Pulmonary Hypertension in Patients with Advanced Lung Disease.” *International Journal of Cardiovascular Imaging* (2017) ;33:825-835. doi:10.1007/s10554-017-1069-3.
- 7- D. Boulate, J. Arthur Ataam, A.J. Connolly, G. Giraldeau, **M. Amsallem**, B. Decante, L. Lamrani, E. Fadel, P. Dorfmueller, F. Perros, F. Haddad, O. Mercier, “Early Development of Right Ventricular Ischemic Lesions in a Novel Large Animal Model of Acute Right Heart Failure in Chronic Thromboembolic Pulmonary Hypertension.” *Journal of Cardiac Failure* (2017) ;23:876-886. doi:10.1016/j.cardfail.2017.08.447.
- 8- F. Haddad, **M. Amsallem**, “Full Circle on Pulmonary Flow Dynamics in Pulmonary Arterial Hypertension.” *Journal of the American College of Cardiology JACC: Cardiovascular Imaging* (2017) ;10:1278-1280. doi:10.1016/j.jcmg.2016.12.022.
- 9- F. Loisel, B. Provost, F. Haddad, J. Guihaire, **M. Amsallem**, B. Vrtovec, E. Fadel, G. Uzan, O. Mercier, “Stem Cell Therapy Targeting the Right Ventricle in Pulmonary Arterial Hypertension: is it a Potential Avenue of Therapy?” *Pulmonary Circulation* (2018) ;8:2045893218755979. doi:10.1177/2045893218755979.
- 10- S. Guimaron, J. Guihaire, **M. Amsallem**, F. Haddad, E. Fadel, O. Mercier, “Current Knowledge and Recent Advances of Right Ventricular Molecular Biology and Metabolism from Congenital Heart Disease to Chronic Pulmonary Hypertension” *Biomed Research International* (2018) ;2018:1981568. doi:10.1155/2018/1981568.
- 11- **M. Amsallem**, H. Lu, X. Tang, NL Do Couto Francisco, Y. Kobayashi, K. Moneghetti, H. Shiran, I. Rogers, I. Schnittger, D. Liang, F. Haddad, “Optimizing Right Ventricular Focused Four-chamber Views using Three-Dimensional imaging, a Comparative Magnetic Resonance Based Study” *International Journal of Cardiovascular Imaging* (2018). doi:10.1007/s10554-018-1356-7.
- 12- **M. Amsallem**, J. Guihaire, J. Arthur Ataam, L. Lamrani, D. Boulate, S. Mussot, D. Fabre, Y. Taniguchi, F. Haddad, O. Sitbon, X. Jais, M. Humbert, G. Simmoneau, O. Mercier, P. Brenot, E. Fadel, “Impact of the Initiation of Balloon Pulmonary Angioplasty Program on Referral of Patients with Chronic

Thromboembolic Pulmonary Hypertension to Surgery” *Journal of Heart Lung Transplantation* (2018) ;37:1102-1110. doi:10.1016/j.healun.2018.05.004.

13- **M. Amsallem**, O. Mercier, Y. Kobayashi, K. Moneghetti, F. Haddad, “Forgotten No More: a Focused Update on the Right Ventricle in Cardiovascular Disease” *Journal of the American College of Cardiology JACC: Heart Failure* (2018), in press.

14- **M. Amsallem**, M. Aymami, W. Hiesinger, S. Zeigler, K. Moneghetti, M. Marques, J. Teuteberg, R. Ha, D. Banerjee, F. Haddad, “Right Ventricular Load Adaptability Metrics in Patients Undergoing Left Ventricular Assist Device Implantation” *The Journal of Thoracic and Cardiovascular Surgery*” (2018), in press.

15- M. Aymami, **M. Amsallem**, J. Adams, K. Sallam, K. Moneghetti, M. Wheeler, W. Hiesinger, J. Teuteberg, D. Weisshaar, J-P. Verhoye, J. Woo, R. Ha, F. Haddad, D. Banerjee, “The Incremental Value of Right Ventricular Size in the Risk Assessment of Right Heart Failure post-Left Ventricular Assist Device Implantation” *Journal of Cardiac Failure* (2018), in revisions.

LIST OF FIGURES

Figure 1. The right heart-pulmonary circulation unit.

Figure 2. The pulmonary resistance-capacitance relationship and clinical implications.

Figure 3. Transpulmonary pressure gradient and mean pulmonary arterial pressure – cardiac output relationship.

Figure 4. Right heart anatomy.

Figure 5. Pulmonary hypertension classification.

Figure 6. Right heart-pulmonary arterial coupling and adaptation.

Figure 7. Right ventricular response to pressure overload and possible treatment strategies.

Figure 8. Main molecular changes underlying right ventricular (RV) adaptation and maladaptation to increased afterload, and main histological patterns of RV remodeling in the setting of chronic pressure overload.

Figure 9. Inflammation and angiogenesis in atherosclerosis, aortic aneurysm, cardiac sarcoidosis and acute heart rejection.

Figure 10. Distinct roles for reparative and dysregulated immunity after vascular injury.

Figure 11. Right heart metrics using two-dimensional trans-thoracic echocardiography.

Figure 12. Myocardial deformation imaging based right ventricular longitudinal strain.

Figure 13. Example of right ventricular focused and unfocused apical 4-chamber views derived from 3-dimensional dataset, in end-diastole, in a patient with normal right ventricular phenotype and in a patient with mild pulmonary arterial hypertension.

Figure 14. Load adaptability indices.

Figure 15. Relationships between right ventricular function or end-systolic size and ventricular afterload.

Figure 16. Freehand drawings and corresponding cine SSFP images on four-chambers and three-chambers views demonstrating normal RV anatomy: moderator band, tendinous cords of tricuspid valve and trabeculations.

Figure 17. Short-axis images from the systolic phase of the cardiac cycle in a patient with PAH.

Figure 18. Severe idiopathic pulmonary hypertension in a 28 year-old man; pulmonary arterial pressure at right catheterization was 70 mmHg.

Figure 19. Four-dimensional flow MRI of a patient with pulmonary valvular disease; patients with pulmonary hypertension compared with a healthy control.

Figure 20. Example of estimation of ventricular dimensions using 4D flow MRI in a 9-year-old male with aortic coarctation.

Figure 21. Illustration of the three most common ELISA methods.

Figure 22. Example of flow cytometry multiplex arrays.

Figure 23. Criteria for assessment of novel cardiovascular biomarkers for clinical use and clinical applications of cardiovascular biomarkers.

Figure 24. Potential reasons for neutral/negative results targeting inflammation in heart failure.

Figure 25. Different aspects associated with deep phenotyping of the right heart in patients with pulmonary hypertension.

Figure 26. Mechanisms underlying the transition from right ventricular adaptation to maladaptation to afterload in pulmonary hypertension.

LIST OF TABLES

Table 1. Definition and clinical importance of metrics assessing right heart afterload in pulmonary hypertension.

Table 2. Summary of studies investigating inflammatory mediators in the right ventricular tissue.

Table 3. Summary of studies evaluating the relationship of circulating inflammatory biomarkers with the parameters of right ventricular performance.

Table 4. Selection of the most relevant right heart imaging metrics.

Table 5. Studies assessing correlation between invasive and echocardiography based right ventricular systolic pressure estimations.

ABBREVIATIONS

2D: two-dimensional

3D: three-dimensional

4D: four-dimensional

CMR: Cardiac Magnetic Resonance

CO: Cardiac Output

CRP: C-Reactive Protein

CTEPH: Chronic Thrombo-Embolic Pulmonary Hypertension

DCE: Delayed Contrast Enhancement

DPAP: Diastolic Pulmonary Arterial Pressure

HFpEF: Heart Failure with preserved Ejection Fraction

HFrfEF: Heart Failure with reduced Ejection Fraction

LV: Left Ventricular

LVEF: Left Ventricular Ejection Fraction

MPAP: Mean Pulmonary Arterial Pressure

PA: Pulmonary Artery

PAH: Pulmonary Arterial Hypertension

PAWP: Pulmonary Arterial Wedge Pressure

PH: Pulmonary Hypertension

PVR: Pulmonary Vascular Resistance

RA: Right Atrial

RAP: Right Atrial Pressure

RHF: Right Heart Failure

RV: Right Ventricular

RVEF: Right Ventricular Ejection Fraction

RVEDA: Right Ventricular End-Diastolic Area

RVESA: Right Ventricular End-Systolic Area

RVFAC: Right Ventricular Fractional Area Change

RVLS: Right Ventricular Free-Wall Longitudinal Strain

RVSP: Right Ventricular Systolic Pressure

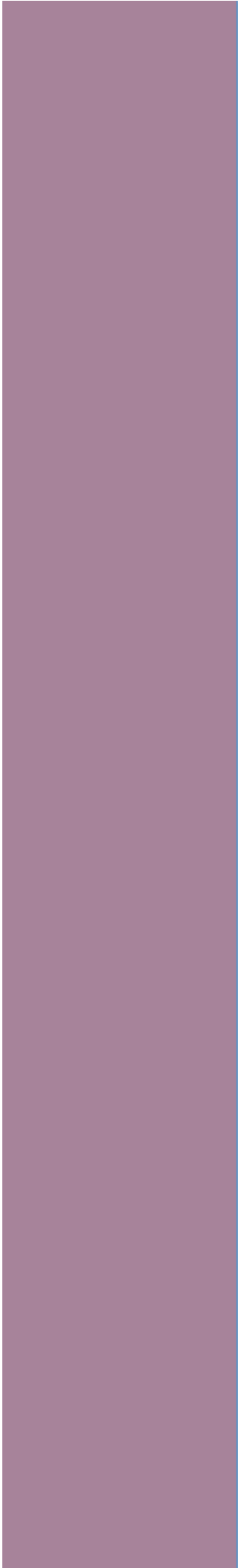
SPAP: Systolic Pulmonary Arterial Pressure

SV: Stroke Volume

TAPSE: Tricuspid Annulr Plane Systolic Excursion

TTE: trans-thoracic echocardiography

TR: Tricuspid Regurgitation



INTRODUCTION

INTRODUCTION

In 2006, a National Heart, Lung and Blood Institute Working Group on Cellular and Molecular Mechanisms of Right Heart Failure report delineated in broad terms the current base of scientific understanding of the right ventricle, identifying future directions of investigation (1).

In the following 12 years, there has been a renewed interest in the right heart. The right ventricle differs from the left ventricle in fundamental ways such as its embryologic origin (the left ventricle deriving from the primary heart field and the right from the secondary heart field (2), metabolism (3) and regulatory pathways (4). The right heart fascinates not only from its ability to adapt to pressure or volume overload but also to reverse remodel and recover from injury. Historically an important step was to move beyond the misconception of the right ventricle as a passive conduit. This was prompted by the observation that the right ventricle may be bypassed in patients with tricuspid aplasia or hypoplastic right heart by the Fontan surgery (5). While it is true that the low-pressure pulmonary system allows the right ventricle to be bypassed, the Fontan circulation remains vulnerable to pulmonary hypertension (PH) and has limited circulatory reserve with exercise (6). The link between right ventricular (RV) dysfunction and poor outcome in PH, left heart failure with preserved or reduced ejection fraction, post-left ventricular assist device implantation and myocardial infarction is now well established (7,8).

The main objective of this thesis is to present the utility of right heart deep phenotyping in the diagnosis, risk stratification and management of patients with PH, and in unraveling the mechanistic pathways underlying right heart failure.

Part 1- PATHOPHYSIOLOGY of the CARDIOPULMONARY UNIT

A comprehensive understanding of right heart function should consider the right heart within the cardiopulmonary unit (9). As shown in **Figure 1**, this includes a better assessment of ventriculo-arterial coupling (matching between the right ventricular RV contractility and afterload), atrio-ventricular coupling and inter-ventricular inter-dependence.

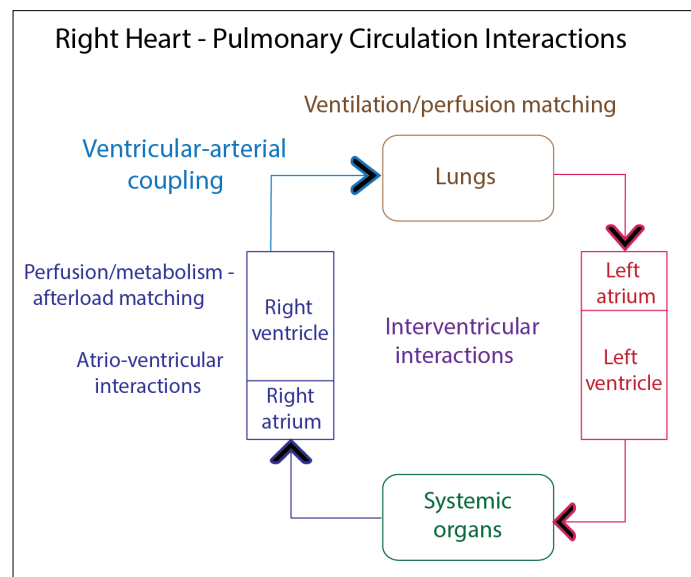


Figure 1. The right heart-pulmonary circulation unit. Schematic representation of the interaction present within the cardio-pulmonary circulation, including right ventricular-arterial coupling, atrio-ventricular interaction, right-left inter-ventricular inter-dependence and right ventricular myocardial perfusion-metabolism matching. (adapted with permission from the Marie Lannelongue Hospital Research Lab).

In this chapter, we will first review the main physiological concepts of the pulmonary circulation, highlighting the main differences with the systemic circulation and the clinical implications. Secondly, we will summarize the main embryological, anatomical, molecular and physiological features of the right ventricle in order to better understand the challenges for right heart imaging as well as the rationale behind right heart failure management. Thirdly, we will define pulmonary hypertension, classification and

consequences on the right heart, in order to approach the concept of ventriculo-arterial coupling and adaptation. Lastly, we will discuss the molecular pathways underlying RV adaptation to afterload in PH.

1.1 Physiology of the Pulmonary Circulation

1.1.a Main definitions

The right heart afterload can be simplified into two components: the resistive afterload (represented by the pulmonary vascular resistance, PVR) and the pulsatile afterload (represented by the pulmonary stiffness) (10).

Several parameters have been developed to provide information on local, regional, or global pulmonary arterial stiffness: pulse pressure, elasticity, distensibility, compliance, capacitance, and stiffness index β (11), as detailed in **Table 1**. Among them, capacitance (invasively estimated as the ratio of stroke volume (SV) divided by pulse pressure) has been associated with RV dysfunction, remodeling, and mortality, independently of the level of resistance, in a wide spectrum of diseases (idiopathic and scleroderma-associated pulmonary arterial hypertension PAH (12,13), heart failure with reduced ejection fraction HFrEF (14,15) and heart failure with preserved ejection fraction HFpEF) (16). Pulmonary arterial elasticity is measured as (maximal pulmonary artery (PA) area - minimum area)/minimum area, using phase-contrast cardiac magnetic resonance (CMR) imaging, on the transverse perpendicular plane. It may be valuable for the detection of exercise-induced PH or earlier stages of pulmonary vascular disease (17).

Table 1. Definition and clinical importance of metrics assessing right heart afterload in pulmonary hypertension.

Metric	Definition	Modality	Key finding	Clinical implications
Transpulmonary pressure gradient	MPAP-PAWP	RHC	Increased	Higher in patients with pre-capillary PH than in those with post-capillary PH
Pulmonary vascular resistance (PVR)	(MPAP-PAWP)/CO	RHC	Increased	Mostly related to arterial tree resistance Can increase up to 4 times in PH as opposed to systemic circulation 50% increase
Total pulmonary resistance (TPR)	MPAP/CO	RHC	Increased	
Pulse pressure (PP)	SPAP-DPAP	RHC	Decreased	Not able to differentiate between a pure decreased in stroke volume or an increased in pressure (i.e. increased in stiffness).
Elasticity	(max PA area – min area) / min area	Phase-contrast MRI, transverse perpendicular plane	Decreased	Different concept than elastance (change in pressure for a given change in volume)
Distensibility	PA elasticity / PP	MRI and RHC	Decreased	Diagnosis of PH >10% is a marker of acute responsiveness to vasodilators in PAH
Compliance	(max area – min area) / PP	MRI and RHC	Decreased	Quantifies local PA stiffness
Capacitance	Stroke Volume/PP	RHC or MRI	Decreased	Quantifies total stiffness Predicts survival independently from resistance level in PAH, HFrEF and HFpEF
Stiffness index beta	log(SPAP/DPAP) / elasticity	MRI and RHC	Increased	Quantifies pressure-independent stiffness

CO: cardiac output; DPAP: diastolic pulmonary arterial pressure; HFpEF: left heart failure with preserved ejection fraction; HFrEF: left heart failure with reduced ejection fraction; LVAD: left ventricular assisting device; MRI: magnetic resonance imaging; PA: pulmonary artery; PAWP: pulmonary arterial wedge pressure; PH: pulmonary hypertension; RAP: right atrial pressure; RHC: right heart catheterization; SPAP: systolic pulmonary arterial pressure.

1.1.b The inverse resistance-capacitance relationship

Understanding the differences between the pulmonary circulation and the systemic circulation is key to understand the pathophysiology of right heart failure (RHF). In contrast to the systemic circulation, the pulmonary circulation is a low resistance-high compliance/capacitance system (18), in which resistance (R) and capacitance (C) are inversely related to each other as follows: $C=\tau/R$ where τ is the RC time constant of the system (**Figure 2A** and **2B**) (19–22). Lankhaar et al. showed that the RC-time, the product of resistance R and compliance C, remains relatively constant in patients treated for PH (22). In mild PH, a decrease in resistance is accompanied by a substantial increase in compliance compared to severe PH (**Figure 2C**). This may explain the clinical observation that patients with mild PH often show a greater hemodynamic improvement after therapy than patients with severe PH, even if their resistance decreases by the same amount. Saouti et al. further demonstrated that the pulsatile component of load remains constant (about 23% of total load) in subjects without PH and patients with PAH over a wide range of pulmonary pressures, in contrast to the systemic circulation (23). As illustrated in **Figure 2B**, the RV relationship is shifted to the left in patients with post-capillary PH (i.e. secondary to left heart failure) (24,25). This may reflect smaller capacitance (i.e. larger stiffness) of the pulmonary vascular circulation in patients with pre-capillary PH than in those with post-capillary PH at a similar level of PVR severity. As suggested by Vonk Noordegraaf et al. in their recent review, it may also be explained by the definition of capacitance, invasively estimated as = stroke volume / pulse pressure, which does not include pulmonary arterial wedge pressure (PAWP) (19).

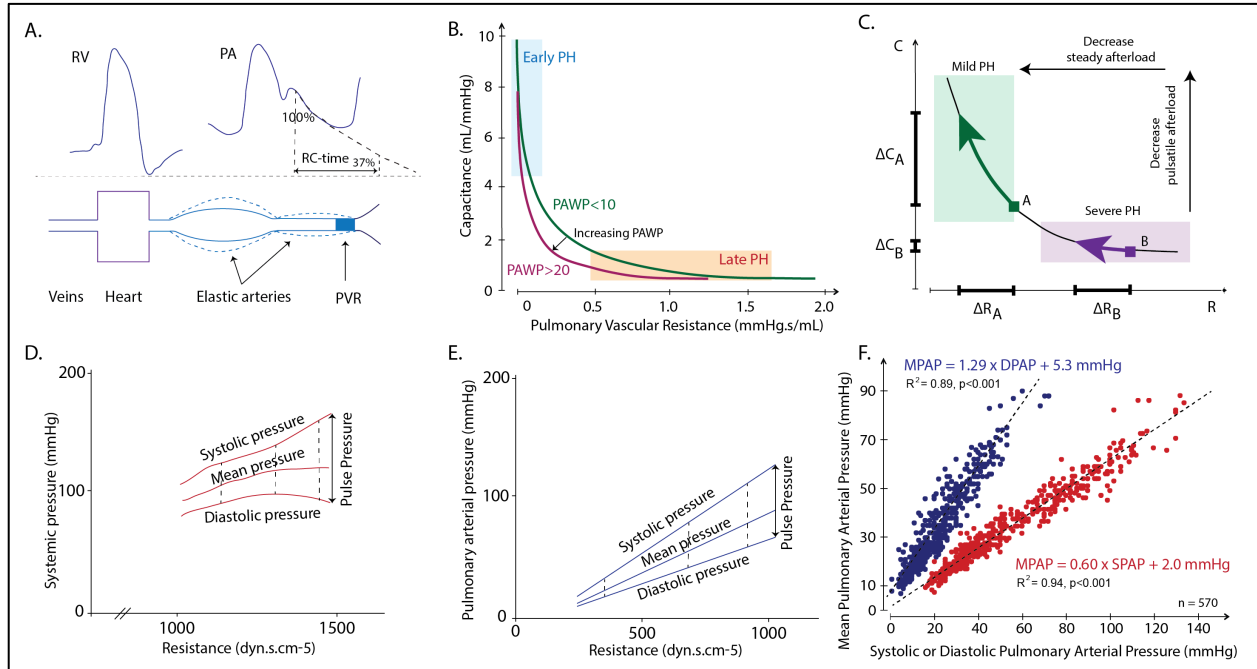


Figure 2. The pulmonary resistance-capacitance relationship and clinical implications. (A) Diagram of the pulmonary system showing the pulsatile and resistive components of resistance to flow (adapted from Saouti et al. *Eur Respir Rev*, 2010). (B) Schematic inverse relation between resistance and capacitance, and influence of PAWP. At normal and low R (early PH, blue), changes in R have a large effect on C. At high R (late PH, orange), a similar change in resistance has little effect on C (adapted from Vonk Noordegraaf et al. *J Am Coll Cardiol*, 2017). (C) Change in afterload with therapy (adapted from Lankhaar et al. *Eur Heart J*, 2008). (D) In the systemic circulation, when pressure increases, systolic, diastolic and mean pressures are not linearly related. (E) In contrast, systolic mean and diastolic pressures increase linearly in pulmonary hypertension. Note also that the ranges in pressures and resistance are extremely large in pulmonary circulation in comparison to systemic circulation (D to E are adapted from Saouti et al. *Eur Respir Rev*, 2010). (F) Linear relationship between mean pulmonary arterial pressure (MPAP) and diastolic (DPAP) or systolic (SPAP) pressures, expressed as Pearson correlation (R²), in 570 patients with pulmonary arterial hypertension or advanced lung disease (adapted from Amsallem et al. *JACC:HF*, 2018). C: capacitance; DPAP: diastolic pulmonary arterial pressure; MPAP: mean pulmonary arterial pressure; PA: pulmonary artery; PAWP: pulmonary arterial wedge pressure; PVR: pulmonary vascular resistance; R: resistance; RV: right ventricle; SPAP: systolic pulmonary arterial pressure.

1.1.c The mean and systolic pulmonary arterial pressures collinearity

Another specific feature of the pulmonary circulation is the linear relationship between the mean pulmonary arterial pressure (MPAP), systolic pulmonary arterial pressure (SPAP) and pulse pressure (**Figure 2D-F**) (20,26,27). First reported by Chemla et al. in 2004 using high fidelity manometers (28), the simple linear equation ($MPAP=0.61 \times SPAP + 2 \text{ mmHg}$) was recently validated by our group in a larger cohort of more than 600 patients with PAH or advanced lung disease (26), as illustrated in **Figure 2F**.

1.1.d Transpulmonary-pressure gradient versus diastolic pulmonary gradient

Although PVR is commonly used in clinical practice, it assumes that the closure pressure (pressure at zero flow) is equal to the pulmonary artery occlusion pressure, and therefore the relationship passes through zero (18). However, this assumption is not accurate and can lead to misinterpretation of dynamic changes in resistance. An increase in calculated PVR (i.e. $MPAP-PAWP/\text{cardiac output}$) may merely reflect a decrease in cardiac output and not necessarily a change in the transpulmonary-pressure gradient ($TPG = MPAP-PAWP$), which reflects the resistive afterload per se. A more physiological albeit less practical method of assessing resistance would be to derive the slope of the transpulmonary-pressure gradient-cardiac index relationship, as presented in **Figure 3A** (18).

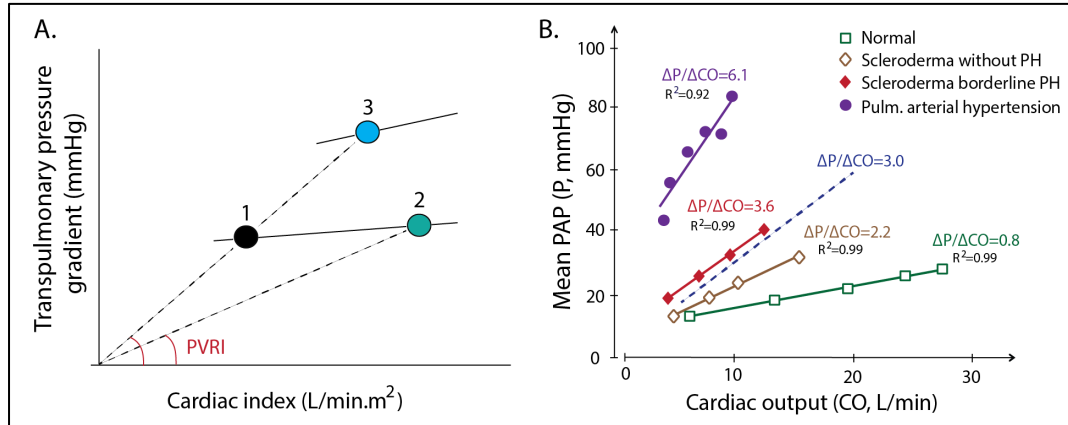


Figure 3. Transpulmonary pressure gradient and mean pulmonary arterial pressure – cardiac output (MPAP-CO) relationship. (A) Pressure-flow relationship: pulmonary vascular resistance index (PVRI) is defined by the transpulmonary pressure gradient over cardiac index ratio (adapted from Chemla et al. Eur Respir J, 2002). The solid line indicates the multipoint pulmonary arterial pressure-flow relationship with closure pressure greater than pulmonary artery occlusion pressure. From 1 to 2, PVRI decreases while functional state of the pulmonary circulation remains essentially unchanged. From 1 to 3, PVRI is unchanged while the increased slope of the relationship attests to worsening of pulmonary hypertension (PH). **(B)** MPAP-CO relationships according to different etiology during incremental exercise. The threshold of >3.0 represents an abnormal pulmonary vascular response to exercise and may be indicative of early pulmonary vasculopathy (adapted from Lewis et al. Circulation, 2013).

Recently, the diastolic pulmonary gradient was proposed to replace the transpulmonary pressure gradient to differentiate post-capillary from pre-capillary PH (29). The diastolic pulmonary gradient (defined as diastolic pulmonary artery pressure - PAWP) is believed to be less affected by left heart failure-induced changes in vascular compliance than the transpulmonary pressure gradient (30). The threshold of 7mmHg has been proposed to differentiate patients with pre-capillary PH (diastolic pulmonary gradient < 7 mmHg and $PVR \leq 3$ Wood units) from those with mixed pre- and post-capillary PH (7). Gerges et al. showed in a large cohort of 1,994 patients with post-capillary PH and transpulmonary pressure gradient > 12 mmHg that a diastolic pressure gradient ≥ 7 mmHg was associated with worse outcome than < 7 mmHg, suggesting that diastolic pressure gradient may reflect more

advanced pulmonary vascular remodeling (31). However, Tampakakis et al. did not validate these findings in a large retrospective of 1,236 evaluated for unexplained cardiomyopathy, in which elevated diastolic pressure gradient was not associated with worse survival whereas elevated transpulmonary pressure gradient and PVR were (32). Perhaps the biggest caveat of using diastolic pressure gradient measured using fluid-filled catheters is that it may be particularly prone to measurement error; given the low absolute value of diastolic pressure gradient, even minor inaccuracies in diastolic pulmonary arterial pressure or PAWP measurements can have a significant effect on diastolic pressure gradient.

1.1.e Rediscovering the pressure – cardiac output, a window to exercise-induced PH

In the pulmonary circulation, the mean pulmonary pressure-cardiac output (MPAP-CO) relationship can be approximated using a linear model, although the “true” relationship is more curvilinear depending on the distensibility coefficient of the pulmonary circulation (**Figure 3B**) (33). This concept was first described in 1985 by Janicki et al. in patient with heart failure and is currently building a framework for a new definition of exercise induced PH (34–36). Prior to the 4th World Symposium on Pulmonary Hypertension guidelines, a MPAP with exercise >30 mmHg was used to define exercise-induced PH. This definition was since removed as this threshold may be reached in older normal subjects (37) or in patients with high cardiac output (38). A MPAP-CO slope >3 is now recognized to define exercise-induced PH, as it was shown to be incremental to MPAP >30mmHg (36,39).

1.2 The Right Ventricle

1.2.a Embryology and anatomy of the right heart

The right ventricle and the left ventricle have distinct embryological origins; the left ventricle first derives from the primary heart field and the right ventricle derives from the secondary heart field (2).

During the fetal period, the right ventricle ejects blood at high pressure into a high-resistance vascular circulation. The RV and left ventricular (LV) wall thickness are similar (about 3.5mm at term) (40). After birth, the pulmonary circulation transition into a low-resistance circuit and the RV wall thickness remains at 4mm, while the LV wall increases at about 10mm to adapt for increased afterload (about 4 times). The features of the fetal heart have been recently reviewed by Guimaron et al. in the **Supplementary article 2** (3).

The right ventricle is classically divided into three parts, as illustrated in **Figure 4**: the inlet, the apical part and the outlet. The RV wall is composed of a superficial apical layer in continuity with the left ventricle, and a deep longitudinal layer (41). The longitudinal component of the RV contraction is prominent, contributing to the high prognostic value of longitudinal metrics of RV function such as RV longitudinal strain.

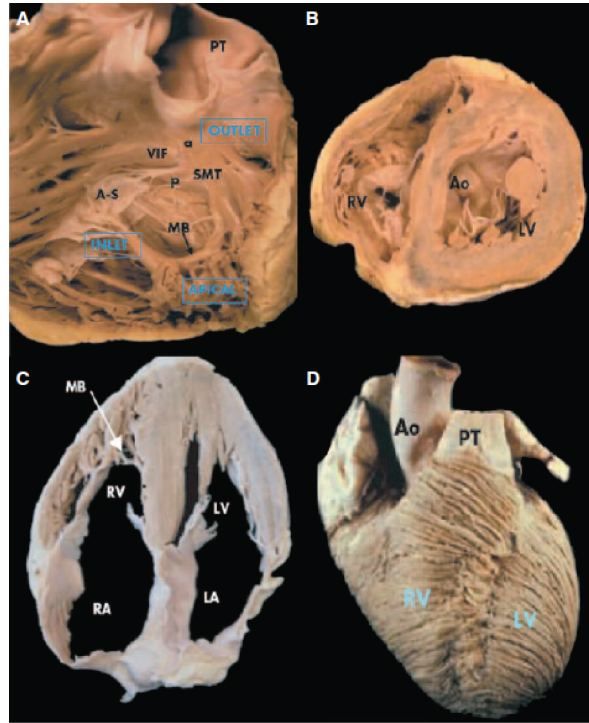


Figure 4. Right heart anatomy. (A) The inlet, trabeculated apical myocardium and infundibulum of the RV. The tricuspid and pulmonary valves are separated by the ventriculo-infundibular fold (VIF). (B) Short-axis plane of the RV demonstrating its crescentic shape. (C) The 4-chamber anatomic plane of the heart showing the moderator band (MB) and the more apical insertion of the tricuspid valve. (D) Superficial muscle layer of the RV. SMT indicates septo-marginal trabeculation with its anterior (a) and posterior (p) arm; A-S, antero-superior leaflet of the tricuspid valve; PT, pulmonary trunk; Ao, aorta; RA, right atrium; and LA, left atrium. Reproduced from Haddad et al. *Circulation*, 2008.

1.2.b Right heart versus left heart

Although the separation between the right and left heart has a clear anatomical and embryological basis, it does not reflect the complexity of the structural and functional relationships and interactions between the heart and the circulation. Anatomically, the right and left ventricles are strongly connected through the septum and myofiber architecture (42). Because of the functional interactions between the ventricles, interpretation of RV performance should always be made in the context of LV function and vice versa. In

the absence of complex congenital heart disease, the effective stroke volume of both ventricles is equal on average. Consequently, RV dysfunction in patients with predominantly “left heart failure” could mainly reflect low stroke volume and not necessarily intrinsic myocardial involvement of the right heart. In addition to systolic interactions, diastolic interactions, neurohormonal factors and interventricular dyssynchrony blur the lines between the right and left heart (43–45).

1.3 Pulmonary Hypertension

1.3.a Definitions

Pulmonary hypertension is defined by a resting invasive MPAP ≥ 25 mmHg (7). The normal value of the MPAP 14 ± 3 mmHg leaves a “gray area” of pressures between 20-24 mmHg. The consequences of these values are still not completely understood, some interpreting them as “pre-PH state”.

The definition of **exercise-induced PH** has recently evolved. Initially defined as MPAP at exercise >30 mmHg, this definition has been removed in the latest European guidelines on PH, as this threshold can be reached with age or high CO (38). Janicki et al. were among the first to report in 1985 the linear relationship between MPAP and CO during exercise, as illustrated in **Figure 3B** (34). More recently, Herve et al. revalidated the MPAP/CO slope (i.e. total pulmonary resistance), showing the incremental value of a >3.0 threshold at exercise to MPAP >30 mmHg to predict the presence of pulmonary vascular disease (20,36).

1.3.b Classification of pulmonary hypertension

The 5th World Symposium on Pulmonary Hypertension consensus (2013) proposed a new clinical classification of PH into 5 categories presented in **Figure 5** (7).

1. Pulmonary Arterial Hypertension Idiopathic Heritable (BMP2 mutation, other mutations) Drugs and toxins induced Associated with: Connective tissue disease Human immunodeficiency virus infection Portal hypertension Congenital heart diseases Schistosomiasis	3. Pulmonary Hypertension due to Lung diseases and/or Hypoxia Chronic obstructive pulmonary disease Interstitial lung disease Other pulmonary diseases with mixed restrictive and obstructive pattern Sleep-disordered breathing Alveolar hypoventilation disorders Chronic exposure to high altitude Developmental lung diseases
1'. Pulmonary veno-occlusive disease and/or pulmonary capillary haemangiomas Idiopathic Heritable (EIF2AK mutation, other mutations) Drugs, toxins and radiation induced Associated with: Connective tissue disease Human immunodeficiency virus infection	4. Chronic Thrombo-Embolic Pulmonary Hypertension and other pulmonary artery obstructions Chronic thrombo-embolic pulmonary hypertension Other pulmonary artery obstructions Angiosarcoma Other intravascular tumors Arteritis Congenital pulmonary arteries stenosis Parasites (hydatidosis)
1". Persistent pulmonary hypertension of the newborn	
2. Pulmonary Hypertension due to left heart disease Left ventricular systolic dysfunction Left ventricular diastolic dysfunction Valvular disease Congenital/acquired left heart inflow/outflow tract obstruction and cardiomyopathies Congenital/acquired pulmonary veins stenosis	5. Pulmonary Hypertension with unclear and/or multifactorial mechanisms Hematological disorders: chronic haemolytic anemia, myeloproliferative disorders, splenectomy Systemic disorders: sarcoidosis, pulmonary histiocytosis, lymphangioleiomyomatosis Metabolic disorders: Gaucher disease, thyroid disorders Others: pulmonary tumoral thrombotic microangiopathy, fibrosis mediastinitis, chronic renal failure (with/without dialysis)

Figure 5. Classification of Pulmonary Hypertension.

Group 1 - Pulmonary arterial hypertension (**PAH**) is characterized by vascular remodeling of the pulmonary arterial tree, vasoconstriction, inflammation, smooth muscle cells proliferation, endothelial resistance to apoptosis leading to obstruction (46).

Group 2 - Pulmonary hypertension due to **left heart diseases**, previously classified as “post-capillary PH”, includes left heart systolic and “diastolic” dysfunction, valvular disease such as mitral stenosis or congenital heart disease, leading to an increase of PAWP \geq 15mmHg. Two presentations can occur: “passive post-capillary PH” or “mixed pre- and post-capillary PH”. With the increase in prevalence of left

HFpEF, often wrongly addressed as “diastolic heart failure”, this category represents the most frequent cases of PH (47).

Group 3 – Pulmonary hypertension due to **lung disease and/or hypoxia** is characterized usually by less severe MPAP elevation than in PAH (MPAP usually less than 35mmHg) (48). Vasoconstriction due to hypoxia is one of the main mechanisms of increased pulmonary pressure, particularly at exercise. One of the challenges presented by this category is being able to detect pulmonary hypertension, as this is associated with poor outcome in patients with advanced lung disease such as chronic obstructive pulmonary disease. Diagnosis of PH can be achieved invasively by right heart catheterization, although exposing patients to vascular complications risks. Non-invasive strategies, such as using echocardiography, present with the advantage of being cheap, accessible, reproducible and harmless. As presented in the imaging section below, PH can be detected using right ventricular systolic pressure (RVSP) estimation from Doppler measurement of the tricuspid regurgitation peak velocity (26). However, the tricuspid regurgitation signal is frequently (less than half of patients) not interpretable in patients with advanced lung disease, due to poor echogenicity or heart axis deviation. An alternative method is to use indirect signs of increase right heart pressures, such as right ventricular or right atrial enlargement or right ventricular dysfunction (49). We recently showed in a large cohort of patients with advanced restrictive or obstructive lung diseases referred for right heart catheterization and echocardiography at Stanford University that using echocardiography for detecting PH was more challenging in this population than in other etiologies of PH, as we found out that several patients had RV enlargement or dysfunction despite normal invasive pressures at rest (48), presented in **Supplementary article 3**. One hypothesis is the presence of PH during exercise associated with hypoxia in these patients.

Group 4 – **Chronic Thrombo-Embolitic Pulmonary Hypertension (CTEPH)** is a rare but severe complication of acute pulmonary embolism leading to RHF and premature mortality. Its cumulative incidence ranges from 0.1–9.1% within the first 2 years after symptomatic acute pulmonary embolism, although probably underestimated due to the lack of systematic follow-up and screening in clinical routine (50–52). The pathophysiology of CTEPH is believed to be the result of fibrotic transformation of

pulmonary artery thrombi causing chronic obstruction in macroscopic pulmonary arteries, associated with microvascular remodeling, inflammation and endothelial dysfunction (53,54).

Despite being associated to different etiology, PH categories have common consequences on the right heart, as presented in the next section.

1.4 Right Heart Adaptation to Pressure Overload

The right ventricle forms a functional unit with the pulmonary circulation and venous return (cardio-pulmonary unit). In order to better understand the adaptation of the right heart to pressure overload, the concept of RV – pulmonary arterial coupling needs to be first defined.

1.4.a Right ventricular – pulmonary arterial coupling

Landmark studies from Dell’Italia et al. have shown that RV function can be approximated using a time varying elastance model, where contractility is estimated using end-systolic pressure-volume relationship and ventriculo-arterial coupling by the ventricular to arterial elastance ratio (E_{es}/E_a) (**Figure 6A**) (55).

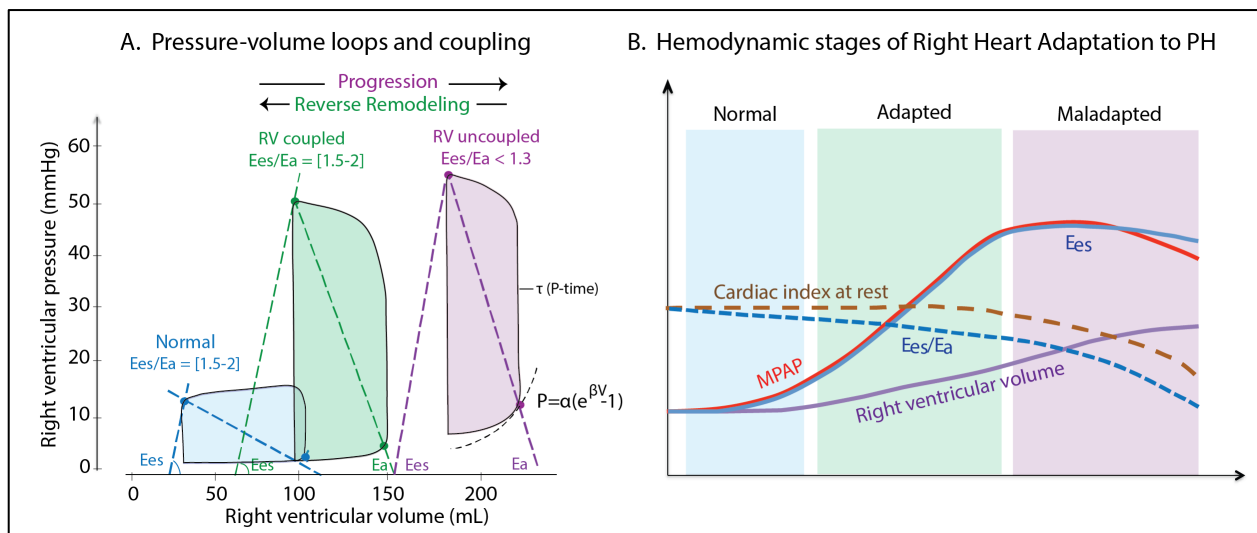


Figure 6. Right heart-pulmonary arterial coupling and adaptation. (A) Examples of pressure-volume loops in an healthy control, patients with coupled and uncoupled pulmonary hypertension (PH). **(B)** Hemodynamic stages of right heart adaptation to increased afterload in patients with pulmonary arterial hypertension. Ea: pulmonary arterial elastance; Ees: ventricular elastance; MPAP: mean pulmonary arterial pressure; PAWP: pulmonary arterial wedge pressure. (Adapted from Amsallem et al. JACC:HF, 2018).

1.4.b Right heart adaptation to pressure overload

Increased afterload of the right ventricle results in an increase in the RV wall-stress. Exposed to this increased wall-stress, the right heart will first adapt by increasing the wall thickness (RV hypertrophy) following Laplace's law. In order to maintain cardiac output, the right heart dilates (following Starling's law) and the heart rate increases (19). This adaptive remodeling initially enables maintaining RV-pulmonary arterial coupling (i.e. Ees/Ea between 1.5 to 2.0), as presented in **Figure 6A**. **Figure 6B** illustrates the natural history of right heart and pulmonary circulation metrics in a patient with PAH. With time, tachycardia and RV enlargement becomes deleterious, increasing the myocardial oxygen consumption, failing to maintain cardiac index and RV uncoupling occurs (i.e. Ees/Ea decreases). Parallel to the decrease in cardiac index, the MPAP decreases. The decrease in MPAP should not be interpreted as an improvement in the pulmonary vascular disease, showing the limitation of using MPAP alone to define afterload (**Figure 6B**). In addition, contrary to the common belief, ventricular elastance (Ees, contractility) is increased in patients with PAH (as illustrated in **Figure 6B**). The ability of the right ventricle to reverse remodel following lung transplantation could be in part explained by its preserved contractility (56).

The vicious circle of RV adaptation to pressure overload has been recently reviewed by Vonk Noordegraaf et al.'s team (19,57) and is summarized in **Figure 7**.

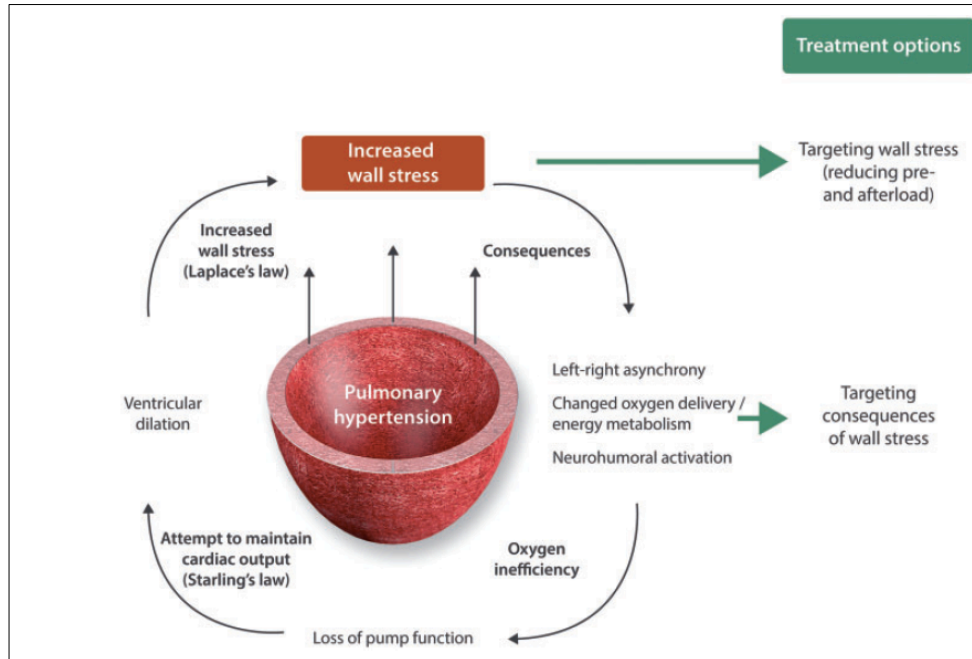


Figure 7. Right ventricular response to pressure overload and possible treatment strategies. Consequences of increased RV wall stress with PH may include left-right asynchrony, changed cardiac oxygen delivery and energy metabolism, and elevates neurohumoral activation. These can in turn cause loss of pump function. In an attempt to maintain cardiac output the RV may dilate, with a further increase in wall stress. Treatment options target elevated wall stress or target the consequences of elevated wall stress. Adapted from Westerhof et al. *Cardiovasc Res*, 2017.

Understanding the increase in wall stress following pressure overload and its consequences is the base to better treat right heart failure. Therapy of the failing right heart is beyond of the scope of the present thesis. This topic has been comprehensively covered in several reviews and state of the art documents (8,57,58).

1.4.c Right ventricular adaptation to PH: beyond increased afterload?

While heart failure has been considered as a hemodynamic story for decades, recent evidence suggests that the heart failure syndrome does not solely rely on hemodynamics, but also involves metabolic, neurohormonal and inflammatory changes. The first evidence is the wide variability in RV adaptation to

increased afterload, with patients presenting with compensated RV phenotypes for years, while others present with rapid onset of right heart failure for the same level of afterload. The second evidence is that among etiology of PH, there is also a wide heterogeneity in RV adaptation. Patients with Eisenmenger syndrome secondary to congenital heart disease present with later onset of RHF for higher pressure than patients with PAH secondary to scleroderma (59,60). Similarly, patients with RV pressure overload without pulmonary vascular disease (such as patients with pulmonary stenosis) tends to have preserved RV contractility for a longer period of time than patients with PAH (61,62). These observations combined overall suggest that there are other mechanisms underlying RV adaptation to PH beyond the increase in RV wall stress.

The heterogeneity between RV adaptations in animal models of PH also suggests the implication of molecular pathways in RV adaptation/maladaptation. The effects of pulmonary artery banding on the right heart in rats are better tolerated than the effects of PH induced by endothelial toxins, such as monocrotaline or Sugen 5416/hypoxic model (Sugen is an antagonist of the vascular endothelial growth factor receptor) (63). This further suggests the role of endothelial dysfunction and inflammation in RV maladaptation to increased overload, which represents two among several targets in the field.

1.4.d Molecular changes underlying right heart adaptation to PH

The molecular changes associated with RV remodeling in PH include metabolic changes, angiogenesis impairment and the potential role of immunity, as illustrated in **Figure 8**.

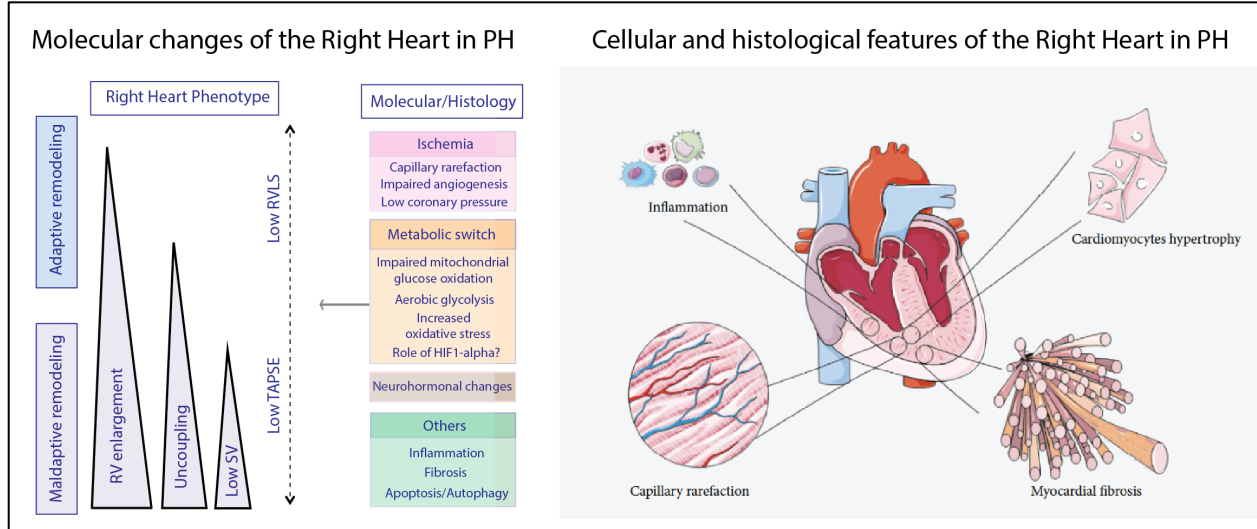


Figure 8. Main molecular changes underlying right ventricular (RV) adaptation and maladaptation to increased afterload (left panel) and main histological patterns of RV remodeling in the setting of chronic pressure overload (right panel, adapted from Guimaron et al. BioMed Res Int, 2018). Inflammation involving mononuclear cells and cardiomyocytes hypertrophy are observed at the early stage. Reduced capillary density and myocardial fibrosis are associated with right ventricular maladaptive phenotype. PH: pulmonary hypertension; RVLS: right ventricular free-wall longitudinal strain; SV: stroke volume; TAPSE: tricuspid annular plane systolic excursion.

1.4.d.i Metabolic changes and the role of the mitochondria

The **metabolic changes** and the role of the **mitochondria** have been recently reviewed by Ryan and Archer (64) and will not be extensively covered in this thesis. Briefly, mitochondria are the main actors of metabolic changes that similarly occur in RV cardiomyocytes and vascular cells in PAH. Glycolysis and glucose oxidation become uncoupled (i.e. aerobic glycolysis), leading to a cancer-like metabolic cellular phenotype. There is an increase in the energetic reliance on aerobic glycolysis (less efficient to produce adenosine triphosphate ATP) while mitochondrial respiration is inhibited (secondary to the activation of transcription factors such as c-Myc or hypoxia inducible factor HIF1-alpha and the inhibition of the phosphodehydrogenase enzyme by the phosphodehydrogenase kinases). Cells are more susceptible to fibrosis and hypertrophy; display increased proliferation rate and apoptosis, and impaired contractility. These changes can be targeted by metabolic modulators restoring depressed glucose oxidation or inhibiting the upregulated fatty acid oxidation and glutaminolysis. These therapies (such as dichloroacetate inhibiting phosphodehydrogenase kinase) have been shown to be beneficial to the hemodynamic and functional states in small animal models (65,66), and have been the focus of a recent clinical trial (NCT01083524, assessing the tolerance of three doses of dichloroacetate: completed, results pending).

1.4.d.ii Myocardial ischemia

The second aspect of RV molecular changes in PH is the presence of **myocardial ischemia**. In hypertrophied right ventricles, the increase in RV wall thickness, the increase in myocardial oxygen consumption and the decrease in oxygen coronary supply are factors contributing to ischemia. In a normal right heart, the RV myocardium is perfused both in diastole and systole, because of the systolic gradient between the aorta and the low RV systolic pressure. In PH, the gradient between the intra-aortic pressure and the RV systolic pressure may be close to zero (annulling the systolic filling of the right coronary artery), and the aortic diastolic pressure – RV diastolic pressure difference may be reduced (reducing the diastolic filling of the right coronary artery) (67). Studies have shown that the threshold of intra-right

coronary artery pressure enabling preserved RV contractile function is 50mmHg (68). The second potential contributor to ischemia is capillary rarefaction observed in right ventricles exposed to increased afterload, associated with impaired angiogenesis. The impairment in angiogenesis may result from decreased expression of genes such as insulin-like growth factor 1, vascular endothelial growth factor VEGF, or angiopoietin-1 (69).

In patients with PAH, ischemia can manifest as angina, troponin elevation or evidence of low myocardial perfusion using nuclear perfusion stress imaging (70). Biopsy or transplanted samples of hearts from patients with congenital heart disease or idiopathic pulmonary arterial hypertension have also supported the ischemic hypothesis showing evidence of histological ischemia within the RV myocardium (71–73), as presented in **Supplementary article 5**. However, there is little evidence on RV ischemia features in patients with other forms of PH such as CTEPH. As evidence is emerging that PAH may involve systemic inflammation and endothelial dysfunction beyond pulmonary vascular remodeling, it can be hypothesized that patients with CTEPH may have specific features that deserve to be studied (46).

Determinants of the **transition from RV adaptive to maladaptive phenotypes** are still not fully understood. In particular, existing evidence on molecular mechanisms and histology features underlying the transition to maladaptive phenotype mainly derives from preclinical studies. Rodent and piglet animal models of PH studies have shown that initially RV hypertrophy is associated with an increase in hypoxic markers, such as HIF1- α , which leads to activation of angiogenesis (through the VEGF-A pathway) (53,71,72,74,75). The increase in angiogenesis is believed to enable maintaining a compensated phenotype. There is less evidence on the molecular pathways associated with a decompensated/maladaptive phenotype. One study in rats with monocrotaline-induced PH and a decompensated RV phenotype (defined by decreased cardiac output) showed that HIF-1 α and angiogenesis markers were decreased, through the activation of p53. Noly et al. further demonstrated in a piglet model of CTEPH that the mismatch between angiogenesis and RV workload (defined by the capillary density to stroke work ratio) was associated with myocardial fibrosis and RV dysfunction,

supporting the ischemic hypothesis (75). As histological evidence is limited in humans, a prospective clinical study (MVD study, clinicaltrial.gov identification number NCT03199131) has recently been completed at our institution comparing the histological features of RV surgical biopsies from 10 patients with CTEPH and 10 controls referred for aortic surgeries (with normal RV phenotype and without coronary arterial disease). This study will provide more insight on histological and molecular changes in the right ventricle of patients with CTEPH, further exploring the changes in RV remodeling post-endarterectomy.

1.4.d.iii Immunity and proteomic biomarkers

Immunity has recently emerged as another strong candidate in the transition from adapted to maladapted RV in PH. The body of evidence supporting the role of inflammation, either acute or chronic, in the pathogenesis, progression and complications of several **vascular diseases** (such as atherosclerosis and aortic aneurysms) has grown exponentially in the past decades (76–80). **Figure 9** illustrates some examples of the different immune actors in cardiovascular disease (81).

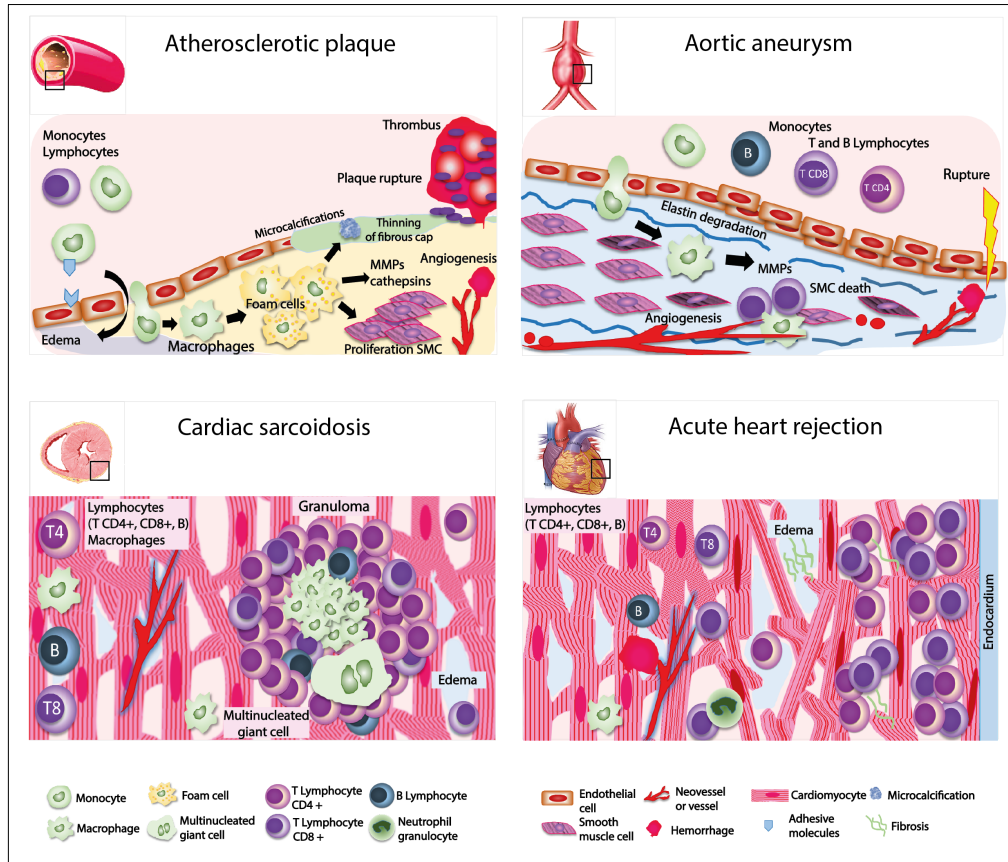


Figure 9. Inflammation and angiogenesis in (A) atherosclerosis, (B) aortic aneurysm, (C) cardiac sarcoidosis and (D) acute heart rejection. MMP, matrix metalloproteinases; SMC, smooth muscle cell. Adapted from Amsallem et al. *Circ J*, 2016.

Immunity has also been extensively demonstrated to be involved in the pathophysiology of **pulmonary vascular remodeling** in **PAH** (46,82–84). High levels of circulating mediators of inflammation (including cytokines) have been associated with worst disease severity, impaired functional status and lower survival in patients with PAH (85–89). **Figure 10** develops some features of the role of inflammation in PAH.

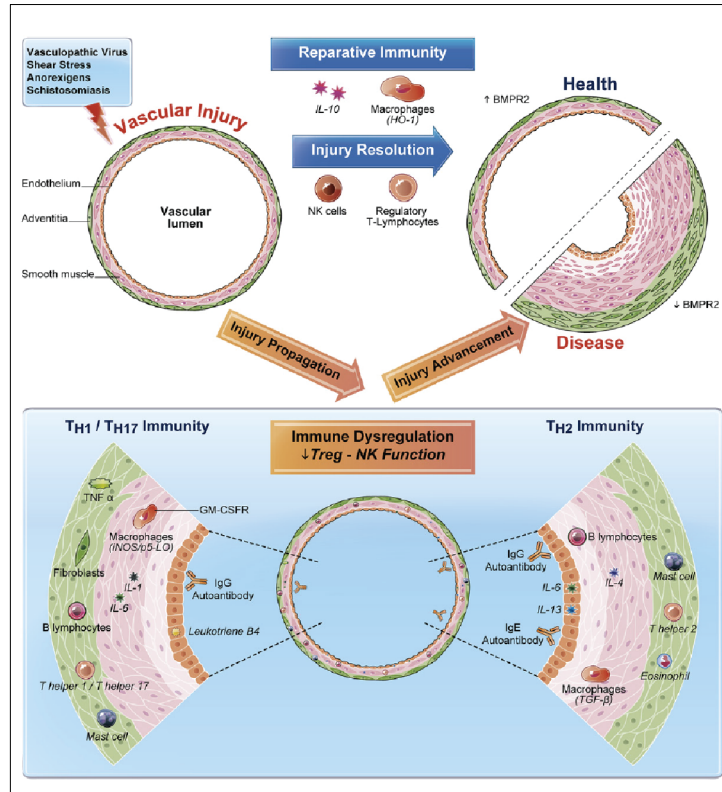


Figure 10. Distinct roles for reparative and dysregulated immunity after vascular injury. A variety of stimuli can be injurious to pulmonary arterioles; a health-promoting immune response will resolve inflammation after the stimulus has been contained and eliminated. With normal reparative immunity, inflammation is prevented from becoming inappropriately exuberant and prolonged by the regulatory activity of natural killer (NK) cells and Tregs. In processes not well understood, adaptive immune responses (T cells, B cells) driven by antigen-specific signals coordinate with evolutionarily ancient innate immune responses (NK cells, macrophages) to dampen immunity once the danger of the vascular injury has passed. This process may involve the skewing of immune responses with anti-inflammatory molecules, such as interleukin (IL)-10 and heme oxygenase 1 (HO-1), and the induction of bone morphogenetic protein receptor 2 (BMPR2); the result is the restoration of vascular health. However, when there is a genetic or acquired predisposition to immune dysregulation, or if the vascular injury itself drives a poorly regulated response (eg, schistosomiasis infection), vascular injury is not quickly resolved. A useful oversimplification of this situation divides the dysregulated response into 2 subtypes: TH1/TH17 and TH2 immunity. In the TH1/TH17-skewed response, the arteriole may be invaded by mononuclear cells, including cytotoxic T cells, autoreactive B cells, autoantibodies, mast cells, and activated macrophages expressing granulocyte-macrophage colony-stimulating

factor (GM-CSFR), inducible nitric oxide synthase (iNOS), and leukotriene B4 (LTB4). Injurious cytokines liberated in this milieu include tumor necrosis factor- α , IL-1, and IL-6.

In TH2-driven responses, there are unique inflammatory patterns. Transforming growth factor- β -mediated immunity, linked closely with enhanced IL-4 and IL-13 activity, drive a destructive eosinophil and mast cell-rich perivascular infiltrate. IL-6 can be vasoprotective in this setting in contrast to the TH1/TH17-skewed response, where it is likely harmful. With unmitigated immune dysregulation, inflammation is not resolved in a health-promoting manner, and pulmonary vascular disease ensues. Adapted from Rabinovitch et al. *Circ Res*, 2014.

Immunity and systemic inflammation are also involved in the pathogenesis of **CTEPH** (90). This was first suggested by the high prevalence of systemic inflammatory comorbidities or splenectomy in patients with CTEPH (91–94) and by evidence on the involvement of staphylococci infection in patients with ventriculo-atrial shunts developing CTEPH (95). Several circulating proteins (such as tumor necrosis factor TNF alpha, C-reactive protein CRP, fibrinogen and interleukin-1 beta IL-1 β) or adhesion molecules have been shown to be increased in patients with CTEPH as compared to controls (85,86,90,96), to influence endothelial dysfunction (97) and to decrease after endarterectomy (96,98). High fibrinogen levels were associated with poor functional status and hemodynamics (as assessed by pulmonary vascular resistance, right atrial pressure and mean pulmonary arterial pressure) in 49 patients with CTEPH (99). Pro-inflammatory circulating biomarkers, such as CRP, have also been shown to be prognostic of long-term outcomes in a recent study conducted on a large cohort of patients with CTEPH, in addition to D-dimers levels, and independently of the pulmonary resistance levels (98). The value of these biomarkers, and particularly CRP, for prediction of perioperative outcomes after endarterectomy to remains to be further explored.

In PH, inflammatory features have not only been described in the pulmonary vasculature or in the systemic bloodstream, but also in the **right ventricle** itself. In addition to *in situ* ventricular inflammation, circulating inflammatory cytokines released by the pulmonary vasculature may have a direct toxic effect

on the right heart, promoting local inflammation, adverse RV remodeling and eventually contributing to right heart maladaptation to pressure overload (100).

Immunity has been shown to be involved in both **acute** and **chronic** pressure overloaded right (as presented in **Table 2**) (100). Indeed, inflammatory cellular infiltration has been reported in the RV wall autopsy tissue samples from patients who died from acute pulmonary embolisms, suggesting that inflammation may be an early feature following acute right heart pressure overload (101,102). Experimental studies, using animal models of acute PH (such as rat models of acute pulmonary embolism induced by infusion of microspheres or pulmonary arterial banding in dogs), have also shown neutrophils and monocytes/macrophages infiltration in the right ventricle (103,104). The expression of several cytokines (including proinflammatory cytokines such as the interleukins IL-1, IL-6 and tumor necrosis factor TNF alpha, and chemokines recruiting leukocytes) have further been reported to be increased in the right ventricle of animal models of acute PH (104), as presented in **Table 2** (100). The overexpression of IL-6 was associated with poor RV-pulmonary arterial coupling (104).

Evidence of the presence of inflammatory cellular infiltration and increased pro-inflammatory mediators in the right ventricle of animal models and patients with **chronic pressure overload** has also been widely reported. These have been summarized in a recent review by Sydykok et al. (**Table 2**) (100).

Table 2. Summary of studies investigating inflammatory mediators in the right ventricular tissue. Adapted from Sydykov et al. Front Physiol, 2018.

Disease model	Species/ subjects	Findings	References
Acute RVF following transient PAB	Dogs	Increased expression of CCL2, CCR2, IL-1 β , TNF- α mRNA.	(104,105)
Acute RVF following PE	Rats	Increased expression of the CC-chemokines (CCL-2, -3, -4, -6, -7, -9, -17, -20, -27), the CXC-chemokines (CXCL-1, -2, -3, -9, -10, -16), the receptors CCR1 and CXCR4, ICAM-1, selectin E, the cytokines IL-1 β and IL-6 mRNA. Elevation of CCL2 protein expression. Increased MPO activity. Accumulation of neutrophils and monocyte/macrophages (CD68).	(103,106–108)
Acute RVF following PE	Autopsy tissues from patients	Increased recruitment of macrophages (CD68).	(102)
Acute RVF following transplantation	Human donors	Eight of 26 recipients (30.8%) developed RVF. Seven of these eight (87.5%) expressed TNF- α , but only 4 of the 18 (22.2%) who did not develop RVF expressed TNF- α . Higher TNF- α protein expression in the myocardium of donor hearts that developed RVF.	(109)
Chronic hypoxic PH	Mice	Increased accumulation of CD68 positive cells.	(110)
Monocrotaline-induced PH	Rats	Increased TNF- α , IL-1, IL-6 mRNA expression. Elevated protein expression of TNF- α , NF- κ B subunits p100/p52, and Rel-B. Increased accumulation of CD45+ cells enhanced MPO activity.	(111–121)
Sugen-injection induced PH	Athymic rats	Macrophage infiltration.	(122)
PH due to blockade of VEGF receptor and exposure to chronic hypoxia	Female ovariectomized rats	Increased IL-6 mRNA expression.	(123)
PH due to prolonged systemic-to-pulmonary shunting	Growing piglets	Increased TNF- α , IL-1- α , IL-1 β and ICAM2 mRNA expression.	(124,125)
Chronic RVF remodeling following PAB	Mice	Increased mRNA expression of CCL-2, CCL-5, CX3CL-1, CXCL-6, CXCL-10, -16, CD45R, CD3, CD4, CD8, IL-6, TNF- α , Fn14, mMCP-2, -4, -5, -6, and CPA3. Increased density and activity of mast cells.	(126–129)
Chronic RVF following PAB	Rats	Increased expression of activated p65 (NF- κ B). Increased density and activity of mast cells, enhanced accumulation of CD68-	

PAH	Autopsy tissues from patients	positive macrophages. Increased tissue content of CD68 positive macrophages.	(110)
SSc-PAH, IPAH and controls	Autopsy tissues from patients	RV's from SSc-PAH patients showed significantly more inflammatory cells than those from IPAH and then controls.	(130)

PE: pulmonary embolism; PAB: pulmonary artery banding; PH: pulmonary hypertension; PAH: pulmonary arterial hypertension; SSc-PAH: PAH due to systemic sclerosis; IPAH: idiopathic PAH; RV: right ventricle; RVF: right ventricular failure; ICAM2: intercellular adhesion molecule 2; CXCL: chemokine (C-X-C motif) ligand; CCL: CC-chemokine; CX3CL: chemokine (C-X3-C motif) ligand; CCR2: chemokine C-C receptor 2; IL: interleukin; TNF-: tumor necrosis factor; NF-kB: nuclear factor “kappa-light-chain-enhancer” of activated B-cells; mMCP: mouse mast cell protease; CPA3: mast cell carboxypeptidase A3; MPO: myeloperoxidase; Fn1: fibroblast growth factor-inducible molecule 14; VEGF: vascular endothelial growth factor.

Several studies have further showed a correlation between circulating inflammatory biomarkers and RV function (assessed by echocardiography or CMR imaging), as presented in **Table 3**, mainly exploring a small number of markers in single-center limited sized cohorts. Cytokines can contribute to ventricular remodeling and dysfunction through various mechanisms, mainly reported in LV heart failure, such as negative inotropic effects, cardiomyocyte hypertrophy and apoptosis, fibrosis, attenuation of nitric oxide production, inhibition of angiogenesis and endothelial dysfunction (131–135).

Table 3. Summary of studies evaluating the relationship of circulating inflammatory biomarkers with the parameters of right ventricular performance. Adapted from Sydykov et al. *Front Physiol*, 2018.

Disease	Sample	Population	Inflammatory mediators	Findings	References
CTEPH and CHF	Serum	Patients with CTEPH (n=49), CHF (n=17), Control (n=34)	TNF- α , sTNFR-1, -2, IL-10, hs-CRP, and NT-proBNP	High serum levels of TNF- α , sTNFR-1, sTNFR-2, NT-proBNP and IL-10 in CTEPH and CHF patients. Correlations between sTNFR-1, sTNFR-2, IL-6, hs-CRP and NT-proBNP and CMR-derived RVEF.	(136)
IPAH	Plasma	Patients with IPAH (n=61), Control (n=20)	CXCL-10, CXCL-12 (SDF-1) and CXCL-16	Association of increased levels of CXCL-10, CXCL-12 and CXCL-16 with RVEF and TAPSE	(137)
PAH	Serum	Patients with PAH (n=40)	IL-6	Inverse correlation of serum IL-6 levels with echocardiography-derived RVFAC, TAPSE and right ventricle-pulmonary artery coupling parameters. Negative relationship between circulating IL-6 and CMR-derived RVEF.	(138)
HF patients presenting with RVF	Serum	HF patients with RVF (n=83), Control (n=15)	TNF- α	Correlation of TNF- α levels with severity of peripheral edema and multigated acquisition (MUGA) technique-derived RVEF.	(139)

CHF: chronic heart failure; CMR: cardiac magnetic resonance imaging; CTEPH: chronic thromboembolic pulmonary arterial hypertension; CXCL: chemokine (C-X-C motif) ligand; hs-CRP, high-sensitivity C-reactive protein; IL: interleukin; IPAH: idiopathic PAH; NT-proBNP: N-terminal pro-B-type natriuretic peptide; PAH: pulmonary arterial hypertension; PTX3: pentraxin 3; RV: right ventricular; RVF: right ventricular failure; RVEF: RV ejection fraction; RVFAC: RV fractional area change; sTNFR: soluble tumor necrosis factor receptors; TAPSE: tricuspid annular plane systolic excursion; TNF- α : tumor necrosis factor alpha.

A large study assessing a wider panel of circulating immune biomarkers and their correlation to right heart adaptation/maladaptation in patients with PH has yet to be done. One of the main limitations to conduct such a screening study on circulating biomarkers of right heart failure derives from the need to a better phenotyping of right heart adaptation/maladaptation in this population.

The following section of the thesis will review the current state-of-the-art in right heart phenotyping, focusing on the two non-invasive imaging techniques: echocardiography and cardiac magnetic resonance.

Part 2- RIGHT HEART IMAGING

Non-invasive imaging enables assessment of the right heart dimensions, function, coupling and metabolism. We recently published a review on “Right heart imaging in heart failure” providing a detailed update in the field (**Supplementary article 6**) (10).

In this chapter, we will review the four main non-invasive imaging modalities used in patients with PH (i.e. echocardiography, CMR imaging, computed tomography, and positron emission tomography PET-CT), focusing on echocardiography and CMR imaging. We will summarize for each modality their advantages, limitations, latest developments and unmet needs delineating future research directions.

2.1 Echocardiography

2.1.a Principles and advantages

Echocardiography is based on the propagation of ultrasounds in the tissues and their reflection at the level of interfaces between two structures with different echogenicity characteristics. Echocardiography remains the mainstay of clinical evaluation, having the advantage of availability, low cost, excellent spatial and temporal resolution, and flow assessment (10).

Two-dimensional (2D) trans-thoracic echocardiography (TTE) enables measurement of right heart dimensions, estimation of RV function, pressures and assessment of valvular stenosis or regurgitation. **Figure 11** illustrates the main 2D TTE metrics providing a comprehensive assessment of the right heart (with the exception of the inferior vena cava not shown in the figure) (8).

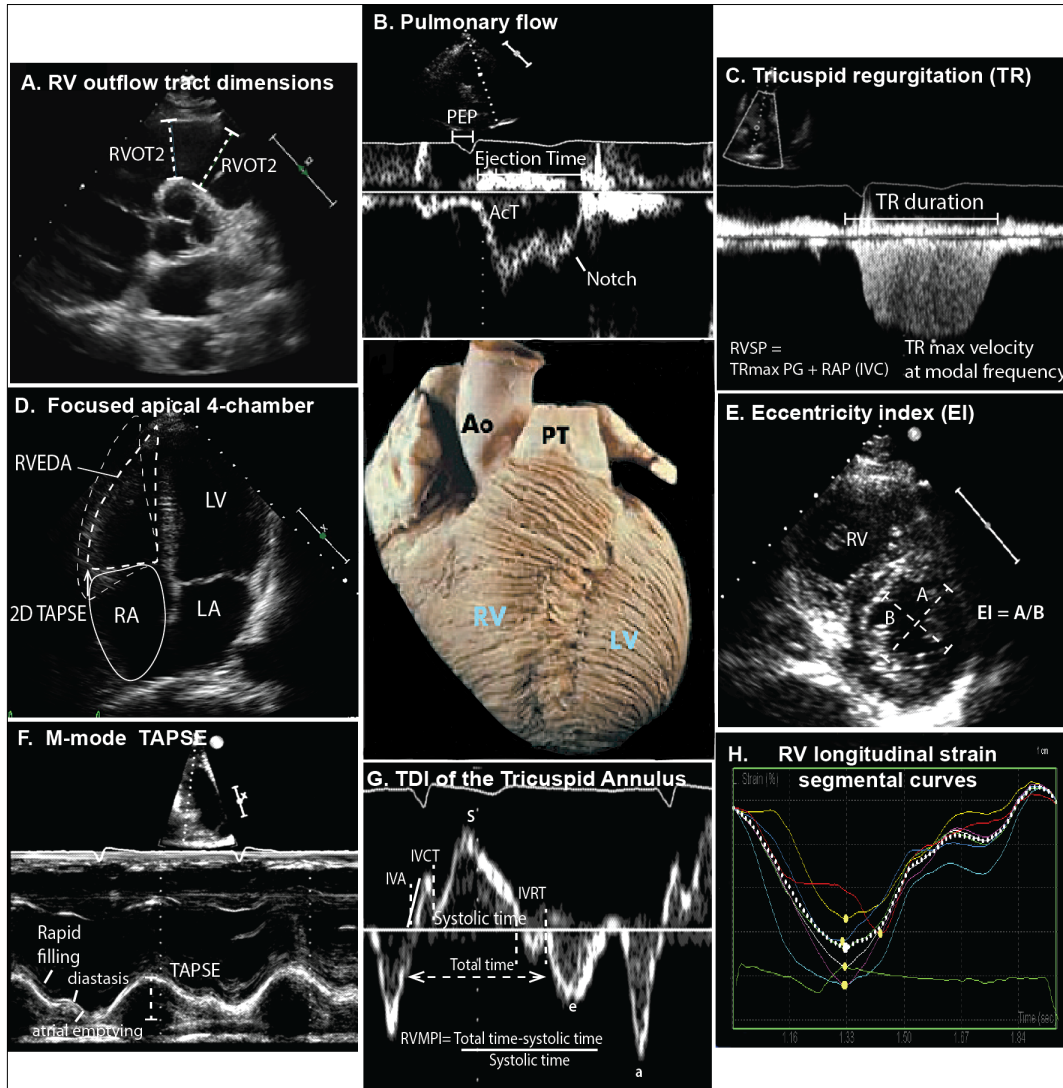


Figure 11. Right heart metrics using two-dimensional trans-thoracic echocardiography. Ao: aorta; IVA: isovolumic acceleration; IVC: inferior vena cava dimensions and collapsibility should also be systematically assessed; IVCT: isovolumic contraction time; IVRT: isovolumic relaxation time; LA: left atrium; LV: left ventricle; PG: pressure gradient; PT: pulmonary artery; RA: right atrium; RAP: right atrial pressure; RV: right ventricle; RVEDA: RV end-diastolic area; RVLS: RV longitudinal strain; RVMPI: RV myocardial performance index; RVSP: RV systolic pressure; TAPSE: tricuspid annular plane systolic excursion. Adapted from Amsallem et al. JACC:HF, 2018.

Right heart dimensions include the RV diameter of the outflow tract (**Figure 11A**), RV transversal diameters on the apical four-chamber view, right atrial maximal area, and ventricular areas in end-diastole (RVEDA) and end-systole (RVESA) (**Figure 11D**) (8,49,140).

RV systolic function can be estimated using RV fractional area change (RVFAC $\% = 100 * [RVEDA - RVESA] / RVEDA$) reflecting the radial and longitudinal component of RV contraction; or metrics assessing more the longitudinal shortening of the RV wall, such as tricuspid annular plane systolic excursion (TAPSE, **Figures 11D** and **11E**), tricuspid annulus peak S' (**Figure 11G**) or RV strain (**Figure 11H**). TAPSE has gained interest from clinicians because of its simplicity, reproducibility and prognostic value in heart failure, PH and congenital heart disease (141,142). However, the caveats of TAPSE should be emphasized. First, it is less sensitive than free-wall longitudinal strain (RVLS), RVFAC or ejection fraction (RVEF) for the early detection of RV systolic dysfunction in PH (10). Second, TAPSE is not reliable in the early post-operative cardiac surgery period, in contrast to RVEF or RVFAC leading to over-diagnosis of ventricular dysfunction (30,143,144). Finally, RVLS or end-systolic RV dimensions are emerging as stronger predictors of outcome than TAPSE or the once popular RV myocardial performance index (145,146). Inter-ventricular interdependence can be assessed by measuring the LV eccentricity index (EI = antero-posterior diameter divided by the latero-septal diameter, using the parasternal short axis view) as illustrated in **Figure 11E**. The eccentricity index reflects septal curvature flattening, classically secondary to volume overload when abnormal in end-diastole or pressure overload when abnormal in end-systole (42).

2D echocardiography-Doppler can also assess flow and estimate pressures within the right heart. Using the Bernoulli equation, RVSP can be estimated using the tricuspid regurgitation (TR) maximal velocity using continuous Doppler and the estimated right atrial pressure (RAP) as follows: $RVSP = 4 * (\text{maximal TR velocity})^2 + \text{estimated RAP}$ (49,140) (**Fig. 11C**). Estimation of RVSP from the TR signal requires an interpretable TR signal and has been the topic of much controversy in the field as detailed below. Mean and diastolic pulmonary arterial pressures (MPAP and DPAP) can also be estimated from

the proto-diastolic and end-diastolic velocities of the pulmonary regurgitation Doppler signal respectively (using continuous Doppler).

Finally, the analysis of the pulmonary anterograde flow signal can provide indirect signs of increased pulmonary pressures, in case of decreased acceleration time and/or systolic notch (**Figure 11B**) (147). Acceleration time has been shown to correlate with MPAP and resistance in patients with chronic obstructive pulmonary disease (both areas under the curve of 0.96) (148), but it was not validated in a recent publication by our team in a more diverse cohort of patients with advanced lung disease (48), **Supplementary article 3**. In 1974, Nanda et al. were the first to observe that the pulmonary valve in patients with PH appeared straight in diastole with rapid opening slopes (>350 mm/s) and prolonged pre-ejection periods (149). Weyman et al. further described the presence of mid-systolic fluttering, closure or notching of the pulmonary valve in most patients with PAH (n= 20) and in none of the controls (150). The changes in pulmonary valve motion and pulmonary flow in PH can be explained by the complex interplay between forward and reflected pulmonary pressure waves (151,152). Under normal conditions, the reflected wave only accounts for a small component of the total pressure wave. In patients with PH, the reflected pressure wave becomes significant and adds to the forward wave, imposing an added pressure burden on a still ejecting right ventricle. The resulting reduction in flow velocity during mid-ejection changes the normal dome-like contour into a notched contour. Although the notched pattern of pulmonary flow was initially believed to be characteristic of PAH, it has been also observed in patients with chronic thromboembolic disease, and is a strong prognostic factor (153). The pulmonary notch has also been shown to be strongly suggestive of elevated pulmonary vascular resistance in patients with predominantly “left heart failure” (154). A recent study has suggested that the ratio of notch wave to main wave velocities is also a reflection of RV function (155). **Table 4** summarizes the main right heart imaging metrics and their normative values.

Table 4. Selection of the most relevant right heart imaging metrics. Adapted from Amsallem et al. *Curr Opin Cardiol*, 2016.

Metrics	Reference values	Clinical relevance and comments
Dimensional indices		
RV volumes	Sex dependent	Increased RV volumes (particularly RV end-systolic volumes) and decreased LV end-diastolic volume are predictors of poor survival in pulmonary hypertension.
- RV end-diastolic volume index (mL/m ²)	Male: 87±12 [63,111]/Female: 78±9 [60,96]	
- RV end-systolic volume index (mL/m ²)	Male: 62±15 [32,92]/ Female: 49±13 [23,75]	
RV mass	Indexed on BSA: 21±4 g/m ²	Hypertrophy is predictor of poor survival in PAH, but of better survival in patients with Eisenmenger.
RA enlargement	> 11.0 cm ² /m ²	>15.4 cm ² /m ² is associated with poor survival in PAH.
Systolic functional indices		
RV ejection fraction	> 50%	< 35% by CMR or SPECT is often used as a threshold to discriminate outcome associated with poor survival in HFrEF and pulmonary hypertension. < 45% by 3-dimensional echocardiography usually reflects abnormal RV systolic function, though laboratory may choose to refer to age and gender-specific values.
RV fractional area change	> 35%	< 25% denotes moderate-to-severe dysfunction.
TAPSE	> 17mm	< 14mm is predictor of poor survival in pulmonary hypertension. Is load-dependent and has limited value after cardiac surgery.
S' peak velocity	> 12cm/s	< 8cm/s is considered abnormal. Is load-dependent.
Deformation indices		
Global longitudinal strain	≤ -20%	Considered severely altered when ≥-15% by speckle tracking. Predictor of survival in pulmonary hypertension.
Systolodiastolic functional index		
RVMPI-puled tissue	< 0.55	> 0.88 predicts poor survival in idiopathic PAH. Can be pseudonormalized in case of severe RV dysfunction.
Diastolic metric		
IVRT (TDI)	< 65ms	> 75ms (value non adjusted for heart rate) has been associated with RV dysfunction. Requires indexation by heart rate (e.g. IVRT

divided by the square root of RR interval); no consensus on the method.

Pulmonary flow

Pulmonary acceleration time > 93ms

Role for screening for pulmonary hypertension, particularly in case of severe tricuspid regurgitation.

Is time-dependent (in theory would require adjustment to the heart rate).

Ventricular interdependency

Left ventricular eccentricity index No normative value Usually < 1

Is predictor of poor survival in pulmonary hypertension (no consensus on the threshold).

End-systolic eccentricity index reflects pressure overload while end-diastolic eccentricity index reflects volume overload.

Data are presented as mean±standard deviation [range]. BSA: body surface area; CMR: cardiac magnetic resonance; HFrEF: left heart failure with reduced ejection fraction; IVRT: isovolumic relaxation time; LV: left ventricle; PA: pulmonary artery; PAH: pulmonary arterial hypertension; PET: positron emission tomography; PH: pulmonary hypertension; RA: right atrium; RV: right ventricle; RVMPI: RV myocardial performance index; SPECT: single photon emission computed tomography; TAPSE: tricuspid annular plane systolic excursion; TDI: tissue Doppler imaging. Normative values and thresholds are from the following references: (49,140,145,146,156–160).

2.1.b Latest developments in echocardiography

2.1.b.i Right ventricular deformation imaging

Myocardial deformation imaging has gathered a lot of attention in recent years, leading to several thousand publications (161). Myocardial deformation encompasses different concepts, including strain, usually expressed as longitudinal, circumferential, or radial strain; strain rate, which represents the deformation over time; and velocity-based parameters. As summarized in a statement study by Voigt et al., strain may refer to either natural strain or Lagrangian strain (161). One of the landmark studies in the field is that of Dumesnil et al., which outlines the principles of axial and transverse shortening of the left ventricle (162). While natural and Lagrangian strain both reflect deformation of the myocardial wall, they differ from the fact that natural strain is expressed relative to the length at a previous time and Lagrangian strain is expressed relative to the initial length as follows: $(\text{end-systolic length} - \text{end-diastolic length}) / \text{end-diastolic length}$. Lagrangian strain is usually assessed using speckle tracking or by manual tracing (**Figure 12**) (163,164). Both concepts are related to each other mathematically, but are not equivalent. Moreover, studying strain adds value to other volumetric metrics, especially in cases of non-dilated ventricles (164). Kobayashi et al. showed that in left heart failure, LV ejection fraction and LV strain are more collinearly related to each other in patients with reduced ejection fraction compared with higher ejection fraction. Primarily developed in the left ventricle, several studies have explored the value of longitudinal shortening of the RV-free wall in patients with advanced heart failure referred for heart transplant and outpatients with heart failure (165,166). The software used for speckle tracking has mainly been developed for the left ventricle. Tracking of the right ventricle may be more challenging and is often more reliable in the basal and mid portion. Recently, Ryo et al. have developed software evaluating both axial and surface RV strain using three-dimensional methodology (167). Finally, it should be highlighted that right heart strain derived by CMR imaging often focuses on the circumferential strain, whereas strain derived by echocardiography focuses on the longitudinal strain.

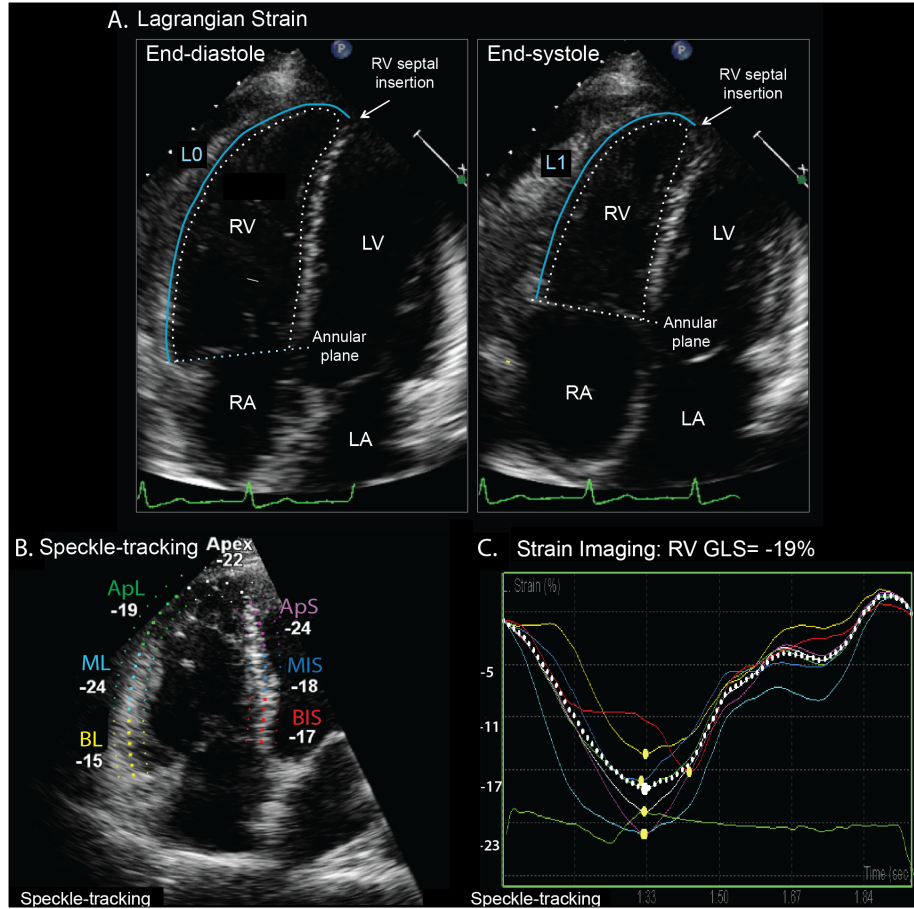


Figure 12. Myocardial deformation imaging based right ventricular longitudinal strain. (A) Lagrangian strain of the right ventricular (RV) free-wall (RVLS, % = $100 * [L1-L0]/L0$), using manual tracing on the apical 4-chamber view focused on the right ventricle. Note the tracing from the annular plane to the septal insertion of the right ventricular free-wall. **(B)** Superposed RV speckle tracking tracing with numbers representing segmental peak strain. Example from Philips tracking (developed for left ventricle and applied to the right ventricle); specific RV tracking has also been developed by other vendors. **(C)** Strain-time curves of the different signals. ApL, apex lateral; ApS, apex septum; BIS, basal interventricular septum; BL, basal lateral; GLS, global longitudinal strain; LA: left atrium; LV, left ventricle; MIS, mid interventricular septum; ML, mid lateral; RA: right atrium; RV, right ventricle. Adapted from Amsallem et al. *Curr Opin Cardiol*, 2018.

2.1.b.ii Three-dimensional echocardiography

As the complex crescent shape of the right ventricle makes 2D echocardiographic limited for estimation of RV dimensions, estimation of volumes and function using CMR remain the gold standard. Three-dimensional (3D) echocardiography opens up the possibility of evaluating RV volumes by overcoming the limitations of conventional two-dimensional echocardiography RV views with regard to orientation and reference points. A meta-analysis has indeed shown the good correlation between CMR and 3D echocardiography for RV volumes and ejection fraction assessment in patients and healthy study participants, with 3D echocardiography slightly underestimating volumes as compared with CMR (160). So far, only one multicenter study provides age, body size, and sex-specific reference values of 3D echocardiography-derived RV volumes and ejection fraction in 507 healthy study participants (168). Overall, women have smaller indexed RV volumes and higher ejection fraction compared with men, whereas older age is associated with smaller RV volumes (a decrement of 5 mL per decade for end-diastolic volume and 3 mL per decade for end-systolic volume) and higher ejection fraction (an increment of 1% per decade) (168). Lastly, a recent quantitative 3D echocardiography study has explored morphological subsets of RV adaption and remodeling in 92 patients with PH, and linked them to clinical outcomes (167). Three-dimensional RV end-systolic volume had indeed significantly better predictive values than end-diastolic volume or global strain to predict the combined endpoint of hospitalization, death, or lung transplantation.

2.1.c Limitations and unmet needs

2.1.c.i Controversy of estimating pulmonary arterial pressure by echocardiography

One of the major controversies in the field of PH is whether echocardiography is reliable to estimate pulmonary pressures. The original 1984 publication from Yock and Popp in 1984 (169) reported an excellent correlation between RVSP measured by right heart catheterization and RVSP simultaneously estimated by echocardiography from the TR maximal velocity and estimated RAP ($r=0.93$, $p<0.001$). This was later confirmed by several other investigators (170–172), as presented in **Table 4**. However, in recent years, the accuracy and reliability of echocardiography for estimating RVSP has been challenged, especially in the field of advanced lung disease and PH. In Fisher et al.'s frequently cited study on 63 subjects with mild or no PH, a weak correlation between invasive and estimated RVSP was reported ($r=0.23$, $p<0.05$), including one third of patients having a difference $>10\text{mmHg}$ (173). Rich et al. more recently reported similar findings (174).

Table 5: Studies assessing correlation between invasive and echocardiography based right ventricular systolic pressure estimations.

Authors, year (reference)	Population	n	% of interpretable TR	Correlation (r)	Significant difference	Limitations
Yock et al., 1984 (169)	Signs of elevated right-sided pressure	62	87%	0.89†	SEE=8mmHg	RAP estimated using JVP
Currie et al., 1985 (170)	PH or no PH	127	87%	0.96	SEE=7mmHg	RAP assumed 10mmHg
Berger et al., 1985 (171)	PH or no PH	69	59%	0.97	SEE=4.9mmHg	-
Laaban et al., 1989 (175)	ALD PH or no PH	41	66%	0.65	SEE=9mmHg	RAP assumed 5mmHg
Tramarin et al., 1991 (176)	ALD PH or no PH	100	30%	0.73	SEE=7.4mmHg	-
Brecker et al., 1994 (177)	Mostly PAH Severe PH	10	-	-	Mean underestimation n=38 ±21mmHg	-
Shapiro et al., 1997 (172)	PAH	69	71%	0.85	-	Comparison with ventricular-atrial gradients
Hinderliter et al., 1997 (178)	PAH	81	86%	0.57	31% >20mmHg difference	RAP assumed 14mmHg
Bach et al., 1998 (179)	ALD	92	27%	0.69	-	-
Arcasoy et al., 2003 (180)	ALD	374	44%	0.69	52% >10mmHg difference	-
Dambrauskaitė et al., 2005 (181)	PH or no PH	66	100%‡	0.79	-	‡Only included interpretable TR
Fisher et al., 2007 (173)	ALD	63	39%	0.23	33% >10mmHg difference	Time delay between RHC and TTE 23 days
Haddad et al., 2009 (182)	PAH	51	-	0.97	2% >20% difference	-
Rich et al., 2011 (174)	PH	160	-	0.68	51% >10mmHg difference	Time delay 30 days
	PH	23	-	0.71	-	-
Lafitte et al., 2013 (183)	PH or no PH	310	-	0.80	-	-
D'Alto et al., 2013 (184)	PH or no PH, mostly PAH or left-sided heart disease	161	94%	-	Bias mean ±SD [95%CI]: -0.5 ±9 [-2;1]	RAP assumed 5mmHg

Correlation between echocardiography-based RVSP and invasive RVSP is presented as Pearson coefficient (r). ALD: advanced lung disease; JVP: jugular venous pressure; PAH: pulmonary arterial hypertension; PH: pulmonary hypertension; RAP: right atrial pressure; RHC: right heart catheterization; SEE: standard error of estimate; TR: tricuspid regurgitation; TTE: trans-thoracic echocardiography; %: percentage. †: after exclusion of one patient with pulmonary stenosis.

The heterogeneity in the findings in previous studies may be related to the fact that the different studies have not always considered the quality of the TR signal. Several methodological pitfalls can lead to misestimating of the TR maximal velocity, including not aligning the Doppler cursor with the TR jet, or failing to pay attention to the shape of the TR signal. This controversy has led to the general consideration in the field that echocardiography is not reliable to detect PH and that the gold standard remains right heart catheterization. However, catheterization is an invasive procedure exposing to rare but severe complications such as pulmonary arterial ruptures or bleeding, with limited accessibility and repeatability.

2.1.c.ii Need for standardization of 2D echocardiography

The crescent shape of the right ventricle makes standardization of 2D echocardiographic RV views challenging. The conventional apical four-chamber view (i.e. focused on the left ventricle) results in considerable variability in the way the right ventricle is sectioned, as illustrated in **Figure 13**. Consequently, RV linear dimensions and areas may vary widely with relatively minor rotations in transducer position. For these reasons, the American Society of Echocardiography/ European Association of Cardiovascular Imaging recommend imaging the right heart using RV focused apical four-chamber view (i.e. four-chamber view passing through the RV maximal transverse diameter) (140).

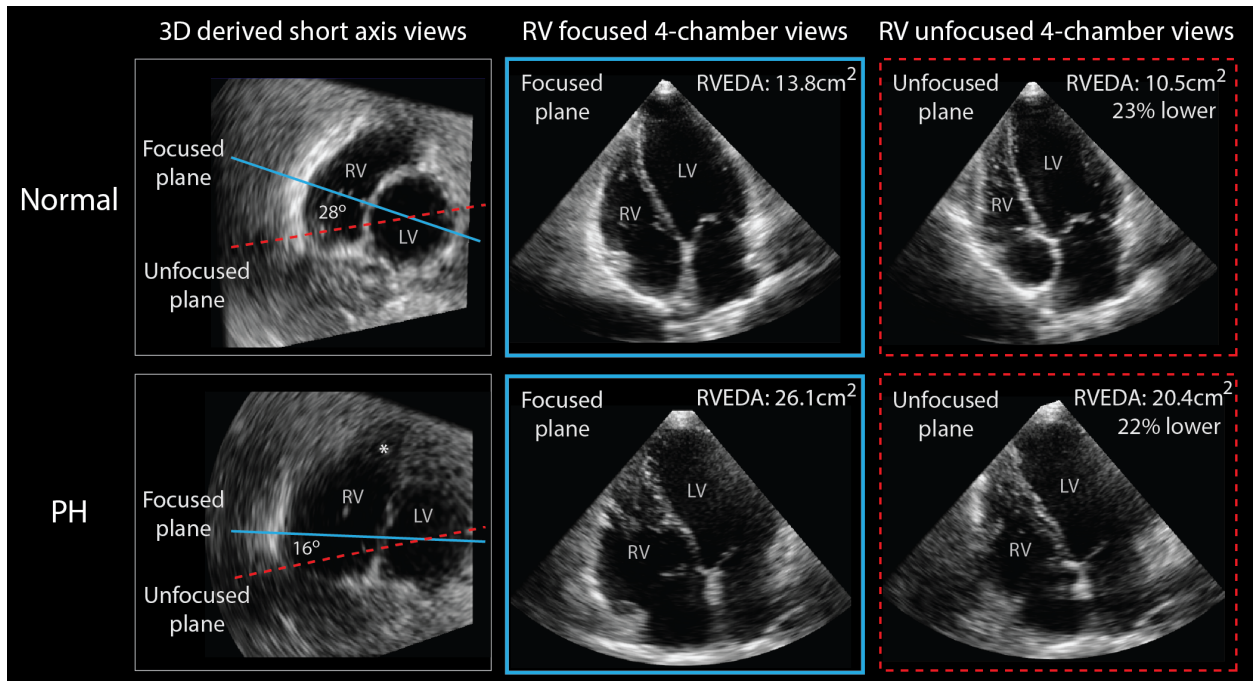


Figure 13. Example of right ventricular focused and unfocused apical 4-chamber views derived from 3-dimensional dataset, in end-diastole, in a patient with normal right ventricular phenotype and in a patient with mild pulmonary arterial hypertension (PH). Unfocused views provided 23% and 22% underestimation of RV end-diastolic area (RVEDA) respectively. *Note the drop in spatial resolution of the RV anterior wall, particularly in the patient with PH. LV: left ventricle; RV: right ventricle. Adapted from Amsallem et al. *Int J Cardiovasc Img*, 2018, **Supplementary article 7**.

Obtaining an RV focused apical four-chamber view may however be challenging without 3D guidance. Although not done routinely, one could verify that the transverse RV diameter obtained in the apical four-chamber view corresponds to the maximal transverse diameter obtained in the short axis view. An alternate method would be to use 3D echocardiography dataset to identify the maximal RV transverse diameter and extract the optimal tomographic RV focused apical view (3D-RV-focused method), **Figure 9**. We recently published a study validating this method comparing it to the gold standard CMR, showing excellent inter- and intra-observer reproducibility and test-retest characteristics (**Supplementary article 7**) (185). We also explore the value of an alternative method based on the rotational matrix technology, iRotate technology (Philips, Amsterdam, The Netherlands), which is an xMATRIX technology that,

instead of manually rotating the transducer, enables rotation of the tomographic ultrasound view through a single acoustic window and fixed transducer position. We show that iRotate can also be used to identify the maximal transverse RV plane.

2.1.c.iii Non-invasive assessment of right heart adaptation to load

A major pitfall in the non-invasive assessment of ventricular function is to equate clinical metrics such as RVEF or TAPSE with contractility. In fact, Guihaire et al. showed in a large animal model of PH that RVFAC or TAPSE are more closely related to ventriculo-arterial coupling (Ees/Ea) than to ventricular elastance (contractility) (186). Mathematically, the Ees/Ea ratio is equal to $[(RVESP - V_0)/RVESV] / [RVESP/SV]$, similarly to the left ventricle (187,188). Usually, the assumption that V_0 is equal to zero is made (i.e. ventricular volume when pressure is equal to zero), which is incorrect in patients with RV enlargement such as in PH (189). The Ees/Ea ratio then becomes equal to $[RVESP/(RVEDV - SV)] * [SV/RVESP] = SV/(RVEDV - SV) = RVEF/(1-RVEF)$. The closer correlation between ventricular function metrics and ventriculo-arterial coupling than with contractility has direct implications for understanding RV recovery in pressure overload states. For example, in severe PAH despite the decrease in RVEF and impaired ventriculo-arterial coupling, RV contractility is usually increased.

There has been an interest in identifying less invasive indices of RV-arterial coupling or load adaptability. Several indices of load adaptability have been proposed, although referring to different concepts: ventriculo-arterial coupling, simple ratio of function and load, or indices assessing whether the RV is well adapted, considering the load being subjected to (**Figure 14**) (21).

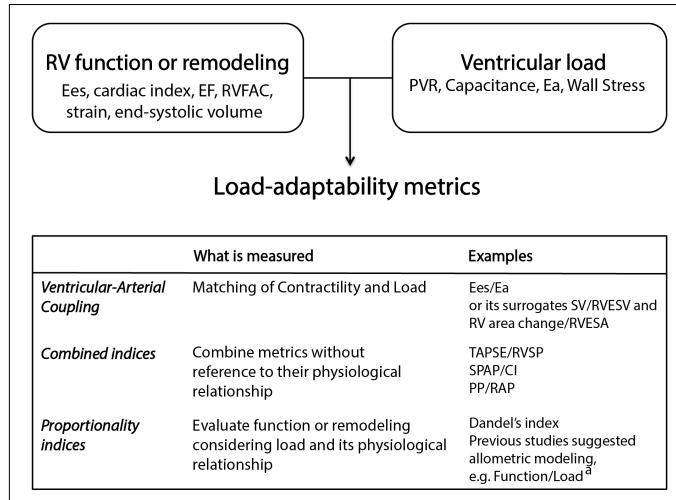


Figure 14. Load adaptability indices. Ea: arterial elastance and Ees: ventricular elastance both derived from pressure-volume loops; EF: ejection fraction; PP: pulse pressure; PVR: pulmonary vascular resistance; RAP: right atrial pressure; RVESV: end-systolic volume; RVESA: end-systolic area; RVFAC: fractional area change; SPAP: systolic pulmonary arterial pressure; SV: stroke volume; TAPSE: tricuspid annular plane systolic excursion.

Simplified, although less accurate, indices of coupling have been proposed, such as the SV divided by end-systolic volume (189), but this latter assumes that volume at pressure 0 passes through the origin (190). Ratiometric indices combining measures of load and function have also been used, but they fail to take into account the physiological dependence of load and function (191,192). The last category assessed whether ventricular dysfunction or enlargement is “proportional or disproportional” to the load imposed on the ventricle. As recently suggested, RV function may follow an allometric function with load in PH (193), and this may have implications when assessing the relationship between load and RV adaptation (**Figure 15**) (10).

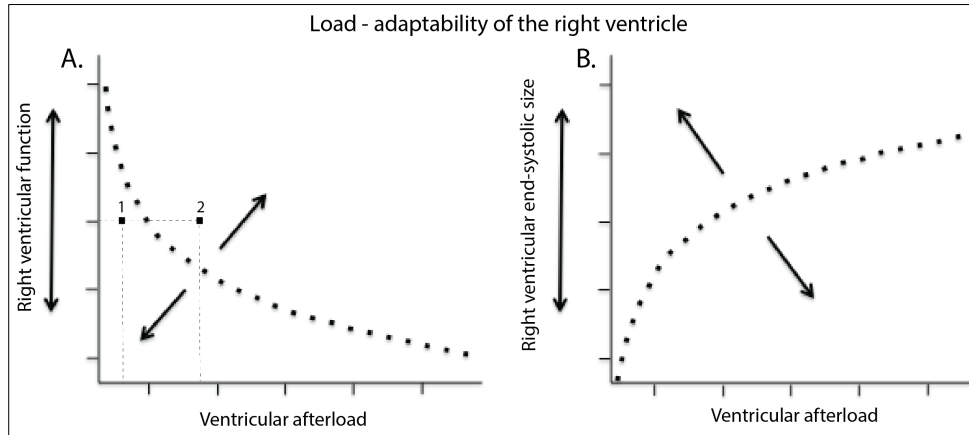


Figure 15. Relationships between right ventricular function (A) or end-systolic size (B) and ventricular afterload. This figure schematically represents the curvilinear fit of the relationships between RV function, or end-systolic dimension, and afterload metrics (such as pressure, resistance, capacitance, or estimation of the RV wall stress). Estimation of the wall stress is more challenging, but better reflects the force opposing ventricular function. The shape of the fit would be reversed if capacitance were used as afterload. Two examples are depicted in this figure (patient 1 and patient 2). Despite similar moderate right ventricular function, patients 1 and 2 differ in terms of RV adaptation. Patient 1 has a disproportional dysfunction, as the function is worse than would be expected for the mild increase in afterload compared with patient 2. Adapted from Amsallem et al. *Curr Opin Cardiol*, 2016.

Overall, these surrogate metrics of load adaptation have conceptual limitations and their incremental prognostic value over simple metrics (such as RV size or function) has not been proven yet.

2.2 Cardiac Magnetic Resonance

2.2.a Principles and advantages

Magnetic resonance imaging is a non-invasive technique based on the interaction of biological tissues with electromagnetic fields. CMR enables volumetric acquisition of the heart and vessels, which provides estimation of RV volumes, mass and RVEF (194). RVEF (%) is defined as $100 \times (\text{RV end-diastolic} / \text{RV end-systolic})$.

volume – RV end-systolic volume)/ RV end-diastolic volume. **Figure 16** presents the anatomical structures visible using CMR (195).

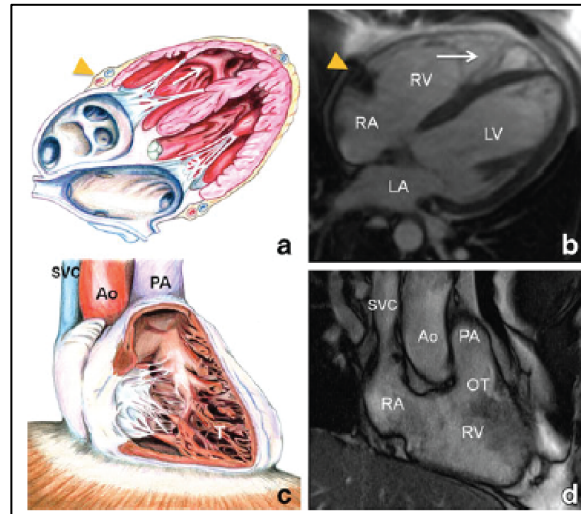


Figure 16. Freehand drawings (a, c) and corresponding cine SSFP images on four-chambers (b) and three-chambers (d) views demonstrating normal RV anatomy: moderator band (arrow), tendinous cords of tricuspid valve and trabeculations (T). RA right atrium, RV right ventricle, LA left atrium, LV left ventricle, orange triangle right atrioventricular groove containing the right coronary artery and small cardiac vein, SVC superior vena cava, Ao aorta, PA pulmonary artery, OT right ventricular outflow tract. Adapted from Galea et al. Insights Imaging, 2013.

As well described by Swift et al. in their recent review, “a standard protocol in the clinical assessment of patients with suspected PH based on current evidence includes a lung volume anatomic scan at breath-hold for localization, volumetric cardiac imaging for assessment of biventricular mass, volume, and function, and stroke volume and cardiac output derived by phase-contrast magnetic resonance imaging at the pulmonary artery and aorta.” (196). **Figure 17** illustrates the short axis medial plane in a patient with PAH across the cardiac cycle, highlighting severe RV enlargement and septal inversion predominant in end-systole in the context of pressure overloaded RV. CMR also enables assessment of pulmonary arterial stiffness, as described in **Table 1**.

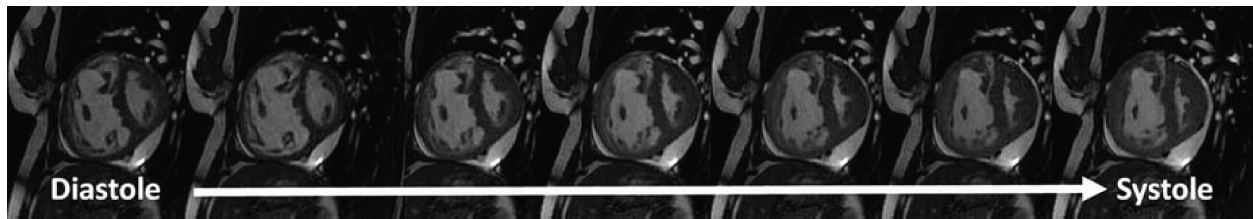


Figure 17. Short-axis images from the systolic phase of the cardiac cycle in a patient with PAH. The interventricular septum is flattened, and there is marked RV dilatation and hypertrophy. Adapted from Swift et al. *J Thorac Imaging*, 2014.

2.2.b Latest developments

2.2.b.i Extracellular matrix – Fibrosis

1. *Delayed contrast enhancement*

Beyond volumetric and functional analysis, CMR also allows tissue characterization. One of the novelties in the field is the ability to assess myocardial fibrosis by delayed contrast enhancement or T1 mapping (81).

Several CMR studies have reported the frequent presence of delayed contrast enhancement (DCE) in patients with PH (197–201). DCE is usually localized at the septal insertion point of the right ventricle, as illustrated in **Figure 18** (197), and is inconsistently found at the inter-ventricular septal level. The pattern of septal RV point DCE is not specific to the etiology of PH, as it has been described in patients with PAH or CTEPH (197,200) or congenital heart disease (201). Interestingly, septal DCE was also found in two patients with exercise-induced PH (202).

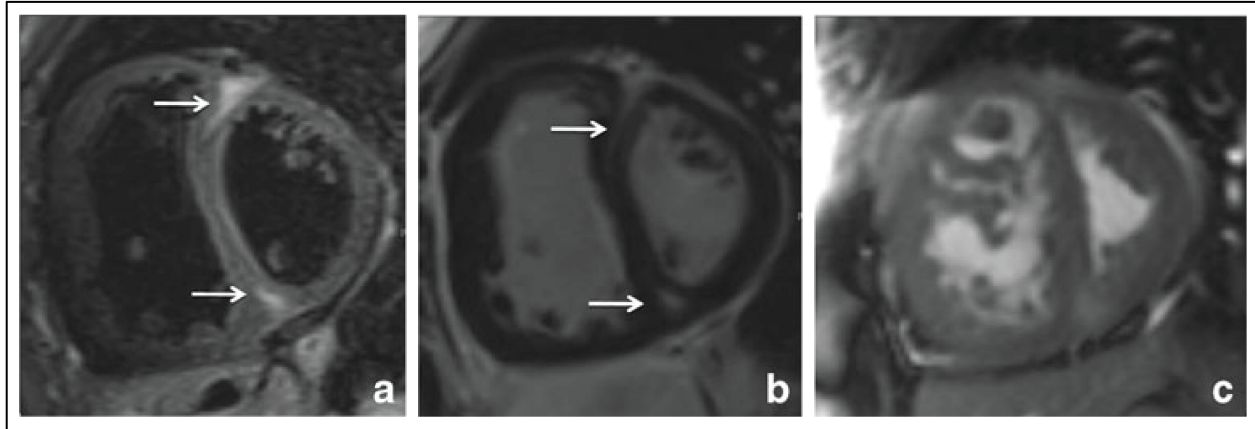


Figure 18. Severe idiopathic pulmonary hypertension in a 28 year-old man; pulmonary arterial pressure at right catheterization was 70 mmHg. Focal areas of hyperintense signal are observed at the level of both ventricular junctions on STIR T2WI (a, arrows) matching mesocardial spots of late enhancement in the same location (b, arrows). Severe concentric RV hypertrophy is observed on short-axis cine-SSFP end-systole image with flattening and inversion of the interventricular septum during contraction (c). Adapted from Galea et al. *Insights Imaging*, 2013.

The mechanisms underlying DCE in pressure overloaded right ventricles are still unclear. The delayed washout of gadolinium in an “unhealthy” myocardium has been extensively reported in the left ventricle, in infarct-related scars or in hypertrophic cardiomyopathy at the inter-ventricular septum level (203,204), and has been linked to fibrosis. However, there is very few evidence linking DCE with pathological findings in the right ventricle. McCann et al. first reported in 2007 the autopsy finding of two patients with PAH who however did not undergo CMR (197). Both patients had similar histological findings: “at the insertion points of the right ventricle to the inter-ventricular septum was seen cardiomyocyte disarray with marked expansion of extracellular spaces adjacent to areas of interstitial or replacement fibrosis and increased fat deposition, beyond the perivascular regions” (197). Bradlow et al. were the only to report the pathological analysis of the heart of a patient who had DCE identified on CMR, showing myocardial disarray with plexiform fibrosis without replacement fibrosis (205).

The predominant localization of delayed contrast enhancement at the RV septal hinge points

(**Figure 18**) is believed to be linked with the myocardial regions that are the most strained with RV increased pressure and enlargement (206,207). The signaling pathways underlying fibrotic deposition in pressure overloaded RVs are poorly known. There is some evidence of distinct pathophysiological pathways between LV and RV fibrosis, precluding generalization of left heart disease findings for the RV (206,208). Hypoxia is also believed to be a trigger of RV fibrosis through the TGF-beta1 signaling pathway and inflammation cytokines such as interleukin IL-6 (209).

Correlations between presence of delayed contrast enhancement and RV metrics, hemodynamics or clinical features have been inconsistent in the literature, mainly due to small samples, heterogeneous etiology, disease severity and PH-specific therapy (197–199,202). In their study conducted in 19 patients with PAH and 6 with CTEPH, Blyth et al. showed the presence of delayed contrast enhancement at the level of the RV septal insertion points in 23/25 patients (198). Estimated delayed contrast enhancement mass correlated significantly with RV dysfunction (using RVEF), RV mass and end-diastolic volume index and MPAP. In McCann et al.'s cohort of 11 patients with idiopathic PAH and 4 scleroderma-associated PAH (receiving PH-specific therapy), RV delayed enhancement (expressed as percentage of myocardial mass) was significantly correlated with RV dysfunction (assessed using RVEF) and stroke volume, but not with hemodynamics or clinical characteristics (197). In contrast, Junquiera et al.'s study found no correlation between presence of RV delayed contrast enhancement (not quantified) and RV size or function, or hemodynamics, but only with duration of the disease in their 13 patients with PAH and 7 with CTEPH (199). In Sanz et al.'s cohort of 55 patients with PH or suspected PH, only SPAP remained significantly associated with the presence of delayed contrast enhancement on multivariate analysis (202).

Whether DCE is more a marker of disease severity than an independent prognostic significance remains unclear. In two cohorts of patients with PH or suspected PH, DCE has been associated with clinical worsening or death in univariable analysis but was not retained in multivariate analysis (210,211).

One of the main pitfalls of delayed contrast enhancement imaging is that it may fail to adequately characterize diffuse interstitial myocardial fibrosis because of reliance on relative signal intensity changes

and nulling of normal-appearing myocardium (212).

2. T1 Mapping

Quantitative assessment of the myocardial longitudinal relaxation time constant (T1) has in parallel emerged as a promising technique to assess for diffuse myocardial changes (81). T1 maps can be produced of non-contrast (native) myocardial T1 values (providing information on both myocytes and the interstitium) or after gadolinium-based contrast administration (enabling quantification of the extracellular space) (213,214). In healthy controls, RV non-contrast T1 values have been shown to be higher than LV values, which may be explained by the higher collagen content of the RV myocardium (215,216). In the setting of RV dysfunction and pulmonary hypertension, RV and hinge point non-contrast T1 and extracellular volume fraction values are elevated, regardless of PH etiology (idiopathic or scleroderma related PAH or CTEPH) (213). Native T1-values of the inter-ventricular insertion points correlated significantly with right atrial pressure, RV end-diastolic and end-systolic volume index, RVEF and NT-proBNP (213). Post-contrast T1 values showed an increase in the myocardial extra-cellular volume that correlates with RV volume and function (216). Finally, several advanced techniques have been proposed to improve T1 quantification of thin-walled structures such as the RV, including imaging in end-systole (215) and higher resolution sequences (216).

2.2.b.ii 4D MRI blood flow

Three-dimensional time-resolved flow magnetic resonance imaging (i.e. 4D flow MRI) is an evolving imaging technique that yields both a vector of blood velocity and the magnitude signal intensity over an imaging volume. It enables simultaneous acquisition of both flow and volume/function information in a single acquisition (about < 10 minutes), without needing detailed operator knowledge of cardiac anatomy (217,218). For each temporal phase of the cardiac cycle, 4D flow MRI allows the evaluation of blood flow, including valvular regurgitation (as shown in **Figure 19**, left panel) (10), quantification of biventricular volumes, function and mass, and visualization of intra-cardiac and extra-cardiac structures (217,219). A recent study demonstrated that RV volume, function, and mass can be quantified with 4D flow MRI with precision and inter-observer agreement comparable to those of cine steady-state free precession (220). Whole heart 4D flow MRI also enables detection and visualization of both normal and abnormal right heart flow patterns (221). In patients with PH, 4D flow MRI often demonstrates a vortex pulmonary artery flow pattern (as shown in **Figure 19**, right panel (222); the relative period of existence of the vortex significantly correlates to the mean pulmonary artery pressure (222,223). Peak systolic velocity, peak flow, stroke volume and wall shear stress by three-dimensional time-resolved flow MRI are significantly lower in patients with PAH compared with healthy study participants (224,225). The prognostic value of three-dimensional time resolved flow MRI still needs to be proven. However, it could offer in the future a noninvasive alternative to catheterization for flow assessment and may help in early detection of RV dysfunction.

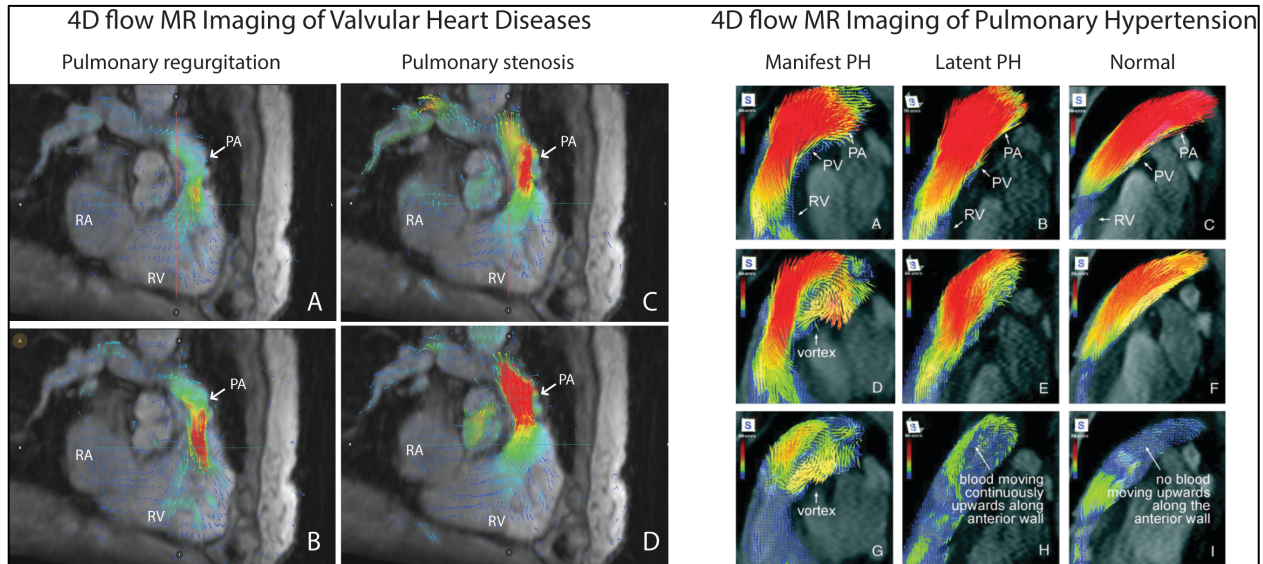


Figure 19. Four-dimensional flow MRI of a patient with pulmonary valvular disease (left); patients with pulmonary hypertension compared with a healthy control (right panel). Left panel: Flow pattern of a patient with both pulmonary regurgitation (a and b, acquired during diastole) and pulmonary stenosis (c and d, acquired during systole). **Right panel:** Typical flow patterns in the RV outflow tract at different cardiac phases for a patient with manifest PH (a, d, and g), a patient with latent PH (b, e, and h), and a normal study participant (c, f, and i). PA, main pulmonary artery; PH, pulmonary hypertension; PV, pulmonary valve; RV, right ventricle. Adapted from Amsallem et al. *Curr Opin in Cardiol*, 2016.

2.2.c Limitations and unmet needs

2.2.c.i Reversibility of DCE after PH surgery

One of the questions warranting further investigation in the field of CMR is whether DCE or T1 mapping abnormalities are reversible after surgical correction of PH. Indeed, reduction of RV fibrosis has been shown in animal models of PH (226). Lung transplantation in PAH and pulmonary arterial endarterectomy in CTEPH have both been shown to be associated with RV reverse remodeling (227–229). However, whether RV reverse remodeling is associated with a reduction in DCE or T1 mapping signal (reflecting an improvement in myocardial disarray and fibrosis) remains to be investigated.

Another potential application of tissue characterization using CMR would be to assess whether the pre-operative DCE or T1 mapping pattern is associated with differential RV reverse remodeling after lung transplantation in PAH or endarterectomy in CTEPH.

2.2.c.ii Validation of MRI 4D flow in PH

While there has been a growing number of studies using 4D blood flow MRI to characterize intra-cardiac or intra-pulmonary artery flow patterns (i.e. vortex), the validity of 4D blood flow sequences to accurately estimate ventricular volumes and mass remains to be explored. If proven to be accurate, one could envision only one 4D flow acquisition in the future (lasting <10 minutes) that would provide estimation of ventricular masses, volumes and ejection fraction, as well as hemodynamics estimation.

To date, the few studies that have shown the accuracy of 4D flow MRI for estimation of volumes and mass have been conducted in young patients with congenital heart disease (217,220). Hanneman et al. has shown the accuracy of ferumoxytol-enhanced 4D flow MRI for estimation of volumes and mass in 22 young patients (age range 0.2–25 years) with congenital heart disease (including one third with Tetralogy of Fallot) (220). Of note, ferumoxytol is an agent used and approved by the FDA for iron-deficient anemia; the use for CMR was an off-label use by the authors. **Figure 20** illustrates the methodology used in the study. The authors found excellent correlations between 4D estimated left ventricular volumes and corresponding volumes estimated using the gold standard cine SSFP acquisitions (correlation coefficient 0.97 for LV end-systolic and end-diastolic volumes, between 0.91 and 0.93 for LV mass and 0.93 for LV ejection fraction). However, RV measurements of end-diastolic and end-systolic volumes were significantly lower when using 4D flow compared to SSFP ($p < 0.05$), with differences of 8.8 mL/m² (8.5% of the mean) and 4.8 mL/m² (6.4% of the mean), respectively. The mean difference in volumes between techniques was within 10% of zero for all measurements, and Bland-Altman relative limits of agreement were between -22% to 20% for the LV and -52% to 34% for the RV. Whether these results are similar in patients with more dilated RV secondary to PAH or CTEPH remains to be explored.

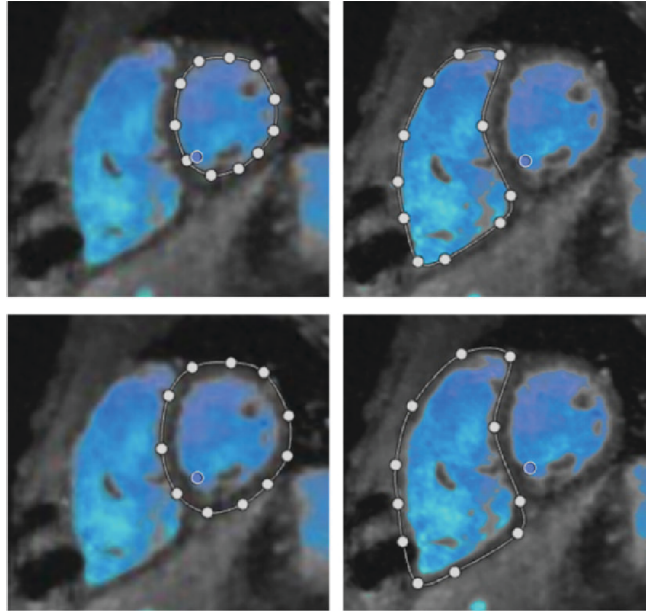


Figure 20. Example of estimation of ventricular dimensions using 4D flow MRI in a 9-year-old male with aortic coarctation. Screen captures of multiple short-axis 4D flow images demonstrating left ventricular (LV) and right ventricular (RV) endocardial (upper row) and epicardial (lower row) end-diastolic contours, with color velocity overlay to facilitate identification of the myocardial blood boundary. Left: LV contours; Right: RV contours. Hanneman et al. JMRI, 2016.

2.3 Multimodality of Right Heart Phenotyping

Although this thesis focuses on echocardiography and CMR, the two modalities mainly used in our studies, there are other imaging modalities providing information on RV phenotype, metabolism and the pulmonary circulation (such as computed tomography and positron emission tomography PET).

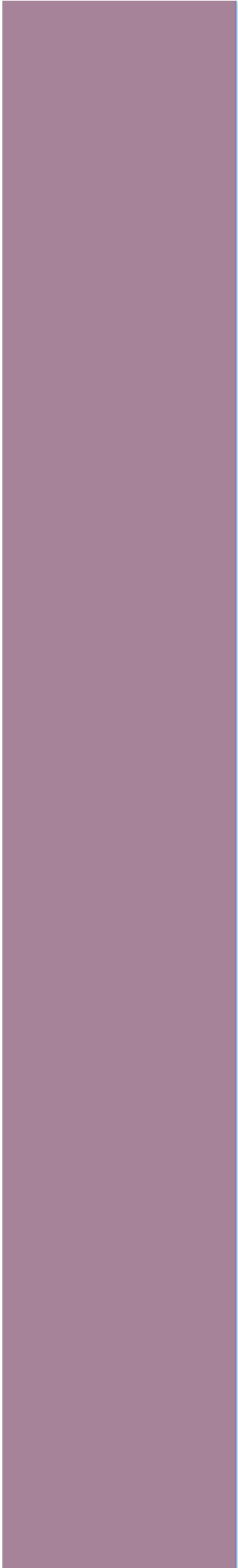
In patients with PH, computed tomography angiography is widely used to rule out CTEPH and underlying lung disease, as well as to characterize precise anatomy in the setting of congenital heart defects (7). A recent study evaluated the utility of routinely performed non-ECG gated chest computed tomography to screen for PH (230). Spruitj et al. showed that both pulmonary arterial dilation (ratio relative to the ascending aorta diameter ≥ 1) and RV enlargement (ratio relative to the left ventricular

diameter ≥ 1.2), measured on the axial view, were incremental for the detection of PH in 51 patients with advanced precapillary PH versus 25 non-PH controls (230). The application of this screening detection in a large population still remains to be done.

As summarized above, multiple molecular changes occur in a failing right ventricle exposed to an increased afterload. Four of them represent potential targets for imaging. The first target derives from the RV metabolic shift from lipolysis toward glycolysis, which has been linked to worse ventricular function and poor survival (231). The increased uptake by the cardiomyocytes of the alternative source of energy (glucose) can be easily quantified using PET 18F-2-deoxy-2-fluoro-D-Glucose. An increase in the RV-to-LV ratio tracer uptake has been reported in patients with PAH (232,233). It remains, however, unclear whether this increased ratio is explained by an increased RV glucose uptake, a decreased LV uptake or both. Moreover, preclinical studies have suggested that this metabolic shift may be transient during progression of RV failure (74), which compromises the relevance of RV PET18F-2-deoxy-2-fluoro-D-Glucose uptake as a routine biomarker in PAH. The second target is the myocardial oxygen consumption, which can be imaged using 15O-labeled tracer or 11C-acetate tracers. An increased resting oxygen consumption by the right ventricle, and hence a reduced efficiency, has been shown in patients with PAH (234). Neurohormonal dysregulation is the third target. There has been growing evidence of the importance of upregulated sympathetic nervous system and renin–angiotensin–aldosterone system in the pathophysiology of right heart failure in PAH (235). Finally, angiogenesis and apoptosis are additional promising targets for detection of maladaptive RV in pulmonary hypertension (236). Although these processes have been imaged in LV diseases (81) and PH animal models, their clinical application in PAH is still pending.

Improving deep phenotyping of the right heart is mandatory to better understand and study mechanisms underlying right heart adaptation/maladaptation. This thesis work will thus be articulated around three main objectives: first validating imaging assessment of the right heart (such as

echocardiography), then identifying the most relevant right heart metrics to define right heart adaptation/maladaptation in PH, finally explore pathophysiology mechanisms (such as immunity) associated with right heart adaptive phenotypes.



HYPOTHESIS AND OBJECTIVES

HYPOTHESIS and OBJECTIVES

Right heart failure is the main cause of mortality and morbidity in patients with PH, regardless of the etiology. Chronic pressure overload of the right ventricle results not only in an increase in RV wall stress leading to remodeling, but also several molecular changes within the right myocardium itself (i.e. metabolic switch, ischemia, active inflammation). Right heart adaptation to pressure overload is very heterogeneous between patients even with similar afterload levels. The mechanisms underlying the progression from RV adaptation to maladaptation in patients with PH remain to be fully elucidated, and they have been identified as a research priority in the latest American Thoracic Society Research Statement (237).

Non-invasive imaging (such as echocardiography) provides information on right heart dimensions, remodeling and function, as well as hemodynamic estimations. However, the accuracy of Doppler-echocardiography for estimation of pulmonary pressures remains controversial. In addition, several right heart imaging metrics (i.e. size, function, load-adaptation metrics) have been published in PH, and it remains unclear which metric better reflects right heart adaptation and outcomes in PH.

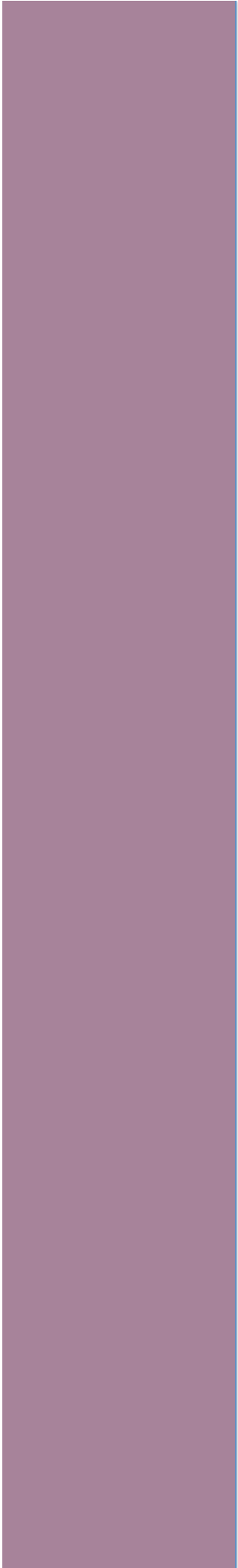
In this thesis, we hypothesized that using non-invasive imaging to improve right heart phenotyping would allow to investigate circulating proteomic biomarkers associated with right heart failure in patients with PH.

In order to test this hypothesis, we articulated this thesis around three main objectives:

- 1- The **first objective** of the thesis was to assess the accuracy and reliability of echocardiography for estimation of pulmonary pressures in a large cohort of patients with pre-capillary PH (groups 1 and 3 of the WHO classification). RV systolic pressure was estimated based on the tricuspid regurgitation maximal velocity using continuous Doppler and estimated right atrial pressure according to the Bernoulli equation, and compared to the gold standard measured by right heart catheterization. In this study, we focused on the quality of the Doppler tricuspid regurgitation signal, aiming to provide a clear methodological checklist to improve accuracy of echocardiography in the following studies on the right heart.

- 2- The **second objective** of the thesis was to identify the best **phenotyping biomarkers** of right heart adaptation/maladaptation in pulmonary hypertension.
 - a. The **first study** compared the **prognostic value** of RV free-wall strain and right ventricular end-systolic remodeling index in a large cohort of patients with idiopathic, familial, drug and toxins or connective tissue disease related pulmonary arterial hypertension, and assessed their incremental value to validated risk scores.
 - b. The **second study** defined the three concepts behind “right heart **load adaptation**” to increased afterload, modeled the physiological relationship between the right ventricle and its afterload, and validated the prognostic value of several previously published load adaptability metrics in pulmonary arterial hypertension.
 - c. The **third study** compared the right heart adaptation to load of patients with **scleroderma**-related pulmonary arterial hypertension to well-matched patients with idiopathic pulmonary arterial hypertension, as patients with scleroderma have been shown to have poor ventricular adaptation to afterload.

- 3- The **third objective** of the thesis was to explore the association between **circulating pro-inflammatory biomarkers** and right heart adaptive phenotypes or outcomes in patients with pulmonary hypertension.
- a. The **first study** assessed the value of preoperative **circulating C-reactive protein** levels for prediction of adverse in-hospital outcomes after pulmonary endarterectomy in two retrospective cohorts of patients with **chronic thromboembolic pulmonary hypertension**. The association between circulating inflammatory markers and right heart phenotype was also explored in a subgroup of patients.
 - b. The **second study** investigated the **circulating proteomics profiles** associated with **right heart failure phenotype** (using the Mayo risk score and the Stanford score determined in objective 2.a.) in two prospective cohorts of patients with pulmonary arterial hypertension. Proteomics profiles were determined using the LUMINEX© technology and included pro-inflammatory cytokines and growth factors.



MATERIAL AND METHODS

MATERIAL and METHODS

This section will present the general methods used in the several studies; the specificities for each study will be detailed in the respective methods section.

1. Study Cohorts

This thesis includes studies performed on several clinical cohorts including patients with predominantly pre-capillary PH, i.e. group 1 (PAH), group 3 (advanced lung disease) or group 4 class (CTEPH) of the WHO classification, and healthy controls.

1.1 Ethical and regulatory aspects

Clinical cohorts were included from patients referred to Stanford University – Stanford Health Care Hospitals (CA, USA) or to Marie Lannelongue Hospital (Le Plessis Robinson, France). All studies were approved by either Stanford University Institutional Review Board (for studies conducted at Stanford) or the Comité de Protection des Personnes and the Agence Nationale de Sécurité du Médicament et des Produits de Santé (for studies conducted at Marie Lannelongue Hospital). All research subjects gave written informed consent before inclusion in the studies, which were performed in agreement with the Helsinki-II declaration.

1.2 Diagnosis of pulmonary hypertension and classification

Pulmonary hypertension was invasively defined as a MPAP \geq 25mmHg using right heart catheterization (7). Group 1 PH (PAH) was defined as mean pulmonary arterial pressure \geq 25 mmHg,

PAWP \leq 15 mmHg and exclusion of other PH groups. In this thesis, idiopathic, familial, drug and toxin related or connective tissue disease-related PAH were included; no study included patients with congenital heart disease related PH. Group 3 PH (advanced lung disease) included patients with chronic obstructive pulmonary disease, interstitial lung diseases, idiopathic pulmonary fibrosis, or cystic fibrosis. Group 4 PH (CTEPH) was defined MPAP \geq 25mmHg, at least 1 segmental perfusion defect detected by lung scanning, and typical lesions of CTEPH on multidetector computed tomographic angiography and/or pulmonary angiography after at least 3 months of effective anticoagulation).

1.3 Demographics, functional status and pulmonary functional testing

In addition to age and sex, patients underwent a clinical examination during which were collected: weight, height, body mass index, body surface area using DuBois formula adjusted for ideal weight (in order to limit the influence of peripheral edema in patients with right heart failure), resting heart rate, non-invasive systemic systolic, diastolic and mean arterial pressure, and presence of symptoms (dyspnea assessed using the New York Heart Association NYHA functional classification from I to IV, syncope, hemoptysis). Functional status was also assessed using the six-minute walk test distance (meters). Results from pulmonary functional tests (including the forced expiratory volume in 1 second FEV1, diffusing capacity of the lungs for carbon monoxide DLCO) and resting arterial blood oxygen were also collected when available.

2. Right Heart Assessment

2.1 Hemodynamics using right heart catheterization

The methodology of invasively measuring hemodynamics using right heart catheterization was similar in both institutions (Stanford Health Care Hospitals and Marie Lannelongue Hospital). A balloon catheter was introduced through the right femoral vein or internal jugular vein after local anesthesia. Patients could be premedicated with 1 to 3 mg of diazepam 30 min before the procedure. The following measurements were obtained: mean right atrial pressure, right ventricular systolic pressure, systolic pulmonary arterial pressure, diastolic pulmonary arterial pressure, mean pulmonary arterial pressure, pulmonary arterial wedge pressure, and cardiac output. Cardiac output was estimated using the thermodilution method, or the Fick method in presence of severe tricuspid regurgitation. To estimate the potential effect of premedication on blood pressure, systolic, diastolic and mean blood pressures were measured at baseline before sedation and during the invasive procedure.

2.2 Resting trans-thoracic echocardiography

Resting two-dimensional trans-thoracic echocardiograms were performed using different vendors, acquiring 3 cardiac cycles or 5 in case of arrhythmia. Echocardiograms were interpreted off-line by a certified cardiologist trained on right heart assessment (MA) and a second reader for inter-observer variability assessment, all blinded to the diagnosis, clinical status and hemodynamics data. The following views were acquired (as presented in the introduction chapter): parasternal long axis view, RV-modified parasternal long axis views centered either on the tricuspid valve or on the pulmonary valve, short axis views, standard apical 4-chamber view, 2-chamber view, 3-chamber view and 3-chamber view, RV-focused apical 4-chamber view, subcostal view and suprasternal view.

Right heart dimension and function were assessed on the RV-focused apical 4-chamber view as recently published (185). Right atrial maximal area was indexed on body surface area. RV dimension metrics included RV end-diastolic area and end-systolic area, both indexed on body surface area. The RV end-systolic remodeling index was calculated as the RV free-wall length / septal height in end-systole as recently published (145).

RV systolic function metric included RV fractional area change (RVFAC), RV free-wall longitudinal Lagrangian strain (RVLS) and the tricuspid annular plane systolic excursion (TAPSE). The RVFAC (%) was defined as $100 * [RV \text{ end-diastolic area} - RV \text{ end-systolic area}] / RV \text{ end-diastolic area}$. The RVLS (%) was derived from manually tracing of the RV free-wall in end-systole and end-diastole, and calculated as $100 * [RV \text{ free-wall end-systolic length} - \text{end-diastolic length}] / RV \text{ end-systolic length}$ (145).

Right ventricular systolic pressure was estimated using the maximal velocity of the tricuspid regurgitation signal using continuous Doppler when interpretable, and the estimation of right atrial pressure based on the size and the compliance of the inferior vena cava following a sniff test, as extensively detailed in our first study (26). Pericardial effusion was considered significant if >5mm in end-diastole.

3. Circulating Biomarkers

3.1 Enzyme-Linked ImmunoSorbent Assay (ELISA)

3.1.a Principles

The ELISA method is a solid-phase enzyme immunoassay enabling detection and/or quantification of an antigen (i.e. protein such as a cytokine) in a liquid sample (i.e. plasma or serum). Among the several different ELISA methods illustrated in **Figure 21**, the double antibody sandwich immunoassay method (R&D Systems® ELISA kits, R&D Systems, Inc., Minneapolis, MN) was used in this thesis for quantification of the following plasmatic protein levels: interleukin-1 β (IL-1 β), interleukin-6 (IL-6) and monocyte chemoattractant protein-1 (MCP-1). This method uses two antibodies, which bind to different sites on the antigen or ligand. The capture antibody is attached to a solid surface. The antigen is then added, followed by addition of a second antibody, the detection antibody, which is linked to an enzyme. The addition of the enzyme's substrate leads to color development. The amount of color (absorbance) is directly proportional to the analyte concentration.

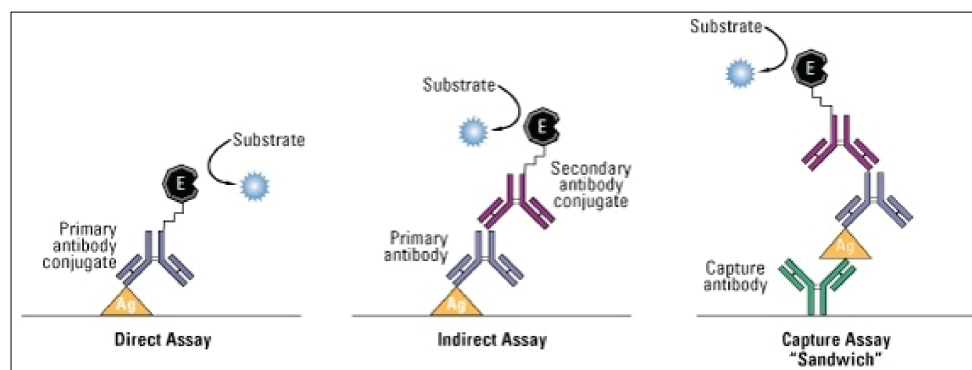


Figure 21. Illustration of the three most common ELISA methods. E: enzyme. Adapted from <https://microbeonline.com/elisa-test-for-antigenantibody-detection>.

3.1.b Advantages

The ELISA method enables accurate and sensitive detection of the antigen, the cytokine of interest, and provides highly quantitative and generally reproducible results (238). Because of these qualities and the long experience with this technology over time, ELISA remains considered as the gold standard cytokine measurement method and is widely utilized in clinical laboratories and biomedical research.

3.1.c Limitations

The ELISA method has however several limitations. First, the ELISA technique allows the measurement of only one cytokine at a time per sample aliquot, requiring large blood volumes and increasing the costs. Second, there can be significant variability on the results deriving from the antibody affinity, quantity, kit manufacturer and operator expertise (239).

3.2 Multiplex Arrays (Luminex®)

3.2.a Principles

Multiplex arrays enable the measurement of multiple cytokines in the same biological sample at the same time, making it the choice method for screening. There are different multiplex arrays methods based on chemoluminescence, electroluminescence or flow cytometry. In this thesis, we used the flow cytometry multiplex arrays, also called bead-based multiplex arrays, from Luminex® (Flexmap 3D® Luminex multi-analyte profiling xMAP technology, Luminex Corporation, Austin, TX). Each bead set is coated with a specific capture antibody, and fluorescence-labeled detection antibodies bind to the specific cytokine-capture antibody complex on the bead set (238). The fluorescent emission detected in each bead is detected using flow cytometric analysis (**Figure 22**).



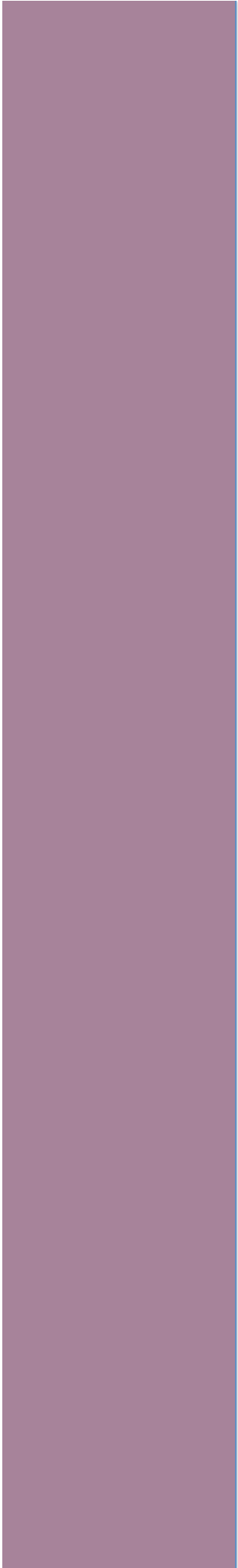
Figure 22. Example of flow cytometry multiplex arrays (Flexmap 3D® Luminex multi-analyte profiling xMAP technology, Luminex® Corporation - HIMC, Stanford University).

3.2.b Advantages

Multiplex arrays allow the quantification of multiple cytokines (up to 96) in the same sample at a given time, requiring smaller sample volume than standard ELISA test. This not only reduces time and costs, but also enable to assess one cytokine in the context of other cytokines. Finally, the multiplex arrays enable detection of different cytokines with different concentrations, without requiring multiple dilution.

3.2.c Limitations

While enabling simultaneous detection of different cytokines, bead-based multiplex arrays expose to the risk of cross-reaction of the secondary antibodies, resulting in false positive reactions. In addition, there is a risk of variability secondary to different experiment times, handlers, plates or reagent lots. This technical heterogeneity referred to as “batch effects” needs to be taken into consideration as they can potentially confound the discovery of real explanatory variables from “big data” such as proteomic-profiling data. The different statistical methods enabling batch effect mitigation are beyond the scope of this thesis. The principles and challenges of batch effect correction methods (i.e. data cleaning approach where batch effects are estimated and removed from the data) have been recently reviewed by Goh et al. (240).



RESULTS

RESULTS

Chapter 1- ACCURACY of ECHOCARDIOGRAPHY for DETECTION of PULMONARY HYPERTENSION

Study 1: Addressing the Controversy of Estimating Pulmonary Arterial Pressure by Echocardiography

Authors: Myriam Amsallem MD MS^{1,2}, Joshua M. Sternbach MD³, Sasikanth Adigopula MD¹, Yukari Kobayashi MD¹, Thu A. Vu RN¹, Roham Zamanian MD PhD³, David Liang MD¹, Gundeep Dhillon MD¹, Ingela Schnittger MD¹, Michael V. McConnell MD MSEE¹, and François Haddad MD¹

Affiliations:

¹ Division of Cardiovascular Medicine – Stanford University School of Medicine, Stanford, USA.

² Marie Lannelongue Hospital – Paris Sud University, Le Plessis Robinson, France.

³ Division of Pulmonary and Critical Care – Stanford University School of Medicine, Stanford, USA.

Communications:

Published in *J Am Soc Echocardiogr*. 2016;29:93-102. doi:10.1016/j.echo.2015.11.001.

Presented at 2016 Journées Européennes de la Société Française de Cardiologie (Paris, France), 2016 Stanford Cardiovascular Institute Conference (Palo Alto, USA).

Summary: This study aimed to address the controversy of the accuracy and reliability of echocardiography to estimate pulmonary pressures and detect PH. As previously developed in the introduction, there has been various studies reporting discrepant correlations between invasive pressures and RVSP estimated from the maximal TR velocity and estimated RAP (**Table 2**). In the present study, we hypothesized that the heterogeneity in the findings noted in previous studies is likely related to the fact that different studies have not always considered TR signal quality. Moreover, there is still no consensus in the literature on which RVSP threshold should be used to classify patients with or without PH (thresholds ranging from 35 to 45 mm Hg) (241). To address these questions, we retrospectively analyzed transthoracic echocardiograms from patients with advanced lung disease (group 3 PH) or idiopathic PAH (group 1 PH) who underwent right heart catheterization. Our first objective was to determine the relationship between MPAP and SPAP in a large hemodynamic cohort to provide guidance for the selection of the best criteria for RVSP. Our second objective was to assess the accuracy of echocardiography in estimating pulmonary artery pressures and analyze the factors associated with under- or overestimation. Our final objective was to compare diagnostic performance for classifying PH using commonly used metrics of RV size and function, in patients with uninterpretable TR signals.

Our study brings new perspective to the controversy. First, our results validate, in the largest series to date, the relationship between MPAP and SPAP described by Chemla et al. (28). Second, our study provides a critical appraisal of the diagnostic performance of echocardiographic estimations of pulmonary artery pressure, providing a practical checklist for methodological quality. Finally, we highlight the limitations of using metrics of RV remodeling or function such as systolic eccentricity index, relative RV size, and TAPSE for classifying PH in patients with advanced lung disease or mild PH. Overall, this study shows that echocardiography provides reliable estimation of RVSP in patients with advanced lung disease or PAH when careful attention is paid to signal quality and proper interpretation of modal frequency.

CLINICAL INVESTIGATIONS
PULMONARY ARTERIAL HYPERTENSION

Addressing the Controversy of Estimating Pulmonary Arterial Pressure by Echocardiography

Myriam Amsallem, MD, Joshua M. Sternbach, MD, Sasikanth Adigopula, MD, Yukari Kobayashi, MD, Thu A. Vu, RN, Roham Zamanian, MD, David Liang, MD, Gundeep Dhillon, MD, Ingela Schnittger, MD, Michael V. McConnell, MD, MSEE, and François Haddad, MD, *Stanford, California*

Background: There is currently controversy over whether echocardiography provides reliable estimations of pulmonary pressures. The objective of this study was to determine the factors influencing the accuracy and reliability of estimating right ventricular systolic pressure (RVSP) using echocardiography in patients with advanced lung disease or pulmonary arterial hypertension.

Methods: Between January 2001 and December 2012, 667 patients with advanced lung disease or pulmonary arterial hypertension underwent right heart catheterization and transthoracic echocardiography. Of those, 307 had both studies within 5 days of each other. The correlation and bias in estimating RVSP according to tricuspid regurgitation (TR) signal quality and reader expertise were retrospectively determined. Reasons for under- and overestimation were analyzed. The diagnostic performance of estimated RVSP, relative right ventricular size, eccentricity index, and tricuspid annular plane systolic excursion was compared for classifying patients with pulmonary hypertension (mean pulmonary artery pressure \geq 25 mm Hg).

Results: Invasive mean and systolic pulmonary artery pressures were strongly correlated ($R^2 = 0.95$, $P < .001$), with mean pulmonary artery pressure = $0.60 \times$ systolic pulmonary artery pressure + 2.1 mm Hg. Among patients undergoing right heart catheterization and transthoracic echocardiography within 5 days, level 3 readers considered only 61% of TR signals interpretable, compared with 72% in clinical reports. Overestimation in the clinical report was related mainly to not assigning peak TR velocity at the modal frequency and underestimation to overreading of uninterpretable signals. When the TR signal was interpretable, the areas under the curve for classifying pulmonary hypertension were 0.97 for RVSP and 0.98 for RVSP and eccentricity index ($P > .05$). When TR signals were uninterpretable, eccentricity index and right ventricular size were independently associated with pulmonary hypertension (area under the curve, 0.77).

Conclusions: Echocardiography reliably estimates RVSP when attention is given to simple quality metrics. (J Am Soc Echocardiogr 2016;29:93-102.)

Keywords: Advanced lung disease, Echocardiography, Pulmonary hypertension, Right ventricular systolic pressure, Right heart catheterization

In the past 30 years, echocardiography has emerged as one of the most useful methods for noninvasively estimating pulmonary artery pressures.^{1,2} One of the main Doppler echocardiographic techniques to assess right ventricular (RV) systolic pressure (RVSP) relies on estimating the RV–right atrial pressure gradient from the tricuspid regurgitation (TR) maximal velocity using the modified

Bernoulli equation, to which is added the estimated right atrial pressure (RAP).³ The original 1984 publication of Yock and Popp⁴ reported an excellent correlation between RVSP measured by right heart catheterization (RHC) and RVSP simultaneously estimated by echocardiography ($r = 0.93$, $P < .001$). This was later confirmed by several other investigators.⁵⁻⁷

However, in recent years, the accuracy and reliability of echocardiography for estimating RVSP have been challenged, especially in the field of advanced lung disease (ALD) and pulmonary hypertension (PH). In the study of Fisher *et al.*⁸ on 63 subjects with mild or no PH, a weak correlation between invasive and estimated RVSP was reported ($r = 0.23$, $P < .05$), including one third of patients having a difference > 10 mm Hg. Rich *et al.*⁹ more recently reported similar findings.

In the present study, we hypothesized that the heterogeneity in the findings noted in previous studies is likely related to the fact that different studies have not always considered TR signal quality. Moreover, there is still no consensus in the literature on which RVSP threshold should be used to classify patients with or without

From the Division of Cardiovascular Medicine (M.A., S.A., Y.K., T.A.V., D.L., G.D., I.S., M.V.M., F.H.) and the Division of Pulmonary and Critical Care (J.M.S., R.Z.), Stanford University School of Medicine, Stanford, California.

Dr Amsallem has received a research fellowship from Fédération Française de Cardiologie.

Reprint requests: Myriam Amsallem, MD, Stanford Cardiovascular Institute, Stanford University School of Medicine, 300 Pasteur Drive, Stanford, CA 94304 (E-mail: mamsalle@stanford.edu).

0894-7317/\$36.00

Copyright 2016 by the American Society of Echocardiography.

<http://dx.doi.org/10.1016/j.echo.2015.11.001>

Abbreviations
ALD = Advanced lung disease
AUC = Area under the curve
EI = Eccentricity index
IQR = Interquartile range
IVC = Inferior vena cava
LV = Left ventricular
MPAP = Mean pulmonary artery pressure
PAH = Pulmonary arterial hypertension
PH = Pulmonary hypertension
RAP = Right atrial pressure
RHC = Right heart catheterization
RV = Right ventricular
RVSP = Right ventricular systolic pressure
SPAP = Systolic pulmonary artery pressure
TAPSE = Tricuspid annular plane systolic excursion
TR = Tricuspid regurgitation

PH (thresholds ranging from 35 to 45 mm Hg).¹⁰ To address these questions, we retrospectively analyzed transthoracic echocardiograms from patients with ALD or idiopathic pulmonary arterial hypertension (PAH) who underwent RHC. Our first objective was to determine the relationship between mean pulmonary artery pressure (MPAP) and systolic pulmonary artery pressures (SPAP) in a large hemodynamic cohort to provide guidance for the selection of the best criteria for RVSP. Our second objective was to assess the accuracy of echocardiography in estimating pulmonary artery pressures and analyze the factors associated with under- or overestimation. Our final objective was to compare diagnostic performance for classifying PH using commonly used metrics of RV size and function, in patients with uninterpretable TR signals.

METHODS

Study Population

After obtaining institutional review board approval, we retrospectively reviewed the charts of all patients aged ≥ 18 years referred to the Stanford University ALD center for RHC between 2001 and 2012 ($n = 704$). Eligible subjects had either ALD (chronic obstructive pulmonary disease, interstitial lung diseases, idiopathic pulmonary fibrosis, or cystic fibrosis) or PAH. For our first objective (hemodynamic correlations), all subjects with complete RHC were included ($n = 667$); for our second objective, subjects with RHC and complete echocardiography within 5 days were included ($n = 307$).

Right Heart Catheterization

A balloon catheter was introduced through the right femoral vein or internal jugular vein after local anesthesia. Patients could be premedicated with 1 to 3 mg of diazepam 30 min before the procedure. The following measurements were obtained: RAP, RVSP, SPAP, diastolic pulmonary artery pressure, MPAP, pulmonary artery wedge pressure, and cardiac output. To estimate the potential effect of premedication on blood pressure, systolic and diastolic blood pressures were measured at baseline before sedation and during the invasive procedure. PH was defined as MPAP on RHC of ≥ 25 mm Hg.^{11,12}

Echocardiography

Resting TTE was performed using the Philips 7500 or iE33 system (Philips Medical Systems, Andover, MA) with 5-MHz transducers by experienced, credentialed cardiac sonographers. RVSP was estimated from the maximal RV-right atrial pressure gradient, using the modified Bernoulli equation⁵: $RVSP = 4 \times (\text{maximal TR velocity})^2 + RAP$, where maximal TR velocity was measured using continuous-

wave Doppler. Windows used to measure maximal TR velocity included parasternal long- and short-axis and RV-modified apical four-chamber views. Only the window with the best quality and highest signal was chosen for peak velocity. TR signals acquired after an ectopic beat or after wide respiratory motion were excluded. In the 26 patients with atrial fibrillation, the third beat after two consecutive relatively equal RR intervals was used, previously reported as the "index-beat method."¹³ Patients with severe dense triangular and early peaking TR were excluded, because SPAP could not be appropriately estimated from the TR signal. RAP was estimated in the subcostal view according to the inferior vena cava (IVC) size and collapsibility following a normal sniff: 3 mm Hg if IVC < 15 mm and collapse $\geq 50\%$, 5 mm Hg if IVC between 15 and 21 mm and collapse $\geq 50\%$, 15 mm Hg if IVC ≥ 21 mm and collapse between 10% and 50%, 20 mm Hg if IVC ≥ 21 mm and collapse $< 10\%$, and 10 mm Hg in all other cases.

In this study, we assessed interpretations of the same studies by comparing measurements from the echocardiography laboratory clinical report with offline reassessment by both a level 3-trained cardiologist certified by the National Board of Echocardiography and a level 2-trained cardiologist, who were blinded to RHC values.¹⁴ We also assessed the potential effect of training by the level 2 reader, who blindly reinterpreted all measurements. Level 2 and 3 readers measured maximal Doppler velocities at the peak modal frequency, adjusting Doppler gain to identify the main complete envelope in order to avoid overestimation of maximal velocities. The quality of the TR signal was classified, as shown in Figure 1A, according to envelope visibility (type 1, complete envelope; type 2, partial envelope but prone to extrapolation; and type 3, unreliable envelope or no signal). TR severity was assessed as absent, mild, moderate, or severe according to American Society of Echocardiography guidelines,¹⁵ integrating the following metrics. Severe TR was defined in the presence of a vena contracta ≥ 7 mm, reversed systolic hepatic vein flow, proximal isovelocity surface area radius > 9 mm, and very large central jet or eccentric wall impinging jet. Mild TR was defined by all of the following parameters: visual small jet, proximal isovelocity surface area radius < 5 mm, and systolic predominance of the hepatic vein flow. Moderate TR was defined as TR not corresponding to the definition of either mild or severe TR. Finally, the beam-to-flow angle between the Doppler cursor and the TR jet was assessed and defined as acceptable when $< 40^\circ$. Contrast methods were not routinely used.

A predefined value of RVSP > 40 mm Hg was considered as abnormal in this study on the basis of the previous studies of Chemla *et al.*¹⁶ and considering the RV outflow tract gradient. Over- and underestimation of echocardiography-based RVSP were defined as a relative difference $> 20\%$ or $< 20\%$ of the RHC value. The following routinely acquired RV size and function metrics were also assessed: end-diastolic basal RV/left ventricular (LV) diameter ratio (> 0.67 defining an abnormal ratio and measured in the apical four-chamber view), LV systolic eccentricity index (EI; > 1.2 defining an abnormal ratio, measured in the short-axis view), and tricuspid annular plane systolic excursion (TAPSE; < 17 mm abnormal).¹⁷⁻¹⁹ Pulmonary acceleration time was not included, because it was available in only 53% of patients.

Statistical Analysis

Quantitative data are expressed as mean \pm SD if normally distributed or as medians and interquartile ranges (IQRs) if not normally distributed; qualitative variables are presented as numbers and percentages. The relation between invasive MPAP and SPAP was

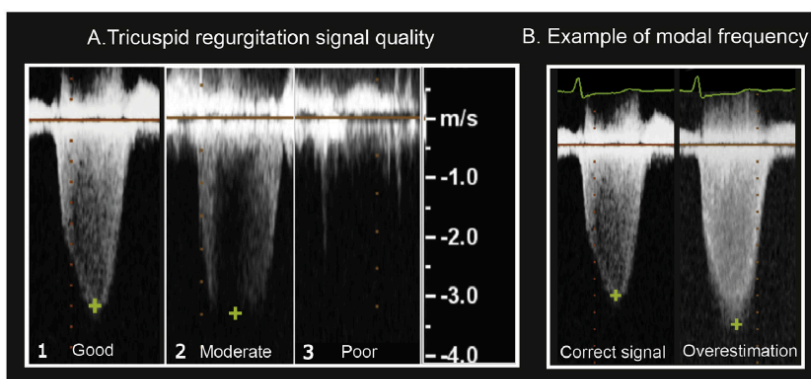


Figure 1 Classification of the TR signal quality using continuous-wave Doppler and example of modal frequency and overestimation. **(A)** An example of each TR signal type from three different patients, according to envelope visibility and quality: complete envelope (1), partial envelope but prone to extrapolation (2), and unreliable envelope (3). **(B)** An example of two TR signals acquired in the same patient. The left signal displays a complete envelope after decreasing the Doppler gain, contrasting with the right signal, in which some additional Doppler signal misread as the TR envelope leads to overestimating peak velocity and consequently RVSP.

assessed by regression analysis in the overall population with available complete RHC data. Comparisons between echocardiographic and invasive RVSP were performed by linear regression analysis (and are presented as Pearson coefficients with 95% CIs) and were then compared using Bland-Altman plots of the difference between RVSPs and the mean value of the two RVSPs (with 95% limits of agreement defined as $\pm 1.96 \times \text{SD}$ of the difference). Systematic differences between two measurements or two groups were assessed using Student's *t* test. The diagnostic performance of echocardiographic estimates of RVSP to identify the presence of PH (defined as invasive MPAP ≥ 25 mm Hg) was assessed by logistic regression and is expressed as the area under the curve (AUC). Intra- and interobserver variability for echocardiography measurements was determined using two-way mixed single-measure intraclass correlation coefficients. *P* values $< .05$ were considered to indicate statistical significance. Statistical analyses were performed using SPSS version 14.0 (SPSS, Inc, Chicago, IL). This study was conducted in agreement with the Declaration of Helsinki and was approved by the Stanford University Institutional Review Board.

RESULTS

Study Population

For the entire cohort referred for RHC, the mean age was 51 ± 13 years, and 54% were women. In the subgroup of patients who underwent RHC and echocardiography within 5 days of each other, the mean age was 50 ± 13 years, 59% were women, and two thirds had PH. Seventy-one percent had ALD, and 29% had PAH. The median time delay between echocardiography and RHC was 2 days (IQR, 1–3 days). Characteristics of the study population are presented in Table 1.

Hemodynamic Relationship between MPAP and SPAP

A strong correlation was noted between invasive MPAP and SPAP ($R^2 = 0.95$, $P < .001$). The linear equation that best described this relation was $\text{MPAP} = .60 \times \text{SPAP} + 2.1$ mm Hg (Figure 2). The MPAP

threshold of 25 mm Hg corresponded to an SPAP of 38 mm Hg. The same equation was observed in the subgroup of subjects undergoing RHC and echocardiography within 5 days.

RVSP Estimation According to Reader Expertise and TR Signal Quality

RVSP was reported more frequently in the clinical reports (72%) than by level 3 (61%) or level 2 readers (56%) ($P < .05$). Figure 3 shows TR signal quality classification according to etiology. In patients with ALD, TR signals were more frequently either uninterpretable or only prone to extrapolation. In contrast, TR signals were considered interpretable in the majority of patients with PAH (75%).

Relationship between Invasive and Echocardiography-Based RVSP Estimation

There were good to excellent correlations between RVSP estimated by RHC and echocardiography: $r = 0.84$ (IQR, 0.79–0.87) for clinical reports, $r = 0.86$ (IQR, 0.82–0.90) for level 2 readers, and $r = 0.96$ (IQR, 0.95–0.97) for level 3 readers ($P < .001$ for all). The correlation for level 3 readers was significantly higher than for level 2 readers or clinical reports ($P < .001$). Correlation between invasive and noninvasive RVSP estimations mentioned in the clinical report did not differ significantly when selecting only patients defined as interpretable by level 2 ($r = 0.85$; IQR, 0.80–0.89) or level 3 ($r = 0.87$; IQR, 0.81–0.91) readers. When selecting only patients who underwent both procedures within 3 days ($n = 287$), correlations were as follows: $r = 0.84$ (IQR, 0.80–0.88) for clinical reports, $r = 0.89$ (IQR, 0.85–0.92) for level 2 readers, and $r = 0.95$ (IQR, 0.93–0.96) for level 3 readers ($P < .001$ for all). Bland-Altman plots of the correlation between RVSP by RHC and all three levels of echocardiography readers for the total population demonstrated good accuracy (with almost no bias, especially for level 2 readers and clinical reports) but wide limits of agreements ($1.96 \times \text{SD}$ up to 33 mm Hg for clinical reports), suggesting low precision (Figure 4). Systolic blood pressure during RHC was 6% lower than systolic blood pressure during echocardiography (median, 115 mm Hg [IQR, 104–131 mm Hg] vs 122 mm Hg [IQR, 110–133 mm Hg]; $P = .001$).

Table 1 Clinical and hemodynamic characteristics of the total population and patients in whom RVSP could be assessed by echocardiography

Variable	Total population (n = 307)	Interpretable signals (n = 172)	Uninterpretable signals (n = 135)	P
Clinical characteristics				
Age (y)	49.5 ± 13.3	49.9 ± 13.2	49.0 ± 13.4	.56
Men	125 (41%)	61 (36%)	64 (47%)	.07
ALD	219 (71%)	104 (60%)	115 (85%)	<.01*
PAH	88 (29%)	68 (40%)	20 (15%)	<.01*
RHC				
HR (beats/min)	81.1 ± 15.8	82.4 ± 15.7	79.8 ± 15.9	.15
SBP (mm Hg)	117.6 ± 18.1	115.8 ± 17.3	119.9 ± 19.0	.05*
MPAP (mm Hg)	36.5 ± 17.8	41.4 ± 18.7	30.3 ± 14.3	<.01*
MPAP ≥ 25 mm Hg	206 (67%)	128 (74%)	78 (58%)	<.01*
RVSP (mm Hg)	56.9 ± 27.3	65.2 ± 28.4	46.7 ± 22.1	<.01*
PCWP (mm Hg)	11.2 ± 6.6	10.8 ± 5.4	11.8 ± 7.8	.19

HR, Heart rate; PCWP, pulmonary capillary wedged pressure; SBP, systolic blood pressure.

Data are expressed as mean ± SD or as number (percentage). Type 1 (complete envelope) and type 2 (partial envelope but prone to extrapolation) TR signals acquired by continuous-wave Doppler and assessed by level 2 readers were considered "interpretable signals." Type 3 (no signal) were considered "uninterpretable signals." P values between patients with interpretable and uninterpretable signals are displayed.

*Statistically significant (P < .05).

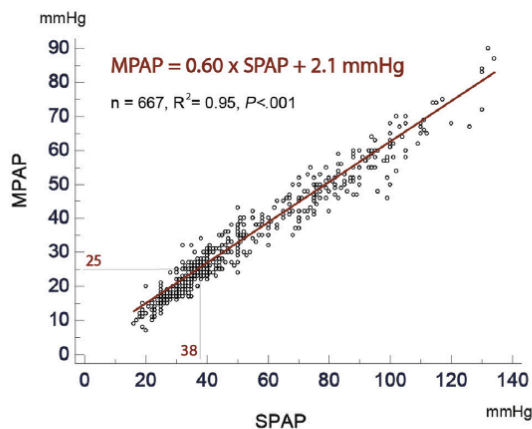


Figure 2 Relationship between invasive MPAP and SPAP in the overall study population. The hemodynamic equation found (MPAP = 0.60 × SPAP + 2.1 mm Hg) validates the equation of Chemla *et al.*¹⁶ An MPAP of 25 mm Hg corresponds to an SPAP of 38 mm Hg.

Reasons for Under- and Overestimation of RVSP

Reassessed by another level 3 reader, the level 3 reader underestimated RVSP in 8.6% of patients and overestimated in 5.4% (Figure 5). Absence of a well-defined TR envelope (88%), time delay between the two examinations, and discrepancies between RAP estimation of >10 mm Hg (although rare, accounting for three patients) were the three main reasons for underestimation, whereas overestimation was associated with poorer TR signal quality (Figure 1B) and a greater delay between RHC and echocardiography.

The clinical report RVSP estimation was underestimated in 11.4% of the population and overestimated in 16.6%. The main reason for

TR signal quality according to etiology

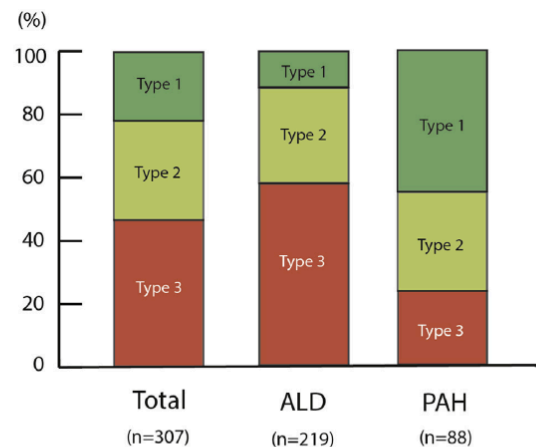


Figure 3 TR signal quality according to etiology. TR signal quality was defined as follows: complete envelope as type 1 (dark green), partial envelope but prone to extrapolation as type 2 (light green), and unreliable envelope or no signal as type 3 (red).

underestimation was the presence of TR envelope incompleteness (94%), including a not well-defined TR signal quality (60%). The main reasons for overestimation were estimation not at TR modal frequency and a not well-defined envelope.

Inter- and Intraobserver Variability of RVSP Estimation

Intraclass correlation coefficients for RVSP estimation were 0.92 (95% CI, 0.86–0.95) between level 3 readers and clinical reports,

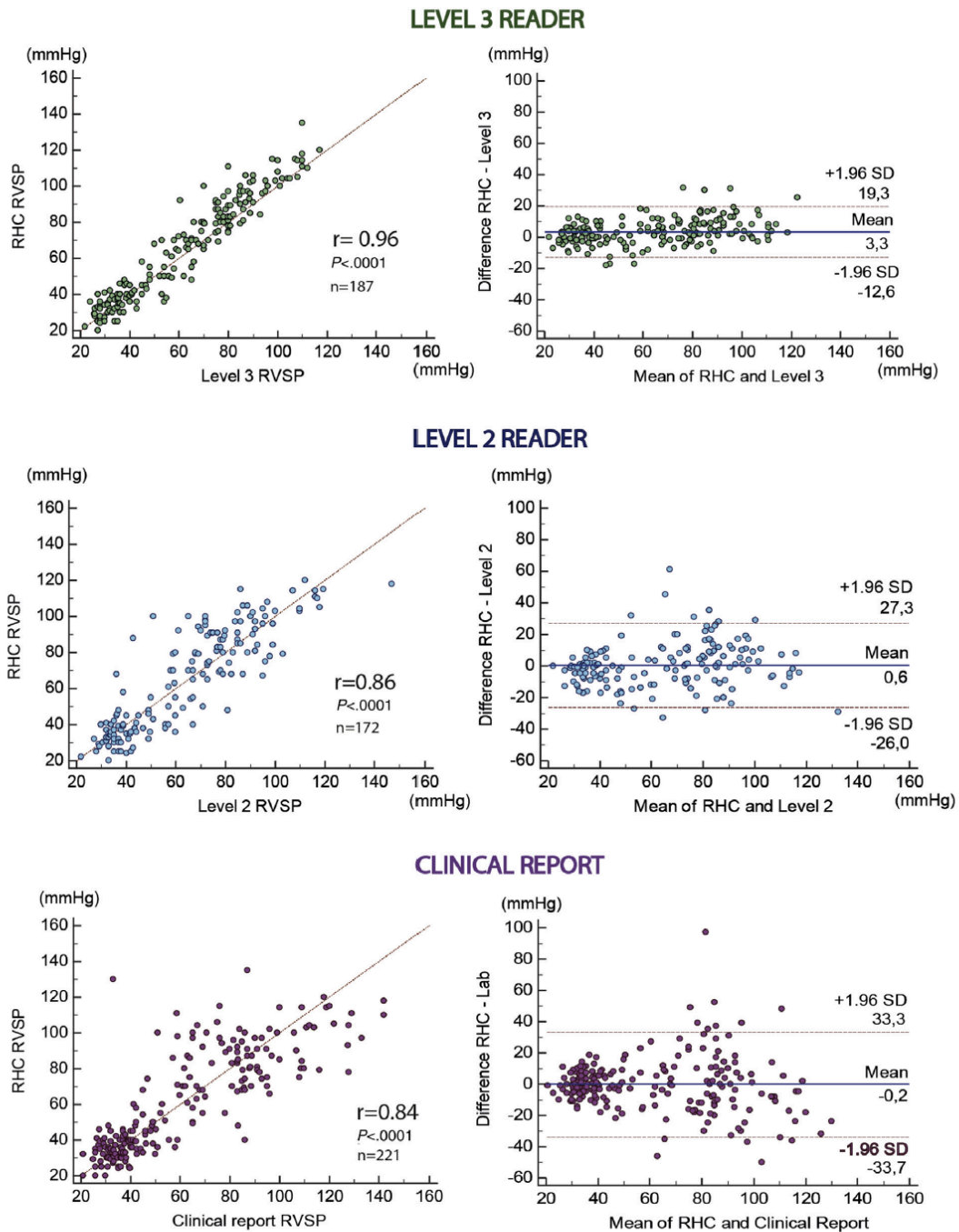


Figure 4 Linear regression (*left*) and Bland-Altman analysis plots (*right*) assessing the correlation between RVSP measured by catheterization and all three levels of echocardiography readers. Level 3 expert reader is displayed in green, level 2 reader in blue, and data from the clinical report in purple. Pearson coefficients are presented as r values. P values $< .05$ were considered to indicate statistical significance.

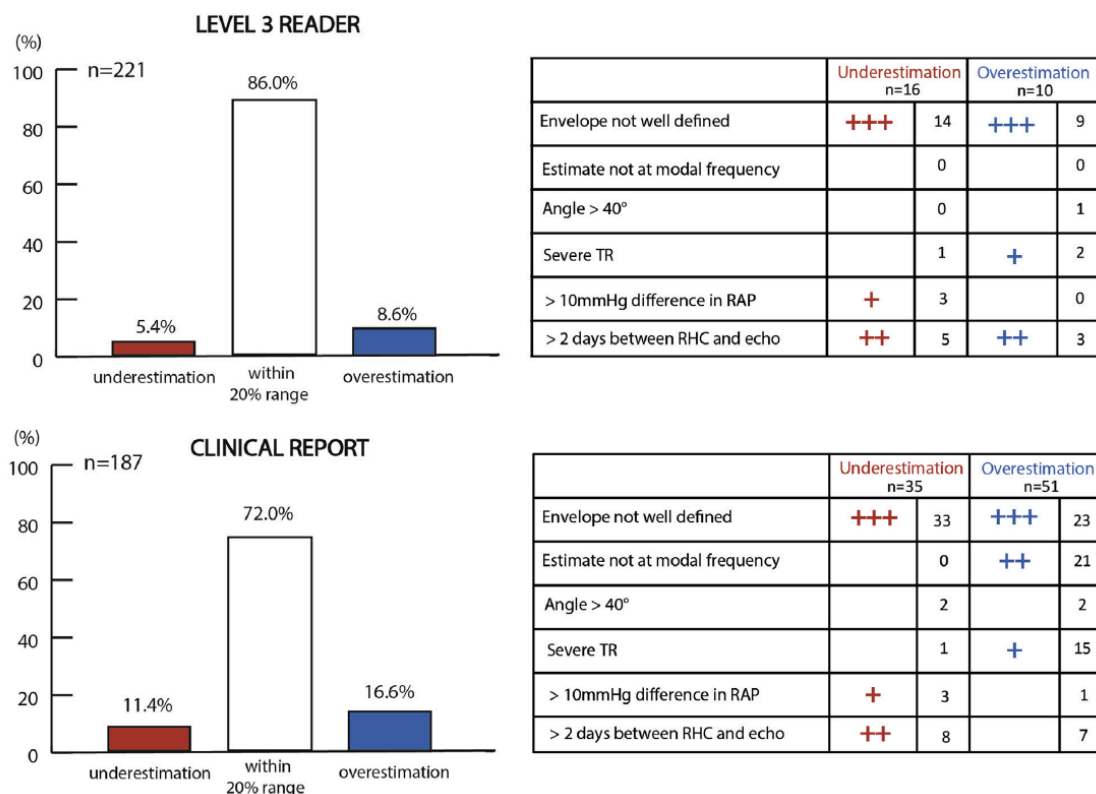


Figure 5 Frequency and etiology of under- and overestimation cases by level 3 reader and the clinical report from the echocardiography laboratory readings. Underestimation (red) and overestimation (blue) of echocardiography-based RVSP were defined as a relative difference > 20% from the RHC value.

0.84 (95% CI, 0.79–0.88) between level 3 and 2 readers, and 0.84 (95% CI, 0.61–0.92) between level 2 readers and clinical reports. Intraobserver variability was excellent for level 2 readers (0.95; 95% CI, 0.94–0.97). There was no significant change with training, for level 2 readers, in RVSP correlation (0.70 [95% CI, 0.63–0.75] before training vs 0.66 [95% CI, 0.60–0.72] after training, $P = .47$). The main modification by training was reclassification of 32 (10.4%) type 2 quality TR signals as uninterpretable type 3 signals.

Right Heart Metric Performance for PH Classification

When considering patients with interpretable signal (i.e., complete or incomplete envelope), the AUC for classifying PH by level 3 readers was excellent (0.97; 95% CI, 0.93–0.99; $P < .001$), as accomplished using our predefined threshold of 40 mm Hg. In comparison, the AUCs were 0.85 (95% CI, 0.80–0.89) for EI, 0.83 (95% CI, 0.78–0.87) for RV/LV ratio, and 0.57 (95% CI, 0.51–0.63) for TAPSE ($P < .01$ for all). After multivariate logistic regression, only RVSP and EI were retained in the model, displaying an AUC of 0.98 (95% CI, 0.94–0.99) if entered as continuous variables or 0.95 (95% CI, 0.91–0.98) if using the predefined thresholds ($P < .001$ for all). These latter AUCs were not statistically different from the AUC for RVSP ($P = .49$ and $P = .36$, respectively). The six patients who had RVSP estimations < 40 mm Hg and EIs < 1.2 despite having PH on RHC had MPAP levels near the threshold of classification of PH (median, 26 mm Hg; IQR, 26–27 mm Hg).

When considering patients with uninterpretable signals, the AUCs for PH classification were 0.75 (95% CI, 0.66–0.82; $P < .001$) for EI, 0.72 (95% CI, 0.63–0.79; $P < .001$) for RV/LV ratio, and 0.52 (95% CI, 0.44–0.61; $P = .66$) for TAPSE. After multivariate logistic regression, only EI and RV/LV ratio were helpful to discriminate PH, displaying an AUC of 0.77 (95% CI, 0.69–0.84) if entered as continuous variables. When the variables were entered using the predefined thresholds, only EI > 1.2 was retained in the model (AUC, 0.68; 95% CI, 0.59–0.76; $P < .001$). The 29 patients who had EIs < 1.2 despite having PH on RHC also had MPAP levels near the threshold of classification of PH (median, 28 mm Hg; IQR, 26–34 mm Hg).

DISCUSSION

Our study brings new perspective to the controversy over estimating pulmonary pressures in patients with ALD or PAH. Our study has three main findings. First, our results validate, in the largest series to date, the relationship between MPAP and SPAP described by Chemla *et al.*¹⁶ Second, our study provides a critical appraisal of the diagnostic performance of echocardiographic estimations of pulmonary artery pressure. Finally, our study highlights the limitations of using systolic EI, relative RV size, and TAPSE for classifying PH in patients with ALD or mild PH.

Although PH is defined as MPAP \geq 25 mm Hg,²⁰ in echocardiography, mainly RVSP is used for classifying PH. Therefore, identifying

Table 2 Studies assessing correlation between invasive and echocardiography based RVSP estimations

Study	Population	n	% of interpretable TR	Correlation (r)	Significant difference	Limitations
Yock <i>et al.</i> (1984) ⁴	Signs of elevated right-sided pressure	62	87	0.89*	SEE = 8 mm Hg	RAP estimated using JVP
Currie <i>et al.</i> (1985) ⁵	PH or no PH	127	87	0.96	SEE = 7 mm Hg	RAP assumed 10 mm Hg
Berger <i>et al.</i> (1985) ⁶	PH or no PH	69	59	0.97	SEE = 4.9 mm Hg	—
Laaban <i>et al.</i> (1989) ²⁷	ALD, PH or no PH	41	66	0.65	SEE = 9 mm Hg	RAP assumed 5 mm Hg
Tramarin <i>et al.</i> (1991) ²⁸	ALD, PH or no PH	100	30	0.73	SEE = 7.4 mm Hg	—
Brecker <i>et al.</i> (1994) ²⁹	Mostly PAH, severe PH	10	—	—	Mean underestimation = 38 ± 21 mm Hg	—
Shapiro <i>et al.</i> (1997) ⁷	PAH	69	71	0.85	—	Comparison with ventricular-atrial gradients
Hinderliter <i>et al.</i> (1997) ³⁰	PAH	81	86	0.57	31% >20 mm Hg difference	RAP assumed 14 mm Hg
Bach <i>et al.</i> (1998) ³¹	ALD	92	27	0.69	—	—
Arcasoy <i>et al.</i> (2003) ²⁴	ALD	374	44	0.69	52% >10 mm Hg difference	—
Dambrauskaitė <i>et al.</i> (2005) ³²	PH or no PH	66	100‡	0.79	—	Included only interpretable TR
Fisher <i>et al.</i> (2007) ⁸	ALD	63	39	0.23	33% >10 mm Hg difference	Time delay between RHC and TTE 23 days
Haddad <i>et al.</i> (2009) ²³	PAH	51	—	0.97	2% >20% difference	—
Rich <i>et al.</i> (2011) ⁹	PH	160	—	0.68	51% >10 mm Hg difference	Time delay 30 days
	PH	23	—	0.71	—	—
Lafitte <i>et al.</i> (2013) ³³	PH or no PH	310	—	0.80	—	—
D'Alto <i>et al.</i> (2013) ²⁵	PH or no PH, mostly PAH or left-sided heart disease	161	94	—	Bias mean ± SD, -0.5 ± 9 (95% CI, -2 to 1)	RAP assumed 5 mm Hg

JVP, Jugular venous pressure; SEE, standard error of estimate; TTE, transthoracic echocardiography.

Correlations between echocardiography-based RVSP and invasive RVSP are presented as Pearson coefficients (r values).

*After exclusion of one patient with pulmonary stenosis.

the best threshold for RVSP that corresponds to MPAP of 25 mm Hg is important for diagnostic purposes. Our study is the first to validate in a large series of patients with ALD and PAH the relationship between MPAP and SPAP first described by Chemla *et al.*'s¹⁶ original equation (MPAP = 0.61 × SPAP + 2 mm Hg) and later confirmed by Steckelberg *et al.*^{20,21} In contrast to the systemic circulation, systolic pressure and mean artery pressure are closely related to each other in the pulmonary circulation because compliance and resistance are more closely linked together.²² According to this equation, a value of SPAP of 38 mm Hg corresponds to an MPAP of 25 mm Hg. Taking into account the RV outflow tract gradient and the potential decrease in pulmonary pressures that occurs with sedation, an echocardiography-based RVSP threshold of 40 to 45 mm Hg in nonsedated subjects would likely best correspond to an MPAP of 25 mm Hg. Lower thresholds used in the literature, such as 35 mm Hg, have the advantage, however, of considering suboptimal insonation angles.

In the literature, there is significant heterogeneity in the studies assessing the reliability of echocardiographic estimations of pulmonary pressures (Table 2). The original work of Yock and Popp⁴ found an excellent relationship between estimated and invasive RVSP, as did more recent studies.^{7,23} However, Arcasoy *et al.*²⁴ found only a moderate correlation between echocardiography and RHC (r = 0.69,

P < .001) in 2003, which was followed by a highly cited 2007 study by Fisher *et al.*⁸ showing an even weaker association (r = 0.23; 95% CI, 0.01–0.44) in 63 patients. The long time delay between RHC and echocardiography in this latter study (mean, 23 days) may account for part of the weaker association.

Our study brings novel insights to this controversy. Although no systematic bias was observed using echocardiography, the precision was variable depending on the level of expertise, with level 3 expert readers having the best precision compared with level 2 readers and clinical reports. Although clinical reports were all read by level 3 readers, the findings highlight the tendency to interpret suboptimal signals in clinical practice as well as a tendency to interpret TR maximal velocities higher than the modal frequency (often because of increased signal gain). Another important observation is that only 56% of TR signals in patients with ALD are optimal for interpretation; consistent with previous literature,^{5,12,15,24} this highlights the greater difficulty in acquiring TR signals in patients with ALD in comparison with those with PAH. This may suggest that more time should be spent to acquire high-quality signals in all possible windows as well as pulmonary regurgitation signals for estimation of pulmonary pressures.

Although the majority of studies on echocardiography have focused on the estimation of pulmonary pressures, the ability to

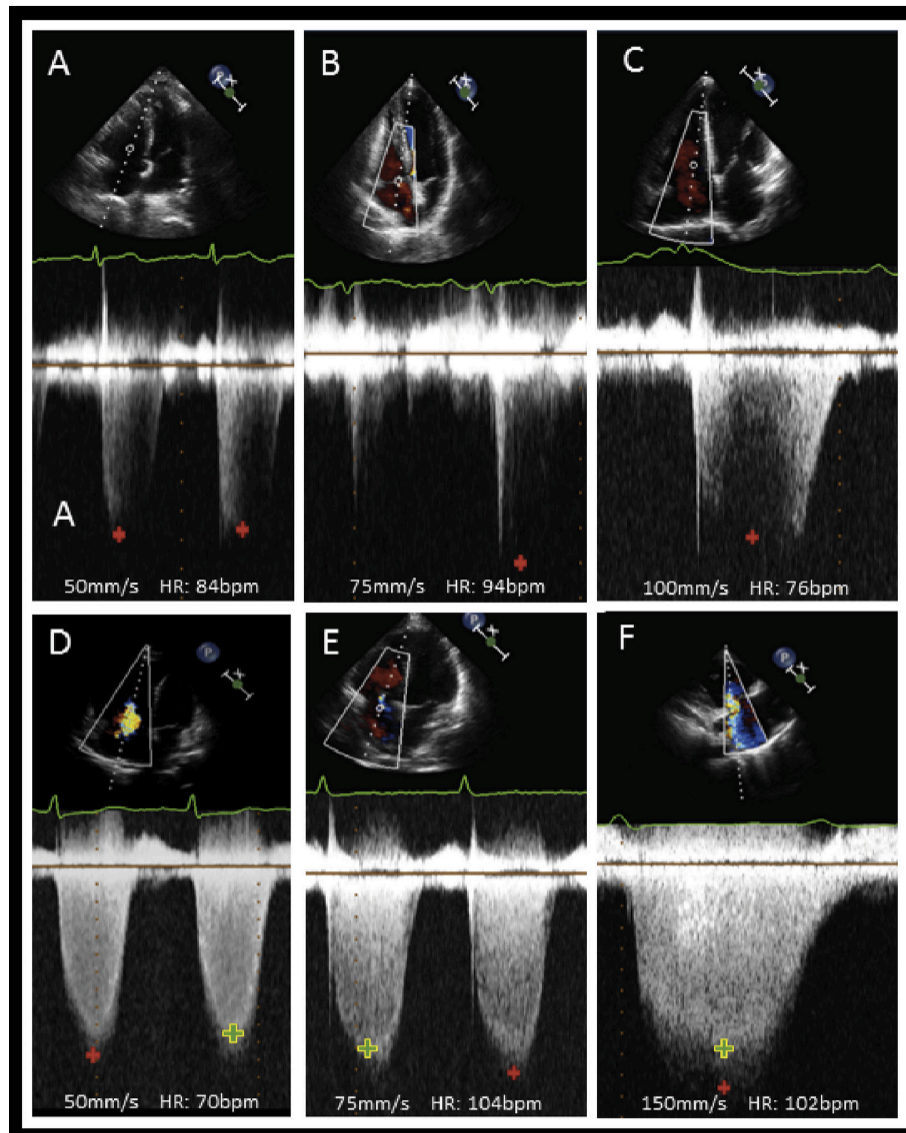


Figure 6 Examples of under- and overestimation of RVSP: common pitfalls. **(A–C)** Continuous-wave Doppler signals of the TR of three different patients, taken from apical four-chamber view. RVSP estimation was underestimated because of the absence of visualization of a sufficient TR envelope. In addition, the angle between the Doppler insonation beam and the TR jet could be improved. **(D–F)** TR signals of three patients in which RVSP was overestimated, mainly because of incorrect adjustment of the Doppler gain. Signals **(D)** and **(E)** are extracted from an apical four-chamber view, while signal **(F)** provides an example of the parasternal long-axis view centered on the RV view. Finally, the overall figure illustrates the importance of adjusting the sweep speed between 75 and 150 mm/sec according to heart rate. The red crosses represent the wrong measurements, and the green crosses outlined in yellow represent the correct measurements.

classify subjects as having PH is often the question asked of echocardiographers. Our study highlights the excellent discrimination provided by RVSP for the classification of PH. Consequently, in patients with interpretable TR signals, routine RV metrics do not appear to provide strong incremental diagnostic value.

When an uninterpretable TR velocity signal precludes estimation of RVSP, other measures of RV structure or function may

be considered; however, in our cohort, these metrics demonstrated lower diagnostic value. As demonstrated by the study of Hilde *et al*,²⁶ patients with chronic obstructive pulmonary disease often have altered structure and function irrespective of the presence of PH. In their study, pulmonary acceleration time was more promising however. Further investigations would be useful to comprehensively assess the role of echocardiographic RV and

flow metrics in PH as well as in ALD patients regardless of presence of PH.

Study Limitations

This study had several limitations that need to be addressed. First, because of its retrospective design, we had no control over the time delay between examinations. However, there was no change in medications during the study period, and Currie *et al.*⁵ previously showed the minimal impact of a 3-day delay between RHC and echocardiography in pulmonary pressure estimation.

Second, RAP was assessed in this study using only the IVC features and following a protocol that differs mildly from the current guidelines but is based on one of our previous studies.²³ In addition, we did not use other parameters, such as tricuspid E/e' ratio or diastolic flow predominance in hepatic veins. Nonetheless, significant differences between RAPs were rarely the cause of misclassification.

Third, the fact we selected a population with a high prevalence of PH and a low prevalence of left-sided heart failure may limit external validity. Quality tips can, however, be generally used in all settings.

Fourth, the optimal cutoff of 40 mm Hg derived from the receiver operating characteristic curve must be viewed with caution, because it requires validation in another cohort, despite having been predefined and based on the equation of Chemla *et al.*¹⁶

Finally, we do not conclude in any way from our study that echocardiography should replace RHC, particularly for the initial diagnosis, as only half of TR signals were interpretable in this patient population. Nevertheless, these results do provide insight on how to improve echocardiography acquisition and interpretation of pulmonary pressures in clinical practice.

Clinical Implications

In view of our results, we can propose the following eight quality points that can improve the estimation of RVSP on the basis of TR maximal Doppler velocity: (1) choose the imaging window with the most optimal insonation angle (this can be found in the parasternal long-axis view centered on the right ventricle, parasternal short-axis view, RV-modified apical four-chamber view, or subcostal view); (2) adjust the sweep speed between 75 and 150 mm/sec according to heart rate; (3) when measuring the maximal velocity, avoid using post-premature ventricular contraction beats, and for patients with atrial fibrillation, use the third beat after two consecutive equal RR intervals; (4) optimize the signal-to-noise ratio by carefully decreasing the Doppler gain, to avoid overestimation of maximal velocities; (5) measure the peak velocity only if the signal is interpretable (avoid overreporting); (6) measure the peak TR velocity using the modal frequency; (7) undertake signal enhancement with saline contrast, which can also improve the signal-to-noise ratio in estimating TR velocities; and (8) use multiple modalities when estimating RAP, and avoid translational motion when assessing the IVC. Figure 6 shows examples of interpretable, overestimated, and underestimated TR signals.

CONCLUSIONS

Echocardiography provides reliable estimation of RVSP in patients with ALD or PAH when careful attention is paid to signal quality and proper interpretation of modal frequency.

ACKNOWLEDGMENTS

We thank the Stanford Cardiovascular Institute and the Vera Moulton Wall Center of Pulmonary Hypertension at Stanford University for their support.

REFERENCES

1. Celermajor DS, Marwick T. Echocardiographic and right heart catheterization techniques in patients with pulmonary arterial hypertension. *Int J Cardiol* 2008;125:294-303.
2. Gupta H, Ghimire C, Naeije R. The value of tools to assess pulmonary arterial hypertension. *Eur Respir Rev* 2011;20:222-35.
3. Milan A, Magnino C, Veglio F. Echocardiographic indexes for the non-invasive evaluation of pulmonary hemodynamics. *J Am Soc Echocardiogr* 2010;23:225-39.
4. Yock PG, Popp RL. Noninvasive estimation of right ventricular systolic pressure by Doppler ultrasound in patients with tricuspid regurgitation. *Circulation* 1984;70:657-62.
5. Currie PJ, Seward JB, Chan KL, Fyfe DA, Hagler DJ, Mair DD, et al. Continuous wave Doppler determination of right ventricular pressure: a simultaneous Doppler-catheterization study in 127 patients. *J Am Coll Cardiol* 1985;6:750-6.
6. Berger M, Haimowitz A, Van Tosh A, Berdoff RL, Goldberg E. Quantitative assessment of pulmonary hypertension in patients with tricuspid regurgitation using continuous wave Doppler ultrasound. *J Am Coll Cardiol* 1985;6:359-65.
7. Shapiro SM, Oudiz RJ, Cao T, Romano MA, Beckmann XJ, Georgiou D, et al. Primary pulmonary hypertension: improved long-term effects and survival with continuous intravenous epoprostenol infusion. *J Am Coll Cardiol* 1997;30:343-9.
8. Fisher MR, Criner GJ, Fishman AP, Hassoun PM, Minai OA, Scharf SM, et al. Estimating pulmonary artery pressures by echocardiography in patients with emphysema. *Eur Respir J* 2007;30:914-21.
9. Rich JD, Shah SJ, Swamy RS, Kamp A, Rich S. Inaccuracy of Doppler echocardiographic estimates of pulmonary artery pressures in patients with pulmonary hypertension: implications for clinical practice. *Chest* 2011;139:988-93.
10. Chemla D, Herve P. Derivation of mean pulmonary artery pressure from systolic pressure: implications for the diagnosis of pulmonary hypertension. *J Am Soc Echocardiogr* 2014;27:107.
11. Kind T, Faes TJC, Vonk-Noordegraaf A, Westerhof N. Proportional relations between systolic, diastolic and mean pulmonary artery pressure are explained by vascular properties. *Cardiovasc Eng Technol* 2011;2:15-23.
12. Badesch DB, Champion HC, Sanchez MAG, Hoepfer MM, Loyd JE, Manes A, et al. Diagnosis and assessment of pulmonary arterial hypertension. *J Am Coll Cardiol* 2009;54:S55-66.
13. Kusunose K, Yamada H, Nishio S, Tomita N, Hotchi J, Bando M, et al. Index-beat assessment of left ventricular systolic and diastolic function during atrial fibrillation using myocardial strain and strain rate. *J Am Soc Echocardiogr* 2012;25:953-9.
14. Quiñones MA, Douglas PS, Foster E, Gorcsan J, Lewis JF, Pearlman AS, et al. ACC/AHA clinical competence statement on echocardiography: a report of the American College of Cardiology/American Heart Association/American College of Physicians-American Society of Internal Medicine Task Force on Clinical Competence. *J Am Coll Cardiol* 2003;41:687-708.
15. Zoghbi WA, Enriquez-Sarano M, Foster E, Grayburn PA, Kraft CD, Levine RA, et al. Recommendations for evaluation of the severity of native valvular regurgitation with two-dimensional and Doppler echocardiography. *J Am Soc Echocardiogr* 2003;16:777-802.
16. Chemla D, Castelain V, Humbert M, Hébert J-L, Simonneau G, Lecarpentier Y, et al. New formula for predicting mean pulmonary artery pressure using systolic pulmonary artery pressure. *Chest* 2004;126:1313-7.

17. Ryan T, Petrovic O, Dillon JC, Feigenbaum H, Conley MJ, Armstrong WF. An echocardiographic index for separation of right ventricular volume and pressure overload. *J Am Coll Cardiol* 1985;5:918-27.
18. Rudski LG, Lai WW, Afilalo J, Hua L, Handschumacher MD, Chandrasekaran K, et al. Guidelines for the echocardiographic assessment of the right heart in adults: a report from the American Society of Echocardiography endorsed by the European Association of Echocardiography, a registered branch of the European Society of Cardiology, and the Canadian Society of Echocardiography. *J Am Soc Echocardiogr* 2010;23:685-713.
19. Lang RM, Badano LP, Mor-Avi V, Afilalo J, Armstrong A, Ernande L, et al. Recommendations for cardiac chamber quantification by echocardiography in adults: an update from the American Society of Echocardiography and the European Association of Cardiovascular Imaging. *J Am Soc Echocardiogr* 2015;28:1-39.
20. McLaughlin VV, Archer SL, Badesch DB, Barst RJ, Farber HW, Lindner JR, et al. ACCF/AHA 2009 expert consensus document on pulmonary hypertension a report of the American College of Cardiology Foundation Task Force on Expert Consensus Documents and the American Heart Association developed in collaboration with the American College of Chest Physicians; American Thoracic Society, Inc.; and the Pulmonary Hypertension Association. *J Am Coll Cardiol* 2009;53:1573-619.
21. Steckelberg RC, Tseng AS, Nishimura R, Ommen S, Sorajja P. Derivation of mean pulmonary artery pressure from noninvasive parameters. *J Am Soc Echocardiogr* 2013;26:464-8.
22. Vonk-Noordegraaf A, Haddad F, Chin KM, Forfia PR, Kawut SM, Lumens J, et al. Right heart adaptation to pulmonary arterial hypertension: physiology and pathobiology. *J Am Coll Cardiol* 2013;62:D22-33.
23. Haddad F, Zamanian R, Beraud A-S, Schnittger J, Feinstein J, Peterson T, et al. A novel non-invasive method of estimating pulmonary vascular resistance in patients with pulmonary arterial hypertension. *J Am Soc Echocardiogr* 2009;22:523-9.
24. Arcasoy SM, Christie JD, Ferrari VA, Sutton MSJ, Zisman DA, Blumenthal NP, et al. Echocardiographic assessment of pulmonary hypertension in patients with advanced lung disease. *Am J Respir Crit Care Med* 2003;167:735-40.
25. D'Alto M, Romeo E, Argiento P, D'Andrea A, Vanderpool R, Corraa A, et al. Accuracy and precision of echocardiography versus right heart catheterization for the assessment of pulmonary hypertension. *Int J Cardiol* 2013;168:4058-62.
26. Hilde JM, Skjorten I, Grøtta OJ, Hansteen V, Melsom MN, Hisdal J, et al. Right ventricular dysfunction and remodeling in chronic obstructive pulmonary disease without pulmonary hypertension. *J Am Coll Cardiol* 2013;62:1103-11.
27. Laaban JP, Diebold B, Zelinski R, Lafay M, Raffoul H, Rochemaure J. Noninvasive estimation of systolic pulmonary artery pressure using Doppler echocardiography in patients with chronic obstructive pulmonary disease. *Chest* 1989;96:1258-62.
28. Tramarin R, Torbicki A, Marchandise B, Laaban JP, Morpurgo M. Doppler echocardiographic evaluation of pulmonary artery pressure in chronic obstructive pulmonary disease. A European multicentre study. Working Group on Noninvasive Evaluation of Pulmonary Artery Pressure. *Eur Heart J* 1991;12:103-11.
29. Brecker SJ, Gibbs JS, Fox KM, Yacoub MH, Gibson DG. Comparison of Doppler derived haemodynamic variables and simultaneous high fidelity pressure measurements in severe pulmonary hypertension. *Br Heart J* 1994;72:384-9.
30. Hinderliter AL, Willis PW, Barst RJ, Rich S, Rubin LJ, Badesch DB, et al. Effects of long-term infusion of prostacyclin (epoprostenol) on echocardiographic measures of right ventricular structure and function in primary pulmonary hypertension. Primary Pulmonary Hypertension Study Group. *Circulation* 1997;95:1479-86.
31. Bach DS, Curtis JL, Christensen PJ, Iannettoni MD, Whyte RI, Kazerooni EA, et al. Preoperative echocardiographic evaluation of patients referred for lung volume reduction surgery. *Chest* 1998;114:972-80.
32. Dambrauskaitė V, Delcroix M, Claus P, Herbots L, Paleček T, D'hooge J, et al. The evaluation of pulmonary hypertension using right ventricular myocardial isovolumic relaxation time. *J Am Soc Echocardiogr* 2005;18:1113-20.
33. Lafitte S, Pillois X, Reant P, Picard F, Arsac F, Dijos M, et al. Estimation of pulmonary pressures and diagnosis of pulmonary hypertension by Doppler echocardiography: a retrospective comparison of routine echocardiography and invasive hemodynamics. *J Am Soc Echocardiogr* 2013;26:457-63.

Chapter 2- RIGHT HEART NON-INVASIVE IMAGING, LOAD ADAPTATION and RISK PREDICTION in PULMONARY HYPERTENSION

Study 1: Right Heart End-Systolic Remodeling Index Strongly Predicts Outcomes in Pulmonary Arterial Hypertension: Comparison With Validated Models

Authors: Myriam Amsallem MD MS^{1,2,3}, Andrew J. Sweatt MD⁴, Marie C. Aymami MD^{1,2}, Tatiana Kuznetsova MD PhD⁵, Mona Selej MD¹, HongQuan Lu MD¹, Olaf Mercier MD PhD³; Elie Fadel MD PhD³, Ingela Schnittger MD^{1,2}, Michael V. McConnell MD MSEE^{1,2}, Marlene Rabinovitch MD PhD^{6,7}, Roham T. Zamanian MD PhD^{4,6*} and Francois Haddad MD^{1,2,6*}

Affiliations:

¹ Division of Cardiovascular Medicine – Stanford University School of Medicine, Stanford, USA.

² Stanford Cardiovascular Institute – Stanford University School of Medicine, Stanford, USA.

³ Research and Innovation Laboratory Inserm U999 and Division of Cardiothoracic Surgery, Marie Lannelongue Hospital, Paris Sud University, Le Plessis Robinson, France.

⁴ Division of Pulmonary and Critical Care Medicine – Stanford University School of Medicine, Stanford, USA.

⁵ Research Unit Hypertension and Cardiovascular Epidemiology, KU Leuven Department of Cardiovascular Sciences, University of Leuven, Belgium.

⁶ Vera Moulton Wall Center at Stanford – Stanford University School of Medicine, Stanford, USA.

⁷ Division of Pediatrics – Stanford University School of Medicine, Stanford, USA.

*both authors contributed equally to the study.

Communications:

Published in *Circ Cardiovasc Imaging*. 2017;10:e005771. doi:10.1161/CIRCIMAGING.116.005771.

Presented as an oral presentation at the 2016 American Heart Association Scientific Sessions (New Orleans, USA). This study was awarded by a finalist position for the 2016 AHA Cournand and Comroe Young Investigator Award. It was also presented at 2017 Stanford Cardiovascular Institute Conference (Palo Alto, USA).

Summary: Right heart failure is the main cause of mortality in patients with PAH. Indices of right heart end-systolic remodeling integrate information of both size and function and are emerging as strong predictors of outcome in patients with PAH. In this longitudinal study, we describe a novel and simple index of RV end-systolic remodeling defined as the RV free wall length divided by septal length. We demonstrate that RV end-systolic remodeling index is centrally connected to other right heart metrics and improves risk prediction based on the REVEAL score and the Pulmonary Hypertension Connection score. Moreover, our study highlights that New York Heart Association functional class, NT-proBNP (N-Terminal Pro-B-Type Natriuretic Peptide) levels, and RV end-systolic remodeling index capture key features of the clinical right heart adaptation continuum in pulmonary arterial hypertension.

This study is also the largest to demonstrate the importance of changes in RV end-systolic remodeling over time showing the increment to baseline remodeling indices and the REVEAL score. Although RV free wall longitudinal strain is predictive of outcome, it does not capture the same level of prediction than RV end-systolic remodeling index and is less reproducible. In terms of clinical impact, our study may simplify clinical risk assessment and offer a simple tool for stratified randomization in clinical trials.

Pulmonary Arterial Hypertension

Right Heart End-Systolic Remodeling Index Strongly Predicts Outcomes in Pulmonary Arterial Hypertension Comparison With Validated Models

Myriam Amsallem, MD, MS; Andrew J. Sweatt, MD; Marie C. Aymami, MD;
Tatiana Kuznetsova, MD, PhD; Mona Selej, MD; HongQuan Lu, MD; Olaf Mercier, MD;
Elie Fadel, MD; Ingela Schnittger, MD; Michael V. McConnell, MD, MSEE;
Marlene Rabinovitch, MD; Roham T. Zamanian, MD;* Francois Haddad, MD*

Background—Right ventricular (RV) end-systolic dimensions provide information on both size and function. We investigated whether an internally scaled index of end-systolic dimension is incremental to well-validated prognostic scores in pulmonary arterial hypertension.

Methods and Results—From 2005 to 2014, 228 patients with pulmonary arterial hypertension were prospectively enrolled. RV end-systolic remodeling index (RVESRI) was defined by lateral length divided by septal height. The incremental values of RV free wall longitudinal strain and RVESRI to risk scores were determined. Mean age was 49 ± 14 years, 78% were female, 33% had connective tissue disease, 52% were in New York Heart Association class \geq III, and mean pulmonary vascular resistance was 11.2 ± 6.4 WU. RVESRI and right atrial area were strongly connected to the other right heart metrics. Three zones of adaptation (adapted, maladapted, and severely maladapted) were identified based on the RVESRI to RV systolic pressure relationship. During a mean follow-up of 3.9 ± 2.4 years, the primary end point of death, transplant, or admission for heart failure was reached in 88 patients. RVESRI was incremental to risk prediction scores in pulmonary arterial hypertension, including the Registry to Evaluate Early and Long-Term PAH Disease Management score, the Pulmonary Hypertension Connection equation, and the Mayo Clinic model. Using multivariable analysis, New York Heart Association class III/IV, RVESRI, and log NT-proBNP (N-Terminal Pro-B-Type Natriuretic Peptide) were retained (χ^2 , 62.2; $P < 0.0001$). Changes in RVESRI at 1 year ($n = 203$) were predictive of outcome; patients initiated on prostanoid therapy showed the greatest improvement in RVESRI. Among right heart metrics, RVESRI demonstrated the best test–retest characteristics.

Conclusions—RVESRI is a simple reproducible prognostic marker in patients with pulmonary arterial hypertension. (*Circ Cardiovasc Imaging*. 2017;10:e005771. DOI: 10.1161/CIRCIMAGING.116.005771.)

Key Words: echocardiography ■ heart failure ■ patient outcome assessment ■ pulmonary hypertension ■ right ventricular dysfunction ■ risk assessment ■ ventricular remodeling

Survival of patients with pulmonary arterial hypertension (PAH) is closely related to right ventricular (RV) function.^{1,2} In 1991, based on a national prospective registry data, D'Alonzo et al³ identified lower cardiac index and higher right atrial pressure (RAP) as important prognostic markers in PAH. Since then, several studies have confirmed the predictive value of right heart remodeling or dysfunction using either imaging biomarkers or circulating blood biomarkers, such as B-Type Natriuretic Peptide. Several echocardiographic parameters have been associated with prognosis in patients with PAH, including tricuspid annular plane systolic excursion, right atrial size, pericardial effusion and, more recently, RV lateral free wall longitudinal strain (RVLS) and RV end-systolic

dimensions.^{4–8} RVLS and RV end-systolic dimensions are emerging as the strongest predictors of outcome in PAH. In the study of Fine et al,⁷ RVLS was found to be an independent predictor of outcomes along with New York Heart Association (NYHA) functional class and serum NT-proBNP (N-Terminal Pro-B-Type Natriuretic Peptide) level in a large cohort of 300 patients with PAH at Mayo Clinic. In contrast, a recent study of Ryo et al⁸ using 3-dimensional (3D) echocardiography found that end-systolic volume was more strongly associated with outcome than 3D determined RVLS.

See Editorial by Samson and Le Jemtel
See Clinical Perspective

Received October 10, 2016; accepted April 12, 2017.

From the Division of Cardiovascular Medicine (M.A., M.C.A., M.S., H.L., I.S., M.V.M., F.H.), Cardiovascular Institute (M.A., M.C.A., H.L., I.S., M.V.M., F.H.), Division of Pulmonary and Critical Care Medicine (A.J.S., R.T.Z.), Vera Moulton Wall Center at Stanford (M.R., R.T.Z., F.H.), and Division of Pediatrics (M.R.), Stanford University School of Medicine, CA; Research Unit Hypertension and Cardiovascular Epidemiology, KU Leuven Department of Cardiovascular Sciences, University of Leuven, Belgium (T.K.); and Division of Cardiothoracic Surgery, Marie Lannelongue Hospital, Le Plessis Robinson, France (O.M., E.F., M.A.).

*Drs Zamanian and Haddad contributed equally to this work.

The Data Supplement is available at <http://circimaging.ahajournals.org/lookup/suppl/doi:10.1161/CIRCIMAGING.116.005771/-/DC1>.

Correspondence to Myriam Amsallem, MD, MS, Division of Cardiovascular Medicine, Stanford School of Medicine, 300 Pasteur Dr, Stanford, CA 94305. E-mail mamsallem@stanford.edu

© 2017 American Heart Association, Inc.

Circ Cardiovasc Imaging is available at <http://circimaging.ahajournals.org>

DOI: 10.1161/CIRCIMAGING.116.005771

Building on the previous studies of Fine et al⁷ and Ryo et al,⁸ we hypothesized that a simple index that would incorporate both the longitudinal component of RV adaptation and end-systolic dimension would carry strong prognostic information in PAH. In this study, we propose a novel and simple RV end-systolic remodeling index (RVESRI) defined as the ratio of end-systolic RV free wall longitudinal length:septal height (RVESRI=end-systolic lateral free wall length/septal height). Internal scaling free wall length to septal length rather than body surface area may have the advantage of scaling using the same dimension (dimensional consistency) and being less influenced by edematous state or obesity. Moreover, we hypothesized that internal scaling to septal height may partially correct for apical foreshortening.

This prospective registry study had 4 main objectives. Our first objective was to assess the connectivity between different right heart parameters and to determine whether RVESRI is centrally connected to other right heart parameters. Our second objective was to determine whether RVESRI would be complementary to well-validated prognostic scores in PAH,^{3,5,9-11} including the Registry to Evaluate Early and Long-Term PAH Disease Management (REVEAL) score and the Pulmonary Hypertension Connection equation. Our third objective was to determine the factors influencing changes in RVESRI at 1 year and relationship with outcome. Finally, our last objective was to compare in a new series the test-retest characteristics of RVESRI and RVLS.

Methods

Between August 2005 and May 2014, 245 patients with PAH were included in the prospective Vera Moulton Wall Center Pulmonary Hypertension Registry at Stanford. Inclusion criteria were diagnosis

of PAH according to the guidelines (mean pulmonary arterial pressure ≥ 25 mmHg and pulmonary arterial wedge pressure ≤ 15 mmHg² and NT-proBNP levels available within 2 weeks of echocardiography in stable condition. Exclusion criteria were the following: congenital systemic-to-pulmonary shunts (n=10); complete echocardiographic study not available for review (n=6); or advanced cancer at baseline (n=1). One-year follow-up echocardiograms were available in 203 patients. By design, patients with pulmonary hypertension WHO classes other than group 1 pulmonary hypertension (PH) were not included in this study.² Stanford University Institutional Review Board approved the study, which was conducted in agreement with the Helsinki-II declaration. All patients gave written informed consent.

Hemodynamic Assessment

Right heart catheterization within 3 months of inclusion (available within a week for 77% of patients) was performed through the internal jugular or right femoral vein. RAP, systolic pulmonary arterial pressure, mean pulmonary arterial pressure and diastolic pulmonary arterial pressures, pulmonary arterial wedge pressure, pulmonary vascular resistance and pulmonary vascular resistance index (measured as transpulmonary gradient divided by cardiac index), and cardiac index (using the thermodilution method) were measured.

Echocardiographic Assessment

Digitized studies were acquired using Hewlett Packard Sonos 5500 or Philips IE 33 ultrasound systems (Philips, Amsterdam, The Netherlands). All measures were averaged over 3 cycles and analyzed according to the latest guidelines by 2 blinded certified readers (M.A. and F.H.).^{12,13} Indices of right heart remodeling and function were measured on the focused RV apical 4-chamber view; measures included end-diastolic and end-systolic areas both indexed to body surface area, maximal right atrial area index, RV fractional area change, tricuspid annular plane systolic excursion, and end-systolic left ventricular eccentricity indices.¹⁴ RV free wall Lagrangian longitudinal strain (RVLS) was measured from midendocardial end-diastolic and end-systolic manually traced lengths and calculated as (end-systolic length–end-diastolic length)/end-diastolic length; values for RVLS

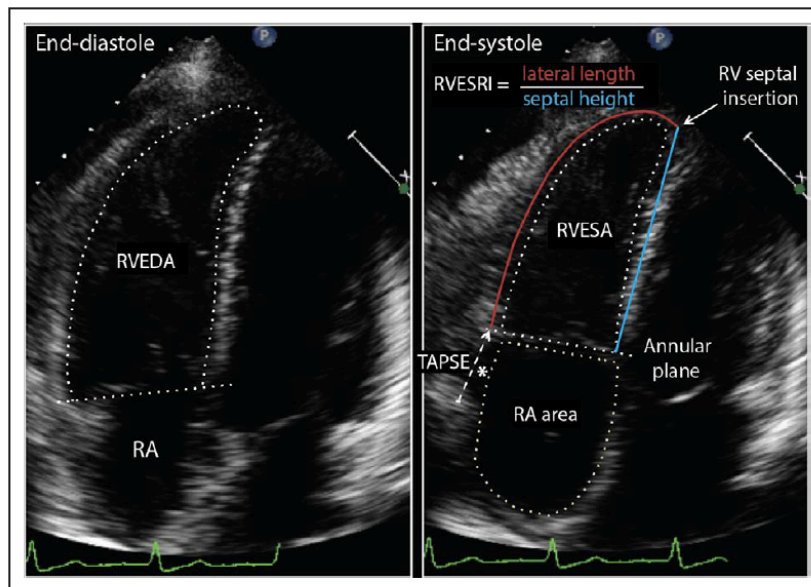


Figure 1. Illustration of measurements of selected right heart metrics in end diastole (left) and end systole (right). Right ventricular end-systolic remodeling index (RVESRI) represents a simple ratio of end-systolic lateral length:septal height (representing RV longitudinal length measured straight from the septal tricuspid annulus point to the RV insertion on the interventricular septum). *Note the exclusion of the right atrial appendage. RA indicates right atrium; RVEDA, RV end-diastolic area; RVESA, RV end-systolic area; and TAPSE, tricuspid annular plane systolic excursion.

Table 1. Baseline Characteristics of the Study Population

Patient Characteristics	N=228
Age, y	48.6±14.1
Female sex	178 (78.1%)
Cause	
Idiopathic	53 (23.2%)
Drugs and toxins	55 (24.1%)
Connective tissue disease	74 (32.5%)
NYHA functional class	
I/II	(48.3%)
III/IV	(51.7%)
Systolic blood pressure, mm Hg	116±14
Heart rate, bpm	81±14
Hemodynamics	
Mean right atrial pressure, mm Hg	8.1±5.2
Mean pulmonary arterial pressure, mm Hg	49.2±16.0
Pulmonary arterial wedge pressure, mm Hg	10.7±4.8
Cardiac index, L min ⁻¹ m ⁻²	2.1±0.7
Stroke volume index, mL/m ²	38.8±12.3
Pulmonary vascular resistance (WU)/indexed	11.2±6.4/19.1±10.2
Laboratory data	
Serum NT-proBNP, pg/mL	296 [93–1194]
Serum creatinine, μmol/L	76.3±22.9
MDRD GFR <60 mL min ⁻¹ 1.73 m ⁻²	78 (50.6%)
Pulmonary functional tests	
CO diffusing capacity (%)	73.3±24.9
Six-min walk test	
Distance, m	419±138
Therapy	
Treatment naïve	82 (36.0%)
Prostanoid therapy	80 (35.1%)
Phosphodiesterase inhibitors	100 (43.9%)
Endothelin receptor blockers	63 (27.6%)

Values are expressed as mean±SD or number (percentage), or median and interquartile range. Right ventricular systolic pressure was estimable from the tricuspid regurgitation signal in 194 (85% patients). GFR indicates glomerular filtration rate; MDRD, Modification of Diet in Renal Disease; NT-proBNP, N-Terminal Pro-B-Type Natriuretic Peptide; and NYHA, New York Heart Association.

are presented in absolute values in the text for consistency with other right heart metrics.¹² As presented in the introduction, RVESRI was defined as the lateral wall:septal wall height ratio (Figure 1). The lateral wall length was measured from the lateral tricuspid annulus to the insertion point of the RV on the interventricular septum. The septal height (representing the RV length at the level of the septum) was measured as a straight line from the septal tricuspid annulus to the RV insertion on the interventricular septum. Other measured of end-systolic dimensions consisted of end-systolic area indexed to either body surface area or height¹⁷, RV free wall length indexed to height or diastolic septal height, minor RV dimension, and minor (ie, lateral to septal) axis:long axis ratio.¹² RAP was estimated from the inferior vena cava size and collapse according to recent guidelines and RV

Table 2. Comparative Echocardiograms of Age- and Sex-Matched Controls and Patients With Pulmonary Arterial Hypertension

Patient Characteristics	Controls (n=80)		PAH (n=228)
		5th–95th Percentile	
Age, y	47.5±10.3	...	48.6±14.1
Female sex	62 (77.5%)	...	178 (78.1%)
Left ventricular internal diameter, mm	50.0±0.4	42.1–58.0	41.6±0.6*
Left ventricular ejection fraction (%)	62.0±4.8	53.7–69.2	60.8±5.9
RV parameters			
End-systolic area, cm ² /m ²	5.2±1.0	3.7–6.9	14.1±5.6*
End-diastolic area, cm ² /m ²	9.2±1.5	6.9–11.8	19.0±6.4*
RVESRI	1.21±0.07	1.11–1.35	1.47±0.19*
Longitudinal strain (%)	25.6±2.4	21.7–28.8	17.1±4.9*
RVFAC (%)	43.7±5.3	36.2–51.1	27.0±7.0*
TAPSE, mm	22.9±3.0	18.4–29.0	17.5±4.6*
RA area index, cm ² /m ²	7.5±1.6	4.8–11.0	12.1±4.7*
Systolic eccentricity index	0.99±0.28	0.95–1.04	1.55±0.47*
RVSP, mm Hg	19.0±3.9	13.6–24.1	77.6±21.1*
RA pressure, mm Hg	3.4±1.4	1.0–5.0	9.9±4.8*
Pericardial effusion	0	...	35 (15.4%)*

Values are expressed as mean±SD or number (percentage), or median and interquartile range (IQR). Right ventricular systolic pressure (RVSP) was estimable from the tricuspid regurgitation signal in 94% of controls and 85% of patients with pulmonary arterial hypertension (PAH). RA indicates right atrium; RV, right ventricle; RVESRI, RV end-systolic remodeling index; RVFAC, RVSP, right ventricular systolic pressure; and TAPSE, tricuspid annular plane systolic excursion.*P value <0.05 for comparison with controls.

systolic pressure from the tricuspid regurgitation maximal velocity and estimated RAP.¹⁵ Pericardial effusion was considered significant if >5 mm in diastole.

Clinical and Laboratory Data

NYHA functional class, six-minute walking distance (m), diffusing capacity of the lung for carbon monoxide, serum creatinine, total bilirubin, and serum NT-proBNP (Roche Diagnostics, Mannheim, Germany) were also available within a month of echocardiography.

Follow-Up and End Points

Patients were prospectively followed after enrollment in the registry. Follow-up was concluded on April 2016. The primary combined end point was death, lung transplantation, or hospitalization for acute right heart failure. Death was verified by through the National Social Security Death Index, whereas lung transplantation and hospitalization for heart failure (defined by >24 hours of hospitalization) was verified through chart review and follow-up. The secondary end point consisted of death or lung transplant.

Risk Scores in PAH

The following scores were calculated for each patient (Table 1 in the Data Supplement): Pulmonary Hypertension Connection,⁹ REVEAL

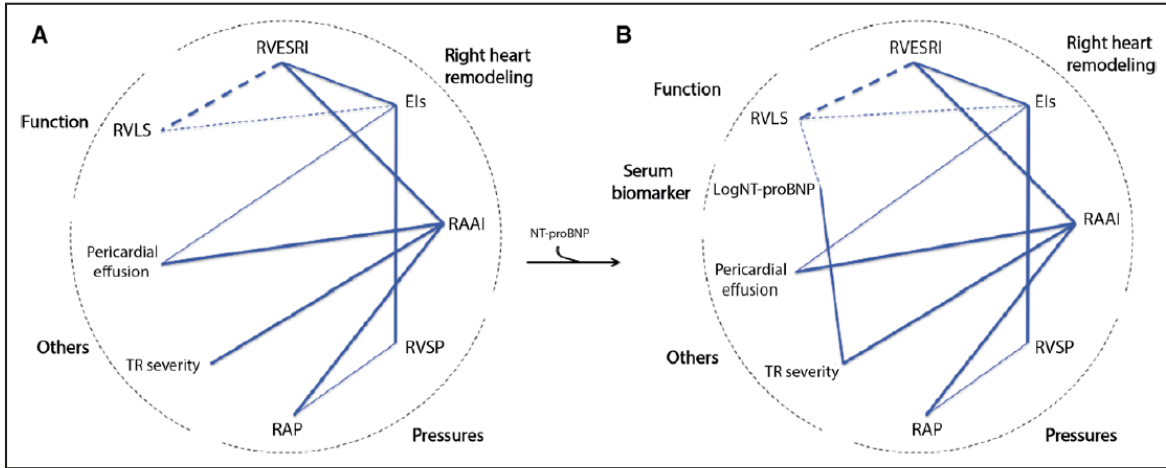


Figure 2. Partial correlation diagrams of right heart metrics showing independent associations between parameters (A); the relationship adding NT-proBNP (N-Terminal Pro-B-Type Natriuretic Peptide; B). Full lines represent significant direct correlations; dashed lines show inverse correlations. Thicker lines show higher statistical significance ($P < 0.001$) than thinner lines. Els indicates systolic eccentricity index; RAAI, right atrial area index; RAP, right atrial pressure; RVESRI, right ventricular end-systolic remodeling index; RVLS, right ventricular longitudinal strain; RVSP, right ventricular systolic pressure; and TR, tricuspid regurgitation.

score,⁵ Scottish composite score,¹⁰ Right Heart score,¹¹ and the Mayo Clinic risk model.⁷ There was 22% overlap between the cohorts evaluated to derive the Right Heart score derived from Stanford cohort and the present cohort.¹¹

Healthy Controls

Eighty healthy controls were selected from the Stanford Healthy Aging research database, with a similar age range and sex ratio as patients with PAH. PH or heart failure was ruled out by a 60-point health questionnaire, physical examination, and echocardiography.

Reproducibility

Intra- and interobserver reproducibility was prospectively assessed in 14 consecutive patients with PAH assessed at Stanford Echocardiography laboratory in the month of November and December 2016. Test-retest was performed using 2 consecutive acquisitions acquired by 2 different sonographers. Using 3D echocardiography and

QLab software analysis, we derived an optimally focused RV apical 4-chamber view (angle 1) and suboptimally focused RV view (angle 2). The suboptimally focused RV plane passed through the smallest transverse RV diameter while still visualizing tricuspid valve opening (angle varied between 15° and 40°).

Statistical Analysis

Data are summarized as mean±SD for continuous variables if following a normal distribution or median and interquartile range otherwise, and number of subjects (%) for categorical variables. Comparisons between groups were performed using 2-sided Student *t*-tests, Mann-Whitney test, or χ^2 test. On the basis of Ryo et al⁸ previous study, we explored the relationship between RV systolic pressure and RVESRI or RVESAI to determine 3 zones of adaptation (ie, adapted, adversely remodeled, and severely adversely remodeled) using polynomial function. Partial correlation analysis was used to determine independent correlations between right heart metrics and their connectivity.¹⁶ Cox proportional hazards regression models were used to define association

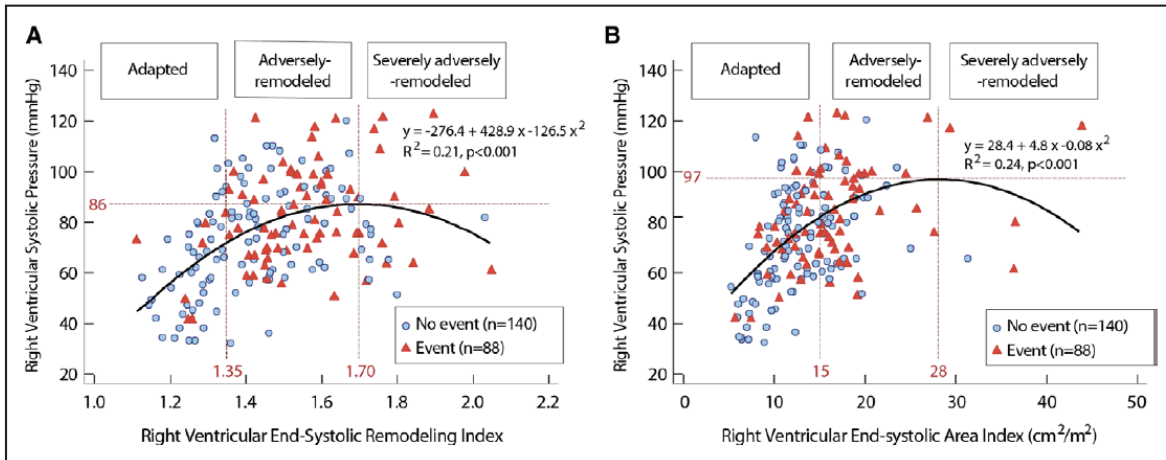


Figure 3. Scatterplot of right ventricular systolic pressure and end-systolic remodeling index (A) or area index (B) showing distribution of patients with and without events. The transition points in the pressure remodeling relationship defined 3 zones of adaptation as follows: the first was the transition between linear and curvilinear relationship (right ventricular end-systolic remodeling index [RVESRI], 1.35), the second was defined by the point when where progressive remodeling was associated with a decrease in RV systolic pressure (RVESRI, 1.7).

Table 3. Univariable and Multivariable Cox Regression Analysis of Correlates of Death or Lung Transplant or Admission for Heart Failure During Follow-Up

	Univariable Analysis			Multivariable Analysis		
	Hazard Ratio*	95% CI	P Value	Hazard Ratio*	95% CI	P Value
Age, y	1.15	0.87–1.52	0.11			
Female sex	1.05	0.63–1.77	0.85			
Incident cases (vs prevalent cases)	1.33	0.83–2.12	0.24			
CTD cause	1.11	0.70–1.75	0.66			
NYHA functional class (III/IV vs I/II)	3.36	2.10–5.38	<0.001	1.96	1.14–3.37	0.01
Systolic blood pressure, mm Hg	0.75	0.65–0.87	0.05			
Systolic blood pressure, <110 mm Hg	1.36	0.81–2.12	0.17			
Heart rate, bpm	1.33	1.00–1.53	0.03			
Echocardiogram						
Right heart remodeling						
RVESRI	2.05	1.66–2.53	<0.001	1.58	1.22–2.04	0.001
RVESAI, cm ² / m ²	1.31	1.18–1.54	<0.001			
RVEDAI, cm ² /m ²	1.29	1.14–1.54	<0.001			
Right atrial area Index, cm ² /m ²	1.37	1.20–1.57	<0.001			
Systolic eccentricity index	1.58	1.28–1.97	<0.001			
Diastolic eccentricity index	1.34	1.15–1.56	<0.001			
Right heart function						
RVFAC (%)	0.64	0.52–0.81	<0.001			
TAPSE, cm	0.16	0.02–1.37	0.09			
RVLS (absolute value, %)	0.63	0.51–0.82	<0.001			
Others						
Tricuspid regurgitation severity	1.44	1.19–1.75	<0.001			
Estimated RAP, mm Hg	1.58	1.26–1.96	<0.001			
Estimated RVSP, mm Hg	1.23	0.81–1.52	0.07			
Pericardial effusion	2.35	1.47–3.75	<0.001			
LVEF (%)	0.89	0.69–1.12	0.28			
Left ventricular longitudinal strain (absolute value, %)	1.20	0.96–1.96	0.11			
Laboratory data						
Log serum NT-proBNP	1.95	1.57–2.42	<0.001	1.32	1.01–1.73	0.04
MDRD GFR <60 mL min ⁻¹ 1.73 m ⁻²	2.63	1.71–4.03	<0.001			
Pulmonary functional tests						
CO diffusing capacity (%)	0.67	0.52–0.84	0.001			
Six-min walk test						
Distance, m	0.57	0.44–0.66	<0.001			

CI indicates confidence interval; CTD, connective tissue disease; GFR, glomerular filtration rate; LVEF, left ventricular ejection fraction; MDRD, Modification of Diet in Renal Disease; NT-proBNP, N-Terminal Pro-B-Type Natriuretic Peptide; NYHA, New York Heart Association; RAP, right atrial pressure; RVEDAI, right ventricular end-diastolic area indexed on body surface area; RVESAI, right ventricular end-systolic area indexed on body surface area; RVESRI, right ventricular end-systolic remodeling index; RVFAC, right ventricular fractional area change; RVLS, right ventricular free wall longitudinal strain; RVSP, right ventricular systolic pressure; and TAPSE, tricuspid annular plane systolic excursion.

*Hazard ratio is adjusted by the SD of the variable considered.

with outcomes. To assess the assumption of proportional hazards, scaled Schoenfeld residuals for each independent variable were plotted against time; these correlations were found to be nonsignificant for all variables included in the multivariable models. Variables with *P* < 0.10

were then entered in the model and selected by a backward procedure with a threshold of *P* = 0.05. Hazard ratios are presented per SD of the considered continuous variables to correct for variations of units. The evaluation of the predictive value of risk scores for death, transplant,

Table 4. Comparison of the Prognostic Value of Right Ventricular End-Systolic Remodeling Indices

Variable	Mean±SD	Prognostic Value				
		HR*	95% CI	P Value	Model† χ^2	P Value
RVESRI	1.47±0.19	2.05	1.66–2.53	<0.0001	62	<0.0001
L1/diastolic septal height	1.29±0.20	1.83	1.53–2.20	<0.0001	59	<0.0001
L1/height	12.42±2.25	1.68	1.40–2.00	<0.0001	53	<0.0001
L1/BSA	12.01±2.75	1.17	1.06–1.30	0.004	47	<0.0001
RVESA/height ^{1,7}	10.31±3.93	1.62	1.35–1.92	<0.0001	52	<0.0001
RVESA/BSA	14.62±5.61	1.31	1.18–1.54	<0.0001	48	<0.0001
RV minor/long axis diameter ratio	0.44±0.07	1.28	1.05–1.56	0.02	47	<0.0001

BSA indicates body surface area adjusted on the ideal body weight; CI, confidence interval; HR, hazard ratio; L1, end-systolic free wall length; RV, right ventricle; RVESA, RV end-systolic area; and RVESRI, RV end-systolic remodeling index.

*HR of the variable using univariable Cox regression analysis of correlates of the primary end point (death or lung transplant or admission for heart failure) during follow-up, adjusted by the SD of the variable considered.

†Multivariable Cox regression models (enter) for the primary end point, including the RV remodeling variable, New York Heart Association classes III/IV and log N-Terminal Pro-B-Type Natriuretic Peptide.

or admission at 3 years was performed using C statistic calculated for a binary outcome. Patients included in 2014 with <3 years follow-up (n=14) were right censored; the outcome at the end of follow-up was used. The incremental value of RVESRI or RVLS to risk scores was assessed by comparison of χ^2 values and C statistics. The added ability of RVESRI to predict events was also assessed using the net reclassification improvement (NRI) as described by Pencina et al.¹⁷ To calculate the continuous NRI, the 3-year risk for the event was predicted for each subject from a Cox model with and without RVESRI and RVLS. P(up/event) was the percentage of patients with events whose predicted probability is increased by adding the echocardiographic variable to the model and P(up/nonevent) the percentage of patients without events whose predicted probability is increased. The NRI was calculated as 2*[P(up/event)–P(up/nonevent)]. Predictive scores for the primary end point were then developed from the final multivariable model and the Mayo Clinic multivariable model. Continuous variables were categorized according to clinically relevant cutoff points, RVLS thresholds from Fine et al⁷ study ($\geq 25\%$, [20–25], [15–20], <15%)⁷ and quartiles for RVESRI. Points were given according to the hazard ratio using multivariable analysis rounded to the nearest integer. Discrimination obtained with the scores was assessed using C statistic and its 95% confidence interval (CI). Change in RVESRI between baseline and 1 year was predefined as improving if >10%, worsening if <–10%, or stable otherwise. Multivariable model was used to determine associates with improvement in RVESRI. Reproducibility was expressed by intraclass correlation coefficient. Results were considered significant when 2-sided P values were <0.05. Statistical analysis was performed using SPSS statistical software (SPSS V.19, Inc, Chicago, IL).

Results

Study Population

In total, 228 patients were included in the study (Table 1). The study population represents patients with PAH over a wide range of disease severity, as shown by mean pulmonary arterial pressure of 49±16 mm Hg, pulmonary vascular resistance index ranging from 3 to 54 WU m², and cardiac index from 1.1 to 6.0 L min^{–1} m^{–2}. No patients were lost during an average follow-up of 3.9±2.4 years (median 3.7 years ranging from 40 days to 10.8 years).

Right Heart Indices and Partial Correlation Analysis

Patients presented a wide range of ventricular size and function (RVLS in absolute value from 7% to 31%, tricuspid

annular plane systolic excursion from 7 to 29 mm, RVESAI from 5 to 45 cm²/m², eccentricity index from 0.9 to 3.2, and RVESRI from 1.1 to 2.1; Tables 1 and 2). Right heart remodeling and function indices were related to each other with the strongest correlations observed between RV fractional area change and RVESAI (–0.65, P<0.0001), RV fractional area change and RVLS (0.49, P<0.0001), RVLS and RVESRI (–0.38, P<0.001), and RVESRI and right atrial area index (0.20, P<0.01). Partial correlation analysis, which highlights the independent associations between parameters, showed that the 2 most connected metrics based on the number of direct connections were RVESRI and right atrial area index. Log NT-proBNP was connected to the network but demonstrated low connectivity, although diastolic wall stress modeling was not assessed in this study (Figure 2).¹⁸

Right Heart Remodeling–Pressure Relationship

The relationship between end-systolic remodeling indices (RVESRI and RVESAI) and RV systolic pressure, estimated using polynomial function, identified different zones of ventricular adaptation (Figure 3). On the basis of the morphology of the polynomial curve, 3 zones could be described, that is, adapted (n=71 patients), adversely remodeled (n=132), and severe adversely remodeled RV (n=25). The first zone was defined by the transition between linear and curvilinear relationship (RVESRI, 1.35), which was equal to the 95th percentile of healthy controls. The second was defined by the point where progressive enlargement was associated with a decrease in RV systolic pressure (RVESRI, 1.70). Similar thresholds were found using the relationships between RVESRI and invasive measurement of pressure (mean pulmonary arterial pressure) and resistance level (pulmonary vascular resistance index), as presented in Figure I in the Data Supplement.

Clinical Outcomes

During a mean follow-up of 3.9±2.4 years, the primary end point of death, transplant, or admission was reached in 88 patients (43 died, 15 were transplanted, and 30 were admitted). Event-free survival rates for the primary end point were 90.6 (CI, 86.7%–94.5%) at 1 year, 78.0 (CI, 72.3%–83.7%)

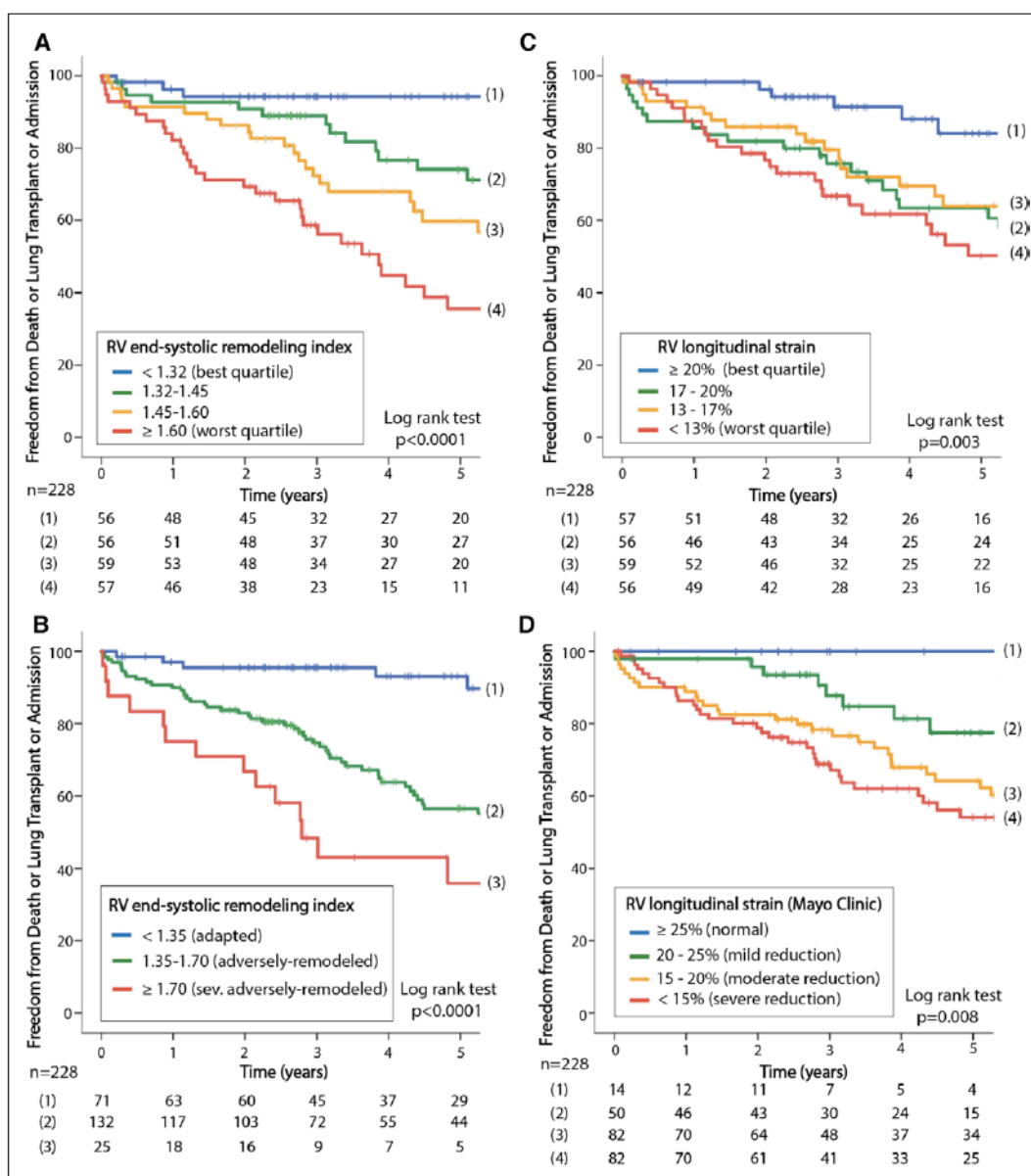


Figure 4. Five-year Kaplan–Meier survival curves of right ventricular (RV) end-systolic remodeling index (A–B) and strain (C–D) for the primary combined end point of death, transplantation, or hospitalization for acute right heart failure.

at 3 years, and 64.8 (CI, 57.5%–72.1%) at 5 years. The secondary end point of death or transplant was reached in 58 patients (43 deaths and 15 transplants). Event-free survival rates (secondary end point) were 91.0 (CI, 87.3%–94.7%) at 1 year, 80.4 (CI, 74.9%–85.9%) at 3 years, and 72.5 (CI, 65.8%–79.2%) at 5 years.

Univariable and Multivariable Analysis

The strongest univariate variables associated with the primary end point included NYHA class, RVESRI, RVLS, and log NT-proBNP (Table 3). Whether a patient had prevalent or incident PAH was not significantly associated with outcome ($P=0.24$), although there was a trend for patients with incident

PAH to have worse outcome. Table II in the [Data Supplement](#) compares the characteristics of patients with or without the primary end point at 3 years. When comparing the different indices of RV end-systolic size or the traverse:longitudinal ratio, RVESRI was more closely associated with outcome (Table 4). Kaplan–Meier survival curves for the primary end point (Figure 4) show the different survival curves according to RVESRI quartiles, RVLS quartiles, thresholds of RVESRI adaptation zones, and RVLS according to previously published thresholds.⁷ Similar results were found when using the secondary end point of death or lung transplant (Figure II in the [Data Supplement](#)). Kaplan–Meier survival curves for the primary end point of NT-proBNP, NYHA classes, and RV

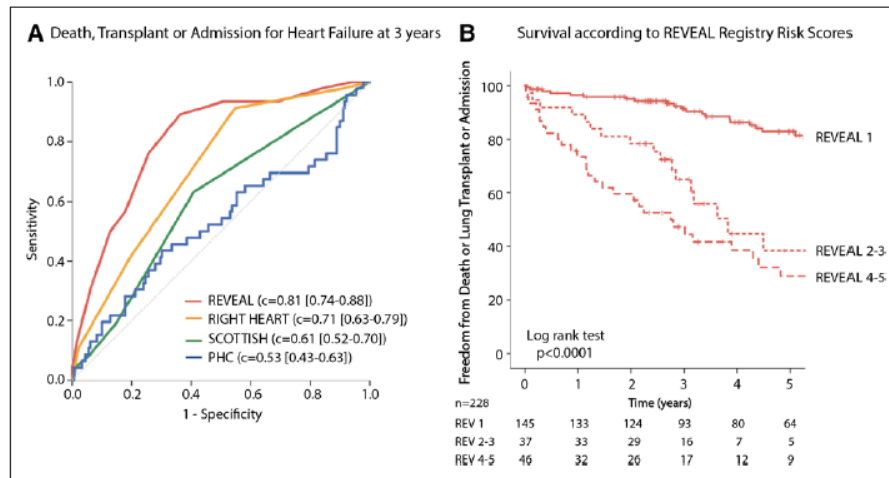


Figure 5. Validation of risk scores for prediction of outcomes in pulmonary arterial hypertension (PAH). **A**, Receiving operating curve for the primary end point at 3 y for the Pulmonary Hypertension Connection (PHC), Registry to Evaluate Early And Long-term PAH Disease Management (REVEAL), Scottish composite, and Right Heart scores. **B**, Kaplan–Meier survival curves of the REVEAL registry risk score categories for the primary combined end point of death, transplantation, or hospitalization for acute right heart failure. Low risk was defined by a score between 0 and 7, average if equal to 8, moderate high if equal to 9, high if equal to 10 or 11 and very high if ≥ 12 . Patients were combined into 3 groups (REVEAL 1=low, REVEAL 2–3=average/moderate high, and REVEAL 4–5=high/very high) instead of the 5 original groups to obtain balanced groups in terms of number of patients.

minor/long axis ratio are presented in Figure III in the [Data Supplement](#).

To minimize overfitting the multivariable model, only 7 variables were included in addition to age and sex: NYHA class, RVESRI, RVLS, log NT-proBNP, pericardial effusion, RAP, and connective tissue disease cause. The choice of variables was based on the following rationale: (1) NYHA class III or IV as previously reported, (2) RVESRI emerged as a strong novel metric, (3) RVLS was also associated to outcomes in the Mayo Clinic cohort,⁷ (4) pericardial effusion, (5) log NT-proBNP emerging in many studies, including the REVEAL registry score, (6) RAP, a validated strong predictor of outcome, and (7) connective tissue disease cause as often found to be associated with poor outcome. Renal dysfunction

had significant interactions with RAP and NT-proBNP ($P<0.0001$) and thus was not included as a covariate in the model. On multivariable analysis, NYHA class III or IV, RVESRI, and log NT-proBNP were retained in the model for the primary end point (χ^2 , 62.2; $P<0.0001$; Table 3). For the secondary end point of death or transplant, RVESRI (1.50; CI, 1.10–2.04) and log NT-proBNP (1.85; CI, 1.32–2.58) were also retained (χ^2 , 42.40; $P<0.0001$).

Incremental Value of RVESRI and RVLS to Risk Scores

In this cohort, validated risk scores were predictive of outcome (Figure 5A) with the strongest score being the REVEAL registry score ($P<0.001$ when compared with the

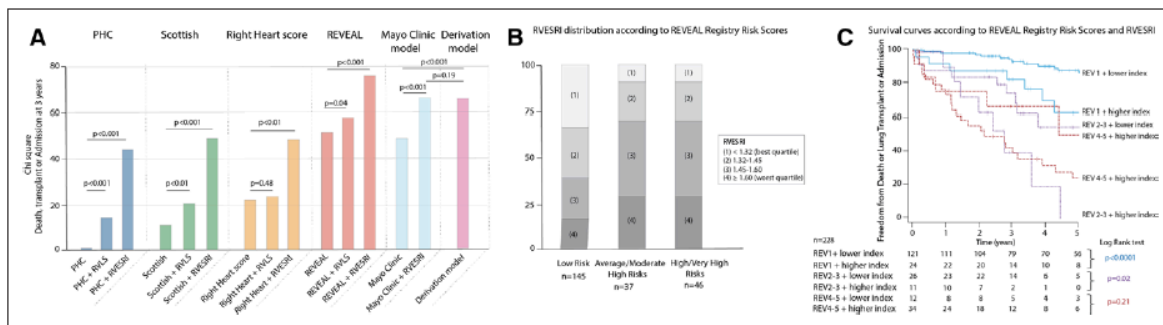


Figure 6. Incremental value of right ventricular end-systolic remodeling index (RVESRI) for prediction of outcomes in pulmonary arterial hypertension (PAH). **A**, χ^2 of scores and RVESRI and RV lateral free wall longitudinal strain (RVLS) for prediction of the primary end point (death, transplant, or admission for heart failure) at 3 y. The Mayo Clinic variables (age, sex, RVLS, New York Heart Association [NYHA] class, and log NT-proBNP [N-Terminal Pro-B-Type Natriuretic Peptide]) were entered in the model using enter mode. The current derivation model was age, sex, RVESRI, NYHA class, and log NT-proBNP. **B**, Distribution of baseline RVESRI according to groups of the Registry to Evaluate Early And Long-term PAH Disease Management (REVEAL) scores (REVEAL 1=low, REVEAL 2–3=average/moderate high, and REVEAL 4–5=high/very high). **C**, Five-year Kaplan–Meier survival curves according to the REVEAL registry score groups and baseline RVESRI. Worst index was defined by RVESRI ≥ 1.60 (worst quartile) and best as <1.60 for REVEAL 1–3; and worst index was defined by RVESRI ≥ 1.45 and best as <1.45 for REVEAL 4–5 because of the small number of patients with best quartile ($n=3$). Similar results were obtained if using 1.60 for REVEAL 4–5.

Table 5. Mayo Clinic–Derived Score and Derivation Model–Derived Score for Prediction of the Primary End Point (ie, Death, Lung Transplant, or Admission) at 3 Years

Mayo Clinic Model		Derivation Model	
Variables	Points	Variables	Points
RV longitudinal strain (%)		RV end-systolic remodeling index	
≥25 (reference)	0	<1.32 (reference)	0
[20–25[3	[1.32–1.45[2
[15–20[5	[1.45–1.60[3
<15	5	≥1.60	5
NT-proBNP, pg/mL		NT-proBNP (pg/mL)	
<1500	0	<1500	0
≥1500	1	≥1500	2
NYHA class		NYHA class	
I or II	0	I or II	0
III or IV	3	III or IV	3
Total	/17	Total	/15

Continuous variables were categorized according to clinically relevant cutoff points, RV free wall longitudinal strain thresholds from Fine et al⁷ study (≥25%, [20–25], [15–20], <15%) and quartiles for RV end-systolic remodeling index. Points were given according to the hazard ratio using multivariable analysis rounded to the nearest integer. In our cohort, the derivation model score ranged from 0 to 10 as follows: 35 patients with 0, 31 with 2, 44 with 4, 1 with 4, 37 with 5, 19 with 6, 7 with 7, 31 with 8, and 23 with a score of 10. NT-proBNP indicates N-Terminal Pro-B-Type Natriuretic Peptide; NYHA, New York Heart Association; and RV, right ventricular.

Pulmonary Hypertension Connection and Scottish scores; $P=0.06$ compared with the Right Heart score). Patients were combined in 3 REVEAL groups (REVEAL 1=low, REVEAL 2–3=average/moderate high, and REVEAL 4–5=high/very high) to balance groups in terms of number of patients. The REVEAL score groups were validated in our cohort (Figure 5B). Adding RVESRI to validated scores, using Cox regression analysis, improved discrimination for the Pulmonary Hypertension Connection, the REVEAL, the Right Heart score, and the Scottish score (Figure 6A). RVLS also improved discrimination of the REVEAL score. The incremental value of RVESRI to the REVEAL score in predicting outcome was also illustrated in the Kaplan–Meier curves divided according to the different strata of risk (low score, average and moderate high score, and high and very high score; Figure 6B and 6C). The NRI (%) of the REVEAL score with RVLS was 1.05 (CI, –31.3% to 33.4%), $P=0.95$, the NRI of the REVEAL score with RVESRI was 45.9 (CI, 14.4%–77.4%), $P<0.01$, and NRI of the REVEAL score with RVLS and RVESRI was 42.6 (CI, 11.0%–74.2%), $P<0.01$. Scores derived from the Mayo Clinic and our derivation models were constructed (Table 5). Five-year Kaplan–Meier survival curve of our derivation score divided into 5 groups according to the distribution of patients is presented in Figure IV in the Data Supplement. The C statistics for the 3-year outcome based on the REVEAL score was not statistically different than the Mayo Clinic score or our derivation model score. C statistics of the REVEAL score was 0.81 (CI, 0.74–0.88), of the REVEAL+RVESRI was 0.83 (CI, 0.77–0.89),

and C statistics of the REVEAL+RVLS was 0.82 (CI, 0.75–0.89). The C statistics of the Mayo model score and our derivation model score were 0.76 (CI, 0.67–0.84) and 0.79 (CI, 0.72–0.86), respectively (both $P<0.0001$).

Change in RVESRI During Follow-Up

Follow-up echocardiograms were available in 203 patients (98% of 1-year survivors). The relative changes in RVESRI showed a normal distribution (Figure 7A). At 1 year, RVESRI was significantly associated with outcome (hazard ratio, 2.22; CI, 1.83–2.70; $P<0.0001$), as did the baseline values (Figure V in the Data Supplement). Moreover, the change in RVESRI over time was also related to outcome (Figure 7B). When dividing patients according to the 3 groups according to the REVEAL registry score, change in RVESRI was significantly incremental for predicting outcome in patients in the low risk or high/very high risk strata (Figure 7C and 7D). Patients in whom prostanoids were initiated during the first year improved to a greater extent their RVESRI than the other patients, as shown in Figure 7E. On multivariable analysis, improvement in RVESRI was associated with new prostanoid therapy (odds ratio, 3.12; 95% CI, 1.08–9.02; $P=0.04$) and baseline RVESRI (OR, 2.65; 95% CI, 1.47–4.75; $P=0.001$) but not the status of incident case ($P=0.08$).

Variability and Reproducibility of RVESRI

Recognizing that a nonfocused RV view can influence the reliability of RV measures, we investigated in a new cohort of patients with PAH the effects of different apical angle planes. In this cohort of 14 patients, RVLS ranged from 7% to 23% and RVESRI varying from 1.2 to 1.9 and was normally distributed. Compared with RVLS and other functional and structural indices, RVESRI was less influenced by different apical 4-chamber views (angle change) and showed the best intra- and interobserver variability assessed by intraclass correlation coefficient and test–retest characteristics (Figure 8; Table III in the Data Supplement).

Discussion

The main finding of our study is that a simple index of RV end-systolic remodeling carries a strong prognostic value in PAH. Our findings also externally validate the prognostic value of RVLS in PAH and confirm the robustness of the REVEAL registry score. Finally, our study is the largest to date to analyze changes in RV remodeling over time and to explore its association with response to therapy.

Our study highlights the importance of RV adaptation in PAH. Research in PAH has often been focused on identifying an adapted and maladapted right heart phenotype.¹⁹ Identifying phenotypes of RV adaptation can, however, be challenging because thresholds may be arbitrary, and rest parameters may not capture the complexity of adaptation. Acknowledging these limitations, we identified similarly to Ryo et al⁸ methodology 3 zones of adaptation based on the RV end-systolic dimension to pressure relationship. The first zone is characterized by minimal RV enlargement in the presence of increasing RV pressure, whereas the third zone is characterized by a failing right heart with progressive RV enlargement and decrease in pressures, reflecting decrease

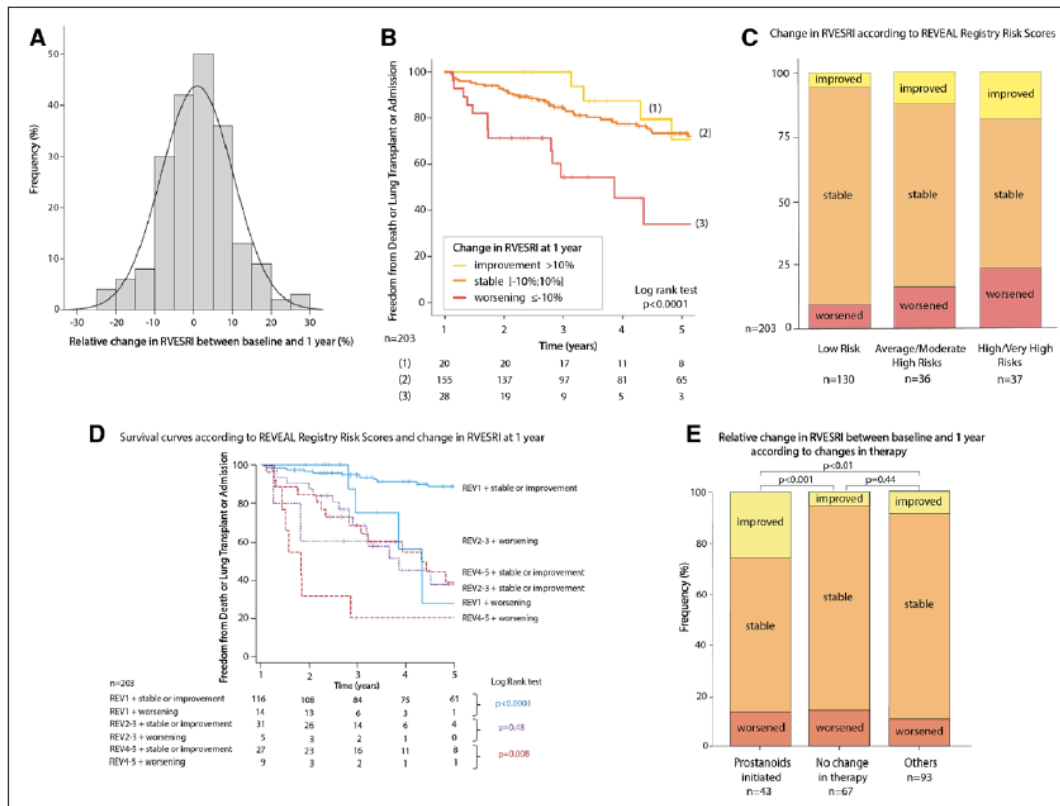


Figure 7. Incremental value of change in right ventricular end-systolic remodeling index (RVESRI) with time and evolution of RVESRI according to medication changes in patients with 1-y follow-up echocardiograms (n=203). **A**, Relative change in RVESRI between baseline and 1 year after a normal distribution. **B**, Five-year Kaplan-Meier survival curves of RVESRI at 1 year according to change in RVESRI for the primary end point; improvement was defined by a decrease in RVESRI of >10%, worsening by an increase of >10%, and stability otherwise. **C**, Change in RVESRI at 1 year according to the REVEAL score groups (REVEAL 1=low, REVEAL 2–3=average/moderate high, and REVEAL 4–5=high/very high). **D**, Three-year Kaplan-Meier survival curves according to the REVEAL registry score groups and change in RVESRI. **E**, Relative change in RVESRI between baseline and 1 y according to changes in therapy specific of pulmonary arterial hypertension (PAH): prostanoids, endothelin receptor blockers, and phosphodiesterase inhibitors.

in cardiac output. This classification in 3 stages seems more appropriate than a simple separation between adapted and maladapted, although more complex analysis should also

take into account the load imposed on the ventricle, diastolic characteristics, and neurohormonal and immunologic components of adaptation.^{19–22} Our multivariable model, as

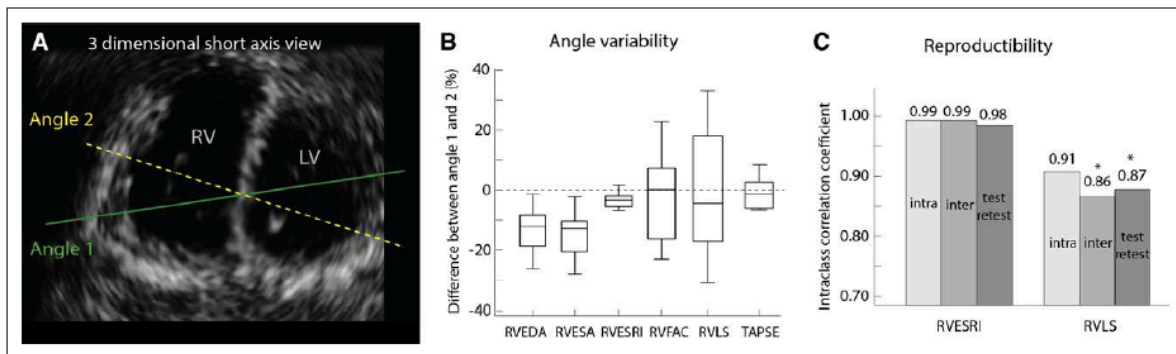


Figure 8. Variability of measurements in patients with pulmonary arterial hypertension (PAH; n=14). Variability of 2-dimensional (2D) measures obtained using 3D imaging standardization at maximal angle difference while still visualizing the tricuspid valve opening; this would represent the maximal changes obtainable while still being on axis (A), expressed as percentage of the difference between values obtained on plane with angle 2 and with angle 1 (B). Intra- and interobserver reproducibility of right ventricular (RV) metrics, including test-retest (C). *P values <0.05 for comparison with respective intraclass correlation coefficient (ICC) of RV end-systolic remodeling index (RVESRI). LV, left ventricle; RVEDA, RV end-diastolic area; RVESA, RV end-systolic area; RVFAC, RV fractional area change; RVLS, RV free wall longitudinal strain; and TAPSE: tricuspid area plane systolic excursion.

well as Fine et al,⁷ proposes the combination of 3 simple parameters (ie, NYHA functional class, NT-proBNP level, and either RV end-systolic remodeling or longitudinal strain) that may help identifying the continuum of RV maladaptation profiles. Our study represents the largest validation of RVLS in an independent cohort. Although strain is a more recent concept in the field, several pioneering works have been done on end-systolic dimensions in left heart failure, including the landmark 1984 study of Carabello et al²³ placing end-systolic dimensions and stress-corrected end-systolic dimensions as the best predictors of postoperative recovery in valvular heart disease.

One important contribution of our study is the demonstration of the connection of RV end-systolic indices to right atrial dimensions and RVLS, which may contribute to their strong relationship with outcome. Although we cannot prove it in our study, one could hypothesize that a strongly connected parameter could carry more prognostic value. The index proposed in our study has the advantage of simplicity and reproducibility. In fact, RVESRI is less influenced by apical planes than other indices and has better test–retest characteristics. We have additionally demonstrated that internally scaling to septal height carries more prognostic information than scaling to height or body surface area. Compared with other remodeling indices, such as RV sphericity, RVESRI is more predictive of outcome in PAH. As RVESRI integrates ventricular enlargement, it can be questioned whether this index would be validated in other conditions, such as left heart failure, in which the range of RV dilation is lower. It is indeed unlikely to be as highly prognostic in patients with heart failure with preserved ejection fraction in whom strain has been validated as an early marker of RV dysfunction.²⁴ Although derived using echocardiography, RVESRI could be applied in PAH using cardiac magnetic resonance imaging 4-chamber plane, which is a more reproducible imaging modality. Several cardiac magnetic resonance metrics have been validated for prognosis in PAH (RV end-systolic volume, ejection fraction, and stroke volume index), and it remains to be assessed whether RVESRI may complement them.^{25,26}

Practically, 1 important question that arises when considering risk models is whether it is time to move beyond prediction in PAH²⁷ because several models have already been published.^{3,5,6,9–11} The REVEAL registry score, derived from multicenter collaborations, emerged as a strong predictor of outcome in our cohort (with similar C statistics), highlighting both its robustness and the representability of our study population.^{5,28} In our opinion, the most important contribution of any novel imaging biomarker will be to simplify the number of parameters needed to build robust prediction score in PAH. Although novel imaging parameters like ours may improve already existing scores, their contribution will indeed likely be relatively moderate. Perhaps, more meaningful will be the contribution of incorporating stability over time or the response to therapy or as this can lead to reclassification of risk, as suggested by our findings. More studies will be needed to confirm and explore the incremental value of dynamic changes in RV end-systolic remodeling, for example, to stratify randomization of clinical trials. Our

results suggest that patient with low REVEAL score but high RV end-systolic index may need closer monitoring of their evolution, and they may benefit from more intensive therapy or combined therapies.

Study Limitations

The first limitation comes from the single-center study design. However, it was primarily intended as a validation of previous studies and a comparison between end-systolic indices and longitudinal strain. Moreover, the population is a representative of major contemporary large cohort (such as the REVEAL registry). The second limitation could emerge from the mixed cohort, including both incident and prevalent cases. However, we found no significant interaction of this status with the results, although there was a trend for worse outcome in incident cases. Third, connective tissue disease cause did not emerge as an independent predictor of outcome in our cohort, contrary to the REVEAL registry. The small number of patients and the exclusion of patients with interstitial lung disease may have precluded our study to capture this risk; some of the risk may have already been accounted by other indices, such as NT-proBNP. Fourth, we assessed the incremental value of change in RVESRI at 1 year using the baseline REVEAL score and not at 1 year because catheterization was not systematically repeated at 1 year (reflecting the majority of clinical practice). Fifth, the score derived from our multivariable analysis is a simple proof-of-concept score that did not undergo calibration and used a simple ponderation, derived from the hazard ratios. Finally, the manual determination of Lagrangian strain may be questioned. In our laboratory, we have found this to be more reproducible because we use careful landmarks and we have previously shown the excellent reliability of manual derived strain values in the left heart.^{29,30} The validation of the normative values of RV strain in our healthy cohort and the validation of the thresholds described by Fine et al⁷ both support the validity of our method.¹²

In conclusion, this study highlights the importance of RV end-systolic remodeling for risk stratification in patients with PAH. More studies will be needed to confirm the incremental value of dynamic changes in RV end-systolic remodeling on the REVEAL score, especially in the intermediate-risk groups and as markers of response to therapy.

Acknowledgments

We would like to thank the Stanford Cardiovascular Institute and the Vera Moulton Wall Center of Pulmonary Hypertension at Stanford for their support and A. Hsi for database management.

Sources of Funding

This study was funded by the NHLBI-HV-10-05 (Dr Rabinovitch) and the ANR-15-RHUS-0002 (Dr Mercier). Dr Amsallem received a Young Investigator Seed Grant from the Vera Moulton Wall Center and Dr Haddad a grant from the Pai Chan Lee research Fund. Dr McConnell previously received cardiac magnetic resonance imaging research support from GE Healthcare and is currently on partial leave of absence while an employee at Verily Life Sciences.

Disclosures

None.

References

- McLaughlin VV, Archer SL, Badesch DB, Barst RJ, Farber HW, Lindner JR, Mathier MA, McGoon MD, Park MH, Rosenson RS, Rubin LJ, Tapson VF, Varga J, Harrington RA, Anderson JL, Bates ER, Bridges CR, Eisenberg MJ, Ferrari VA, Grines CL, Hlatky MA, Jacobs AK, Kaul S, Lichtenberg RC, Lindner JR, Moliterno DJ, Mukherjee D, Pfoh GM, Rosenson RS, Schofield RS, Shubrooks SJ, Stein JH, Tracy CM, Weitz HH, Wesley DJ; ACCF/AHA. ACCF/AHA 2009 expert consensus document on pulmonary hypertension: a report of the American College of Cardiology Foundation Task Force on Expert Consensus Documents and the American Heart Association: developed in collaboration with the American College of Chest Physicians, American Thoracic Society, Inc., and the Pulmonary Hypertension Association. *Circulation*. 2009;119:2250–2294. doi: 10.1161/CIRCULATIONAHA.109.192230.
- Galiè N, Humbert M, Vachiery JL, Gibbs S, Lang I, Torbicki A, Simonneau G, Peacock A, Vonk Noordegraaf A, Beghetti M, Ghofrani A, Gomez Sanchez MA, Hansmann G, Klepetko W, Lancellotti P, Matucci M, McDonagh T, Pierard LA, Trindade PT, Zompatori M, Hoeper M, Aboyans V, Vaz Carneiro A, Achenbach S, Agewall S, Allanore Y, Asteghiano R, Paolo Badano L, Albert Barberà J, Bouvaist H, Bueno H, Byrne RA, Carerj S, Castro G, Erol Ç, Falk V, Funck-Brentano C, Gorenflo M, Granton J, Jung B, Kiely DG, Kirchhof P, Kjellström B, Landmesser U, Lekakis J, Lionis C, Lip GY, Orfanos SE, Park MH, Piepoli MF, Ponikowski P, Revel MP, Rigau D, Rosenkranz S, Völler H, Luis Zamorano J. 2015 ESC/ERS Guidelines for the diagnosis and treatment of pulmonary hypertension: The Joint Task Force for the Diagnosis and Treatment of Pulmonary Hypertension of the European Society of Cardiology (ESC) and the European Respiratory Society (ERS): Endorsed by: Association for European Paediatric and Congenital Cardiology (AEPC), International Society for Heart and Lung Transplantation (ISHLT). *Eur Heart J*. 2016;37:67–119. doi: 10.1093/eurheartj/ehv317.
- D'Alonzo GE, Barst RJ, Ayres SM, Bergofsky EH, Brundage BH, Detre KM, Fishman AP, Goldring RM, Groves BM, Kernis JT. Survival in patients with primary pulmonary hypertension. Results from a national prospective registry. *Ann Intern Med*. 1991;115:343–349.
- Ghio S, Recusani F, Klersy C, Sebastiani R, Laudisa ML, Campana C, Gavazzi A, Tavazzi L. Prognostic usefulness of the tricuspid annular plane systolic excursion in patients with congestive heart failure secondary to idiopathic or ischemic dilated cardiomyopathy. *Am J Cardiol*. 2000;85:837–842.
- Benza RL, Miller DP, Gomberg-Maitland M, Frantz RP, Foreman AJ, Coffey CS, Frost A, Barst RJ, Badesch DB, Elliott CG, Liou TG, McGoon MD. Predicting survival in pulmonary arterial hypertension: insights from the Registry to Evaluate Early and Long-Term Pulmonary Arterial Hypertension Disease Management (REVEAL). *Circulation*. 2010;122:164–172. doi: 10.1161/CIRCULATIONAHA.109.898122.
- Humbert M, Sitbon O, Yaici A, Montani D, O'Callaghan DS, Jaïs X, Parent F, Savale L, Natali D, Günther S, Chaouat A, Chabot F, Cordier JF, Habib G, Gressin V, Jing ZC, Souza R, Simonneau G; French Pulmonary Arterial Hypertension Network. Survival in incident and prevalent cohorts of patients with pulmonary arterial hypertension. *Eur Respir J*. 2010;36:549–555. doi: 10.1183/09031936.00057010.
- Fine NM, Chen L, Bastiansen PM, Frantz RP, Pellikka PA, Oh JK, Kane GC. Outcome prediction by quantitative right ventricular function assessment in 575 subjects evaluated for pulmonary hypertension. *Circ Cardiovasc Imaging*. 2013;6:711–721. doi: 10.1161/CIRCIMAGING.113.000640.
- Ryo K, Goda A, Onishi T, Delgado-Montero A, Tayal B, Champion HC, Simon MA, Mathier MA, Gladwin MT, Gorcsan J. Characterization of right ventricular remodeling in pulmonary hypertension associated with patient outcomes by 3-dimensional wall motion tracking echocardiography. *Circ Cardiovasc Imaging*. 2015;8:e003176.
- Thenappan T, Shah SJ, Rich S, Tian L, Archer SL, Gomberg-Maitland M. Survival in pulmonary arterial hypertension: a reappraisal of the NIH risk stratification equation. *Eur Respir J*. 2010;35:1079–1087. doi: 10.1183/09031936.00072709.
- Lee WT, Ling Y, Sheares KK, Pepke-Zaba J, Peacock AJ, Johnson MK. Predicting survival in pulmonary arterial hypertension in the UK. *Eur Respir J*. 2012;40:604–611. doi: 10.1183/09031936.00196611.
- Haddad F, Spruijt OA, Denault AY, Mercier O, Brunner N, Furman D, Fadel E, Bogaard HJ, Schnitger I, Vrtovec B, Wu JC, de Jesus Perez V, Vonk-Noordegraaf A, Zamanian RT. Right heart score for predicting outcome in idiopathic, familial, or drug- and toxin-associated pulmonary arterial hypertension. *JACC Cardiovasc Imaging*. 2015;8:627–638. doi: 10.1016/j.jcmg.2014.12.029.
- Lang RM, Badano LP, Mor-Avi V, Afilalo J, Armstrong A, Ernande L, Flachskampf FA, Foster E, Goldstein SA, Kuznetsova T, Lancellotti P, Muraru D, Picard MH, Rietzschel ER, Rudski L, Spencer KT, Tsang W, Voigt JU. Recommendations for cardiac chamber quantification by echocardiography in adults: an update from the American Society of Echocardiography and the European Association of Cardiovascular Imaging. *J Am Soc Echocardiogr*. 2015;28:1.e14–39.e14. doi: 10.1016/j.echo.2014.10.003.
- Rudski LG, Lai WW, Afilalo J, Hua L, Handschumacher MD, Chandrasekaran K, Solomon SD, Louie EK, Schiller NB. Guidelines for the echocardiographic assessment of the right heart in adults: a report from the American Society of Echocardiography endorsed by the European Association of Echocardiography, a registered branch of the European Society of Cardiology, and the Canadian Society of Echocardiography. *J Am Soc Echocardiogr*. 2010;23:685–713; quiz 786. doi: 10.1016/j.echo.2010.05.010.
- Haddad F, Guhnaire J, Skhiri M, Denault AY, Mercier O, Al-Halabi S, Vrtovec B, Fadel E, Zamanian RT, Schnitger I. Septal curvature is marker of hemodynamic, anatomical, and electromechanical ventricular interdependence in patients with pulmonary arterial hypertension. *Echocardiography*. 2014;31:699–707. doi: 10.1111/echo.12468.
- Amsallem M, Sternbach JM, Adigopula S, Kobayashi Y, Vu TA, Zamanian R, Liang D, Dhillon G, Schnitger I, McConnell MV, Haddad F. Addressing the controversy of estimating pulmonary arterial pressure by echocardiography. *J Am Soc Echocardiogr*. 2016;29:93–102. doi: 10.1016/j.echo.2015.11.001.
- Kuznetsova T, Haddad F, Knez J, Rosenberg-Hasson Y, Sung J, Cauwenberghs N, Thijs L, Karakikes I, Maecker H, Mahaffey KW, Wu JC, Staessen JA. Cytokines profile in hypertensive patients with left ventricular remodeling and dysfunction. *J Am Soc Hypertens*. 2015;9:975.e3–984.e3. doi: 10.1016/j.jash.2015.10.003.
- Pencina MJ, D'Agostino RB Sr, Steyerberg EW. Extensions of net reclassification improvement calculations to measure usefulness of new biomarkers. *Stat Med*. 2011;30:11–21. doi: 10.1002/sim.4085.
- Rain S, Handoko ML, Trip P, Gan CT, Westerhof N, Stienen GJ, Paulus WJ, Ottenheijm CA, Marcus JT, Dorfmueller P, Guignabert C, Humbert M, Macdonald P, Dos Remedios C, Postmus PE, Saripalli C, Hidalgo CG, Granzier HL, Vonk-Noordegraaf A, van der Velden J, de Man FS. Right ventricular diastolic impairment in patients with pulmonary arterial hypertension. *Circulation*. 2013;128:2016–2025. 1. doi: 10.1161/CIRCULATIONAHA.113.001873.
- Amsallem M, Kuznetsova T, Hanneman K, Denault A, Haddad F. Right heart imaging in patients with heart failure: a tale of two ventricles. *Curr Opin Cardiol*. 2016;31:469–482. doi: 10.1097/HCO.0000000000000315.
- Vonk-Noordegraaf A, Galiè N. The role of the right ventricle in pulmonary arterial hypertension. *Eur Respir Rev*. 2011;20:243–253. doi: 10.1183/09059180.00006511.
- Vonk-Noordegraaf A, Haddad F, Chin KM, Forfia PR, Kawut SM, Lumens J, Naeije R, Newman J, Oudiz RJ, Provencher S, Torbicki A, Voelkel NF, Hassoun PM. Right heart adaptation to pulmonary arterial hypertension: physiology and pathobiology. *J Am Coll Cardiol*. 2013;62(suppl 25):D22–D33. doi: 10.1016/j.jacc.2013.10.027.
- Ryan JJ, Huston J, Kutty S, Hatton ND, Bowman L, Tian L, Herr JE, Johri AM, Archer SL. Right ventricular adaptation and failure in pulmonary arterial hypertension. *Can J Cardiol*. 2015;31:391–406. doi: 10.1016/j.cjca.2015.01.023.
- Carabello BA, Spann JF. The uses and limitations of end-systolic indexes of left ventricular function. *Circulation*. 1984;69:1058–1064.
- Morris DA, Krisper M, Nakatani S, Köhncke C, Otsuji Y, Belyavskiy E, Radha Krishnan AK, Kropf M, Osmanoglou E, Boldt LH, Blaschke F, Edelmann F, Haverkamp W, Tschöpe C, Pieske-Kraigher E, Pieske B, Takeuchi M. Normal range and usefulness of right ventricular systolic strain to detect subtle right ventricular systolic abnormalities in patients with heart failure: a multicentre study. *Eur Heart J Cardiovasc Imaging*. 2017;18:212–223. doi: 10.1093/ehjci/ehw011.
- van de Veerdonk MC, Kind T, Marcus JT, Mauritz G-J, Heymans MW, Bogaard H-J, Boonstra A, Marques KJM, Westerhof N, Vonk-Noordegraaf A. Progressive right ventricular dysfunction in patients with pulmonary arterial hypertension responding to therapy. *J Am Coll Cardiol*. 2011;58:2511–2519.
- van de Veerdonk MC, Marcus JT, Westerhof N, de Man FS, Boonstra A, Heymans MW, Bogaard H-J, Vonk-Noordegraaf A. Signs of right ventricular deterioration in clinically stable patients with pulmonary arterial hypertension. *Chest*. 2015;147:1063–1071.

13 Amsallem et al RV Systolic Remodeling in PAH

27. Nasir K. Cardiovascular imaging research: time to think beyond risk prediction? *JACC Cardiovasc Imaging*. 2015;8:957–959. doi: 10.1016/j.jcmg.2015.06.009.
28. Farber HW, Miller DP, Poms AD, Badesch DB, Frost AE, Muros-Le Rouzic E, Romero AJ, Benton WW, Elliott CG, McGoon MD, Benza RL. Five-year outcomes of patients enrolled in the REVEAL Registry. *Chest*. 2015;148:1043–1054. doi: 10.1378/chest.15-0300.
29. Tuzovic M, Adigopula S, Amsallem M, Kobayashi Y, Kadoch M, Boulate D, Krishnan G, Liang D, Schnittger I, Fleischmann D, McConnell MV, Haddad F. Regional right ventricular dysfunction in acute pulmonary embolism: relationship with clot burden and biomarker profile. *Int J Cardiovasc Imaging*. 2016;32:389–398. doi: 10.1007/s10554-015-0780-1.
30. Kobayashi Y, Ariyama M, Kobayashi Y, Giraldeau G, Fleischman D, Kozelj M, Vrtovec B, Ashley E, Kuznetsova T, Schnittger I, Liang D, Haddad F. Comparison of left ventricular manual versus automated derived longitudinal strain: implications for clinical practice and research. *Int J Cardiovasc Imaging*. 2016;32:429–437. doi: 10.1007/s10554-015-0804-x.

CLINICAL PERSPECTIVE

Right heart failure is the main cause of mortality in patients with pulmonary arterial hypertension. Indices of right heart end-systolic remodeling integrate information of both size and function and are emerging as strong predictors of outcome in patients with pulmonary arterial hypertension. In this longitudinal study, we describe a novel and simple index of right ventricular (RV) end-systolic remodeling defined as the RV free wall length divided by septal length. We demonstrate that RV end-systolic remodeling index is centrally connected to other right heart metrics and improves risk prediction based on the REVEAL score and the Pulmonary Hypertension Connection score. Moreover, our study highlights that New York Heart Association functional class, NT-proBNP (N-Terminal Pro-B-Type Natriuretic Peptide) levels, and RV end-systolic remodeling index capture key features of the clinical right heart adaptation continuum in pulmonary arterial hypertension. The study is also the largest to demonstrate the importance of changes in RV end-systolic remodeling over time showing the increment to baseline remodeling indices and the REVEAL score. Although RV free wall longitudinal strain is predictive of outcome, it does not capture the same level of prediction than RV end-systolic remodeling index and is less reproducible. In terms of clinical impact, our study may simplify clinical risk assessment and offer a simple tool for stratified randomization in clinical trials.

Right Heart End-Systolic Remodeling Index Strongly Predicts Outcomes in Pulmonary Arterial Hypertension: Comparison With Validated Models

Myriam Amsallem, Andrew J. Sweatt, Marie C. Aymami, Tatiana Kuznetsova, Mona Selej, HongQuan Lu, Olaf Mercier, Elie Fadel, Ingela Schnittger, Michael V. McConnell, Marlene Rabinovitch, Roham T. Zamanian and Francois Haddad

Circ Cardiovasc Imaging. 2017;10:

doi: 10.1161/CIRCIMAGING.116.005771

Circulation: Cardiovascular Imaging is published by the American Heart Association, 7272 Greenville Avenue, Dallas, TX 75231

Copyright © 2017 American Heart Association, Inc. All rights reserved.

Print ISSN: 1941-9651. Online ISSN: 1942-0080

The online version of this article, along with updated information and services, is located on the World Wide Web at:

<http://circimaging.ahajournals.org/content/10/6/e005771>

Data Supplement (unedited) at:

<http://circimaging.ahajournals.org/content/suppl/2017/06/07/CIRCIMAGING.116.005771.DC1>

Permissions: Requests for permissions to reproduce figures, tables, or portions of articles originally published in *Circulation: Cardiovascular Imaging* can be obtained via RightsLink, a service of the Copyright Clearance Center, not the Editorial Office. Once the online version of the published article for which permission is being requested is located, click Request Permissions in the middle column of the Web page under Services. Further information about this process is available in the [Permissions and Rights Question and Answer](#) document.

Reprints: Information about reprints can be found online at:

<http://www.lww.com/reprints>

Subscriptions: Information about subscribing to *Circulation: Cardiovascular Imaging* is online at:

<http://circimaging.ahajournals.org/subscriptions/>

SUPPLEMENTARY MATERIAL

Table S1. Risk scores in Pulmonary Arterial Hypertension and Mayo Clinic model including right ventricular strain.

Risk scores	Variables included in the score
Pulmonary Hypertension Connection Registry	Mean pulmonary arterial pressure Invasive mean right atrial pressure Invasive cardiac index
REVEAL Registry	Etiology of pulmonary arterial hypertension Male sex, aged >60 years Chronic renal disease NYHA functional class Systolic blood pressure Heart rate Six-minute minute walk distance N-terminal pro-brain natriuretic peptide (NT-proBNP) Pericardial effusion Diffusing capacity of the lung for carbon monoxide Invasive mean right atrial pressure Pulmonary vascular resistance
Scottish Composite Score	Age, Sex Etiology Six-minute minute walk distance Invasive mean right atrial pressure Invasive cardiac output
Right Heart Score	Right ventricular function, using fractional area change Right atrial enlargement index Systolic blood pressure
Mayo Clinic model	Age, Sex Dyspnea functional class* Log NT-proBNP* Right ventricular free-wall strain*

*significant parameters in model.

Table S2. Comparative characteristics of patients with or without the primary endpoint at 3 years.

Patient Characteristics	Event	No event	p*
	N=46	N=182	
Age (years)	50.2 ±13.6	48.2 ±14.2	0.40
Female sex	35 (76.1%)	143 (78.6%)	0.72
Etiology			
Idiopathic	9 (19.6%)	44 (24.2%)	0.64
Drugs and toxins	16 (34.8%)	39 (21.4%)	0.09
Connective tissue disease	16 (34.8%)	58 (31.9%)	0.84
NYHA functional class	I-II (21.7%); III-IV (78.3%)	I-II (56.0%); III-IV (44.0%)	<0.001
Systolic blood pressure (mmHg)	111 ±14	117 ±14	<0.001
Heart rate (bpm)	84 ±15	80 ±14	0.06
Hemodynamics			
Mean Right atrial pressure (mmHg)	9.8 ±6.8	7.7 ±4.6	0.01
Mean pulmonary arterial pressure (mmHg)	55.2 ±15.1	47.9 ±16.0	<0.01
Pulmonary arterial wedge pressure (mmHg)	11.8 ±5.5	10.5 ±4.5	0.10
Cardiac Index (L/min/m ²)	2.2 ±0.9	2.1 ±0.6	0.37
Stroke volume index (mL/m ²)	37.7 ±14.3	39.0 ±11.7	0.52
Pulmonary vascular resistance (WU) / indexed	13.3 ±7.5 / 23.0 ±11.1	10.7 ±6.0 / 18.1 ±9.7	0.01 <0.01
Echocardiograms			
Left ventricular ejection fraction (%)	60.7 ±6.2	60.8 ±5.9	0.92
Left ventricular longitudinal strain (absolute value, %)	17.3 ±3.9	17.7 ±3.6	0.51
Right atrial area index (cm ² /m ²)	14.4 ±4.5	11.6 ±4.4	<0.001
RVEDAI (cm ² /m ²)	22.8 ±7.2	18.1 ±5.8	<0.001
RVESAI (cm ² /m ²)	17.5 ±6.3	13.2 ±5.1	<0.001
RVFAC (%)	23.7 ±6.0	27.8 ±7.0	<0.001
TAPSE (mm)	16.5 ±4.0	17.8 ±4.7	0.09
RVLS (absolute value, %)	14.8 ±3.9	17.7 ±4.9	<0.001

RVESRI	1.60 ±0.18	1.43 ±0.17	<0.001
Systolic eccentricity index	1.80 ±0.61	1.48 ±0.41	<0.001
Moderate to severe TR	17 (37.0%)	28 (15.4%)	<0.01
RVSP (mmHg)	85.8 ±18.6	75.3 ±21.2	<0.01
Right atrial pressure (mmHg)	12.2 ±5.0	9.3 ±4.6	<0.001
Pericardial effusion	15 (32.6%)	20 (11.0%)	<0.001
Laboratory data			
Serum NT-proBNP (pg/mL)	1335 [414-3416]	232 [78-834]	<0.001
Serum creatinine (µmol/L)	83.9 ±22.9	76.3 ±22.9	0.04
MDRD GFR < 60mL/min/1.73m ²	26 (56.5%)	52 (28.6%)	<0.001
Pulmonary functional tests			
CO diffusing capacity (%)	64.0 ±20.7	73.1 ±20.9	<0.01
Six minutes walk test			
Distance (m)	357.1 ±136.0	432.9 ±135.1	<0.001
Therapy			
Treatment naive	13 (28.3%)	69 (37.9%)	0.30
Prostanoid Therapy	25 (54.3%)	55 (30.0%)	<0.01
Phosphodiesterase Inhibitors	23 (50.0%)	77 (42.3%)	0.44
Endothelin Receptor Blockers	13 (28.3%)	50 (27.5%)	0.94

Values are expressed as mean ±SD or number (percentage), or median and interquartile range [IQ]. *p-value for comparison using Student *t*-test or Chi-square test. Patients included in 2014 with less than 3 years follow-up (n=14) were right-censored; the outcome at the end of follow-up was used. RVSP was estimable from the tricuspid regurgitation signal in 91% of patients with outcomes and 84% without outcomes. GFR: glomerular filtration rate; NYHA: New York Heart Association; RV: right ventricular; RVEDAI, RVESAI: RV end-diastolic/systolic area indexed on BSA; RVESRI: RV end-systolic remodeling index; RVFAC: fractional area change; RVLS: free-wall longitudinal strain; RVSP: right ventricular systolic pressure; TAPSE: tricuspid annular plane systolic excursion.

Table S3. Reproducibility of right heart metrics measurements.

Metrics	Intraclass correlation coefficient	95% Confidence Interval
Intraobserver variability		
RV end-diastolic area	0.98	0.95 – 0.99
RV end-systolic area	0.99	0.97 – 0.99
RV end-systolic remodeling index	0.99	0.95 – 0.99
RV fractional area change	0.97	0.91 – 0.99
RV longitudinal strain	0.91	0.74 – 0.97
TAPSE	0.85	0.61 – 0.95
Interobserver variability		
RV end-diastolic area	0.94	0.81 – 0.98
RV end-systolic area	0.97	0.91 – 0.99
RV end-systolic remodeling index	0.99	0.97 – 0.99
RV fractional area change	0.94	0.83 – 0.98
RV longitudinal strain	0.86	0.56 – 0.95
TAPSE	0.73	0.35 – 0.90
Test-retest		
RV end-diastolic area	0.89	0.69 – 0.96
RV end-systolic area	0.95	0.84 – 0.98
RV end-systolic remodeling index	0.98	0.94 – 0.99
RV fractional area change	0.89	0.69 – 0.96
RV longitudinal strain	0.87	0.59 – 0.94
TAPSE	0.70	0.45 – 0.94

RV: right ventricle; TAPSE: tricuspid annular plane systolic excursion.

Figure S1. Scatterplots of invasive mean pulmonary arterial pressure and RV end-systolic remodeling index (left panel) or pulmonary vascular resistance index (right panel). Polynomial functions are displayed.

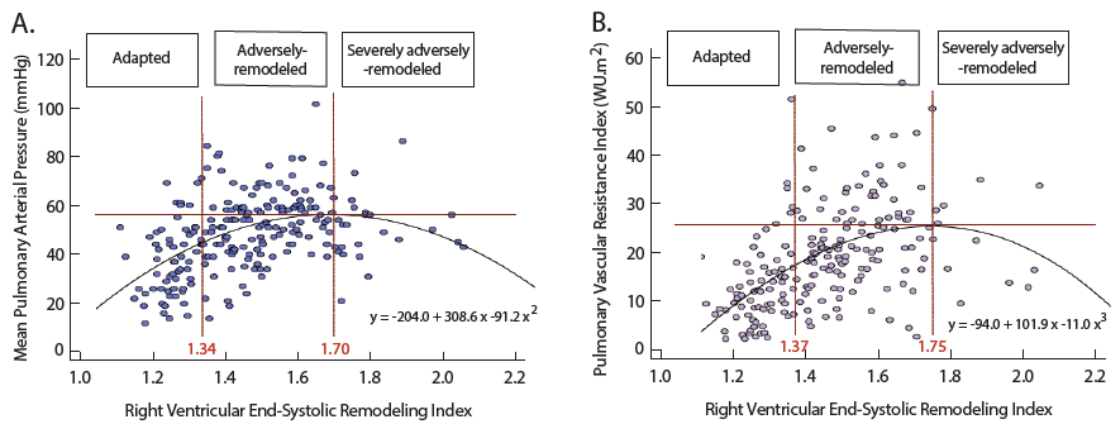


Figure S2. Five-year Kaplan Meier survival curves of right ventricular end-systolic remodeling index (RVESRI) and longitudinal strain (RVLS) quartiles for the secondary endpoint of death or transplant.

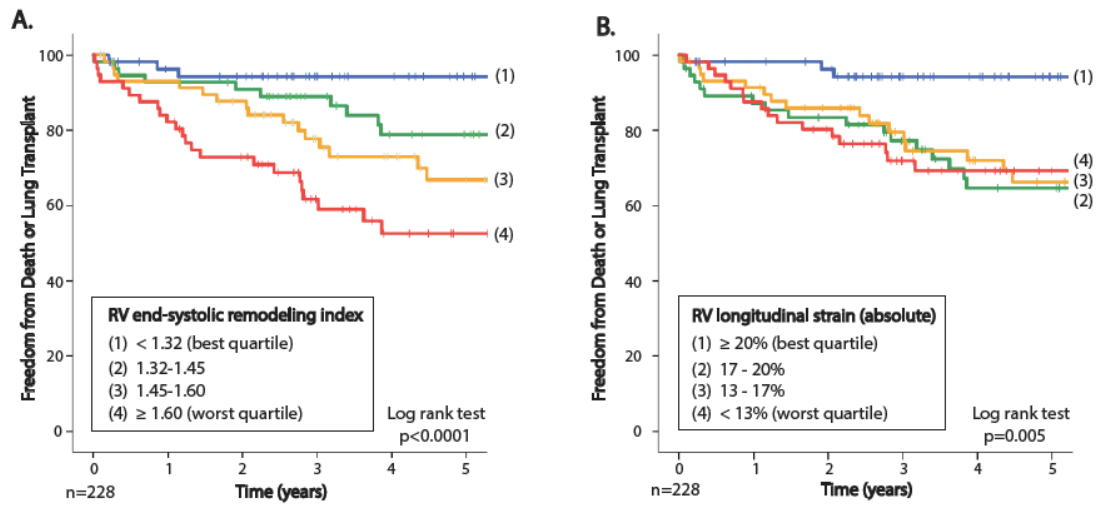


Figure S3. Five-year Kaplan Meier survival curves of logNT-proBNP (A), NYHA functional classes (B) and RV end-systolic minor/long axis ratio quartiles (C) for the primary endpoint of death, transplant or admission.

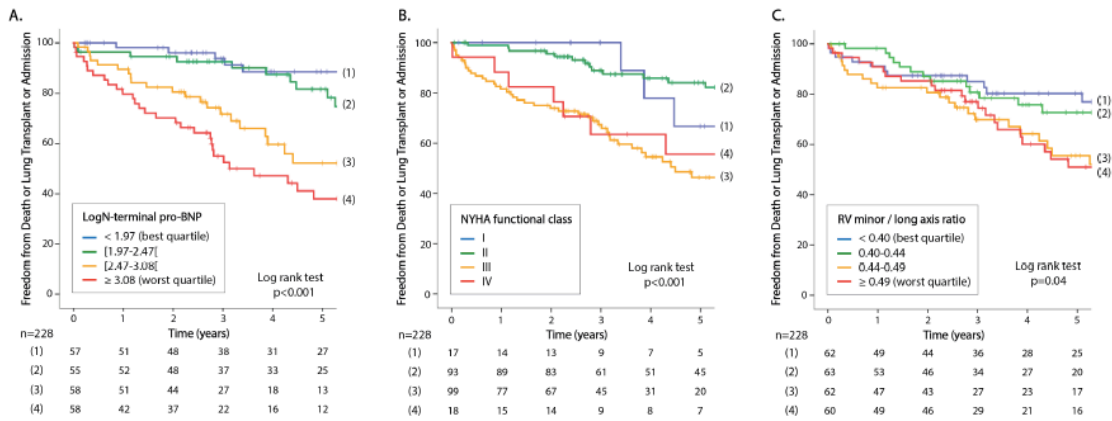


Figure S4. Five-year Kaplan Meier survival curve of the derivation score. In our cohort, the score ranged from 0 to 10/15 as follows: 35 patients with 0, 31 with 2, 44 patients with 4, one patient with 4, 37 with 5, 19 with 6, 7 with 7, 31 with 8 and 23 with a score of 10. Patients were divided into 5 groups to balance the number of patients in each group as follows: 0-2 (n=66), 3-4 (n=45), 5-6 (n=56), 7-8 (n=38) and ≥ 9 (n=23).

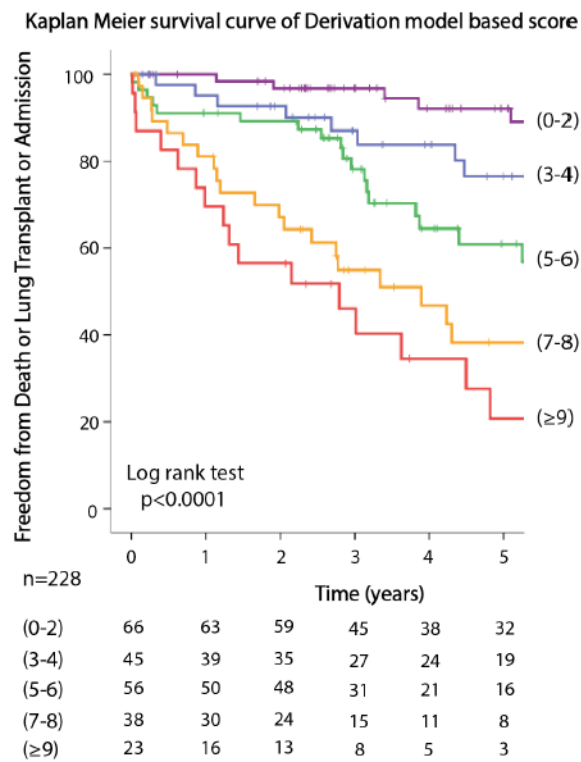
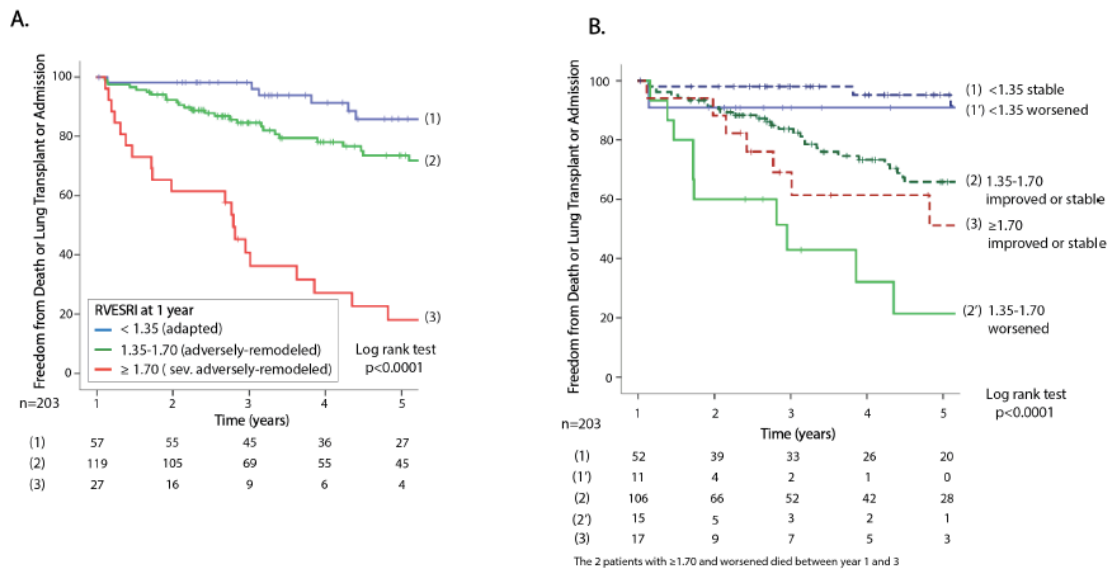


Figure S5. Five-year Kaplan Meier survival curves of RVESRI at 1 year according to RVESRI thresholds of adaptation for the primary endpoint of death, transplant or admission (A) and according to baseline RVESRI adaptation groups (B).



Study 2: Load Adaptability in Patients With Pulmonary Arterial Hypertension.

Authors: Myriam Amsallem MD MS^{1,2,3}, David Boulate MD PhD³, Marie Aymami MD MS^{1,2}, Julien Guihaire MD PhD³, Mona Selej MD MS^{1,4}, Jennie Huo MD^{1,2}, Andre Denault MD PhD⁵, Michael V. McConnell MD MSEE^{1,2}, Ingela Schnittger MD^{1,2}, Elie Fadel MD PhD³, Olaf Mercier MD PhD³, Roham T. Zamanian MD PhD^{4,6*} and Francois Haddad MD^{1,2,6*}

Affiliations:

¹ Division of Cardiovascular Medicine – Stanford University School of Medicine, Stanford, USA.

² Stanford Cardiovascular Institute – Stanford University School of Medicine, Stanford, USA.

³ Research and Innovation Laboratory Inserm U999 and Division of Cardiothoracic Surgery, Marie Lannelongue Hospital, Paris Sud University, Le Plessis Robinson, France.

⁴ Division of Pulmonary and Critical Care Medicine – Stanford University School of Medicine, Stanford, USA.

⁵ Department of Anesthesiology and Critical Care Division, Centre Hospitalier de l'Université de Montréal and Montreal Heart Institute, Montreal, Quebec, Canada

⁶ Vera Moulton Wall Center at Stanford – Stanford University School of Medicine, Stanford, USA.

Communications:

Published in *Am J Cardiol.* 2017;120:874-82. doi:10.1016/j.amjcard.2017.05.053.

Presented as a poster presentation at the 2016 American Heart Association Scientific Sessions (New Orleans, USA).

Summary: Several indices of right heart load adaptability have been proposed, although referring to different concepts: ventriculo-arterial coupling, simple ratio of function and load, or indices assessing whether the RV is well adapted, considering the load being subjected to. As recently suggested, RV function may follow an allometric function with load in PH (193).

In this study we hypothesized that using allometric modeling (i.e., $RV \text{ function or size} = a \cdot \text{Load}^b$, where a and b are constants) enables derivation of ratios of “proportional” load adaptability. This study is the first to critically evaluate and compare the different concepts associated with load-adaptability in a derivation and a validation cohort of patients with PAH. Our findings confirm the allometric relation between RV function-dimension and load, defining a method to quantify proportionality of adaptation. Patients with moderate dysfunction at a lower degree of elevation of resistance may warrant closer attention and more intense or combined specific therapies than other patients with moderate dysfunction at a higher degree of load. The clinical implication is the need to use allometric correction to load in multivariate models.

Our study is also the first to compare the prognostic value of right load adaptability metrics, including our validated allometric-based method to quantify the proportionality of RV adaptation. Although end-systolic-based load-adaptability metrics are helpful in risk stratifying patients, their incremental value to end-systolic structural indices is modest reinforcing the prognostic value of simple RV end-systolic structural indices in PAH.

Load Adaptability in Patients With Pulmonary Arterial Hypertension



Myriam Amsallem, MD, MS^{a,b,c,*}, David Boulate, MD, MS^c, Marie Aymami, MD, MS^{a,b}, Julien Guihaire, MD, PhD^c, Mona Selej, MD, MS^{a,d}, Jennie Huo, MD^{a,b}, Andre Y. Denault, MD, PhD^e, Michael V. McConnell, MD, MSEE^{a,b}, Ingela Schnittger, MD^{a,b}, Elie Fadel, MD, PhD^c, Olaf Mercier, MD, PhD^c, Roham T. Zamanian, MD, PhD^{d,f}, and Francois Haddad, MD^{a,b}

Right ventricular (RV) adaptation to pressure overload is a major prognostic factor in patients with pulmonary arterial hypertension (PAH). The objectives were first to define the relation between RV adaptation and load using allometric modeling, then to compare the prognostic value of different indices of load adaptability in PAH. Both a derivation (n = 85) and a validation cohort (n = 200) were included. Load adaptability was assessed using 3 approaches: (1) surrogates of ventriculo-arterial coupling (e.g., RV area change/end-systolic area), (2) simple ratio of function and load (e.g., tricuspid annular plane systolic excursion/right ventricular systolic pressure), and (3) indices assessing the proportionality of adaptation using allometric pressure-function or size modeling. Proportional hazard modeling was used to compare the hazard ratio for the outcome of death or lung transplantation. The mean age of the derivation cohort was 44 ± 11 years, with 80% female and 74% in New York Heart Association class III or IV. Mean pulmonary vascular resistance index (PVRI) was 24 ± 11 with a wide distribution (1.6 to 57.5 WU/m²). Allometric relations were observed between PVRI and RV fractional area change (R² = 0.53, p < 0.001) and RV end-systolic area indexed to body surface area right ventricular end-systolic area index (RVESAI) (R² = 0.29, p < 0.001), allowing the derivation of simple ratiometric load-specific indices of RV adaptation. In right heart parameters, RVESAI was the strongest predictor of outcomes (hazard ratio per SD = 1.93, 95% confidence interval 1.37 to 2.75, p < 0.001). Although RVESAI/PVRI^{0.35} provided small incremental discrimination on multivariate modeling, none of the load-adaptability indices provided stronger discrimination of outcome than simple RV adaptation metrics in either the derivation or the validation cohort. In conclusion, allometric modeling enables quantification of the proportionality of RV load adaptation but offers small incremental prognostic value to RV end-systolic dimension in PAH. © 2017 Elsevier Inc. All rights reserved. (Am J Cardiol 2017;120:874–882)

Right ventricular (RV) adaptation is a key determinant of survival in pulmonary arterial hypertension (PAH).^{1–3} Several indices of load adaptability have been proposed, although referring to different concepts: ventriculo-arterial coupling, simple ratio of function and load, or indices

assessing whether the RV is well adapted, considering the load being subjected to (Figure 1).⁴ Ventriculo-arterial coupling is measured as the ratio of ventricular to arterial elastance using pressure-volume loop analysis.^{5,6} Simplified, although less accurate, indices of coupling have been proposed, such as stroke volume (SV) divided by end-systolic volume, but this latter assumes that volume at pressure 0 passes through the origin.⁷ Ratiometric indices combining measures of load and function have also been used, but they fail to take into account the physiological dependence of load and function.^{8,9} The last category assessed whether ventricular dysfunction or enlargement is “proportional or disproportional” to the load imposed on the ventricle. As recently suggested, RV function may follow an allometric function with load in pulmonary hypertension (PH).¹⁰ We hypothesized that using allometric modeling (i.e., RV function or size = a·Load^b, where a and b are constants) enables derivation of ratios of “proportional” load adaptability. Our first objective was to confirm the allometric relation in multiple indices of RV function or remodeling and load in a derivation prospective cohort of patients with PAH undergoing almost simultaneous echocardiography and catheterization. Our second objective

^aDivision of Cardiovascular Medicine, Stanford University School of Medicine, Stanford, California; ^bCardiovascular Institute, Stanford University School of Medicine, Stanford, California; ^cDivision of Cardiothoracic Surgery, Marie Lannelongue Hospital, Le Plessis Robinson, France; ^dDivision of Pulmonary and Critical Care Medicine, Stanford University School of Medicine, Stanford, California; ^eDepartment of Anesthesiology and Critical Care Division, Centre Hospitalier de l'Université de Montréal and Montreal Heart Institute, Montreal, Quebec, Canada; and ^fVera Moulton Wall Center at Stanford, Stanford University School of Medicine, Stanford, California. Manuscript received March 14, 2017; revised manuscript received and accepted May 31, 2017.

Grant support: M. Amsallem received a Young Investigator Seed Grant from the Vera Moulton Wall Center, Stanford, USA, and O. Mercier received funding from the French National Research Agency (ANR-15-RHUS-0002).

See page 881 for disclosure information.

*Corresponding author: Tel: +1 (650) 799 0373; fax: (650) 725-1599. E-mail address: mamsalle@stanford.edu (M. Amsallem).

0002-9149/\$ - see front matter © 2017 Elsevier Inc. All rights reserved.
<http://dx.doi.org/10.1016/j.amjcard.2017.05.053>

www.ajconline.org

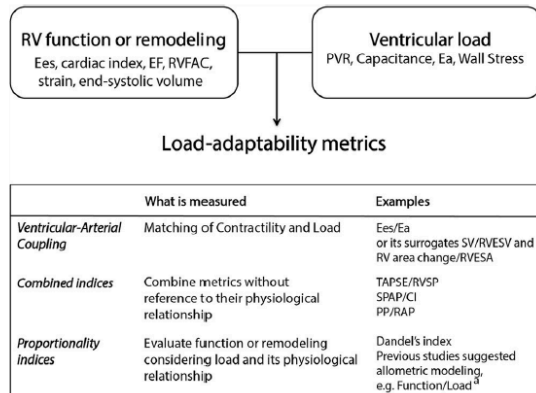


Figure 1. Load adaptability indices. Ea = arterial elastance and Ees = ventricular elastance both derived from pressure-volume loops; EF = ejection fraction; PP = pulse pressure; PVR = pulmonary vascular resistance; RAP = right atrial pressure; RVESV = end-systolic volume; RVESA = end-systolic area; RVFAC = fractional area change; SPAP = systolic pulmonary arterial pressure; SV = stroke volume; TAPSE = tricuspid annular plane systolic excursion.

was to compare the prognostic value of load-adaptability indices in the derivation and a validation cohort.

Methods

Two prospective cohorts of patients with established diagnosis of PAH (i.e., mean pulmonary arterial pressure [MPAP] ≥ 25 mm Hg and pulmonary arterial wedge pressure ≤ 15 mm Hg) referred to Stanford University Hospital and Clinics were included. The derivation cohort included 85 patients with idiopathic PAH or PAH of familial, drug, and toxin or connective tissue disease etiology who underwent, from August 2007 to June 2009, echocardiogram within 3 hours before catheterization (enabling close assessment of RV metrics and load). From 101 patients enrolled, 7 patients with congenital heart disease, 3 patients who required escalation of PH therapy between echocardiography and catheterization, 2 patients with technically difficult echocardiographic studies, 3 patients with active infection, and 1 with incomplete invasive data were excluded. Treatment and decision of lung transplantation was left to the discretion of the physicians according to clinical practice. To compare the derivation cohort with controls, we also included 1:1 age- and sex-matched healthy controls from the Stanford Healthy Aging research database in whom PH or heart failure was excluded by a 60-point health questionnaire, physical examination, and echocardiography. The validation cohort included 200 patients with idiopathic PAH or PAH of familial, drug, and toxin or connective tissue disease etiology who underwent both examinations within 3 months, from January 2007 to January 2014 (excluding patients from the derivation cohort). One-year follow-up echocardiograms were available in 179 patients. This study was approved by the Stanford University Institutional Review Board and conducted in agreement with the Helsinki II declaration, with written informed consent obtained from all participants.

Catheterization was performed through the internal jugular or right femoral vein, after local anesthesia, using mild se-

Table 1
Characteristics of patients with pulmonary arterial hypertension

Variable	n = 85
Age (years)	44 \pm 11
Women	68 (80%)
Body surface area (m ²)	1.84 \pm 0.23
Etiology	
- Idiopathic	31 (36%)
- Drugs and toxins	34 (40%)
- Connective tissue disease	20 (24%)
New York Heart Association functional class	II (26%); III (60%); IV (14%)
Diabetes mellitus	6 (7%)
Systemic hypertension	6 (7%)
Heart rate (bpm)	81 \pm 15
Systolic blood pressure (mmHg)	110 \pm 15
Right atrial pressure (mmHg)	12 \pm 7
Mean pulmonary arterial pressure (mmHg)	53 \pm 14
Mean pulmonary arterial pressure/Mean arterial pressure	0.64 \pm 0.17
Pulmonary capillary wedge pressure (mmHg)	10 \pm 4
Cardiac Index (L/min/m ²)	2.0 \pm 0.5
Stroke volume index (mL/m ²)	25 \pm 8
Pulmonary vascular resistance (WU)/indexed (WU.m ²)	13 \pm 6 / 24 \pm 11
Pulmonary capacitance (mL/mmHg)/indexed	1.0 \pm 0.6 / 0.56 \pm 0.32
Resistance Compliance time constant (s)	0.67 \pm 0.15
Pulmonary arterial elastance (mmHg/mL)	1.92 \pm 0.97
Serum creatinine (mg/dL)	1.04 \pm 0.36
Serum sodium (mEq/L)	137 \pm 3
Serum N-terminal pro B-type natriuretic peptide* (pg/mL)	869.5 [300.0–2023.3]
Prostanoid Therapy	33 (39%)
Phosphodiesterase Inhibitors	34 (40%)
Endothelin Receptor Blockers	22 (26%)
Warfarin	25 (29%)

Values are expressed as mean \pm SD or number (percentage) or median and interquartile range.

* NT-proBNP levels were available only for 56/85 patients.

dition as required.¹¹ Afterload was assessed by MPAP, pulmonary vascular resistance, capacitance, and arterial elastance (Ea). Pulmonary vascular resistance index (PVRI) was measured as transpulmonary gradient divided by cardiac index (CI). Capacitance was estimated as SV divided by pulse pressure (PP, i.e., difference between systolic and diastolic PAP).¹² Pulmonary arterial capacitance index was defined by indexing SV by the body surface area (using Du Bois formula). Pulmonary Ea was defined as systolic PAP \times 0.9 divided by SV.^{13,14} Pulmonary arterial wedge pressure was measured at the end of expiration; cardiac output was determined using the thermodilution method (or Fick method in case of severe tricuspid regurgitation), and right atrial pressure (RAP) was averaged over the cardiac cycle.

Digitized echocardiographic studies were acquired using Hewlett Packard Sonos 7500 or Philips IE 33 ultrasound systems (Philips, Andover, MA). All measures were averaged over 3 cycles according to latest guidelines^{15,16} by 2 blinded certified readers. Right heart dimensions were assessed using RV end-diastolic area, end-systolic area, and right atrial maximal area; all dimensions were indexed to body surface area (right ventricular end-diastolic area index

Table 2
Comparative echocardiographic characteristics and load adaptation of controls and patients with pulmonary arterial hypertension

Variable	Controls (n = 85)		Pulmonary Arterial Hypertension (n = 85)	
	Mean \pm SD	5 th -95 th perc.	Mean \pm SD	Ratio [†]
Age (years)	44 \pm 13	-	44 \pm 11	-
Women	68 (80%)	-	68 (80%)	-
Body surface area (m ²)	1.76 \pm 0.20	-	1.84 \pm 0.23*	-
Baseline Echocardiography				
Left ventricular internal diameter (mm)	50.0 \pm 4.4	42.6-58.7	40.5 \pm 6.2*	0.95
Left ventricular internal diameter indexed to height (mm/m)	30.0 \pm 2.3	25.5-33.4	24.3 \pm 3.6*	0.95
Left ventricular ejection fraction (%)	62.1 \pm 4.8	53.7-70.0	62.4 \pm 11.3	-
RV end-diastolic area index (cm ² /m ²)	9.3 \pm 1.6	6.9-11.6	18.3 \pm 5.5*	1.58
RV end-systolic area index (cm ² /m ²)	5.2 \pm 1.0	3.7- 6.9	14.5 \pm 4.7*	2.10
Right atrial area index (mL/m ²)	7.5 \pm 1.6	4.8-10.9	14.8 \pm 5.8*	1.36
End-systolic eccentricity index	0.99 \pm 0.10	0.95-1.04	2.5 \pm 0.8*	2.50
RV fractional area change (%)	43.6 \pm 5.2	36.3-50.9	22.9 \pm 6.8*	0.63
Tricuspid annular plane systolic excursion (mm)	23.0 \pm 3.0	18.0-29.2	14.3 \pm 4.1*	0.79
RV free-wall longitudinal strain (absolute value, %)	25.7 \pm 2.4	21.7-29.1	13.4 \pm 4.0*	0.62
RV systolic pressure (mmHg)	19.4 \pm 2.5	15.0-24.0	81.0 \pm 19.7*	3.38
Right atrial pressure (mmHg)	3.4 \pm 1.3	1.0- 5.0	11.4 \pm 6.0*	2.28
Ventricular-Arterial Coupling indices				
RV area change/RV end-systolic area	0.8 \pm 0.2	0.6- 1.0	0.3 \pm 0.1*	0.50
Combined indices				
Tricuspid annular plane systolic excursion/RV systolic pressure	1.2 \pm 0.2	0.9- 1.6	0.2 \pm 0.1*	0.22
Systolic pulmonary arterial pressure/Cardiac index	-	-	47.3 \pm 18.7	-
Mean pulmonary arterial pressure/Cardiac index	-	-	29.6 \pm 11.9	-
Pulse pressure/ Right atrial pressure	-	-	5.9 \pm 4.2	-
Mean pulmonary arterial pressure/Right atrial pressure	-	-	6.0 \pm 3.7	-
Proportionality indices				
Diastolic Dandel's index	28.0 \pm 6.1	18.1-38.1	34.7 \pm 10.8*	0.91
Systolic Dandel's index	39.6 \pm 9.6	26.2-57.6	39.4 \pm 12.3	-

Values are expressed as mean \pm standard deviation, or median and interquartile range when appropriate, or number (percentage).

* p values < 0.05 for comparison between pulmonary arterial hypertension and controls were considered significant.

[†] Ratio of the mean PAH value divided by the 5th or the 95th percentile of controls when appropriate. RV: right ventricle. The tricuspid regurgitation signal was interpretable in 93% of controls and 86% of patients with pulmonary arterial hypertension.

[RVEDAI], right ventricular end-systolic area index [RVESAI], and right atrial area index [RAI]) and measured in the RV-focused apical 4-chamber view. End-systolic RV wall thickness was measured in end-systole in the subcostal view. RV systolic function was quantified using fractional area change (RVFAC), tricuspid annular systolic excursion (TAPSE), and free-wall Lagrangian longitudinal strain (RVLS).^{16,17} Pericardial effusion was considered significant when >0.5 cm in diastole. RV systolic pressure (RVSP) was estimated based on the modified Bernoulli equation applied to the peak tricuspid regurgitation velocity and estimated RAP.^{11,18} End-systolic RV wall stress was estimated as (RVSP \times RV end-systolic radius \times 0.5)/(RV end-systolic wall thickness), with radius being approximated by dividing the area (end-systolic area [RVESA]) by the length in end-systole.^{19,20}

The following load adaptation indices were assessed (Figure 1). RV area change/RVESA ratio was measured, similarly to the SV/end-systolic volume ratio, surrogate of the ventricular elastance to Ea ratio.²¹ Ratiometric included TAPSE/RVSP ratio,⁸ systolic pulmonary arterial pressure/CI ratio,²² MPAP/CI ratio, pulmonary artery pulsatility index (PP/RAP), and MPAP/RAP ratio.⁹ Proportionality indices included the Dandel index as the velocity-time integral of the tricuspid regurgitation signal normalized for the average RV radius described

in end-diastole (velocity-time integral of the tricuspid regurgitation signal \times RVED length/RVEDA)²³ and the modified systolic Dandel index using the same formula in end-systole.

The primary combined end point was all-cause mortality or need for lung transplantation during follow-up. Death was verified by an independent investigator through the Stanford Pulmonary Hypertension database and the National Social Security Death Index; transplantation was verified through chart review. Patients who underwent transplantation were censored at the time of surgery. All patients from the derivation cohort completed 5-year follow-up. As the last patient from the validation cohort was included in January 2014, we decided to assess outcomes at 3 years for the validation cohort.

Statistical analysis was performed using SPSS Statistics 19 (SPSS Inc, Chicago, IL). Data are summarized as mean \pm SD for continuous variables (if normally distributed) and number of subjects (%) for categorical variables. Comparisons between groups were performed using 2-sided Student *t* tests if normally distributed or Mann-Whitney if not. The relations between RV size or function and afterload were modeled using allometric function and compared with linear and logarithmic functions. Regression analysis was used to determine the correlation coefficient (R²). Load adaptability using allometric modeling was measured as RV function or

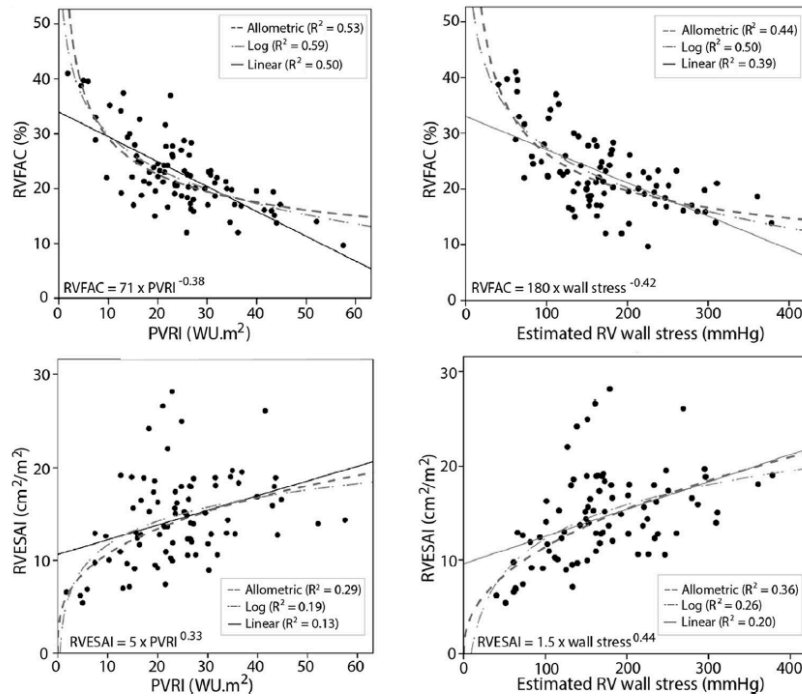


Figure 2. Modeling of the relationship between right ventricular function (RVFAC) or size (RVESAI) and afterload ($n = 85$). Linear (line), logarithmic (dot-line-dot), and allometric function (dashed line) curves are expressed by the regression coefficient (R^2 , all $p < 0.001$). Allometric functions ($Function = a \times Load^b$) were preferably used over logarithmic models ($Function = c + d \times \log(Load)$) to define load-adaptation indices, because of the absence of constant (c), enabling use of simple ratios ($Function/Load^b$) for the following analyses. Allometric formulas are displayed on each panel. PVRI = pulmonary vascular resistance index; RVESAI = right ventricular end-systolic area index; RVFAC = RV fractional area change.

size divided by the load^b, where b is the allometric coefficient of survivors as we hypothesized that survivor relation would represent “adapted” RV. The coefficient of the total population was similar and gave consistent results. Cox proportional hazard models were used to determine correlates of outcome in the derivation cohort at 5 years and in the validation cohort at 3 years. Hazard ratios were normalized for 1 SD. The incremental value of load adaptation indices to function or size indices was assessed by comparison of the chi-square values. Correlates of progression in RV dilation at 1 year (defined as increase in $>15\%$ in RVESAI) was assessed using univariate and multivariate regression model (using forward stepwise mode), and expressed as odds ratio per SD (OR^{SD}). The results were considered significant when 2-sided p values were <0.05 . There was a good concordance between measures of RV parameters ($n = 20$ patients) performed at 3-month intervals: intraclass coefficient was 0.84 for RVFAC and 0.93 for RVESAI.

Results

The mean age of the derivation cohort ($n = 85$) was 44 ± 11 years with 80% of women (Table 1). Patients had a wide range of disease severity: PVRI (1.6 to 57.5 WU/m²), RVFAC (9.7% to 46.8%), and SV index (9.9 to 51.2 ml/m²).

During the 5-year follow-up, 24 patients had a primary event (7 underwent lung transplantations of whom 3 died and 21 patients died), and no patient was lost to follow-up. Estimated survival rates (death or need of transplant) were 84.7% at 1 year, 75.3% at 2 years, 71.8% at 3 years, and 63.5% at 5 years. Patients with PAH had worse load adaptability indices than controls (Table 2). Figure 2 shows allometric modeling of the relation between RV function (RVFAC) or size (RVESAI) and afterload (resistance or estimated wall stress). We used the allometric coefficients of the relations of transplant-free survivors at 5 years ($n = 54$), making the assumption that it would correspond to a better-compensated state (Figure 3). A high-resistance adaptation $RVESAI/PVRI^{0.35}$ index indicated RV enlargement higher than what would be expected for the given level of resistance. Similarly, a low $RVFAC/PVRI^{-0.38}$ indicated lower function than what would be expected for the level of resistance. Median $RVESAI/PVRI^{0.35}$ was 4.7 (3.8 to 5.7) and median $RVFAC/PVRI^{-0.38}$ was 71.3 (63.1 to 80.2). Although allometric adjustment was able to correct for the influence of load (PVRI), it did not correct for differences in baseline size or function, as illustrated by the colinear relation between $RVESAI/PVRI^{0.35}$ and RVESAI ($R^2 = 0.74$, $p < 0.0001$) in Figure 3. Finally, variability of the load-adaptation index $RVESAI/PVRI^{0.35}$ was higher in

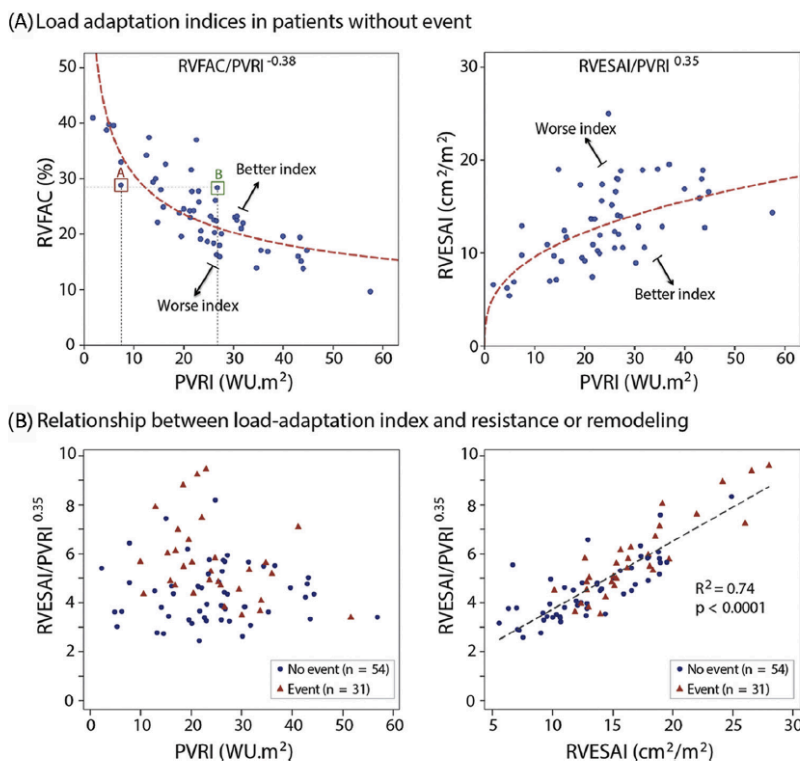


Figure 3. Relationships between right ventricular function (RVFAC), size (RVESAI), and pulmonary resistance (PVRI) in transplant-free survivors at 5 years (n = 54), defining load-adaptation indices (A). Relationship between load adaptation index and PVRI and RVESAI (B). (A) Despite having more severe pulmonary hypertension (as demonstrated with higher PVRI 26.8WU/m² for patient B vs 7.4WU/m² for patient A), patient B has a similar function to patient A (RVFAC of 28%). The load adaptation ratio (RVFAC/PVRI^{-0.38}) could help to differentiate these patients: for RVFAC/PVRI^{-0.38} = 98.9 for B vs 61.8 for A). (B) Pearson correlation is shown as R². Load adaptation is not correlated to PVRI (p = 0.24) but remains correlated with RVESAI.

patients with moderate load, moderate RV enlargement (Figure 3), or moderate RV dysfunction.

Univariate correlates of death or lung transplant at 5 years for clinical, echocardiographic, and hemodynamic variables (Table 3) and load-adaptation indices (Table 4) were performed in the derivation cohort. In contrast to structural and functional parameters, afterload parameters (PVRI, pulmonary artery capacitance index, Ea, and RV wall stress) were not associated with outcomes. Relative pressure (MPAP/MAP) and RAP were the 2 hemodynamic metrics strongly associated with outcomes. When these were considered into a multivariate model, they were independently associated with outcomes. Figure 4 shows the incremental value of echocardiographic metrics to the model (MPAP/MAP and RAP). Models that included load adaptation indices had better incremental prognostic value than models including RVFAC or RVESAI. RVESAI/PVRI^{0.35} had higher chi-square value than RVFAC/PVRI^{-0.38}.

The mean age of the validation cohort (n = 200) was 49 ± 14 years with 78% of women (Table 5). Patients had a wide range of disease severity: PVRI (2.7 to 54.4 WU/m²), RVFAC (10.8% to 49.7%), and cardiac index (1.1 to 4.8 L/min/m²). At 3-year follow-up, 37 patients had a primary event (11 underwent lung

transplantation of whom 3 died and 26 additional patients died), and 3 patients were lost to follow-up. Estimated single-year survival rates (death or need of transplant) were 90.8% at 1 year, 86.1% at 2 years, and 79.9% at 3 years. RV end-systolic remodeling index (RVESAI and RVESAI/PVRI^{0.35}) were also strongly associated with outcomes (Table 5). Load adaptation indices RV area change/RVESA, TAPSE/RVSP, and Dandel indices were significantly associated with outcomes. Figure 4 shows the small incremental predictive value of RVESAI/PVRI^{0.35} and RVESAI over the MPAP/MAP and RAP model (both p ≤ 0.01). Both the allometric indices RVESAI/PVRI^{0.35} (OR^{SD} = 1.52 [1.04 to 2.21], p = 0.03) and RVESAI (OR^{SD} = 1.51 [1.02 to 2.22], p = 0.04) were significantly associated with RV enlargement progression at 1 year in the 179 patients with echocardiogram follow-up. When we put RVESAI and RVESAI/PVRI^{0.35} in a bivariate model, RVESAI/PVRI^{0.35} was retained in the model (chi-square = 129.3).

Discussion

This study critically evaluates the different concepts associated with load-adaptability in PAH, validating an

Table 3
Univariate Cox regression analysis of correlates of death or lung transplant at 5 years in patients with pulmonary arterial hypertension (n = 85)

Variable	Hazard ratio*	95% CI	p value
Age (years)	0.71	0.50–1.12	0.09
Women	0.48	0.23–1.15	0.06
Connective tissue disease	1.18	0.53–2.63	0.69
New York Heart Association functional class (III/IV vs. II)	1.88	0.72–4.89	0.20
Systolic blood pressure (mmHg)	0.86	0.63–1.35	0.43
Systolic blood pressure <110 mmHg	1.76	0.81–3.81	0.16
Heart rate (bpm)	1.78	1.16–2.36	<0.01
Laboratory data			
Hyponatremia (<136 mEq/L)	2.72	1.23–6.12	0.01
Renal dysfunction [†]	1.82	0.90–3.70	0.09
Log N-terminal proB-type natriuretic peptide	1.73	1.03–2.98	0.04
Echocardiogram			
RV end-diastolic area index (cm ² /m ²)	1.87	1.31–2.61	<0.001
RV end-systolic area index (cm ² /m ²)	1.93	1.37–2.75	<0.001
Right atrial area index (cm ² /m ²)	1.40	1.08–1.92	0.01
Systolic Eccentricity Index	1.49	1.06–2.08	0.02
RV fractional area change (%)	0.65	0.41–0.93	0.03
Tricuspid annular plane systolic excursion (cm)	0.75	0.52–1.10	0.14
RV longitudinal strain (absolute value, %)	0.71	0.49–1.00	0.06
RV myocardial performance index	1.25	0.86–1.81	0.25
Estimated RV wall stress (mmHg)	1.00	0.49–2.03	0.17
Severe tricuspid regurgitation	2.60	1.28–5.27	<0.01
Estimated right atrial pressure (mmHg)	1.68	1.19–2.44	<0.01
Estimated right ventricular systolic pressure (mmHg)	1.10	1.00–2.17	0.04
Pericardial effusion	1.50	0.72–3.14	0.28
Hemodynamics			
Mean pulmonary arterial pressure (mmHg)	1.50	1.00–2.22	0.05
Mean pulmonary arterial pressure/Mean arterial pressure	1.60	1.11–2.31	0.01
Pulmonary vascular resistance index (Wood Units.m ²)	1.00	0.65–1.37	0.82
Capacitance index (mL/mmHg/m ²)	0.86	0.58–1.28	0.45
Arterial elastance (mmHg/mL)	1.03	0.73–1.44	0.88
Stroke volume index (mL/m ²)	0.92	0.65–1.39	0.73
Cardiac index (L/min/m ²)	1.20	0.87–1.66	0.27
Mean right atrial pressure (mmHg)	1.75	1.33–2.44	<0.001

* Hazard ratios are presented as HR per standard deviation for continuous variables and calculated as HR^{SD}.

[†] Renal dysfunction was defined as creatinine clearance <60 mL/min using the MDRD formula.

RV = right ventricle.

allometric-based method to quantify the proportionality of RV adaptation. Although end-systolic-based load-adaptability metrics are helpful in risk stratifying patients, their incremental value to end-systolic structural indices is modest.

Previous studies have highlighted the great variability of ventricular adaptation to load particularly in patients with moderate elevation of pulmonary load.^{5,6,10,23} Patients with the worst adaptation do not have necessarily the highest load. However, most of the studies assessing the proportionality of load adaptation used linear modeling. Stevens et al first suggested, using cardiac magnetic resonance in diverse etiologies of PH, that RV function and load can be approximated using allometric relations.⁹ Interestingly, their allometric coefficients were in a similar range to the one we found, although with different populations. As in Stevens et al's cohort, our coefficients of determination were higher for functional parameters than for remodeling parameters. In addition to confirming this allometric relation, our study proposes a derived method to assess proportionality of adaptation. Allometric-adjusted indices (such as RVESAI/PVRI^{0.35}) enabled adjustment from load but remained colinear to the dimension or function metric. We

further explored the implications of allometric correction for risk stratification. The cohorts are representative of prevalent PAH cohorts as illustrated by the survival similar to the REVEAL cohort's²⁴ and because many of the predictors of outcome in REVEAL or others' risk scores were found. Allometric RVESAI/PVRI^{0.35} was significantly associated with outcomes in both cohorts, but its incremental value to MPAP/MAP, RAP, and RVESAI appeared modest. In addition, RVESAI/PVRI^{0.35} showed value in predicting RV enlargement progression at 1 year in the validation cohort.

There was a recent interest in simple combined indices of load adaptability such as TAPSE/RVSP⁸ or the pulsatility index.⁹ The first index reflects RV length-force relation. It was validated in left heart failure with reduced or preserved ejection fraction, but it does not take into account the physiological dependence of load and function, as TAPSE usually decreases with increasing load.⁸ Although related to outcome in our second cohort, TAPSE/RVSP did not have a stronger predictive value than RV size or function. Dandel et al proposed in 2013 a diastolic index associated with RV function recovery after left ventricular assist device implantation,²²

Table 4

Univariate Cox regression analysis of load adaptation correlates of death or lung transplant at 5 years in patients with pulmonary arterial hypertension (n = 85)

Variable	Hazard ratio*	95% CI	p value
Ventricular-Arterial Coupling			
RV area change/RV end-systolic area	0.77	0.52–1.14	0.19
Combined indices			
Tricuspid annular plane systolic excursion/RV systolic pressure	0.58	0.30–1.11	0.10
Pulse pressure/Right atrial pressure	0.51	0.30–0.89	0.02
Mean pulmonary arterial pressure /Right atrial pressure	0.61	0.37–0.99	0.048
Systolic pulmonary arterial pressure/Cardiac index	0.93	0.66–1.30	0.66
Mean pulmonary arterial pressure/Cardiac index	0.99	0.70–1.39	0.93
Proportional indices			
Diastolic Dandel's index	0.66	0.44–1.00	0.05
Modified systolic Dandel's index	0.68	0.44–1.04	0.07
RVESAI/PVRI ^{0.35}	1.95	1.44–2.65	<0.0001
RVESAI/ wall stress ^{0.48}	1.71	1.26–2.32	0.001
RVFAC/PVRI ^{-0.38}	0.61	0.41–0.89	0.01
RVFAC/wall stress ^{-0.46}	0.83	0.57–1.15	0.27

* Hazard ratios are presented as HR per standard deviation for continuous variables and calculated as HR^{SD}. P-values >0.10 were considered as significant. PVRI = pulmonary vascular resistance index; RV = right ventricle; RVESAI: end-systolic area indexed on body surface area; RVFAC = fractional area change. The tricuspid regurgitation was interpretable in 86% of patients and thus Tricuspid annular plane systolic excursion/RV systolic pressure and Dandel's indices were available in only 86% of patients.

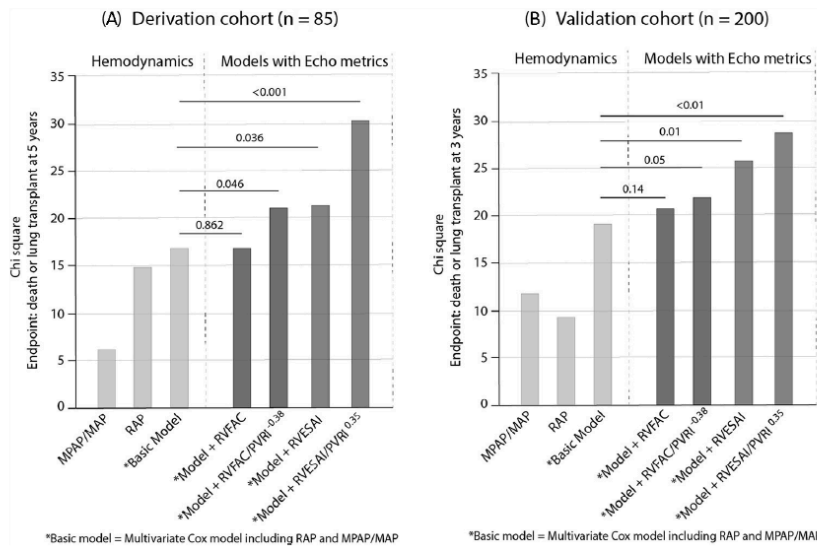


Figure 4. Incremental value of RVFAC, RVESAI, or respective load-adaptation metrics for prediction of outcomes at 5 years in the derivation cohort (A) or at 3 years in the validation cohort (B). Variables are entered in multivariate Cox model using enter mode. MAP = mean arterial pressure; MPAP = mean pulmonary arterial pressure; PVRI = pulmonary vascular resistance index; RAP = right atrial pressure; RVESAI = right ventricular end-systolic area index; RVFAC = fractional area change.

further validated in 79 patients with PAH awaiting lung transplantation as it was associated with the risk of RV failure and transplant-free survival at 1 and 3 years.²³ Although the original diastolic index and modified systolic index were both validated in our cohorts, these indices require the presence of an interpretable tricuspid regurgitation Doppler signal, which is not available in all patients.

This study is also the first to date to compare previously described load-adaptation indices. The variability in statis-

tical significance of association between indices and outcome between our 2 cohorts highlights the importance of validation in a field in which most metrics have been reported in single-derivation cohorts. Overall, a consistent finding in both cohorts is the strong prognostic value of RV end-systolic dimension (simple echocardiographic metric). The importance of end-systolic remodeling, first described by Carabello et al, is consistent with recent magnetic resonance and 3-dimensional echocardiographic studies.^{25–27}

Table 5
Characteristics of the validation cohort (n = 200) and univariate Cox regression analysis of correlates of death or lung transplant at 5 years

Variable	Mean \pm SD	Hazard ratio*	95% CI	p value
Age (years)	49 \pm 14	1.26	0.95 – 1.67	0.11
Women	156 (78%)	1.00	0.52 – 1.92	0.99
Connective tissue disease	68 (34%)	1.26	0.71 – 2.21	0.43
New York Heart Association functional class (III/IV vs. II)	I (8%); II (40%); III (45%); IV (7%)	3.00	1.64 – 5.52	<0.001
Echocardiogram				
RV end-diastolic area index (cm ² /m ²)	18.8 \pm 6.0	1.68	1.38 – 2.06	<0.001
RV end-systolic area index (cm ² /m ²)	13.9 \pm 5.3	1.66	1.36 – 2.03	<0.001
Right atrial area index (cm ² /m ²)	12.2 \pm 4.5	1.62	1.30 – 2.03	<0.001
RV fractional area change (%)	27.1 \pm 7.0	0.61	0.45 – 0.81	0.001
Tricuspid annular plane systolic excursion (mm)	17.6 \pm 4.6	0.77	0.58 – 1.03	0.08
RV longitudinal strain (absolute value, %)	17.2 \pm 4.8	1.64	1.21 – 2.22	0.001
Estimated RV systolic pressure (mmHg)	77.3 \pm 20.6	1.50	1.13 – 1.99	0.01
Hemodynamics				
Mean pulmonary arterial pressure (mmHg)	49.6 \pm 15.9	1.27	1.00 – 1.60	0.048
Mean pulmonary arterial pressure/Mean arterial pressure	0.59 \pm 0.22	1.65	1.26 – 2.16	<0.001
Pulmonary vascular resistance index (Wood Units.m ²)	19.2 \pm 10.3	1.31	1.02 – 1.70	0.03
Cardiac index (L/min/m ²)	2.1 \pm 0.7	1.11	0.83 – 1.49	0.47
Mean right atrial pressure (mmHg)	8.4 \pm 5.3	1.49	1.17 – 1.91	0.001
Load adaptation indices				
RV area change/RV end-systolic area	0.4 \pm 0.1	0.56	0.38 – 0.78	0.001
Tricuspid annular plane systolic excursion/RV systolic pressure	0.3 \pm 0.1	0.90	0.38 – 0.86	0.01
Pulse pressure/Right atrial pressure	8.5 \pm 7.4	0.78	0.55 – 1.12	0.17
Mean pulmonary arterial pressure/Right atrial pressure	8.6 \pm 7.9	0.76	0.52 – 1.12	0.17
Systolic pulmonary arterial pressure/Cardiac index	40.9 \pm 17.4	1.27	0.84 – 1.67	0.07
Mean pulmonary arterial pressure/Cardiac index	25.2 \pm 10.6	1.30	0.90 – 1.68	0.06
Diastolic Dandel's index	36.7 \pm 9.9	0.64	0.47 – 0.88	0.01
Modified systolic Dandel's index	43.5 \pm 12.6	0.61	0.45 – 0.85	0.01
RVESA/PVRI ^{0.35}	5.2 \pm 1.8	1.55	1.28 – 1.88	<0.001
RVFAC/PVRI ^{0.38}	77.9 \pm 18.4	0.82	0.63 – 1.10	0.17

* Hazard ratios are presented as HR per SD for continuous variables and calculated as HR^{SD}.

PVRI = pulmonary vascular resistance index; RV = right ventricle; RVESA = RV end-systolic area; RVFAC = RV fractional area change.

The first clinical implication of this study is to confirm the allometric relation between RV function-dimension and load, defining a method to quantify proportionality of adaptation. Patients with moderate dysfunction at a lower degree of elevation of resistance may warrant closer attention and more intense or combined specific therapies than other patients with moderate dysfunction at a higher degree of load. The second implication is the need to use allometric correction to load in multivariate models.

The first limitation derives from the fact that there is no ideal population to study RV adaptation; we chose 2 populations with prevalent PAH and wide ranges of disease severity. The second limitation comes from the delay between echocardiograms and catheterization: <3 hours in the derivation cohort (reducing the risk of variability); it was up to 3 months in the validation cohort. This enabled to first assess accurately physiology of the relation between ventricular metrics and load in the derivation cohort, and then more in a “clinical practice” setting in the validation cohort, as catheterization is often not performed at each assessment. The third limitation may come from the use of the allometric coefficient of survivors to define load adaptability indices, hypothesizing that the relation in survivor would better approximate RV adaptation. The coefficients of the total population were similar than the coefficients of the survivors, and provided the same results in terms of prognosis.

In conclusion, this study confirms the allometric relation between RV size or function and load, enabling quantification of the proportionality of ventricular adaptation. Although associated with outcomes, the incremental value of allometric-derived metrics to RV end-systolic dimension is modest, reinforcing the prognostic value of simple RV end-systolic structural indices in PAH.

Acknowledgment: The authors would like to thank the Stanford Cardiovascular Institute and the Vera Moulton Wall Center of Pulmonary Hypertension at Stanford for their support, and Zoe Kooreman and Guillaume Fadel for their help in collecting data. M. Amsallem received a Young Investigator Seed Grant from the Vera Moulton Wall Center. F. Haddad received funds from Pai Chan Lee Research fund. O. Mercier received funds from the French National Research Agency (ANR-15-RHUS-0002). M.V. McConnell previously received cardiac MRI research support from GE Healthcare and is currently on partial leave of absence while an employee at Verily Life Sciences. None of the authors have any potential conflicts of interest relative to the study.

Disclosures

The authors have no conflicts of interest to disclose.

- Vonk-Noordegraaf A, Haddad F, Chin KM, Forfia PR, Kawut SM, Lumens J, Naeije R, Newman J, Oudiz RJ, Provencher S, Torbicki A, Voelkel NF, Hassoun PM. Right heart adaptation to pulmonary arterial hypertension: physiology and pathobiology. *J Am Coll Cardiol* 2013;62:22–33.
- Galiè N, Humbert M, Vachiery J-L, Gibbs S, Lang I, Torbicki A, Simonneau G, Peacock A, Vonk-Noordegraaf A, Beghetti M, Ghofrani A, Gomez Sanchez MA, Hansmann G, Klepetko W, Lancellotti P, Matucci M, McDonagh T, Pierard LA, Trindade PT, Zompatori M, Hoeper M, Aboyans V, Vaz Carneiro A, Achenbach S, Agewall S, Allanore Y, Asteggiano R, Paolo Badano L, Albert Barberà J, Bouvaist H, Bueno H, Byrne RA, Carerj S, Castro G, Erol Ç, Falk V, Funck-Brentano C, Gorenflo M, Granton J, Jung B, Kiely DG, Kirchhof P, Kjellström B, Landmesser U, Lekakis J, Lionis C, Lip GYH, Orfanos SE, Park MH, Piepoli MF, Ponikowski P, Revel M-P, Rigau D, Rosenkranz S, Völler H, Luis Zamorano J. 2015 ESC/ERS Guidelines for the diagnosis and treatment of pulmonary hypertension: the Joint Task Force for the Diagnosis and Treatment of Pulmonary Hypertension of the European Society of Cardiology (ESC) and the European Respiratory Society (ERS). Endorsed by: Association for European Paediatric and Congenital Cardiology (AEPC), International Society for Heart and Lung Transplantation (ISHLT). *Eur Heart J* 2016;37:67–119.
- Amsallem M, Kuznetsova T, Hanneman K, Denault A, Haddad F. Right heart imaging in patients with heart failure: a tale of two ventricles. *Curr Opin Cardiol* 2016;31:469–482.
- Sanz J, Garcia-Alvarez A, Fernández-Friera L, Nair A, Mirelis JG, Sawit ST, Pinney S, Fuster V. Right ventriculo-arterial coupling in pulmonary hypertension: a magnetic resonance study. *Heart* 2012;98:238–243.
- Vanderpool RR, Pinsky MR, Naeije R, Deible C, Kosaraju V, Bunner C, Mathier MA, Lacomis J, Champion HC, Simon MA. RV-pulmonary arterial coupling predicts outcome in patients referred for pulmonary hypertension. *Heart* 2015;101:37–43.
- Trip P, Kind T, van de Veerdonk MC, Marcus JT, de Man FS, Westerhof N, Vonk-Noordegraaf A. Accurate assessment of load-independent right ventricular systolic function in patients with pulmonary hypertension. *J Heart Lung Transplant* 2013;32:50–55.
- Guazzi M, Bandera F, Pelissero G, Castelvécchio S, Menicanti L, Ghio S, Temporelli PL, Arena R. Tricuspid annular plane systolic excursion and pulmonary arterial systolic pressure relationship in heart failure: an index of right ventricular contractile function and prognosis. *Am J Physiol Heart Circ Physiol* 2013;305:1373–1381.
- Kang G, Ha R, Banerjee D. Pulmonary artery pulsatility index predicts right ventricular failure after left ventricular assist device implantation. *J Heart Lung Transplant* 2016;35:67–73.
- Stevens GR, Garcia-Alvarez A, Sahni S, Garcia MJ, Fuster V, Sanz J. RV dysfunction in pulmonary hypertension is independently related to pulmonary artery stiffness. *JACC Cardiovasc Imaging* 2012;5:378–387.
- Amsallem M, Sternbach JM, Adigopula S, Kobayashi Y, Vu TA, Zamanian R, Liang D, Dhillon G, Schnittger I, McConnell MV, Haddad F. Addressing the controversy of estimating pulmonary arterial pressure by echocardiography. *J Am Soc Echocardiogr* 2016;29:93–102.
- Mahapatra S, Nishimura RA, Sorajja P, Cha S, McGoon MD. Relationship of pulmonary arterial capacitance and mortality in idiopathic pulmonary arterial hypertension. *J Am Coll Cardiol* 2006;47:799–803.
- Kelly RP, Ting CT, Yang TM, Liu CP, Maughan WL, Chang MS, Kass DA. Effective arterial elastance as index of arterial vascular load in humans. *Circulation* 1992;86:513–521.
- Chemla D, Antony I, Lecarpentier Y, Nitenberg A. Contribution of systemic vascular resistance and total arterial compliance to effective arterial elastance in humans. *Am J Physiol Heart Circ Physiol* 2003;285:614–620.
- Rudski LG, Lai WW, Afalalo J, Hua L, Handschumacher MD, Chandrasekaran K, Solomon SD, Louie EK, Schiller NB. Guidelines for the echocardiographic assessment of the right heart in adults: a report from the American Society of Echocardiography endorsed by the European Association of Echocardiography, a registered branch of the European Society of Cardiology, and the Canadian Society of Echocardiography. *J Am Soc Echocardiogr* 2010;23:685–788.
- Lang RM, Badano LP, Mor-Avi V, Afalalo J, Armstrong A, Ernande L, Flachskampf FA, Foster E, Goldstein SA, Kuznetsova T, Lancellotti P, Muraru D, Picard MH, Rietzschel ER, Rudski L, Spencer KT, Tsang W, Voigt J-U. Recommendations for cardiac chamber quantification by echocardiography in adults: an update from the American Society of Echocardiography and the European Association of Cardiovascular Imaging. *J Am Soc Echocardiogr* 2015;28:1–39.
- Voigt J-U, Pedrizzetti G, Lysyansky P, Marwick TH, Houle H, Baumann R, Pedri S, Ito Y, Abe Y, Metz S, Song JH, Hamilton J, Sengupta PP, Koliaas TJ, d'Hooge J, Aurigemma GP, Thomas JD, Badano LP. Definitions for a common standard for 2D speckle tracking echocardiography: consensus document of the EACVI/ASE/Industry Task Force to standardize deformation imaging. *Eur Heart J Cardiovasc Imaging* 2015;16:1–11.
- Amsallem M, Boulate D, Kooreman Z, Zamanian RT, Fadel G, Schnittger I, Fadel E, McConnell MV, Dhillon G, Mercier O, Haddad F. Investigating the value of right heart echocardiographic metrics for detection of pulmonary hypertension in patients with advanced lung disease. *Int J Cardiovasc Imaging* 2017;33:825–835. doi:10.1007/s10554-017-1069-3.
- Norton JM. Toward consistent definitions for preload and afterload. *Adv Physiol Educ* 2001;25:53–61.
- Lurz P, Puranik R, Nordmeyer J, Muthurangu V, Hansen MS, Schievano S, Marek J, Bonhoeffer P, Taylor AM. Improvement in left ventricular filling properties after relief of right ventricle to pulmonary artery conduit obstruction: contribution of septal motion and interventricular mechanical delay. *Eur Heart J* 2009;30:2266–2274.
- Boulate D, Mercier O, Guihaire J, Fadel E, Naeije R, Haddad F, Richard F. Pulmonary circulatory—right ventricular uncoupling: new insights into pulmonary hypertension pathophysiology. In: *Pulmonary Hypertension: Basic Science to Clinical Medicine*. Switzerland: Springer International Publishing; 2016.
- Saydain G, Awan A, Manickam P, Kleinow P, Badr S. Pulmonary hypertension an independent risk factor for death in intensive care unit: correlation of hemodynamic factors with mortality. *Clin Med Insights Circ Respir Pulm Med* 2015;9:27–33.
- Dandel M, Knosalla C, Kemper D, Stein J, Hetzer R. Assessment of right ventricular adaptability to loading conditions can improve the timing of listing to transplantation in patients with pulmonary arterial hypertension. *J Heart Lung Transplant* 2015;34:319–328.
- Dandel M, Potapov E, Krabatsch T, Stepanenko A, Löw A, Vierecke J, Knosalla C, Hetzer R. Load dependency of right ventricular performance is a major factor to be considered in decision making before ventricular assist device implantation. *Circulation* 2013;128:14–23.
- Benza RL, Miller DP, Gomberg-Maitland M, Frantz RP, Foreman AJ, Coffey CS, Frost A, Barst RJ, Badesch DB, Elliott CG, Liou TG, McGoon MD. Predicting survival in pulmonary arterial hypertension: insights from the Registry to Evaluate Early and Long-Term Pulmonary Arterial Hypertension Disease Management (REVEAL). *Circulation* 2010;122:164–172. doi:10.1161/CIRCULATIONAHA.109.898122.
- Carabello BA, Spann JF. The uses and limitations of end-systolic indexes of left ventricular function. *Circulation* 1984;69:1058–1064.
- Ryo K, Goda A, Onishi T, Delgado-Montero A, Tayal B, Champion HC, Simon MA, Mathier MA, Gladwin MT, Gorcsan J. Characterization of right ventricular remodeling in pulmonary hypertension associated with patient outcomes by 3-dimensional wall motion tracking echocardiography. *Circ Cardiovasc Imaging* 2015;8:e003176.
- Amsallem M, Sweatt AJ, Aymami MC, Kuznetsova T, Selej M, Lu H, Mercier O, Fadel E, Schnittger I, McConnell MV, Rabinovitch M, Zamanian RT, Haddad F. Right heart end-systolic remodeling index strongly predicts outcomes in pulmonary arterial hypertension: comparison with validated models. *Circ Cardiovasc Imaging* 2017;10:pii: e005771.

Study 3: Non-invasive Right Ventricular Load Adaptability in Patients with Scleroderma-Associated Pulmonary Arterial Hypertension

Authors: Myriam Amsallem MD MS^{1*}, Sarah French MD^{2*}, Nadia Ouazani MD^{1*}, Shufeng Li³, Kristina Kudelko, MD⁴, Roham T. Zamanian MD^{4,5}, Francois Haddad MD MS^{1**} and Lorinda Chung MD MS^{6,7**}

Affiliations:

¹Division of Cardiovascular Medicine, Stanford University Medical Center, Stanford, CA, USA

²Division of Internal Medicine, Stanford University Medical Center, Stanford, CA, USA

³Division of Biostatistics, Stanford University Medical Center, Stanford, CA, USA

⁴Division of Pulmonary and Critical Care Disease, Stanford University Medical Center, Stanford, CA, USA

⁵Vera Moulton Wall Center for Pulmonary Hypertension at Stanford, Stanford, Palo Alto, CA, USA

⁶Division of Rheumatology, Stanford University Medical Center, Stanford, CA, USA

⁷Division of Rheumatology, Palo Alto VA Healthcare System, Palo Alto, CA, USA

* and ** Authors contributed equally to the study.

Communications:

Published in *Pulmonary Circulation* 2018;8(3):2045894018788268. doi:10.1177/2045894018788268.

Presented as a poster presentation at the 2016 American College of Rheumatology/ARHP Annual Meeting (Washington DC, USA).

Summary: Systemic sclerosis (i.e. scleroderma) is a connective tissue disease characterized by fibrosis and vascular remodeling that can affect multiple organ systems, including the pulmonary arterial tree. Scleroderma-associated pulmonary arterial hypertension (SSc-PAH) occurs in 8-13% of patients and is associated with a median survival of 3 years after diagnosis (13,242,243). Despite similar level of afterload, SSc-PAH has been associated with worse outcomes than other forms of PAH including idiopathic PAH (IPAH), as well as PAH secondary to other connective tissue diseases as shown in the REVEAL Registry (Registry to Evaluate Early And Long-term PAH Disease Management) (60,244–246).

Different non-invasive indices of load adaptability have been proposed in the literature in patients with heart failure or pulmonary hypertension. The first objective of this study was to compare right heart size, function and RV load adaptability between patients with incident SSc-PAH or IPAH. The second objective was to compare therapeutic response in terms of right heart remodeling and load adaptability indices in the two groups. Finally, our third objective was to explore potential difference in clinical outcomes in the SSc-PAH or IPAH groups, recognizing the limitation due to small sample size.

Our study is one of the first providing “deep” RV adaptation phenotyping of patients with incident scleroderma-associated PAH. Resting load-adaptability metrics do not significantly differ between SSc-PAH and IPAH and do not appear to capture the increased risk of heart failure and mortality in SSc-PAH. Consistent with previous studies, our exploratory analysis suggests worse 1-year outcomes in SSc-PAH and shows less improvement in RV remodeling in response to therapy in SSc-PAH than IPAH. In conclusion, resting non-invasive load adaptability indices at baseline and 1 year follow-up do not appear to capture the complexity of ventricular adaptation and increased risk of heart failure in patients with SSc-PAH, and other modalities such as exercise testing or CMR should be assessed in future studies.

Non-invasive right ventricular load adaptability indices in patients with scleroderma-associated pulmonary arterial hypertension

Sarah French¹, Myriam Amsallem^{2,3}, Nadia Ouazani², Shufeng Li⁴, Kristina Kudelko⁵, Roham T. Zamanian^{5,6}, Francois Haddad² and Lorinda Chung^{7,8}

¹Division of Internal Medicine, Stanford University Medical Center, USA; ²Division of Cardiovascular Medicine, Stanford University Medical Center, USA; ³Research and Innovation Unit, INSERM U999, DHU Torino, Paris Sud University, Marie Lannelongue Hospital, France; ⁴Division of Biostatistics, Stanford University Medical Center, USA; ⁵Division of Pulmonary and Critical Care Disease, Stanford University Medical Center, USA; ⁶Vera Moulton Wall Center for Pulmonary Hypertension at Stanford, Palo Alto, USA; ⁷Division of Rheumatology, Stanford University Medical Center, USA; ⁸Division of Rheumatology, Palo Alto VA Healthcare System, Palo Alto, USA

Abstract

Scleroderma-associated pulmonary arterial hypertension (SSc-PAH) is associated with worse outcome than idiopathic pulmonary arterial hypertension (IPAH), potentially due to worse right ventricular adaptation to load as suggested by pressure–volume loop analysis. The value of non-invasive load-adaptability metrics has not been fully explored in SSc-PAH. This study sought to assess whether patients with incident SSc-PAH have worse echocardiographic load-adaptability metrics than patients with IPAH. Twenty-two patients with incident SSc-PAH were matched 1:1 with IPAH based on pulmonary vascular resistance. Echocardiographic load-adaptability indices were divided into: surrogates of ventriculo-arterial coupling (e.g. right ventricular area change/end-systolic area), indices reflecting the proportionality of load adaptation (e.g. tricuspid regurgitation velocity-time integral normalized for average right ventricular radius), and simple ratios (e.g. tricuspid annular plane systolic excursion/right ventricular systolic pressure). The prognostic value of these indices for clinical worsening (i.e. death, transplant, or hospitalization for heart failure) at one year was explored. The two groups were comprised of patients of similar age, with similar cardiac index, pulmonary resistance, capacitance and NT-proBNP levels ($p > 0.10$). There was no difference in baseline right ventricular dimension, function or load-adaptability indices. At one year, eight (36.4%) SSc-PAH patients had experienced clinical worsening (eight hospitalizations and two deaths) versus one hospitalization in the IPAH group. Load adaptation at one year in survivors was not worse in SSc-PAH ($p > 0.33$). Patients with IPAH responded better to therapy than SSc-PAH in terms of reduction of right ventricular areas at one year ($p < 0.05$). Right ventricular load-adaptability echocardiographic indices do not appear to capture the increased risk of negative outcomes at one year associated with SSc-PAH.

Keywords

connective tissue disease, echocardiography, outcomes, pulmonary arterial hypertension, right ventricle, scleroderma

Date received: 2 April 2018; accepted: 20 June 2018

Pulmonary Circulation 2018; 8(3) 1–11

DOI: 10.1177/2045894018788268

Introduction

Systemic sclerosis (i.e. scleroderma) is a connective tissue disease characterized by excess fibrosis and vascular remodeling that can affect multiple organ systems, including the pulmonary arterial tree.¹ Scleroderma-associated pulmonary arterial hypertension (SSc-PAH) occurs in 8–13% of patients and is associated with a median survival of three

years after diagnosis.^{2–4} Despite a similar level of afterload, SSc-PAH has been associated with worse outcomes than other forms of pulmonary arterial hypertension including idiopathic (IPAH) as well as pulmonary arterial

Corresponding author:

Myriam Amsallem, 300 Pasteur Drive, CA 94305, Stanford, USA.

Email: mamsalle@stanford.edu

 Creative Commons Non Commercial CC BY-NC: This article is distributed under the terms of the Creative Commons Attribution-NonCommercial 4.0 License (<http://www.creativecommons.org/licenses/by-nc/4.0/>) which permits non-commercial use, reproduction and distribution of the work without further permission provided the original work is attributed as specified on the SAGE and Open Access pages (<https://us.sagepub.com/en-us/nam/open-access-at-sage>).

© The Author(s) 2018.
Reprints and permissions:
sagepub.co.uk/journalsPermissions.nav
journals.sagepub.com/home/pul



hypertension secondary to other connective tissue diseases, as shown in the Registry to Evaluate Early And Long-term PAH Disease Management (REVEAL Registry).⁵⁻⁹

Several factors have been alleged to contribute to this increased mortality: increased prevalence of left ventricular dysfunction and comorbidities such as renal impairment, but also intrinsically worse right ventricular (RV) adaptation to load.^{4,5,7,10} A mechanistic and invasive study by Tedford et al. compared the RV pressure-volume relation in seven patients with SSc-PAH and five with IPAH, suggesting altered ventriculo-arterial coupling in SSc-PAH.¹¹ Coupling, which refers to matching between contractility and afterload, was invasively measured as the ventricular elastance (Ees) over arterial elastance (Ea) ratio (Ees/Ea).¹² However, a recent larger study has failed to replicate these results when assessing coupling using an invasive and magnetic resonance imaging combined Ees/Ea ratio.⁹

Different non-invasive indices of right load adaptability have been proposed in the literature in patients with heart failure or pulmonary hypertension.^{13,14} These indices can be divided into three categories (as presented in Fig. 1): surrogates of ventriculo-arterial coupling, indices assessing the proportionality of adaptation, and simple ratio of function and load.¹⁵⁻¹⁷ The present study tested the hypothesis that patients with SSc-PAH have worse resting right load adaptability using echocardiography than patients with IPAH matched for load (using pulmonary vascular resistance). The value of these indices of load adaptability has not been compared between patients with incident SSc-PAH and IPAH.

The first objective was to compare baseline right heart dimensions, function and RV load adaptability between patients with incident SSc-PAH or IPAH. The second objective was to compare therapeutic response in terms of right heart remodeling and load-adaptability indices in the two groups. The third objective was to explore potential differences in clinical outcomes in the SSc-PAH or IPAH groups and the prognostic value of load-adaptation indices.

Methods

Patients with pulmonary arterial hypertension

Between November 2002 and April 2015, 56 patients with SSc-PAH were included in the prospective observational Vera Moulton Wall Center Pulmonary Hypertension database at Stanford. Stanford University Institutional Review Board approved the study, which was conducted in agreement with the Helsinki-II-Declaration; all patients gave written informed consent. This study first included all consecutive adults with incident SSc-PAH (SSc-PAH group) and 1:1 pulmonary vascular resistance-matched patients with incident IPAH (IPAH group), who all underwent right heart catheterization during this period, as presented in Fig. 2. Inclusion criteria were: diagnosis of pulmonary arterial hypertension according to latest guidelines (mean pulmonary arterial pressure (MPAP) ≥ 25 mmHg and pulmonary arterial wedge pressure ≤ 15 mmHg)¹⁸ and baseline echocardiogram available within three months of catheterization. Patients in the SSc-PAH group met American College of Rheumatology/European League Against

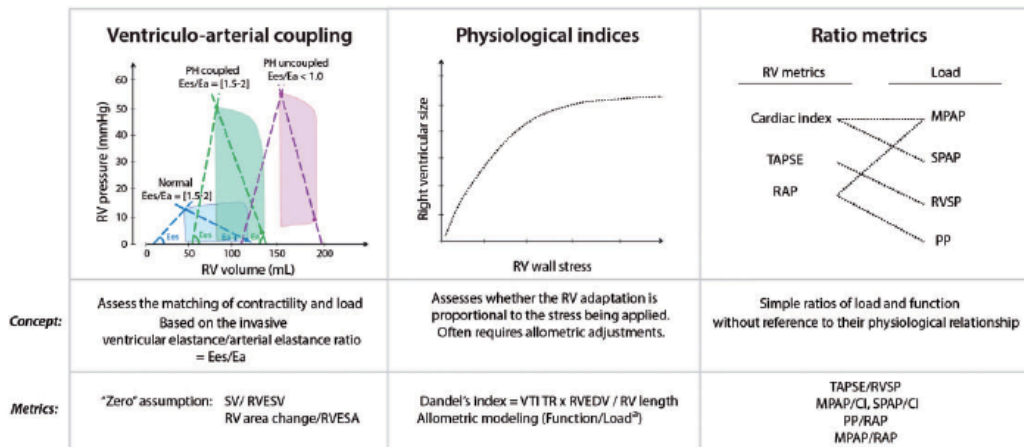


Fig. 1. Right ventricular load-adaptability indices.

CI: cardiac index; Ea: arterial elastance; Ees: ventricular elastance; MPAP: mean pulmonary arterial pressure; PH: pulmonary hypertension; PP: pulse pressure; RAP: right atrial pressure; RV: right ventricular; RVEDV: right ventricular end-diastolic volume; RVESA: right ventricular end-systolic area; RVESV: right ventricular end-systolic volume; RVSP: right ventricular systolic pressure; SPAP: systolic pulmonary arterial pressure; SV: stroke volume; TAPSE: tricuspid annular plane systolic excursion; VTI TR: velocity time integral using continuous Doppler signal of the tricuspid regurgitation

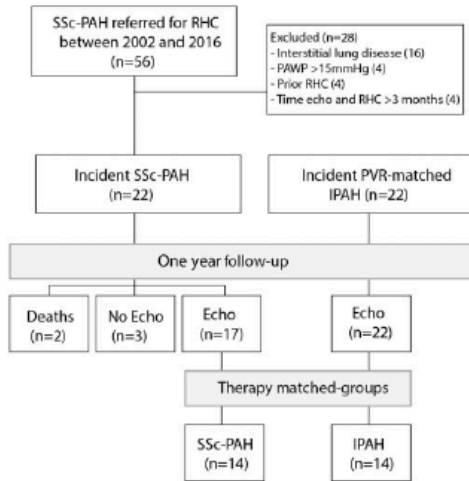


Fig. 2. Study design.

echo: follow-up echocardiogram available at one year; IPAH: idiopathic pulmonary arterial hypertension; PAWP: pulmonary arterial wedge pressure; PVR: pulmonary vascular resistance; RHC: right heart catheterization; SSc-PAH: scleroderma-associated pulmonary arterial hypertension

Rheumatism 2013 criteria for scleroderma.¹⁹ Patients were excluded from the study if they had evidence of severe interstitial lung disease (defined as having moderate or severe interstitial lung disease on chest X-ray or high resolution computed tomography and pulmonary function tests with at least moderate restriction defined as forced vital capacity and/or total lung capacity <70% of the predicted value) or if they had evidence of increase left ventricular filling pressure (pulmonary arterial wedge pressure >15 mmHg). Treatments and decisions regarding referral for lung transplantation were left to the discretion of the treating physicians according to current clinical practice.

Healthy controls

In order to compare the incident SSc-PAH cohort with controls, we also included 1:1 age- and sex-matched healthy controls from the Stanford Healthy Aging research database, in whom pulmonary hypertension or heart failure was excluded by a 60-point health questionnaire, physical exam and echocardiography.

Right heart catheterization

Catheterization was performed through the internal jugular or right femoral vein, after local anesthesia, using mild sedation as required.²⁰ Right atrial pressure, MPAP, systolic (SPAP) and diastolic pulmonary arterial pressures, and cardiac output were measured. Pulmonary arterial wedge pressure was measured at the end of expiration.

Pulmonary vascular resistance was measured as transpulmonary gradient divided by cardiac output and indexed to body surface area using the DuBois formula adjusted to the ideal weight and gender (PVRI). Pulmonary arterial capacitance was estimated as stroke volume divided by pulse pressure (difference between SPAP and diastolic pulmonary arterial pressures), and indexed on body surface area.²¹ Pulmonary arterial elastance was defined as SPAP \times 0.9 divided by stroke volume.^{22,23}

Echocardiography

Resting echocardiographic studies were acquired using Philips IE 33 ultrasound systems (Philips, Andover, MA, USA). All measures were averaged over three cycles and performed according to latest guidelines.^{24,25} Two blinded cardiologists measured all echocardiograms. Right heart dimensions were measured on RV-focused apical four-chamber view using RV end-diastolic area, RV end-systolic area (RVESA) and right atrial maximal area; all indexed to body surface area. RV systolic function was quantified using fractional area change (RVFAC), tricuspid annular plane systolic excursion (TAPSE), and free-wall Lagrangian longitudinal strain (RVLS). Pericardial effusion was considered significant when >0.5 cm in diastole.²⁶ RV systolic pressure (RVSP) was estimated based on the modified Bernoulli equation applied to the peak tricuspid regurgitation velocity and estimated right atrial pressure.²⁰ Inter-observer variability for RV measurements in our laboratory has been recently published.²⁶

Right load adaptation

As a surrogate of ventriculo-arterial coupling, we measured the RV area change/RVESA ratio, similar to the previously reported stroke volume/end-systolic volume ratio.¹² Proportionality indices included the Dandel's index described in end-diastole (velocity-time integral of the tricuspid regurgitation signal \times RV length/RV area)¹⁷ and the index derived from the allometric relation between RV function (RVFAC or RVLS) and load (PVRI) as recently published:¹⁴ RV function/load^{coefficient}. The allometric modeling of the function/load relationship was first demonstrated by Stevens et al. in a magnetic resonance based study in patients with suspected pulmonary hypertension, and recently confirmed in patient with PAH.^{14,27} Simple ratio metrics included the TAPSE/RVSP ratio,¹⁵ the SPAP/cardiac index ratio,²⁸ the MPAP/cardiac index ratio, the pulmonary artery pulsatility index (pulse pressure/right atrial pressure), and the MPAP/right atrial pressure ratio.²⁹

Clinical and laboratory characteristics

New York Heart Association functional class, six-minute walking distance (m), diffusing capacity of the lung for

carbon monoxide, serum creatinine and derived MDRD calculation of creatinine clearance, and serum N-terminal pro-B type natriuretic peptide (NT-proBNP; Roche Diagnostics, Mannheim, Germany) were also collected when available within one year of inclusion. The REVEAL score was calculated as previously published⁶ in patients with all criteria available. Low risk was defined by a score between 0 and 7, average if equal to 8, moderately high if equal to 9, high if equal to 10 or 11 and very high if ≥ 12 . Patients were combined into three groups (REVEAL 1=low, REVEAL 2–3=average/moderate–high, and REVEAL 4–5=high/very high) instead of the five original groups to obtain balanced groups in terms of number of patients. A modified REVEAL score was calculated excluding the connective tissue disease criteria, and classified as modified REVEAL I=low (0–6), REVEAL II–III=average/moderate high (7–8) and REVEAL IV–V=high/very high (≥ 9).

Exploratory outcomes analysis

Follow-up was concluded in September 2016. The combined end-point of clinical worsening was defined as death, lung transplantation or hospitalization for acute right heart failure (defined by more than 24 h of hospitalization). The secondary end-point consisted of death or lung transplant. One-year follow-up echocardiograms were available in 39 patients (93% of survivors). Patients were matched for therapy at one year in order to compare right heart remodeling, function and load adaptation in the two groups according to four categories: single oral agent, dual oral agent, intravenous (i.v.) prostacyclins and i.v. prostacyclins plus additional oral therapy. Inhaled prostacyclins ($n=1$ SSc-PAH and $n=4$ IPAH) were classified as “oral” agents.

Statistical analysis

Continuous variables are presented as median and interquartile range for values that were not normally distributed using the Wilcoxon–Mann–Whitney test and mean \pm standard deviation for normally distributed variables using Student’s *t*-test. Normality was assessed using the Shapiro–Wilk test. Categorical data are presented as number and percentage and compared using Fischer’s exact test. Cox proportional hazards regression univariate models were used to define association between SSc-PAH etiology, REVEAL score, RV dimension and function at baseline, and all load-adaptability indices at baseline with the primary endpoint and presented as hazard ratios and their 95% confidence intervals (95% CIs). In order to assess the influence of excluding the two patients who died before one year in the one-year analysis, sensitivity analyses were performed using imputation of the RV metrics from the latest echocardiography available prior to death (one month prior to death for both). All statistical analyses were performed using SPSS version 23.0 (IBM SPSS, Inc.,

Armonk, NY, USA). The results were considered significant when two-sided *p* values were < 0.05 .

Results

Baseline characteristics

Of the 56 SSc-PAH patients originally referred for catheterization, 22 SSc-PAH met inclusion criteria, matched to 22 IPAH (Figure 2). The average scleroderma disease duration from first non-Raynaud phenomenon symptom was 5.1 ± 2.4 years with a majority of patients with limited cutaneous scleroderma (90.9%); half displayed positive anti-centromere antibody. Baseline clinical characteristics and resting hemodynamics of patients with SSc-PAH and IPAH are presented in Table 1. Hemodynamics showed severe pulmonary hypertension in both groups, with significantly higher MPAP in patients with IPAH, despite being matched for pulmonary resistance and having similar moderately decreased cardiac index ($p=0.19$), capacitance or arterial elastance ($p>0.78$). There were no statistically significant differences in the six-minute walk distance, NT-proBNP or prevalence of renal insufficiency (\geq stage 3 of chronic kidney disease). A higher percentage of patients with SSc-PAH had high-risk REVEAL scores, even after excluding the connective tissue disease criteria. No patients were receiving treatment for pulmonary hypertension at baseline; however, two SSc-PAH patients were being treated with phosphodiesterase inhibitors for severe Raynaud’s phenomenon. As shown in Table 1, both groups had similarly increased right heart dimension and RV dysfunction. Most patients had moderate to severe RV dysfunction at baseline: 63.6% of SSc-PAH and 72.7% of IPAH using RVFAC ($\leq 25\%$) and 68.2% in both groups using RVLS (absolute value $\leq 15\%$). Despite similar left ventricular ejection fractions, patients with SSc-PAH had a larger left atrial dimension than IPAH patients ($p=0.01$).

Load-adaptation in SSc-PAH versus IPAH

Fig. 3 illustrates the variability of RV function (using RVFAC and RVLS) and afterload (using pulmonary vascular resistance), which can be modeled by a curvilinear relation, as previously demonstrated.^{14,27} The allometric relation allowed to derive indices of proportionality of load adaptation as previously reported:¹⁴ $RVFAC/PVRI^{-0.29}$ and $RVLS/PVRI^{-0.34}$. Among the several load-adaptability indices, the Dandel’s index tended to be better in patients with SSc-PAH than IPAH ($p=0.049$). None of the other indices were significantly different between the two groups (Table 1). The normalized values compared with the healthy reference group (95th or 5th percentile) are presented in Fig. 4. End-systolic dimensions presented on average a higher increase than end-diastolic dimensions. Values of the healthy cohort can be found in Supplementary Material Table S1 online.

Table 1. Comparative baseline clinical and echocardiographic characteristics of patients with incident idiopathic or scleroderma-associated pulmonary arterial hypertension.

	Scleroderma-associated PAH n = 22	Idiopathic PAH n = 22	p-value
Age, years	61.6 (53.4; 68.0)	52.0 (43.8; 66.1)	0.10
Female sex (%)	21 (95.5)	17 (77.3)	0.08
Adjusted body surface area, m ²	1.67 (1.55; 1.74)	1.75 (1.67; 1.83)	0.04
New York Heart Association functional class (%)			
I	1 (4.5)	0 (0)	0.32
II	2 (9.1)	8 (36.4)	0.03
III	13 (59.1)	10 (45.5)	<0.01
IV	6 (27.3)	4 (18.2)	0.48
6MWT distance, m	304.8 (182.9; 499.8)	411.5 (185.9; 518.2)	0.30
REVEAL score			
I (%)	4 (22.2)	9 (50.0)	0.09
2–3 (%)	2 (11.1)	5 (27.8)	0.21
4–5 (%)	12 (66.7)	4 (22.2)	<0.01
Modified REVEAL score ^a			
I (%)	4 (22.2)	6 (33.3)	0.46
II–III (%)	2 (11.1)	7 (38.9)	0.06
IV–V (%)	12 (66.7)	5 (27.8)	0.02
Hemodynamics			
Heart rate >92 beats/min	7 (31.8)	5 (22.7)	0.50
Systolic blood pressure <110 mmHg	5 (22.7)	1 (4.5)	0.08
Right atrial pressure, mmHg	6.5 (3.8; 12.3)	7.5 (4.8; 12.3)	0.67
Mean PAP, mmHg	47.5 (39.8; 52.3)	56.0 (45.8; 60.0)	0.01
Systolic PAP, mmHg	79.5 (63.0; 87.0)	94.0 (77.5; 101.3)	<0.01
Diastolic PAP, mmHg	27.5 (23.0; 35.0)	30.0 (29.0; 40.3)	0.11
Pulmonary arterial wedge pressure, mmHg	8.5 (6.0; 10.0)	9.5 (7.0; 12.3)	0.40
Cardiac index, L/min per m ²	1.9 (1.6; 2.0)	2.0 (1.8; 2.2)	0.19
Pulmonary vascular resistance, WU	12.1 (8.3; 15.7)	12.5 (8.8; 14.7)	0.99
Pulmonary vascular resistance indexed, WU.m ²	19.8 (14.6; 26.0)	21.6 (15.3; 25.8)	0.78
Pulmonary arterial capacitance, mL/mmHg	0.74 (0.63–1.06)	0.81 (0.65–1.09)	0.78
Pulmonary arterial capacitance indexed, mL.m ² per mmHg	1.22 (1.03–1.92)	1.41 (1.05–1.95)	0.61
Pulmonary arterial elastance, mmHg/mL	1.95 (1.40–2.29)	1.68 (1.36–2.87)	0.92
Laboratory data			
Anti-nuclear antibodies (%)	20 (91.0)	0	N/A
Anti-centromere antibodies (%)	11 (50.0)	0	N/A
Anti-Scl-70 antibodies (%)	1 (4.5)	0	N/A
Log(NT-proBNP)	7.7 (6.4; 7.9)	6.0 (4.8; 7.7)	0.52
Serum creatinine, mg/dL	1.1 (0.9; 1.2)	1.1 (0.9; 1.3)	0.97
Renal insufficiency (%)	12 (54.5)	7 (31.8)	0.13
Baseline therapy			
Phosphodiesterase inhibitors ^b	2 (9.1)	0 (0)	0.49
Echocardiography data			
RV end-diastolic area index, cm ² /m ²	15.8 (11.4; 18.8)	18.3 (13.5; 22.1)	0.10
RV end-systolic area index, cm ² /m ²	11.6 (7.6; 14.9)	14.8 (9.0; 18.4)	0.14
Right atrial area index, cm ² /m ²	13.0 (10.4; 16.1)	13.0 (9.9; 14.8)	0.74
RVFAC, %	25.0 (20.2; 27.6)	22.3 (19.4; 29.3)	0.47
TAPSE, mm	15.5 (11.8; 22.0)	17.0 (14.0; 18.3)	0.47

(continued)

Table 1. Continued

	Scleroderma-associated PAH n=22	Idiopathic PAH n=22	p-value
RVLS, absolute value, %	13.2 (9.7; 17.7)	12.8 (9.9; 18.0)	0.94
RVSP, mmHg	57.3 (40.6; 68.7)	62.7 (42.4; 70.4)	0.41
Left ventricular ejection fraction (%)	63.9 (54.7; 66.8)	63.1 (55.8; 69.2)	0.98
Left atrial area index, cm ² /m ²	9.8 (7.5; 11.9)	7.8 (6.5; 9.3)	0.01
Pericardial effusion	7 (31.8)	2 (9.1)	0.07
Ventricular-arterial coupling indices			
RV area change/RVESA	0.33 (0.25; 0.38)	0.29 (0.24; 0.41)	0.47
Combined indices			
TAPSE/RVSP	0.27 (0.19; 0.39)	0.27 (0.22; 0.40)	0.81
SPAP/cardiac index	42.7 (32.3; 49.8)	48.1 (33.2; 53.4)	0.39
MPAP/cardiac index	26.7 (20.1; 30.7)	26.4 (20.9; 30.4)	0.69
Pulse pressure/right atrial pressure	6.3 (4.2; 12.1)	7.5 (4.9; 10.9)	0.47
MPAP/right atrial pressure	6.0 (4.3; 10.6)	7.2 (4.3; 10.9)	0.67
Proportionality indices			
Dandel's index	42.9 (34.9; 47.1)	30.2 (27.2; 45.7)	0.049
RVFAC/PVRI ^{0.29}	57.2 (49.4; 65.0)	57.6 (42.8; 67.8)	0.80
RVLS/PVRI ^{-0.34}	37.9 (25.7; 42.1)	36.0 (28.0; 48.1)	0.66

Values are expressed as median (interquartile range) or number (percentage). Renal insufficiency was defined by stage 3 or more of chronic kidney disease. NT-proBNP levels were not available for five patients, REVEAL score in eight patients and 6MWT distance in two.

^aThe modified REVEAL score included all criteria except for the connective tissue disease criteria.

^bTwo patients were being treated with phosphodiesterase inhibitors for severe Raynaud phenomenon.

6MWT: six-minute walk test; MPAP: mean pulmonary arterial pressure; NT-proBNP; N-terminal pro-B type natriuretic peptide; PAH: pulmonary arterial hypertension; PAP: pulmonary arterial pressure; PVRI: pulmonary vascular resistance index; RV: right ventricular; RVESA: right ventricular end-systolic area; RVFAC: fractional area change; RVLS: RV free-wall longitudinal strain; RVSP: right ventricular systolic pressure; SPAP: systolic pulmonary arterial pressure; TAPSE: tricuspid annular plane systolic excursion

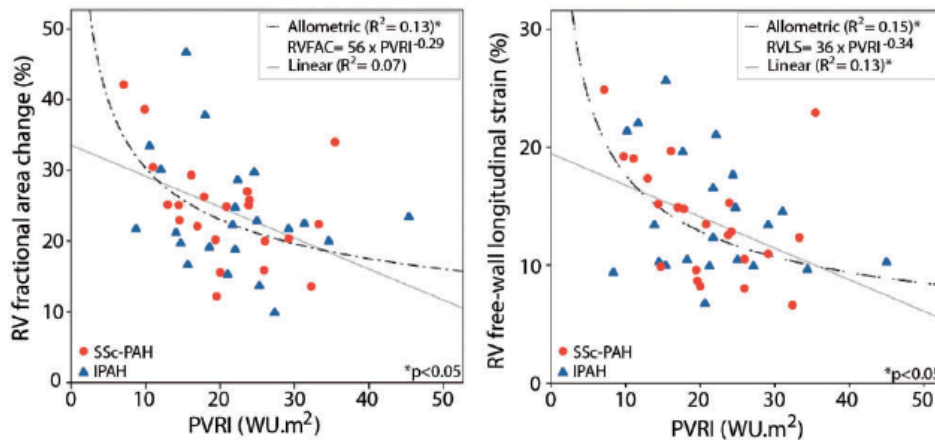


Fig. 3. Allometric relationship between load and right ventricular function in incident patients with SSc-PAH (dots) or IPAH (triangles).

IPAH: idiopathic pulmonary arterial hypertension; PVRI: pulmonary vascular resistance index; RV: right ventricular; RVFAC: right ventricular fractional area change; RVLS: right ventricular longitudinal strain; SSc-PAH: scleroderma-associated PAH

Exploratory outcome analysis

The mean follow-up was 3.0 ± 2.6 years. No patient was lost to follow-up at one year. The primary endpoint of death,

transplant or hospitalization was reached in eight (36.4%) patients in the SSc-PAH group (eight hospitalizations and two deaths) and one (4.6%) in the IPAH group (one hospitalization) at one year ($p = 0.02$). Event-free survival rate for

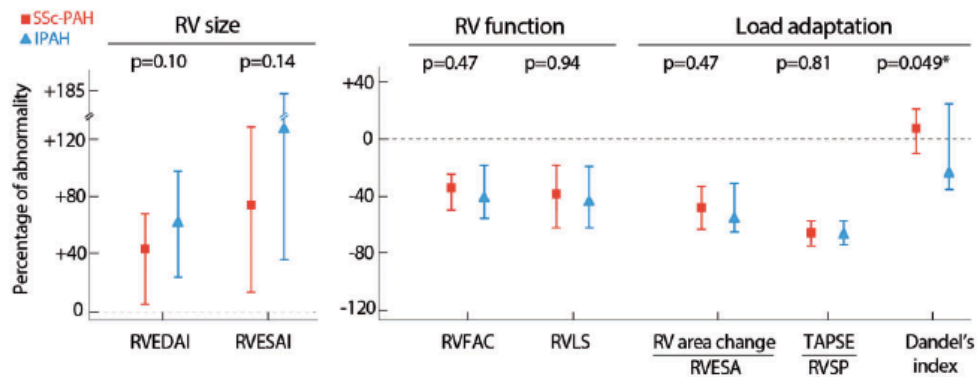


Fig. 4. Percentage of abnormal right ventricular size, function and adaptation to load in patients with incident SSc-PAH or IPAH. The percentage of abnormality was calculated according to the 95th or 5th percentile of the healthy controls ($n=22$), presented as median and interquartile range and compared using the Mann–Whitney test. Dandel's index is defined in end-diastole as [velocity-time integral of the tricuspid regurgitation signal \times RV length/RV area].

IPAH: idiopathic pulmonary arterial hypertension; RV: right ventricular; RVEDA: right ventricular end-diastolic area index; RVESA: right ventricular end-systolic area; RVESA: RVESA index; RVFAC: fractional area change; RVLS: right ventricular free-wall longitudinal strain; RVSP: right ventricular systolic pressure; SSc-PAH: scleroderma-associated pulmonary arterial hypertension; TAPSE: tricuspid annular plane systolic excursion

the primary endpoint (\pm standard error) was 79.5 ± 6.3 % at one year: 63.6 ± 10.5 % for patients with SSc-PAH and 95.5 ± 4.4 % patients with IPAH. The secondary end-point of death or transplant at one year was reached in two (9.1%) patients with SSc-PAH and none in patients with IPAH ($p=0.15$). In univariate analysis, only SSc-PAH etiology (hazard ratio 9.5, 95% confidence interval (1.2–76.1), $p=0.03$) and REVEAL score (hazard ratio 1.4 (1.1–1.9), $p < 0.01$) were significantly associated with the primary endpoint, while none of the baseline or changes in echocardiographic parameters including load-adaptability indices were associated with clinical worsening. None of the changes in RV metrics between baseline and follow-up echocardiography were significantly associated with the primary endpoint, even when performing imputation for the two non-survivors at one year (all $p > 0.13$).

One-year follow-up

At one year, in each group, five patients received a single oral agent, seven dual oral agents and two i.v. prostacyclins. There was no significant difference in terms of right heart dimensions at one year between the two groups in therapy-matched patients ($n=14$ SSc-PAH vs. 14 IPAH) as presented in Table 2. Both SSc-PAH and IPAH demonstrated improvement in RV function (as assessed by all metrics) and reverse right heart remodeling at one year. Patients with IPAH had better RV reverse remodeling at one year (as shown by RV areas) than SSc-PAH despite similar functional improvement and load reduction. Non-invasive load-adaptability metrics did not differ between the two groups at one year, while the Dandel's index improved in patients with IPAH. Similar results were found in

non-therapy matched patients with available follow-up echocardiogram at one year (17 SSc-PAH versus 22 IPAH), as presented in Supplementary Table S2. The two patients with SSc-PAH who died before one year (at eight months and 10.5 months) underwent echocardiography one month prior to death. Follow-up echocardiography showed marked RV enlargement ($+21$ % and $+8$ % increase in RV end-systolic area index) in the context of increased RVSP ($+144$ % and $+8$ %) outside the range of survivors with SSc-PAH (Supplementary Table S3). Among load-adaptability indices, only the TAPSE/RVSP ratio seemed to reflect RV worsening in these patients when compared with other patients with SSc-PAH. Sensitivity analysis imputing RV metrics (including load-adaptability indices) for the two non-survivors is presented in Supplementary Table S4, showing significant difference in changes in the Dandel's index between patients with SSc-PAH and IPAH.

Discussion

Our study is one of the first providing comprehensive RV adaptation phenotyping of patients with incident SSc-PAH using echocardiography. Indices of RV load-adaptability do not appear to capture the increased risk of heart failure and mortality in SSc-PAH. Consistent with previous studies, our exploratory analysis suggests worse one-year outcomes in SSc-PAH and shows less improvement in RV remodeling in response to therapy in SSc-PAH than in IPAH.^{7,30,31}

Our main hypothesis was that worse clinical outcomes in SSc-PAH might be partially explained by poor ventricular adaptation to pulmonary vascular load in comparison with other forms of pulmonary hypertension. Recent studies using hemodynamic monitoring with pressure–volume

Table 2. Evolution of right heart size, function and load adaptation at one year in therapy-matched patients with scleroderma-associated or idiopathic pulmonary arterial hypertension.

	Scleroderma-associated PAH <i>n</i> = 14	Idiopathic PAH <i>n</i> = 14	<i>p</i> -value
RV end-diastolic area index, cm ² /m ²	17.1 (10.9; 21.2)	14.2 (11.8; 17.3)	0.60
RV end-systolic area index, cm ² /m ²	12.3 (7.0; 17.0)	9.3 (7.5; 11.7)	0.57
Right atrial area index, cm ² /m ²	12.1 (8.6; 17.7)	10.4 (8.8; 11.2)	0.08
RVFAC, %	27.4 (17.7; 35.1)	33.3 (23.6; 36.5)	0.33
TAPSE, mm	18.0 (16.5; 20.8)	19.5 (17.8; 22.3)	0.29
RVLS, absolute value, %	17.4 (8.7; 21.5)	20.9 (14.6; 22.3)	0.18
RVSP, mmHg	51.8 (34.4; 74.7)	52.5 (38.1; 64.5)	0.98
Left ventricular ejection fraction, %	67.4 (64.8; 69.0)	66.6 (63.9; 68.9)	0.45
Left atrial area index, cm ² /m ²	10.1 (7.3; 12.2)	9.2 (7.9; 11.0)	0.67
Pericardial effusion	2 (14.3)	0 (0)	0.15
Load-adaptability indices at one year			
RV area change/RVESA	0.38 (0.21; 0.54)	0.50 (0.31; 0.58)	0.33
TAPSE/RVSP	0.31 (0.22; 0.58)	0.38 (0.32; 0.62)	0.40
Dandel's index	36.2 (31.1; 43.2)	41.4 (28.7; 55.5)	0.64
Delta change between one year and baseline			
Delta RV end-diastolic area index, %	-4.4 (-13.0; 10.8)	-13.0 (-37.1; -4.0)	0.04
Delta RV end-systolic area index, %	-13.3 (-18.6; 12.7)	-30.5 (-46.9; -5.3)	0.03
Delta right atrial area index, %	-3.8 (-19.4; 21.4)	-15.5 (-28.8; -3.1)	0.15
Delta RVFAC, %	21.9 (0.2; 33.0)	45.9 (-0.2; 92.5)	0.10
Delta TAPSE, %	16.7 (0; 53.5)	15.0 (0; 49.5)	0.95
Delta RVLS, %	15.4 (-7.6; 47.7)	50.6 (-2.0; 125.7)	0.18
Delta RVSP, %	-8.3 (-40.5; 15.4)	-1.7 (-22.6; 6.2)	0.98
Delta left ventricular ejection fraction, %	8.4 (0.3; 23.4)	5.3 (-6.1; 16.5)	0.08
Delta left atrial area index, %	3.1 (-1.6; 27.0)	16.3 (-5.6; 61.1)	0.45
Delta RV area change/RVESA, %	27.7 (0.3; 47.1)	69.3 (-0.12; 142.6)	0.15
Delta TAPSE/RVSP, %	33.3 (2.4; 111.8)	41.8 (-5.9; 98.1)	0.87
Delta Dandel's index, %	-3.9 (-19.2; 7.3)	15.6 (-0.5; 31.9)	0.03
6MWT at one year	<i>n</i> = 9	<i>n</i> = 14	
6MWT distance, m	322 (230; 402)	466 (320; 549)	0.31
Absolute delta 6MWT distance, m	48 (-25; 138)	284 (51; 459)	0.03
Laboratory data at one year	<i>n</i> = 8	<i>n</i> = 11	
NT-proBNP level, pg/mL	540 (138; 2241)	58 (46; 473)	0.08
Delta NT-proBNP level, %	-10 (-60; -10)	-90 (-100; -70)	0.09

Values are expressed as median (interquartile range) or number (percentage).

6MWT: six-minute walk test; NT-proBNP: N-terminal pro-B-type natriuretic peptide; PAH: pulmonary arterial hypertension; RV: right ventricular; RVESA: right ventricular end-systolic area; RVFAC: fractional area change; RVLS: right ventricular free-wall longitudinal strain; RVSP: right ventricular systolic pressure; TAPSE: tricuspid annular plane systolic excursion.

loop analysis have shown differences in contractility between SSc-PAH patients and other forms of PAH, both at rest and with exercise.^{11,8,32} Tedford et al. compared the pressure-volume relationship using right heart catheterization with Valsalva in seven patients with SSc-PAH and five with IPAH, showing altered RV coupling in SSc-PAH (Ees/Ea ratio 1.0 ± 0.5) compared with IPAH (Ees/Ea 2.1 ± 1.0, *p* = 0.03) despite similar afterload and cardiac index.¹¹ Hsu et al. performed a similar analysis of RV contractility during

exercise to compare contractile reserve in SSc-PAH versus IPAH.³² Despite similar resting RV function and morphology, SSc-PAH subjects had depressed RV functional reserve during exercise. Finally, Kelemen et al. showed that SSc-PAH patients (*n* = 35) had lower RV mass than IPAH patients (*n* = 18) with similar pulmonary resistance, reflecting a potential difference in adaptive hypertrophy.⁸

There has been recent interest in focusing on non-invasive surrogate markers of RV load adaptability. The RV area

change/RVESA ratio, similar to the previously reported stroke volume/end-systolic volume ratio as a surrogate of the Ees/Ea ratio, failed to distinguish SSc-PAH from IPAH in our study, showing the complexity of RV geometry. Ratio metrics (such as TAPSE/RVSP) address the question of how to best combine right heart function and load metrics into a simple index, to more accurately assess RV function and pulmonary hypertension. The TAPSE/RVSP ratio, proposed by Guazzi et al., is a simplified index of RV length-force relationship.¹⁵ A value less than 0.36 mm/mmHg was associated with an increased cardiovascular mortality (hazard ratio of 10.4 (5.4–19.8), $p < 0.001$) in 293 patients with heart failure with reduced or preserved ejection fraction.¹⁵ However, simple ratios may not address the question of disproportionality of adaptation, as the relationship between function and afterload follows a non-linear and often inverse fit.^{14,27} Dandel et al. proposed an index defined as delta pressure between the RV and the right atrium divided by the end-diastolic volume/length ratio.^{16,17} First demonstrated for the assessment of RV function recovery in patients with end-stage left heart failure on left ventricular assist devices,¹⁶ the prognostic value of this index was validated in 79 patients with PAH (including <8% with connective tissue disease) awaiting lung transplantation.¹⁷ A low index (reflecting excessive RV dilation and high right atrial pressure with relative low RV pressure) indicated impaired right heart adaptation to load and was associated with an increased risk of RV failure and worse transplant-free survival at one and three years.¹⁷ Although we found in our cohort a borderline significance ($p = 0.049$) for a higher Dandel's index at baseline in patients with SSc-PAH than in those with IPAH (which would suggest a better adaptation), taking into account the multiple comparison analysis performed, we can only conclude that this index was not able to capture the increased risk of patients with SSc-PAH in our cohort.

Although negative, our study has several features of originality including being the first to provide complete resting ventricular function and remodeling data in incident SSc-PAH and IPAH patients. In a field in which numerous RV metrics of remodeling, function and load adaptation are available, comparing those metrics head to head is necessary in order to understand which provide the most accurate prognostication for patients. Consistent with previous studies, our study did not show a difference in terms of echocardiographic simple RV functional metrics.¹⁰ However, unlike previous studies in which RV function was usually assessed by qualitative right heart dilation from reports or by the TAPSE (which gives limited information on lateral basal contraction),^{10,33} our study analyzed quantitative indices of right heart remodeling and function including novel indices of ventricular function such as RV longitudinal strain.^{34,35} In addition, our study comprehensively explored previously reported non-invasive load-adaptability metrics. Finally, the longitudinal assessment of these metrics at one year after introduction of therapy enables us to explore the

value of these metrics as markers of response to therapy, although larger randomized studies are needed.

Potential explanations for the worse intrinsic RV function in SSc-PAH need further investigation, but include the presence of myocardial fibrosis, inflammation, depressed sarcomeric function, microvascular disease or neurohumoral effectors.^{36,37} Cardiac magnetic resonance enabling extra-cellular matrix imaging by contrast enhancement or T1 mapping sequences could be potentially useful for detection of intrinsic RV differences in SSc-PAH and IPAH patients. Exercise or dobutamine echocardiography may also provide an alternative means to identify early RV dysfunction non-invasively, as exercise has been shown to detect those with early PAH^{38,39} and unmask ventriculo-arterial uncoupling in SSc-PAH.³²

This study has several limitations. First, it is a retrospective study performed in a prospective cohort with missing imaging data at one year in three survivors with SSc-PAH. Second, the stringent matching by resistance and pulmonary hypertension therapy resulted in a relatively small sample size, which may have hindered our ability to detect subtle differences in RV dysfunction and load adaptation. Similarly, the small number of patients and events during follow-up limits our confidence in interpreting relationship with outcomes. Third, pulmonary vascular resistance was used to match for load acknowledging that RV afterload is a dynamic interplay between resistance, capacitance and wave reflections. However, capacitance and estimation of arterial elastance did not significantly differ between the two groups at baseline. Lastly, in this cohort, patients did not undergo cardiac magnetic resonance imaging, thus RV mass could not be accurately assessed.

In conclusion, resting non-invasive right load-adaptability indices at baseline and one-year follow-up do not appear to capture the complexity of ventricular adaptation and increased risk of heart failure in patients with SSc-PAH. Other modalities such as exercise testing or extracellular imaging using cardiac magnetic resonance imaging should be assessed in future studies.

Acknowledgements

The authors would like to thank the Vera Moulton Wall Center at Stanford and Stanford Cardiovascular Institute for their support. Ethical approval: all procedures performed in studies involving human participants were approved by Stanford University Institutional Review Board in accordance with the ethical standards of the institutional and/or national research committee and with the 1964 Helsinki declaration and its later amendments or comparable ethical standards. Informed consent was obtained from all individual participants included in the study. Author contribution: SF, MA, FH and LC contributed equally to the study. SF and MA (co-first authors) have both equally contributed to the conception and design of the study, analysis and interpretation of data, drafting of the manuscript, and final approval of the version to be submitted. NO has contributed to collection of echocardiographic data and final approval of the manuscript. SL has contributed to the design of the study, statistical analysis and final

approval of the manuscript. KK and RTZ have contributed to the conception and design of the study, revising the article critically and final approval of the article. FH and LC (co-senior authors) have both equally contributed to the conception and design of the study, interpretation of data, revising the article critically and final approval of the manuscript.

Conflict of interest

The authors declare that there is no conflict of interest.

Funding

This work was supported by the Vera Moulton Wall Center (Young Investigator Seed Grant), the French National Research Agency as part of the second Investissements d'Avenir program (ANR-15-RHUS-0002) and the Pai Chan Lee Research Fund.

References

- Sundaram SM and Chung L. An update on systemic sclerosis-associated pulmonary arterial hypertension: A review of the current literature. *Curr Rheumatol Rep* 2018; 20: 10.
- Mukerjee D, St George D, Coleiro B, et al. Prevalence and outcome in systemic sclerosis associated pulmonary arterial hypertension: Application of a registry approach. *Ann Rheum Dis* 2003; 62: 1088–1093.
- Wigley FM, Lima JAC, Mayes M, et al. The prevalence of undiagnosed pulmonary arterial hypertension in subjects with connective tissue disease at the secondary health care level of community-based rheumatologists (the UNCOVER study). *Arthritis Rheum* 2005; 52: 2125–2132.
- Campo A, Mathai SC, Le Pavec J, et al. Hemodynamic predictors of survival in scleroderma-related pulmonary arterial hypertension. *Am J Respir Crit Care Med* 2010; 182: 252–260.
- Kawut SM, Taichman DB, Archer-Chicko CL, et al. Hemodynamics and survival in patients with pulmonary arterial hypertension related to systemic sclerosis. *Chest* 2003; 123: 344–350.
- Benza RL, Miller DP, Gomberg-Maitland M, et al. Predicting survival in pulmonary arterial hypertension: Insights from the Registry to Evaluate Early and Long-Term Pulmonary Arterial Hypertension Disease Management (REVEAL). *Circulation* 2010; 122: 164–172.
- Chung L, Farber HW, Benza R, et al. Unique predictors of mortality in patients with pulmonary arterial hypertension associated with systemic sclerosis in the REVEAL registry. *Chest* 2014; 146: 1494–1504.
- Kelemen BW, Mathai SC, Tedford RJ, et al. Right ventricular remodeling in idiopathic and scleroderma-associated pulmonary arterial hypertension: Two distinct phenotypes. *Pulm Circ* 2015; 5: 327–334.
- Swift AJ, Capener D, Johns C, et al. Magnetic resonance imaging in the prognostic evaluation of patients with pulmonary arterial hypertension. *Am J Respir Crit Care Med* 2017; 196: 228–239.
- Fisher MR, Mathai SC, Champion HC, et al. Clinical differences between idiopathic and scleroderma-related pulmonary hypertension. *Arthritis Rheum* 2006; 54: 3043–3050.
- Tedford RJ, Mudd JO, Giris RE, et al. Right ventricular dysfunction in systemic sclerosis-associated pulmonary arterial hypertension. *Circ Heart Fail* 2013; 6: 953–963.
- Boulate D, Mercier O, Guihaire J, et al. Pulmonary circulatory – right ventricular uncoupling: New insights into pulmonary hypertension pathophysiology. In: Maron BA, Zamanian RT and Waxman AB. (eds) *Pulmonary hypertension: Basic science to clinical medicine*. Basel, Switzerland: Springer International Publishing, 2016.
- Amsallem M, Kuznetsova T, Hanneman K, et al. Right heart imaging in patients with heart failure: A tale of two ventricles. *Curr Opin Cardiol* 2016; 31: 469–482.
- Amsallem M, Boulate D, Aymami M, et al. Load adaptability in patients with pulmonary arterial hypertension. *Am J Cardiol* 2017; 120: 874–882.
- Guazzi M, Bandera F, Pelissero G, et al. Tricuspid annular plane systolic excursion and pulmonary arterial systolic pressure relationship in heart failure: An index of right ventricular contractile function and prognosis. *Am J Physiol Heart Circ Physiol* 2013; 305: 1373–1381.
- Dandel M, Potapov E, Krabatsch T, et al. Load dependency of right ventricular performance is a major factor to be considered in decision making before ventricular assist device implantation. *Circulation* 2013; 128: 14–23.
- Dandel M, Knosalla C, Kemper D, et al. Assessment of right ventricular adaptability to loading conditions can improve the timing of listing to transplantation in patients with pulmonary arterial hypertension. *J Heart Lung Transplant* 2015; 34: 319–328.
- Galiè N, Humbert M, Vachiery J-L, et al. 2015 ESC/ERS Guidelines for the diagnosis and treatment of pulmonary hypertension: The Joint Task Force for the Diagnosis and Treatment of Pulmonary Hypertension of the European Society of Cardiology (ESC) and the European Respiratory Society (ERS): Endorsed by Association for European Paediatric and Congenital Cardiology (AEPC), International Society for Heart and Lung Transplantation (ISHLT). *Eur Heart J* 2016; 37: 67–119.
- Van den Hoogen F, Khanna D, Fransen J, et al. 2013 classification criteria for systemic sclerosis: An American College of Rheumatology/European League against Rheumatism collaborative initiative. *Arthritis Rheum* 2013; 65: 2737–2747.
- Amsallem M, Sternbach JM, Adigopula S, et al. Addressing the controversy of estimating pulmonary arterial pressure by echocardiography. *J Am Soc Echocardiogr* 2016; 29: 93–102.
- Mahapatra S, Nishimura RA, Sorajja P, et al. Relationship of pulmonary arterial capacitance and mortality in idiopathic pulmonary arterial hypertension. *J Am Coll Cardiol* 2006; 47: 799–803.
- Kelly RP, Ting CT, Yang TM, et al. Effective arterial elastance as index of arterial vascular load in humans. *Circulation* 1992; 86: 513–521.
- Chemla D, Antony I, Lecarpentier Y, et al. Contribution of systemic vascular resistance and total arterial compliance to effective arterial elastance in humans. *Am J Physiol Heart Circ Physiol* 2003; 285: 614–620.
- Rudski LG, Lai WW, Afilalo J, et al. Guidelines for the echocardiographic assessment of the right heart in adults: A report from the American Society of Echocardiography endorsed by the European Association of Echocardiography, a registered branch of the European Society of Cardiology, and the Canadian Society of Echocardiography. *J Am Soc Echocardiogr* 2010; 23: 685–713.

25. Lang RM, Badano LP, Mor-Avi V, et al. Recommendations for cardiac chamber quantification by echocardiography in adults: An update from the American Society of Echocardiography and the European Association of Cardiovascular Imaging. *J Am Soc Echocardiogr* 2015; 28: 1–39.e14.
26. Amsallem M, Sweatt AJ, Aymami MC, et al. Right heart end-systolic remodeling index strongly predicts outcomes in pulmonary arterial hypertension: Comparison with validated models. *Circ Cardiovasc Imaging* 2017; 10: pii:e005771.
27. Stevens GR, Garcia-Alvarez A, Sahni S, et al. RV dysfunction in pulmonary hypertension is independently related to pulmonary artery stiffness. *JACC Cardiovasc Imaging* 2012; 5: 378–387.
28. Saydain G, Awan A, Manickam P, et al. Pulmonary hypertension an independent risk factor for death in intensive care unit: Correlation of hemodynamic factors with mortality. *Clin Med Insights Circ Respir Pulm Med* 2015; 9: 27–33.
29. Kang G, Ha R and Banerjee D. Pulmonary artery pulsatility index predicts right ventricular failure after left ventricular assist device implantation. *J Heart Lung Transplant* 2016; 35: 67–73.
30. Rubin LJ, Badesch DB, Barst RJ, et al. Bosentan therapy for pulmonary arterial hypertension. *N Engl J Med* 2002; 346: 896–903.
31. McLaughlin V, Channick RN, Ghofrani H-A, et al. Bosentan added to sildenafil therapy in patients with pulmonary arterial hypertension. *Eur Respir J* 2015; 46: 405–413.
32. Hsu S, Houston BA, Tampakakis E, et al. Right ventricular functional reserve in pulmonary arterial hypertension. *Circulation* 2016; 133: 2413–2422.
33. Mathai SC, Sibley CT, Forfia PR, et al. Tricuspid annular plane systolic excursion is a robust outcome measure in systemic sclerosis-associated pulmonary arterial hypertension. *J Rheumatol* 2011; 38: 2410–2418.
34. Haecck MLA, Scherptong RWC, Marsan NA, et al. Prognostic value of right ventricular longitudinal peak systolic strain in patients with pulmonary hypertension. *Circ Cardiovasc Imaging* 2012; 5: 628–636.
35. Fine NM, Chen L, Bastiansen PM, et al. Outcome prediction by quantitative right ventricular function assessment in 575 subjects evaluated for pulmonary hypertension. *Circ Cardiovasc Imaging* 2013; 6: 711–721.
36. Overbeek MJ, Mouchaers KTB, Niessen HM, et al. Characteristics of interstitial fibrosis and inflammatory cell infiltration in right ventricles of systemic sclerosis-associated pulmonary arterial hypertension. *Int J Rheumatol* 2010; 2010: 604615.
37. Hsu S, Kokkonen-Simon KM, Kirk JA, et al. Right ventricular myofilament functional differences in humans with systemic sclerosis-associated versus idiopathic pulmonary arterial hypertension. *Circulation* 2018; 137: 2360–2370.
38. Callejas-Rubio JL, Moreno-Escobar E, de la Fuente PM, et al. Prevalence of exercise pulmonary arterial hypertension in scleroderma. *J Rheumatol* 2008; 35: 1812–1816.
39. Steen V, Chou M, Shanmugam V, et al. Exercise-induced pulmonary arterial hypertension in patients with systemic sclerosis. *Chest* 2008; 134: 146–151.

Chapter 3- RIGHT HEART REMODELING AND IMMUNITY

Study 1: Preoperative C-Reactive Protein Predicts Early Postoperative Outcomes After Pulmonary Endarterectomy in Patients with Chronic ThromboEmbolic Pulmonary Hypertension

Summary: Chronic thromboembolic pulmonary hypertension (CTEPH) is a rare but severe complication of acute pulmonary embolism, characterized by progressive intraluminal thrombus organization, fibrosis and vascular inflammatory remodeling. Patients with CTEPH have features of systemic inflammation such as increased circulating levels of cytokines. This study assesses whether high preoperative C-reactive protein (CRP) levels are associated with in-hospital outcomes post-endarterectomy (PEA).

Using the French prospective registry of patients referred for PEA, this study had three objectives. The first objective was to evaluate the association between high preoperative CRP levels and hemodynamics, functional and RV adaptive phenotype in a first derivation cohort of 161 patients with CTEPH. The second objective was to map the preoperative circulating inflammatory network in this cohort. The third objective was to explore the association between high preoperative CRP levels and in-hospital adverse outcomes (i.e. death or lung transplant or extracorporeal membrane oxygenation need or extensive inotropic or catecholamine need) post-PEA in the derivation cohort and in a validation cohort of 241 patients.

Our study confirms that high preoperative plasmatic CRP levels are associated with severe preoperative hemodynamics in patients with CTEPH referred for PEA. In addition, CRP levels $\geq 10\text{mg/L}$ are associated with adverse in-hospital outcomes after PEA, independently of the pulmonary disease severity, in both the derivation and the validation cohorts. Patients with high preoperative CRP levels require more vasopressor support than those with low CRP, potentially secondary to inflammation-triggered systemic vasodilation. Closer perioperative hemodynamic monitoring of patients displaying preoperative features of systemic inflammation is recommended.

ABSTRACT

Background: Patients with chronic thromboembolic pulmonary hypertension (CTEPH) display features of systemic inflammation. This study assesses whether high preoperative C-reactive protein (CRP) levels are associated with in-hospital outcomes post-endarterectomy.

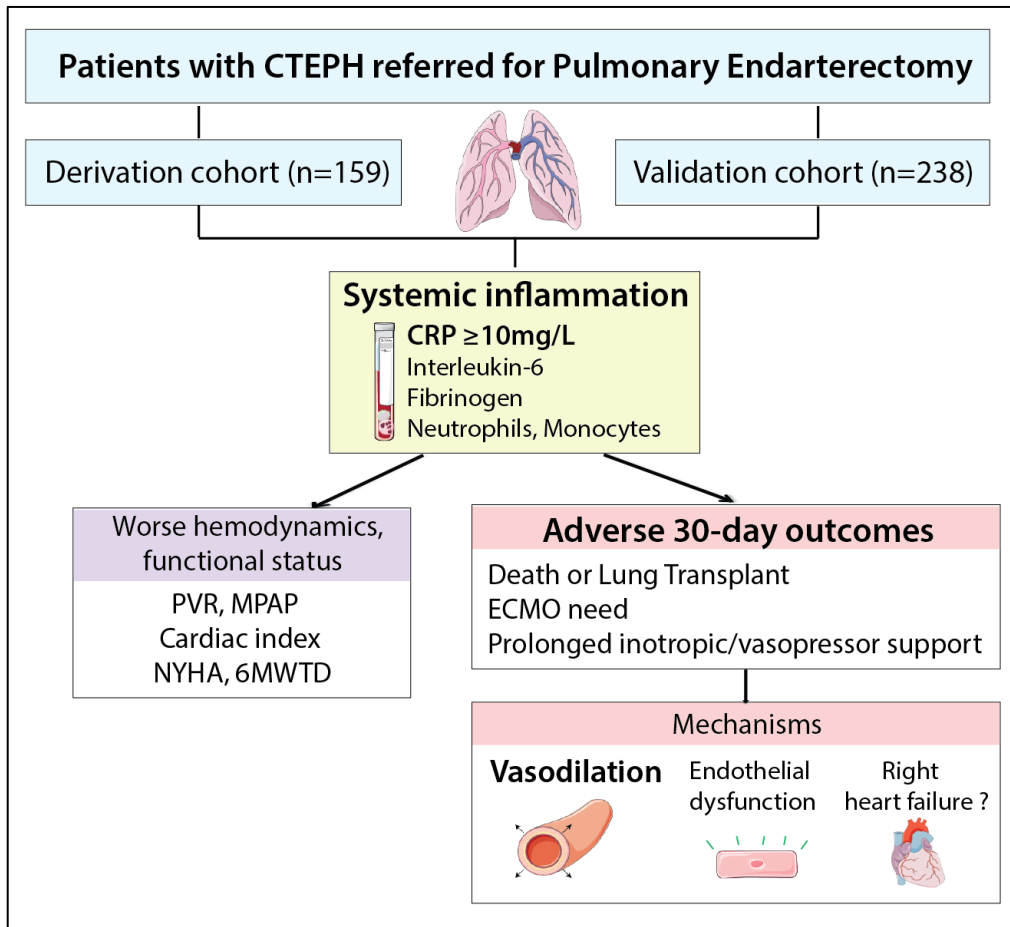
Methods: Using the French prospective CTEPH registry, this study included 159 patients who underwent endarterectomy from 2009 to 2013 (derivation cohort) and 238 patients from 2015 to 2016 (validation cohort). The correlations between pro-inflammatory markers (CRP, interleukins 1 and 6, fibrinogen and leukocytes) and hemodynamics were assessed in the derivation cohort. Pre-, perioperative characteristics and 30-day outcomes (primary endpoint: death or lung transplant or extracorporeal membrane oxygenation need or inotropic or vasopressor need ≥ 3 days) of patients with high or low CRP levels were compared.

Results: Median age of the derivation cohort was 63 [52-73] years with 48% of female, 80% in NYHA class III/IV. CRP levels moderately correlated with fibrinogen, interleukin-6 and neutrophils count (r range 0.28-0.47). The validation cohort had similar demographics and disease severity. Patients with high CRP had higher resistance levels and lower cardiac index than those with low CRP in both cohorts. The primary endpoint was reached in 38% (derivation) and 42% (validation) of patients. In multivariable logistic regression analysis, CRP ≥ 10 mg/L was associated with the primary endpoint in both the derivation cohort (odd ratio = 2.49 [1.11-5.61], independently of NYHA class IV and aortic clamping duration) and the validation cohort (odd ratio = 1.89 [1.09-3.61], independently of age and aortic clamping duration).

Conclusion: Preoperative CRP levels ≥ 10 mg/L are independently associated with adverse early outcomes post-endarterectomy.

KEYWORDS: C-reactive protein; endarterectomy; inflammation; outcomes; pulmonary hypertension.

GRAPHICAL ABSTRACT



6MWT: six-minute walk test distance; CRP: C-reactive protein; CTEPH: chronic thromboembolic pulmonary hypertension; ECMO: extracorporeal membrane oxygenation; MPAP: mean pulmonary arterial pressure; NYHA: New York Heart Association functional class; PVR: pulmonary vascular resistance.

INTRODUCTION

Chronic thromboembolic pulmonary hypertension (CTEPH) is a severe complication of acute pulmonary embolism, characterized by progressive intraluminal thrombus organization, fibrosis and vascular inflammatory remodeling (54,90). Pulmonary endarterectomy (PEA) enables luminal desobstruction, reduction of pulmonary vascular resistance and survival improvement (7,247). However, PEA is frequently associated with perioperative hemodynamic instability, particularly due to profound systemic vasodilation (96).

The role of immunity in the pathogenesis of CTEPH is first suggested by the high prevalence of systemic inflammatory comorbidities and splenectomy in these patients (91–94) and evidence of the involvement of staphylococci infection in patients with ventriculo-atrial shunts who have developed CTEPH (95). In addition, patients with CTEPH frequently display features of systemic inflammation, including high plasmatic pro-inflammatory mediators levels (i.e. fibrinogen, interleukin-1 or C-reactive protein CRP) (85,96,99). High fibrinogen levels have been associated with poor functional status and hemodynamics (i.e. pulmonary vascular resistance, right atrial pressure RAP and mean pulmonary arterial pressure MPAP) in 49 patients with CTEPH (99). CRP is an acute-phase protein produced by the liver in response to infection, inflammation or tissue injury (248). It is a sensitive but nonspecific marker of inflammation that responds rapidly to changes in underlying inflammatory disease activity, making it an optimal clinical biomarker to detect and monitor systemic inflammation (249). There is little evidence to date on the value of preoperative CRP levels for prediction of perioperative outcomes post-PEA in patients with CTEPH, particularly on right heart failure and hemodynamic instability. In this study we hypothesized that high preoperative CRP levels would be associated with worse in-hospital outcomes in patients undergoing PEA for CTEPH.

Using the national prospective PEA registry, this study had three objectives. The first objective was to evaluate the association between high preoperative CRP levels and hemodynamics, functional and right ventricular (RV) adaptive phenotype in a cohort of 161 patients with CTEPH referred for PEA from 2009 to 2013 (derivation cohort). The second objective was to map the preoperative circulating

inflammatory network in this cohort. The third objective was to explore the association between high preoperative CRP levels and in-hospital adverse outcomes (i.e. death or lung transplant or extracorporeal membrane oxygenation need or extensive inotropic or catecholamine need) post-PEA in the derivation cohort and in a validation cohort of patients who underwent PEA from 2015 to 2016.

METHODS

This retrospective study is based on the prospective registry of patients with CTEPH undergoing PEA at Marie Lannelongue Hospital (Le Plessis Robinson, France), the only French center performing this procedure (250)(15). Marie Lannelongue Institutional Review Board approved the study, which was conducted in agreement with the Helsinki-II-declaration. Two cohorts were included: a derivation and a validation cohort.

Derivation cohort

Between January 2009 and December 2013, 529 consecutive patients underwent elective PEA for suspected CTEPH (i.e. MPAP \geq 25 mmHg, at least one segmental perfusion defect detected by lung scanning, and typical lesions of CTEPH on multi-detector computed tomographic angiography and/or pulmonary angiography after at least 3 months of effective anticoagulation) (7). Indications of surgery were weekly discussed by an expert multidisciplinary CTEPH team, including at least one experienced surgeon (250). Patients were considered operable if presenting with sufficient surgically accessible thromboembolic material relating to pulmonary hemodynamics and absence of high-risk comorbidities precluding surgery (251). Among them, 161 patients who gave their informed written consent for inclusion in this study exploring the value circulating biomarkers in patients with operable CTEPH had preoperative serum samples available (**Figure 1a**). The exclusion criterion was pulmonary artery sarcoma on pathological analysis of the surgical sample (n=2).

Validation cohort

Between January 2015 and December 2016, 238 patients were included (**Figure 1b**). Exclusion criteria were: pulmonary artery sarcoma (n=3) and unavailable complete postoperative inotropic or catecholamine support data (n=5).

Inflammatory biomarkers

Blood samples were collected on EDTA within 24 hours of surgery and plasma was prepared. No patient had clinically active infection at the time of preoperative blood sampling. CRP levels were measured using Dimension® Xpand Plus (Siemens, Munich, Germany) with an upper limit of normal of 10mg/L during the first period (2009-2013) and 5mg/L during the second period (2015-2016). Fibrinogen was measured using the HemosIL® Fibrinogen-C kit and D-dimers using HemosIL® D-dimer HS 500 kit (Instrumentation Laboratory - Werfen, Austria). In the derivation cohort, plasma levels of inflammatory cytokines (monocyte chemoattractant protein-1, interleukin-1 β , and interleukin-6) were measured using a sandwich enzyme-linked immunosorbent assay Quantikine ELISA kit (R&D Systems, Minneapolis, MN), according to the manufacturer's instruction. Other routine preoperative laboratory data performed at the hospital laboratory were collected.

Preoperative characteristics

Clinical, functional and pulmonary functional tests data available within a month of surgery were collected. Screening for autoimmune and haematological disorders was not systematic, as left at the discretion of the referring physicians.

Hemodynamics, obtained by right heart catheterization, included: mean RAP, MPAP, pulmonary artery wedge pressure, cardiac output (using thermodilution, or direct Fick method in case of severe tricuspid regurgitation), total pulmonary resistance (defined as MPAP/cardiac output) and pulmonary vascular resistance. Total pulmonary resistance was preferred to pulmonary vascular resistance as wedge pressure was not measurable in all patients particularly in case of proximal obstruction.

Echocardiograms available within one month of surgery were interpreted offline by a certified cardiologist (MA) using GE EchoPAC ultrasound workstation software (GE Healthcare, NY). Right heart metrics, measured on RV focused-apical 4-chamber view, included right atrial maximal area, RV end-

diastolic and end-systolic areas indexed on body surface area, RV fractional area change, tricuspid annular plane systolic excursion and RV free-wall longitudinal strain (145). RV systolic pressure was estimated from the tricuspid regurgitation maximal velocity using continuous Doppler and estimated RAP (26).

Perioperative characteristics

The PEA procedure did not change during the study period and was performed as previously described (252). Cardiopulmonary bypass was first established between the ascending aorta and the two vena cava; body temperature was decreased to 20°C before cross-clamping of the aorta. Right, and then left endarterectomy procedures were performed with sequential circulatory arrests for distal pulmonary arterial recanalization. Thrombus type and location was classified according to the Jamieson's classification (253). Duration of cardiopulmonary bypass, aortic clamping, circulatory arrest and need of extracorporeal membrane oxygenation assistance at the end of surgery were collected. Postoperative inotropic (dobutamine) and catecholamine support (norepinephrine, epinephrine) was left at the discretion of the physicians, targeting a central venous pressure < 15mmHg, mean arterial pressure > 65mmHg and cardiac index > 2 L/min/m² in the operative room and during the postoperative phase. In case of predominant cardiogenic shock, dobutamine was initiated at the dose of 5µg/kg/min and increased by 2.5µg/kg/min every hour, up to 20µg/kg/min if needed. In case of predominant or associated systemic vasodilation, noradrenaline was initiated, and in case of severe shock, adrenaline would be preferred. In the intensive care unit, inotropic and vasopressor supports were weaned as the heart recovered, based on invasive monitoring and echocardiography. A mean arterial pressure of 65-90mmHg was targeted to support renal perfusion with a central venous pressure < 15mmHg while maintaining a cardiac index > 2 L/min/m².

Early postoperative outcomes

The primary endpoint was the composite early (within 30-day post-PEA) outcome of postoperative hemodynamic failure defined as all-cause death, or heart-lung or double-lung transplantation for persistent pulmonary hypertension, or ECMO need immediately after surgery, or inotropic or

catecholamine support need for ≥ 3 days post-PEA. The secondary endpoints included: [1] early all-cause death or heart-lung or double-lung transplantation, and [2] early all-cause death, or heart-lung or double-lung transplantation, or ECMO need post-PEA. All-cause mortality was verified through chart review.

Statistical analysis

Continuous variables are summarized as median and interquartile range; categorical variables are presented as number (%). Comparisons between groups were performed using non-parametric independent Mann-Whitney test for continuous variables and Chi-square test for categorical data. Spearman correlation coefficients (r) were used to express the correlation between immune markers. Logistic regression analyses were performed on preoperative variables to identify correlates of the primary endpoint or the secondary endpoints occurring within 30 days of surgery. Odds ratios of continuous variables are presented per standard deviation of the considered variable for comparison purposes. P-values <0.05 were considered statistically significant. Statistical analyses were performed using SPSS v.23.0 (SPSS, Chicago, IL).

RESULTS

Derivation cohort – preoperative characteristics

Median age was 63 [52-73] years with 48% of females; 80% were in NYHA functional class III or IV (**Table 1**). Patients with preoperative CRP $\geq 10\text{mg/L}$ ($n=37$) had significantly lower cardiac index and higher MPAP and higher resistance levels than patients with CRP $< 10\text{mg/L}$ ($n=122$) without any difference in terms of PH-specific or statins therapy. Three patients received immunosuppressive therapy for history of systemic inflammatory disease (1 with Lupus treated by hydroxychloroquine, 1 with Crohn disease treated by methotrexate, azathioprine and corticosteroids and 1 with Wegener treated by azathioprine and corticosteroids); their CRP level was below 10mg/L . In the subgroup of patients with complete preoperative echocardiographic data ($n=59$), patients with CRP $\geq 10\text{mg/L}$ ($n=18$) had similar

resistance and cardiac index than those with CRP < 10mg/L (n=41, **Table 2**). In these two subgroups with similar hemodynamics, RV size and systolic function were similar (all p>0.23).

Patients with CRP \geq 10mg/L had higher neutrophils and monocytes counts than patients with normal CRP levels, which translated into higher neutrophil to lymphocyte ratio (**Table 3**). No patient had high CRP but normal other inflammatory markers because of liver failure. **Figure 2** illustrates the correlation heatmap of immune markers, highlighting the moderate correlation between CRP levels and fibrinogen, interleukin-6, neutrophils and monocytes count (all p<0.01). CRP levels were also significantly correlated with D-dimers levels (r=0.27, p<0.01), but not with resistance or cardiac index.

Derivation cohort – perioperative characteristics

The Jamieson classification did not significantly differ between patients with preoperative CRP \geq 10mg/L and those with low CRP level (p=0.11). There was no significant difference between the groups in term of cardiopulmonary bypass, aortic clamping or circulatory arrest duration (all p>0.68, supplementary **Table S1**).

Derivation cohort – outcomes

At 30-days, 8 patients from the derivation cohort had died (**Figure 1a**). Causes of death included persistent pulmonary hypertension associated with refractory right heart failure in 3 patients, sepsis in 3 patients and severe hemorrhage in 2 patients. One patient underwent emergent heart-lung transplantation for refractory right heart failure but died on day-1 of the transplant. Median duration of intensive care unit stay was 8.0 [5.0-15.0] days; 57 patients (35.4%) required prolonged (\geq 3 days) inotropic or catecholamine support post-surgery. Median in-hospital stay duration was 18.0 [11.0-46.3] days. The primary composite endpoint was reached in 60/159 (37.7%) patients, more frequently in patients with preoperative high CRP (n=21, 56.8%) than in those with low CRP (n=39, 32.0%, p<0.01). Patients with CRP \geq 10mg/L required more frequently norepinephrine for \geq 3 days (45.9% versus 21.3%, p<0.01), while there was no difference for epinephrine (5.4% versus 2.5%, p=0.38) and dobutamine need (10.8% versus 11.5%, p=0.83) than those with low CRP (**Figure 3a**). Regarding the secondary endpoints, 8 patients (5.0%) died or required heart-lung transplant, including 3 (8.1%) in the high CRP group versus 5

(4.1%) in the low CRP group ($p=0.33$). Twelve patients (7.5%) reached the endpoint of “death or heart-lung transplant or ECMO need”; 4 (10.8%) in the high CRP group versus 8 (6.6%) in the low CRP group ($p=0.42$). There was no statistical difference between the groups in term of intensive care unit stay duration (9.0 [5.0-16.0] days in the high CRP group versus 8.0 [5.0-15.0] in the low CRP group), or mechanical ventilation duration (2.0 [1.0-7.0] days versus 1.0 [1.0-3.0] respectively).

Table 4 presents the univariable analyses for correlates of the primary endpoint. Short preoperative 6-minute walk test distance, NYHA class IV, high invasive RAP and RV enlargement were associated with worse postoperative outcome. A CRP level ≥ 10 mg/L was associated with a three-fold increased risk of the primary endpoint. To minimize overfitting the multivariable model, only 5 variables were included in addition to age and sex: NYHA class IV, invasive RAP, total pulmonary resistance, CRP ≥ 10 mg/L and aortic clamping duration. The choice of variables was based on the following rationale: [1] NYHA class IV as previously reported, [2] RAP is a strong predictor of outcomes in pulmonary hypertension, [3] total pulmonary vascular resistance as a reflection of the disease severity (a similar model including pulmonary vascular resistance provided the same results), [4] CRP ≥ 10 mg/L, and [5] aortic clamping duration reflecting the duration of the procedure associated with the accessibility of lesions. On multivariable analysis in the total cohort ($n=159$), CRP ≥ 10 mg/L (odds ratio = 2.49 [1.11-5.61], $p=0.04$), NYHA class IV (4.98 [1.54-16.12], $p<0.01$) and aortic clamping duration (1.55 [1.14-2.39], $p<0.01$) were retained in the model for the primary endpoint ($\chi^2=23.7$; $p<0.001$). An alternative model including RV end-systolic area index (which emerged as one of the strongest echocardiographic metric in univariable analysis) in the subgroup with echocardiographic data available ($n=59$), retained female sex (6.44 [1.09-38.20], $p=0.04$), CRP ≥ 10 mg/L (7.62 [1.34 – 43.31], $p=0.02$), RAP (2.13 [1.01-4.36], $p=0.046$) and aortic clamping duration (3.65 [1.55-10.19], $p<0.01$) for the primary endpoint ($\chi^2=29.2$, $p<0.0001$). High CRP levels (≥ 10 mg/L) were not significantly associated with any of the secondary endpoints.

Validation cohort – pre and perioperative characteristics

Patients from the validation cohort (n=238) had similar demographics (median age 63.5 [50.0-70.0] years, with 46% of female) and disease severity as assessed using hemodynamics or functional parameters (supplementary **Table S2**). Patients were more frequently treatment naïve than in the derivation cohort (88.7% versus 80.7%, p=0.03). Patients with preoperative CRP \geq 5mg/L had significantly higher RAP and MPAP levels and higher resistance levels than patients with $<$ 5 mg/L (supplementary **Table S2**). Fifty-eight patients had CRP levels \geq 10mg/L, representing 24.4% of the total validation cohort and 55.8% of the CRP \geq 5mg/L subgroup.

Validation cohort - outcomes

At 30-days, 11 patients from the validation cohort had died (**Figure 1b**). Causes of death included persistent pulmonary hypertension associated with refractory right heart failure in 5 patients, sepsis in 4 patients, severe hemorrhage in 1 patients and acute pancreatitis in 1 patient. One patient underwent double-lung transplantation for refractory right heart failure within the same index hospitalization after 30-days. Median in-hospital stay was 16.0 [11.0-24.5] days). Median duration of intensive care unit stay was 11.0 [4.0-18.0] days; 99 patients (41.6%) required prolonged inotropic or catecholamine support (**Figure 3b**). Overall, 104 (43.7%) patients reached the primary endpoint. Using univariable analysis (**Table 5**), CRP \geq 10mg/L was associated with the primary endpoint (1.85 [1.02-3.36], p=0.03) while CRP \geq 5mg/L did not reach significance (p=0.05). On multivariable analysis using the same variables as in the derivation cohort, age, CRP \geq 10mg/L and aortic clamping duration were retained in the model for the primary endpoint ($\chi^2=33.0$, p<0.001, **Table 5**). Patients with high CRP required more frequently norepinephrine (46% if CRP \geq 10, 4% if [5-10], 37% if $<$ 5mg/L, p<0.001) or epinephrine for \geq 3 days (7%, 0% and 0% respectively, p<0.01) than in those with low CRP levels (**Figure 3b**); while there was no difference for dobutamine need (7%, 13% and 6% respectively, p=0.28). Regarding the secondary endpoint of death or lung transplantation (reached in n=11 patients, 4.6%), when testing the same variables in multivariable analysis, CRP \geq 10mg/L (6.55 [1.22 – 35.11], p=0.03), aortic clamping duration (3.31 [1.63-5.25], p<0.01) and NYHA class IV (10.18 [1.52-68.11], p=0.02) were retained in the model ($\chi^2=32.5$; p<0.001).

DISCUSSION

Our study confirms that high preoperative plasmatic CRP levels are associated with severe preoperative hemodynamics in patients with CTEPH referred for PEA. In addition, CRP levels $\geq 10\text{mg/L}$ are associated with adverse early outcomes after PEA, independently of the pulmonary disease severity, in both the derivation and the validation cohorts.

CRP is a pentameric protein of hepatic origin whose plasmatic levels rise in response to inflammation. The main factor influencing the plasmatic level of CRP is its rate of hepatic production by the liver (248). In our study, no patient had high CRP levels because of isolated liver failure without features of inflammation using other markers, or because of renal failure, confirming that high CRP levels reflects systemic inflammation in CTEPH. Interestingly, patients with high CRP levels had more frequently congestive liver features, which can be related to more severe disease and secondary right heart failure. The expression of CRP is predominantly under transcriptional control by the cytokine interleukin-6, and to a lesser extent interleukin-1 and tumor necrosis factor, secretion by macrophages and T cells (254). As illustrated in our heatmap, CRP levels consistently correlated with interleukin-6 level, fibrinogen level and neutrophils and monocytes counts, confirming the activation of these pro-inflammatory pathways in CTEPH.

There is a strong body of evidence on the value of CRP as a prognostic biomarker in cardiovascular diseases, such as atherosclerosis (77,249), left heart failure (255–257) and pulmonary arterial hypertension. Elevated circulating levels of interleukin-6 and CRP have been reported to be associated with adverse outcomes in several cohorts of patients with pulmonary arterial hypertension, and membrane-bound interleukin-6 receptor has been recently shown to plays a role in the prosurvival phenotype of smooth muscle cells in these patients. There have been fewer studies conducted in CTEPH (85,98). Quarck et al. reported elevated plasmatic levels of high sensitive CRP in 79 patients with CTEPH (including 44 undergoing PEA) (85). CRP levels, however, did not correlate with the disease severity and

were not predictive of outcomes in this study that may have been underpowered. Recently, Skoro-Sajer et al. have shown in a large CTEPH cohort (n=289, including 157 undergoing PEA) that high CRP levels negatively correlated with the six-minute walk test distance and RV function assessed using tricuspid annular plane systolic excursion (98). CRP levels superior to 10mg/L (determined by the receiver operating characteristic curve) were further associated with death or lung transplant need during the 57 [45-69] months follow-up, independently of pulmonary resistance levels. Our study further validates the prognostic value of CRP for prediction of early outcomes post-endarterectomy independently of pulmonary resistance levels and duration of surgery.

In our derivation cohort, the association between high CRP levels ($\geq 10\text{mg/L}$) and the primary composite endpoint was mainly driven by the “prolonged catecholamine support” component of the endpoint, suggesting a strong link between preoperative systemic inflammation and perioperative hemodynamic instability characterized by profound vasoplegia. This finding was confirmed in the validation cohort (with the same threshold of 10mg/L). This latter had sufficient statistical power to further demonstrate the association between CRP $\geq 10\text{mg/L}$ and 30-day mortality post-endarterectomy. The effect of pro-inflammatory circulating cytokines (such as interleukin-6 and tumor necrosis factor) on perioperative hemodynamic instability has been first investigated in a cohort of 14 patients undergoing PEA, reporting the positive correlation between perioperative maximum vasopressor support and peak levels of interleukin-6 that was also released during surgery ($r = 0.82$), suggesting cytokines-triggered vasoregulation (96). CRP was however not investigated in this study.

In CTEPH, the vascular effect of CRP has been mainly explored at the pulmonary arterial level. *In vitro* studies have shown that CRP stimulates pulmonary smooth muscle cells proliferation, induces endothelial dysfunction by increasing the expression of adhesion molecules (such as intercellular adhesion molecule-1) resulting in increased monocytes adhesion to pulmonary arterial endothelial cells (53,97,258). When incubated with endothelial cells, CRP directly decreases nitric oxide (NO) production through post-transcriptional effects on endothelial NO synthase mRNA stability, further inhibiting angiogenesis (259). A recent study further showed that the effect of CRP on NO production by

endothelial cells differed according to the isoform: the native CRP reducing NO production while monomeric CRP increases it (260).

The main originality of our study is to assess the relationship between preoperative pro-inflammatory marker CRP and adverse early outcomes post-endarterectomy, focusing on postoperative hemodynamic instability and mortality. Our results have practical clinical implication to recommend closer perioperative hemodynamic monitoring of patients with preoperative biological features of systemic inflammation. To date, there are no strong guidelines on perioperative hemodynamic management or indications of ECMO after PEA, which remains left at the discretion of anesthesiologists, surgeons and intensivists based on general hemodynamic thresholds. Increasing the level of evidence on perioperative management post-endarterectomy faces the same design trial challenges than perioperative management post-cardiac surgery (such as left ventricular assist device implantation). Further studies should explore whether the level of mechanical and drug support post-endarterectomy would be stratified according to pre- and perioperative pro-inflammatory biomarkers levels.

This study has several limitations. The first limitation comes from the limited echocardiographic data that was available in a subset of 59 patients, whose characteristics were different than the total population, limiting the extrapolation of RV phenotyping results. Recent studies have reported a negative correlation between CRP levels and RV function (either assessed by cardiac magnetic resonance-derived ejection fraction or by echocardiographic tricuspid annular plane systolic excursion), although not adjusting for pulmonary vascular resistance levels (98,136). In our subgroup with available echocardiographic data, patients with high CRP had similar hemodynamics than those with low CRP, and similar RV size and function as assessed by comprehensive RV parameters including strain. Further investigations are needed to assess whether, after matching for afterload, patients with high CRP have different RV function or remodeling than those with low CRP. The second limitation is the absence of data on dynamic changes in CRP levels during and after surgery. Langer et al. previously demonstrated that, in addition to preoperative increased levels of pro-inflammatory cytokines (such as interleukin-6), endarterectomy resulted in the release of these cytokines, particularly following deep hypothermic

circulatory arrest (96). Regarding CRP, evidence is missing on early postoperative levels as data available have only been reported at 12 months after PEA (85,98). Finally, data on maximal doses of catecholamine and dobutamine are not available in all patients, as it was not prospectively recorded in the CTEPH registry. The current study thus used prolonged inotropic/vasopressor support to reflect hemodynamic instability.

In conclusion, preoperative CRP plasmatic levels $\geq 10\text{mg/L}$ are associated with worse hemodynamics and adverse early outcomes post-endarterectomy in CTEPH. Patients with high preoperative CRP levels require more vasopressor support than those with low CRP, potentially secondary to inflammation-triggered systemic vasodilation. Closer perioperative hemodynamic monitoring of patients displaying preoperative features of systemic inflammation is recommended.

CONFLICTING INTERESTS

None of the authors has anything to disclose relative to this study.

FUNDING SOURCES

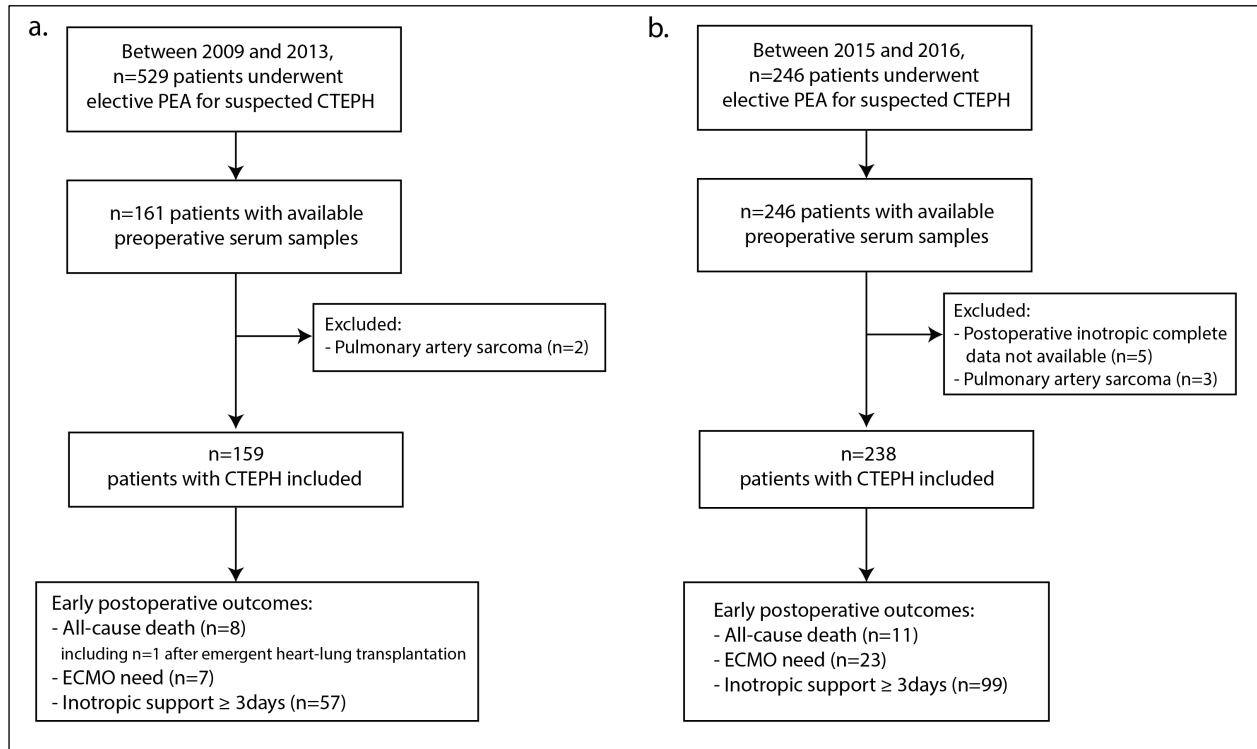
The prospective endarterectomy registry was funded by the Programme Hospitalier de Recherche Clinique National 2009 of the French Ministry of Health; RCB 2009-A0098057. This study was supported by a public grant overseen by the French National Research Agency as part of the second Investissements d’Avenir program (ANR-15-RHUS-0002). None of the funding organizations directly had a role in the collection of data, its analysis and interpretation, and in the right to approve or disapprove publication of the finished manuscript.

ACKNOWLEDGMENTS

The authors would like to thank Lilia Lamrani, Florence Lecerf and Farah Hapiot (Marie Lannelongue Hospital) for their help with data collection.

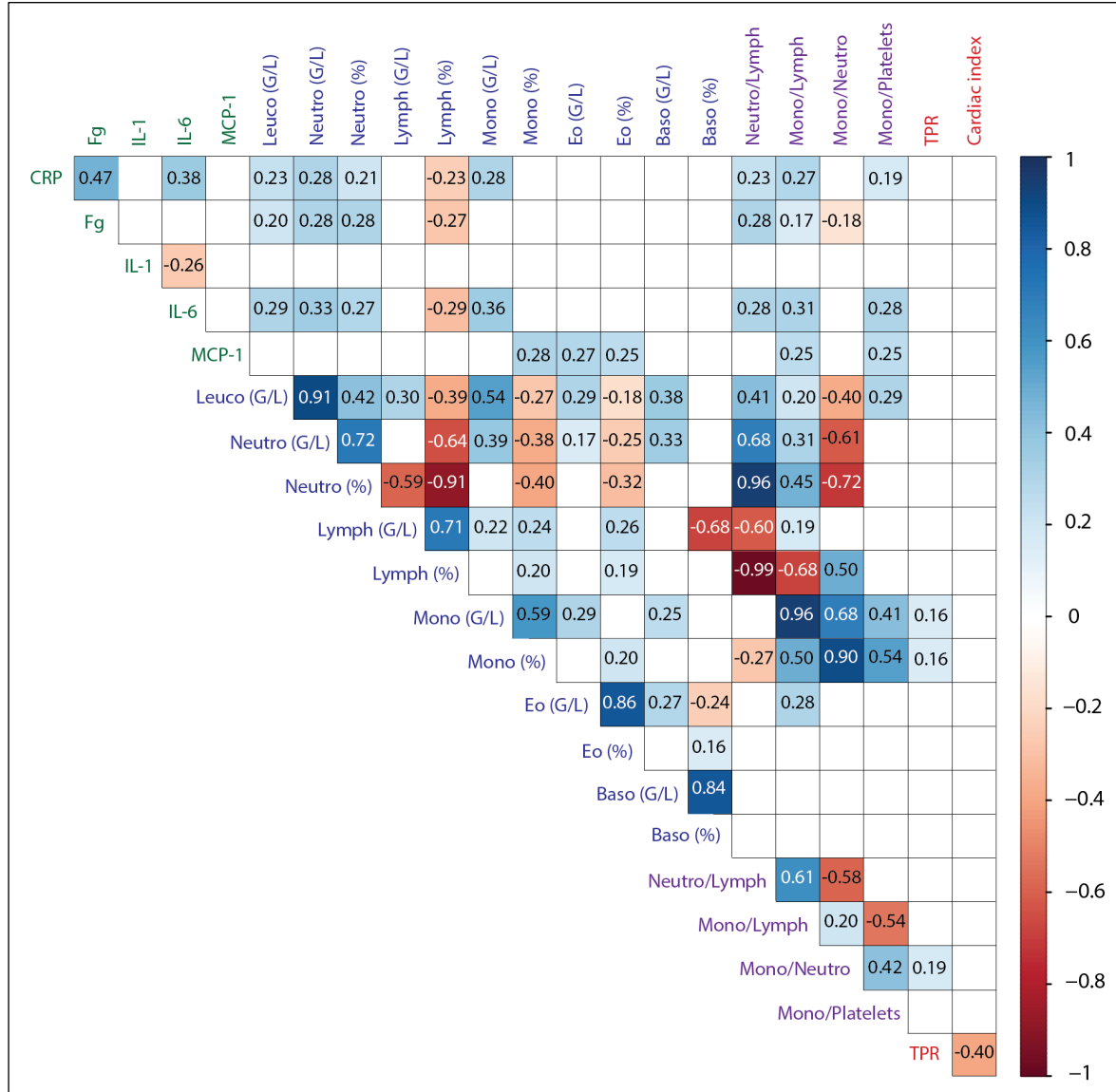
FIGURES

Figure 1. Flow chart of the derivation (a) and validation cohorts (b) and their respective early postoperative outcomes.



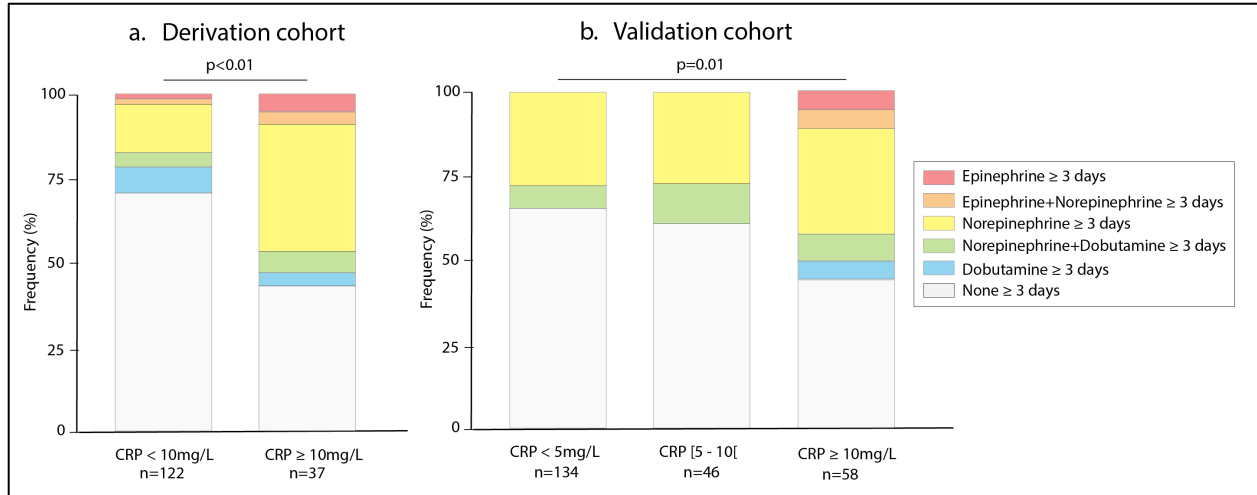
CTEPH: chronic thromboembolic pulmonary hypertension; ECMO: extracorporeal membrane oxygenation; PEA: pulmonary arterial endarterectomy.

Figure 2. Correlation heatmap of immune markers and hemodynamics in the derivation cohort.



Correlations are expressed using Spearman (rho) correlations between variables in all patients (n=159), except for correlations with IL-1, IL-6 and MCP-1 only available in n=72 patients. Only statistically significant correlations (p values <0.05) are shown. Baso: basophils; CRP: C-reactive protein; Eo: eosinophils; Fg: fibrinogen; IL-1: interleukin-1; IL-6: interleukin-6; Leuco: leucocytes; Lymph: lymphocytes; MCP-1: monocyte chemoattractant protein-1; Mono: monocytes; Neutro: neutrophils; TPR: total pulmonary resistance. Correlations were similar when using pulmonary vascular resistance.

Figure 3. Frequency and type of inotropic (dobutamine) or catecholamine (norepinephrine and epinephrine) support ≥ 3 days post-endarterectomy in the derivation (a) and validation cohorts (b), according to the preoperative plasmatic level of C-reactive protein (CRP).



P-value for comparison between CRP groups using Chi-square test.

TABLES

Table 1. Comparative preoperative characteristics of the derivation cohort according to preoperative CRP levels.

	Total cohort n=159	CRP <10mg/L n=122	CRP ≥10mg/L n=37	p value*
Age (years)	63.1 [51.7-72.9]	63.0 [52.0-73.0]	65.50 [53.0-73.9]	0.49
Female sex (%)	76 (47.8)	60 (49.2)	16 (43.2)	0.52
Body mass index (kg/m ²)	25.6 [23.2-28.8]	25.6 [23.8-29.0]	24.9 [22.0-28.8]	0.45
Body surface area (m ²)	1.81 [1.69-1.98]	1.84 [1.69-1.99]	1.75 [1.70-1.92]	0.56
History of deep venous thrombosis or acute pulmonary embolism (%)	117 (73.6)	92 (75.4)	25 (67.6)	0.35
Inferior vena cava filter (%)	9 (5.7)	9 (7.4)	0	0.18
Presence of endovascular device** (%)	10 (6.3)	6 (4.9)	4 (10.8)	0.20
History of splenectomy (%)	3 (1.9)	3 (2.5)	0	0.76
Thrombophilia or blood disorder (%)	23 (14.5)	20 (16.4)	3 (8.1)	0.21
Chronic inflammatory systemic disease (%)	3 (1.9)	3 (2.5)	0	0.76
Active or recent (<3 years) smoker (%)	12 (7.5)	9 (7.4)	3 (8.1)	0.89
New York Heart Association functional class				
II	32 (20.1)	25 (20.5)	7 (18.9)	
III	105 (66.0)	84 (68.9)	21 (56.8)	0.11
IV	22 (13.8)	13 (10.7)	9 (24.3)	
Hemoptysis on admission (%)	5 (3.1)	4 (3.3)	1 (2.7)	0.86
Six-minute walk test distance (m)	(n=86) 400.0 [305.5-462.0]	(n=65) 404.0 [342.5-480.0]	(n=21) 346.0 [251.0-442.0]	0.08

Therapies				
Treatment naïve (%)	128 (80.5)	97 (79.5)	31 (83.8)	0.56
Double therapy (%)	12 (7.5)	10 (8.2)	2 (5.4)	0.78
Prostanoid therapy (%)	1 (0.6)	1 (0.8)	0	0.55
Phosphodiesterase inhibitors (%)	19 (11.9)	14 (11.5)	5 (13.5)	0.95
Endothelin receptor blockers (%)	23 (14.5)	20 (16.4)	3 (8.1)	0.28
Statins (%)	21 (13.2)	20 (16.4)	1 (2.7)	0.05
Hemodynamics				
RAP (mmHg)	7.0 [4.0-10.0]	7.0 [4.0-10.0]	8.0 [4.0-10.0]	0.31
Mean PAP (mmHg)	45.0 [38.0-53.0]	44.0 [38.0-52.0]	50.0 [43.0-56.0]	0.01
PAWP (mmHg)	(n=156)	(n=121)	(n=35)	
	5.0 [3.0-7.0]	5.0 [3.0-7.0]	5.0 [3.0-8.0]	0.42
Cardiac Index (L/min/m ²)	2.5 [2.1-2.9]	2.6 [2.2-2.9]	2.3 [1.9-2.8]	0.02
Total Pulmonary Resistance (WU)	10.1 [7.0-11.5]	9.3 [6.8-11.9]	11.6 [10.3-14.1]	<0.01
Total Pulmonary Resistance index (WU/m ²)	18.1 [13.4-22.8]	16.7 [12.9-21.7]	20.6 [17.4-26.4]	<0.01
Pulmonary Vascular Resistance (WU)	(n=156)	(n=121)	(n=35)	<0.01
	8.7 [6.1-11.5]	8.2 [5.9-10.2]	9.8 [9.1-12.6]	
Pulmonary Vascular Resistance index (WU/m ²)	(n=156)	(n=121)	(n=35)	<0.01
	15.5 [11.6-20.5]	14.4 [11.0-19.6]	18.8 [15.1-23.3]	
Pulmonary functional tests				
DLCO (%)	(n=76)	(n=62)	(n=15)	
	64.9 [51.0-75.5]	65.5 [51.0-75.4]	64.1 [47.9-82.4]	0.73
Resting paO ₂ (mmHg)	(n=121)	(n=95)	(n=26)	
	64.0 [57.3-74.0]	64.1 [57.8-72.8]	61.9 [55.4-77.5]	0.87

*Comparison between the two subgroups preoperative CRP levels lower or higher than the detection threshold (10mg/L) (using Mann-Whitney test or Chi-square test). **Including implantable port, pacemakers, ventricular-arterial derivation. DLCO: diffusing capacity for carbon monoxide); PAP: pulmonary arterial pressure; PAWP: pulmonary arterial wedge pressure; RAP: right atrial pressure.

Table 2. Comparative preoperative characteristics of the subgroup with available echocardiography data according to preoperative CRP levels.

	Total cohort with echo n=59	CRP <10mg/L n=41	CRP ≥10mg/L n=18	p value*
Age (years)	62.3 [50.3-72.3]	63.1 [48.4-72.3]	61.2 [48.9-73.4]	0.97
Female sex (%)	24 (40.7)	17 (41.5)	7 (38.9)	0.85
Body surface area (m ²)	1.8 [1.6-2.0]	1.8 [1.6-2.0]	1.8 [1.7-2.0]	0.90
New York Heart Association functional class				0.31
II	16 (27.1)	11 (26.8)	5 (27.8)	
III	38 (64.4)	28 (68.3)	10 (55.6)	
IV	5 (8.5)	2 (4.9)	3 (16.7)	
RAP (mmHg)	7.0 [4.0-10.3]	6.0 [3.5-11.0]	8.0 [5.0-10.0]	0.67
Mean PAP (mmHg)	45.0 [35.0-53.0]	42.0 [35.0-52.5]	50.0 [44.5-55.3]	0.15
Cardiac Index (L/min/m ²)	2.5 [2.1-3.0]	2.5 [2.2-3.0]	2.4 [2.0-2.9]	0.77
Total Pulmonary Resistance (WU)	10.4 [7.4-13.8]	10.1 [6.8-13.9]	11.2 [10.2-13.6]	0.20
Pulmonary Vascular Resistance (WU)	9.5 [6.6-11.2]	8.2 [6.0-11.7]	9.8 [8.9-11.3]	0.22
RV end-diastolic area index (cm ² /m ²)	17.1 [14.1-19.6]	17.3 [13.5-19.8]	16.9 [14.3-19.4]	0.91
RV end-systolic area index (cm ² /m ²)	12.4 [9.8-15.2]	12.8 [9.8-15.2]	12.0 [9.8-15.5]	0.74
RV end-systolic remodeling index	1.35 [1.24-1.43]	1.31 [1.23-1.43]	1.36 [1.24-1.45]	0.49
RV fractional area change (%)	24.9 [20.7-28.7]	24.8 [21.4-27.9]	25.5 [18.9-30.1]	0.74
RV longitudinal strain (%)	16.3 [12.4-19.2]	16.0 [12.7-19.7]	16.4 [11.8-18.4]	0.77
Tricuspid annular plane systolic excursion (mm)	15.0 [12.7-18.0]	15.3 [12.8-18.0]	15.0 [10.8-19.4]	0.93
Right atrial area index (cm ² /m ²)	11.6 [9.0-14.4]	12.6 [8.9-14.8]	10.0 [9.2-13.6]	0.48

Severe tricuspid regurgitation (%)	1 (0.6)	1 (0.8)	0	0.55
Estimated RAP (mmHg)	10.0 [10.0-15.0]	10.0 [10.0-15.0]	10.0 [10.0-17.5]	0.92
Estimated RVSP (mmHg)	n=57	n=40	n=17	
	85.0 [66.0-99.5]	80.5 [65.5-97.3]	92.0 [72.5-107.5]	0.23
Left ventricular ejection fraction (%)	60.0 [60.0-65.0]	60.0 [60.0-65.0]	60.0 [60.0-65.0]	0.65

*Comparison between the two subgroups preoperative CRP levels lower or higher than the detection threshold (10mg/L) (using Mann-Whitney test or Chi-square test). PAP: pulmonary arterial pressure; PAWP: pulmonary arterial wedge pressure; RAP: right atrial pressure; RV: right ventricular; RVSP: RV systolic pressure.

Table 3. Comparative preoperative biological characteristics of the derivation cohort according to preoperative CRP levels.

	Total cohort n=159	CRP <10mg/L n=122	CRP ≥10mg/L n=37	p value*
Leucocytes (G/L)	6.7 [5.6-8.1]	6.7 [5.4-7.9]	7.6 [6.0-9.6]	0.03
Neutrophils (%)	63.5 [56.4-70.9]	62.6 [55.2-69.9]	68.5 [58.3-72.9]	0.04
Neutrophils (G/L)	4.2 [3.2-5.6]	4.0 [3.2-5.0]	4.7 [4.0-7.0]	<0.01
Lymphocytes (%)	25.7 [18.1-31.7]	26.3 [20.0-31.9]	21.1 [16.7-30.3]	0.03
Lymphocytes (G/L)	1.7 [1.3-2.1]	1.8 [1.4-2.1]	1.6 [1.2-2.1]	0.34
Monocytes (%)	7.1 [5.8-9.0]	7.0 [5.6-9.0]	7.5 [6.1-9.4]	0.31
Monocytes (G/L)	0.5 [0.4-0.6]	0.5 [0.4-0.6]	0.6 [0.5-0.7]	<0.01
Eosinophils (%)	2.0 [1.4-3.1]	2.0 [1.4-3.2]	1.8 [1.3-3.1]	0.34
Eosinophils (G/L)	0.1 [0.1-0.2]	0.1 [0.1-0.2]	0.2 [0.1-0.2]	0.76
Basophils (%)	0.8 [0.6-1.0]	0.8 [0.6-1.1]	0.7 [0.5-0.9]	0.23
Basophils (G/L)	0.05 [0.04-0.07]	0.05 [0.03-0.07]	0.05 [0.04-0.07]	0.99
Red blood cells (G/L)	4.8 [4.3-5.2]	4.8 [4.3-5.2]	4.8 [4.1-5.2]	0.67
Hemoglobin (g/dL)	14.4 [13.4-15.9]	14.4 [13.3-15.9]	14.6 [13.5-16.0]	0.73
Platelet count (G/L)	244.0 [190.1- 303.5]	236.0 [189.8- 292.8]	265.0 [190.5- 314.5]	0.33
Neutrophil/Lymphocyte ratio	2.5 [1.9-3.9]	2.4 [1.8-3.5]	3.3 [1.9-4.4]	0.03
Monocyte/Lymphocyte ratio	0.29 [0.22-0.41]	0.27 [0.21-0.37]	0.34 [0.28-0.51]	<0.01
Monocyte/Neutrophil ratio	0.12 [0.09-0.15]	0.12 [0.09-0.16]	0.10 [0.09-0.15]	0.64
Fibrinogen (mg/dL)	4.0 [3.3-4.6]	3.7 [3.2-4.3]	4.8 [4.3-5.5]	<0.001
Interleukin-1 (ng/mL)	n=72 1.7 [0.6-4.3]	n=50 1.6 [0.6-4.2]	n=22 1.8 [0.7-4.6]	0.77
Interleukin-6 (ng/mL)	n=78 10.2 [2.9-39.9]	n=54 6.3 [2.4-36.7]	n=24 24.1 [9.2-56.6]	<0.01
MCP-1 (ng/mL)	n=72 399.5 [251.0- 649.6]	n=50 416.2 [227.7- 671.1]	n=22 352.6 [279.7- 622.1]	0.79

D-dimers (ng/mL)	372.0 [239.8-677.3]	350.0 [224.3-596.8]	564.0 [315.0-1135.8]	<0.01
Antithrombin III (%)	103.0 [92.0-111.0]	101.5 [92.0-111.0]	104.0 [93.0-113.0]	0.78
Blood urea nitrogen (mg/dL)	7.3 [5.8-9.5]	7.0 [5.6-9.2]	8.2 [6.8-10.5]	<0.01
Creatinine clearance (mL/min)				
≥60mL/min	52 (32.7)	42 (34.4)	10 (27.0)	
59 - 30mL/min	103 (64.8)	77 (63.1)	26 (70.2)	0.70
<30mL/min	4 (2.5)	3 (2.5)	1 (2.7)	
Aspartate transaminase (U/L)	28.0 [22.0-36.5]	26.0 [21.0-36.0]	31.0 [24.0-39.0]	0.04
Alanine transaminase (U/L)	25.0 [19.0-34.0]	25.0 [19.0-34.5]	24.0 [20.0-33.0]	0.61
Gamma-glutamyl transferase (U/L)	64.5 [35.0-119.5]	58.0 [33.8-105.0]	89.5 [51.3-157.5]	0.04
Alkaline phosphatase (U/L)	77.0 [61.5-100.5]	73.0 [60.0-97.0]	89.5 [65.5-105.0]	0.13
Total bilirubin (μmol/L)	14.0 [10.0-21.0]	14.0 [10.0-21.0]	14.5 [11.0-21.0]	0.34
Conjugated bilirubin (μmol/L)	3.0 [2.0-4.0]	2.0 [2.0-4.0]	3.0 [2.0-5.8]	<0.01
Lactate dehydrogenase (U/L)	247.0 [209.0-283.0]	236.0 [202.8-275.0]	264.0 [231.5-305.5]	0.01
Creatine phosphokinase (U/L)	84.0 [54.8-127.0]	78.0 [55.0-135.5]	86.0 [51.5-117.0]	0.77
BNP (pg/mL)	132.0 [39.5-393.5]	115.0 [31.8-319.5]	280.0 [101.0-626.0]	0.04

*Comparison between the two subgroups with preoperative CRP levels lower or higher than the detection threshold (10mg/L) (using Mann-Whitney test or Chi-square test). BNP: B-type natriuretic peptide; MCP-1: monocyte chemoattractant protein-1.

Table 4. Univariate analysis of correlates of the primary endpoint (early death or heart-lung transplant or ECMO need or prolonged inotropic/catecholamine support) in the derivation cohort (n=159).

Variables	Odd ratio*	95% confidence interval	p-value
Age (years)	1.33	0.98 – 1.75	0.20
Female sex	1.04	0.55 – 1.97	0.92
History of splenectomy	3.38	0.30 – 38.09	0.33
History of endovascular device	1.11	0.30 – 4.10	0.88
Active or <3 year smoking	0.81	0.23 – 2.86	0.74
NYHA class (reference class = II)			0.02
III	1.18	0.51 – 2.75	0.70
IV	4.38	1.67 – 11.50	<0.01
6-minute walk test distance (m)	0.60	0.40 – 1.00	0.04
Preoperative right heart catheterization (n=159)			
Heart rate (bpm)	1.75	0.69 – 4.42	0.24
Right atrial pressure (mmHg)	1.39	1.05 – 1.96	0.04
Mean pulmonary arterial pressure (mmHg)	1.30	0.93 – 1.69	0.15
Cardiac index (mmHg)	0.97	0.69 – 1.33	0.82
Total pulmonary resistance (WU)	1.06	0.78 – 1.43	0.71
Pulmonary vascular resistance (WU)	1.10	0.79 – 1.50	0.56
Preoperative laboratory data (n=159)			
CRP \geq 10 mg/L (%)	2.79	1.32 – 5.93	<0.01
CRP levels (<10; [10;20[and \geq 20 mg/L)	1.82	1.10 – 3.00	0.02
LogCRP	1.42	1.02 – 1.97	0.04
Fibrinogen (mg/dL)	0.84	0.71 – 1.40	0.96
Interleukin-1 (ng/mL) n=72	0.61	0.28 – 1.39	0.24
Interleukin-6 (ng/mL) n=78	1.94	1.25 – 3.70	0.01
MCP-1 (ng/mL) n=72	1.00	0.03 – 1.00	0.84
D-dimers (ng/mL)	1.00	0.99 – 1.79	0.93
Antithrombin III (%)	1.15	0.75 – 1.75	0.64
Leucocytes (G/L)	1.54	1.01 – 2.32	0.04
Neutrophils (G/L)	1.46	1.04 – 2.02	0.03

Monocytes (G/L)	1.43	1.02 – 2.01	0.04
Neutrophil/Lymphocyte ratio	1.26	0.81 – 1.96	0.31
Hemoglobin (g/dL)	0.79	0.56 – 1.10	0.16
Platelets (G/L)	1.00	0.41 – 1.00	0.83
Blood urea nitrogen (mg/dL)	1.03	0.87 – 1.22	0.74
Creatinine clearance < 60 mL/min	2.03	0.99 – 1.11	0.05
Aspartate transaminase (U/L)	1.52	0.79 – 2.96	0.21
Alanine transaminase (U/L)	0.49	0.24 – 0.98	0.04
Gamma-glutamyl transferase (U/L)	0.77	0.46 – 1.47	0.47
Alkaline phosphatase (U/L)	1.38	0.82 – 2.33	0.23
Total bilirubin (µmol/L)	1.60	0.88 – 2.94	0.13
Conjugated bilirubin (µmol/L)	0.72	0.33 – 1.56	0.41
BNP (pg/mL)	1.55	1.00 – 1.09	0.28
Preoperative echocardiograms (n=59)			
RV end-diastolic area index (cm ² /m ²)	2.75	1.34 – 5.41	<0.01
RV end-systolic area index (cm ² /m ²)	2.59	1.32 – 4.89	<0.01
RV end-systolic remodeling index	3.46	1.57 – 7.63	<0.01
RV fractional area change (%)	0.56	0.30 – 1.08	0.08
RV longitudinal strain (absolute %)	0.68	0.38 – 1.17	0.18
Tricuspid annular plane systolic excursion (mm)	0.69	0.40 – 1.24	0.23
Right atrial area index (mmHg)	2.28	0.96 – 2.91	0.08
Perioperative data (n=159)			
Jamieson classification (reference group = 1)			0.01
Group 2	2.76	0.58 – 13.15	0.20
Group 3	6.57	1.31 – 32.86	0.02
Group 4	12.00	1.56 – 92.29	0.02
Associated cardiac procedure (%)	1.72	0.53 – 5.61	0.37
Cardiopulmonary bypass duration (min)	2.08	1.45 – 2.99	0.02
Aortic clamping duration (min)	1.55	1.25 – 1.93	0.01
Circulatory arrest duration (min)	1.22	0.82 – 1.63	0.31

*Odd ratios are presented as odd ratio adjusted by the standard deviation of the continuous variable (OR^{SD}) for comparison purposes. CRP: C-reactive protein; MCP-1: monocyte chemoattractant protein-1; RV: right ventricular.

Table 5. Logistic regression analysis of correlates of the primary endpoint (early death or heart-lung transplant or ECMO need or prolonged inotropic/catecholamine support) in the validation cohort (n=238).

Variables	Univariate analysis			Multivariate analysis		
	Odd ratio*	95% CI	p-value	Odd ratio*	95% CI	p-value
Age (years)	1.73	1.32 – 2.57	<0.01	1.73	1.32 – 2.25	<0.01
Female sex	0.76	0.45 – 1.27	0.29	-	-	-
Body mass index (kg/m ²)	0.80	0.60 – 1.06	0.08			
NYHA class (reference = I)			<0.01			
II	0.36	0.05 – 2.80	0.33			
III	0.93	0.13 – 6.80	0.94			
IV	1.29	0.16 – 10.30	0.81	-	-	-
6-minute walk test distance (m)	0.29	0.28 – 3.46	0.16			
Right heart catheterization						
Right atrial pressure (mmHg)	1.09	0.84 – 1.46	0.58	-	-	-
Mean pulmonary arterial pressure (mmHg)	1.97	1.41 – 2.45	<0.01			
Cardiac index (mmHg)	0.65	0.48 – 0.87	<0.01			
Total pulmonary resistance (WU)	1.82	1.33 – 2.43	<0.01	-	-	-
Pulmonary vascular resistance (WU)	1.66	1.19 – 2.25	<0.01			
Laboratory data						
CRP ≥ 5 mg/L (%)	1.58	0.99 – 2.65	0.05			
CRP ≥ 10 mg/L (%)	1.85	1.02 – 3.36	0.03	1.89	1.09 – 3.61	0.04
LogCRP	1.37	1.05 -1.92	0.02			
Creatinine clearance < 60 mL/min	2.99	1.68 – 5.34	<0.01			
Perioperative data						
Jamieson classification						

(reference group = 1)							
Group 2		0.73	0.21 – 2.62	0.63			
Group 3		0.79	0.21 – 2.98	0.73			
Group 4		2.00	0.24 – 16.36	0.52			
Cardiopulmonary bypass duration (min)		1.44	1.09 – 1.84	<0.01			
Aortic clamping duration (min)		2.06	1.28 – 3.31	<0.01	1.63	1.28 – 2.06	<0.01
Circulatory arrest duration (min)		1.10	0.85 – 1.43	0.47			

*Odd ratios are presented as odd ratio adjusted by the standard deviation of the continuous variable (OR^{SD}) and their adjusted confidence interval (95% CI) for comparison purposes. CRP: C-reactive protein.

SUPPLEMENTARY MATERIALS

Supplementary Table S1. Perioperative characteristics of the total study population and comparison between patients with low versus high preoperative CRP levels.

	Total cohort n=159	CRP <10mg/L n=122	CRP ≥10mg/L n=37	p value*
Jamieson classification				
Group 1 (%)	14 (8.8)	10 (8.2)	4 (10.8)	0.11
Group 2 (%)	92 (57.9)	73 (59.8)	19 (51.4)	
Group 3 (%)	44 (27.7)	35 (28.7)	9 (24.3)	
Group 4 (%)	9 (5.7)	4 (3.3)	5 (13.5)	
Associated surgical procedure (%)**	12 (7.5)	10 (8.2)	2 (5.4)	0.78
Cardiopulmonary bypass duration (min)	222.0 [199.0-244.0]	222.0 [200.0-242.5]	222.0 [196.0-249.0]	0.68
Aortic clamping duration (min)	96.0 [85.0-112.3]	98.0 [85.5-111.5]	96.0 [83.0-119.5]	0.91
Circulatory arrest duration (min)	28.0 [23.0-35.5]	27.5 [23.0-35.0]	29.0 [22.0-36.0]	0.79

*Comparison between the two subgroups with negative or positive preoperative CRP levels (using Mann-Whitney test or Chi-square test). **Including coronary arterial bypass graft or ascending aortic procedures.

Supplementary Table S2. Characteristics of the validation cohort and comparison between patients with low and high preoperative CRP levels.

	Total cohort n=238	CRP <5mg/L n=134	CRP ≥5mg/L n=104	p value*
Age (years)	63.5 [50.0-70.0]	65.4 [51.8-71.1]	61.0 [48.6-69.0]	0.11
Female sex (%)	110 (46.2)	59 (44.0)	51 (49.0)	0.56
Body mass index (kg/m ²)	25.8 [23.0-29.4]	26.0 [23.2-29.4]	25.5 [22.9-31.1]	0.78
Presence of endovascular device** (%)	8 (3.4)	3 (2.2)	5 (4.8)	0.27
History of splenectomy (%)	4 (6.7)	1 (0.7)	3 (2.9)	0.19
New York Heart Association functional class				
I	4 (6.7)	2 (1.5)	2 (1.9)	
II	60 (25.2)	38 (28.4)	22 (21.2)	0.21
III	141 (59.2)	81 (60.4)	60 (57.7)	
IV	32 (13.4)	13 (9.7)	19 (18.3)	
Six-minute walk test distance (m)	(n=106) 384.5 [293.5-460.0]	(n=68) 390.0 [293.3-460.8]	(n=38) 371.5 [291.0-460.0]	0.86
Hemodynamics				
RAP (mmHg)	8.0 [5.0-10.0]	7.5 [5.0-10.0]	9.0 [5.0-11.0]	0.04
Mean PAP (mmHg)	45.0 [38.0-53.0]	43.0 [35.0-50.0]	49.0 [40.0-55.0]	<0.01
Cardiac Index (L/min/m ²)	2.4 [2.0-2.8]	2.5 [2.1-2.8]	2.3 [2.0-2.8]	0.05
Total Pulmonary Resistance (WU) / index (WU/m ²)	10.0 [7.3-13.3]/ 17.7 [13.9-24.3]	9.4 [6.8-12.6]/ 16.8 [12.8-22.8]	10.4 [8.4-13.5]/ 19.7 [14.5-27.2]	0.04/ <0.01
Pulmonary Vascular Resistance (WU)/index (WU/m ²)	(n=189) 7.6 [5.0-10.8]/ 13.6 [10.1-19.7]	(n=112) 7.3 [4.8-9.2]/ 13.1 [9.6-17.9]	(n=77) 8.0 [5.7-11.7]/ 15.3 [10.5-22.6]	0.09/ 0.08

Therapies				
Treatment naïve (%)	211 (88.7)	123 (91.8)	88 (84.6)	0.08
Double therapy (%)	9 (3.8)	7 (5.2)	2 (1.9)	0.19
Triple therapy (%)	2 (0.8)	0	2 (1.9)	0.11
Prostanoid therapy (%)	9 (3.8)	0	9 (8.7)	<0.01
Phosphodiesterase inhibitors (%)	8 (3.4)	4 (3.0)	4 (3.8)	0.73
Endothelin receptor blockers (%)	15 (6.3)	8 (6.0)	7 (6.7)	0.83
Riociguat (%)	8 (3.4)	2 (1.5)	6 (5.8)	0.07
Statins (%)	29 (12.2)	14 (10.4)	15 (14.4)	0.35
Laboratory data				
Creatinine clearance (mL/min)				
≥60mL/min	165 (69.3)	97 (72.4)	68 (65.4)	
59 - 30mL/min	68 (28.6)	34 (25.4)	34 (32.7)	0.22
<30mL/min	0	0	0	
Jamieson classification				
Group 1 (%)	10 (4.2)	4 (3.0)	6 (5.8)	
Group 2 (%)	154 (64.7)	85 (63.4)	69 (66.3)	0.56
Group 3 (%)	68 (28.6)	42 (31.3)	26 (25.0)	
Group 4 (%)	6 (2.5)	3 (2.2)	3 (2.9)	
Associated cardiac procedure (%)**	12 (5.0)	2 (0.7)	10 (9.6)	<0.01
Cardiopulmonary bypass duration (min)	218.0 [193.5-251.0]	212.0 [194.0-250.0]	223.5 [193.3-255.3]	0.35
Aortic clamping duration (min)	97.0 [82.0-110.5]	97.0 [81.5-109.0]	98.0 [83.0-117.0]	0.23
Circulatory arrest duration (min)	30.0 [22.0-38.0]	30.5 [22.8-38.3]	28.0 [21.0-36.0]	0.19

*Comparison between the two subgroups with preoperative CRP levels lower or higher than the detection threshold (5mg/L) (using Mann-Whitney test or Chi-square test). **Including implantable port,

pacemakers, ventricular-arterial derivation. None of the patients had chronic inflammatory disease. PAP: pulmonary arterial pressure; RAP: right atrial pressure; RV: right ventricular.

Study 2: Proteomics of Right Heart Failure in Patients with Pulmonary Arterial Hypertension.

Summary: Immunity plays a major role in the pathogenesis and progression of pulmonary vascular remodeling in PAH. Having previously defined right heart maladaptive phenotyping in part 2 of the results section, this study aimed to identify the immune proteomic profile associated with right heart maladaptation in patients with PAH. Two clinical prospective cohorts from the Stanford Vera Moulton Wall center who underwent plasmatic proteomic profiling using 48-plex flow cytometry multiplex Luminex® (including interleukins, chemokines and growth factors) were included. Right heart maladaptive phenotype was defined using two prognostic right heart scores: the Mayo right heart score (based on right ventricular RV longitudinal strain, NYHA class and NT-proBNP) and the Stanford right heart score (based on RV end-systolic remodeling index, NYHA class and NT-proBNP).

This screening proteomics study identified three circulating cytokines to be associated with right heart maladaptive features in a discovery and validation cohort of patients with PAH. High plasmatic levels of hepatic growth factor (HGF), nerve growth factor (NGF) and stem cell growth factor (SCGF β) were significantly associated with worst Mayo and Stanford right heart scores, RV dysfunction based on RVLS, RV adverse end-systolic remodelling based on RVESRI, worst NYHA functional class and higher NT-proBNP levels. These cytokine levels were not associated with pulmonary hemodynamic severity, suggesting these biomarkers to reflect the compromised right ventricle itself rather than pulmonary vascular disease.

These exploratory results illustrate the use of right heart phenotyping including non-invasive imaging biomarkers to explore circulating biomarkers and molecular pathways associated with right heart failure. Flow cytometry multiplex arrays enable to screen a wide range of plasmatic cytokines in a limited blood volume. Validation of the value of these circulating biomarkers and their role in right heart remodeling and failure in PAH remains to be proven.

ABSTRACT

Background: Immunity has extensively been demonstrated to play a major role in the pathophysiology of pulmonary vascular remodeling in pulmonary arterial hypertension (PAH). There has also been increasing evidence of the presence of inflammation within pressure-overloaded right ventricle, suggesting a link between immunity and right heart adaptation to increased overload. To date, most of the proteomics studies have focused on the pulmonary vasculature rather than on the right ventricle itself.

Objective: To determine the circulating immune proteomic profile associated with right heart maladaptive phenotype in patients with PAH.

Methods: This study included 121 patients with PAH from 2008 to 2011 (discovery cohort) and 76 patients from 2011 to 2014 (validation cohort), who underwent plasmatic proteomic profiling using 48-plex flow cytometry multiplex Luminex® (including interleukins, chemokines and growth factors). Right heart maladaptive phenotype was defined using two prognostic right heart scores: the Mayo right heart score (based on right ventricular RV longitudinal strain, NYHA class and NT-proBNP) and the Stanford right heart score (based on RV end-systolic remodeling index, NYHA class and NT-proBNP). The association between cytokines and right heart maladaptive phenotype was assessed using partial least square (PLS) regression analysis.

Results: The median age of the discovery cohort was 50 [39 – 59] years, with a majority of female (74%), and connective tissue disease as the most frequent etiology of PAH (33%). Patients from the validation cohort were more frequently female ($p=0.04$) and had more severe features (lower six minute walk test distance, lower cardiac index and higher levels of NT-proBNP) than patients from the discovery cohort, while pulmonary vascular resistance levels and right heart echocardiography metrics were similar. Using PLS analysis, high levels of hepatic growth factor (HGF), stem cell growth factor beta (SCGF β) and nerve growth factor (NGF) were significantly associated with worst Mayo scores and worst Stanford scores but not with pulmonary vascular resistance or mean pulmonary arterial pressure, in both cohorts. No cytokine was consistently associated with favorable right heart scores in our study.

Conclusion: High plasmatic levels of HGF, SCGF β and NGF are associated with right heart adaptive phenotypes beyond pulmonary resistance in patients with PAH. Validation of the expression of these biomarkers and their receptors in the right ventricle remains to be performed.

KEYWORDS: Biomarkers; Immunity; Proteomics; Right Heart Failure; Pulmonary Hypertension.

INTRODUCTION

Pulmonary arterial hypertension (PAH) is characterized by the progressive remodeling and narrowing of the pulmonary arterial tree, leading to pulmonary hypertension, right heart remodeling and eventually right heart failure (RHF) and death in the absence of transplant (244). Right heart failure is a cornerstone in the natural history of the disease. Recent non-invasive imaging studies have improved right heart adaptive phenotyping, identifying right ventricular (RV) end-systolic remodeling and RV deformation imaging-based strain using as the two strongest prognostic markers of RV adaptation to afterload, in association with the New York Heart Association (NYHA) functional class and the N-terminal pro b-type natriuretic peptide (NT-proBNP) (145,146,261).

Better understanding the pathophysiology underlying the progression from RV adaptation to maladaptation to increased afterload in PAH is essential to improve early detection of RHF and identify potential targets for RV-focused therapies (262,19,263). Immunity has extensively been demonstrated to be involved in the pathophysiology of pulmonary vascular remodeling in PAH (46,82–84). High levels of circulating mediators of inflammation (such as the interleukin-1 cytokine) have been associated with worst disease severity, impaired functional status and lower survival (85–88,264). Inflammatory features have not only been reported in the pulmonary vasculature or in the systemic bloodstream, but also in the right ventricle itself (100,137,138). In addition to *in situ* ventricular inflammation, circulating cytokines released by the pulmonary vasculature may have a direct toxic effect on the right heart, promoting local inflammation, adverse right ventricular remodeling and eventually contributing to right heart maladaptation to pressure overload (100).

To our knowledge, there has been no proteomics screening study focusing on the right heart in PAH, partially because of the longstanding challenges of RV phenotyping. In this study, we used the recently published right heart risk scores based on the Mayo Clinic model (i.e. RV strain, NYHA class and NT-proBNP) and the Stanford model (i.e. RV end-systolic remodeling index, NYHA class and NT-proBNP) to define right heart maladaptive phenotypes (145,146). We hypothesized that patients with

PAH would express a specific blood circulating biomarker profile according to right heart maladaptive phenotype, beyond the pulmonary vascular disease severity.

Using the Stanford Vera Moulton Wall Center prospective registry of patients with PAH, this study sought to identify the circulating immune and growth factor biomarkers profile associated with right heart maladaptive phenotype in a discovery and a validation cohort, using flow cytometry multiplex arrays.

METHODS

Study population

This study includes patients from the prospective registry for PAH of the Vera Moulton Wall Center for Pulmonary Hypertension at Stanford (CA, USA). Between 2008 and 2014, 245 consecutive patients were included in the registry. Inclusion criteria were: diagnosis of PAH according to the latest guidelines (mean pulmonary arterial pressure MPAP \geq 25mmHg and pulmonary arterial wedge pressure PAWP \leq 15mmHg (7); plasmatic proteomics profiling using flow cytometry multiplex arrays and NT-proBNP levels available within 2 weeks of echocardiography. Exclusion criteria were the following: 1) proteomics data not available (n=30); 2) congenital systemic-to-pulmonary shunts (n=10); 3) complete echocardiographic study not available for review (n=6), 4) advanced cancer at baseline (n=1). The cohort was divided in a discovery cohort (121 patients included between 2008 and 2011, in whom proteomics were analysed in 2012, and a validation cohort (76 patients included from 2011 to 2014, in whom proteomics were analysed in 2014). Baseline was defined by the date of blood sampling. Stanford University Institutional Review Board approved the study, which was conducted in agreement with the Helsinki-II-declaration. All patients gave written informed consent.

Sample Preparation and Cytokine Analysis

Blood samples were collected, and plasma was prepared. To measure a panel of cytokines, we used a 48-plex flow cytometry multiplex arrays Luminex® bead kit (Affymetrix, Santa Clara, CA, USA), presented in **Table 1** and supplementary **Table S1**. Each sample was measured in duplicate. Plates were read using

a Luminex LabMap200 instrument with a lower bound of 100 beads per sample per measured cytokine. The Luminex LabMap200 outputs the fluorescence intensity of each bead measured for a given cytokine in a sample. For each well, we considered the median fluorescence intensity (MFI) of all beads measured for a given cytokine and average the MFI of the two duplicates.

Clinical, Laboratory and Hemodynamic assessment

New York Heart Association (NYHA) functional class, six minute walking distance (m), diffusing capacity of the lung for carbon monoxide, glomerular filtration rate calculated using the MDRD formula based on serum creatinine and NT-proBNP (Roche Diagnostics, Mannheim, Germany) within a month of inclusion were collected. Right heart catheterization, within 3 months of inclusion (available within a week for 77% of patients), was performed through the internal jugular or right femoral vein. The following measurements were collected: right atrial pressure, MPAP, PAWP, pulmonary vascular resistance (PVR, measured as transpulmonary gradient divided by cardiac output) and cardiac index (using the thermodilution method or the Fick method in case of severe tricuspid regurgitation).

Echocardiographic assessment

Digitized echocardiographic studies were acquired by the Stanford Biomarker and Phenotypic Laboratory, using Hewlett Packard Sonos 5500 or Philips IE 33 ultrasound systems (Philips, Amsterdam, The Netherlands). All measures were averaged over three cycles, performed according to latest guidelines (49,140) and assessed off-line by two blinded certified readers, as recently described (145). Right heart dimensions and functional metrics were measured on RV-focused apical 4-chamber views (185). RV end-systolic area was indexed on ideal body weight-adjusted body surface area (RVESAI). RV end-systolic remodeling index (RVESRI) was defined by the lateral wall to septal height ratio (145). RV function was assessed using free-wall Lagrangian longitudinal strain (RVLS, measured from mid-endocardial end-diastolic and end-systolic manually traced lengths), RV fractional area change (RVFAC) and tricuspid annular plane systolic excursion (TAPSE).

Right heart risk scores

Right heart adaptive phenotypes were defined using the two following right heart scores predicting outcomes in PH (presented in supplementary **Table S2**): the Mayo Clinic score, derived from Fine et al.'s model in patients with suspected or confirmed pulmonary hypertension, including RVLS, NYHA class and NT-proBNP (146), and the Stanford score derived from the Vera Moulton Wall Center PAH cohort model (including the presented study cohort) integrating RVESRI, NYHA class and NT-proBNP (145). The REVEAL score was also calculated: low risk was defined by a score between 0 and 7, average if equal to 8, moderate high if equal to 9, high if equal to 10 or 11 and very high if ≥ 12 (244).

Statistical analysis

Data are summarized as median and interquartile range for continuous variables, and number of subjects (%) for categorical variables. Comparisons between groups were performed using Mann-Whitney test and Chi-square test respectively. Mean fluorescent intensity (MFI) of Luminex® data were averaged (duplicates) and logarithmically transformed to normalize its distribution prior to analysis. In addition, pre-processing also include normalization for plate-effect and non-specific binding. Identification of cytokines associated with Mayo right heart score and Stanford right heart score (as continuous variables) was performed using sparse partial least squares discriminant analysis (sPLSDA) in both cohorts. Identification of cytokines associated with the components of the scores (RVLS, NYHA, NT-proBNP and RVESRI) and pulmonary hemodynamics (MPAP and pulmonary vascular resistance) was also performed using the same methodology in both cohorts. Results were considered significant when two-sided p values were <0.05 . Statistical analysis was performed using SPSS® statistical software (SPSS V.19, Inc, Chicago, IL) and RStudio Version 1.0.136 (© 2009-2016 RStudio, Inc).

RESULTS

Study cohorts

In total, 198 patients were included in the study, 121 in the discovery cohort and 76 in the validation cohort. Comparative baseline characteristics of the two cohorts are presented in **Table 2**. The median age of the discovery cohort was 50 [39 – 59] years, with a majority of female (74%), and connective tissue

disease as the most frequent etiology of PAH (33%). Patients from the validation cohort were more frequently female ($p=0.04$) and had more severe features (lower six minute walk test distance, lower cardiac index and higher levels of NT-proBNP) than patients from the discovery cohort. As patients from the validation cohort were more frequently incidental cases, they were less frequently treated by PAH therapies. The PVR and echocardiographic metrics did not significantly differ from the two cohorts. The REVEAL risk categories repartition was similar in the two cohorts: 61.2% were classified low risk in the discovery cohort versus 60.5% in the validation cohort, 14.0% versus 19.7% were classified as average/moderately high risk, and 24.8% versus 19.7% were classified as high/very high risk respectively ($p=0.48$). Similarly, the repartition of the right heart risk scores did not differ between the two groups. Regarding the Mayo risk score, 47.1% patients had a low score (0-5) in the discovery cohort versus 43.4% in the validation cohort, 33.1% versus 36.8% had an intermediate score (6-8), and 19.8% versus 19.7% had a score higher than 9 ($p=0.85$). Regarding the Stanford risk score, 40.5% patients had a low score (0-2) in the discovery cohort versus 39.5% in the validation cohort, 38.0% versus 34.2% had an intermediate score (3), and 21.5% versus 26.3% had a score higher than 4 ($p=0.72$).

Proteomics profiling of right heart maladaptation

The circulating biomarkers significantly associated with right heart metrics using partial least square regression analyses in the discovery cohort ($n=121$) are presented in **Table 3** and **Figure 1**. High levels of HGF, SCGF β and NGF were significantly associated with worst Mayo risk score, worst Stanford risk score, RV dysfunction based on RVLS, RV adverse remodelling based on RVESRI, higher NT-proBNP and NYHA functional class, but not with pulmonary disease severity (mean pulmonary arterial pressure and PVR). High SDF1a levels were significantly associated with worst Mayo and Stanford scores and RV dysfunction. None of the cytokines was consistently and significantly associated with favorable right heart metrics. Supplementary **Figure S1** presents the raw Volcano plots of the partial least square analyses.

When performing partial least square regression analyses in the validation cohort ($n=76$), high levels of HGF, SCGF β and NGF were significantly associated with worst Mayo score, worst Stanford risk

score and RV dysfunction based on RVLS (**Table 3** and **Figure 1**). High HGF levels were also associated with adverse RV end-systolic remodeling and high NT-proBNP, and high SCGF β levels were associated with high NT-proBNP. None of the cytokines was consistently and significantly associated with favorable right heart metrics.

DISCUSSION

This screening proteomics study identifies three circulating cytokines to be associated with right heart maladaptive features in a discovery and validation cohort of patients with PAH. High plasmatic levels of HGF, NGF and SCGF β were significantly associated with worst Mayo and Stanford right heart scores, RV dysfunction based on RVLS, RV adverse end-systolic remodelling based on RVESRI, worst NYHA functional class and higher NT-proBNP levels. These cytokine levels were not associated with pulmonary hemodynamic severity, suggesting these biomarkers to reflect the compromised right ventricle itself rather than pulmonary vascular disease. Finally, none of the cytokines screened was consistently associated with favorable right heart metrics in both cohorts.

HGF (hepatic growth factor) is a mesenchymal-derived pleiotropic cytokine controlling cell migration, morphogenesis, apoptosis and proliferation. HGF binds to its tyrosine kinase receptor Met, the product of the c-Met proto-oncogene, expressed in different cell types such as epithelial, endothelial and mesenchymal cells (265). During embryogenesis, HGF influences cardiomyocyte proliferation and differentiation (266). In the adult heart, HGF/Met signaling controls homeostasis and prevents oxidative stress in normal cardiomyocytes (265). HGF is also a strong angiogenic growth factor; exogenous HGF has been shown to increase myocardial capillary density in rats before and after myocardial infarction (267). Overall, activating HGF and its receptor Met after myocardial infarction are thought to be cardioprotective through pro-survival (anti-apoptotic and anti-autophagic) effects in cardiomyocytes, increased angiogenesis, inhibition of fibrosis, anti-inflammatory and immunomodulatory effects, as well as increasing regeneration through activation of cardiac stem cells (268–270). Regarding its effects on the endothelium, HGF has been shown to inhibit vascular permeability and inflammation, while increasing

levels of VEGF (promoter of endothelial permeability and oedema) (271). HGF has also anti-fibrotic properties, reported in animal models of myocardial infarction and left cardiomyopathy (272–274), through the inhibition of the transforming growth factor- β 1 production (275). In addition, HGF has anti-inflammatory properties, decreasing the expression of adhesion molecules (such as intercellular adhesion molecule ICAM-1) on endothelial cells, thus decreasing recruitment of leukocytes by the endothelium (276). HGF is also an immunomodulator, promoting the differentiation of macrophages into dendritic cells and regulating T-cells (277). **Figure 2**, adapted from Gallo et al.'s excellent review, summarizes all the cardioprotective functions of HGF/Met axis that has been reported in the left heart (265).

Evidence on the role of HGF in the right heart is sparse. Several studies using different small animal PH models (e.g. rats with monocrotaline-induced PH, rabbits with shunt flow-induced PH) have shown that exogenous HGF or HGF gene transfection reduced the development of PH in these animals, which presented with lower MPAP associated with less marked right heart hypertrophy and lower inflammatory profiles (lower IL-6 levels and higher IL-10 levels) than shams (278–281). In humans, higher levels of HGF have been reported in patients with scleroderma-associated PAH than in healthy controls (282), as well as in a small cohort of patients with PAH from diverse etiology or idiopathic PAH in whom HGF positively correlated with MPAP (283). HGF has been described to increase expression of the Bone Morphogenetic Protein Receptor 2, a pathway found to be mutated in the familial form of PAH and downregulated in non-genetic forms (284), which was shown to be beneficial in PAH and RV failure when activated (285).

Despite all the cardioprotective effects of HGF mentioned previously, several studies have reported the association between high circulating levels of HGF and left ventricular remodeling and dysfunction and adverse outcomes in several pressure overloaded cardiac diseases, such as hypertension and aortic stenosis, or advanced left heart failure secondary to ischemic cardiomyopathy (286–288). In our study, we show that high levels of HGF are associated with right heart adverse remodeling and maladaptation, beyond the pulmonary vascular disease, in patients with PAH. As it promotes tissue repair, the increase of HGF can be expected in pressure overload or heart failure conditions, but it can be

hypothesized that high circulating levels of HGF may become detrimental eventually, potentially through down-regulation of the Met receptor (289). The potential beneficial role of HGF as a therapy in PAH has also been discussed (290), but the role of HGF in the right heart remains to be first elucidated. While the extensive literature on HGF and its role in the left heart provides a valuable external validation for the finding of this cytokine in our study, further validation is required to explore its role in the pressure-overloaded right heart.

NGF (nerve growth factor), discovered in 1976 by Rita Levi-Montalcini who was later awarded a Nobel Prize for her discovery, is the main neurotrophic factor that increases cardiac sympathetic activity (291–293). NGF binds to two receptors: the high-affinity tropomyosine-related receptor kinase A (TrkA) and the low-affinity NGF receptor (LNGFR/p75NTR). The pro-survival effects of NGF on cardiomyocytes has been reported through its binding to the TrkA receptor downstream signalling (294). Regarding the right heart – pulmonary circulation, a previous study documented higher secretion and endothelial expression of NGF from pulmonary arteries of patients with PH secondary to chronic obstructive pulmonary disease than controls without PH (295). However, there was no significant increase in the secretion or lung expression of NGF in patients with idiopathic PAH. In this study, the authors showed that NGF induced hyperreactivity to vasoconstrictors in rat and human isolated pulmonary arteries, proliferation and migration of human pulmonary arterial smooth muscle cells and endothelial cells, and secretion of the proinflammatory cytokines IL-1 β and TNF- α (295). Anti-NGF blocking antibodies has been shown to reverse PH in the animal models of PH, decreasing pulmonary vascular remodeling, hyperreactivity and inflammation, suggesting the potential of NGF as a therapy target in PH (295). Recently, an experimental study demonstrated rats with RV hypertrophy secondary to monocrotaline-induced PH demonstrated NGF upregulation associated with deterioration of neuronal cellular function (296). Two studies have shown that NGF is downregulated in patients with end-stage left heart failure (297,298), suggesting a time-variability of this factor in heart failure, highlighting the need to further explore the involvement and role of NGF in the right ventricle of patients with PAH.

SCGF β (stem cell growth factor beta, also known as C-type lectin domain family 11 member A) is a human growth factor whose function and downstream signalling pathways remains underexplored. Higher plasmatic concentrations of SCGF β has been documented in patients with idiopathic and scleroderma-associated PAH than in patients with scleroderma without PAH (299). Higher plasmatic levels of SCGF β have also been reported in patients with dilated cardiomyopathy and Chagas disease, without a link with outcomes (300). Taken together with our results suggest further investigations on the role of SCGF β in right heart failure. Finally, in our study, SDF1a (stromal cell-derived factor 1, also known as the chemokine CXCL12) was significantly associated with worst right heart scores in the discovery cohort but not in the validation cohort. Increased plasmatic levels of SDF1a has been previously reported in 61 patients with idiopathic PAH as compared to healthy controls; SDF1a levels also correlated with NT-proBNP and RV function (assessed by tricuspid annular plane systolic excursion and RV ejection fraction) (137).

Clinical implications

A recent multicentered study by Rhodes et al. has analyzed the plasmatic proteomics associated with survival in 4 cohorts of patients with PAH using DNA-based aptamer reagents, known as SOMAmers (301). The study identified among a panel of 1129 proteins (including HGF, NGF and SCGF β) 9 proteins associated with adverse outcomes, independently from NT-proBNP and the REVEAL score (301,302). The authors can be commended for their precise and robust methodology enabling to offer a large screening in PAH.

To our knowledge, our study is the first to screen proteomics profiles associated with specific right heart features of maladaptation to pressure overload in two cohorts of patients with PAH. Including two cohorts differing in terms of demographics, prevalence/incidence repartition, and functional severity strengthens the results, suggesting that the biomarkers identified are associated to right ventricular adaptation, across PAH etiology. These exploratory results illustrate the use of right heart phenotyping including non-invasive imaging biomarkers to explore circulating biomarkers and molecular pathways

associated with right heart failure. Flow cytometry multiplex arrays enable to screen a wide range of plasmatic cytokines in a limited blood volume. Validation of the value of these circulating biomarkers and their role in right heart remodeling and failure in PAH remains to be proven.

Study limitations

This study has several limitations. The first limitation derives from its single-center design. This study includes two separate and independent cohorts, providing internal clinical validation. The fact that the two cohorts were collected and analysed at two different time points, excluding the risk of batch effect in the proteomics analysis, contributes to increase the confidence in the results. The current preliminary results however remain exploratory and required external clinical validation and/or translational validation. Indeed, the second and main limitation of this proteomics study is its screening nature, providing biomarkers candidate associated with right heart adverse remodeling in PAH. These results should be seen as hypothesis generating, leading to several validation studies that will be developed in the following section. However, the purpose of this work in the present thesis is to illustrate an application of the right heart deep phenotyping methods that have been presented in the previous chapter.

PERSPECTIVES – FURTHER INVESTIGATIONS

Our clinical screening study has identified three circulating biomarkers levels to be associated with right heart maladaptive phenotype in patients with PAH.

The following step is to experimentally demonstrate the expression of HGF, NGF and SCGF β and their receptors within the right ventricle of patients with PAH. Indeed, one cannot exclude for example that high circulating levels of HGF are not related to the heart itself but to hepatic congestion related to right heart failure. In order to study the cardiac expression of these biomarkers in PAH, we will use right and left ventricular samples from patients with PAH who underwent heart and lung transplantation at Marie Lannelongue Hospital, and compare them with samples from controls. Using immunofluorescence and Western blot analyses, we will compare the expression and localization of HGF, Met, NGF, TrKA and SCGF β (as its receptor has not been identified yet) in patients with end-stage right

heart failure and controls. We are aware that choosing patients who underwent heart-lung transplantation for PAH, likely presenting with end-stage right heart maladaptive phenotype, will only provide information on the expression of these markers in end-stage right heart failure.

We will consequently explore these markers, and specifically the HGF/Met signalling pathway, in a small animal model of PH. Recent single-cell RNA-sequencing (scRNAseq) in healthy mouse tissue (Tabula Muris Consortium “Mouse atlas”) shows only mildly expressed HGF in the heart at baseline in fibroblasts (PDGFRa) as well as smooth muscle cells (Acta2), whereas c-Met is expressed in inflammatory cells (Ptprc) as well as smooth muscle cells (Acta 2) (**Figure 3**) (303). In the liver, at baseline HGF is predominantly expressed in endothelial cells, whereas c-Met is mainly expressed in different subtypes of hepatocytes (303). In order to further explore the role of HGF in RV failure in pulmonary hypertension, we will study the expression of HGF and its receptor in the mouse model of pulmonary artery banding. Finally, the ongoing prospective clinical PRINCEPT study will provide information on the circulating levels of these biomarkers before and after endarterectomy in patients with chronic thromboembolic pulmonary hypertension and in patients undergoing lung transplantation for PAH.

CONCLUSION

This screening proteomic study identified high plasmatic levels of HGF, SCGF β and NGF to be associated with right heart adaptive phenotypes beyond pulmonary resistance in patients with PAH. Validation of the expression of these biomarkers and their receptors in the right ventricle remains to be performed.

ACKNOWLEDGMENTS

The authors would like to thank the Stanford Cardiovascular Institute and the Vera Moulton Wall Center of Pulmonary Hypertension at Stanford for their support. The authors would like to thank Andrew Hsi for database management. M. Amsallem received a Young Investigator Seed Grant from the Vera Moulton Wall Center and has been supported by a public grant overseen by the French National Research Agency as part of the second Investissement d'Avenir program (ANR-15-RHUS-0002). None of the authors have any potential conflicts of interest relative to the study.

FIGURES

Figure 1. Variable Importance in Projection (VIP) scores and correlations for each cytokine with respect to right heart scores and metrics in both cohorts.

MPAP: mean pulmonary arterial hypertension; NYHA: New York Heart Association; PVR: pulmonary vascular resistance; RVLS: right ventricular free-wall longitudinal strain is presented in absolute value (lowest values indicate worst right ventricular dysfunction); RVESRI: right ventricular end-systolic remodeling index. For cytokines abbreviations, please see **Table 1** and supplementary **Table S1**.

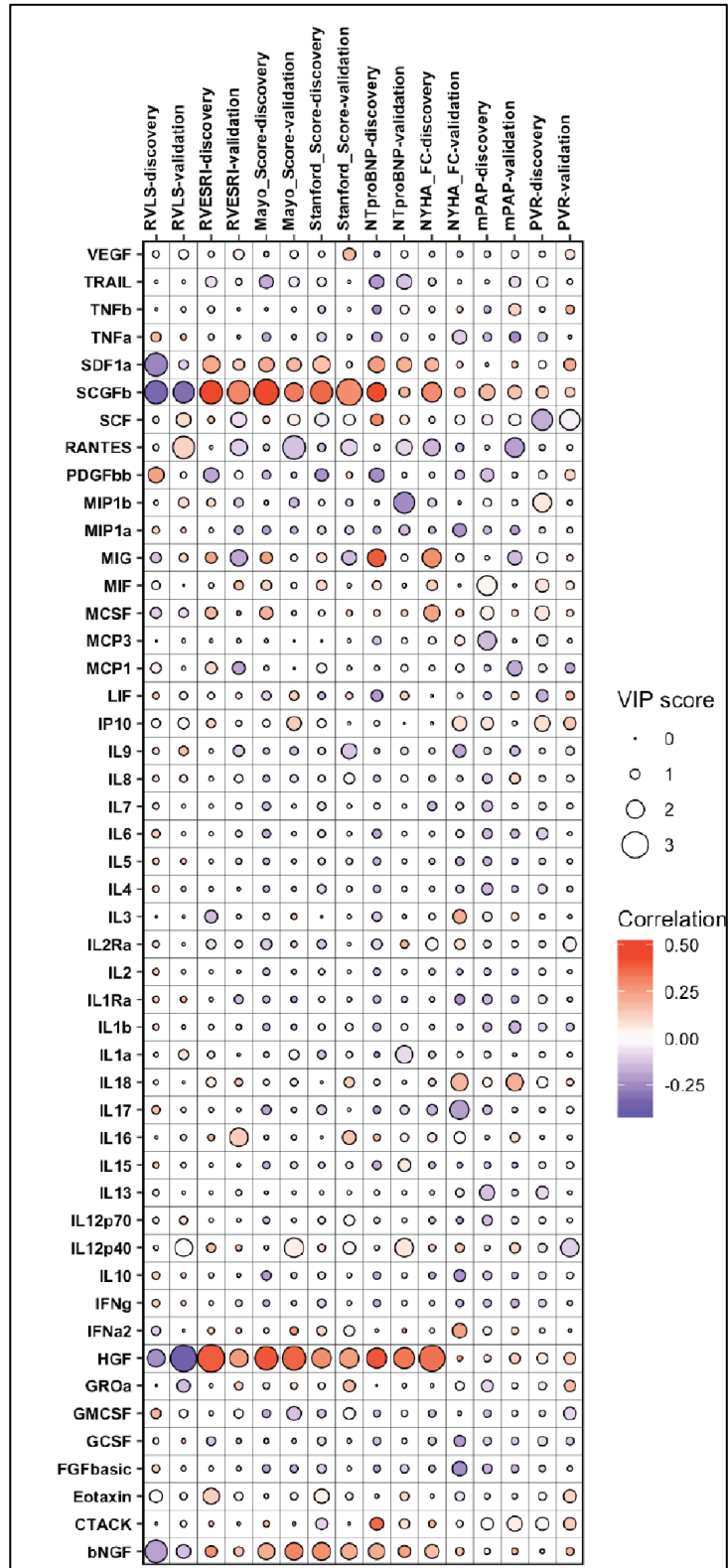
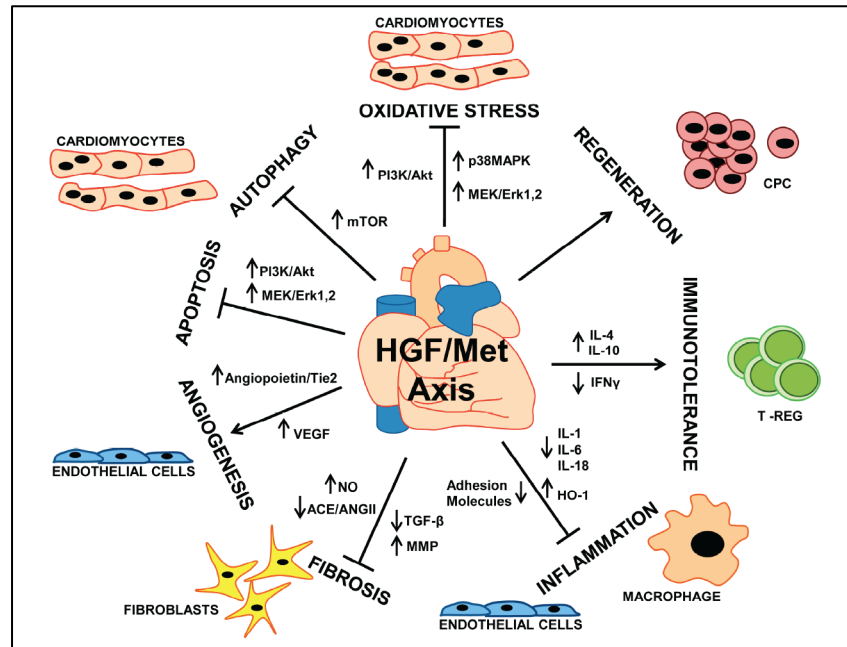
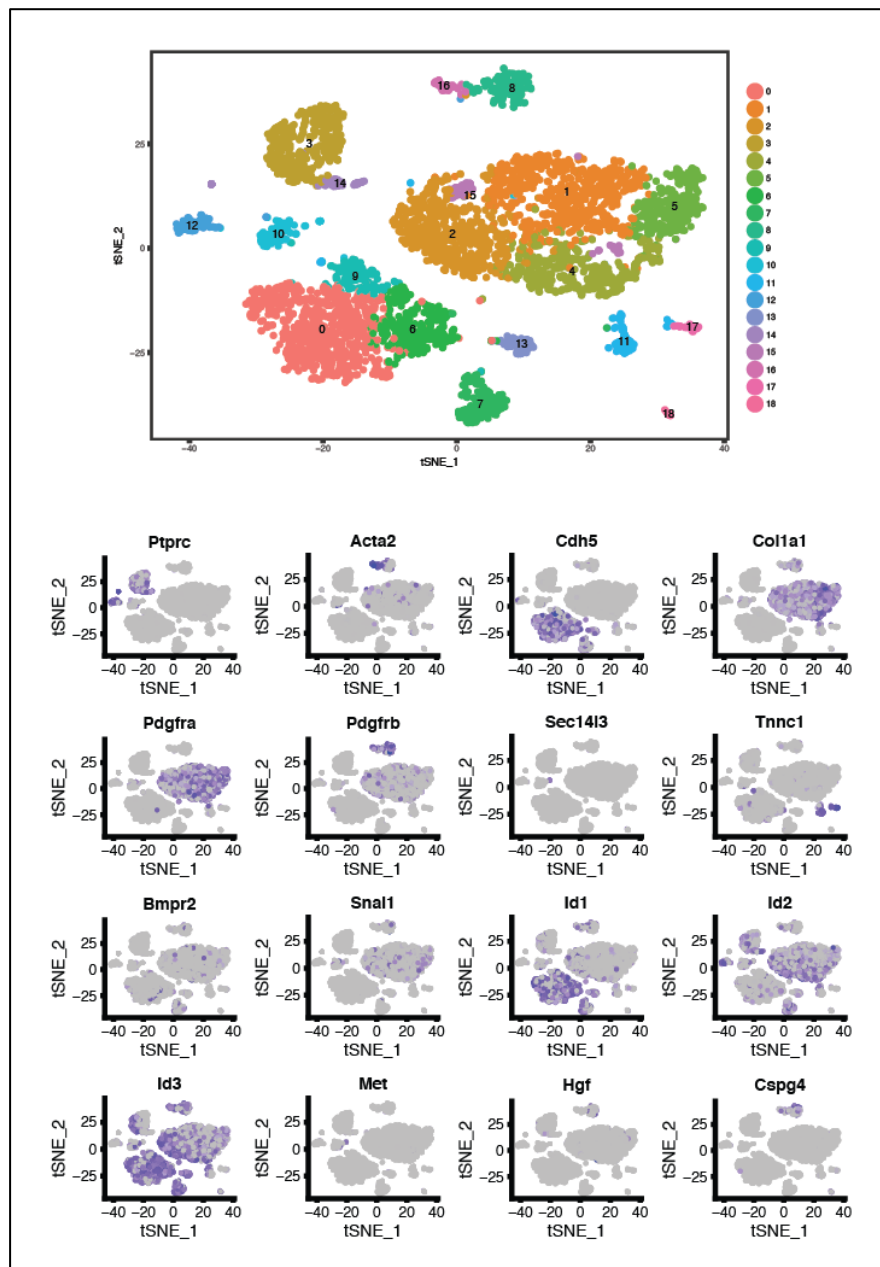


Figure 2. Existing evidence on the cardioprotective functions of HGF/Met axis in the left heart,
Adapted from Gallo et al. (265).



Schematic representation of the cardioprotective roles played by HGF mainly studied in the left heart. HGF/Met axis acts on the different cell populations of the cardiac tissue. HGF exerts anti-oxidant, anti-autophagic and anti-apoptotic effects in cardiomyocytes. It has a mitogenic effect on endothelial cells, leading to induction of angiogenesis, and inhibits fibrosis. Furthermore, HGF/Met presents an anti-inflammatory action, through modification of endothelial cells and macrophages. It also promotes expansion of regulatory T cells (T-REG), leading to immune tolerance. Finally, HGF activates cardiac progenitor cells (CPC) to induce regeneration of injured heart.

Figure 3. Unsupervised clustering and tSNE (t-distributed stochastic neighbor embedding) visualization of Single cell RNA Sequencing data revealing distinct types of cells (18 groups) in normal mouse heart tissue (Mouse atlas, Tabula Muris – upper panel) and **tSNE plots for selected genes from single cell RNA seq** of normal mouse heart (Mouse atlas) including Hepatocyte Growth Factor (HGF), Met-Receptor, endothelial cell markers (Cdh5), smooth muscle cell markers (Acta2), mesenchymal markers (Col1a1, Pdgfra), inflammatory markers (Ptprc), BMPR2, downstream targets of BMPR2 (Id1, Id2, Id3) and Cardiomyocyte marker (Tnnc1).



TABLES

Table 1. Circulating proteomic biomarkers assessed in the study using flow cytometry multiplex arrays.

Class	Biomarkers
Interleukins	IL-1 α , -1 β , -2, -3, -4, -5, -6, LIF, IL-7, -9, -10, -12p70, - 13, -15, -16, -17, -18
Interleukin receptors	IL-1R α , -2R α
Chemokines	MCP1=CCL2, MIP1 α =CCL3, MIP1 β =CCL4, RANTES=CCL5, MCP3=CCL7, CTACK=CCL27, Eotaxin, GRO α =CXCL1, IL-8=CXCL8, MIG=CXCL9, IP10=CXCL10, SDF1=CXCL12
Growth factors	MCSF (Macrophage colony-stimulating factor)=CSF1 (Colony stimulating factor 1), NGF (Nerve growth factor), SCF (Stem cell factor), SCGF β (Stem cell growth factor beta), TNF α (Transforming growth factor alpha), TNF β (Transforming growth factor beta 1), HGF (Hepatic growth factor), PDGFbb (Platelet-derived growth factor bb), FGF2=FGF β (Basic fibroblast growth factor), GCSF (Granulocyte colony- stimulating factor), GMCSF (Granulocyte-macrophages colony- stimulating factor), VEGF-A (Vascular endothelial growth factor-A)
Other cytokines	MIF (Macrophage migration inhibitory factor), TRAIL (TNF- related apoptosis-inducing ligand), IFNA2 (Interferon alpha-2), IFN γ (Interferon gamma)

Table 2. Comparative baseline characteristics of the discovery and validation cohorts.

Variables	Discovery cohort n=121	Validation cohort n=76	p value
Age (years)	50 [39 – 59]	52 [43 – 61]	0.20
Female sex	90 (74.4)	66 (86.8)	0.04
Body mass index (kg/m ²)	26.9 [22.5 – 31.9]	27.4 [24.7 – 33.5]	0.12
PAH etiology			0.40
Connective tissue disease	40 (33.1)	31 (40.8)	
Idiopathic	34 (28.1)	14 (18.4)	
Drugs and toxins	21 (17.4)	18 (23.7)	
Congenital heart disease	13 (10.7)	7 (9.2)	
Portal pulmonary hypertension	11 (9.1)	5 (6.6)	
Heritable PAH	2 (1.7)	1 (1.3)	
NYHA functional class			0.26
Class I	8 (6.6)	5 (6.6)	
Class II	48 (39.7)	20 (26.3)	
Class III	50 (41.3)	41 (53.9)	
Class IV	15 (12.4)	10 (13.2)	
Six minute walk distance (m)	427 [342 – 537]	392 [299 – 476]	0.03
NT-proBNP (pg/mL)	235 [67 – 977]	536 [150 – 1441]	0.04
DLCO (% predicted)	73 [60 – 86]	69 [53 – 92]	0.91
GFR (mL/min/1.73m ²)	68 [53 – 90]	66 [54 – 79]	0.21
Hemodynamics			
Right atrial pressure (mmHg)	7 [5 – 11]	7 [5 – 12]	0.49
Mean pulmonary arterial pressure (mmHg)	50 [40 – 59]	49 [40 – 58]	0.78
Pulmonary arterial wedge pressure (mmHg)	10 [8 – 13]	10 [7 – 14]	0.72
Pulmonary vascular resistance (WU)	9/9 [6.1 – 14.2]	10.3 [6.8 – 15.7]	0.56
Cardiac Index (L/min/m ²)	2.2 [1.8 – 2.5]	2.0 [1.6 – 2.3]	0.03

Echocardiographic metrics

RVESAI (cm ² /m ²)	12.7 [10.5 – 16.4]	12.9 [10.2 – 16.2]	0.81
RVESRI	1.4 [1.3 – 1.6]	1.5 [1.3 – 1.6]	0.43
RVLS (absolute value, %)	16.9 [13.9 – 20.0]	16.6 [13.2 – 21.1]	0.93
RVFAC (%)	27.1 [22.7 – 30.7]	26.6 [23.1 – 32.8]	0.91
TAPSE (cm)	1.8 [1.4 – 2.1]	1.7 [1.3 – 2.0]	0.20

PAH Therapy

Therapy extent			<0.01
Treatment naive	35 (28.9)	38 (50.0)	
Monotherapy	34 (28.1)	24 (31.6)	
Dual therapy	36 (29.8)	12 (15.8)	
Triple therapy	16 (13.2)	2 (2.6)	
Phosphodiesterase-5 inhibitors	62 (51.2)	28 (36.8)	0.04
Endothelin receptor antagonists	39 (32.2)	12 (15.8)	0.01
Prostanoid therapy	53 (43.8)	14 (18.4)	<0.01

Values are expressed as mean ±SD or number (percentage), or median and interquartile range (IQ). RVSP was estimable from the TR signal in 194 (85% patients). NYHA: New York Heart Association; PAH: pulmonary arterial hypertension; RV: right ventricular; RVESAI: RV end-diastolic area indexed on BSA; RVFAC: fractional area change; RVLS: free-wall longitudinal strain; RVSP: right ventricular systolic pressure; TAPSE: tricuspid annular plane systolic excursion.

Table 3. Biomarkers with significant partial least square regression coefficients for association with right heart metrics.

	High cytokine level associated with “unfavorable” metric		High cytokine level associated with “favorable” metric	
	Discovery	Validation	Discovery	Validation
Mayo right heart score	SCGFβ	HGF	TRAIL	None
	HGF	SCGFβ	IL2R α	
	NGF	NGF		
	MCSF			
	SDF1a			
	MIG			
Stanford right heart score	SCGFβ	SCGFβ	None	None
	HGF	HGF		
	NGF	NGF		
	SDF1a	VEGF		
	Eotaxin			
RVLS	SCGFβ	HGF	PDGF β	
	HGF	SCGFβ	GMCSF	None
	SDF1a	NGF	TNF α	
	NGF			
RVESRI	HGF	SCGFβ	PDGF β	None
	SCGFβ	HGF	IL3	
	NGF		GCSF	
	MCP1			
	Eotaxin			
NT-proBNP (log)	HGF	HGF	TRAIL	None
	SCGFβ		ILR2 α	
	NGF		PDGF β	
	MIG		LIF	
	SDF1a		IL3	
NYHA class	HGF	None	None	None
	SCGFβ			

	MIG			
	MCSF			
MPAP	None	None	MCP3	None
PVR	None	None	SCF	SCF
				IL12

P values <0.05 using Jackknife test were considered significant. MPAP: mean pulmonary arterial pressure; PVR: pulmonary vascular resistance; NT-proBNP: N-terminal pro-b type natriuretic peptide; NYHA: New York Heart Association; RVESRI: right ventricular end-systolic remodeling index; RVLS: right ventricular free-wall longitudinal strain. For circulating biomarkers abbreviations, please see **Table 1**.

SUPPLEMENTARY MATERIALS

Figure S1. Volcano plots of the partial least square regression analyses of the circulating proteomic biomarkers associated with right heart scores and metrics in both cohorts. The y-axis represents the VIP scores and the x-axis the Spearman correlation coefficient. Red: higher cytokine levels correlate with less favorable risk score or right heart metric (as continuous variables). Green: higher cytokine levels correlate with more favorable risk score or right heart metric. MPAP: mean pulmonary arterial hypertension; NYHA: New York Heart Association; PVR: pulmonary vascular resistance; RVLS: right ventricular free-wall longitudinal strain is presented in absolute value (lowest values indicate worst right ventricular dysfunction); RVESRI: right ventricular end-systolic remodeling index. For cytokines abbreviations, please see **Table 1** and supplementary **Table S1**.

Figure S1.



Table S1. Circulating proteomic biomarkers assessed in the study using flow cytometry multiplex arrays (Luminex®). PAH: pulmonary arterial hypertension; PH: pulmonary hypertension.

Abbreviation	Full name	Selected features
Interleukins and receptors		
IL1 α	Interleukin-1 alpha	<ul style="list-style-type: none"> - Pro-inflammatory cytokine - Produced by macrophages, neutrophils and endothelial cells - Induced TNFα release by endothelial cells - Stimulates hepatocytes for CRP secretion - Binds to the interleukin-1 receptor
IL1 β	Interleukin-1 beta	<ul style="list-style-type: none"> - Produced by activated macrophages as a proprotein, which is proteolytically processed to its active form from caspase 1 - Cell proliferation, differentiation and apoptosis
IL2	Interleukin-2	<ul style="list-style-type: none"> - Promotes the differentiation of immature T-cells into regulatory T-cells, effector T-cells or memory T-cells
IL3	Interleukin-3	<ul style="list-style-type: none"> - Stimulates proliferation of all cells in the myeloid lineage
IL4	Interleukin-4	<ul style="list-style-type: none"> - Induces the differentiation of naïve helper T-cells (Th0 cells) to Th2 cells - Decreases the production of Th1 cells and macrophages, promotes M2 repair macrophages > M1
IL5	Interleukin-5	<ul style="list-style-type: none"> - Produced by type-2 T helper cells and mast cells - Associated with eosinophil and allergy
IL6	Interleukin-6	<ul style="list-style-type: none"> - Acts as both a pro-inflammatory cytokine (secreted by macrophages and stimulating acute phase protein synthesis and production of neutrophils) and an anti-inflammatory myokine (through inhibitory effects on TNF-alpha and IL-1, and activation of IL-1ra and IL-10)
LIF	Leukemia inhibitory factor	<ul style="list-style-type: none"> - Interleukin-6 class cytokine - Affects cell growth by inhibiting differentiation - Role in cachexia and inflammation
IL7	Interleukin-7	<ul style="list-style-type: none"> - Hematopoietic growth factor, role in lymphocyte maturation
IL9	Interleukin-9	<ul style="list-style-type: none"> - Secreted by CD4+ helper cells that acts as a regulator of a variety of hematopoietic cells - Stimulates cell proliferation and prevents apoptosis
IL10	Interleukin-10	<ul style="list-style-type: none"> - Anti-inflammatory cytokine
IL12p70	Interleukin-12 (p70=active	<ul style="list-style-type: none"> - Produced by dendritic cells, macrophages, and neutrophils - Promotes the differentiation of naive T cells into Th1 cells, involved in the activation of NK cells and T-cells - Stimulates production of IFNγ and TNFα - Anti-angiogenic activity
IL12p40	heterodimer) (p40=homodimer)	
IL13	Interleukin-13	<ul style="list-style-type: none"> - Involved in allergic inflammation
IL15	Interleukin-15	<ul style="list-style-type: none"> - Secreted by mononuclear phagocytes - Induces cell proliferation of NK cells
IL16	Interleukin-16	<ul style="list-style-type: none"> - Pleiotropic cytokine that functions as a chemoattractant and a modulator of T cell activation
IL17	Interleukin-17	<ul style="list-style-type: none"> - Proinflammatory cytokine, acts in synergy with IL1 and TNFα
IL18	Interleukin-18	<ul style="list-style-type: none"> - Proinflammatory cytokine - Produced by macrophages and other cells

IL1R α	Interleukin-1 receptor alpha chain	<ul style="list-style-type: none"> - Secreted by immune and epithelial cells - Natural inhibitor of the pro-inflammatory effect of IL1β
IL2R α	Interleukin-2 receptor alpha chain	<ul style="list-style-type: none"> - Transmembrane protein present on activated T-cells and B-cells - Soluble form elevated in T-cell lymphoma/leukemia used for disease monitoring.
Chemokines		
MCP1 = CCL2	Chemokine (C-C motif) ligand 2	<ul style="list-style-type: none"> - Recruits monocytes, memory T cells, and dendritic cells to the sites of inflammation - Implicated in the pathogenesis of atherosclerosis, CTEPH
MIP1 α = CCL3	Chemokine (C-C motif) ligand 3	<ul style="list-style-type: none"> - Produced by macrophages after stimulation by bacterial endotoxin - Activates granulocytes (neutrophils, eosinophils and basophils) leading to acute neutrophilic inflammation - Induces secretion of IL-1, -6 and TNF-α from fibroblasts and macrophages - Idem than CCL3.
MIP1 β = CCL4	Chemokine (C-C motif) ligand 4	<ul style="list-style-type: none"> - Recruits T cells, eosinophils, and basophils, - Plays an active role in recruiting leukocytes into inflammatory sites
RANTES = CCL5	Chemokine (C-C motif) ligand 5	<ul style="list-style-type: none"> - Specifically attracts monocytes, and regulates macrophage function
MCP3 = CCL7	Chemokine (C-C motif) ligand 7	<ul style="list-style-type: none"> - Plays a role in T-cell mediated inflammation of the skin
CTACK = CCL27	Chemokine (C-C motif) ligand 27	<ul style="list-style-type: none"> - Elicits chemotactic effect by binding to the chemokine receptor CCR10
Eotaxins	Chemokine (C-C motif) ligand 11, 24, 26	<ul style="list-style-type: none"> - Recruits eosinophils
GRO α = CXCL1	Chemokine (C-X-C motif) ligand 1	<ul style="list-style-type: none"> - Expressed by macrophages, neutrophils and epithelial cells - Has neutrophil chemoattractant activity, is involved in angiogenesis, inflammation - Has his action through receptor CXCR2
IL8 = CXCL8	Chemokine (C-X-C motif) ligand 8 = Interleukin-8	<ul style="list-style-type: none"> - Produced by macrophages and endothelial cells - Has neutrophil chemoattractant activity and potently promotes angiogenesis
MIG = CXCL9	Chemokine (C-X-C motif) ligand 9	<ul style="list-style-type: none"> - Chemoattractant for T-cells
IP10 = CXCL10	Chemokine (C-X-C motif) ligand 10	<ul style="list-style-type: none"> - Chemoattraction for monocytes/macrophages, T cells, NK cells, and dendritic cells - Promotes T cell adhesion to endothelial cells - Inhibits bone marrow colony formation and angiogenesis
SDF1 α = CXCL12	Chemokine (C-X-C motif) ligand 12	<ul style="list-style-type: none"> - Has lymphocyte chemoattractant activity - Role in angiogenesis - Associated with risk of coronary disease
Growth factors		
MCSF = CSF1	Macrophage colony-stimulating factor = Colony stimulating factor 1	<ul style="list-style-type: none"> - Hematopoietic growth factor involved in the proliferation, differentiation, and survival of monocytes, macrophages, and bone marrow progenitor cells - Involved in the development and progression of atherosclerosis
NGF	Nerve growth factor	<ul style="list-style-type: none"> - Involved in the growth, maintenance, proliferation, and survival of neurons - Role in the regulation of the immune system - Released in high concentrations by mast cells, playing a role in pain perception in areas under

			inflammation
			- Released by CD4+ T cell clones, inducing a cascade of maturation of T cells under infection
			- The expression of NGF is increased in inflammatory diseases such as asthma where it suppresses inflammation
			- Role in cardiovascular disease (reduced levels of NGF in acute coronary syndromes)
			- Increased in the right ventricle of mice with PH model
SCF	Stem cell factor		- Role in hematopoiesis
			- Cardiomyocyte-specific overexpression of transmembrane SCF promotes stem cell migration and improves cardiac function and animal survival after myocardial infarction
SCGFβ	Stem cell growth factor beta		- Hematopoietic growth factors
TNFα	Transforming growth factor alpha		- Mainly produced by activated macrophages
			- Proinflammatory cytokine
			- Promotes the development of PAH by reducing BMPR2 expression, promoting BMPR-II cleavage in vascular cells, and driving inappropriate proliferation of smooth muscle cells in pulmonary arteries
TNFβ	Transforming growth factor beta 1		- Role in immunoregulation
			- Negative autocrine growth factor
HGF	Hepatic growth factor		- Paracrine factor normally produced by cells of mesenchymal origin (fibroblasts, macrophages)
			- Role in normal embryogenesis and development, and in adults, role in tissue repair
			- Cardioprotective properties reported in the left heart
			- High circulating associated levels in left pressure overloaded disease and left heart failure
PDGFbb	Platelet-derived growth factor bb		- Role in angiogenesis
			- Produced by platelets upon activation, smooth muscle cells, activated macrophages, and endothelial cells
FGF2 = FGFβ	Basic fibroblast growth factor		- Mitogenic, involved in cell survival activities and angiogenesis
GCSF	Granulocyte colony-stimulating factor		- Stimulates the bone marrow to produce granulocytes and stem cells and release them into the bloodstream
			- Stimulates the survival, proliferation, differentiation, and function of neutrophils precursors and mature neutrophils
GMCSF	Granulocyte-macrophages colony-stimulating factor		- Secreted by macrophages, T cells, mast cells, natural killer cells, endothelial cells and fibroblasts
			- Promotes neutrophil, macrophages and eosinophil proliferation and maturation
VEGF-A	Vascular endothelial growth factor-A		- Role in angiogenesis and vasodilation
			- Chemotactic for granulocytes and macrophages
Other cytokines			
MIF	Macrophage migration inhibitory factor		- Proinflammatory cytokine
			- Involved in cell-mediated immunity, immunoregulation, and inflammation
			- In PAH: elevated concentrations of MIF
			- In mouse models of PH: antagonism of MIF inhibits hypoxia-induced smooth cell proliferation
TRAIL	TNF-related apoptosis-inducing ligand		- Induces apoptosis
IFNA2	Interferon alpha-2		- Potent antitumor activity, activation of the immune system which can eliminate tumor cell

IFN γ

Interferon gamma

- Important role for innate and adaptive immunity against viral, bacterial and protozoal infections
 - Activator of macrophages and MHC II
-

Table S2. Right heart risk scores. Mayo Clinic derived-score and Stanford-derived score for prediction of death, lung transplant or admission at 3 years in the recently published Vera Moulton Wall Center cohort (145).

Mayo Clinic score		Stanford score	
Variables	Points	Variables	Points
RV longitudinal strain (%)		RV end-systolic remodeling index	
≥25 (reference)	0	<1.32 (reference)	0
[20 – 25[3	[1.32 - 1.45[2
[15 – 20[5	[1.45 - 1.60[3
<15	5	≥1.60	5
NT-proBNP (pg/mL)		NT-proBNP (pg/mL)	
< 1500	0	< 1500	0
≥ 1500	1	≥ 1500	2
NYHA class		NYHA class	
I or II	0	I or II	0
III or IV	3	III or IV	3
Total	/17	Total	/15

NYHA: New York Heart Association; RV: right ventricular.

DISCUSSION

DISCUSSION

Right heart failure remains the major cause of morbi-mortality in patients with PH, despite remarkable improvements in the understanding of the importance of RV adaptation and in the management of patients with PH (237). The transition between RV adaptation to pressure overload to RV maladaptation remains a complex and not fully understood process (19). In this thesis, we demonstrated the utility of non-invasive imaging (such as echocardiography) to provide right heart adaptive deep phenotyping and to contribute to unravel the molecular pathways associated with right heart failure in PH.

The first chapter of this thesis has been dedicated to assess and improve the **methodology** of using resting trans-thoracic echocardiography to detect PH in patients with suspected pre-capillary PH (26). We first confirmed in the largest cohort to date the linear relationship between invasive mean and systolic pulmonary arterial pressures, first reported by Chemla et al. over a decade ago (28). As the definition of PH relies on a mean pulmonary arterial pressure above 25mmHg, this validation reinforced the relevance of using RVSP estimation to detect PH. We then proposed a simple classification of the quality of the tricuspid regurgitation signal envelope using continuous Doppler to avoid over- and underestimation of RVSP. The main pitfalls were the tendency of over reporting RVSP in the presence of an incomplete envelope and the overestimation of RVSP in the presence of extra-echogenicity on top of the envelope (often referred to as the “hair” of the envelope). However, while applying these simple methodological tips improved the accuracy of the estimation of pulmonary pressures, our study highlighted the residual variability of echocardiography for pressure estimation. Overall, it should be kept in mind that the aim of this study was not to demonstrate the superiority of echocardiography over right heart catheterization for estimation of pulmonary pressures, but to improve the methodology of using echocardiography to routinely detect PH. As right heart catheterization will remain the gold standard to measure pulmonary pressures, echocardiography remains the cornerstone of clinical screening for PH,

particularly in patients with left heart disease or advanced lung disease. Published in the Journal of the American Society of Echocardiography, our study has been chosen as part of the American Society of Echocardiography Continuous Medical Education program. In our institution (Marie Lannelongue Hospital), the methodological protocol used in this study has been implemented and adopted in both the clinical and the research echo laboratories.

While trans-thoracic echocardiography is the most routinely used imaging technique to assess cardiac function, size and estimate hemodynamics parameters, its limitations for estimation of RV size and ejection fraction have to be highlighted. In a supplementary article, our group has demonstrated that using RV focused apical 4-chamber view improved the accuracy of RV areas and function estimation (185). Cardiac magnetic resonance remains the gold standard for evaluation of RV volumes, mass and ejection fraction, despite its limited clinical availability. The evolution of the research field of right heart non-invasive assessment goes towards using novel sequences such as the 4D blood flow, still requiring validation in patients with PH (8). Our team is conducting an ongoing study aiming to validate the accuracy of 4D blood flow for estimation of cardiac volumes, mass and function in a prospective cohort of patients with CTEPH undergoing endarterectomy or patients with PAH undergoing lung transplantation (PRINCEPT study, ClinicalTrials.gov Identifier: NCT03205085).

The second chapter of this thesis has enabled to identify, among the multiple **right heart non-invasive imaging metrics**, RV end-systolic remodeling indices as the strongest prognostic biomarkers in patients with PAH, consistently across etiologies. Combined with the NYHA functional class and NT-proBNP levels, the RV end-systolic remodeling index was predictive of long-term outcomes (i.e. death, lung transplantation or readmission for right heart failure) during follow-up in a prospective cohort of 228 patients with incident or prevalent PAH, beyond well-validated existing risk scores (such as the REVEAL score) (145). In addition to its strong prognostic value, our study suggested that the RV end-systolic remodeling index (simple ratio of the end-systolic RV free-wall length divided by the septal height on the

RV focused apical 4-chamber view) can be used as a predictor of response to therapy, if validated in future studies.

The second part of the chapter was dedicated to redefine the three physiological concepts behind the term of “right heart load adaptability”. In the two studies conducted in patients with PAH or patients with scleroderma-associated PAH, previously published complex **load adaptability metrics** did not provide incremental prognostic value beyond simple metrics such as the RV end-systolic area index (21,304), reinforcing the “simple is better” trend in cardiovascular imaging. Overall, the strong and consistent prognostic value of RV end-systolic indices in the pressure overloaded right heart refers to the landmark physiological study from Carabello and Spann in left heart disease (305), showing that the wall-stress is the highest in end-systole in pressure overloaded heart failure. In PH, the evolution of RV remodeling is characterized by cardiomyocyte hypertrophy, alterations in the interstitial matrix eventually associated with chamber dilatation. Hence, the finding of RV end-systolic remodeling as a strong prognostic marker is not surprising, as it is supported by pathophysiological evidence.

The third chapter of this thesis has explored the role of **immune circulating biomarkers** in patients with PH. The first study demonstrated the prognostic value of high preoperative CRP plasmatic levels for prediction of early postoperative outcomes (i.e. death or transplant or ECMO need or prolonged inotropic or vasopressor support) after endarterectomy in operable patients with CTEPH. Particularly, preoperative systemic inflammation was associated with postoperative hemodynamic instability associated with peripheral vasodilation. In this study, we failed to demonstrate a significant correlation between the plasmatic level of CRP and right heart adaptation to PH using echocardiography in a subgroup of patients with high or low CRP, and similar pulmonary resistance levels. This negative result contrast from the previous findings of the link between systemic inflammation and right heart function in patients with CTEPH, however without matching for afterload (98,136). Further investigations are needed to assess whether, after matching for afterload, operable patients with CTEPH and high CRP have different RV function or remodeling than those with low CRP.

The second study provides a practical application of right heart deep phenotyping to determine the circulating immune **proteomic profile** associated with right heart failure in patients with PAH. This hypothesis-generating screening proteomics study has identified high plasmatic levels of hepatic growth factor, nerve growth factor and stem cell growth factor beta to be associated with right heart maladaptation in two cohorts with PAH beyond the pulmonary disease severity. The role of these biomarkers within the right ventricle itself remains to be fully explored, and ongoing validation is being conducted.

Biomarker (“biological markers”) has been defined in 1998 by the National Institutes of Health Biomarkers Definitions Working Group as “a characteristic that is objectively measured and evaluated as an indicator of normal biological processes, pathogenic processes, or pharmacologic responses to a therapeutic intervention.” In PH, circulating biomarkers can serve as non-invasive tools for diagnosis, assessment of the severity of the disease, prognosis and response to therapy, as well as generate hypothesis for mechanistic studies exploring molecular pathways underlying pathogenesis or progression of the disease (306). Morrow and de Lemos have defined in 2007 the three criteria that a “good biomarker” needs to fulfill in order to be implemented in routine practice (307). These criteria can be structured by three fundamental questions, illustrated in **Figure 23**: [1] Can the clinician measure it? [2] Does it add new information? [3] Does it help the clinician to manage patients?

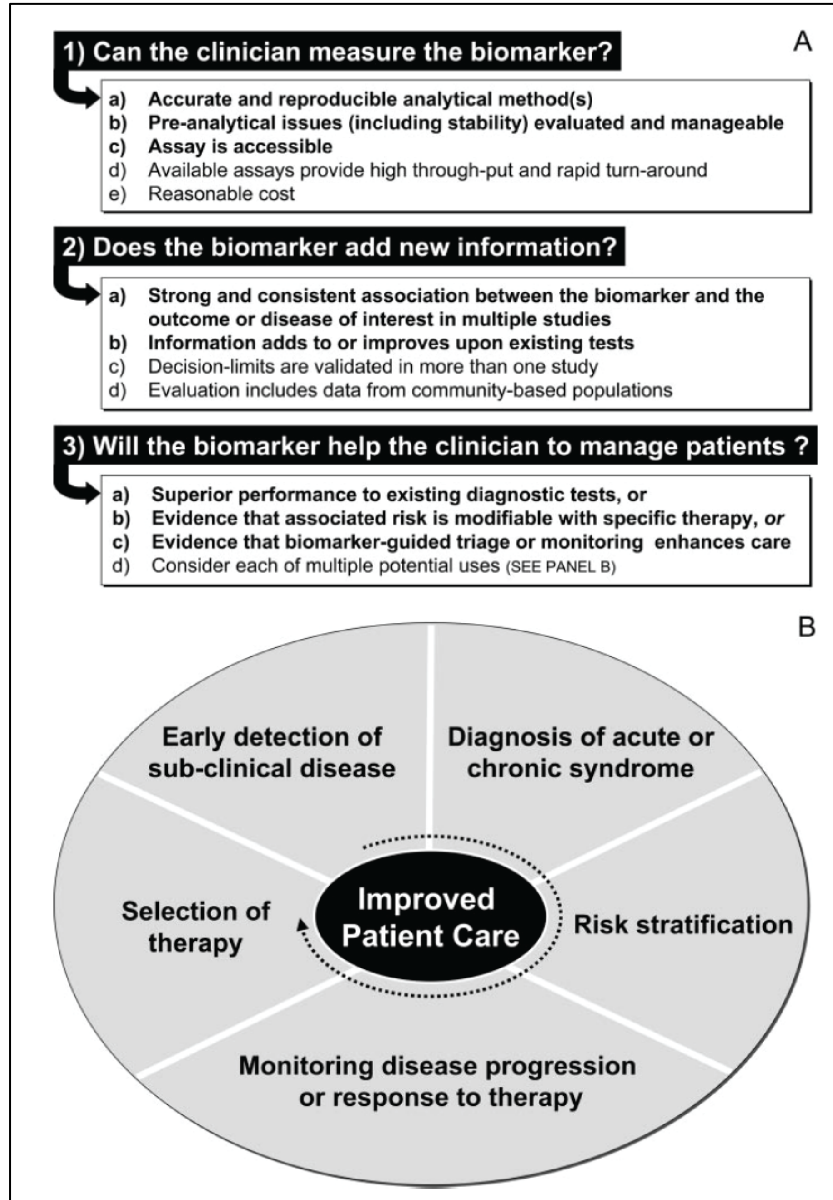


Figure 23. Criteria for assessment of novel cardiovascular biomarkers for clinical use (A) and clinical applications of cardiovascular biomarkers (B). Adapted from Morrow and de Lemos, *Circulation*, 2007.

Regarding the value of circulating immune or growth factors in patients with PH, several questions remain unanswered, as highlighted by the 2018 American Thoracic Society Research Statement (237). First, whether inflammation is a cause or consequence of right heart failure in patients with PH is unclear. Similarly, it is unknown whether a certain degree of inflammation is beneficial for repair and

cardiac adaptation (and if so, how much), and whether targeting inflammation would be beneficial in PH (308). Many studies targeting inflammation in left heart failure have provided neutral or negative results, as recently reviewed by Mann (309). **Figure 24** summarizes the potential reasons underlying these results.

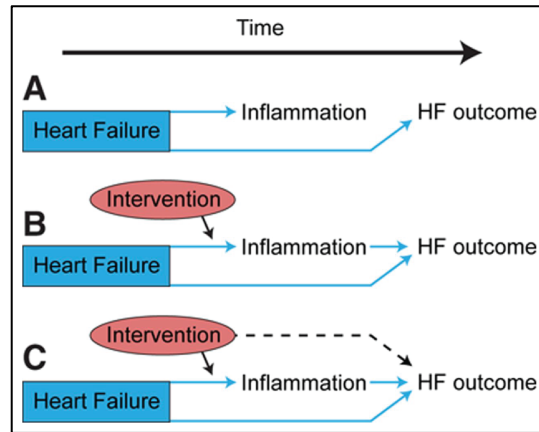
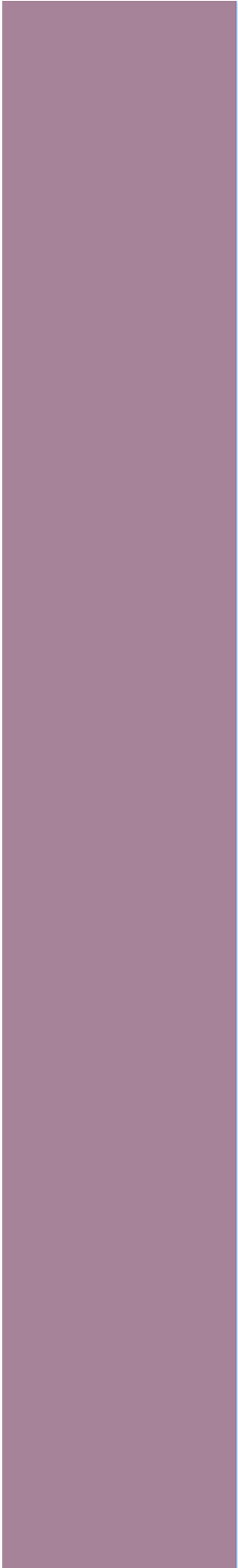


Figure 24. Potential reasons for neutral/negative results targeting inflammation in heart failure. Adapted from Mann et al. *Circ Res*, 2015. (A) Inflammation is not in the causal pathway of heart failure. (B) Of several causal pathways of heart failure, anti-inflammatory therapy targets a pathway that contributes to the syndrome of heart failure, but is not directly related to clinical outcomes (ie, is a disease modifier). (C) Of several causal pathways of heart failure, anti-inflammatory therapy targets a pathway that contributes to the clinical outcomes, but has direct side effects that lead to worsening heart failure. Dotted lines, off-target mechanism(s) of action that might exist. HF: heart failure.

It can be expected that targeting inflammation in right heart failure faces the same caveats, and a better understanding of the timeline and immune actors involved is a needed pre-requirement.



CONCLUSION AND PERSPECTIVES

CONCLUSION AND PERSPECTIVES

This thesis illustrates the utility of right heart deep phenotyping to early detect PH and right heart adaptation, risk stratify the prognostic and response to therapy, as well as to contribute to explore the molecular pathways associated with right heart failure in PH.

Figure 25 summarizes the different aspects associated with right heart deep phenotyping in PH that have been highlighted in our thesis.

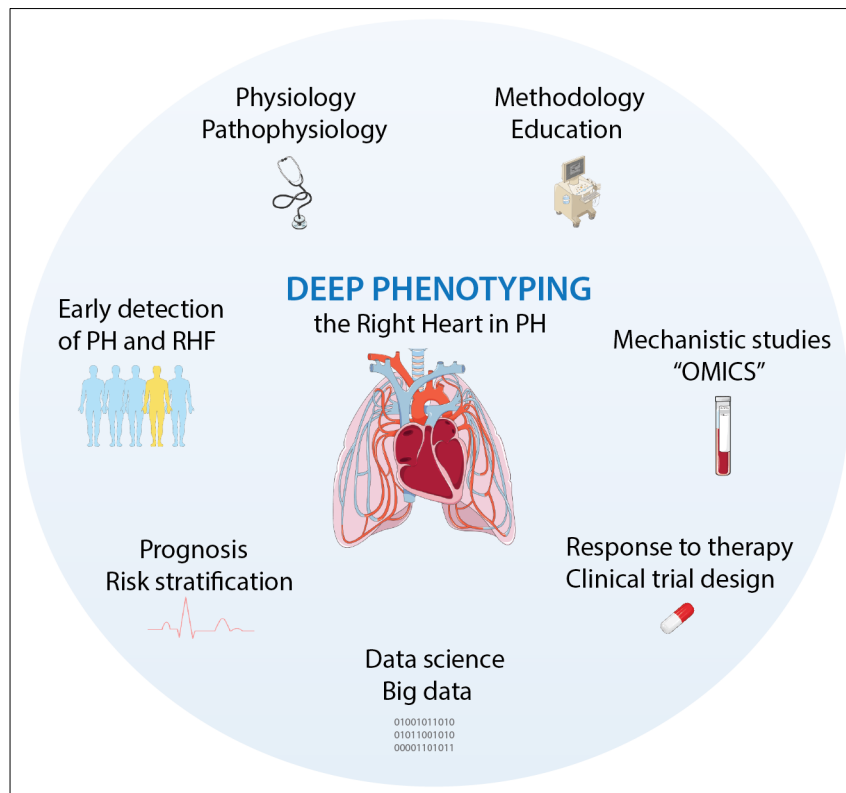


Figure 25. Different aspects associated with deep phenotyping of the right heart in patients with pulmonary hypertension. PH: pulmonary hypertension; RHF: right heart failure.

Despite recent improvements, PH remains frequently diagnosed at a late stage of the disease. Early detection of PH is associated with better outcome, enabling early management. While right heart catheterization remains the gold standard, the first chapter of our thesis has enabled to provide simple tools to improve the accuracy of echocardiography to detect PH. Our results have highlighted the importance of training and education to improve the methodology.

Integrating physiological concepts of the cardio-pulmonary unit as well as the pathophysiology of RV adaptation to afterload, deep phenotyping of the right heart has identified end-systolic remodeling indices to be the strongest prognostic markers in PH (145,261,305). Beyond risk stratification, the current challenge is to use non-invasive imaging to identify predictors of response to therapy among patients with PAH. Indeed, as current risk scores such as the REVEAL score already has a high prediction value (c-statistics above 0.80 as illustrated in the second chapter of this thesis), it is expected that novel imaging indices will not be able to provide incremental prognostic value. Identification of imaging biomarkers as surrogate markers of response to therapy in PH is thus an unmet need. These surrogate imaging markers could help designing novel clinical trials focusing on right heart adaptation as well as reduction of the afterload in PH.

Finally the third aspect of improving RV deep phenotyping is to enable better assessment of the mechanisms underlying RV adaptation. The third chapter of this thesis explores the immune proteomics markers associated with RV adaptive phenotypes. Similar studies can be performed exploring other “OMICS”, such as metabolomics (MVD study, Clinicaltrial.gov Identifier NCT03199131). As illustrated in our last study, the current trend of cardiovascular research including “OMICS” studies is to provide numerous data points, referred to as “big data”, requiring advanced statistical analysis and collaborations with data scientists.

Among the several potential perspectives deriving from our results, the study of right heart reverse remodeling post-surgery of PH is the most promising. Indeed, one of the remarkable specificity of the right heart is its ability to reverse remodel and recover from injury. Several studies have reported the reverse remodeling of the right heart following pulmonary endarterectomy in patients with CTEPH (247,310,311) or lung transplantation in patients with PAH (227,228).

Studying the molecular pathways involved in the recovery of the right heart can provide insights into pathways potentially involved in the transition from adapted to maladapted RV in PH, and can help identify targets for RV specific therapies (**Figure 26**).

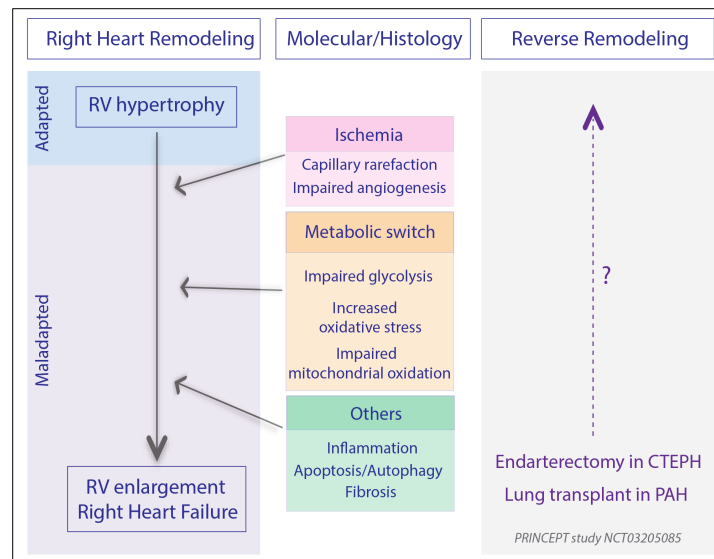
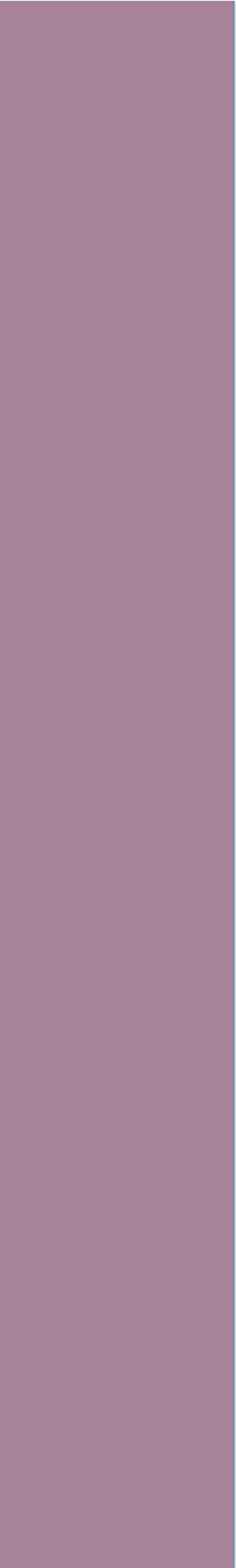


Figure 26. Mechanisms underlying the transition from right ventricular adaptation to maladaptation to afterload in pulmonary hypertension. CTEPH: chronic thromboembolic pulmonary hypertension; PAH: pulmonary arterial hypertension; RV: right ventricular.

This thesis has also been dedicated to set up and initiate at Marie Lannelongue Hospital a prospective clinical study, the PRINCEPT study (Determinants of Postoperative Right Heart Remodeling IN Patients with Chronic Thrombo-Embolic Pulmonary Hypertension after Endarterectomy, or Pulmonary Arterial Hypertension after Lung Transplantation), aiming to study the reverse remodeling of

the right heart after reduction of afterload in PH. This single centered study (Clinicaltrial.gov Identifier NCT03205085 – Primary Investigator: Prof. Olaf Mercier) will include 100 patients with CTEPH before endarterectomy and 50 patients with PAH referred for double lung transplantation, and will follow them up for 6 months after surgery. All patients will undergo a complete right heart deep phenotyping (including echocardiography and cardiac magnetic resonance with 4D blood flow sequence) and biological bio banking at inclusion (before surgery) and at 6 months after surgery. It can be hypothesized that the molecular changes observed after surgery can reflect the pathways involved in right heart failure in PH. This ongoing study has already included a third of the patients and is expected to provide results in 2020.



REFERENCES

REFERENCES

1. Voelkel NF., Quaife RA., Leinwand LA., et al. Right ventricular function and failure: report of a National Heart, Lung, and Blood Institute working group on cellular and molecular mechanisms of right heart failure. *Circulation* 2006;114:1883–91.
2. Srivastava D., Olson EN. A genetic blueprint for cardiac development. *Nature* 2000;407:221–6.
3. Guimaron S., Guihaire J., Amsallem M., Haddad F., Fadel E., Mercier O. Current Knowledge and Recent Advances of Right Ventricular Molecular Biology and Metabolism from Congenital Heart Disease to Chronic Pulmonary Hypertension. *BioMed Res Int* 2018;2018:1981568.
4. Batkai S., Bär C., Thum T. MicroRNAs in right ventricular remodelling. *Cardiovasc Res* 2017;113:1433–40.
5. Fontan F., Baudet E. Surgical repair of tricuspid atresia. *Thorax* 1971;26:240–8.
6. Senzaki H., Masutani S., Ishido H., et al. Cardiac rest and reserve function in patients with Fontan circulation. *J Am Coll Cardiol* 2006;47:2528–35.
7. Galiè N., Humbert M., Vachiery J-L., et al. 2015 ESC/ERS Guidelines for the diagnosis and treatment of pulmonary hypertension: The Joint Task Force for the Diagnosis and Treatment of Pulmonary Hypertension of the European Society of Cardiology (ESC) and the European Respiratory Society (ERS): Endorsed by: Association for European Paediatric and Congenital Cardiology (AEPC), International Society for Heart and Lung Transplantation (ISHLT). *Eur Heart J* 2016;37:67–119.
8. Amsallem M., Mercier O., Kobayashi Y., Moneghetti K., Haddad F. Forgotten No More: a Focused Update on the Right Ventricle in Cardiovascular Disease. *JACC Heart Fail* 2018;6:891-903.
9. Vonk Noordegraaf A., Haddad F., Bogaard HJ., Hassoun PM. Noninvasive imaging in the assessment of the cardiopulmonary vascular unit. *Circulation* 2015;131:899–913.
10. Amsallem M., Kuznetsova T., Hanneman K., Denault A., Haddad F. Right Heart Imaging in Patients with Heart Failure: A Tale of Two Ventricles. *Curr Opin Cardiol* 2016;31:469–82.
11. Sanz J., Kariisa M., Dellegrottaglie S., et al. Evaluation of pulmonary artery stiffness in pulmonary hypertension with cardiac magnetic resonance. *JACC Cardiovasc Imaging* 2009;2:286–95.
12. Mahapatra S., Nishimura RA., Sorajja P., Cha S., McGoon MD. Relationship of pulmonary arterial capacitance and mortality in idiopathic pulmonary arterial hypertension. *J Am Coll Cardiol* 2006;47:799–803.
13. Campo A., Mathai SC., Le Pavec J., et al. Hemodynamic predictors of survival in scleroderma-related pulmonary arterial hypertension. *Am J Respir Crit Care Med* 2010;182:252–60.

14. Dupont M., Mullens W., Skouri HN., et al. Prognostic role of pulmonary arterial capacitance in advanced heart failure. *Circ Heart Fail* 2012;5:778–85.
15. Pellegrini P., Rossi A., Pasotti M., et al. Prognostic relevance of pulmonary arterial compliance in patients with chronic heart failure. *Chest* 2014;145:1064–70.
16. Al-Naamani N., Preston IR., Paulus JK., Hill NS., Roberts KE. Pulmonary Arterial Capacitance Is an Important Predictor of Mortality in Heart Failure With a Preserved Ejection Fraction. *JACC Heart Fail* 2015;3:467–74.
17. Saydain G., Awan A., Manickam P., Kleinow P., Badr S. Pulmonary Hypertension an Independent Risk Factor for Death in Intensive Care Unit: Correlation of Hemodynamic Factors with Mortality. *Clin Med Insights Circ Respir Pulm Med* 2015;9:27–33.
18. Chemla D., Castelain V., Hervé P., Lecarpentier Y., Brimiouille S. Haemodynamic evaluation of pulmonary hypertension. *Eur Respir J* 2002;20:1314–31.
19. Vonk Noordegraaf A., Westerhof BE., Westerhof N. The Relationship Between the Right Ventricle and its Load in Pulmonary Hypertension. *J Am Coll Cardiol* 2017;69:236–43.
20. Saouti N., Westerhof N., Postmus PE., Vonk-Noordegraaf A. The arterial load in pulmonary hypertension. *Eur Respir Rev* 2010;19:197–203.
21. Amsallem M., Boulate D., Aymami M., et al. Load Adaptability in Patients with Pulmonary Arterial Hypertension. *Am J Cardiol* 2017;120:874-82.
22. Lankhaar J-W., Westerhof N., Faes TJC., et al. Pulmonary vascular resistance and compliance stay inversely related during treatment of pulmonary hypertension. *Eur Heart J* 2008;29:1688–95.
23. Saouti N., Westerhof N., Helderma F., et al. Right ventricular oscillatory power is a constant fraction of total power irrespective of pulmonary artery pressure. *Am J Respir Crit Care Med* 2010;182:1315–20.
24. Tedford RJ., Hassoun PM., Mathai SC., et al. Pulmonary capillary wedge pressure augments right ventricular pulsatile loading. *Circulation* 2012;125:289–97.
25. Gerges M., Gerges C., Pistrutto A-M., et al. Pulmonary Hypertension in Heart Failure. Epidemiology, Right Ventricular Function, and Survival. *Am J Respir Crit Care Med* 2015;192:1234–46.
26. Amsallem M., Sternbach JM., Adigopula S., et al. Addressing the Controversy of Estimating Pulmonary Arterial Pressure by Echocardiography. *J Am Soc Echocardiogr* 2016;29:93-102.
27. Kind T., Faes TJC., Vonk-Noordegraaf A., Westerhof N. Proportional Relations Between Systolic, Diastolic and Mean Pulmonary Artery Pressure are Explained by Vascular Properties. *Cardiovasc Eng Technol* 2011;2:15–23.
28. Chemla D., Castelain V., Humbert M., et al. New formula for predicting mean pulmonary artery pressure using systolic pulmonary artery pressure. *Chest* 2004;126:1313–7.

29. Haddad F., Kudelko K., Mercier O., Vrtovec B., Zamanian RT., de Jesus Perez V. Pulmonary hypertension associated with left heart disease: characteristics, emerging concepts, and treatment strategies. *Prog Cardiovasc Dis* 2011;54:154–67.
30. Haddad F., Elmi-Sarabi M., Fadel E., Mercier O., Denault AY. Pearls and pitfalls in managing right heart failure in cardiac surgery. *Curr Opin Anaesthesiol* 2016;29:68–79.
31. Gerges C., Gerges M., Lang MB., et al. Diastolic pulmonary vascular pressure gradient: a predictor of prognosis in “out-of-proportion” pulmonary hypertension. *Chest* 2013;143:758–66.
32. Tampakakis E., Leary PJ., Selby VN., et al. The diastolic pulmonary gradient does not predict survival in patients with pulmonary hypertension due to left heart disease. *JACC Heart Fail* 2015;3:9–16.
33. Naeije R., Vanderpool R., Dhakal BP., et al. Exercise-induced pulmonary hypertension: physiological basis and methodological concerns. *Am J Respir Crit Care Med* 2013;187:576–83.
34. Janicki JS., Weber KT., Likoff MJ., Fishman AP. The pressure-flow response of the pulmonary circulation in patients with heart failure and pulmonary vascular disease. *Circulation* 1985;72:1270–8.
35. Lewis GD., Bossone E., Naeije R., et al. Pulmonary vascular hemodynamic response to exercise in cardiopulmonary diseases. *Circulation* 2013;128:1470–9.
36. Herve P., Lau EM., Sitbon O., et al. Criteria for diagnosis of exercise pulmonary hypertension. *Eur Respir J* 2015;46:728–37.
37. Kovacs G., Olschewski A., Berghold A., Olschewski H. Pulmonary vascular resistances during exercise in normal subjects: a systematic review. *Eur Respir J* 2012;39:319–28.
38. Oliveira RKF., Agarwal M., Tracy JA., et al. Age-related upper limits of normal for maximum upright exercise pulmonary haemodynamics. *Eur Respir J* 2016;47:1179–88.
39. Kovacs G., Herve P., Barbera JA., et al. An official European Respiratory Society statement: pulmonary haemodynamics during exercise. *Eur Respir J* 2017;50.
40. Firpo C., Hoffman JL., Silverman NH. Evaluation of fetal heart dimensions from 12 weeks to term. *Am J Cardiol* 2001;87:594–600.
41. Haddad F., Hunt SA., Rosenthal DN., Murphy DJ. Right ventricular function in cardiovascular disease, part I: Anatomy, physiology, aging, and functional assessment of the right ventricle. *Circulation* 2008;117:1436–48.
42. Haddad F., Guihaire J., Skhiri M., et al. Septal curvature is marker of hemodynamic, anatomical, and electromechanical ventricular interdependence in patients with pulmonary arterial hypertension. *Echocardiogr* 2014;31:699–707.

43. Atherton JJ., Moore TD., Lele SS., et al. Diastolic ventricular interaction in chronic heart failure. *Lancet* 1997;349:1720–4.
44. Belenkie I., Smith ER., Tyberg JV. Ventricular interaction: from bench to bedside. *Ann Med* 2001;33:236–41.
45. Gan CT-J., Lankhaar J-W., Marcus JT., et al. Impaired left ventricular filling due to right-to-left ventricular interaction in patients with pulmonary arterial hypertension. *Am J Physiol Heart Circ Physiol* 2006;290:1528-33.
46. Rabinovitch M., Guignabert C., Humbert M., Nicolls MR. Inflammation and immunity in the pathogenesis of pulmonary arterial hypertension. *Circ Res* 2014;115:165–75.
47. Vachiéry J-L., Adir Y., Barberà JA., et al. Pulmonary hypertension due to left heart diseases. *J Am Coll Cardiol* 2013;62:100-8.
48. Amsallem M., Boulate D., Kooreman Z., et al. Investigating the value of right heart echocardiographic metrics for detection of pulmonary hypertension in patients with advanced lung disease. *Int J Cardiovasc Imaging* 2017;33:825–35.
49. Rudski LG., Lai WW., Afilalo J., et al. Guidelines for the echocardiographic assessment of the right heart in adults: a report from the American Society of Echocardiography endorsed by the European Association of Echocardiography, a registered branch of the European Society of Cardiology, and the Canadian Society of Echocardiography. *J Am Soc Echocardiogr* 2010;23:685–713.
50. Lang IM., Pesavento R., Bonderman D., Yuan JX-J. Risk factors and basic mechanisms of chronic thromboembolic pulmonary hypertension: a current understanding. *Eur Respir J* 2013;41:462–8.
51. Kim NH., Delcroix M., Jenkins DP., et al. Chronic thromboembolic pulmonary hypertension. *J Am Coll Cardiol* 2013;62:92-9.
52. Guérin L., Couturaud F., Parent F., et al. Prevalence of chronic thromboembolic pulmonary hypertension after acute pulmonary embolism. Prevalence of CTEPH after pulmonary embolism. *Thromb Haemost* 2014;112:598–605.
53. Mercier O., Arthur Ataam J., Langer NB., et al. Abnormal pulmonary endothelial cells may underlie the enigmatic pathogenesis of chronic thromboembolic pulmonary hypertension. *J Heart Lung Transplant* 2017;36:305-14.
54. Simonneau G., Torbicki A., Dorfmüller P., Kim N. The pathophysiology of chronic thromboembolic pulmonary hypertension. *Eur Respir Rev* 2017;26.pii:160112.
55. Dell'Italia LJ., Walsh RA. Application of a time varying elastance model to right ventricular performance in man. *Cardiovasc Res* 1988;22:864–74.
56. Kusunose K., Tsutsui RS., Bhatt K., et al. Prognostic value of RV function before and after lung transplantation. *JACC Cardiovasc Imaging* 2014;7:1084–94.

57. Westerhof BE., Saouti N., van der Laarse WJ., Westerhof N., Vonk Noordegraaf A. Treatment strategies for the right heart in pulmonary hypertension. *Cardiovasc Res* 2017;113:1465–73.
58. Kapur NK., Esposito ML., Bader Y., et al. Mechanical Circulatory Support Devices for Acute Right Ventricular Failure. *Circulation* 2017;136:314–26.
59. Hopkins WE., Ochoa LL., Richardson GW., Trulock EP. Comparison of the hemodynamics and survival of adults with severe primary pulmonary hypertension or Eisenmenger syndrome. *J Heart Lung Transplant* 1996;15:100–5.
60. Kawut SM., Taichman DB., Archer-Chicko CL., Palevsky HI., Kimmel SE. Hemodynamics and survival in patients with pulmonary arterial hypertension related to systemic sclerosis. *Chest* 2003;123:344–50.
61. Oosterhof T., Tulevski II., Vliegen HW., Spijkerboer AM., Mulder BJM. Effects of volume and/or pressure overload secondary to congenital heart disease (tetralogy of fallot or pulmonary stenosis) on right ventricular function using cardiovascular magnetic resonance and B-type natriuretic peptide levels. *Am J Cardiol* 2006;97:1051–5.
62. Hopkins WE., Waggoner AD. Severe pulmonary hypertension without right ventricular failure: the unique hearts of patients with Eisenmenger syndrome. *Am J Cardiol* 2002;89:34–8.
63. Oka M., Homma N., Taraseviciene-Stewart L., et al. Rho kinase-mediated vasoconstriction is important in severe occlusive pulmonary arterial hypertension in rats. *Circ Res* 2007;100:923–9.
64. Ryan JJ., Archer SL. The right ventricle in pulmonary arterial hypertension: disorders of metabolism, angiogenesis and adrenergic signaling in right ventricular failure. *Circ Res* 2014;115:176–88.
65. McMurtry MS., Bonnet S., Wu X., et al. Dichloroacetate prevents and reverses pulmonary hypertension by inducing pulmonary artery smooth muscle cell apoptosis. *Circ Res* 2004;95:830–40.
66. Michelakis ED., McMurtry MS., Wu X-C., et al. Dichloroacetate, a metabolic modulator, prevents and reverses chronic hypoxic pulmonary hypertension in rats: role of increased expression and activity of voltage-gated potassium channels. *Circulation* 2002;105:244–50.
67. van Wolferen SA., Marcus JT., Westerhof N., et al. Right coronary artery flow impairment in patients with pulmonary hypertension. *Eur Heart J* 2008;29:120–7.
68. Bian X., Williams AG., Gwartz PA., Downey HF. Right coronary autoregulation in conscious, chronically instrumented dogs. *Am J Physiol* 1998;275:169-75.
69. Piao L., Fang Y-H., Parikh K., Ryan JJ., Toth PT., Archer SL. Cardiac glutaminolysis: a maladaptive cancer metabolism pathway in the right ventricle in pulmonary hypertension. *J Mol Med* 2013;91:1185–97.
70. Gómez A., Bialostozky D., Zajarias A., et al. Right ventricular ischemia in patients with primary pulmonary hypertension. *J Am Coll Cardiol* 2001;38:1137–42.

71. Nagendran J., Sutendra G., Paterson I., et al. Endothelin axis is upregulated in human and rat right ventricular hypertrophy. *Circ Res* 2013;112:347–54.
72. Nagendran J., Archer SL., Soliman D., et al. Phosphodiesterase type 5 is highly expressed in the hypertrophied human right ventricle, and acute inhibition of phosphodiesterase type 5 improves contractility. *Circulation* 2007;116:238–48.
73. Boulate D., Arthur Ataam J., Connolly AJ., et al. Early Development of Right Ventricular Ischemic Lesions in a Novel Large Animal Model of Acute Right Heart Failure in Chronic Thromboembolic Pulmonary Hypertension. *J Card Fail* 2017;23:876–86.
74. Sutendra G., Dromparis P., Paulin R., et al. A metabolic remodeling in right ventricular hypertrophy is associated with decreased angiogenesis and a transition from a compensated to a decompensated state in pulmonary hypertension. *J Mol Med* 2013;91:1315–27.
75. Noly P-E., Haddad F., Arthur-Ataam J., et al. The importance of capillary density-stroke work mismatch for right ventricular adaptation to chronic pressure overload. *J Thorac Cardiovasc Surg* 2017;154:2070–9.
76. Ross R. Atherosclerosis--an inflammatory disease. *N Engl J Med* 1999;340:115–26.
77. Libby P. Inflammation in atherosclerosis. *Nature* 2002;420:868–74.
78. Libby P., Ridker PM., Hansson GK., Leducq Transatlantic Network on Atherothrombosis. Inflammation in atherosclerosis: from pathophysiology to practice. *J Am Coll Cardiol* 2009;54:2129–38.
79. Dale MA., Ruhlman MK., Baxter BT. Inflammatory cell phenotypes in AAAs: their role and potential as targets for therapy. *Arterioscler Thromb Vasc Biol* 2015;35:1746–55.
80. Hellenthal FAMVI., Buurman WA., Wodzig WKWH., Schurink GWH. Biomarkers of abdominal aortic aneurysm progression. Part 2: inflammation. *Nat Rev Cardiol* 2009;6:543–52.
81. Amsallem M., Saito T., Tada Y., Dash R., McConnell MV. Magnetic Resonance Imaging and Positron Emission Tomography Approaches to Imaging Vascular and Cardiac Inflammation. *Circ J* 2016;80:1269–77.
82. Dorfmueller P., Perros F., Balabanian K., Humbert M. Inflammation in pulmonary arterial hypertension. *Eur Respir J* 2003;22:358–63.
83. Hassoun PM., Mouthon L., Barberà JA., et al. Inflammation, growth factors, and pulmonary vascular remodeling. *J Am Coll Cardiol* 2009;54:10-9.
84. Price LC., Wort SJ., Perros F., et al. Inflammation in pulmonary arterial hypertension. *Chest* 2012;141:210–21.
85. Quarck R., Nawrot T., Meyns B., Delcroix M. C-reactive protein: a new predictor of adverse outcome in pulmonary arterial hypertension. *J Am Coll Cardiol* 2009;53:1211–8.

86. Soon E., Holmes AM., Treacy CM., et al. Elevated levels of inflammatory cytokines predict survival in idiopathic and familial pulmonary arterial hypertension. *Circulation* 2010;122:920–7.
87. Cracowski J-L., Chabot F., Labarère J., et al. Proinflammatory cytokine levels are linked to death in pulmonary arterial hypertension. *Eur Respir J* 2014;43:915–7.
88. Heresi GA., AYTEKIN M., Hammel JP., Wang S., Chatterjee S., Dweik RA. Plasma interleukin-6 adds prognostic information in pulmonary arterial hypertension. *Eur Respir J* 2014;43:912–4.
89. Humbert M., Monti G., Brenot F., et al. Increased interleukin-1 and interleukin-6 serum concentrations in severe primary pulmonary hypertension. *Am J Respir Crit Care Med* 1995;151:1628–31.
90. Quarck R., Wynants M., Verbeken E., Meyns B., Delcroix M. Contribution of inflammation and impaired angiogenesis to the pathobiology of chronic thromboembolic pulmonary hypertension. *Eur Respir J* 2015;46:431–43.
91. Bonderman D., Jakowitsch J., Adlbrecht C., et al. Medical conditions increasing the risk of chronic thromboembolic pulmonary hypertension. *Thromb Haemost* 2005;93:512–6.
92. Hoeper MM., Niedermeyer J., Hoffmeyer F., Flemming P., Fabel H. Pulmonary hypertension after splenectomy? *Ann Intern Med* 1999;130:506–9.
93. Jaïs X., Ios V., Jardim C., et al. Splenectomy and chronic thromboembolic pulmonary hypertension. *Thorax* 2005;60:1031–4.
94. Frey MK., Alias S., Winter MP., et al. Splenectomy is modifying the vascular remodeling of thrombosis. *J Am Heart Assoc* 2014;3:e000772.
95. Bonderman D., Jakowitsch J., Redwan B., et al. Role for staphylococci in misguided thrombus resolution of chronic thromboembolic pulmonary hypertension. *Arterioscler Thromb Vasc Biol* 2008;28:678–84.
96. Langer F., Schramm R., Bauer M., Tscholl D., Kuniyama T., Schäfers H-J. Cytokine response to pulmonary thromboendarterectomy. *Chest* 2004;126:135–41.
97. Wynants M., Quarck R., Ronisz A., et al. Effects of C-reactive protein on human pulmonary vascular cells in chronic thromboembolic pulmonary hypertension. *Eur Respir J* 2012;40:886–94.
98. Skoro-Sajer N., Gerges C., Gerges M., et al. Usefulness of thrombosis and inflammation biomarkers in chronic thromboembolic pulmonary hypertension-sampling plasma and surgical specimens. *J Heart Lung Transplant* 2018;37:1067-74.
99. Hennigs JK., Baumann HJ., Lüneburg N., et al. Fibrinogen plasma concentration is an independent marker of haemodynamic impairment in chronic thromboembolic pulmonary hypertension. *Sci Rep* 2014;4:4808.

100. Sydykov A., Mamazhakypov A., Petrovic A., et al. Inflammatory Mediators Drive Adverse Right Ventricular Remodeling and Dysfunction and Serve as Potential Biomarkers. *Front Physiol* 2018;9:609.
101. Begieneman MPV., van de Goot FRW., van der Bilt I a. C., et al. Pulmonary embolism causes endomyocarditis in the human heart. *Heart* 2008;94:450–6.
102. Iwadate K., Doi M., Tanno K., et al. Right ventricular damage due to pulmonary embolism: examination of the number of infiltrating macrophages. *Forensic Sci Int* 2003;134:147–53.
103. Watts JA., Zagorski J., Gellar MA., Stevinson BG., Kline JA. Cardiac inflammation contributes to right ventricular dysfunction following experimental pulmonary embolism in rats. *J Mol Cell Cardiol* 2006;41:296–307.
104. Dewachter C., Dewachter L., Rondelet B., et al. Activation of apoptotic pathways in experimental acute afterload-induced right ventricular failure. *Crit Care Med* 2010;38:1405–13.
105. Dewachter C., Belhaj A., Rondelet B., et al. Myocardial inflammation in experimental acute right ventricular failure: Effects of prostacyclin therapy. *J Heart Lung Transplant* 2015;34:1334–45.
106. Watts JA., Gellar MA., Stuart LK., Obratzsova M., Kline JA. Proinflammatory events in right ventricular damage during pulmonary embolism: effects of treatment with ketorolac in rats. *J Cardiovasc Pharmacol* 2009;54:246–52.
107. Zagorski J., Gellar MA., Obratzsova M., Kline JA., Watts JA. Inhibition of CINC-1 decreases right ventricular damage caused by experimental pulmonary embolism in rats. *J Immunol* 2007;179:7820–6.
108. Zagorski J., Sanapareddy N., Gellar MA., Kline JA., Watts JA. Transcriptional profile of right ventricular tissue during acute pulmonary embolism in rats. *Physiol Genomics* 2008;34:101–11.
109. Birks EJ., Owen VJ., Burton PB., et al. Tumor necrosis factor-alpha is expressed in donor heart and predicts right ventricular failure after human heart transplantation. *Circulation* 2000;102:326–31.
110. Nergui S., Fukumoto Y., Do E Z., et al. Role of endothelial nitric oxide synthase and collagen metabolism in right ventricular remodeling due to pulmonary hypertension. *Circ J* 2014;78:1465–74.
111. Handoko ML., de Man FS., Happé CM., et al. Opposite effects of training in rats with stable and progressive pulmonary hypertension. *Circulation* 2009;120:42–9.
112. Campian ME., Hardziyenka M., de Bruin K., et al. Early inflammatory response during the development of right ventricular heart failure in a rat model. *Eur J Heart Fail* 2010;12:653–8.
113. de Man FS., Handoko ML., van Ballegoij JJM., et al. Bisoprolol delays progression towards right heart failure in experimental pulmonary hypertension. *Circ Heart Fail* 2012;5:97–105.

114. Ahmed LA., Obaid AAZ., Zaki HF., Agha AM. Role of oxidative stress, inflammation, nitric oxide and transforming growth factor-beta in the protective effect of diosgenin in monocrotaline-induced pulmonary hypertension in rats. *Eur J Pharmacol* 2014;740:379–87.
115. Moreira-Gonçalves D., Ferreira R., Fonseca H., et al. Cardioprotective effects of early and late aerobic exercise training in experimental pulmonary arterial hypertension. *Basic Res Cardiol* 2015;110:57.
116. Paulin R., Sutendra G., Gurtu V., et al. A miR-208-Mef2 axis drives the decompensation of right ventricular function in pulmonary hypertension. *Circ Res* 2015;116:56–69.
117. Nogueira-Ferreira R., Moreira-Gonçalves D., Silva AF., et al. Exercise preconditioning prevents MCT-induced right ventricle remodeling through the regulation of TNF superfamily cytokines. *Int J Cardiol* 2016;203:858–66.
118. Rice KM., Manne NDPK., Kolli MB., et al. Curcumin nanoparticles attenuate cardiac remodeling due to pulmonary arterial hypertension. *Artif Cells Nanomedicine Biotechnol* 2016;44:1909–16.
119. Wang J-J., Zuo X-R., Xu J., et al. Evaluation and Treatment of Endoplasmic Reticulum (ER) Stress in Right Ventricular Dysfunction during Monocrotaline-Induced Rat Pulmonary Arterial Hypertension. *Cardiovasc Drugs Ther* 2016;30:587–98.
120. Alencar AK., Montes GC., Montagnoli T., et al. Activation of GPER ameliorates experimental pulmonary hypertension in male rats. *Eur J Pharm Sci* 2017;97:208–17.
121. Brown MB., Neves E., Long G., et al. High-intensity interval training, but not continuous training, reverses right ventricular hypertrophy and dysfunction in a rat model of pulmonary hypertension. *Am J Physiol Regul Integr Comp Physiol* 2017;312:197–210.
122. Guihaire J., Deuse T., Wang D., et al. Pulmonary hypertension: macrophage infiltration correlates with right ventricular remodeling in an experimental model of pulmonary hypertension. *J Heart Lung Transplant* 2017;36:370–370.
123. Frump AL., Goss KN., Vayl A., et al. Estradiol improves right ventricular function in rats with severe angioproliferative pulmonary hypertension: effects of endogenous and exogenous sex hormones. *Am J Physiol Lung Cell Mol Physiol* 2015;308:873-90.
124. Rondelet B., Dewachter C., Kerbaul F., et al. Prolonged overcirculation-induced pulmonary arterial hypertension as a cause of right ventricular failure. *Eur Heart J* 2012;33:1017–26.
125. Belhaj A., Dewachter L., Kerbaul F., et al. Heme oxygenase-1 and inflammation in experimental right ventricular failure on prolonged overcirculation-induced pulmonary hypertension. *PloS One* 2013;8:e69470.
126. Vistnes M., Waehre A., Nygård S., et al. Circulating cytokine levels in mice with heart failure are etiology dependent. *J Appl Physiol* 2010;108:1357–64.

127. Waehre A., Vistnes M., Sjaastad I., et al. Chemokines regulate small leucine-rich proteoglycans in the extracellular matrix of the pressure-overloaded right ventricle. *J Appl Physiol* 2012;112:1372–82.
128. Luitel H., Sydykov A., Schymura Y., et al. Pressure overload leads to an increased accumulation and activity of mast cells in the right ventricle. *Physiol Rep* 2017;5.pii:e13146.
129. Olivetti G., Lagrasta C., Ricci R., Sonnenblick EH., Capasso JM., Anversa P. Long-term pressure-induced cardiac hypertrophy: capillary and mast cell proliferation. *Am J Physiol* 1989;257:1766-72.
130. Overbeek MJ., Mouchaers KTB., Niessen HM., et al. Characteristics of interstitial fibrosis and inflammatory cell infiltration in right ventricles of systemic sclerosis-associated pulmonary arterial hypertension. *Int J Rheumatol* 2010;2010.pii:604615.
131. Torre-Amione G., Kapadia S., Benedict C., Oral H., Young JB., Mann DL. Proinflammatory cytokine levels in patients with depressed left ventricular ejection fraction: a report from the Studies of Left Ventricular Dysfunction (SOLVD). *J Am Coll Cardiol* 1996;27:1201–6.
132. Hegewisch S., Weh HJ., Hossfeld DK. TNF-induced cardiomyopathy. *Lancet* 1990;335:294–5.
133. Finkel MS., Oddis CV., Jacob TD., Watkins SC., Hattler BG., Simmons RL. Negative inotropic effects of cytokines on the heart mediated by nitric oxide. *Science* 1992;257:387–9.
134. Pasceri V., Willerson JT., Yeh ET. Direct proinflammatory effect of C-reactive protein on human endothelial cells. *Circulation* 2000;102:2165–8.
135. Verma S., Li S-H., Badiwala MV., et al. Endothelin antagonism and interleukin-6 inhibition attenuate the proatherogenic effects of C-reactive protein. *Circulation* 2002;105:1890–6.
136. von Haehling S., von Bardeleben RS., Kramm T., et al. Inflammation in right ventricular dysfunction due to thromboembolic pulmonary hypertension. *Int J Cardiol* 2010;144:206–11.
137. Yang T., Li Z-N., Chen G., et al. Increased levels of plasma CXC-Chemokine Ligand 10, 12 and 16 are associated with right ventricular function in patients with idiopathic pulmonary arterial hypertension. *Heart Lung J Crit Care* 2014;43:322–7.
138. Prins KW., Archer SL., Pritzker M., et al. Interleukin-6 is independently associated with right ventricular function in pulmonary arterial hypertension. *J Heart Lung Transplant* 2018;37:376–84.
139. Odeh M., Sabo E., Oliven A. Circulating levels of tumor necrosis factor-alpha correlate positively with severity of peripheral oedema in patients with right heart failure. *Eur J Heart Fail* 2006;8:141–6.
140. Lang RM., Badano LP., Mor-Avi V., et al. Recommendations for cardiac chamber quantification by echocardiography in adults: an update from the American Society of Echocardiography and the European Association of Cardiovascular Imaging. *J Am Soc Echocardiogr* 2015;28:1-39.e14.

141. Damy T., Kallvikbacka-Bennett A., Goode K., et al. Prevalence of, associations with, and prognostic value of tricuspid annular plane systolic excursion (TAPSE) among out-patients referred for the evaluation of heart failure. *J Card Fail* 2012;18:216–25.
142. Ghio S., Pica S., Klersy C., et al. Prognostic value of TAPSE after therapy optimisation in patients with pulmonary arterial hypertension is independent of the haemodynamic effects of therapy. *Open Heart* 2016;3.
143. Wranne B., Pinto FJ., Hammarström E., St Goar FG., Puryear J., Popp RL. Abnormal right heart filling after cardiac surgery: time course and mechanisms. *Br Heart J* 1991;66:435–42.
144. Tamborini G., Muratori M., Brusoni D., et al. Is right ventricular systolic function reduced after cardiac surgery? A two- and three-dimensional echocardiographic study. *Eur J Echocardiogr* 2009;10:630–4.
145. Amsallem M., Sweatt AJ., Aymami MC., et al. Right Heart End-Systolic Remodeling Index Strongly Predicts Outcomes in Pulmonary Arterial Hypertension: Comparison With Validated Models. *Circ Cardiovasc Imaging* 2017;10pii:e005771.
146. Fine NM., Chen L., Bastiansen PM., et al. Outcome prediction by quantitative right ventricular function assessment in 575 subjects evaluated for pulmonary hypertension. *Circ Cardiovasc Imaging* 2013;6:711–21.
147. Haddad F., Amsallem M. Full Circle on Pulmonary Flow Dynamics in Pulmonary Arterial Hypertension. *JACC Cardiovasc Imaging* 2017;10:1278–80.
148. Hilde JM., Skjørten I., Grøtta OJ., et al. Right ventricular dysfunction and remodeling in chronic obstructive pulmonary disease without pulmonary hypertension. *J Am Coll Cardiol* 2013;62:1103–11.
149. Nanda NC, Gramiak R, Robinson TI, Shah PM Echocardiographic evaluation of pulmonary hypertension. *Circulation* 1974;50:575-81.
150. Weyman AE., Dillon JC., Feigenbaum H., Chang S. Echocardiographic patterns of pulmonic valve motion with pulmonary hypertension. *Circulation* 1974;50:905–10.
151. Parker KH., Jones CJ. Forward and backward running waves in the arteries: analysis using the method of characteristics. *J Biomech Eng* 1990;112:322–6.
152. Chemla D., Castelain V., Simonneau G., Lecarpentier Y., Hervé P. Pulse wave reflection in pulmonary hypertension. *J Am Coll Cardiol* 2002;39:743–4.
153. Castelain V., Hervé P., Lecarpentier Y., Duroux P., Simonneau G., Chemla D. Pulmonary artery pulse pressure and wave reflection in chronic pulmonary thromboembolism and primary pulmonary hypertension. *J Am Coll Cardiol* 2001;37:1085–92.

154. Arkles JS., Opotowsky AR., Ojeda J., et al. Shape of the right ventricular Doppler envelope predicts hemodynamics and right heart function in pulmonary hypertension. *Am J Respir Crit Care Med* 2011;183:268–76.
155. Takahama H., McCully RB., Frantz RP., Kane GC. Unraveling the RV Ejection Doppler Envelope: Insight Into Pulmonary Artery Hemodynamics and Disease Severity. *JACC Cardiovasc Imaging* 2017;10:1268–77.
156. Haddad F., Spruijt OA., Denault AY., et al. Right Heart Score for Predicting Outcome in Idiopathic, Familial, or Drug- and Toxin-Associated Pulmonary Arterial Hypertension. *JACC Cardiovasc Imaging* 2015;8:627–38.
157. Ghio S., Klersy C., Magrini G., et al. Prognostic relevance of the echocardiographic assessment of right ventricular function in patients with idiopathic pulmonary arterial hypertension. *Int J Cardiol* 2010;140:272–8.
158. Tei C., Dujardin KS., Hodge DO., et al. Doppler echocardiographic index for assessment of global right ventricular function. *J Am Soc Echocardiogr* 1996;9:838–47.
159. Zimbarra Cabrera I., Ruísánchez C., Grapsa J., et al. Validation of the isovolumetric relaxation time for the estimation of pulmonary systolic arterial blood pressure in chronic pulmonary hypertension. *Eur Heart J Cardiovasc Imaging* 2013;14:51–5.
160. Shimada YJ., Shiota M., Siegel RJ., Shiota T. Accuracy of right ventricular volumes and function determined by three-dimensional echocardiography in comparison with magnetic resonance imaging: a meta-analysis study. *J Am Soc Echocardiogr* 2010;23:943–53.
161. Voigt J-U., Pedrizzetti G., Lysyansky P., et al. Definitions for a common standard for 2D speckle tracking echocardiography: consensus document of the EACVI/ASE/Industry Task Force to standardize deformation imaging. *Eur Heart J Cardiovasc Imaging* 2015;16:1–11.
162. Dumesnil JG., Shoucri RM., Laurenceau JL., Turcot J. A mathematical model of the dynamic geometry of the intact left ventricle and its application to clinical data. *Circulation* 1979;59:1024–34.
163. Dandel M., Lehmkuhl H., Knosalla C., Suramashvili N., Hetzer R. Strain and strain rate imaging by echocardiography - basic concepts and clinical applicability. *Curr Cardiol Rev* 2009;5:133–48.
164. Kobayashi Y., Ariyama M., Kobayashi Y., et al. Comparison of left ventricular manual versus automated derived longitudinal strain: implications for clinical practice and research. *Int J Cardiovasc Imaging* 2016;32:429–37.
165. Cameli M., Righini FM., Lisi M., et al. Comparison of right versus left ventricular strain analysis as a predictor of outcome in patients with systolic heart failure referred for heart transplantation. *Am J Cardiol* 2013;112:1778–84.

166. Iacoviello M., Citarelli G., Antoncechi V., et al. Right Ventricular Longitudinal Strain Measures Independently Predict Chronic Heart Failure Mortality. *Echocardiogr* 2016;33:992-1000.
167. Ryo K., Goda A., Onishi T., et al. Characterization of right ventricular remodeling in pulmonary hypertension associated with patient outcomes by 3-dimensional wall motion tracking echocardiography. *Circ Cardiovasc Imaging* 2015;8.pii:e003176.
168. Maffessanti F., Muraru D., Esposito R., et al. Age-, body size-, and sex-specific reference values for right ventricular volumes and ejection fraction by three-dimensional echocardiography: a multicenter echocardiographic study in 507 healthy volunteers. *Circ Cardiovasc Imaging* 2013;6:700–10.
169. Yock PG., Popp RL. Noninvasive estimation of right ventricular systolic pressure by Doppler ultrasound in patients with tricuspid regurgitation. *Circulation* 1984;70:657–62.
170. Currie PJ., Seward JB., Chan KL., et al. Continuous wave Doppler determination of right ventricular pressure: a simultaneous Doppler-catheterization study in 127 patients. *J Am Coll Cardiol* 1985;6:750–6.
171. Berger M., Haimowitz A., Van Tosh A., Berdoff RL., Goldberg E. Quantitative assessment of pulmonary hypertension in patients with tricuspid regurgitation using continuous wave Doppler ultrasound. *J Am Coll Cardiol* 1985;6:359–65.
172. Shapiro SM., Oudiz RJ., Cao T., et al. Primary pulmonary hypertension: improved long-term effects and survival with continuous intravenous epoprostenol infusion. *J Am Coll Cardiol* 1997;30:343–9.
173. Fisher MR., Criner GJ., Fishman AP., et al. Estimating pulmonary artery pressures by echocardiography in patients with emphysema. *Eur Respir J* 2007;30:914–21.
174. Rich JD., Shah SJ., Swamy RS., Kamp A., Rich S. Inaccuracy of Doppler echocardiographic estimates of pulmonary artery pressures in patients with pulmonary hypertension: implications for clinical practice. *Chest* 2011;139:988–93.
175. Laaban JP., Diebold B., Zelinski R., Lafay M., Raffoul H., Rochemaure J. Noninvasive estimation of systolic pulmonary artery pressure using Doppler echocardiography in patients with chronic obstructive pulmonary disease. *Chest* 1989;96:1258–62.
176. Tamarin R., Torbicki A., Marchandise B., Laaban JP., Morpurgo M. Doppler echocardiographic evaluation of pulmonary artery pressure in chronic obstructive pulmonary disease. A European multicentre study. Working Group on Noninvasive Evaluation of Pulmonary Artery Pressure. European Office of the World Health Organization, Copenhagen. *Eur Heart J* 1991;12:103–11.

177. Brecker SJ., Gibbs JS., Fox KM., Yacoub MH., Gibson DG. Comparison of Doppler derived haemodynamic variables and simultaneous high fidelity pressure measurements in severe pulmonary hypertension. *Br Heart J* 1994;72:384–9.
178. Hinderliter AL., Willis PW., Barst RJ., et al. Effects of long-term infusion of prostacyclin (epoprostenol) on echocardiographic measures of right ventricular structure and function in primary pulmonary hypertension. Primary Pulmonary Hypertension Study Group. *Circulation* 1997;95:1479–86.
179. Bach DS., Curtis JL., Christensen PJ., et al. Preoperative echocardiographic evaluation of patients referred for lung volume reduction surgery. *Chest* 1998;114:972–80.
180. Arcasoy SM., Christie JD., Ferrari VA., et al. Echocardiographic assessment of pulmonary hypertension in patients with advanced lung disease. *Am J Respir Crit Care Med* 2003;167:735–40.
181. Dambrauskaite V., Delcroix M., Claus P., et al. The evaluation of pulmonary hypertension using right ventricular myocardial isovolumic relaxation time. *J Am Soc Echocardiogr* 2005;18:1113–20.
182. Haddad F., Zamanian R., Beraud A-S., et al. A novel non-invasive method of estimating pulmonary vascular resistance in patients with pulmonary arterial hypertension. *J Am Soc Echocardiogr* 2009;22:523–9.
183. Lafitte S., Pillois X., Reant P., et al. Estimation of pulmonary pressures and diagnosis of pulmonary hypertension by Doppler echocardiography: a retrospective comparison of routine echocardiography and invasive hemodynamics. *J Am Soc Echocardiogr* 2013;26:457–63.
184. D’Alto M., Romeo E., Argiento P., et al. Accuracy and precision of echocardiography versus right heart catheterization for the assessment of pulmonary hypertension. *Int J Cardiol* 2013;168:4058–62.
185. Amsallem M., Lu H., Tang X., et al. Optimizing Right Ventricular Focused Four-Chamber Views using Three-Dimensional Imaging, a comparative Magnetic Resonance based study. *Int J Cardiovasc Imaging* 2018;34:1409-17.
186. Guihaire J., Haddad F., Boulate D., et al. Non-invasive indices of right ventricular function are markers of ventricular-arterial coupling rather than ventricular contractility: insights from a porcine model of chronic pressure overload. *Eur Heart J Cardiovasc Imaging* 2013;14:1140–9.
187. Cohen-Solal A., Faraggi M., Czitrom D., Le Guludec D., Delahaye N., Gourgon R. Left ventricular-arterial system coupling at peak exercise in dilated nonischemic cardiomyopathy. *Chest* 1998;113:870–7.
188. Gourgon R., Cohen-Solal A., Himbert D., Dahan M. Is ejection fraction an index of left ventricular function and/or of the condition of the arterial system? *Arch Mal Coeur Vaiss* 1993;86:97–9.

189. Sanz J., García-Alvarez A., Fernández-Friera L., et al. Right ventriculo-arterial coupling in pulmonary hypertension: a magnetic resonance study. *Heart* 2012;98:238–43.
190. Trip P., Kind T., van de Veerdonk MC., et al. Accurate assessment of load-independent right ventricular systolic function in patients with pulmonary hypertension. *J Heart Lung Transplant* 2013;32:50–5.
191. Guazzi M., Bandera F., Pelissero G., et al. Tricuspid annular plane systolic excursion and pulmonary arterial systolic pressure relationship in heart failure: an index of right ventricular contractile function and prognosis. *Am J Physiol Heart Circ Physiol* 2013;305:1373–81.
192. Kang G., Ha R., Banerjee D. Pulmonary artery pulsatility index predicts right ventricular failure after left ventricular assist device implantation. *J Heart Lung Transplant* 2016;35:67–73.
193. Stevens GR., Garcia-Alvarez A., Sahni S., Garcia MJ., Fuster V., Sanz J. RV dysfunction in pulmonary hypertension is independently related to pulmonary artery stiffness. *JACC Cardiovasc Imaging* 2012;5:378–87.
194. Alfakih K., Reid S., Jones T., Sivananthan M. Assessment of ventricular function and mass by cardiac magnetic resonance imaging. *Eur Radiol* 2004;14:1813–22.
195. Galea N., Carbone I., Cannata D., et al. Right ventricular cardiovascular magnetic resonance imaging: normal anatomy and spectrum of pathological findings. *Insights Imaging* 2013;4:213–23.
196. Swift AJ., Wild JM., Nagle SK., et al. Quantitative magnetic resonance imaging of pulmonary hypertension: a practical approach to the current state of the art. *J Thorac Imaging* 2014;29:68–79.
197. McCann GP., Gan CT., Beek AM., Niessen HWM., Vonk Noordegraaf A., van Rossum AC. Extent of MRI delayed enhancement of myocardial mass is related to right ventricular dysfunction in pulmonary artery hypertension. *AJR Am J Roentgenol* 2007;188:349–55.
198. Blyth KG., Groenning BA., Martin TN., et al. Contrast enhanced-cardiovascular magnetic resonance imaging in patients with pulmonary hypertension. *Eur Heart J* 2005;26:1993–9.
199. Junqueira FP., Macedo R., Coutinho AC., et al. Myocardial delayed enhancement in patients with pulmonary hypertension and right ventricular failure: evaluation by cardiac MRI. *Br J Radiol* 2009;82:821–6.
200. Bessa LGP., Junqueira FP., Bandeira ML da S., et al. Pulmonary arterial hypertension: use of delayed contrast-enhanced cardiovascular magnetic resonance in risk assessment. *Arq Bras Cardiol* 2013;101:336–43.
201. Babu-Narayan SV., Goktekin O., Moon JC., et al. Late gadolinium enhancement cardiovascular magnetic resonance of the systemic right ventricle in adults with previous atrial redirection surgery for transposition of the great arteries. *Circulation* 2005;111:2091–8.

202. Sanz J., Dellegrottaglie S., Kariisa M., et al. Prevalence and correlates of septal delayed contrast enhancement in patients with pulmonary hypertension. *Am J Cardiol* 2007;100:731–5.
203. Wagner A., Mahrholdt H., Holly TA., et al. Contrast-enhanced MRI and routine single photon emission computed tomography (SPECT) perfusion imaging for detection of subendocardial myocardial infarcts: an imaging study. *Lancet* 2003;361:374–9.
204. He D., Ye M., Zhang L., Jiang B. Prognostic significance of late gadolinium enhancement on cardiac magnetic resonance in patients with hypertrophic cardiomyopathy. *Heart Lung J Crit Care* 2018;47:122–6.
205. Bradlow WM., Assomull R., Kilner PJ., Gibbs JSR., Sheppard MN., Mohiaddin RH. Understanding late gadolinium enhancement in pulmonary hypertension. *Circ Cardiovasc Imaging* 2010;3:501–3.
206. Egemnazarov B., Crnkovic S., Nagy BM., Olschewski H., Kwapiszewska G. Right ventricular fibrosis and dysfunction: Actual concepts and common misconceptions. *Matrix Biol* 2018;68:507-21.
207. Shehata ML., Lossnitzer D., Skrok J., et al. Myocardial delayed enhancement in pulmonary hypertension: pulmonary hemodynamics, right ventricular function, and remodeling. *Am J Roentgenol* 2011;196:87–94.
208. Herpel E., Singer S., Flechtenmacher C., et al. Extracellular matrix proteins and matrix metalloproteinases differ between various right and left ventricular sites in end-stage cardiomyopathies. *Virchows Arch Int J Pathol* 2005;446:369–78.
209. Wang J-H., Zhao L., Pan X., et al. Hypoxia-stimulated cardiac fibroblast production of IL-6 promotes myocardial fibrosis via the TGF- β 1 signaling pathway. *Lab Invest* 2016;96:839-52.
210. Freed BH., Gomberg-Maitland M., Chandra S., et al. Late gadolinium enhancement cardiovascular magnetic resonance predicts clinical worsening in patients with pulmonary hypertension. *J Cardiovasc Magn Reson* 2012;14:11.
211. Swift AJ., Rajaram S., Capener D., et al. LGE patterns in pulmonary hypertension do not impact overall mortality. *JACC Cardiovasc Imaging* 2014;7:1209–17.
212. Azevedo CF., Nigri M., Higuchi ML., et al. Prognostic significance of myocardial fibrosis quantification by histopathology and magnetic resonance imaging in patients with severe aortic valve disease. *J Am Coll Cardiol* 2010;56:278–87.
213. Spruijt OA., Vissers L., Bogaard H-J., Hofman MBM., Vonk-Noordegraaf A., Marcus JT. Increased native T1-values at the interventricular insertion regions in precapillary pulmonary hypertension. *Int J Cardiovasc Imaging* 2016;32:451–9.
214. Baksi AJ., Pennell DJ. T1 mapping in heart failure: from technique to prognosis, toward altering outcome. *Circ Cardiovasc Imaging* 2013;6:861–3.

215. Kawel-Boehm N., Dellas Buser T., Greiser A., Bieri O., Bremerich J., Santini F. In-vivo assessment of normal T1 values of the right-ventricular myocardium by cardiac MRI. *Int J Cardiovasc Imaging* 2014;30:323–8.
216. Mehta BB., Auger DA., Gonzalez JA., et al. Detection of elevated right ventricular extracellular volume in pulmonary hypertension using Accelerated and Navigator-Gated Look-Locker Imaging for Cardiac T1 Estimation (ANGIE) cardiovascular magnetic resonance. *J Cardiovasc Magn Reson* 2015;17:110.
217. Hsiao A., Lustig M., Alley MT., et al. Rapid pediatric cardiac assessment of flow and ventricular volume with compressed sensing parallel imaging volumetric cine phase-contrast MRI. *Am J Roentgenol* 2012;198:250-9.
218. Markl M., Chan FP., Alley MT., et al. Time-resolved three-dimensional phase-contrast MRI. *J Magn Reson Imaging* 2003;17:499–506..
219. Frydrychowicz A., Wieben O., Niespodzany E., Reeder SB., Johnson KM., François CJ. Quantification of thoracic blood flow using volumetric magnetic resonance imaging with radial velocity encoding: in vivo validation. *Invest Radiol* 2013;48:819–25.
220. Hanneman K., Kino A., Cheng JY., Alley MT., Vasanawala SS. Assessment of the precision and reproducibility of ventricular volume, function, and mass measurements with ferumoxytol-enhanced 4D flow MRI. *J Magn Reson Imaging* 2016;44:383-92.
221. François CJ., Srinivasan S., Schiebler ML., et al. 4D cardiovascular magnetic resonance velocity mapping of alterations of right heart flow patterns and main pulmonary artery hemodynamics in tetralogy of Fallot. *J Cardiovasc Magn Reson* 2012;14:16.
222. Reiter G., Reiter U., Kovacs G., et al. Magnetic resonance-derived 3-dimensional blood flow patterns in the main pulmonary artery as a marker of pulmonary hypertension and a measure of elevated mean pulmonary arterial pressure. *Circ Cardiovasc Imaging* 2008;1:23–30.
223. Reiter U., Reiter G., Kovacs G., et al. Evaluation of elevated mean pulmonary arterial pressure based on magnetic resonance 4D velocity mapping: comparison of visualization techniques. *PLoS One* 2013;8:e82212.
224. Barker AJ., Roldán-Alzate A., Entezari P., et al. Four-dimensional flow assessment of pulmonary artery flow and wall shear stress in adult pulmonary arterial hypertension: results from two institutions. *Magn Reson Med* 2015;73:1904–13.
225. Truong U., Fonseca B., Dunning J., et al. Wall shear stress measured by phase contrast cardiovascular magnetic resonance in children and adolescents with pulmonary arterial hypertension. *J Cardiovasc Magn Reson* 2013;15:81.

226. de Raaf MA., SchaliJ I., Gomez-Arroyo J., et al. SuHx rat model: partly reversible pulmonary hypertension and progressive intima obstruction. *Eur Respir J* 2014;44:160–8.
227. Sarashina T., Nakamura K., Akagi S., et al. Reverse Right Ventricular Remodeling After Lung Transplantation in Patients With Pulmonary Arterial Hypertension Under Combination Therapy of Targeted Medical Drugs. *Circ J* 2017;81:383–90.
228. Kasimir M-T., Seebacher G., Jaksch P., et al. Reverse cardiac remodelling in patients with primary pulmonary hypertension after isolated lung transplantation. *Eur J Cardio-Thorac Surg* 2004;26:776–81.
229. Rensing BJ., McDougall JC., Breen JF., Vigneswaran WT., McGregor CG., Rumberger JA. Right and left ventricular remodeling after orthotopic single lung transplantation for end-stage emphysema. *J Heart Lung Transplant* 1997;16:926–33.
230. Spruijt OA., Bogaard H-J., Heijmans MW., et al. Predicting pulmonary hypertension with standard computed tomography pulmonary angiography. *Int J Cardiovasc Imaging* 2015;31:871–9.
231. Nagaya N., Goto Y., Satoh T., et al. Impaired regional fatty acid uptake and systolic dysfunction in hypertrophied right ventricle. *J Nucl Med* 1998;39:1676–80.
232. Lundgrin EL., Park MM., Sharp J., et al. Fasting 2-deoxy-2-[18F]fluoro-D-glucose positron emission tomography to detect metabolic changes in pulmonary arterial hypertension hearts over 1 year. *Ann Am Thorac Soc* 2013;10:1–9.
233. Kluge R., Barthel H., Pankau H., et al. Different mechanisms for changes in glucose uptake of the right and left ventricular myocardium in pulmonary hypertension. *J Nucl Med* 2005;46:25–31.
234. Wong YY., Ruitter G., Lubberink M., et al. Right ventricular failure in idiopathic pulmonary arterial hypertension is associated with inefficient myocardial oxygen utilization. *Circ Heart Fail* 2011;4:700–6.
235. de Man FS., Handoko ML., Guignabert C., Bogaard HJ., Vonk-Noordegraaf A. Neurohormonal axis in patients with pulmonary arterial hypertension: friend or foe? *Am J Respir Crit Care Med* 2013;187:14–9.
236. Paffett ML., Hesterman J., Candelaria G., et al. Longitudinal in vivo SPECT/CT imaging reveals morphological changes and cardiopulmonary apoptosis in a rodent model of pulmonary arterial hypertension. *PloS One* 2012;7:e40910.
237. Lahm T., Douglas IS., Archer SL., et al. Assessment of Right Ventricular Function in the Research Setting: Knowledge Gaps and Pathways Forward. An Official American Thoracic Society Research Statement. *Am J Respir Crit Care Med* 2018;198:e15–43.

238. Leng SX., McElhaney JE., Walston JD., Xie D., Fedarko NS., Kuchel GA. ELISA and multiplex technologies for cytokine measurement in inflammation and aging research. *J Gerontol A Biol Sci Med Sci* 2008;63:879–84.
239. Aziz N., Nishanian P., Mitsuyasu R., Detels R., Fahey JL. Variables that affect assays for plasma cytokines and soluble activation markers. *Clin Diagn Lab Immunol* 1999;6:89–95.
240. Goh WWB., Wang W., Wong L. Why Batch Effects Matter in Omics Data, and How to Avoid Them. *Trends Biotechnol* 2017;35:498–507.
241. Chemla D., Herve P. Derivation of mean pulmonary artery pressure from systolic pressure: implications for the diagnosis of pulmonary hypertension. *J Am Soc Echocardiogr* 2014;27:107.
242. Mukerjee D., St George D., Coleiro B., et al. Prevalence and outcome in systemic sclerosis associated pulmonary arterial hypertension: application of a registry approach. *Ann Rheum Dis* 2003;62:1088–93.
243. Wigley FM., Lima JAC., Mayes M., McLain D., Chapin JL., Ward-Able C. The prevalence of undiagnosed pulmonary arterial hypertension in subjects with connective tissue disease at the secondary health care level of community-based rheumatologists (the UNCOVER study). *Arthritis Rheum* 2005;52:2125–32.
244. Benza RL., Miller DP., Gomberg-Maitland M., et al. Predicting survival in pulmonary arterial hypertension: insights from the Registry to Evaluate Early and Long-Term Pulmonary Arterial Hypertension Disease Management (REVEAL). *Circulation* 2010;122:164–72.
245. Chung L., Farber HW., Benza R., et al. Unique predictors of mortality in patients with pulmonary arterial hypertension associated with systemic sclerosis in the REVEAL registry. *Chest* 2014;146:1494–504.
246. Kelemen BW., Mathai SC., Tedford RJ., et al. Right ventricular remodeling in idiopathic and scleroderma-associated pulmonary arterial hypertension: two distinct phenotypes. *Pulm Circ* 2015;5:327–34.
247. Jenkins D., Madani M., Fadel E., D'Armini AM., Mayer E. Pulmonary endarterectomy in the management of chronic thromboembolic pulmonary hypertension. *Eur Respir Rev* 2017;26.pii:16011.
248. Rhodes B., Fürnrohr BG., Vyse TJ. C-reactive protein in rheumatology: biology and genetics. *Nat Rev Rheumatol* 2011;7:282–9.
249. Ridker PM., Hennekens CH., Buring JE., Rifai N. C-reactive protein and other markers of inflammation in the prediction of cardiovascular disease in women. *N Engl J Med* 2000;342:836–43.

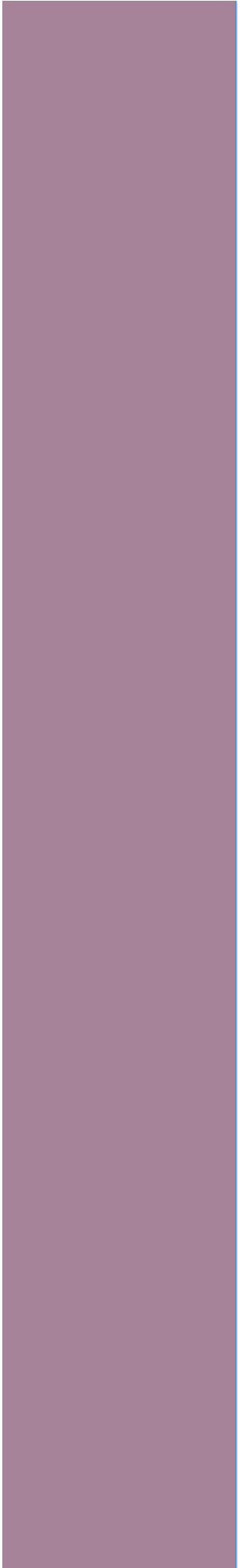
250. Amsallem M., Guihaire J., Arthur Ataam J., et al. Impact of the initiation of balloon pulmonary angioplasty program on referral of patients with chronic thromboembolic pulmonary hypertension to surgery. *J Heart Lung Transplant* 2018;37:1102-10.
251. Pepke-Zaba J., Delcroix M., Lang I., et al. Chronic thromboembolic pulmonary hypertension (CTEPH): results from an international prospective registry. *Circulation* 2011;124:1973–81.
252. Dartevelle P., Fadel E., Mussot S., et al. Chronic thromboembolic pulmonary hypertension. *Eur Respir J* 2004;23:637–48.
253. Thistlethwaite PA., Mo M., Madani MM., et al. Operative classification of thromboembolic disease determines outcome after pulmonary endarterectomy. *J Thorac Cardiovasc Surg* 2002;124:1203–11.
254. Ganter U., Arcone R., Toniatti C., Morrone G., Ciliberto G. Dual control of C-reactive protein gene expression by interleukin-1 and interleukin-6. *EMBO J* 1989;8:3773–9.
255. Pye M., Rae AP., Cobbe SM. Study of serum C-reactive protein concentration in cardiac failure. *Br Heart J* 1990;63:228–30.
256. Kaneko K., Kanda T., Yamauchi Y., et al. C-Reactive protein in dilated cardiomyopathy. *Cardiology* 1999;91:215–9.
257. Matsumoto M., Tsujino T., Lee-Kawabata M., et al. Serum interleukin-6 and C-reactive protein are markedly elevated in acute decompensated heart failure patients with left ventricular systolic dysfunction. *Cytokine* 2010;49:264–8.
258. Wynants M., Vengethasamy L., Ronisz A., Meyns B., Delcroix M., Quarck R. NF-κB pathway is involved in CRP-induced effects on pulmonary arterial endothelial cells in chronic thromboembolic pulmonary hypertension. *Am J Physiol Lung Cell Mol Physiol* 2013;305:934-42.
259. Verma S., Wang C-H., Li S-H., et al. A self-fulfilling prophecy: C-reactive protein attenuates nitric oxide production and inhibits angiogenesis. *Circulation* 2002;106:913–9.
260. Sproston NR., El Mohtadi M., Slevin M., Gilmore W., Ashworth JJ. The Effect of C-Reactive Protein Isoforms on Nitric Oxide Production by U937 Monocytes/Macrophages. *Front Immunol* 2018;9:1500.
261. Swift AJ., Capener D., Johns C., et al. Magnetic Resonance Imaging in the Prognostic Evaluation of Patients with Pulmonary Arterial Hypertension. *Am J Respir Crit Care Med* 2017;196:228–39.
262. Vonk Noordegraaf A., Galiè N. The role of the right ventricle in pulmonary arterial hypertension. *Eur Respir Rev* 2011;20:243–53.
263. Voelkel NF., Gomez-Arroyo J., Abbate A., Bogaard HJ., Nicolls MR. Pathobiology of pulmonary arterial hypertension and right ventricular failure. *Eur Respir J* 2012;40:1555–65.

264. Humbert M., Monti G., Brenot F., et al. Increased interleukin-1 and interleukin-6 serum concentrations in severe primary pulmonary hypertension. *Am J Respir Crit Care Med* 1995;151:1628–31.
265. Gallo S., Sala V., Gatti S., Crepaldi T. HGF/Met Axis in Heart Function and Cardioprotection. *Biomedicines* 2014;2:247–62.
266. Rappolee DA., Iyer A., Patel Y. Hepatocyte growth factor and its receptor are expressed in cardiac myocytes during early cardiogenesis. *Circ Res* 1996;78:1028–36.
267. Aoki M., Morishita R., Taniyama Y., et al. Angiogenesis induced by hepatocyte growth factor in non-infarcted myocardium and infarcted myocardium: up-regulation of essential transcription factor for angiogenesis, ets. *Gene Ther* 2000;7:417–27.
268. Nakamura T., Mizuno S., Matsumoto K., Sawa Y., Matsuda H., Nakamura T. Myocardial protection from ischemia/reperfusion injury by endogenous and exogenous HGF. *J Clin Invest* 2000;106:1511–9.
269. Sala V., Crepaldi T. Novel therapy for myocardial infarction: can HGF/Met be beneficial? *Cell Mol Life Sci* 2011;68:1703–17.
270. Gallo S., Gatti S., Sala V., et al. Agonist antibodies activating the Met receptor protect cardiomyoblasts from cobalt chloride-induced apoptosis and autophagy. *Cell Death Dis* 2014;5:e1185.
271. Min J-K., Lee Y-M., Kim JH., et al. Hepatocyte growth factor suppresses vascular endothelial growth factor-induced expression of endothelial ICAM-1 and VCAM-1 by inhibiting the nuclear factor-kappaB pathway. *Circ Res* 2005;96:300–7.
272. Azuma J., Taniyama Y., Takeya Y., et al. Angiogenic and antifibrotic actions of hepatocyte growth factor improve cardiac dysfunction in porcine ischemic cardiomyopathy. *Gene Ther* 2006;13:1206–13.
273. Chen X-H., Minatoguchi S., Kosai K., et al. In vivo hepatocyte growth factor gene transfer reduces myocardial ischemia-reperfusion injury through its multiple actions. *J Card Fail* 2007;13:874–83.
274. Nakamura T., Matsumoto K., Mizuno S., Sawa Y., Matsuda H., Nakamura T. Hepatocyte growth factor prevents tissue fibrosis, remodeling, and dysfunction in cardiomyopathic hamster hearts. *Am J Physiol Heart Circ Physiol* 2005;288:2131-9.
275. Taniyama Y., Morishita R., Aoki M., et al. Angiogenesis and antifibrotic action by hepatocyte growth factor in cardiomyopathy. *Hypertens* 2002;40:47–53.

276. Mizuno S., Nakamura T. Prevention of neutrophil extravasation by hepatocyte growth factor leads to attenuations of tubular apoptosis and renal dysfunction in mouse ischemic kidneys. *Am J Pathol* 2005;166:1895–905.
277. Rutella S., Bonanno G., Procoli A., et al. Hepatocyte growth factor favors monocyte differentiation into regulatory interleukin (IL)-10⁺⁺IL-12^{low}/neg accessory cells with dendritic-cell features. *Blood* 2006;108:218–27.
278. Chen J., Zhang H., Zhang R., et al. Transfer of human hepatocyte growth factor reduces inflammation and prevents pulmonary arterial remodeling in monocrotaline-induced. *Int J Clin Exp Pathol* 2014;7:8763–9.
279. Ono M., Sawa Y., Mizuno S., et al. Hepatocyte growth factor suppresses vascular medial hyperplasia and matrix accumulation in advanced pulmonary hypertension of rats. *Circulation* 2004;110:2896–902.
280. Ono M., Sawa Y., Fukushima N., et al. Gene transfer of hepatocyte growth factor with prostacyclin synthase in severe pulmonary hypertension of rats. *Eur J Cardio-Thorac Surg* 2004;26:1092–7.
281. Wang W., Liu K., Zhang F., et al. Recombinant human hepatocyte growth factor transfection alleviates hyperkinetic pulmonary artery hypertension in rabbit models. *J Thorac Cardiovasc Surg* 2013;146:198–205.
282. Riccieri V., Stefanantoni K., Vasile M., et al. Abnormal plasma levels of different angiogenic molecules are associated with different clinical manifestations in patients with systemic sclerosis. *Clin Exp Rheumatol* 2011;29:46-52.
283. Liang M., Pang Y., Zhang S., Zhang M. Utility of Hepatocyte Growth Factor as a Biomarker for Early Diagnosis of Pulmonary Artery Hypertension. *Mol Diagn Ther* 2016;20:463–8.
284. Ye L., Lewis-Russell JM., Davies G., Sanders AJ., Kynaston H., Jiang WG. Hepatocyte growth factor up-regulates the expression of the bone morphogenetic protein (BMP) receptors, BMPR-IB and BMPR-II, in human prostate cancer cells. *Int J Oncol* 2007;30:521–9.
285. Spiekerkoetter E., Tian X., Cai J., et al. FK506 activates BMPR2, rescues endothelial dysfunction, and reverses pulmonary hypertension. *J Clin Invest* 2013;123:3600–13.
286. Kuznetsova T., Haddad F., Knez J., et al. Cytokines profile in hypertensive patients with left ventricular remodeling and dysfunction. *J Am Soc Hypertens* 2015;9:975-84.
287. Kim JB., Kobayashi Y., Kuznetsova T., et al. Cytokines profile of reverse cardiac remodeling following transcatheter aortic valve replacement. *Int J Cardiol* 2018;270:83-8.
288. Rychli K., Richter B., Hohensinner PJ., et al. Hepatocyte growth factor is a strong predictor of mortality in patients with advanced heart failure. *Heart* 2011;97:1158–63.

289. Leo C., Sala V., Morello M., et al. Activated Met signalling in the developing mouse heart leads to cardiac disease. *PLoS One* 2011;6:e14675.
290. Guo Y-H., Su L-X., Guo N., Liu C-T. Novel therapy for idiopathic pulmonary arterial hypertension: Can hepatocyte growth factor be beneficial? *J Geriatr Cardiol* 2012;9:211–2.
291. Levi-Montalcini R. The nerve growth factor: its role in growth, differentiation and function of the sympathetic adrenergic neuron. *Prog Brain Res* 1976;45:235–58.
292. Hassankhani A., Steinhilber ME., Soonpaa MH., et al. Overexpression of NGF within the heart of transgenic mice causes hyperinnervation, cardiac enlargement, and hyperplasia of ectopic cells. *Dev Biol* 1995;169:309–21.
293. Ieda M., Kanazawa H., Ieda Y., et al. Nerve growth factor is critical for cardiac sensory innervation and rescues neuropathy in diabetic hearts. *Circulation* 2006;114:2351–63.
294. Caporali A., Sala-Newby GB., Meloni M., et al. Identification of the prosurvival activity of nerve growth factor on cardiac myocytes. *Cell Death Differ* 2008;15:299–311.
295. Freund-Michel V., Cardoso Dos Santos M., Guignabert C., et al. Role of Nerve Growth Factor in Development and Persistence of Experimental Pulmonary Hypertension. *Am J Respir Crit Care Med* 2015;192:342–55.
296. Kimura K., Ieda M., Kanazawa H., et al. Cardiac sympathetic rejuvenation: a link between nerve function and cardiac hypertrophy. *Circ Res* 2007;100:1755–64.
297. Kaye DM., Vaddadi G., Gruskin SL., Du XJ., Esler MD. Reduced myocardial nerve growth factor expression in human and experimental heart failure. *Circ Res* 2000;86:80–4.
298. Qin F., Vulapalli RS., Stevens SY., Liang C-S. Loss of cardiac sympathetic neurotransmitters in heart failure and NE infusion is associated with reduced NGF. *Am J Physiol Heart Circ Physiol* 2002;282:363–71.
299. Stefanantoni K., Sciarra I., Vasile M., et al. Elevated serum levels of macrophage migration inhibitory factor and stem cell growth factor β in patients with idiopathic and systemic sclerosis associated pulmonary arterial hypertension. *Reumatismo* 2015;66:270–6.
300. Wang Y., Khan A., Heringer-Walther S., Schultheiss H-P., Moreira M da CV., Walther T. Prognostic value of circulating levels of stem cell growth factor beta (SCGF beta) in patients with Chagas' disease and idiopathic dilated cardiomyopathy. *Cytokine* 2013;61:728–31.
301. Rhodes CJ., Wharton J., Ghataorhe P., et al. Plasma proteome analysis in patients with pulmonary arterial hypertension: an observational cohort study. *Lancet Respir Med* 2017;5:717–26.
302. Ganz P., Heidecker B., Hveem K., et al. Development and Validation of a Protein-Based Risk Score for Cardiovascular Outcomes Among Patients With Stable Coronary Heart Disease. *JAMA* 2016;315:2532–41.

303. Tabula Muris Consortium., Quake S., Wyss-Coray T., Darmanis S. Transcriptomic characterization of 20 organs and tissues from mouse at single cell resolution creates a Tabula Muris. *Nature*; in press, published online in bioRxiv.
304. French S., Amsallem M., Ouazani N., et al. Non-invasive right ventricular load adaptability indices in patients with scleroderma-associated pulmonary arterial hypertension. *Pulm Circ* 2018;8:2045894018788268.
305. Carabello BA., Spann JF. The uses and limitations of end-systolic indexes of left ventricular function. *Circulation* 1984;69:1058–64.
306. Foris V., Kovacs G., Tscherner M., Olschewski A., Olschewski H. Biomarkers in pulmonary hypertension: what do we know? *Chest* 2013;144:274–83.
307. Morrow DA., de Lemos JA. Benchmarks for the assessment of novel cardiovascular biomarkers. *Circulation* 2007;115:949–52.
308. Quarck R., Delcroix M. Is inflammation a potential therapeutic target in chronic thromboembolic pulmonary hypertension? *Eur Respir J* 2014;44:842–5.
309. Mann DL. Innate immunity and the failing heart: the cytokine hypothesis revisited. *Circ Res* 2015;116:1254–68.
310. Berman M., Gopalan D., Sharples L., et al. Right ventricular reverse remodeling after pulmonary endarterectomy: magnetic resonance imaging and clinical and right heart catheterization assessment. *Pulm Circ* 2014;4:36–44.
311. Li Y., Wang Y., Zhai Z., et al. Relationship between echocardiographic and cardiac magnetic resonance imaging-derived measures of right ventricular function in patients with chronic thromboembolic pulmonary hypertension. *Thromb Res* 2015;135:602–6.



SUPPLEMENTARY MATERIALS

SUPPLEMENTARY ARTICLE 1

ARTICLE IN PRESS

JACC: HEART FAILURE
© 2018 BY THE AMERICAN COLLEGE OF CARDIOLOGY FOUNDATION
PUBLISHED BY ELSEVIER

VOL. ■, NO. ■, 2018

STATE-OF-THE-ART PAPER

Forgotten No More A Focused Update on the Right Ventricle in Cardiovascular Disease

Myriam Amsellem, MD, MS,^{a,b,c,d} Olaf Mercier, MD, PhD,^{d,e} Yukari Kobayashi, MD,^{a,b}
Kegan Moneghetti, MBBS (HONS),^{a,b} Francois Haddad, MD^{a,b,c}

ABSTRACT

In the last decade, there has been renewed interest in the study of the right ventricle. It is now well established that right ventricular function is a strong predictor of mortality, not only in heart failure but also in pulmonary hypertension, congenital heart disease, and cardiothoracic surgery. The right ventricle is part of a cardiopulmonary unit with connections to the pulmonary circulation, venous return, atria, and left ventricle. In this context, ventriculoarterial coupling, interventricular interactions, and pericardial constraint become important to understand right ventricular adaptation to injury or abnormal loading conditions. This state-of-the-art review summarizes major advances that occurred in the field of right ventricular research over the last decade. The first section focuses on right ventricular physiology and pulmonary circulation. The second section discusses the emerging data on right ventricular phenotyping, highlighting the importance of myocardial deformation (strain) imaging and assessment of end-systolic dimensions. The third section reviews recent clinical trials involving patients at risk for or with established right ventricular failure, focusing on beta blockade, phosphodiesterase inhibition, and mechanical support of the failing right heart. The final section presents a perspective on active areas of research that are most likely to translate in clinical practice in the next decade. (J Am Coll Cardiol HF 2018;■:■-■) © 2018 by the American College of Cardiology Foundation.

The right ventricle has been the focus of renewed interest in the last 10 years. Historically, the perception of the right ventricle has fluctuated between an essential and a nonessential ventricle. At one end, in patients with tricuspid atresia and low-pressure pulmonary system, the right ventricle can be bypassed while still maintaining circulation (Fontan circulation) (1). The Fontan circulation remains, however, vulnerable to increases in pulmonary arterial wedge pressure and pulmonary hypertension (PH) and has limited circulatory reserve with exercise (Online Ref. 1). At the other end, contemporary studies have demonstrated the strong

prognostic value of right ventricular (RV) dysfunction in left heart failure, PH, and congenital heart disease (2-5) (Online Refs. 2-5). Explanations for this apparent paradox were provided by physiological studies published in the 1980s. Using a dog model of acute RV myocardial infarction, Goldstein et al. (Online Ref. 6) demonstrated that opening the pericardium significantly improved hemodynamics, highlighting the importance of pericardial constraint and ventricular interdependence in the setting of acute RV enlargement and dysfunction. Further physiological studies demonstrated the importance of ventricular interdependence in the setting of acute pulmonary

From the ^aDivision of Cardiovascular Medicine, Stanford University School of Medicine, Stanford, California; ^bStanford Cardiovascular Institute, Stanford, California; ^cVera Moulton Wall Center at Stanford, Stanford, California; ^dResearch and Innovation Unit, INSERM U999, DHU Torino, Paris Sud University, Marie Lannelongue Hospital, Le Plessis Robinson, France; and the ^eDepartment of Cardiothoracic Surgery, Marie Lannelongue Hospital, Le Plessis Robinson, France. Drs. Amsellem, Mercier, and Haddad are supported by a public grant overseen by the French National Research Agency as part of the second Investissements d'Avenir program (ANR-15-RHUS-0002). This work is also supported by funding from the Vera Moulton Center for Pulmonary Vascular Disease. All other authors have reported that they have no relationships relevant to the contents of this paper to disclose.

Manuscript received March 25, 2018; revised manuscript received May 17, 2018, accepted May 30, 2018.

ISSN 2213-1779/\$36.00

<https://doi.org/10.1016/j.jchf.2018.05.022>

REV 5.50 DTD ■ JCHF935_proof ■ 28 August 2018 ■ 11:43 pm ■ ce

ABBREVIATIONS AND ACRONYMS

3D = 3-dimensional
CMR = cardiac magnetic resonance
DCE = delayed contrast enhancement
Ees = ventricular elastance
MPAP = mean pulmonary arterial pressure
PAH = pulmonary arterial hypertension
PH = pulmonary hypertension
RHF = right heart failure
RV = right ventricular
RVLS = right ventricular free-wall longitudinal strain
TAPSE = tricuspid annular plane systolic excursion

embolism and mechanical ventilation (Online Refs. 7,8). The concept of “cardiopulmonary unit” was born, emphasizing the importance of ventriculoarterial coupling, ventricular interactions, and pericardial constraint in understanding RV adaptation to injury or abnormal loading conditions.

The objective of the current review is to highlight recent advances in RV physiology, phenotyping, and management of right heart failure (RHF). We present selected studies and advances likely to influence practice and conclude by giving a perspective on future directions in the field of right heart research.

DEFINING RHF, EFFORTS TOWARD A COMMON LANGUAGE

Several definitions of RHF have been proposed in the last decade (Table 1) (6–8). The definition proposed by the International Right Heart Failure Foundation Scientific Working Group has the advantage of considering both low and high output failure, impairment of blood filling or ejection, and the different anatomic subgroups of RHF (i.e., subpulmonic or systemic right ventricle) (6). RHF may also be prominent during exercise or periods of increased physiological needs, such as pregnancy.

ADVANCES IN RV PHYSIOLOGY

Pressure-volume loop analysis has proven to be valuable in understanding RV adaptation to injury or abnormal loading conditions. In 1988, Dell’Italia and Walsh (9) have shown that a time varying elastance model can be applied to the right ventricle, similar to the left ventricle. In this model, RV end-systolic elastance (Ees) estimates contractility, arterial elastance measures RV afterload, and ventriculoarterial coupling (Ees arterial elastance) estimates matching between contractility and afterload or more specifically energy transfer efficiency between the right ventricle and the pulmonary circulation (Figure 1A) (10). Because PH is the most common cause of RV dysfunction, effort has been devoted to better understand mechanisms of adaptation of the pressure-overloaded right ventricle. Vonk Noordegraaf et al. (10) have recently summarized the changes in RV physiology that can occur with the progression of pre-capillary chronic PH (Figure 1B). In the early stages of chronic PH, RV elastance usually increases and ventriculoarterial coupling is maintained despite the elevation in afterload (adapted phenotype of the pressure-overloaded ventricle). With the progression of pulmonary vascular disease,

despite the increase in ventricular elastance, ventriculoarterial uncoupling occurs leading to an eventual decrease in ejection fraction and later effective stroke volume (maladapted phenotype of RHF) (10). As part of the Frank-Starling mechanism of adaptation, RV enlargement is usually observed early in the pressure-overloaded right ventricle (10). RV enlargement also emerges as an important prognostic factor in pulmonary arterial hypertension (PAH) and congenital heart disease (4,5,11,12) (Online Ref. 3). Although in clinical practice systolic performance indices, such as ejection fraction, are sometimes equated with contractility, pressure-volume loop analyses have clearly demonstrated that these are separate concepts, with the latter reflecting an intrinsic myocardial property. This was recently highlighted by Guilhaire et al.’s study, using a piglet model of pulmonary artery ligation subsegmental pulmonary embolisms (Online Refs. 9,10), demonstrating that indices of systolic performance, such as fractional area change or tricuspid annular plane systolic excursion (TAPSE), are more closely associated with ventriculoarterial coupling (Ees/arterial elastance) than contractility (Ees) (13).

In recent years, isolated human cardiomyocyte studies have provided further insights on RV adaptation to pressure overload. As highlighted by the Hsu et al. (14) recent study, the increase in RV contractility in PH may not be uniform across etiologies. Cardiomyocytes isolated from 11 patients with systemic sclerosis-associated PAH had decreased maximal calcium-activated force when compared with control subjects, whereas patients with idiopathic PAH had increased maximal calcium-activated force (14). This suggests that intrinsic myocardial dysfunction may be present in patients with systemic sclerosis-associated PAH in contrast to patients with idiopathic PAH and could explain part of their poor outcome. Single RV myocyte-based studies also provided insights on RV diastolic adaptation (Online Refs. 11,12). In isolated single myocyte studies of patients undergoing heart-lung transplantation and nonfailing donors, Rain et al. (Online Ref. 11) demonstrated that the passive tension at different sarcomere lengths was significantly higher in patients with PAH and was associated with reduced titin phosphorylation. A subsequent study on isolated RV trabecular strips of pressure-overloaded rats demonstrated that both myofibril- and fibrosis-mediated stiffness contribute to increased RV myocardial stiffness in more severe RHF (Online Ref. 12). Only few pathologic studies have quantified the degree of RV fibrosis in patients with PAH (15) (Online Refs. 11,13,14). In Rain et al.’s

study, RV fibrosis in patient undergoing heart-lung transplantation was quantified at $9.6 \pm 0.7\%$ compared with $7.2 \pm 0.6\%$ in donors, whereas other studies report interstitial fibrosis ranging from 10% to 15% (15) (Online Refs. 11,13,14). In comparison, studies in patients with aortic stenosis observe a greater extent of interstitial fibrosis (Online Refs. 15,16). More recently, Rommel et al. (Online Ref. 17) observed increased RV stiffness in patients with heart failure with preserved ejection fraction in 24 patients undergoing conductance catheter studies.

RV reserve has also been the focus of recent studies in PH and cardiovascular disease. Nootens et al. (Online Ref. 18) demonstrated that the RV response to exercise is blunted in PAH, showing minimal increase in ejection fraction with exercise. More recently, Hsu et al. (Online Ref. 19) have observed that RV enlargement with exercise may reflect more severely uncoupled ventricles. Their study further investigated the RV force-frequency relationship by measuring the geometric rate of decay in contractile potentiation following abrupt cessation of atrial pacing (recirculation fraction). The recirculation fraction, which reflects recycling of calcium into and out of the sarcoplasmic reticulum, was more preserved in idiopathic PAH in contrast to systemic scleroderma-associated PAH (Online Ref. 19). Online Table S1 and the Online Appendix presents the importance of RV reserve with exercise for outcome in cardiovascular diseases.

In the past decade, several studies have been dedicated to better understand the load imposed on the right ventricle. Lankhaar et al. (16) have demonstrated that resistance and compliance are closely related to each other with a relatively stable resistance compliance time constant in pre-capillary PH (Figure 1C). They further showed that improvement in stroke volume with therapy in PAH was more closely related to changes in compliance than to changes in resistance (16). Although this was initially interpreted as the RV being more responsive to changes in pulsatile load than resistance, Saouti et al. (17) later demonstrated using hydraulic power analysis (integrative of pressure and cardiac output) that the oscillatory power was relatively constant at 23% in non-PH and idiopathic PAH. This constant fraction can explain why mean pulmonary artery pressure (MPAP) is more closely related to systolic and diastolic pressure in the pulmonary circulation. The greater improvement in RV stroke volume observed with greater absolute changes in compliance may rather reflect threshold reduction needed in pulmonary vascular load to observe significant improvement stroke volume. More recent studies

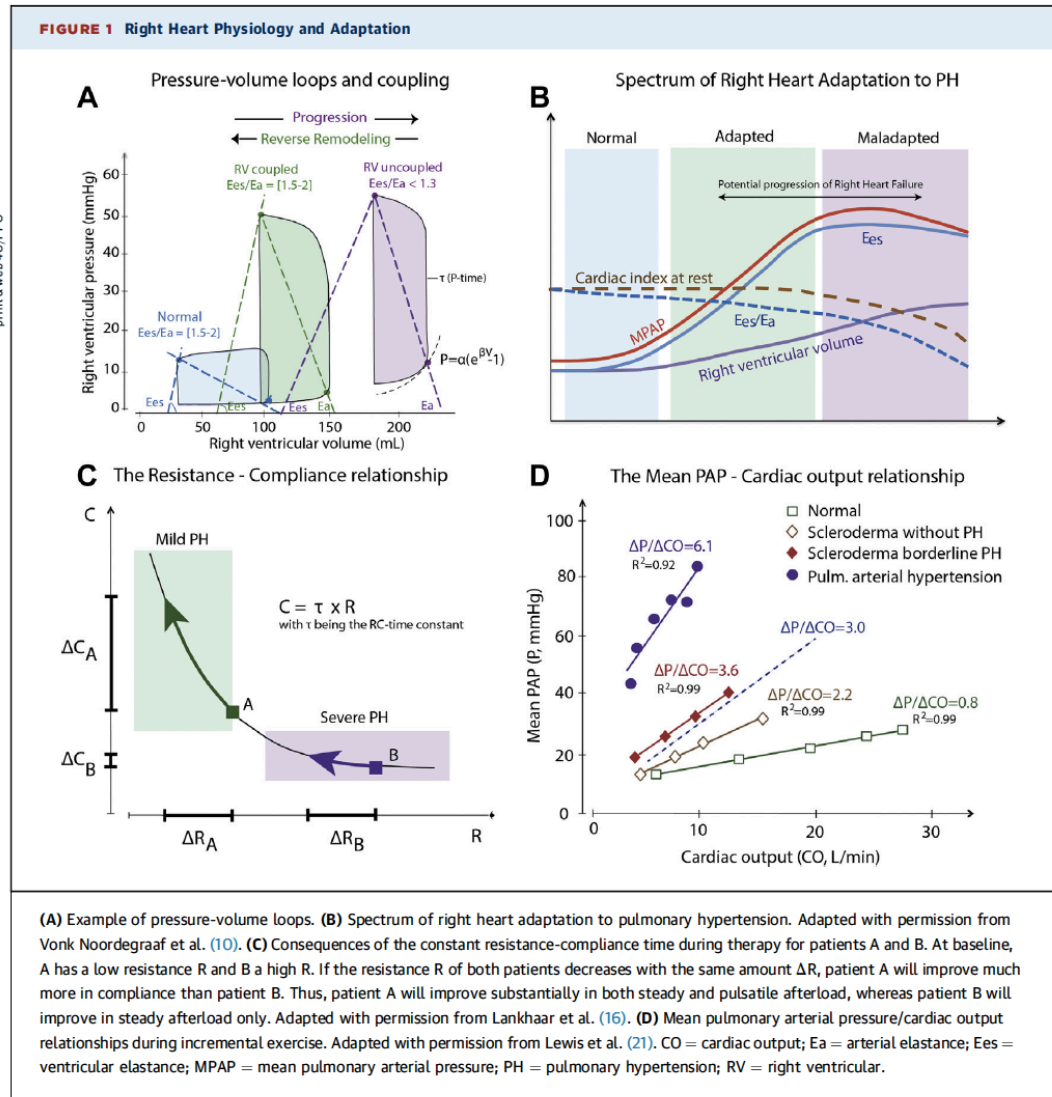
TABLE 1 RHF and Dysfunction

RHF definitions	
2014 International Right Heart Failure Foundation Scientific Working Group	Clinical syndrome caused by an alteration of structure and/or function of the right heart circulatory system that leads to suboptimal delivery of blood flow (high or low) to the pulmonary circulation and/or elevated venous pressures at rest or with exercise.
Ventricular dysfunction	Term often reserved to objectively describe RV function or to refer to asymptomatic stages of RHF.
Specific definitions	
2013 World Symposium on Pulmonary Hypertension	RHF in patients with pulmonary hypertension can be defined as a complex clinical syndrome caused by suboptimal delivery of blood and/or elevated systemic venous pressure at rest or exercise as a consequence of elevated RV afterload.
2014 INTERMACS definition for patients with left ventricular assist device.	The diagnosis of RV failure requires the documentation of elevated central venous pressure >16 mm Hg and manifestation of elevated central venous pressure including end-organ dysfunction. Four levels of RV failure are considered (mild, moderate, severe, and severe-acute) depending on the duration of inotropic support or the need for RV assist device implantation.
RHF = right heart failure; RV = right ventricular.	

have highlighted that the resistance compliance time can be influenced by tachycardia or elevated pulmonary arterial wedge pressure (decreasing the resistance compliance time constant) (Online Figure S1, Online Appendix) (18).

Significant progress has also been made in the field of exercise-induced PH. This issue often arises when assessing a patient with unexplained dyspnea or mild RV enlargement and normal resting pulmonary pressure. The previous definition (i.e., MPAP >30 mm Hg with exercise) was abandoned because it failed to take into account the contribution of cardiac output on pulmonary pressures with exercise. Pulmonary pressures can indeed increase significantly with cardiac output in the absence of pulmonary vascular disease (19). In 1985, Janicki et al. (20) first highlighted that MPAP and cardiac output during exercise can be approximated using a linear relationship irrespective of the pre-capillary or post-capillary origin of PH. The slope of the MPAP/cardiac output relation differs according to PH etiology (Figure 1D) (21). Herve et al. (22) recently showed that a MPAP >30 mm Hg with a total pulmonary resistance of >3.0 mm Hg/l/min could help differentiate patients with pulmonary vascular disease from control subjects. Exercise-related PH has recently been the subject of excellent reviews and society statements (Online Refs. 20,21) and will be addressed in the upcoming reports from the World Symposium on Pulmonary Hypertension.

The right ventricle has a major ability to recover. In fact, RV recovery has been reported in most patients

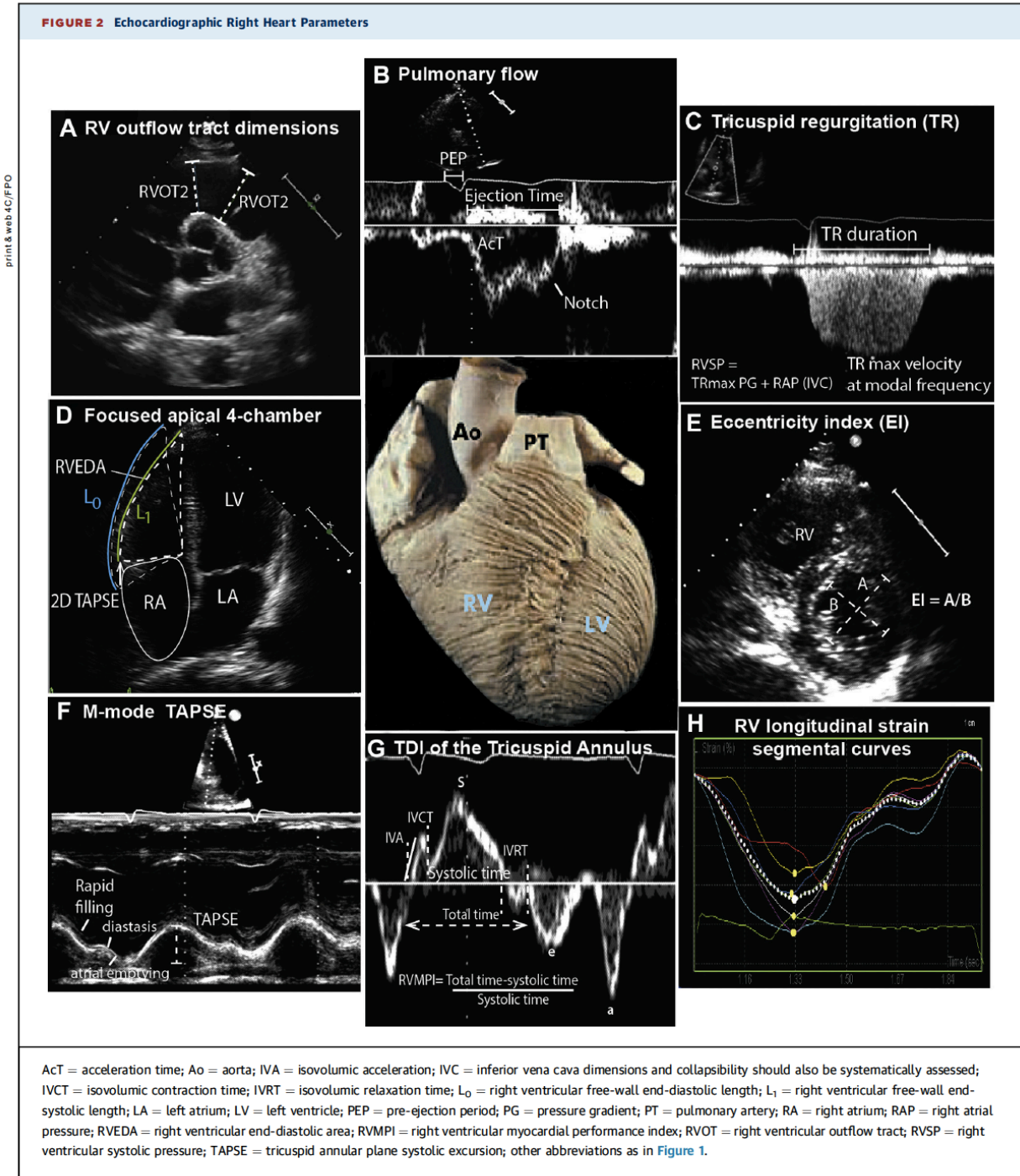


with PAH undergoing lung transplantation (23-25) and in patients with chronic thromboembolic PH undergoing pulmonary arterial endarterectomy (26) or balloon angioplasty (27). Physiologically, it is important to note that in contrast to patients with dilated “left” cardiomyopathy, RV contractility in PAH or chronic thromboembolic PH is usually preserved or increased; this preserved contractility and the relatively low-percent fibrosis of the RV could explain its ability to recover once the afterload is reduced, although further studies are needed in this area. RV plasticity has led transplant surgeons to favor double lung transplantation rather than heart-lung transplant in most patients with PAH (Online Ref. 22). The pressure-overloaded right ventricle may, however, be

susceptible to failure in the early post-operative period (28). Moreover, patients with depressed myocardial contractility or more extensive fibrosis may not have the same ability to reverse remodel. Therefore, selected patients with PAH are still considered for heart-lung transplantation and ongoing studies will refine the selection criteria (Online Ref. 22).

ADVANCES IN RIGHT HEART IMAGING AND PHENOTYPING

Combining hemodynamics, cardiac magnetic resonance (CMR), molecular imaging, and biomarkers provides new opportunities for right heart phenotyping (29). Echocardiography remains the mainstay of



clinical assessment of the right ventricle. **Figure 2** outlines important components of the echocardiographic assessment of the cardiopulmonary unit. CMR is particularly useful when precise structural and

functional assessment of the right heart are needed and is the modality of choice when assessing RV size or function in clinical trials. Molecular imaging provides novel insights on perfusion, metabolism, oxygen

TABLE 2 Selected Recent Imaging Studies Assessing the Value of Noninvasive Right Heart Metrics

First Author, Journal, Year	Population	n	Design	Metrics	Conclusions
Pulmonary hypertension					
Forfia et al., <i>Am J Respir Crit Care Med</i> , 2006	Group 1, 3, 4 PH	63	Prospective	TAPSE	TAPSE <18 mm was associated with 4-fold increased risk of death during follow-up.
Fine et al., <i>Circ Cardiovasc Imaging</i> , 2013	Group 1, 3, 4 PH vs. no PH	406 vs. 169	Prospective	RVLS	Large study on prognostic value of RV strain in PH. Multivariate model: NYHA, strain, NT-proBNP for death at 18 months.
Ryo et al., <i>Circ Cardiovasc Imaging</i> , 2015	Pre-capillary PH	92 vs. 20	Prospective	RVESVI 3D RVLS	3D echocardiography study showing prognostic value of RVESVI (≥ 114 ml/m ²) for PH-related hospitalization, death, or lung transplantation or endarterectomy at 6 months.
Amsallem et al., <i>Circ Cardiovasc Imaging</i> , 2017	PAH	228	Prospective	RV end-systolic area and remodeling index RVLS	Comparative study showing the equivalent prognostic value of RV end-systolic remodeling index, NYHA, NT-proBNP to validated risk scores, such as the REVEAL score.
Swift et al., <i>Am J Respir Crit Care Med</i> , 2017	PAH	576	Prospective	RVESVI Relative area change of the pulmonary artery	Largest magnetic resonance study confirming RV end-systolic volume as a strong and independent RV prognostic metric in PAH.
Congenital heart disease					
Lee et al., <i>J Am Coll Cardiol</i> , 2012	Repaired tetralogy of Fallot	67	Retrospective	RVESVI RVEDVI	CMR study: pulmonary valve replacement should be considered before RVEDVI >163 ml/m ² or RVESVI >80 ml/m ² , with more attention to RVESVI.
HFpEF					
Lam et al., <i>J Am Coll Cardiol</i> , 2009	LVEF $\geq 50\%$ Framingham criteria	244	Prospective	Echo estimated RVSP >35 mm Hg	Study showing the prognostic value of PH in HFpEF. RVSP ≥ 48 mm Hg had worse all-cause mortality than RVSP <48 mm Hg (p < 0.01) during 2.4 \pm 1.2 yrs follow-up.
Aschauer et al., <i>Eur J Heart Fail</i> , 2016	LVEF >50% Signs or symptoms of heart failure NT-proBNP >220 pg/ml LV diastolic dysfunction	171	Prospective	RVEF RVFAC TAPSE	RV systolic dysfunction (RVEF <45% using CMR) was independently associated with event-free survival (HR: 4.90 [95% CI: 2.46-9.75]). RVEF was superior to RVFAC and TAPSE for prediction of cardiac events.
Freed et al., <i>Circ Cardiovasc Imaging</i> , 2016	LVEF $\geq 50\%$ Framingham criteria	308	Prospective	RVFAC <35% TAPSE <16 mm RVLS >20%	RV strain was associated with outcome (univariate HR: 1.30 [95% CI: 1.07-1.58]). Using multivariate analysis, RV strain was not retained, whereas LA strain and LA stiffness were.
Tampakakis et al., <i>Circ Heart Fail</i> , 2018	HFREF or HFpEF with pulmonary hypertension	1,036	Retrospective	Pulmonary arterial compliance, elastance, resistance	Pulmonary arterial compliance and elastance were more strongly associated with outcome than resistance or transpulmonary gradient
HFREF					
Ghio et al., <i>Eur J Heart Fail</i> , 2013	LVEF <45%	658	Prospective	SPAP ≥ 40 mm Hg TAPSE ≤ 14 mm	SPAP ≥ 40 mm Hg and TAPSE ≤ 14 mm were associated with worst outcome (death, urgent heart transplant, ventricular fibrillation). Their combination improved risk stratification.
Moneghetti et al., <i>Eur Heart J Cardiovasc Imaging</i> , 2017	Dilated cardiomyopathy	208	Retrospective	RA volume index	RA volume index is complementary to well-validated heart failure risk scores, which highlights the importance of exercise performance in dilated cardiomyopathy.
Carluccio et al., <i>Circ Cardiovasc Imaging</i> , 2018	HFREF with TAPSE >16 mm	200	Prospective	RVLS	RVLS >-15.3% was associated with outcomes and reclassified patients with TAPSE >16 mm.

Continued on the next page

consumption, and neurohormonal regulation, which may be particularly useful in translational studies or for clinical trial design.

Major recent advances in echocardiography include RV myocardial deformation imaging and improved 3-dimensional (3D) imaging allowing better assessment of RV volume and 3D strain (30). RV free-wall longitudinal strain (RVLS) measures longitudinal

shortening of the RV wall during systole. Although RVLS is usually measured using speckle tracking, Amsallem et al. (4) have demonstrated the feasibility of the manual tracing of RV free-wall length in both diastole and systole, following the Lagrangian definition. RVLS has been recently reported to carry prognostic information in PH, congenital heart disease, and heart failure (Table 2, Online Tables 2 to 5,

TABLE 2 Continued

First Author, Journal, Year	Population	n	Design	Metrics	Conclusions
LVAD					
Soliman et al., <i>Circulation</i> , 2017	Patients referred for continuous-flow LVAD	2,988	Prospective	RV dysfunction assessed semiquantitatively	RV dysfunction was independently associated with risk of right heart failure post-LVAD in one of the largest study in LVAD.
Bellavia et al., <i>Eur J Heart Fail</i> , 2017	Patients referred for LVAD	4,428	Meta-analysis (36 studies)	RVLS	Low RVLS was associated with outcome, but with heterogeneity in the methodology. The complementarity with RV end-systolic size remains to be assessed.
Pulmonary hemodynamics					
Arkles et al., <i>Am J Respir Crit Care Med</i> , 2011	PH vs. HFrEF and PH	88 vs. 32	Retrospective	RV outflow tract Doppler flow velocity envelope	Presence of mid-systolic notch was associated with high pulmonary resistance.
Takahama et al., <i>J Am Coll Cardiol Img</i> , 2017	PAH	159	Retrospective	Comprehensive analysis of the Doppler pulmonary anterograde flow envelope.	Pulmonary flow patterns reflect not only pulmonary impedance ("resistance" to flow) but also right ventricular adaptation to the increased load.
Amsallem et al., <i>J Am Soc Echocardiogr</i> , 2016	Group 1, 3 PH	337	Retrospective		Tricuspid regurgitation derived estimation of RV systolic pressure is reliable when careful attention is given to the quality of the Doppler signal.

3D = 3-dimensional; CI = confidence interval; CMR = cardiac magnetic resonance; HFpEF = heart failure preserved ejection fraction; HFrEF = heart failure reduced ejection fraction; LA = left atrial; LV = left ventricular; LVAD = left ventricular assist device; LVEF = left ventricular ejection fraction; NT-proBNP = N-terminal pro-B-type natriuretic peptide; NYHA = New York Heart Association; PAH = pulmonary arterial hypertension; PH = pulmonary hypertension; RVEDVI = right ventricular end-diastolic volume index; RVESVI = right ventricular end-systolic volume index; RVEF = right ventricular ejection fraction; RVFAC = right ventricular fractional area change; RVLS = right ventricular free-wall longitudinal strain; RVSP = right ventricular systolic pressure; SPAP = systolic pulmonary arterial pressure; TAPSE = tricuspid annular plane systolic excursion; other abbreviations as in Table 1.

Online Appendix) (3-5,12) (Online Refs. 2-4,23-33). In a large study of patients with suspected PH, Fine et al. (3) have demonstrated RVLS, N-terminal pro-B-type natriuretic peptide and New York Heart Association functional class provide independent prognostic value. These findings were confirmed in PAH by Amsallem et al. (4) who further found that measures of RV end-systolic remodeling may carry slightly

more prognostic information. In both these studies, RVLS carried more prognostic information than TAPSE, which represents 1 of the most widely used indices of RV systolic performance. Compared with RVLS, TAPSE has the advantage of being more simple and reproducible. Unlike RV ejection fraction or fractional area change, both TAPSE and RVLS decrease following pericardiectomy, leading to

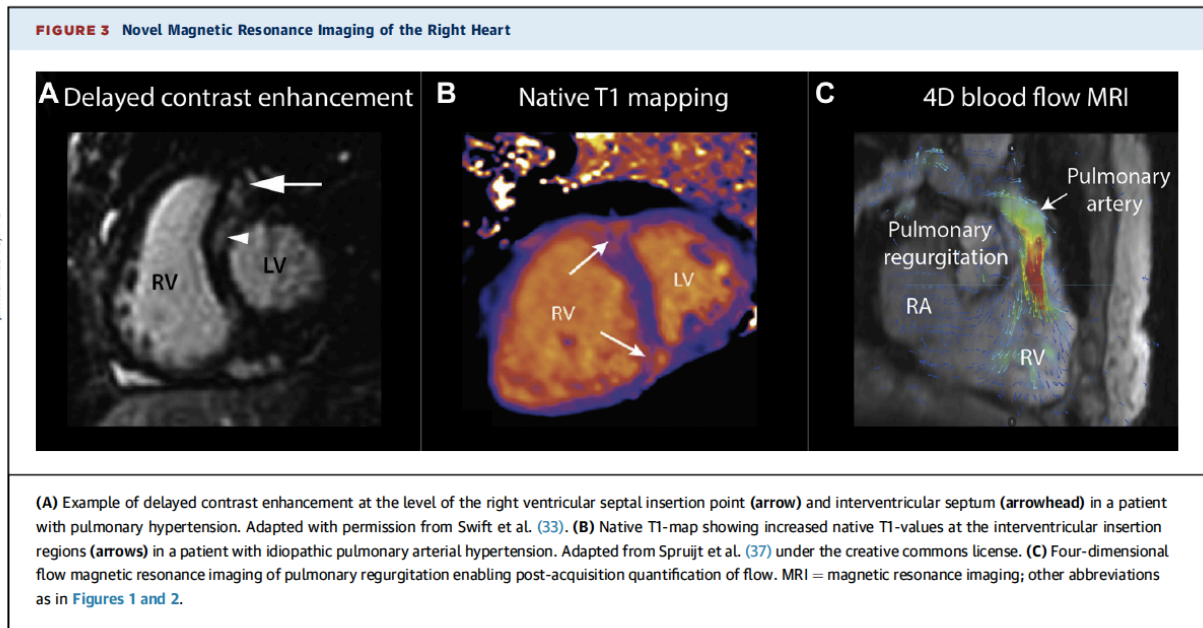


TABLE 3 Selected Therapeutic Studies of the Cardiopulmonary Arterial Unit

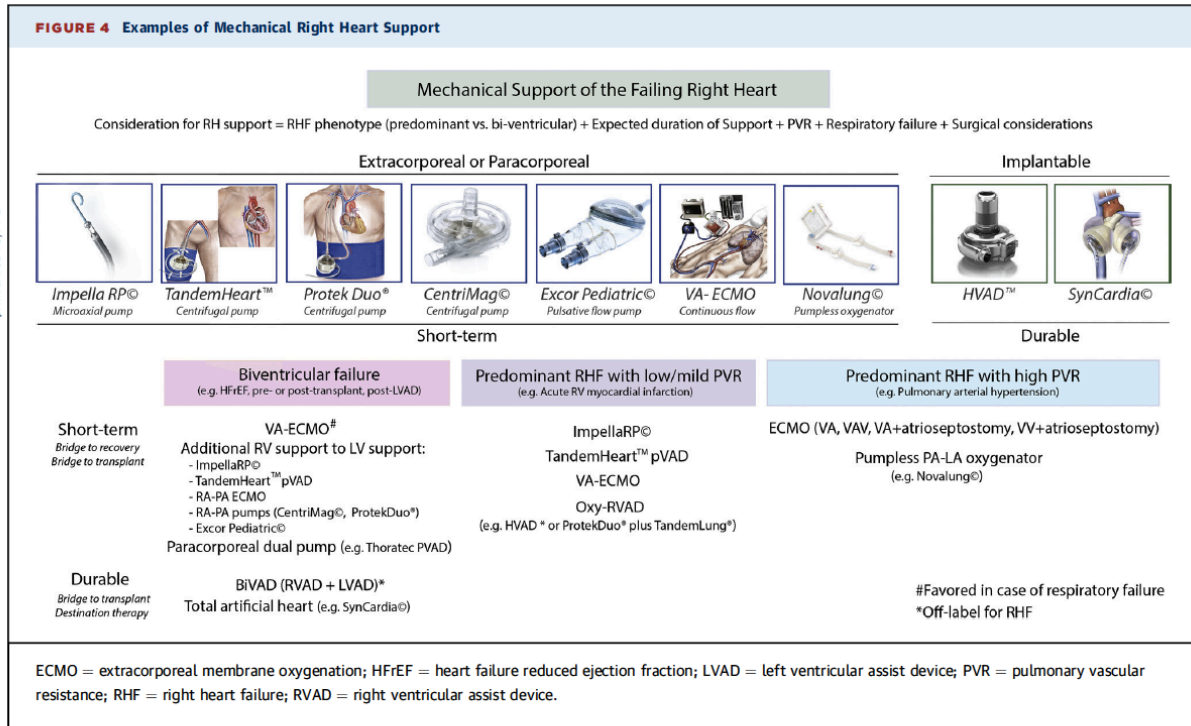
First Author, Journal, Year	Molecule	Population	Design	Results
Phosphodiesterase 5 inhibitors				
Lewis et al., <i>Circulation</i> , 2007	Sildenafil	HFREF (LVEF <40%) and MPAP >25 mm Hg (n = 34)	Phase 3 (randomized vs. placebo)	At 12 weeks, sildenafil reduced PVR and increased cardiac output with exercise, improved peak VO ₂ and RV ejection fraction.
Guazzi et al., <i>Circulation</i> , 2011	Sildenafil	HFpEF and SPAP >40 mm Hg (n = 44)	Phase 3 (randomized vs. placebo)	At 6 months, sildenafil reduced SPAP and improved RV function.
Hoendermis et al., <i>Eur Heart J</i> , 2015	Sildenafil	HFpEF and MPAP >25 mm Hg, PAWP >15 mm Hg (n = 52)	Phase 3 (randomized vs. placebo)	At 12 weeks, no change in MPAP (primary endpoint), cardiac output or peak VO ₂ .
Hussain et al., <i>Circ Heart Fail</i> , 2016	Sildenafil	HFpEF (RELAX criteria) and SPAP measurement available (n = 138)	Ancillary study of the phase 3 RELAX study	In the subgroup of patients with RV dysfunction and impaired RV-PA coupling, sildenafil did not improve RV function, exercise capacity, or ventilatory efficiency.
Bermejo et al., <i>Eur Heart J</i> , 2017	Sildenafil	Successful valve replacement or repair (more than 1 yr before study) and MPAP ≥30 mm Hg (n = 200)	Phase 3 (randomized vs. placebo) SIOVAC study	Sildenafil was associated with worse outcome (death, hospital admission for heart failure, change in functional class, and patient global self-assessment) than placebo.
Endothelin receptor antagonist				
Vachiéry et al., <i>Eur Respir J</i> , 2018	Macicentan	PH related to left heart disease and diastolic pressure gradient ≥7 mm Hg and pulmonary vascular resistance >3 WU (n = 63)	Phase 3 MELODY-1 trial (randomized controlled trial)	No difference in terms of significant fluid retention or worsening in New York Heart Association functional class from baseline at 12 weeks.
Inhaled prostacyclins				
Denault et al., <i>Can J Anesth</i> , 2016	Milrinone	High-risk cardiac surgery (2+ valvular surgery or CABG) patients with pre-operative PH (n = 124)	Phase 3	Prophylactic use of inhaled milrinone was associated with improvement in hemodynamics but did not reduce the incidence of difficult or complex separation from cardiopulmonary bypass.
Betablockade				
Grinnan et al., <i>Am J Respir Crit Care Med</i> , 2014	Carvedilol	PAH (n = 10)	Phase 1 (safety)	No major event, 4 discontinuations. Patients included (n = 6) had significant improvement in RVEF and reduction in RV end-systolic volume. The results of phase 2 study (NCT02120339) are pending.
Van Campen et al., <i>Eur Respir J</i> , 2016	Bisoprolol	Idiopathic PAH (n = 18)	Phase 2	Significantly reduced heart rate was not associated with a significant change in RVEF, but reduction in cardiac index. Study failed to enroll the targeted 25 patients.
Aldosterone receptor antagonist				
Maron et al., <i>Am J Cardiol</i> , 2013	Spirolactone Ambrisentan	PAH (n = 393)	Phase 3 (randomized double controlled)	Spirolactone + ambrisentan improved exercise capacity. The effects of spiro lactone on chronic right heart failure will be assessed in a coming phase 4 study (NCT03344159).
Cardiac resynchronization therapy				
Dubin et al., <i>Circulation</i> , 2003	Right-left synchronization	RV dysfunction and right bundle branch block (n = 7)	Phase 2	Improvement in RV contractility and left ventricular stroke volume. Larger trials needed.

CABG = coronary arterial bypass graft; MPAP = mean pulmonary arterial pressure; PA = pulmonary artery; PAWP = pulmonary arterial wedge pressure; PVR = pulmonary vascular resistance; other abbreviations as in Tables 1 and 2.

overdiagnosis of perioperative ventricular dysfunction (31).

CMR has been a transformative technology in the assessment of the right heart. RV ejection fraction and RV volumes carry strong prognostic information in PAH, congenital heart disease, and heart failure (Table 2, Online Tables 2 to 5, Online Appendix) (3–5,12) (Online Refs. 2–4,23–33). In a recent large study, Swift et al. (5) confirmed the independent predictive value of normalized RV end-systolic volumes, along with CMR-derived pulmonary artery pulsatility in PAH (Online Ref. 26). Novel CMR sequences (e.g., delayed contrast enhancement [DCE]

and T1 mapping) have enabled progress in tissue characterization, although their importance in directly guiding prognosis or therapy still remains to be proven (32,33). Patients with PH frequently have DCE localized at the RV insertion point of the interventricular septum (Figure 3A) corresponding to higher fiber stress zones (34,35,33) (Online Refs. 13,14). The mechanisms underlying DCE (myocardial disarray and/or plexiform fibrosis) remains to be elucidated (36). DCE has been associated with RV enlargement, systolic dysfunction, and severe hemodynamic profiles in small cohorts (34,36) (Online Refs. 34,35). One potential pitfall of DCE imaging is



failing to detect diffuse interstitial myocardial fibrosis, because it relies on relative signal intensity changes and nulling of normal-appearing myocardium (Online Ref. 36). Quantitative assessment of the myocardial longitudinal relaxation time constant (T1), either from noncontrast (native) myocardial T1 values (providing information on both myocytes and interstitium) or after gadolinium-based contrast administration (enabling extracellular space quantification), emerges as an alternative technique (37) (Online Ref. 37). In the setting of RV dysfunction and PH, RV hinge point noncontrast T1 and extracellular volume estimation values are elevated (Figure 3B) (37) (Online Ref. 37). Studies using T1 mapping for RV assessment remain limited by the RV wall thickness exposing to the risk of partial volume effect; therefore, further validation is needed before its implementation in clinical practice. Future studies will also help determine the yield of 3D time-resolved flow magnetic resonance sequence (i.e., 4-dimensional blood flow sequence). Four-dimensional blood flow is an evolving imaging technique integrating both a vector of blood velocity and the magnitude signal intensity over an imaging volume (Figure 3C). It enables off-line 3D assessment of blood flow and detection of flow turbulence within the pulmonary artery (Online Ref. 38,39).

MANAGING RHF

This section presents an overview of misconceptions and recent trials relevant to management of RHF. One common misconception in managing acute RHF is to assume that patients would benefit from volume loading. This is based on the assumption that patients are on the pre-load-dependent zone of the Frank-Starling relationship (38). However, studies have clearly demonstrated that volume loading can worsen pericardial constraint, increase left ventricular filling pressure and decrease effective cardiac output, particularly in case of severe RV enlargement (39) (Online Refs. 8,40,41).

There has been great interest in identifying novel therapeutics in patients with RHF. Interpretation of these clinical trials may, however, be challenging for several reasons (40-44) (Online Refs. 42-47). First, many of these trials focus on PH rather than RV dysfunction per se. Second, trials in pediatrics have often included patients with both subpulmonic and systemic right ventricles. Third, trials are often underpowered for exercise capacity let alone mortality or heart failure hospitalization. Table 3 summarizes selected recent trials focusing on PH specific medications (i.e., phosphodiesterase inhibition, endothelin receptor blockade) or neurohormonal modulation (i.e.,

TABLE 4 Selected Recent Clinical Studies on the Use of ECMO or Pumpless Oxygenator

First Author, Journal, Year	Population	Support	Results
Boulate et al., <i>Ann Thorac Surg</i> , 2016	CTEPH with persistent cardiorespiratory failure post-endarterectomy (n = 31)	VA-ECMO or central pulmonary arterial - left atrial oxygenator (Novalung)	This single-center study shows the feasibility of using ECMO or Novalung to support patients after endarterectomy either to recover or to salvage transplantation.
Todd et al., <i>J Thorac Cardiovasc Surg</i> , 2017	Patients referred for lung transplantation (n = 93)	VA- or VV-ECMO	12 patients received bridge to transplant and 81 did not. 1-yr survival was excellent: 100% in the bridge to transplant group and 91% in the nonbridge group.
Tsiouris et al., <i>ASAIO J</i> , 2017	37 U.S. lung transplant centers	ECMO	Multicenter survey of 33/57 U.S. transplant centers: 22 use ECMO as bridge to transplant, including 18 using VV-ECMO
Biscotti et al., <i>Ann Thorac Surg</i> , 2017	Patients referred for lung transplantation with ECMO as bridge to transplant (n = 72)	ECMO	Of the 72 patients, 40 (55.6%) underwent lung transplantation, 37 (92.5%) survived to discharge, and 21 (84.0%) survived for 2 yrs.
Ius et al., <i>Eur J Cardiothorac Surg</i> , 2018	Patients referred for lung transplantation with ECMO as bridge to transplant (n = 68 including awake in 57)	ECMO	Among the 917 patients transplanted in that large center, patients requiring ECMO as bridge to transplant had lower survival than those who did not require ECMO. However, use of ECMO pre-transplant did not significantly impact graft survival.
Hoetzenecker et al., <i>J Thorac Cardiovasc Surg</i> , 2018	Patients referred for lung transplantation with bridge to transplant ECMO (n = 71)	ECMO including 23 with dual lumen venous canula, 9 Novalung	Among the 71 patients, 13 had pulmonary hypertension, including 9 had Novalung. 1-yr survival was 66%. Survival was lower in patients who had ECMO as a bridge to retransplantation.

CTEPH = chronic thromboembolic pulmonary hypertension; ECMO = extracorporeal membrane oxygenation; VA = venous-arterial; VV = venovenous.

beta blockade or mineralocorticoid receptor blockade) (40-44) (Online Refs. 42-47).

PHOSPHODIESTERASE INHIBITION. Recent studies have tempered the enthusiasm of using phosphodiesterase inhibition in patients with PH and left heart disease. Guazzi et al. (41) showed significant

response to sildenafil in 44 patients with heart failure with preserved ejection fraction and elevated systolic pulmonary arterial pressure (>40 mm Hg), most having elevated right atrial pressure. The more recent Phosphodiesterase-5 Inhibition to Improve CLinical Status And EXercise Capacity in Diastolic Heart Failure (RELAX) trial failed to identify benefits of sildenafil in the overall population and in the subgroup of patients stratified according to the TAPSE/RV systolic pressure ratio (42). In the recent Sildenafil for Improving Outcomes after Valvular Correction (SIOVAC) study in patients with corrected valvular heart disease and persistent PH, sildenafil was, however, associated with worse outcome (death, hospital admission for heart failure, change in functional class, and patient global self-assessment) than placebo, highlighting the need of further trials exploring the safety and efficacy of sildenafil (44). In 34 patients with heart failure with reduced ejection fraction and PH, Lewis et al. (40) have observed improvement in hemodynamics during exercise (peak VO₂ and RV ejection fraction) with sildenafil when compared with placebo.

BETA-BLOCKADE. Despite positive results from preclinical studies, a recent small phase 2 clinical trial using bisoprolol in patients with PAH and RHF failed to demonstrate short-term benefits of bisoprolol on RV remodeling and 6-min-walk distance (43). Because patients with PH and RHF have significantly decreased contractile reserve, it is unclear whether the potential benefits of beta

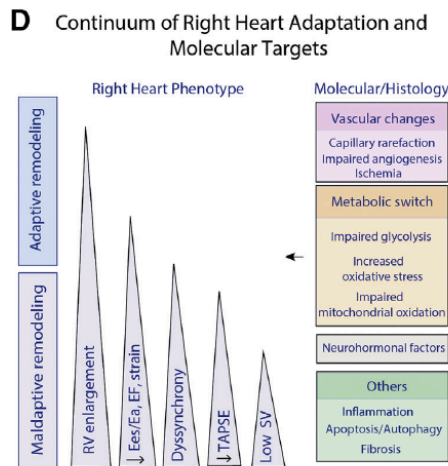
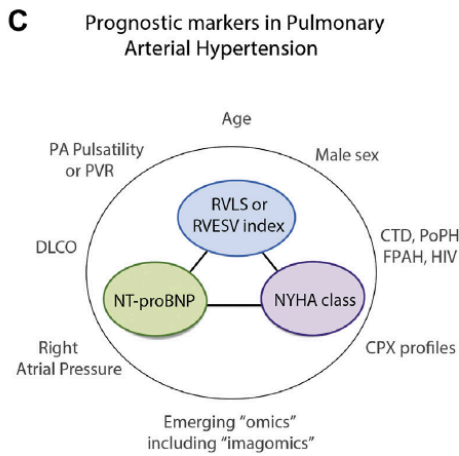
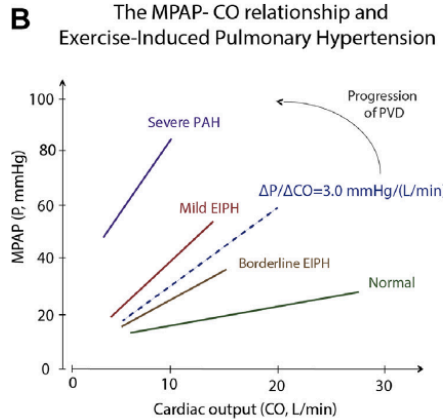
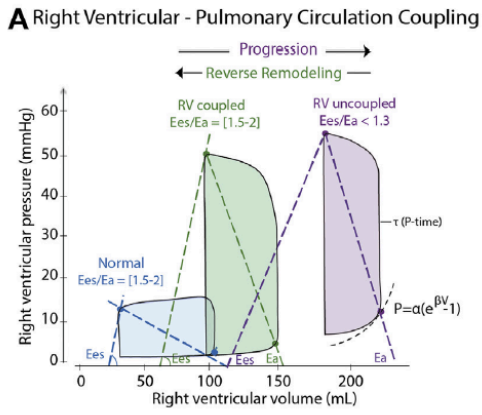
TABLE 5 Perspectives on Future Right Heart Research

Field	Areas of future research
Computational methods	Use of computational methods to develop efficient diagnostic, prognostic, and management algorithms in RHF. Automation of image analysis will also likely emerge in the next 10 yrs especially using magnetic resonance imaging.
Biomarkers	Identifying the most complementary biomarkers for detection, risk stratification, and disease phenotyping. Identifying biomarkers predicting of response to therapy in PAH
Imaging	Further development of deformation imaging (improving its reliability), 3D echocardiography, magnetic resonance tissue characterization (T1 mapping, magnetic resonance spectroscopy), 4D blood flow, computed tomography, and positron emission tomography (molecular imaging).
Management strategies	Develop efficient strategies for the monitoring and management of patients with RHF. Better define the role of invasive surveillance of patient with RHF and pulmonary hypertension.
Recovery	Identification of markers of irreversible RV remodeling and dysfunction. Identification of patients with PAH most likely to benefit from a heart-lung transplantation vs. double lung transplant.
Translations	Develop representative large animal models of chronic and acute pressure overload. Develop RV specific in vivo cellular models allowing further investigation of specific molecular transducers of RHF.
Clinical trials and therapeutics	Develop enriched clinical trials based on molecular imaging (e.g., metabolism imaging) or physiological phenotypes. Design RV-based therapeutic trials in pulmonary hypertension or congenital heart disease. Design novel mechanical support system for the failing right heart.

4D = 4-dimensional; other abbreviations as in Tables 1 and 2.

print & web 4C/FPO

CENTRAL ILLUSTRATION Summary of the Latest Advances in Physiology



Amsallem, M. et al. *J Am Coll Cardiol HF*. 2018; ■(■): ■-■.

Summary of the latest advances in physiology including assessment of right ventricular-pulmonary arterial coupling using pressure-volume loops (A) and the importance of the mean pulmonary arterial pressure/cardiac output to detect exercise-induced pulmonary hypertension (B). Schematic representation of predictive factors in pulmonary arterial hypertension; recent imaging-based studies highlighted the importance of right ventricular longitudinal strain or end-systolic dimensions, N-terminal pro-B-type natriuretic peptide, and functional class to determine prognosis (C), and the importance of pulmonary arterial pulsatility as an independent predictive factor (3-5). Continuum of right heart adaptation/maladaptation in pulmonary hypertension and molecular targets (D). CO = cardiac output; CPX = cardiopulmonary exercise testing; CTD = connective tissue disease; DLCO = diffusing capacity of the lung for carbon monoxide; Ea = arterial elastance; Ees = ventricular elastance; EIPH = exercise-induced pulmonary hypertension; FPAH = familial PAH; MPAP = mean pulmonary arterial pressure; NT-proBNP = N-terminal pro-B-type natriuretic peptide; NYHA = New York Heart Association; PA = pulmonary artery; PAH = pulmonary arterial hypertension; PH = pulmonary hypertension; PoPH = portal pulmonary hypertension; PVD = pulmonary vascular disease; PVR = pulmonary vascular resistance; RV = right ventricular; RVLS = RV longitudinal strain; SV = stroke volume; TAPSE = tricuspid annular plane systolic excursion.

blockade would offset the decrease in chronotropic response (Online Ref. 48). Small pilot observations using carvedilol in PAH seem encouraging, but larger clinical trials are needed (Online Ref. 45). In patients with congenital heart disease, the effects

of beta-blockers on a systemic RV have not been fully elucidated, because a recent negative trial assessing carvedilol in pediatrics only included a small proportion of patients with a systemic RV (Online Ref. 49).

MINERALOID RECEPTOR ANTAGONIST. Spironolactone is also being investigated in PAH. A recent clinical trial has demonstrated the benefits of spironolactone and ambrisentan on exercise capacity (Table 3) (Online Ref. 47), and a phase 4 study is ongoing (NCT02253394).

MECHANICAL SUPPORT OF THE FAILING RIGHT HEART

The field of right mechanical support has witnessed major advances in the last 15 years, largely because of improvement in oxygenators used in extracorporeal membrane oxygenation and the emergence of dedicated expert teams (Online Ref. 50). Several considerations are involved in choosing mechanical right heart support options in a given patient, including type of RHF, expected duration of support, the presence of concomitant respiratory failure, and a variety of surgical considerations (Figure 4). Advances in extracorporeal membrane oxygenation have made possible successful bridging to lung transplantation or recovery in severe RHF (Table 4) (28,45) (Online Refs. 51-54). Better oxygenator design has also led to the development of pumpless oxygenators, which can be used in patients with respiratory failure and preserved cardiac output (28,45). Pumpless oxygenators with central cannulation have also been used in PAH or chronic thromboembolic PH, in which the unloaded right ventricle (often with preserved contractility) can pump within the circuit (28,45). The reader is referred to the excellent recent review of Kapur et al. (Online Ref. 54) and Online Table S6

(Online Appendix), which further discuss challenges and solution for RHF support.

RESEARCH PERSPECTIVES ON THE NEXT 10 YEARS

The right ventricle will continue to be the focus of intensive research as it challenges both clinicians and scientists. Ongoing precision medicine initiatives will help better understand the transition from the adapted to the maladapted right heart and define criteria for irreversible RHF. Computational methods will likely contribute to improve diagnosis and risk stratification algorithms for RHF and contribute to automation of image analysis. Moreover, enriched clinical trial designs using right heart imaging and molecular phenotyping will likely help tailor precision therapeutics. Table 5 and the Central Illustration summarize some active areas of right heart research. Statements from the World Pulmonary Hypertension Meeting and American Thoracic Society workgroup on the right heart will also provide complementary perspectives on the field. As the field has entered the new era of right heart research, the right heart is truly forgotten no more.

ACKNOWLEDGEMENTS The authors thank Sharon Hunt and Jeffrey Teuteberg (Stanford) and Julien Guihaire (Marie Lannelongue Hospital) for their advice on this review.

ADDRESS FOR CORRESPONDENCE: Dr. Francois Haddad, Stanford University School of Medicine, 300 Pasteur Drive, Stanford, California 94304. E-mail: fhaddad@stanford.edu.

REFERENCES

- Fontan F, Baudet E. Surgical repair of tricuspid atresia. *Thorax* 1971;26:240-8.
- Mehta SR, Eikelboom JW, Natarajan MK, et al. Impact of right ventricular involvement on mortality and morbidity in patients with inferior myocardial infarction. *J Am Coll Cardiol* 2001;37:37-43.
- Fine NM, Chen L, Bastiansen PM, et al. Outcome prediction by quantitative right ventricular function assessment in 575 subjects evaluated for pulmonary hypertension. *Circ Cardiovasc Imaging* 2013;6:711-21.
- Amsallem M, Sweatt AJ, Aymami MC, et al. Right heart end-systolic remodeling index strongly predicts outcomes in pulmonary arterial hypertension: comparison with validated models. *Circ Cardiovasc Imaging* 2017;10:e005771.
- Swift AJ, Capener D, Johns C, et al. Magnetic resonance imaging in the prognostic evaluation of patients with pulmonary arterial hypertension. *Am J Respir Crit Care Med* 2017;196:228-39.
- Mehra MR, Park MH, Landzberg MJ, Lala A, Waxman AB. Right heart failure: toward a common language. *Pulm Circ* 2013;3:963-7.
- Lampert BC, Teuteberg JJ. Right ventricular failure after left ventricular assist devices. *J Heart Lung Transplant* 2015;34:1123-30.
- Galiè N, Simonneau G. The Fifth World Symposium on Pulmonary Hypertension. *J Am Coll Cardiol* 2013;62:D1-3.
- Dell'Italia LJ, Walsh RA. Application of a time varying elastance model to right ventricular performance in man. *Cardiovasc Res* 1988;22:864-74.
- Vonk Noordegraaf A, Westerhof BE, Westerhof N. The relationship between the right ventricle and its load in pulmonary hypertension. *J Am Coll Cardiol* 2017;69:236-43.
- Amsallem M, Boulate D, Aymami M, et al. Load adaptability in patients with pulmonary arterial hypertension. *Am J Cardiol* 2017;120:874-82.
- Ryo K, Goda A, Onishi T, et al. Characterization of right ventricular remodeling in pulmonary hypertension associated with patient outcomes by 3-dimensional wall motion tracking echocardiography. *Circ Cardiovasc Imaging* 2015;8:e003176.
- Guihaire J, Haddad F, Boulate D, et al. Non-invasive indices of right ventricular function are markers of ventricular-arterial coupling rather than ventricular contractility: insights from a porcine model of chronic pressure overload. *Eur Heart J Cardiovasc Imaging* 2013;14:1140-9.
- Hsu S, Kokkonen-Simon KM, Kirk JA, et al. Right ventricular myofilament functional differences in humans with systemic sclerosis-associated versus idiopathic pulmonary arterial hypertension. *Circulation* 2018;137:2360-70.
- Overbeek MJ, Mouchaers KTB, Niessen HM, et al. Characteristics of interstitial fibrosis and inflammatory cell infiltration in right ventricles of systemic sclerosis-associated pulmonary arterial hypertension. *Int J Rheumatol* 2010 Sep 30 [E-pub ahead of print].

16. Lankhaar J-W, Westerhof N, Faes TJC, et al. Pulmonary vascular resistance and compliance stay inversely related during treatment of pulmonary hypertension. *Eur Heart J* 2008;29:1688-95.
17. Saouti N, Westerhof N, Helderma F, et al. Right ventricular oscillatory power is a constant fraction of total power irrespective of pulmonary artery pressure. *Am J Respir Crit Care Med* 2010;182:1315-20.
18. Tedford RJ, Hassoun PM, Mathai SC, et al. Pulmonary capillary wedge pressure augments right ventricular pulsatile loading. *Circulation* 2012;125:289-97.
19. Oliveira RKF, Agarwal M, Tracy JA, et al. Age-related upper limits of normal for maximum upright exercise pulmonary haemodynamics. *Eur Respir J* 2016;47:1179-88.
20. Janicki JS, Weber KT, Likoff MJ, Fishman AP. The pressure-flow response of the pulmonary circulation in patients with heart failure and pulmonary vascular disease. *Circulation* 1985;72:1270-8.
21. Lewis GD, Bossone E, Naeije R, et al. Pulmonary vascular hemodynamic response to exercise in cardiopulmonary diseases. *Circulation* 2013;128:1470-9.
22. Herve P, Lau EM, Sitbon O, et al. Criteria for diagnosis of exercise pulmonary hypertension. *Eur Respir J* 2015;46:728-37.
23. Kasimir M-T, Seebacher G, Jaksch P, et al. Reverse cardiac remodeling in patients with primary pulmonary hypertension after isolated lung transplantation. *Eur J Cardiothorac Surg* 2004;26:776-81.
24. Sarashina T, Nakamura K, Akagi S, et al. Reverse right ventricular remodeling after lung transplantation in patients with pulmonary arterial hypertension under combination therapy of targeted medical drugs. *Circ J* 2017;81:383-90.
25. Gorter TM, Verschuuren EAM, van Veldhuisen DJ, et al. Right ventricular recovery after bilateral lung transplantation for pulmonary arterial hypertension. *Interact Cardiovasc Thorac Surg* 2017;24:890-7.
26. Berman M, Gopalan D, Sharples L, et al. Right ventricular reverse remodeling after pulmonary endarterectomy: magnetic resonance imaging and clinical and right heart catheterization assessment. *Pulm Circ* 2014;4:36-44.
27. Fukui S, Ogo T, Morita Y, et al. Right ventricular reverse remodeling after balloon pulmonary angioplasty. *Eur Respir J* 2014;43:1394-402.
28. Boulate D, Mercier O, Mussot S, et al. Extracorporeal life support after pulmonary endarterectomy as a bridge to recovery or transplantation: lessons from 31 consecutive patients. *Ann Thorac Surg* 2016;102:260-8.
29. Vonk Noordegraaf A, Haddad F, Bogaard HJ, Hassoun PM. Noninvasive imaging in the assessment of the cardiopulmonary vascular unit. *Circulation* 2015;131:899-913.
30. Amsallem M, Kuznetsova T, Hanneman K, Denault A, Haddad F. Right heart imaging in patients with heart failure: a tale of two ventricles. *Curr Opin Cardiol* 2016;31:469-82.
31. Haddad F, Elmi-Sarabi M, Fadel E, Mercier O, Denault AY. Pearls and pitfalls in managing right heart failure in cardiac surgery. *Curr Opin Anaesthesiol* 2016;29:68-79.
32. Freed BH, Gomberg-Maitland M, Chandra S, et al. Late gadolinium enhancement cardiovascular magnetic resonance predicts clinical worsening in patients with pulmonary hypertension. *J Cardiovasc Magn Reson* 2012;14:11.
33. Swift AJ, Rajaram S, Capener D, et al. LGE patterns in pulmonary hypertension do not impact overall mortality. *J Am Coll Cardiol Img* 2014;7:1209-17.
34. Blyth KG, Groenning BA, Martin TN, et al. Contrast enhanced-cardiovascular magnetic resonance imaging in patients with pulmonary hypertension. *Eur Heart J* 2005;26:1993-9.
35. Bradlow WM, Assomull R, Kilner PJ, Gibbs JSR, Sheppard MN, Mohiaddin RH. Understanding late gadolinium enhancement in pulmonary hypertension. *Circ Cardiovasc Imaging* 2010;3:501-3.
36. McCann GP, Gan CT, Beek AM, Niessen HWM, Vonk Noordegraaf A, van Rossum AC. Extent of MRI delayed enhancement of myocardial mass is related to right ventricular dysfunction in pulmonary artery hypertension. *AJR Am J Roentgenol* 2007;188:349-55.
37. Spruijt OA, Vissers L, Bogaard H-J, Hofman MBM, Vonk Noordegraaf A, Marcus JT. Increased native T1-values at the interventricular insertion regions in precapillary pulmonary hypertension. *Int J Cardiovasc Imaging* 2016;32:451-9.
38. Piazza G, Goldhaber SZ. The acutely decompensated right ventricle: pathways for diagnosis and management. *Chest* 2005;128:1836-52.
39. Monnet X, Marik PE, Teboul J-L. Prediction of fluid responsiveness: an update. *Ann Intensive Care* 2016;6:111.
40. Lewis GD, Shah R, Shahzad K, et al. Sildenafil improves exercise capacity and quality of life in patients with systolic heart failure and secondary pulmonary hypertension. *Circulation* 2007;116:1555-62.
41. Guazzi M, Vicenzi M, Arena R, Guazzi MD. Pulmonary hypertension in heart failure with preserved ejection fraction: a target of phosphodiesterase-5 inhibition in a 1-year study. *Circulation* 2011;124:164-74.
42. Hussain I, Mohammed SF, Forfia PR, et al. Impaired right ventricular-pulmonary arterial coupling and effect of sildenafil in heart failure with preserved ejection fraction: an ancillary analysis from the Phosphodiesterase-5 Inhibition to Improve Clinical Status And Exercise Capacity in Diastolic Heart Failure (RELAX) Trial. *Circ Heart Fail* 2016;9:e002729.
43. van Campen JSJA, de Boer K, van de Veerdonk MC, et al. Bisoprolol in idiopathic pulmonary arterial hypertension: an explorative study. *Eur Respir J* 2016;48:787-96.
44. Bermejo J, Yotti R, Garcia-Orta R, et al. Sildenafil for improving outcomes in patients with corrected valvular heart disease and persistent pulmonary hypertension: a multicenter, double-blind, randomized clinical trial. *Eur Heart J* 2018;39:1255-64.
45. Hoetzenecker K, Donahoe L, Yeung JC, et al. Extracorporeal life support as a bridge to lung transplantation-experience of a high-volume transplant center. *J Thorac Cardiovasc Surg* 2018;155:1316-28.

KEY WORDS heart failure, imaging, pulmonary hypertension, right heart, ventricular-assist devices

APPENDIX For supplemental tables and figures, please see the online version of this paper.

Review Article

Current Knowledge and Recent Advances of Right Ventricular Molecular Biology and Metabolism from Congenital Heart Disease to Chronic Pulmonary Hypertension

Samantha Guimaron,¹ Julien Guihaire ,^{1,2} Myriam Amsallem,¹ François Haddad,^{1,3} Elie Fadel,^{1,4} and Olaf Mercier^{1,4}

¹Research and Innovation Unit, RHU BioArt Lung 2020, Marie Lannelongue Hospital, Paris-Sud University, Le Plessis-Robinson, France

²Cardiac Surgery, Marie Lannelongue Hospital, Paris-Sud University, Le Plessis-Robinson, France

³Division of Cardiovascular Medicine, Stanford Cardiovascular Institute, Stanford University School of Medicine, Stanford, CA, USA

⁴Thoracic and Vascular Surgery and Heart and Lung Transplantation, Marie Lannelongue Hospital, Paris-Sud University, Le Plessis-Robinson, France

Correspondence should be addressed to Julien Guihaire; julienguihaire@gmail.com

Received 1 September 2017; Accepted 20 December 2017; Published 17 January 2018

Academic Editor: Utako Yokoyama

Copyright © 2018 Samantha Guimaron et al. This is an open access article distributed under the Creative Commons Attribution License, which permits unrestricted use, distribution, and reproduction in any medium, provided the original work is properly cited.

Studies about pulmonary hypertension and congenital heart diseases have introduced the concept of right ventricular remodeling leading these pathologies to a similar outcome: right ventricular failure. However right ventricular remodeling is also a physiological process that enables the normal fetal right ventricle to adapt at birth and gain its adult phenotype. The healthy mature right ventricle is exposed to low pulmonary vascular resistances and is compliant. However, in the setting of chronic pressure overload, as in pulmonary hypertension, or volume overload, as in congenital heart diseases, the right ventricle reverts back to a fetal phenotype to sustain its function. Mechanisms include angiogenic changes and concomitant increased metabolic activity to maintain energy production. Eventually, the remodeled right ventricle cannot resist the increased afterload, leading to right ventricular failure. After comparing the fetal and adult healthy right ventricles, we sought to review the main metabolic and cellular changes occurring in the setting of PH and CHD. Their association with RV function and potential impact on clinical practice will also be discussed.

1. Introduction

Recent emphasis on pulmonary hypertension (PH) has underscored the need for a better knowledge of the right ventricle mainly because studies have shown that left ventricular (LV) failure pathophysiology cannot be extrapolated to the right ventricle [1, 2]. Right ventricular (RV) physiology in health and disease has been gained thanks to studies in patients with pulmonary hypertension (PH) [3] and congenital heart disease (CHD) [4–6]. Even if PH is still defined as dramatic changes in pulmonary hemodynamics with mean pulmonary arterial pressure (mPAP) ≥ 25 mmHg at rest [7], right ventricular (RV) function is known as the major factor of functional capacity and prognosis in PH. PH is a global entity regrouping many subsets with different etiologies.

Regardless of PH etiology, chronic pressure overload results in RV remodeling and adaptation and eventually leads to dysfunction and death in absence of lung transplantation. In a study investigating the immediate prognosis of RV failure in PH patients, the overall mortality was 14% but rose to 46% for patients requiring inotropic support and 49% for patients in the intensive care unit [8]. On the other hand, the mortality associated with LV failure requiring inotropic support is usually lower than 15% [9, 10]. Similarly, Humbert et al. reported survival rates of 85,7% at 1 year, 69,6% at 2 years, and 54,9% at 3 years, in patients with WHO group I PH admitted for RV failure [11].

Right heart failure in patients with PH is the result of insufficient blood delivery to the heart and/or increased

systemic venous pressure secondary to elevated RV afterload represented by pulmonary arterial pressure or pulmonary vascular load [12]. The chronic RV pressure overload state results in myocardial remodeling, mainly characterized by a compensated hypertrophy. At the early stage, this adaptive right ventricle already presents with impaired bioenergetics, altered immunological response, and increased adrenergic response. This phenotype resembles the fetal RV phenotype; however, these adaptive mechanisms may lead to systolic dysfunction and cavities enlargement, representing the maladaptive right ventricle [13]. Clinical symptoms of peripheral edema, distended jugular veins, dyspnea, and syncope are consequences of increased filling pressures, diastolic dysfunction, and decreased cardiac output [3, 14, 15]. The transition from adaptive to maladaptive phenotype remains poorly understood and clinically unpredictable. Authors have been dividing this evolution into these 2 phenotypes, but there is a growing evidence for continuum between them: the adaptive right ventricle accumulates molecular and metabolic abnormalities until a point where it cannot overcome the persistent pressure overload and therefore becomes maladaptive.

Pulmonary arterial hypertension (PAH) associated with CHD belongs to group 1 of the WHO clinical classification of PH [7]. The evolution of this subset is characterized by dysfunction of the endothelial cells and hypertrophy and proliferation of the smooth muscle cells in the pulmonary circulation. Consequent obstruction of small arteries then occurs because of a narrowing of their diameter and plexiform lesions, the hallmark lesion of PAH. In this condition, pulmonary vascular resistances (PVR) progressively increase [16]. One of the difficulties to better appraise the natural history of RV failure is the variability of RV adaptation among patients exposed to chronic PH according to the etiology of PH. As an example, patients with PH related to untreated congenital cardiac defect or persistent ductus arteriosus may have a reversal of the left-to-right shunt, known as Eisenmenger syndrome. They tend to keep better RV function for a longer period and higher survival rate compared to patients with idiopathic PAH for a similar level of PVR and their survival is better [17–19]. Among the reasons to explain these different outcomes, the long-lasting fetal hypertrophied RV phenotype may prevent RV dilation and therefore its bowing towards the left ventricle. Second, persistent right to left shunts through septal defects enable tolerance of suprasystemic pulmonary hypertension [16].

The present review sought to summarize the current knowledge of RV metabolism and molecular physiology as studied in CHD and adult PH, in order to better understand RV failure associated with these diseases. After a brief overview of the fetal and adult right ventricle in health, we will review insights from experimental studies about pathophysiological evolution of RV remodeling in CHD and adult PH. Finally, we will develop the potential role of RV molecular biology and metabolism in the diagnosis, prognosis, and therapeutic approaches of RV dysfunction in PH. Inflammatory pattern of RV remodeling will be not described here as it has been recently well reviewed elsewhere [20, 21].

2. Right Ventricle in Health: From the Fetal Right Ventricle to the Adult Phenotype

2.1. Physiological Transition from the Fetal to the Adult Right Ventricle. The human heart originates from 3 main sources of cells: the first heart field, the second heart field and the neural crest cells. The first heart field gives the primitive left ventricle, a small part of the atria, and the atrioventricular canal myocardium resulting in the primary heart tube. The second heart field gives the complete right ventricle including the RV side of the ventricular septum and the RV outflow tract or pulmonary trunk. Finally, the neural crest cells participate in the constitution of the cardiac conduction system, as well as the RV outflow tract [22]. In utero, the right ventricle is not completely connected to the pulmonary circulation as it remains exposed to a high afterload and is not compliant. At this stage, the right ventricle plays the role of a systemic ventricle because of high PVR and low systemic vascular resistance in the placental circulation [22]. At birth, with the first breaths, fetal lung fluid is evacuated, partial O₂ pressure increases, both creating an air-liquid interface, and ventilation occurs. These events result in increased shear stress in the pulmonary circulation leading to vasodilation secondary to the release of vasodilators, such as prostacyclin and nitric oxide, and decreased secretion of vasoconstrictors, such as endothelin-1. Since the placental circulation in utero is under high PVR and low systemic vascular resistance, clamping the umbilical cord at birth will therefore separate the newborn from the low resistance placental circulation, leading to a decrease in PVR and increase in systemic vascular tone. Concomitantly, patent ductus arteriosus progressively closes leading the right ventricle to eject only in the pulmonary arterial tree. As a result of these events occurring at birth, RV wall thickness progressively decreases and LV mass increases [22, 23]. This physiological transition occurs with important molecular, structural, and functional changes. Eventually, the right ventricle becomes more compliant and gains its adult phenotype, with normal relation and interdependence to the left ventricle.

2.2. Features of the Normal Fetal Right Ventricle. The fetal right ventricle is exposed to a low oxygen environment. Carbohydrates substrates are preferentially used to produce energy from the glycolytic pathway such as glucose, lactate, and pyruvate. The major signaling pathway expressed is the hypoxia inducible factor 1 α (HIF1 α) and vascular endothelial growth factor (VEGF) pathway, promoting angiogenesis. It is associated with upregulated glycolysis. Both of these mechanisms lead the fetal right ventricle to better tolerate hypoxia compared to the adult right ventricle [19, 22–24]. Moreover, because of patent ductus arteriosus, the fetal right ventricle is more sensitive to systemic vascular resistances than to PVR. Fisher et al. studied regional blood flow in fetal ($n = 16$), newborn ($n = 12$), and adult ($n = 9$) sheep, using radionuclide-labeled microsphere imaging [25]. He observed in all fetal lambs that regional blood flow was significantly higher in the right ventricular free wall compared to the left ventricular free wall, respectively, 213 ± 13 ml/min versus 162 ± 12 ml/min ($p < 0.001$). Similarly, the right side of the

TABLE 1: Main characteristics of healthy phenotypes of fetal and adult right ventricles.

Characteristics	Fetal phenotype	Adult phenotype
<i>Environment</i>		
Oxygen environment	Low	High
Main blood circulation	Placental circulation	Systemic circulation
Ductus arteriosus	Opened	Closed
PVR	High	Low
Main vascularized heart regions	Right ventricular free wall, Right side of the IVS	Left ventricular free wall, Left side of the IVS
Systemic ventricle	Right ventricle	Left ventricle
<i>Genetics</i>		
Gene pattern expression	β -MHC	α -MHC
<i>Metabolic features</i>		
Mitochondrial function	Normal/adapted	Normal/adapted
mROS production	Adapted to heart activity	Adapted to heart activity
Energetic substrates	Carbohydrates	Fatty acids
<i>Hypoxia-induced factors</i>		
(i) HIF1 α	Expressed	Not expressed
(ii) VEGF		
Ca ²⁺ homeostasis	Immature	Mature
<i>Cellular features</i>		
Myocytes diameter	5–7 μ m	15–25 μ m
Myocytes/nonmyocytes ratio	30%	70%
Sarcomeres	Disoriented	Parallel
Capillary density	Preserved	Preserved
Fibrosis	Absent	Absent

PVR: pulmonary vascular resistance; MHC: myosin heavy chain; mROS: mitochondrial reactive oxygen species; HIF-1 α : hypoxia inducible factor 1 alpha; VEGF: vascular endothelial growth factor; Ca²⁺: calcium.

interventricular septum had a higher blood flow compared to the left side, respectively, 190 \pm 13 ml/min versus 147 \pm 12 ml/min ($p < 0.05$) [25]. Finally, microscopic features of the fetal right ventricle include small myocytes ranging from 5 to 7 μ m, a predominance of 70% of noncontractile mass represented of nuclei, cell membranes and mitochondria (30% of cardiomyocytes) [4], and disoriented sarcomeres with immature calcium homeostasis (Ca²⁺ pumps and transporters) and therefore immature contractility with genetic expression of β -myosin heavy chain (β -MHC) [24, 26, 27].

2.3. Features of the Normal Adult Right Ventricle. The adult right ventricle is exposed to a high oxygen environment with the adapted metabolic pathway including fatty acids oxidation, which produces more ATP than glycolysis [24]. Depending on injury or stress, there is an adaptation of metabolic substrates from fatty acids to glucose oxidation known as the Randle cycle. The HIF1 α -angiogenesis signaling pathway and the glycolytic phenotype are no longer expressed in these conditions. In fact there are adult isoforms of enzymes such as pyruvate dehydrogenase kinase (PDK), especially the cardiac specific PDK4, which are responsible for glycolysis inhibition and promotion of glucose oxidation [21, 28]. In their study [25], Fisher et al. reported that, after birth, regional blood flow was higher in the left ventricular free wall compared to the right ventricular free wall,

respectively, 204 \pm 18 ml/min versus 140 \pm 15 ml/min ($p < 0.01$). They explained this reversal in blood flow delivery by a change in oxygen requirements occurring after birth. In fact, because of the dramatic fall of PVR after birth, and therefore the decrease in right ventricular afterload, there is a major decrease in oxygen requirements for the right ventricle, with increased oxygen needs for the left ventricle being exposed to high systemic pressure [25]. Considering cellular features, myocytes are larger (from 15 to 25 μ m), sarcomeres are parallel, Ca²⁺ homeostasis is mature, and β -MHC gene is expressed [26], leading to a more efficient contractility [4, 27]. Table 1 summarizes the main differences between the normal fetal right ventricle and the normal adult right ventricle.

3. The Parallel between RV Remodeling in Pulmonary Hypertension and Congenital Heart Disease

3.1. Insights of Right Heart Failure in CHD. In conditions such as tetralogy of Fallot, surgically and congenitally corrected transposition of the great vessels, Ebstein anomaly, or late Fontan circulation, RV dysfunction is frequent because the right ventricle is chronically exposed to pressure overload. In the early phases, the right ventricle responds to increased

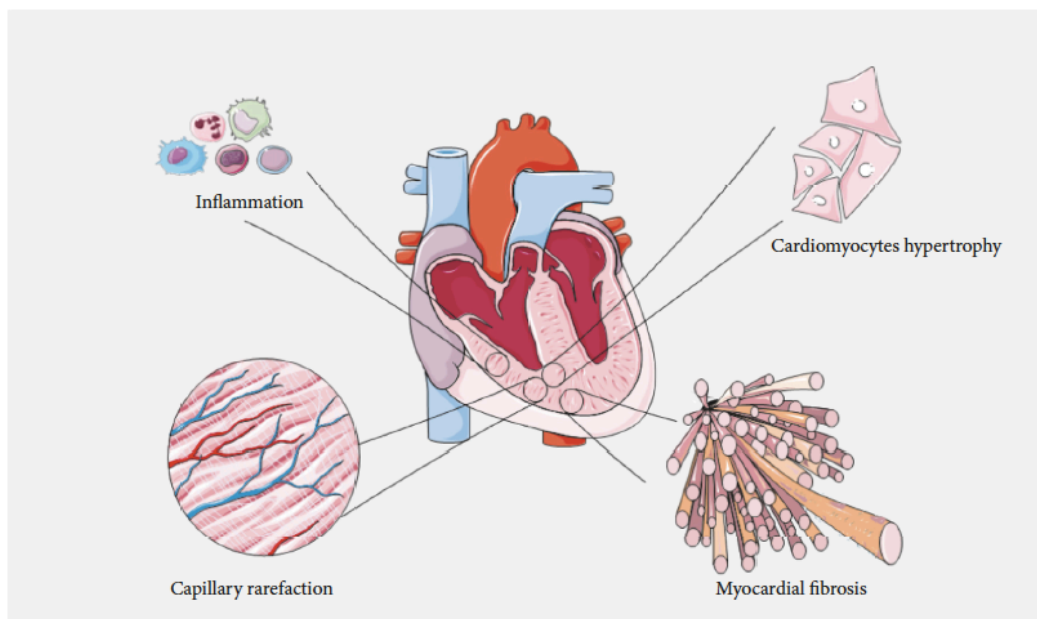


FIGURE 1: Main histological patterns of right ventricular remodeling in the setting of chronic pressure overload. Inflammation involving mononuclear cells and cardiomyocytes hypertrophy are observed at the early stage. Reduced capillary density and myocardial fibrosis are associated with right ventricular maladaptive phenotype.

wall stress with RV hypertrophy. It carries the role of a systemic ventricle characterized by coarse trabeculation, hypertrophied muscular band, and an abnormal septal tricuspid leaflet [29]. It increases its mitochondrial activity and carbohydrates use for energy production. Long-term evolution is characterized by substrates deprivation and energy loss. In addition, tricuspid regurgitation (congenitally corrected transposition of the great vessels and Ebstein anomaly), pulmonary regurgitation (Tetralogy of Fallot and RV dilation), and arrhythmias may occur [5]. Reasons for these evolution are multiple [29]. First of all, the right ventricle is characterized by a longitudinal contractile pattern compared to the circumferential pattern of the left ventricle (both radial and longitudinal). That makes the right ventricle unable to have a twisting and torsion component necessary to deal with high pressure overload. Second, RV tissue samples obtained in surgical CHD have shown decreased angiogenesis and marked fibrosis associated with arrhythmia, decreased RV ejection fraction, and increased RV wall stress [29, 30]. Third, studies showed that the hypertrophied right ventricle, because of its increased mass, has an impaired coronary flow and is therefore exposed to ischemia [19, 29, 30]. Finally, metabolic events include accumulation of mitochondrial reactive oxygen species (mROS) and of p53 protein responsible for HIF-1 α signaling pathway inhibition and ventricular dilation as reported by Sano et al. in a mice model of transverse aortic constriction. At 14 days, maximum hypertrophy was reached, followed by loss of microvessels, ventricular dilation, and failure. When these mice were p53 knocked out, ventricular hypertrophy was sustained with high number of microvessels [31]. Another molecular

feature has been described by Wu et al. on RV tissues from children with tetralogy of Fallot, hypoxia and hypertrophy (HH group), pulmonary stenosis, hypertrophy (H group), and small isolated ventricular septal defect compared to a control group. They reported that contractile dysfunction was linked to increased mROS associated with the decreased mRNA expression of a Ca²⁺-regulatory protein responsible for calcium homeostasis, as known as sarcoplasmic reticulum Ca²⁺-ATPase 2a (SERCA2a) [27].

3.2. Insights into Right Heart Failure in PH. Numerous experimental studies of RV remodeling in the setting of PH have been conducted in rodents including the fawn-hooded rat model [32] and then in the pulmonary arterial banding model, the hypoxia-induced PH [33], the angioproliferative PH, and the monocrotaline models [19]. The main histological features of RV tissular remodeling are summarized in Figure 1. Two phenotypes are usually described: “adaptive” versus “maladaptive” RV remodeling, or “compensated” RV hypertrophy (cRDVH) versus “decompensated” RV hypertrophy (dRDVH). That has been well described by Sutendra et al. especially by comparing baseline animals versus cRVH and dRVH in the same animals over time [19, 28, 34].

cRHV is characterized by numerous normal shaped hyperpolarized mitochondria, with low but continuous production of mROS, which does not allow p53 protein expression. This state is associated with high expression of HIF-1 α pathway, increased levels of glucose transporter Glut-1, PDK4 enzyme, and therefore glucose uptake. These changes are responsible for a switch from a mitochondria-based glucose oxidation to a glycolytic status, as well as increased

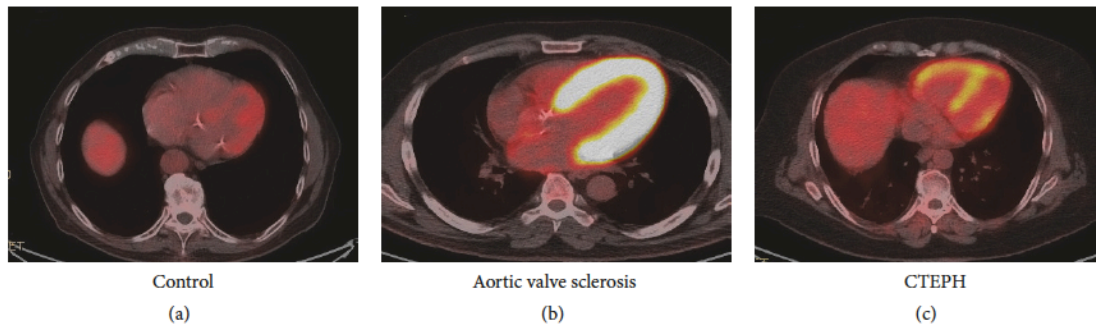


FIGURE 2: 18-Fluorodeoxyglucose Positron Emission Tomography in a control healthy patient (a), in a patient with aortic valve sclerosis (b), and in a chronic thromboembolic pulmonary hypertension patient (CTEPH) (c). Images show 4 chambers views. Control imaging shows no right ventricular uptake, but presence of left ventricular uptake. Picture (b) shows increased glucose uptake localized on the left ventricular free wall and on the interventricular septum in a patient with marked hypertrophy of the left ventricle due to aortic sclerosis.

angiogenesis/VEGF expression [19]. Progressively accumulation of mROS leads to reduced number of mitochondria, sometimes clustered together, and usually with abnormal shapes and sizes [33, 35]. Finally, energy supply is insufficient with substrates deprivation and therefore dRVH. Activation of p53 protein and inhibition of HIF1 α are key elements resulting in decreased angiogenesis and are associated with decreased PDK expression and glucose uptake leading to a reversed glycolytic shift. This last element was reflected by ¹⁸Fluorodeoxyglucose Positron Emission Tomography (¹⁸FDG-PET) showing increased glucose uptake in cRVH and reverse uptake in dRVH. In summary, a protective glycolytic shift appears to be associated with cRVH and reversed in dRVH because of excessive oxidative stress, substrates starvation, and mitochondrial loss of function [19, 34].

Concomitant of metabolic features, impaired angiogenesis is crucial in the pathology. Because of increased RV wall stress, myocardial oxygen consumption increases and therefore leads to loss of microvessels and reduced right coronary artery perfusion pressure (below 50 mmHg). This leads to an increased RV mass without compensatory angiogenesis and therefore results in ischemia [14, 36, 37]. Gómez et al. studied RV ischemia in patients with primary PH using stress technetium 99 m myocardial scintigraphy. RV ischemia was significantly correlated to increased RV end-diastolic pressure and increased right atrial pressure [14]. Bogaard et al. compared an isolated RV pressure overloaded rodent model (pulmonary arterial banding) versus a model with progressive pressure overload due to angioproliferative PH secondary to hypoxia and VEGF receptors blockage. In the context of angioproliferative PH, RV failure occurred with apoptosis, fibrosis, decreased VEGF gene and protein expressions, and decreased RV capillary density [36]. Finally, Tian et al. recently showed that RV ischemia causes mitochondrial-mediated fission that was responsible for diastolic dysfunction. When inhibiting mitochondrial fission, they showed a preserved RV function [38]. It is important to acknowledge that molecular and metabolic changes are a continuous process, starting as early as cRVH or “adaptive” RV remodeling. The precise role of the glycolytic shift, either protective or

detrimental, remains a matter of debate and requires further investigations. Table 2 summarizes characteristics of RV remodeling in CHD and PH. Figure 3 depicts evolution of RV failure in CHD and PH.

Recent emphasis has been observed about the concept of right ventricular-pulmonary arterial (RV-PA) coupling as a relevant marker of cardiac performance and energetics for the right ventricle. It represents the maximal efficiency between stroke work and myocardial oxygen consumption. RV-PA coupling can be assessed using pressure-volume loops as the ratio between RV end-systolic elastance (Ees) and pulmonary arterial elastance (Ea) [2, 39]. Ventricular-arterial uncoupling is defined as Ees/Ea ratio below 1. At the early stage of PH, RV-PA coupling may be decreased, despite preserved RV function and increased contractility. When the elevated afterload is too high, RV stroke volume and RV ejection fraction decrease. Uncoupling therefore occurs, followed by RV dilation and failure [2, 40, 41]. Because pressure-volume loops assessment is invasive and time-consuming and may be dangerous for PH patients because of the need for transient but repeated occlusions of the inferior vena cava, this remains dedicated to experimental studies.

4. Clinical Perspectives

4.1. What Do RV Metabolic and Molecular Features Add to the Diagnosis of PH Related RV Dysfunction? The glycolytic shift associated with RV remodeling is characterized by an upregulation of glucose uptake, shown by the increased uptake of ¹⁸FDG-PET [19, 37, 42, 43]. Figure 2 illustrates the hypermetabolism of hypertrophied RV observed in PH patients. Glucose uptake has been correlated with invasive PVR, mean pulmonary artery pressure, right atrial pressure, and RV wall stress [24, 44]. In addition, Lundgrin et al. showed the correlation between 18-FDG uptake and echocardiographic markers of systolic dysfunction (i.e., altered TAPSE, dilated RV, and RV fraction area change) and HIF-1 α activation [45].

Brittain et al. hypothesized that alterations of FA metabolism were due to a decrease in FA oxidation. They focused on FA in blood samples, RV tissue samples, and their

TABLE 2: Common features of functional and dysfunctional remodeled right ventricles in congenital heart disease and pulmonary hypertension.

Characteristics	Functional remodeled right ventricle	Dysfunctional remodeled right ventricle
<i>Morphology</i>		
Chambers size	Normal	Dilated (i.e., RV/LV > 0,6)
Free wall thickness	Thick (>5 mm)	Thin
IVS motion	Normal	End-diastolic bowing in the left ventricle
Pericardial effusion	Absent or minimal	Moderate to important
Coarse trabeculation		
CHD common features	Hypertrophied and muscular moderator band	
	Abnormal tricuspid septal leaflet insertion (mitral valve proximity)	
<i>Function</i>		
RVEF	Preserved	Decreased
Contractility	Hypercontractility	Decreased
Cardiac index	Preserved	Decreased Bad prognosis < 2l/min/m ²
RV-arterial coupling	Preserved	Uncoupling
Rhythm	Mostly preserved	Arrhythmias
CHD common features	Tricuspid and pulmonary regurgitations prior to dilation	
<i>Metabolic features</i>		
Mitochondria	Adapted sizes and shapes	Small, abnormal shapes, clustered
Mitochondrial function	Increased	Decreased
mROS production	Continuous and Low	High accumulation
Signaling pathway	Down-regulation of p53 Up-regulation of HIF1 α -VEGF pathway	Up-regulation of p53 Inhibition of HIF1 α -VEGF pathway
Energetic substrates	Carbohydrates > fatty acids High use of PDK4, Glut1 = glycolytic shift	Total substrates deprivation Energy starvation = reversed glycolytic shift
<i>Cellular and Tissular features</i>		
Myocytes	Hypertrophied	?
Capillary density	Increased Present	Rarefaction
Ischemia	With role of CHD-associated coronary malformations	Present
Fibrosis	Absent	Present

IVS: inter entricular septum; RVEF: right ventricular ejection fraction; CHD: congenital heart disease; RV-arterial coupling: right ventricular arterial coupling; mROS: mitochondrial reactive oxygen species; p53: p53 protein; HIF-1 α : hypoxia inducible factor 1 alpha; VEGF: vascular endothelial growth factor; PDK4: pyruvate dehydrogenase kinase 4; Glut1: glucose transporter 1.

association with proton magnetic resonance spectroscopy. They observed increased levels of FA in the blood stream and in RV tissue samples. These findings were associated with cardiac steatosis and lipotoxicity on spectroscopy [46]. Studies investigating oxidative stress showed the key role of continuous mROS accumulation over time in the evolution of the pathology [19].

4.2. What Do RV Metabolic and Molecular Features Add to the Prognosis of PH Related RV Dysfunction? The glycolytic shift observed in animal models of PH might be a marker for RV remodeling. Authors have studied PET imaging in PH patients in order to find a prognostic value of the observed metabolic changes. As previously mentioned, correlations between glucose uptake seen using 18FDG-PET imaging and

hemodynamic have been reported, as well as association with echocardiographic findings and functional parameters such as the 6-minute walking test and NYHA status [47–49]. Moreover, there is evidence for the additional value of metabolic imaging for long-term follow-up of PH patients under treatment. Changes in FDG uptake over time seem to be related to varying expression of proangiogenic factors and different degrees of HIF-1 α activation [45, 50]. Recently, Li et al. studied 45 patients with idiopathic PAH using PET imaging during fasting and glucose-loading conditions. They reported that increased RV to LV 18-FDG uptake ratio significantly predicted mortality [51]. These clinical findings therefore agree on the fact that PET imaging enables strong association between metabolism, mass, and RV function. Finally, in an ongoing clinical trial conducted by our team,

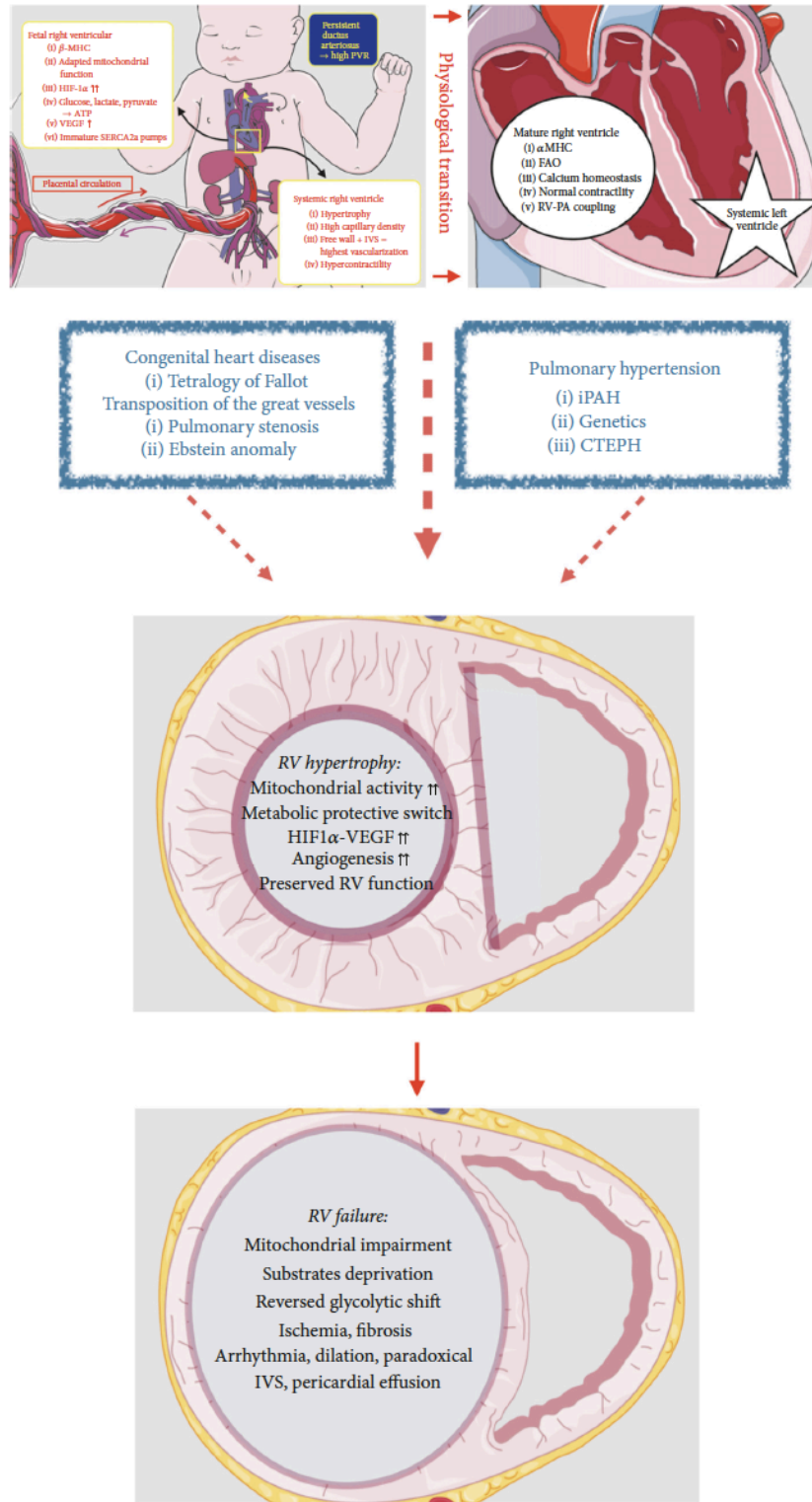


FIGURE 3: Right ventricular remodeling in congenital heart disease and pulmonary hypertension. β MHC: β -myosin heavy chain; HIF1 α : hypoxia inducible factor 1 α ; VEGF: vascular endothelial growth factor; SERCA2a: sarcoplasmic/endoplasmic reticulum Ca²⁺ ATPase 2a; IVS: interventricular septum; α MHC: α -myosin heavy chain; FAO: fatty acids oxidation; RV-PA coupling: right ventricular-pulmonary arterial coupling; PVR: pulmonary vascular resistances; RV: right ventricular; iPAH: idiopathic pulmonary arterial hypertension; CTEPH: chronic thromboembolic pulmonary hypertension.

we have been able to see significant correlations between decreased capillary density in human RV tissues and altered RV function (assessed by CMR and echocardiography) in the setting of chronic thromboembolic PH, as well as correlations with PET imaging.

4.3. What Do RV Metabolic and Molecular Features Add to Therapeutic Strategies of PH Related RV Dysfunction? Phosphodiesterase-5, endothelin inhibitors, and prostaglandin D2 (PGD2) agonists have been shown to reduce RV pressure overload in patients with PH. However, their effects on the right ventricle are poorly explored. Authors hypothesized that myocardial substrates usage (such as glucose oxidation) can be modulated with pharmacologic inhibitors [24, 52]. Piao et al. studied the effect of PDK inhibitor, dichloroacetate, in two rat models of RV hypertrophy: monocrotaline-induced PH and pulmonary artery banding without PH. In the first model, dichloroacetate increased glucose oxidation and cardiac stroke work. Long-term use showed improved RV function. In RV compensated hypertrophy induced by pulmonary artery banding, the glycolytic shift could be reversed with dichloroacetate as well. These effects of dichloroacetate were greater in monocrotaline-induced RV hypertrophy associated with PH. Dichloroacetate might therefore correct vascular changes and RV remodeling [42]. These findings suggest that glycolysis is not detrimental for the overload right ventricle. Similarly, the same authors showed that long-term use of dichloroacetate inhibited FOXO1, a transcriptional regulatory factor of PDK. Consequent downregulation of PDK 4 (an isoform of PDK) restored glucose oxidation and improved bioenergetics and RV function [53].

The link between RV remodeling and fatty acid oxidation (the main energy source in healthy adult myocardium) still remains unclear. Fang et al. used partial inhibitors of FA oxidation such as ranolazine and trimetazidine in experimental pulmonary artery banding. They reported abnormal levels of FA oxidation with reduced RV function at baseline. Under ranolazine and trimetazidine treatment, they reported decreased FA oxidation and restored glucose oxidation resulting in increased cardiac output and improved exercise capacity [54]. Another metabolic-oriented therapy, as described earlier, which might be targeting mROS production with p53 protein inhibition might be an alternative [27]. Finally, beneficial effects might be possible by modulating mi-RNA expression in the heart in CHD or in the pulmonary arteries in PAH [6].

5. Conclusion

RV adaptation to pressure overload is a key determinant of survival in patients with PH and CHD. RV failure occurring in these conditions has similar features such as glycolytic shift and altered angiogenesis. A relationship between metabolic changes and RV function is strongly supported by recent experimental findings. Translational approaches of RV metabolism as well as noninvasive assessment of RV-PA coupling are needed to better discriminate the RV phenotype in the setting of chronic pressure overload. Pharmacological support to modulate RV energetics and to restore RV capillary

density might be promising approaches to improve the condition of PH patients.

Conflicts of Interest

The authors declare that there are no conflicts of interest regarding the publication of this paper.

Acknowledgments

This work was supported by a public grant overseen by the French National Research Agency (ANR) as part of the second Investissements d'Avenir Program (Reference ANR-15-RHUS-0002).

References

- [1] J. Guihaire, H. Bogaard, E. Flécher et al., "Experimental models of right heart failure: a window for translational research in pulmonary hypertension," *Seminars in Respiratory and Critical Care Medicine*, vol. 34, no. 5, pp. 689–699, 2013.
- [2] J. Guihaire, P. E. Noly, S. Schrepfer, and O. Mercier, "Advancing knowledge of right ventricular pathophysiology in chronic pressure overload: Insights from experimental studies," *Archives of Cardiovascular Diseases*, vol. 108, no. 10, pp. 519–529, 2015.
- [3] N. F. Voelkel, R. A. Quaife, L. A. Leinwand et al., "Right ventricular function and failure: report of a National Heart, Lung, and Blood Institute working group on cellular and molecular mechanisms of right heart failure," *Circulation*, vol. 114, no. 17, pp. 1883–1891, 2006.
- [4] W. F. Friedman, "The intrinsic physiologic properties of the developing heart," *Progress in Cardiovascular Diseases*, vol. 15, no. 1, pp. 87–111, 1972.
- [5] L. Lopez, M. S. Cohen, R. H. Anderson et al., "Unnatural history of the right ventricle in patients with congenitally malformed hearts," *Cardiology in the Young*, vol. 20, supplement 3, pp. 107–112, 2010.
- [6] D. Iacobazzi, M.-S. Suleiman, M. Ghorbel, S. J. George, M. Caputo, and R. M. Tulloh, "Cellular and molecular basis of RV hypertrophy in congenital heart disease," *Heart*, vol. 102, no. 1, pp. 12–17, 2016.
- [7] N. Galie, M. Humbert, J. L. Vachiery et al., "2015 ESC/ERS Guidelines for the diagnosis and treatment of pulmonary hypertension: the joint task force for the diagnosis and treatment of pulmonary hypertension of the European society of cardiology (ESC) and the European respiratory society (ERS)," in *European Heart Journal*, Association for European Paediatric and Congenital Cardiology (AEPC) and International Society for Heart and Lung Transplantation (ISHLT), Eds., vol. 37, pp. 67–119, 2016.
- [8] B. Sztrymf, R. Souza, L. Bertoletti et al., "Prognostic factors of acute heart failure in patients with pulmonary arterial hypertension," *European Respiratory Journal*, vol. 35, no. 6, pp. 1286–1293, 2010.
- [9] W. T. Abraham, K. F. Adams, G. C. Fonarow et al., "In-hospital mortality in patients with acute decompensated heart failure requiring intravenous vasoactive medications: an analysis from the acute decompensated heart failure national registry (ADHERE)," *Journal of the American College of Cardiology*, vol. 46, no. 1, pp. 57–64, 2005.
- [10] J. J. Ryan and S. L. Archer, "The right ventricle in pulmonary arterial hypertension: disorders of metabolism, angiogenesis

- and adrenergic signaling in right ventricular failure," *Circulation Research*, vol. 115, no. 1, pp. 176–188, 2014.
- [11] M. Humbert, O. Sitbon, A. Chaouat et al., "Survival in patients with idiopathic, familial, and anorexigen-associated pulmonary arterial hypertension in the modern management era," *Circulation*, vol. 122, no. 2, pp. 156–163, 2010.
- [12] A. Vonk-Noordegraaf, F. Haddad, K. M. Chin et al., "Right heart adaptation to pulmonary arterial hypertension: physiology and pathobiology," *Journal of the American College of Cardiology*, vol. 62, no. 25, pp. D22–D33, 2013.
- [13] M. Amsellem, T. Kuznetsova, K. Hanneman, A. Denault, and F. Haddad, "Right heart imaging in patients with heart failure: a tale of two ventricles," *Current Opinion in Cardiology*, vol. 31, no. 5, pp. 469–482, 2016.
- [14] A. Gómez, D. Bialostozky, A. Zajarias et al., "Right ventricular ischemia in patients with primary pulmonary hypertension," *Journal of the American College of Cardiology*, vol. 38, no. 4, pp. 1137–1142, 2001.
- [15] A. Vonk-Noordegraaf and N. Galiè, "The role of the right ventricle in pulmonary arterial hypertension," *European Respiratory Review*, vol. 20, no. 122, pp. 243–253, 2011.
- [16] J. Guihaire, F. Haddad, O. Mercier, D. J. Murphy, J. C. Wu, and E. Fadel, "The right heart in congenital heart disease, mechanisms and recent advances," *Journal of Clinical & Experimental Cardiology*, vol. 1, no. 8, pp. 1–11, 2012.
- [17] W. E. Hopkins, L. L. Ochoa, G. W. Richardson, and E. P. Trulock, "Comparison of the hemodynamics and survival of adults with severe primary pulmonary hypertension or Eisenmenger syndrome," *The Journal of Heart and Lung Transplantation*, vol. 15, no. 1 I, pp. 100–105, 1996.
- [18] B. Rondelet, C. Dewachter, F. Kerbaul et al., "Prolonged overcirculation-induced pulmonary arterial hypertension as a cause of right ventricular failure," *European Heart Journal*, vol. 33, no. 8, pp. 1017–1026, 2012.
- [19] G. Sutendra, P. Dromparis, R. Paulin et al., "A metabolic remodeling in right ventricular hypertrophy is associated with decreased angiogenesis and a transition from a compensated to a decompensated state in pulmonary hypertension," *Journal of Molecular Medicine*, vol. 91, no. 11, pp. 1315–1327, 2013.
- [20] N. F. Voelkel, J. Gomez-Arroyo, A. Abbate, H. J. Bogaard, and M. R. Nicolls, "Pathobiology of pulmonary arterial hypertension and right ventricular failure," *European Respiratory Journal*, vol. 40, no. 6, pp. 1555–1565, 2012.
- [21] J. J. Ryan and S. L. Archer, "Emerging concepts in the molecular basis of pulmonary arterial hypertension. Part I: metabolic plasticity and mitochondrial dynamics in the pulmonary circulation and right ventricle in pulmonary arterial hypertension," *Circulation*, vol. 131, no. 19, pp. 1691–1702, 2015.
- [22] N. F. Voelkel, "The right ventricle in health and disease," *Respiratory Medicine*, 2015.
- [23] R. G. Kelly, "Building the right ventricle," *Circulation Research*, vol. 100, no. 7, pp. 943–945, 2007.
- [24] S. E. Altin and P. C. Schulze, "Metabolism of the right ventricle and the response to hypertrophy and failure," *Progress in Cardiovascular Diseases*, vol. 55, no. 2, pp. 229–233, 2012.
- [25] D. J. Fisher, M. A. Heymann, and A. M. Rudolph, "Regional myocardial blood flow and oxygen delivery in fetal, newborn, and adult sheep," *American Journal of Physiology-Heart and Circulatory Physiology*, vol. 243, no. 5, pp. H729–H731, 1982.
- [26] B. D. Lowes, W. Minobe, W. T. Abraham et al., "Changes in gene expression in the intact human heart: downregulation of α -myosin heavy chain in hypertrophied, failing ventricular myocardium," *The Journal of Clinical Investigation*, vol. 100, no. 9, pp. 2315–2324, 1997.
- [27] Y. Wu, W. Feng, H. Zhang et al., "Ca²⁺-regulatory proteins in cardiomyocytes from the right ventricle in children with congenital heart disease," *Journal of Translational Medicine*, vol. 10, no. 1, article 67, 2012.
- [28] P. Dromparis, G. Sutendra, and E. D. Michelakis, "The role of mitochondria in pulmonary vascular remodeling," *Journal of Molecular Medicine*, vol. 88, no. 10, pp. 1003–1010, 2010.
- [29] S. Shah, T. Gupta, and R. Ahmad, "Managing heart failure in transposition of the great arteries," *The Ochsner Journal*, vol. 15, no. 3, pp. 290–296, 2015.
- [30] E. Di Pietro, M. C. De Angelis, F. Esposito et al., "An imbalance between protective and detrimental molecular pathways is associated with right ventricular dysfunction in congenital heart diseases with outflow obstruction," *International Journal of Cardiology*, vol. 172, no. 3, pp. e519–e521, 2014.
- [31] M. Sano, T. Minamino, H. Toko et al., "p53-induced inhibition of Hif-1 causes cardiac dysfunction during pressure overload," *Nature*, vol. 446, 2007.
- [32] S. Bonnet, E. D. Michelakis, C. J. Porter et al., "An Abnormal mitochondrial-hypoxia inducible factor-1 α -Kv channel pathway disrupts oxygen sensing and triggers pulmonary arterial hypertension in fawn hooded rats: Similarities to human pulmonary arterial hypertension," *Circulation*, vol. 113, no. 22, pp. 2630–2641, 2006.
- [33] J. Gomez-Arroyo, S. Mizuno, K. Szczepanek et al., "Metabolic gene remodeling and mitochondrial dysfunction in failing right ventricular hypertrophy secondary to pulmonary arterial hypertension," *Circulation: Heart Failure*, vol. 6, no. 1, pp. 136–144, 2013.
- [34] G. Sutendra, P. Dromparis, A. Kinnaird et al., "Mitochondrial activation by inhibition of PDKII suppresses HIF1 α signaling and angiogenesis in cancer," *Oncogene*, vol. 32, no. 13, pp. 1638–1650, 2013.
- [35] H. J. Bogaard, K. Abe, A. V. Noordegraaf, and N. F. Voelkel, "The right ventricle under pressure: cellular and molecular mechanisms of right-heart failure in pulmonary hypertension," *CHEST*, vol. 135, no. 3, pp. 794–804, 2009.
- [36] H. J. Bogaard, R. Natarajan, S. C. Henderson et al., "Chronic pulmonary artery pressure elevation is insufficient to explain right heart failure," *Circulation*, vol. 120, no. 20, pp. 1951–1960, 2009.
- [37] S. L. Archer, Y. Fang, J. J. Ryan, and L. Piao, "Metabolism and bioenergetics in the right ventricle and pulmonary vasculature in pulmonary hypertension," *Pulmonary Circulation*, vol. 3, no. 1, pp. 144–152, 2013.
- [38] L. Tian, M. Neuber-Hess, J. Mewburn et al., "Ischemia-induced Drp1 and Fis1-mediated mitochondrial fission and right ventricular dysfunction in pulmonary hypertension," *Journal of Molecular Medicine*, vol. 95, no. 4, pp. 381–393, 2017.
- [39] K. Sagawa, "The end-systolic pressure-volume relation of the ventricle: definition, modifications and clinical use," *Circulation*, vol. 63, no. 6 I, pp. 1223–1227, 1981.
- [40] B. A. Maron, R. T. Zamanian, and A. B. Waxman, "Pulmonary hypertension," *Basic Science to Clinical Medicine*, pp. 1–371, 2015.
- [41] D. Boulate, O. Mercier, J. Guihaire et al., "Pulmonary circulatory—right ventricular uncoupling: new insights into pulmonary hypertension pathophysiology," *Pulmonary Hypertension: Basic Science to Clinical Medicine*, 2016.

- [42] L. Piao, Y.-H. Fang, V. J. J. Cadete et al., "The inhibition of pyruvate dehydrogenase kinase improves impaired cardiac function and electrical remodeling in two models of right ventricular hypertrophy: resuscitating the hibernating right ventricle," *Journal of Molecular Medicine*, vol. 88, no. 1, pp. 47–60, 2010.
- [43] G. Hagan, M. Southwood, C. Treacy et al., "(18)FDG PET imaging can quantify increased cellular metabolism in pulmonary arterial hypertension: A proof-of-principle study," *Pulmonary Circulation*, vol. 1, no. 4, pp. 448–455, 2011.
- [44] M. Oikawa, Y. Kagaya, H. Otani et al., "Increased [18F]fluorodeoxyglucose accumulation in right ventricular free wall in patients with pulmonary hypertension and the effect of epoprostenol," *Journal of the American College of Cardiology*, vol. 45, no. 11, pp. 1849–1855, 2005.
- [45] E. L. Lundgrin, M. M. Park, J. Sharp et al., "Fasting 2-deoxy-2-[18F]fluoro-D-glucose positron emission tomography to detect metabolic changes in pulmonary arterial hypertension hearts over 1 year," *Annals of the American Thoracic Society*, vol. 10, no. 1, pp. 1–9, 2013.
- [46] E. L. Brittain, M. Talati, J. P. Fessel et al., "Fatty acid metabolic defects and right ventricular lipotoxicity in human pulmonary arterial hypertension," *Circulation*, vol. 133, no. 20, pp. 1936–1944, 2016.
- [47] S. Bokhari, A. Raina, E. B. Rosenweig et al., "PET imaging may provide a novel biomarker and understanding of right ventricular dysfunction in patients with idiopathic pulmonary arterial hypertension," *Circulation: Cardiovascular Imaging*, vol. 4, no. 6, pp. 641–647, 2011.
- [48] M. M. Can, C. Kaymaz, I. H. Tanboga et al., "Increased right ventricular glucose metabolism in patients with pulmonary arterial hypertension," *Clinical Nuclear Medicine*, vol. 36, no. 9, pp. 743–748, 2011.
- [49] S. Tatebe, Y. Fukumoto, M. Oikawa-Wakayama et al., "Enhanced [18F]fluorodeoxyglucose accumulation in the right ventricular free wall predicts long-term prognosis of patients with pulmonary hypertension: a preliminary observational study," *European Heart Journal—Cardiovascular Imaging*, vol. 15, no. 6, pp. 666–672, 2014.
- [50] G. Marsboom, C. Wietholt, C. R. Haney et al., "Lung ¹⁸F-fluorodeoxyglucose positron emission tomography for diagnosis and monitoring of pulmonary arterial hypertension," *American Journal of Respiratory and Critical Care Medicine*, vol. 185, no. 6, pp. 670–679, 2012.
- [51] W. Li, L. Wang, C.-M. Xiong et al., "The prognostic value of 18F-FDG uptake ratio between the right and left ventricles in idiopathic pulmonary arterial hypertension," *Clinical Nuclear Medicine*, vol. 40, no. 11, pp. 859–863, 2015.
- [52] R. M. Tuder, L. A. Davis, and B. B. Graham, "Targeting energetic metabolism: a new frontier in the pathogenesis and treatment of pulmonary hypertension," *American Journal of Respiratory and Critical Care Medicine*, vol. 185, no. 3, pp. 260–266, 2012.
- [53] L. Piao, V. K. Sidhu, Y.-H. Fang et al., "FOXO1-mediated upregulation of pyruvate dehydrogenase kinase-4 (PDK4) decreases glucose oxidation and impairs right ventricular function in pulmonary hypertension: therapeutic benefits of dichloroacetate," *Journal of Molecular Medicine*, vol. 91, no. 3, pp. 333–346, 2013.
- [54] Y.-H. Fang, L. Piao, Z. Hong et al., "Therapeutic inhibition of fatty acid oxidation in right ventricular hypertrophy: exploiting Randle's cycle," *Journal of Molecular Medicine*, vol. 90, no. 1, pp. 31–43, 2012.



Investigating the value of right heart echocardiographic metrics for detection of pulmonary hypertension in patients with advanced lung disease

Myriam Amsallem^{1,5} · David Boulate² · Zoe Kooreman¹ · Roham T. Zamanian^{3,4} · Guillaume Fadel¹ · Ingela Schnittger¹ · Elie Fadel² · Michael V. McConnell¹ · Gundeep Dhillon³ · Olaf Mercier² · François Haddad¹

Received: 18 November 2016 / Accepted: 10 January 2017 / Published online: 24 January 2017
© Springer Science+Business Media Dordrecht 2017

Abstract This study determined whether novel right heart echocardiography metrics help to detect pulmonary hypertension (PH) in patients with advanced lung disease (ALD). We reviewed echocardiography and catheterization data of 192 patients from the Stanford ALD registry and echocardiograms of 50 healthy controls. Accuracy of echocardiographic right heart metrics to detect PH was assessed using logistic regression and area under the ROC curves (AUC) analysis. Patients were divided into a derivation (n=92) and validation cohort (n=100). Experimental validation was assessed in a piglet model of mild PH followed longitudinally. Tricuspid regurgitation (TR) was not interpretable in 52% of patients. In the derivation cohort, right atrial maximal volume index (RAVI), ventricular end-systolic area index (RVESAI), free-wall longitudinal strain

and tricuspid annular plane systolic excursion (TAPSE) differentiated patients with and without PH; 20% of patients without PH had moderate to severe RV enlargement by RVESAI. On multivariate analysis, RAVI and TAPSE were independently associated with PH (AUC=0.77, $p<0.001$), which was confirmed in the validation cohort (0.78, $p<0.001$). Presence of right heart metrics abnormalities did not improve detection of PH in patients with interpretable TR ($p>0.05$) and provided moderate detection value in patients without TR. Only two patients with more severe PH (mean pulmonary pressure 35 and 36 mmHg) were missed. The animal model confirmed that right heart enlargement discriminated best pigs with PH from shams. This study highlights the frequency of right heart enlargement and dysfunction in ALD irrespectively from presence of PH, therefore limiting their use for detection of PH.

Myriam Amsallem and David Boulate have contributed equally to this work.

Electronic supplementary material The online version of this article (doi:10.1007/s10554-017-1069-3) contains supplementary material, which is available to authorized users.

✉ Myriam Amsallem
mamsalle@stanford.edu

- ¹ Division of Cardiovascular Medicine, Stanford University School of Medicine, Stanford, CA, USA
- ² Laboratoire de Recherche Chirurgicale, Marie Lannelongue Hospital, University of Paris Sud, Le Plessis Robinson, France
- ³ Division of Pulmonary and Critical Care Medicine, Stanford University School of Medicine, Stanford, CA, USA
- ⁴ Vera Moulton Wall Center for Pulmonary Vascular Disease, Stanford University School of Medicine, Stanford, CA, USA
- ⁵ Stanford Cardiovascular Institute, 300 Pasteur Drive, Stanford, CA 94305, USA

Keywords Echocardiography · Lung disease · Pulmonary hypertension · Right heart failure · Strain

Introduction

Detection of pulmonary hypertension (PH) in patients with advanced lung disease (ALD) plays an important role, particularly in pre-lung transplant evaluation. It is part of the Lung Allocation Score that was developed with the objective of decreasing wait-list mortality. PH represents in addition a well-established prognostic factor in patients with ALD, including chronic obstructive pulmonary disease (COPD) or interstitial lung disease (ILD).

PH is invasively defined by mean pulmonary arterial pressure (MPAP) ≥ 25 mmHg. Echocardiography remains the main noninvasive tool for assessment of pulmonary artery pressures in clinical practice. The latest European

guidelines strongly rely on the maximal velocity of the tricuspid regurgitation (TR) signal for the diagnosis of PH [1]. However, several studies have reported that the Doppler TR signal is interpretable in only 30–45% of patients with ALD compared to 60–85% in those without ALD [2–4]. The main reasons alleged are hyperinflation of the lungs, heart rotation and limited acoustic windows. Taking into account the limitations of TR signals, several teams have investigated whether right heart or pulmonary flow metrics are useful in detecting PH [5–7]. Right ventricular (RV) isovolumic relaxation time has been shown to be associated with severe PH but has not been well validated in patients with ALD [8]. There also has been a growing interest in novel metrics such as deformation imaging based RV longitudinal strain (RVLS). Hilde et al. recently reported in a cohort of patients with COPD that free-wall strain differed between those with PH and those without PH [9]. However, the value of RV strain to detect PH in patients with ALD has not been validated in other independent cohorts.

In this study, we hypothesized that right heart and pulmonary flow metrics would not have good discrimination value for detection of PH in patients with ALD, who have lower levels of pressure and may have right heart remodeling or dysfunction independently of PH.

The first objective was to identify which metric of right heart size, function or pulmonary flow would best discriminate PH in patients with ALD (using a derivation and a validation cohort), as well as in a large animal model of progressive mild PH. The second objective was to assess by which extent these right metrics could complement the current approach of detection of PH using echocardiography (i.e. TR Doppler signal and estimation of the right ventricular systolic pressure).

Methods

After approval by Stanford University Institutional Review Board, we retrospectively selected 200 consecutive patients with ALD (aged ≥ 18 years old), referred to Stanford University Division of Pulmonary and Critical Care from 2006 to 2012, who underwent echocardiography and right heart catheterization within 48 h of each other. Pre-lung transplant evaluation was the main indication for catheterization. Diagnosis of ALD covered a wide range of etiology: ILD with or without pulmonary fibrosis secondary to connective tissue diseases (such as systemic sclerosis, Sjögren's syndrome, rheumatoid arthritis or mixed); severe COPD (GOLD 3 or 4); and cystic fibrosis (CF). Pulmonary functional tests (forced expiratory volume FEV1% and forced vital capacity FVC%, expressed as % of the predicted value) were collected. The cohort was randomly divided into a derivation (n = 100) and a validation (n = 100) cohort.

Eight patients of the derivation cohort were later excluded because of suboptimal echocardiographic studies (i.e. foreshortening precluding measurements of RV areas or not enough visibility of the RV free-wall precluding assessment of strain). Fifty healthy controls were additionally selected from the Stanford Healthy Aging research database, with a similar age range and sex ratio as ALDs. PH or heart failure was ruled out by a 60-point health questionnaire, physical exam and echocardiography. The study was conducted in agreement with the Helsinki-II-declaration; all patients gave written informed consent.

Catheterization

A balloon catheter was introduced through the internal jugular or right femoral vein after local anaesthesia. Right atrial pressure (RAP), systolic, mean (MPAP) pulmonary arterial pressures, pulmonary artery wedge pressure, pulmonary vascular resistance, total pulmonary resistance index (TPRI) and cardiac index were measured. PH was defined by $MPAP \geq 25$ mmHg at rest [10].

Echocardiography

Resting echocardiograms were performed using Philips 7500 or iE33 ultrasound systems (Philips Medical Systems, Andover, MA) with 5 MHz transducers, and measured off-line by a blinded certified cardiologist. Right heart size was assessed by: RV end-diastolic (RVEDAI), end-systolic areas (RVESAI), RA end-systolic volume (RAVI), all indexed to body surface area (BSA). RV function was assessed by tricuspid annular plane systolic excursion (TAPSE), RV fractional area change (RVFAC) and RV free-wall longitudinal strain (RVLS). Septal curvature (left ventricular end-systolic eccentricity index EI), pulmonary acceleration time, right and left ventricular isovolumic relaxation times (normalized for heart rate by dividing by \sqrt{RR} , RV-IVRTi and LV-IVRTi) were measured. The following pre-defined thresholds were used according to the guidelines [11, 12] or, to our control population 98% percentile when not provided by guidelines. RAVI was abnormal if >32.5 mL/m², RVESAI if >7.8 cm²/m², RVEDAI if >13.6 cm²/m², RVLS if $>-20\%$, RVFAC if $<35\%$, TAPSE if <17 mm. The quality of the TR Doppler signal was assessed and the TR was considered to be interpretable in presence of a complete envelope or a partial envelope prone to extrapolation, or not interpretable otherwise, as recently published [4]. When the TR was interpretable, RVSP was estimated based on the modified Bernoulli equation applied to the peak TR velocity and estimated RAP. Contrast methods were not routinely used.

Experimental validation

We then assessed whether the same metrics would emerge in a large animal model of progressive and mild PH independently of lung disease. We chose a piglet model that enables longitudinal assessment of right heart dimensions and function over time in the setting of moderate elevation of pulmonary pressures (similar to the pressure range found in patients with ALD) [13, 14]. Eight 6-week old “large white” pigs (15–20 kg, Entrepise Lebeau, Gambais, France) were randomized (1:1) to experimental or sham groups (Online Resource 1). Experimental pigs underwent left pulmonary artery ligation by thoracotomy without pericardial opening, followed by weekly (from week 1 to 3) embolization of the right lower lobe with embucrylate (Histoacryl[®], BBraun Medical, France). Pigs developed mild subacute PH by week 4 and chronic PH by week 16 [13, 14]. Echocardiograms were performed at week 0, 4, and 16 for PH pigs and at week 4 for SHAMS, using a Vivid 9 console (GE Healthcare, Fairfield, CT, USA). Measurements were acquired as detailed above: RVEDAI, RVESAI, RA maximal area (RAAI), EI. RV function was assessed by RVFAC, TAPSE, peak of tricuspid lateral annular systolic velocity and RVLS. This study was approved by the Institutional Animal Care Committee of Marie Lannelongue Hospital (Paris-Sud University, France).

Statistical analysis

Quantitative variables were expressed as mean \pm standard deviation (SD) and compared using Student's *t* test, or median, interquartile range [25th–75th] and Mann–Whitney test otherwise. Qualitative variables were presented as number and percentages. Multiple groups were compared using analysis of covariance with Bonferroni correction, and distributions of metrics using Chi square test. Correlations between metrics were explored by partial correlation diagram. Stepwise multivariate logistic regression was used to identify metrics associated with PH or severe PH (MPAP \geq 35 mmHg). Receiver operating characteristic (ROC) curves were constructed to determine the diagnostic accuracy of echocardiographic metrics to detect PH (expressed by area under the curve AUC). Net reclassification improvement index was calculated to assess the reclassification value of right heart metrics over RVSP estimation from the TR signal (PH was defined by RVSP \geq 40 mmHg). Intraobserver variability determined in 20% of subjects using intraclass correlation coefficients was 0.90 [0.77–0.96] for RVFAC, 0.92 [0.83–0.97] for RVLS, 0.72 [0.37–0.88] for TAPSE, 0.97 [0.95–0.98] for RVESAI and 0.97 [0.93–0.99] for RAVI. A *p*-value $<$ 0.05 was considered significant. Statistical analyses were performed using SPSS[®] (version 14.0, SPSS, Inc., Chicago, IL).

Results

Clinical derivation cohort (n=92)

MPAP was 34.1 ± 8.4 mmHg, 51% had PH including 23% with severe PH (MPAP \geq 35 mmHg). The majority of patients had pre-capillary PH (75%) while 25% had mixed PH (PAWP 20.9 ± 3.2 mmHg). Restrictive and obstructive etiologies were balanced: 54% patients had ILD, 33% COPD (including 40% GOLD 4) and 13% cystic fibrosis. MPAP was not significantly different among subgroups: ILD (26.5 ± 10.2 mmHg), COPD (26.0 ± 10.2 mmHg) and CF (25.0 ± 7.5 mmHg), *p* = 0.33. Prevalence of PH did not differ between obstructive (COPD and CF) and restrictive (ILD) patients (55 vs. 48%, *p* = 0.64).

The TR signal was interpretable in 49% of patients with ALD without PH and in 47% of those with PH (Table 1). When compared to well-matched controls, patients with ALD without PH had significantly higher RV dimensions (RVEDAI, RVESAI), worst systolic function (TAPSE, RVFAC, RVLS), prolonged indexed RV-IVRTi and acceleration time (Table 1). When comparing ALD patients with or without PH, RAVI, RVESAI and RVLS were the only metrics statistically different. Figure 1a shows the partial correlation map of right heart metrics used to define enlargement or dysfunction, illustrating the interdependence between metrics, except for RAVI and TAPSE. Figure 1b, c display the distribution of main RV metrics according to presence or not of PH. Results were similar according to ALD etiology (obstructive versus restrictive). Right heart enlargement and dysfunction were frequent in patients with ALD without PH. Seven patients (16%) had all normal following right echo metrics (RAVI, RVESAI, RVFAC, RVLS and TAPSE), 27% had only one abnormal parameter, 31% two abnormal parameters and the rest (26%) had \geq 3 abnormal metrics.

In multivariable analysis including variables with *p* $<$ 0.20 listed in Table 2, RAVI (AUC 0.67 [0.57–0.77]) and TAPSE (0.58 [0.47–0.68]) were independently associated with PH (Fig. 2). The RAVI threshold of 15.7 mL/m² had a sensitivity of 70% and a specificity of 56%, while the TAPSE threshold of 18.5 mm had a sensitivity of 53% and a specificity of 42%. Multivariate analysis found RAVI (AUC 0.75 [0.65–0.83], *p* $<$ 0.01) to be the only independent correlate of severe PH (MPAP \geq 35 mmHg).

Clinical validation cohort (n = 100)

Characteristics were similar to the derivation cohort's (mean age 52.3 ± 13.5 years, 43% of male, 48% of ILD, 39% of COPD, 13% of CF and 49% had PH). Performances of echocardiographic metrics to detect PH were also similar, with RAVI and TAPSE demonstrating moderate AUCs

Table 1 Characteristics of controls and patients with advanced lung disease

	Controls (n=50)	Advanced lung disease	
		Without PH (n=45)	With PH (n=47)
Age (years)	52.4 ± 13.4	52.5 ± 14.0	52.6 ± 13.6
Male sex	25 (50)	18 (40)	31 (66)
Body surface area (m ²)	1.78 ± 0.18	1.75 ± 0.24	1.82 ± 0.27
Hemodynamics			
Cardiac index (L/min/m ²)	–	2.81 ± 0.81	2.75 ± 0.75
Mean pulmonary arterial pressure (mmHg) [min; max]	–	19.3 ± 3.8 [10.0; 24.0]	34.1 ± 8.4 [25.0; 52.0] †
Pulmonary vascular resistance (WU)	–	2.03 ± 0.03	4.71 ± 0.71 [†]
Pulmonary arterial wedge pressure (mmHg)	–	8.8 ± 0.8	12.1 ± 2.1 [†]
Echocardiography			
LVEF (%)	62.6 ± 5.5	60.6 ± 7.8	62.3 ± 7.0
RAAI (cm ² /m ²)	9.04 ± 1.55	7.36 ± 1.81	9.17 ± 4.27
RAVI (mL/m ²)	22.7 ± 5.7	17.2 ± 7.4	28.8 ± 20.8* [†]
RVEDAI (cm ² /m ²)	9.80 ± 1.90	13.06 ± 2.93*	15.08 ± 4.04*
RVESAI (cm ² /m ²)	5.53 ± 1.15	8.23 ± 2.05*	10.35 ± 4.15* [†]
Eccentricity Index	1.01 ± 0.03	1.15 ± 0.17	1.33 ± 0.30 *
TAPSE (cm)	2.35 ± 0.36	2.03 ± 0.51*	1.85 ± 0.46*
RVFAC (%)	43.37 ± 6.40	36.93 ± 8.78*	33.02 ± 10.03*
RVLS (%)	−30.18 ± 3.07	−23.85 ± 4.69*	−20.72 ± 6.92* [†]
Peak S' velocity (cm/s)	13.6 ± 2.2	12.7 ± 3.3	12.1 ± 3.4*
RV-IVRTi	2.03 ± 0.67	3.26 ± 0.92*	3.65 ± 0.93*
Acceleration time (ms)	154 ± 24	82 ± 20*	78 ± 20*
Acceleration time/√RR	6.0 ± 0.7	3.0 ± 0.8*	2.9 ± 0.7*
RVSP (mmHg)	19.2 ± 6.4	39.3 ± 9.5*	60.0 ± 16.3* [†]
Interpretable TR signal enabling RVSP estimation (%)	45 (90)	22 (49)*	22 (47) [†]
RAP estimated (mmHg)	4.1 ± 1.4	5.0 ± 2.6	7.8 ± 5.3 [†]

RAAI right atrial end-systolic area indexed, RAVI right atrial end-systolic volume indexed, RVFAC right ventricular fractional area change, RV-IVRTi RV isovolumic relaxation time divided by √RR, RVLS RV lateral wall longitudinal strain, RVSP right ventricular systolic pressure

*p < 0.05 compared to controls, [†]p < 0.05 ALD without PH versus ALD with PH. All ANOVA p-value were significant except for left ventricular ejection fraction LVEF (p = 0.13).

(Fig. 2). The RAVI threshold of 15.7 mL/m² (derived from the derivation cohort) was associated with a sensitivity of 65% and a specificity of 75%, while the TAPSE threshold of 18.5 mm was associated with a sensitivity of 65% and a specificity of 39%.

Animal validation (n = 8)

At week 4, RVEDAI, RVESAI, RAAI and EI were higher in PH pigs than in SHAMS (p < 0.05, Table 3; Fig. 3a). A prolonged RV-IVRT was the only functional metric significantly different from SHAMS, while there was a non-significant trend for RVFAC, RVLS and TAPSE to be altered in PH. During the 16-week follow-up, MPAP and resistance increased in PH pigs (p < 0.01). RAVI and RVESAI increased over time and tended to stabilize between weeks 4 and 16 (Fig. 3b), while RV-IVRTi continuously increased

(p < 0.01). No significant difference in time was observed for functional indices (Online Resource 2).

Echocardiographic probability of PH

Having previously verified the homogeneity of the two clinical cohorts, the additional diagnostic value of right heart metrics in combination with TR signal maximal velocity or estimated RVSP was then assessed. There was excellent correlation between RVSP estimated from the TR signal and invasively measured RVSP (R² = 0.88, p < 0.0001), as shown in Fig. 4. Similarly, there was excellent correlation between maximal TR velocity and invasively measured RVSP (R² = 0.81, p < 0.0001).

In the total population (n = 192), RAVI and TAPSE were the independent metrics retained from Table 2 variables to be associated with PH (Chi² 51.0, p < 0.0001). The AUC

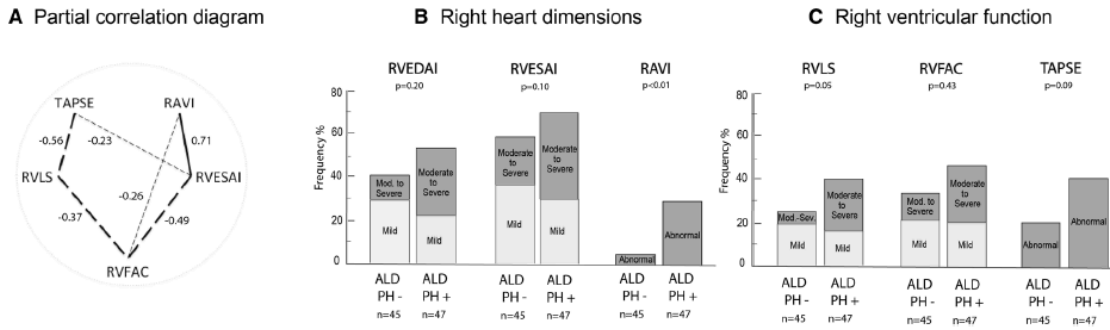


Fig. 1 Correlation between right heart metrics (a); prevalence of right heart enlargement or dysfunction (b, c) according to presence or not of pulmonary hypertension (PH). a Partial correlation diagram between right heart echocardiographic metrics. Full lines represent significant ($p \leq 0.01$ for all) direct correlations; dashed lines show significant inverse correlation. Thicker lines show stronger relationships ($p < 0.001$). b and c RAVI (mL/m²) was considered as abnormal if > 32.5 . RVESAI or RVEDAI were considered normal if $<$ mean value + 2SD of the healthy cohort, and thresholds were derived by section of 20% range. RVESAI (cm²/m²) was normal if ≤ 7.8 , mildly between 7.8–9.4 included, moderately if between 9.4–10.9 and

severely enlarged if > 10.9 . RVEDAI (cm²/m²) was normal if ≤ 13.6 , mildly between 13.6–16.3 included, moderately if between 16.3–19.0 and severely enlarged if > 19.0 . RVLS (%) was normal if ≤ -20 , mildly if between -20 and -16 included, moderately if between -16 and -12 included and severely altered if > -12 . RVFAC (%) was normal if ≥ 35 , mildly if between 35–28 included, moderately if between 28–21 included and severely altered if < 21 . TAPSE was considered abnormal if < 17 mm. RAVI right atrial volume index, RVEDAI RV end-diastolic area index, RVESAI RV end-systolic area index, RVFAC RV fractional area change, RVLS RV lateral wall longitudinal strain, TAPSE tricuspid annular plane systolic excursion

Table 2 Multivariable logistic regression for correlates of pulmonary hypertension in the derivation cohort (n = 92)

Variables	Univariate	p	Multivariable	p
RAVI	5.83 [1.68–15.16]	<0.01	15.16 [2.16–115.52]*	0.02
RVESAI	3.13 [1.38–6.92]	<0.01		
RVEDAI	1.84 [1.15–3.01]	0.66		
RVFAC	0.68 [0.40–1.00]	0.05		
RVLS	2.05 [1.13–3.71]	0.08		
TAPSE	0.68 [0.44–1.05]	0.08	0.37 [0.18–0.77]*	0.03
Obstructive lung disease	1.31 [0.58–2.99]	0.52		
FEV1%	0.99 [0.65–1.53]	0.98		
FVC%	1.12 [0.73–1.72]	0.62		
Minimal SaO ₂ during 6 min walk test	0.97 [0.91–1.03]	0.29		

*Model adjusted for sex. Age did not correlate with RAVI. Variables with p-value < 0.20 were included in multivariable analysis. As RAVI was co-linear to RVESAI ($R^2 = 0.59$) and RVEDAI ($R^2 = 0.53$), these latter were not included in model. Continuous variables are expressed as Odds Ratio per SD unit (OR^{SD}) and their 95% confidence interval [95% CI], and OR [95% CI] for discrete variables

FEV1%: Forced Expiratory Volume exhaled at the end of the first second, FVC%: Forced Vital Capacity; other abbreviations please see Table 1

of the RAVI divided by TAPSE ratio (RAVI/TAPSE) was 0.74 [0.67–0.81]. In patients with interpretable TR signal (n = 92), RAVI and TAPSE were also associated with PH (Chi² 30.6, $p < 0.0001$); the AUC of RAVI/TAPSE was 0.79 [0.70–0.89]. In patients with uninterpretable TR signal (n = 100), RAVI and RVLS were the two retained metrics (Chi² 21.4, $p < 0.0001$); the AUC of RAVI/TAPSE was 0.69 [0.59–0.79].

As the AUCs were at best moderate, we then assessed how taking into account multiple right heart metrics

could help detecting PH. Using similar European guidelines methodology [1], Fig. 5 presents the echocardiographic probability of PH according to TR signal, and presence or not of ≥ 2 right heart alterations among RV size, function and RA metrics. In patients with interpretable TR signal (n = 92), TR maximal velocity was able to discriminate between the different probabilities of PH ($p < 0.0001$). Prevalence of PH in patients with maximal TR velocity ≤ 2.8 m/s was 17.6%, in patients with TR between 2.9–3.4 was 53.8% and in those with > 3.4 was

A Correlates of PH in patients with advanced lung disease

Variables	AUC	95%CI
ALD derivation cohort (n=92)		
RAVI	0.67	0.57-0.77
TAPSE	0.58	0.47-0.68
RAVI+TAPSE	0.77	0.67-0.85
ALD validation cohort (n=100)		
RAVI	0.77	0.67-0.84
TAPSE	0.59	0.49-0.69
RAVI+TAPSE	0.78	0.69-0.86

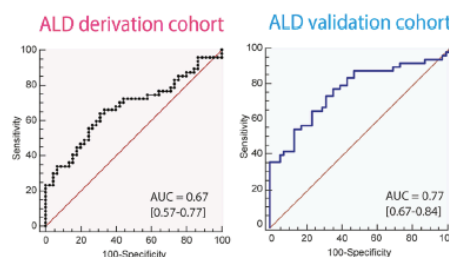
B ROC curves of RA volume index for PH detection

Fig. 2 Accuracy of echocardiographic metrics for detection of pulmonary hypertension. **a** AUC of RA volume index (RAVI) and TAPSE (as continuous variables) for classification of PH (MPAP \geq 25 mmHg) using logistic regression analysis; all p-values

were <0.01 . There was no difference between respective AUCs of the derivation and validation cohorts ($p=0.16$ for RAVI, 0.90 for TAPSE and 0.88 for the model RAVI+TAPSE). **b** ROC of RAVI for PH in both cohorts

96.9%. Adding the presence of ≥ 2 right heart alteration did not significantly add to the risk stratification of PH (p ranging from 0.22 to 0.77). Prevalence of PH in patients with uninterpretable signal ($n=100$) was 47.0%. In these patients, presence of ≥ 2 right heart alteration was able to discriminate between the two risk levels ($p<0.0001$). Similar results were found when considering estimated RVSP (Online Resource 3). In patients in whom the TR was interpretable, the net reclassification index of presence of ≥ 2 right heart alteration over RVSP ≥ 40 mmHg was negative (-0.17), implying worsening in PH classification. Finally, absence of RV enlargement or dysfunction in our cohort was found in only two patients with more severe PH (MPAP 35–36 mmHg).

Exploring the “gray zone” of MPAP 20–24 mmHg

Overall 52/192 patients with ALD (27%) had a MPAP between 20–24 mmHg. Using the thresholds defined in Fig. 1, only one patient had right atrial enlargement, three (6%) had moderate and five (10%) had severe RV enlargement using RVESAI. Two patients (12%) had moderate to severe RV dysfunction using strain and 16 (31%) had an abnormal TAPSE.

Discussion

Our study highlights the frequency of right heart enlargement and dysfunction in patients with lung disease, irrespective of the presence of PH. Non-invasive pulmonary flow or cardiac metrics (including novel modalities such as

strain) consequently provide moderate discriminative ability for PH detection.

Echocardiography and detection of PH

The most studied metrics reported to be markers of elevated pulmonary pressures include acceleration time, IVRT, and strain [15]. Acceleration time has been shown to correlate with MPAP and resistance in COPD (both AUCs of 0.96) [16]. IVRT has also been associated with either invasively assessed ($r=0.87$, $p<0.001$) [17] or echocardiographic estimated systolic pulmonary arterial pressure SPAP ($r=0.52$ – 0.74 , $p<0.001$) [18]. An IVRT >75 ms demonstrated excellent sensitivity (94%) and specificity (97%) in 196 patients with severe PH (SPAP 81 ± 25 mmHg) [8]. Both acceleration time and IVRT were not validated in our cohort (either non-adjusted or adjusted to heart rate), further questioning the optimal way to correct these time metrics by heart rate. Strain has recently attracted increasing interest [19]. Basal and mid RV free wall longitudinal strain were shown to moderately correlate with SPAP ($r=0.53$; $p<0.001$) and pulmonary vascular resistance ($r=0.68$; $p<0.001$) in 50 patients with severe PH (SPAP 86 ± 28 mmHg) [20]. Strain was not found to be as strong in our cohort. This discrepant finding can be due to the fact that a large majority of studies assessing echocardiography in PH has been performed in patients with higher level of pulmonary pressures compared to healthy controls. This may have improved the discrimination performance of those metrics, contrary to our study comparing patients with ALD who have lower pressure levels.

The extent of right heart dilation and dysfunction has been recently reported in patients with COPD [9, 21]. RV

Table 3 Characteristics of piglet models of right ventricular pressure overload (PH) and SHAM at week 4

	SHAM (n= 4)	PH (n= 4)	p
Body weight (kg)	26 [26; 26]	21 [19; 23]	0.02
Body surface area (m ²)	0.64 [0.64; 0.64]	0.56 [0.52; 0.60]	0.02
Right heart catheterization			
Mean pulmonary arterial pressure (mmHg)	10.5 [9.5; 12.5]	20.0 [16.5; 23.5]	0.03
Central venous pressure (mmHg)	1.0 [1.0; 1.5]	1.5 [1.0; 3.5]	0.44
Cardiac index (L/min/m ²)	5.7 [4.8; 6.6]	4.1 [3.9; 5.1]	0.31
Stroke volume index (L/m ²)	0.07 [0.06; 0.07]	0.07 [0.05; 0.06]	0.49
Heart rate (/min)	86 [84; 94]	76 [72; 84]	0.20
Left ventricular end-diastolic pressure (mmHg)	5.5 [4.3; 7.5]	9.5 [7.5; 12.7]	0.06
Total pulmonary resistance index (WU.m ²)	2.0 [1.6; 2.4]	4.2 [4.1; 5.0]	0.02
Pulmonary vascular resistance index (WU.m ²)	1.0 [0.8; 1.0]	2.0 [1.8; 3.0]	0.03
Echocardiogram			
Right heart dimensions			
RV end-diastolic wall thickness indexed (mm/m ²)	3.3 [2.4–4.2]	4.2 [3.4–5.0]	0.04
RV end-systolic wall thickness indexed (mm/m ²)	5.1 [3.8–6.4]	6.1 [4.9–7.4]	0.12
RVEDAI (cm ² /m ²)	16.1 [13.9; 17.0]	21.4 [18.9; 23.1]	0.03
RVESAI (cm ² /m ²)	8.9 [8.1; 9.6]	11.3 [10.9; 13.4]	0.03
RVEDA/LVEDA	0.55 [0.44; 0.64]	0.60 [0.53; 0.67]	0.34
RVESA/LVESA	0.49 [0.47; 0.54]	0.64 [0.57; 0.77]	0.06
RAAI (cm ² /m ²)	9.7 [8.0; 10.6]	14.3 [13.3; 15.3]	0.03
Ventricular interaction			
Diastolic eccentricity index	1.00 [0.99; 1.00]	1.01 [0.99; 1.05]	0.37
Systolic eccentricity index	1.00 [1.00–1.00]	1.05 [1.03–1.09]	0.02
RV systolic and diastolic functions			
RV fractional area change (%)	40.5 [40.0; 45.5]	36.5 [32.8; 46.3]	0.17
Free-wall RV longitudinal strain (%)	−43.8 [−46.2; −35.4]	−34.8 [−38.0; −28.8]	0.20
Tricuspid annular plane systolic excursion (mm)	24 [22; 24]	20 [17; 22]	0.06
Peak S' velocity (cm/s)	9 [9; 11]	8 [6; 13]	0.31
RV-IVRT (ms)	33.7 [22.7; 46.0]	70 [57.5; 85.0]	0.03
RV-IVRTi	1.3 [0.9; 1.7]	2.4 [2.0–2.9]	0.03
LV-IVRT (ms)	74.0 [56.2; 98.5]	80.5 [76.0; 90.5]	0.89
LV-IVRTi	2.9 [2.1–3.8]	3.0 [2.7–3.2]	1.00
E' velocity (m/s)	0.12 [0.11; 0.13]	0.09 [0.09–0.12]	0.25
Indirect pressure estimation			
RV acceleration time (ms)	28.5 [25.5; 33.5]	27.0 [23.5; 32.0]	0.69
RV acceleration time/√RR	0.05 [0.04; 0.05]	0.03 [0.03; 0.04]	0.20
RV–LV acceleration time (ms)	12.0 [3.5; 13.5]	8.5 [6.0; 13.5]	0.89
RV–LV acceleration time/√RR	0.02 [0.01; 0.02]	0.01 [0.01; 0.02]	0.69

Values are expressed as median [interquartile range]

LV-IVRTi left ventricular isovolumic relaxation time divided by $\sqrt{\text{RR}}$, *RAAI* right atrial end-systolic area index, *RVEDAI* right ventricular end-diastolic area index, *RVESAI* end-systolic area index, *RV-IVRTi*: RV-IVRT divided by $\sqrt{\text{RR}}$

impairment, hypertrophy and enlargement were found even at slight elevations of MPAP (18 ± 3 mmHg) in patients without PH [9]. In our cohort, 20% of patients without PH had moderate to severe RV enlargement. Our study further explores the practical consequences on the detection of PH by echocardiography. The originality of our study is threefold. First, a diverse range of lung disease etiologies

(obstructive and restrictive) was included, allowing expansion of previous finding in COPD. Second, our study comprehensively assessed the value of right heart echocardiographic metrics to detect PH in patients with ALD. Right atrial enlargement and TAPSE appeared to be the best independent metrics to detect PH. The simple ratio of RAVI/TAPSE correlated with presence of PH but provided

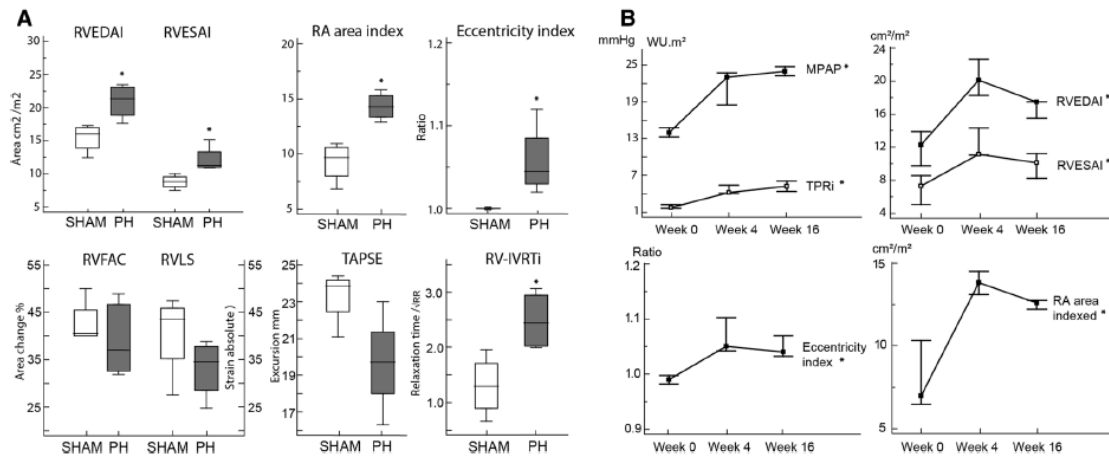
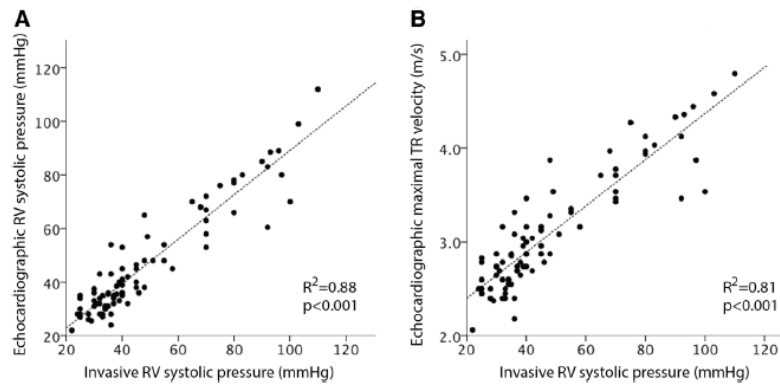


Fig. 3 Characteristics of piglet models of right ventricular pressure overload PH (n=4) versus SHAMS (n=4) at week 4 (a); and evolution of PH pigs over time (b). * p<0.05 or ** p<0.05 as compared to SHAMS. Values are presented as median and interquartile range.

Mean pulmonary arterial pressure (MPAP) and total pulmonary resistance index (TPRi) were obtained from catheterization. Abbreviations please see Table 1

Fig. 4 Pearson correlation between echocardiographic-estimated and invasively measured right ventricular systolic pressures. TR tricuspid regurgitation



moderate diagnosis value. Therefore, the next step was to evaluate whether integrating multiple metrics (including emerging ones such as strain) to the analysis of the TR signal would help PH detection. However, these metrics also showed moderate incremental value. The third originality of our study is the inclusion of a large animal model of mild RV pressure overload that provided experimental confirmation of right heart enlargement to be the most sensitive metric to detect mild PH consistently over time.

Clinical implications

This study has several clinical implications that can influence practice. Our study confirms that RVSP estimation from the TR signal is reliable for detection of PH in patients with advanced lung disease in presence of a good

TR signal envelope [4, 22]. According to the ASE society and in our practice, reliable TR signals are defined by either a complete signal or a signal that can be clearly extrapolated. Caveats to respect include acquiring the signal at the most optimal insonation angle and measuring the peak TR velocity using the modal frequency. The most common mistake is to over-gain the signal, which leads to overestimation of the TR peak velocity. In the absence of interpretable TR signal (i.e. in half of patients with ALD), the combination of abnormal right heart metrics is mainly useful for detection of more severe PH. Based on our findings, it would be logical to avoid catheterization in patients with perfect TR signal and normal to mildly decreased RV function. However, as the Lung Allocation Score includes invasively determined

A

Peak tricuspid regurgitation velocity (m/s)	n	Prevalence of PH	Presence of right heart alteration	n	Prevalence of PH
≤ 2.8	34	17.6%	No	28	17.9%
			Yes	6	16.7%
2.9 to 3.4	26	53.8%	No	17	52.9%
			Yes	9	55.6%
> 3.4	32	96.9%	No	7	71.4%
			Yes	25	96.0%
Not measurable	100	47.0%	No	76	34.2%
			Yes	24	87.5%

B

Ventricular size	Ventricular function	Right atrial metrics
RV end-systolic area index > 7.8 cm ² /m ²	TAPSE < 17mm	RA end-systolic volume index > 32.5 cm ² /m ²
	RV free-wall longitudinal strain > -20%	Estimated RA pressure ≥ 15mmHg

Fig. 5 Prevalence of pulmonary hypertension in patients with advanced lung disease (n=192) according to echocardiographic findings. **a** Prevalence of PH according to tricuspid regurgitation (TR) maximal velocity and presence of right heart alteration. **b** Echocardiographic signs suggesting pulmonary hypertension (PH) used to assess the probability of PH in addition to the TR velocity measure-

ment. Signs from at least two different categories (ventricular size, ventricular function or right atrial metrics) should be present to alter the level of echocardiographic probability of PH. *Green*: low, *yellow*: intermediate, *red*: high probability of PH. *RA* right atrial, *RV* right ventricle, *TAPSE* tricuspid annular plane systolic excursion

pulmonary pressures, it is unlikely that this will change the current practice. The only thing that could change practice would be to determine whether pre-transplant RV enlargement/failure versus presence of PH influence post-transplantation outcome in patients with lung disease [23]. If the prognostic value of right heart failure would be confirmed over pulmonary pressures, it could shift the interest from RHC towards imaging of the right heart. Echocardiography would be a modality of choice with magnetic resonance imaging, although one has to recognize the variable expertise of echocardiography among echo labs. Finally, when patients are not considered for lung transplant, our results suggest that presence

of 2 or more echocardiographic abnormalities would recommend performing catheterization.

Limitations

These results are limited to a severe subset of patients with ALD referred for lung transplantation. The spectrum of the main current indications for lung transplantation (COPD, ILD and CF) was however represented, and results were confirmed in a validation cohort. Second, it can be pointed out that we used a large animal model of mild increased afterload and not a model of chronic hypoxemia. This, however, allowed us to address specifically the ability of RV and flow metrics to discriminate mild right pressure

overload, independently from hypoxemia, and to longitudinally validate these metrics over time. Third, contrast methods were not routinely used. Signal enhancement with saline contrast can improve the signal-to-noise ratio in estimating TR velocities.

Conclusion

This study provides comprehensive critical assessment of noninvasive right heart and pulmonary flow metrics for detection of PH in patients with advanced lung disease. Because of the frequency of right heart enlargement or failure irrespectively of the presence of PH, echocardiographic metrics can be used to precise the pretest probability of PH before catheterization, but cannot replace it as invasively pressures remain part of the Lung Allocation Score.

Acknowledgements The authors would like to thank the Stanford Cardiovascular Institute and Vera Moulton Wall Center of Pulmonary Hypertension at Stanford for their support.

Funding This study was funded by the Stanford Cardiovascular Institute, the Vera Moulton Wall Center of Pulmonary Hypertension at Stanford and the French National Research Agency (ANR-15-RHUS-0002).

Compliance with ethical standards

Conflict of interest The authors declare that they have no conflict of interest. MA received a Young Investigator Seed Grant from the Vera Moulton Wall Center. MVM previously received cardiac MRI research support from GE Healthcare and is currently on partial leave of absence while at Verily. FH received funds from Pai Chan Lee Research fund.

Ethical approval All applicable international, national, and/or institutional guidelines for the care and use of animals were followed (Institutional Animal Care Committee of Marie Lannelongue Hospital, Paris-Sud University, France). All procedures performed in studies involving human participants were approved by Stanford University Institutional Review Board in accordance with the ethical standards of the institutional and/or national research committee and with the 1964 Helsinki declaration and its later amendments or comparable ethical standards. Informed consent was obtained from all individual participants included in the study.

References

- Galiè N, Humbert M, Vachiery J-L, Gibbs S, et al. (2015) ESC/ERS Guidelines for the diagnosis and treatment of pulmonary hypertension: the joint task force for the diagnosis and treatment of pulmonary hypertension of the European Society of Cardiology (ESC) and the European Respiratory Society (ERS): endorsed by: Association for European Paediatric and Congenital Cardiology (AEPC), International Society for Heart and Lung Transplantation (ISHLT). *Eur Respir J* 46:903–975.
- Fisher MR, Criner GJ, Fishman AP et al (2007) Estimating pulmonary artery pressures by echocardiography in patients with emphysema. *Eur Respir J* 30:914–921
- Nathan SD, Shlobin OA, Barnett SD et al (2008) Right ventricular systolic pressure by echocardiography as a predictor of pulmonary hypertension in idiopathic pulmonary fibrosis. *Respir Med* 102:1305–1310
- Amsallem M, Sternbach JM, Adigopula S et al (2015) Addressing the controversy of estimating pulmonary arterial pressure by echocardiography. *J Am Soc Echocardiogr* 29:93–102
- Raymond RJ, Hinderliter AL, Willis PW et al (2002) Echocardiographic predictors of adverse outcomes in primary pulmonary hypertension. *J Am Coll Cardiol* 39:1214–1219
- Ghio S, Klersy C, Magrini G et al (2010) Prognostic relevance of the echocardiographic assessment of right ventricular function in patients with idiopathic pulmonary arterial hypertension. *Int J Cardiol* 140:272–278
- Vonk Noordegraaf A, Galiè N (2011) The role of the right ventricle in pulmonary arterial hypertension. *Eur Respir Rev* 20:243–253
- Zimbarra Cabrera I, Ruisanchez C, Grapsa J et al (2013) Validation of the isovolumetric relaxation time for the estimation of pulmonary systolic arterial blood pressure in chronic pulmonary hypertension. *Eur Heart J Cardiovasc Imaging* 14:51–55
- Hilde JM, Skjorten I, Grøtta OJ et al (2013) Right ventricular dysfunction and remodeling in chronic obstructive pulmonary disease without pulmonary hypertension. *J Am Coll Cardiol* 62:1103–1111
- McLaughlin VV, Archer SL, Badesch DB et al (2009) ACCF/AHA 2009 expert consensus document on pulmonary hypertension: a report of the American College of Cardiology Foundation Task Force on Expert Consensus Documents and the American Heart Association: developed in collaboration with the American College of Chest Physicians, American Thoracic Society, Inc., and the Pulmonary Hypertension Association. *Circulation* 119:2250–2294
- Rudski LG, Lai WW, Afilalo J et al (2010) Guidelines for the echocardiographic assessment of the right heart in adults: a report from the American Society of Echocardiography endorsed by the European Association of Echocardiography, a registered branch of the European Society of Cardiology, and the Canadian Society of Echocardiography. *J Am Soc Echocardiogr* 23:685–788
- Lang RM, Badano LP, Mor-Avi V et al (2015) Recommendations for cardiac chamber quantification by echocardiography in adults: an update from the American Society of Echocardiography and the European Association of Cardiovascular Imaging. *J Am Soc Echocardiogr* 28:1–39
- Mercier O, Fadel E (2013) Chronic thromboembolic pulmonary hypertension: animal models. *Eur Respir J* 41:1200–1206
- Guihaire J, Haddad F, Boulate D et al (2014) Right ventricular plasticity in a porcine model of chronic pressure overload. *J Heart Lung Transplant* 33:194–202
- Jurcut R, Giusca S, La Gerche A et al (2010) The echocardiographic assessment of the right ventricle: what to do in 2010? *Eur J Echocardiogr* 11:81–96
- Hilde JM, Skjorten I, Hansteen V et al (2016) Assessment of right ventricular afterload in COPD. *COPD* 13:176–185
- Bréchet N, Gambotti L, Lafitte S et al (2008) Usefulness of right ventricular isovolumic relaxation time in predicting systolic pulmonary artery pressure. *Eur J Echocardiogr* 9:547–554
- Dambrauskaitė V, Delcroix M, Claus P et al (2005) The evaluation of pulmonary hypertension using right ventricular

- myocardial isovolumic relaxation time. *J Am Soc Echocardiogr* 18:1113–1120
19. Fukuda Y, Tanaka H, Sugiyama D et al (2011) Utility of right ventricular free wall speckle-tracking strain for evaluation of right ventricular performance in patients with pulmonary hypertension. *J Am Soc Echocardiogr* 24:1101–1108
 20. Utsunomiya H, Nakatani S, Okada T et al (2011) A simple method to predict impaired right ventricular performance and disease severity in chronic pulmonary hypertension using strain rate imaging. *Int J Cardiol* 147:88–94
 21. Rice JL, Stream AR, Fox DL et al (2016) Speckle tracking echocardiography to evaluate for pulmonary hypertension in chronic obstructive pulmonary disease. *COPD* 13:1–6
 22. Greiner S, Jud A, Aurich M, et al. (2014) Reliability of non-invasive assessment of systolic pulmonary artery pressure by Doppler echocardiography compared to right heart catheterization: analysis in a large patient population. *J Am Heart Assoc* 3(4):e001103.
 23. Haddad F, Fadel E (2014) RV dysfunction after lung transplantation: a new prognostic marker or mainly a correlate of lung allograft function? *JACC Cardiovasc Imaging* 7:1095–1097



ELSEVIER

The Journal of
Heart and Lung
Transplantation

<http://www.jhltonline.org>

ORIGINAL CLINICAL SCIENCE

Impact of the initiation of balloon pulmonary angioplasty program on referral of patients with chronic thromboembolic pulmonary hypertension to surgery

Myriam Amsallem, MD, MSc,^{a,b,c} Julien Guihaire, MD, PhD,^{b,d}
Jennifer Arthur Ataam, PhD,^b Lilia Lamrani, MSc,^b David Boulate, MD, MSc,^d
Sacha Mussot, MD, MSc,^d Dominique Fabre, MD, PhD,^d Yu Taniguchi, MD,^e
Francois Haddad, MD, MSc,^c Olivier Sitbon, MD, PhD,^e Xavier Jais, MD,^e
Marc Humbert, MD, PhD,^e Gérald Simonneau, MD, PhD,^e
Olaf Mercier, MD, PhD,^{b,d} Philippe Brenot, MD,^{a,1} and Elie Fadel, MD, PhD^{b,d,1}

From the ^aDepartment of Cardiovascular Imaging, Marie Lannelongue Hospital, Le Plessis Robinson, France; ^bResearch and Innovation Unit, INSERM U999, DHU Torino, Paris Sud University, Marie Lannelongue Hospital, Le Plessis Robinson, France; ^cDivision of Cardiovascular Medicine, Stanford University, Stanford, California, USA; ^dDepartment of Cardiothoracic Surgery, Marie Lannelongue Hospital, Le Plessis Robinson, France; and the ^eDepartment of Pulmonary Diseases, Kremlin Bicêtre Hospital-APHP, Kremlin Bicêtre, France.

KEYWORDS:

angioplasty;
epidemiology;
endarterectomy;
outcome;
pulmonary
hypertension

BACKGROUND: Balloon pulmonary angioplasty (BPA) is a technique proposed for inoperable patients with chronic thromboembolic pulmonary hypertension (CTEPH). In this study we aimed to determine whether initiation of the BPA program has modified the characteristics and outcome of patients undergoing pulmonary endarterectomy (PEA), and compared the characteristics of patients undergoing one or the other procedure.

METHODS: This prospective registry study included all patients with CTEPH who underwent PEA in the French National Reference Center before (2012 to 2013) and after (2015 to 2016) BPA program initiation (February 2014). Pre-operative clinical and hemodynamics profiles, peri-operative (Jamieson classification, surgery duration, need of assistance) characteristics of both groups, and all-cause mortality were compared using the *t*-test or chi-square test. Characteristics of patients subjected to surgery or BPA since February 2014 were also compared.

RESULTS: The total number of patients referred to the CTEPH team increased in the BPA era ($n = 291$ vs $n = 484$). The pre-operative characteristics of patients from the pre-BPA era ($n = 240$) were similar to those from the BPA era ($n = 246$). Despite more Jamieson Type 3 cases (29%) in the second period, 30- and 90-day mortality remained stable (both $p > 0.30$). Patients subjected to BPA ($n = 177$) were older than those subjected to PEA ($n = 364$) (64 ± 14 vs 60 ± 14 years, respectively), and had

¹These (senior) authors contributed equally to this study.

Reprint requests: Myriam Amsallem, MD, MSc, Department of Cardiovascular Imaging, Marie Lannelongue Hospital, 133 avenue de la Résistance, Le Plessis Robinson, France. Telephone: +33140942800. Fax: +33140256732.

E-mail address: myriam.amsallem@gmail.com

higher rates of splenectomy (10% vs 1%) or implantable port (9% vs 3%), lower total pulmonary resistance, better cardiac index, and better renal function (all $p < 0.01$).

CONCLUSIONS: This study shows the influence of the initiation of the BPA program on the profile of patients with CTEPH undergoing PEA.

J Heart Lung Transplant 000;000:1–9

© 2018 International Society for Heart and Lung Transplantation. All rights reserved.

Chronic thromboembolic pulmonary hypertension (CTEPH) is a rare but severe complication of acute pulmonary embolism, leading to right heart failure and premature mortality. Its cumulative incidence ranges from 0.1% to 9.1% within the first 2 years after symptomatic acute pulmonary embolism, although this is probably an underestimation due to the lack of systematic follow-up and screening in the clinical routine.^{1–3}

The pathophysiology of CTEPH is believed to be the result of fibrotic transformation of pulmonary artery thrombi causing chronic obstruction in macroscopic pulmonary arteries, associated with microvascular remodeling, inflammation, and endothelial dysfunction.^{4,5} Pulmonary endarterectomy (PEA) enables surgical removal of macroscopic material and offers the best chance of symptomatic and prognostic improvement in operable patients. PEA has shown good results in expert centers, making it the treatment of choice for patients with CTEPH, as highlighted in the latest European guidelines on pulmonary hypertension (PH).^{6,7} However, up to a third of patients with CTEPH are not candidates for surgery, according to an international 2007 to 2009 registry, due to non-operability.⁸

In parallel, balloon pulmonary angioplasty (BPA) has emerged as a new therapeutic technique in inoperable CTEPH. First reported by Feinstein et al in 2001 in 18 patients with CTEPH, BPA showed improvement in long-term functional parameters.⁹ However, 61% of patients developed reperfusion edema, including one third who required mechanical ventilation. Since then, technical material (i.e. size of balloons) and angioplasty strategy (i.e. dilation of 1 or 2 segments per procedure) have improved, reducing the rate of complications and increasing the place of BPA in the arsenal of inoperable patients with CTEPH.^{10–12} Aoki et al recently confirmed, in a cohort of 77 inoperable patients with CTEPH who underwent BPA, the safety and effectiveness of the technique in terms of reduction of resistance and improvement in functional status, with a 5-year survival rate of 98.4%.¹³

Using the French National Reference Center (Kremlin Bicêtre University Hospital–Marie Lannelongue Hospital) CTEPH prospective registry, this study had 2 objectives. The first was to determine whether the profile and outcome of patients with CTEPH subjected to PEA has been influenced by the initiation of the BPA program (2014). The second objective was to compare the baseline characteristics of patients undergoing one or the other procedure since 2014.

Methods

Surgical cohort

In this study, we compared the characteristics of patients before (2012 to 2013) and after (2015 to 2016) the year that angioplasty was initiated in our center (2014). Between January 2012 and December 2016, 626 consecutive patients underwent PEA at Marie Lannelongue Hospital (Le Plessis Robinson, France) for suspected CTEPH (i.e. mean pulmonary arterial pressure [mPAP] ≥ 25 mm Hg, at least 1 segmental perfusion defect detected by lung scanning, and typical lesions of CTEPH on multidetector computed tomographic angiography and/or pulmonary angiography after at least 3 months of effective anti-coagulation).⁷ This cohort represents the totality of PEA procedures performed in France (prevalent and incident cases). Patients with differential diagnoses were excluded: pulmonary artery sarcoma ($n = 17$) and pulmonary hypertension caused by tumor embolism ($n = 3$). Indications for surgery were discussed weekly by an experienced multidisciplinary team at the National Reference Center for PH in Kremlin Bicêtre University Hospital (Paris Sud University, France), including at least 1 experienced surgeon and 1 expert in BPA.⁷ The French National Reference Center enables referral of patients from a network of French centers, and access to the latest up-to-date range of medical and interventional therapies, including PEA since 1995 and BPA since 2014. During the 2 study periods, surgery would be considered as the first line of interventional therapy. Patients were considered operable by the CTEPH team if presenting with sufficient surgically accessible thromboembolic material relating to the pulmonary hemodynamics and absence of high-risk comorbidities precluding surgery.⁸ PEA was performed as previously described; the surgical procedure did not change during the study period.¹⁴ Briefly, cardiopulmonary bypass was first established between the ascending aorta and the 2 vena cavae; body temperature was decreased to 20°C before cross-clamping of the aorta. Right, and then left endarterectomy procedures were performed with sequential circulatory arrests for distal pulmonary arterial recanalization. Emergent PEAs were defined as procedures performed in patients with acute severe right heart failure and more than 1 end-organ failure requiring amines support (dobutamine, noradrenaline, or adrenaline) within 24 hours of their admission to our institution. Associated cardiac surgical procedures included coronary artery bypass graft and/or valvular heart surgery.

Balloon pulmonary angioplasty cohort

The program of angioplasty was initiated in February 2014 at our institution, which is the largest center for BPA in France. Indications of BPA were discussed weekly by the CTEPH team for inoperable patients including distal lesions inaccessible to endarterectomy, contraindications for surgery (such as poor physical condition), and patients' refusal for surgery. In addition, we

included patients who underwent BPA after PEA for residual or persistent symptomatic pulmonary hypertension. "Rescue BPA" was defined as BPA performed during the same hospital admission as PEA, due to residual hemodynamic or respiratory instability after surgery. Angioplasty was performed as described previously,¹⁰ but without discontinuation of anti-vitamin K therapy and per-procedural addition of heparin according to patient's weight. Briefly, a catheter was introduced through the right or left femoral vein. Each procedure would begin with right heart catheterization and measurement of cardiac output using the thermodilution method, or the direct Fick method in cases of severe tricuspid regurgitation. Based on the Feinstein et al cohort, each procedure would treat 1 or 2 territories during the first sessions.

Pre-operative or pre-procedure characteristics

The institutional review board at Marie Lannelongue Hospital approved the study, which was conducted in agreement with the Helsinki II Declaration. All patients gave written informed consent. Clinical, functional, and pulmonary functional testing and biologic data available within 1 month of surgery or procedure were collected. Medical conditions that increase the risk of CTEPH were also collected, including lupus anti-coagulant, anti-phospholipid antibodies, splenectomy, myeloproliferative disorders, and endovascular devices (implantable ports for intravenous chemotherapy, ventriculoatrial shunts, and cardiac pacemakers).^{15,16} Screening for coagulation, autoimmune, and hematologic disorders was not systematic, and was left at the discretion of the referring physicians. Hemodynamics were obtained by catheterization and included mean right atrial pressure, mPAP, pulmonary artery wedge pressure (PAWP), cardiac index, and total pulmonary resistance (defined as mPAP / cardiac output). Cardiac output was measured using the thermodilution method, or the direct Fick method in cases of severe tricuspid regurgitation. Total pulmonary resistance was preferred over pulmonary vascular resistance, as PAWP was not measurable in all patients, particularly in cases of proximal obstruction.

Peri-operative characteristics and outcomes

Thrombus type and location was classified according to the Jamieson classification.¹⁷ Data pertaining to duration of cardiopulmonary bypass, aortic clamping, and need for extracorporeal membrane oxygenation assistance at the end of surgery were collected. The number of patients who underwent double-lung transplantation during the index hospitalization after PEA because of persistent PH was determined. All-cause mortality at 30 days and 90 days after non-emergent PEA (without combined cardiac surgery) was compared. Comprehensive results on post-PEA and post-BPA follow-up and outcome of our cohort are not presented here, as they will be addressed in a separate study.

Statistical analysis

Data are summarized as mean \pm standard deviation (SD) for continuous variables, and number of subjects (%) for categorical variables. Comparisons between groups were performed using 2-sided Student's *t*-tests for continuous variables according to the central limit theorem, or by chi-square test for categorical variables. Results were considered significant when 2-sided *p*-values were <0.05 . Statistical analysis was performed using SPSS version 19 (IBM SPSS, Inc., Armonk, NY).

Results

Surgical cohort

Since initiation of the BPA program, the total number of patients with confirmed CTEPH referred to our institution increased (Figure 1). Although the absolute number of patients undergoing PEA remained stable between the 2 eras, the respective proportion of patients operated among the total cohort of patients with CTEPH decreased ($p < 0.01$). Pre-operative characteristics of patients are compared in Table 1, showing similar levels of disease severity and comorbidities. Patients operated during the BPA era more frequently received prostanoids. Peri-operative characteristics are compared in Table 2. Patients in the BPA era more often had Jamieson Type 3 disease (29%) compared with patients in the pre-BPA era (18%, $p < 0.01$). Surgical procedure was slightly shorter in the BPA era even after exclusion of patients with combined cardiac procedures: cardiopulmonary bypass duration of 231 ± 38 in the pre-BPA era ($n = 222$) vs 221 ± 42 minutes in the BPA era ($n = 234$) and aortic clamping duration of 103 ± 25 vs 97 ± 23 minutes (both $p = 0.02$), whereas circulatory arrest time was not different. Duration of hospital stay was similar in the 2 groups (19.2 ± 13.9 in the pre-BPA era vs 21.1 ± 18.2 in the BPA era, $p = 0.19$). One patient from the pre-BPA era and 2 patients from the BPA era underwent urgent double-lung transplantation within 10 days of PEA for persistent PH and right heart failure.

The all-cause mortality of patients who underwent non-emergent PEA (without combined cardiac surgery) during the BPA era was 4.0% at 30 days and 4.4% at 90 days, which did not differ from the mortality of patients operated during the pre-BPA era (5.7% and 5.8%, respectively; $p =$ not statistically significant for both). The 3 main causes of death at 90 days were similar, including septic shock (50% in the BPA era vs 42% in the pre-BPA era), failure of PEA (30% vs 36%), and intracerebral hemorrhage or massive hemoptysis (10% vs 16%). During the last study year (2016, $n = 112$), 30-day mortality rate was 1.9% and 90-day mortality rate was 2.7%.

Balloon pulmonary angioplasty cohort

Since initiation of the program, 177 patients underwent BPA at our center (Figure 1). Indications for BPA were most frequently the presence of distal lesions ($n = 138$, 78.0%) and contraindication or refusal for surgery ($n = 25$, 15.8%). BPA was performed in 14 patients (7.9%), either after surgery (including 8 patients who had "rescue BPA" for hemodynamic or respiratory instability after surgery: 4 within the 72 first hours and 4 between Days 7 and 16 after PEA) or in association with surgery (in 1 patient who underwent unilateral endarterectomy after angioplasty of the other lung). Comparative pre-procedure characteristics of patients who underwent BPA or PEA are presented in Table 3. Patients who underwent surgery were younger with more severe disease as reflected by higher resistance,

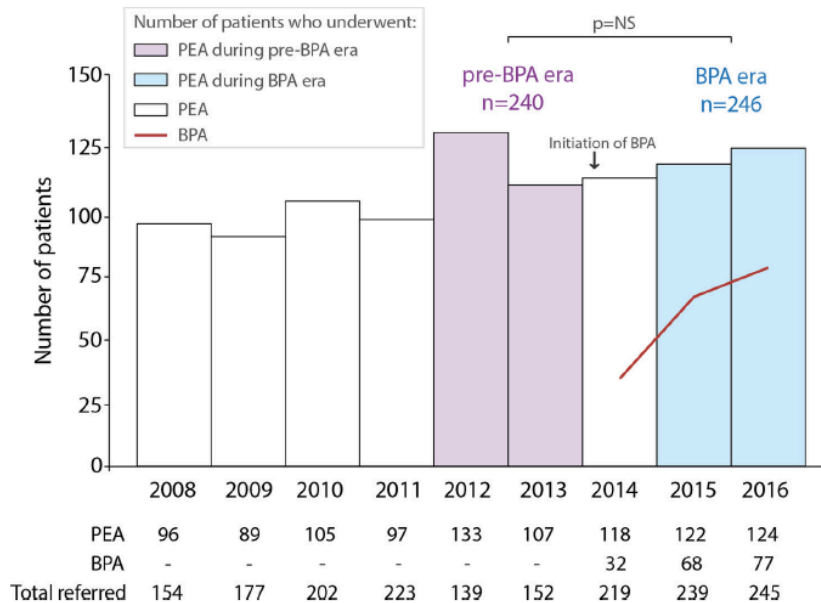


Figure 1 Number of patients with chronic thromboembolic pulmonary hypertension (CTEPH) who underwent pulmonary endarterectomy (PEA) before (pre-BPA era, in purple) and after (BPA era, in blue) initiation of angioplasty at our center. The number of patients who underwent BPA is also displayed as the red line. The total number of patients referred to the National Reference Center is also displayed. BPA, balloon pulmonary angioplasty; NS, difference not statistically significant.

lower cardiac index, and worse dyspnea class, and more frequently had renal insufficiency. In contrast, there was a higher prevalence of patients with history of splenectomy or patients with endovascular devices in patients who underwent BPA, and these latter patients more frequently underwent PH-specific therapy.

Discussion

This prospective study shows the influence of the initiation of the BPA program on the PEA program at our National Reference Center. Since initiation of the BPA program, the total number of patients with confirmed CTEPH referred to our institution increased. Although the absolute number of patients undergoing PEA remained stable between the 2 eras, the respective proportion of patients operated among the total cohort of patients with CTEPH decreased. Despite more distal forms in the BPA era than in the pre-BPA era, post-operative short-term outcomes remained stable. Overall, our experience reinforces the need for patients to be referred to expert centers and assessed by a multidisciplinary team including all experts of the field.

Our large CTEPH cohort is representative of previously published cohorts including the 2011 International Registry, as illustrated by sex-balanced patients in their sixth decade of life with a majority of them having history of acute pulmonary embolism and/or deep venous thrombosis.^{8,16,18,19}

Overall, our findings show that initiation of the BPA program has increased the number of patients with CTEPH

referred to the National Reference Center, particularly by increasing the number of patients with distal disease. This increase may also be due to the fact that several patients who were not eligible for PEA (either decided previously by the CTEPH team or by referring centers) were referred to the CTEPH team for indication of BPA as soon as the program was initiated.

Although the characteristics of patients undergoing PEA has been well reported,¹⁸ several surgical aspects can be discussed in the light of our recent cohort. The first finding is the shorter duration of cardiopulmonary bypass and aortic clamping times in the BPA era than in the pre-BPA era, although limited in terms of clinical relevance (10 and 5 minutes, respectively). The improvement in cardiopulmonary and aortic clamping times, along with the similar circulatory arrest times, can be explained by improved anesthesia environment over time, such as replacement of cold crystalloid plegia by potassium-induced cardioplegia in 2015. Interestingly, the circulatory arrest time was not different between the 2 groups, despite more distal lesions in the recent era. One could expect that complex lesions would be associated with more blood flow coming from distal pulmonary arteries. However, the relationship between the bronchial blood flow and the difficulty of surgical removal of vascular obstruction has not yet been established.

The second finding is the surprising increased proportion of patients with predominantly Jamieson Type 3 (i.e., distal) disease in the BPA era. This evolution is consistent with the evolution of another large surgical CTEPH cohort from the University of California, San Diego (UCSD), in

Table 1 Comparative Pre-operative Characteristics of Patients With CTEPH Who Underwent Pulmonary Endarterectomy in the Pre-BPA and BPA Era

	Pre-BPA era (n = 240)	BPA era (n = 246)	p-value
Age (years)	61.4 ± 15.0	60.0 ± 14.2	0.29
Female sex (%)	119 (49.6)	116 (47.2)	0.60
Body mass index (kg/m ²)	26.2 ± 4.8	26.7 ± 5.6	0.24
Body surface area (m ²)	1.83 ± 0.24	1.86 ± 0.23	0.14
History of deep venous thrombosis (%)	98 (40.8)	95 (38.6)	0.62
History of acute pulmonary embolism (%)	159 (66.3)	197 (80.1)	<0.01 ^a
Inferior vena cava filter (%)	10 (4.2)	3 (1.2)	0.04 ^a
Presence of endovascular device (%)	7 (2.9)	8 (3.3)	0.80
Implantable port (%)	4 (1.7)	5 (2.0)	0.81
Pacemaker (%)	3 (1.3)	3 (1.2)	0.92
Ventricular–arterial derivation (%)	0	0	—
History of splenectomy (%)	5 (2.1)	4 (1.6)	0.68
History of recent (<5 years) cancer (%)	12 (5.0)	9 (3.7)	0.48
Thrombophilia or blood disorder (%)	27 (11.3)	46 (18.7)	0.03 ^a
including anti-phospholipids antibodies (%)	10 (4.2)	7 (2.8)	0.40
NYHA Class III or IV (%)	183 (76.3)	179 (72.7)	0.15
6-minute walk test distance (m)	377 ± 118 (n = 128)	367 ± 124 (n = 111)	0.51
Hemodynamics			
Right atrial pressure (mm Hg)	7.7 ± 4.7	8.6 ± 4.4	0.05
Mean PAP (mm Hg)	44.9 ± 12.2	45.9 ± 11.7	0.36
PAWP (mm Hg)	9.3 ± 11.1 (n = 114)	10.0 ± 3.8 (n = 200)	0.41
Cardiac index (liters/min/m ²)	2.5 ± 0.6	2.5 ± 0.7	0.25
Total pulmonary resistance (WU)	10.3 ± 4.2	10.9 ± 4.9	0.18
Total pulmonary resistance index (WU/m ²)	18.6 ± 7.0	19.8 ± 8.2	0.10
Pulmonary functional tests			
FEV ₁ (%)	87.9 ± 21.3 (n = 224)	85.2 ± 18.1 (n = 219)	0.15
DLCO (%)	65.3 ± 15.7 (n = 157)	62.7 ± 17.6 (n = 159)	0.18
Resting PaO ₂ (mm Hg)	65.7 ± 13.5 (n = 191)	67.4 ± 12.9 (n = 165)	0.21
Echocardiography			
Left ventricular ejection fraction (%)	62.4 ± 8.4	61.6 ± 7.1	0.26
Left ventricular ejection fraction <45%	8 (3.3)	5 (2.0)	0.37
Biologic data			
Creatinine clearance (ml/min)			
≥60 ml/min	146 (60.8)	170 (69.1)	0.06
59 to 30 ml/min	92 (38.3)	76 (30.9)	
<30 ml/min	2 (0.8)	0	
Pulmonary hypertension–specific therapies			
Treatment naïve (%)	197 (82.1)	217 (88.2)	0.06
Double therapy (%)	15 (6.3)	9 (3.7)	0.19
Triple therapy (%)	0	3 (1.2)	0.09
Prostanoid therapy (%)	1 (0.4)	11 (4.5)	<0.01 ^a
Phosphodiesterase inhibitors (%)	21 (8.8)	9 (3.7)	0.02 ^a
Endothelin receptor blockers (%)	37 (15.4)	16 (6.5)	<0.01 ^a
Riociguat (%)	0	8 (3.3)	<0.01 ^a

Data are presented as mean and standard deviation or number and percent, and compared using *t*-test or chi-square test, respectively. Not all data were available for all variables. DLCO, diffusing capacity of the lung for carbon monoxide; FEV₁, forced expiratory volume in 1 second; LVEF, left ventricular ejection fraction; NYHA, New York Heart Association; PaO₂, partial pressure of oxygen; PAP, pulmonary arterial pressure; PAWP, pulmonary arterial wedge pressure.

^a*p* < 0.05 (statistically significant).

which the proportion of patients with Type 3 disease was 28% in the first half of 2000s and 39% in the second half (*p* < 0.01).²⁰ In our study, the increase in patients with distal disease operated may also reflect an increase in the referral of patients with CTEPH to our National Reference Center since the development of another interventional therapy. Indeed, patients who may have previously been

considered as distal, and thus not indicated for surgery by the primary or secondary center, were evaluated by the multidisciplinary team and subjected to PEA. The dichotomy between proximal and distal lesions still relies on the landmark post-operative classification established by Jamieson et al.¹⁸ Recently, there has been increased demand for a more “anatomical” classification that could

Table 2 Comparative Peri-operative Characteristics of Patients With CTEPH Who Underwent Endarterectomy in the Pre-BPA and BPA Era

	Pre-BPA era (n = 240)	BPA era (n = 246)	p-value
Emergent endarterectomy (%)	5 (2.1)	6 (2.4)	0.82
Associated cardiac procedures ^a (%)	18 (7.5)	12 (4.9)	0.23
Jamieson classification			
Group 1 (%)	13 (5.4)	10 (4.1)	0.50
Group 2 (%)	177 (73.7)	160 (65.0)	0.04 ^b
Group 3 (%)	42 (17.5)	70 (28.5)	<0.01 ^b
Group 4 (%)	8 (3.3)	6 (2.4)	0.55
Cardiopulmonary bypass duration (min)	231.4 ± 37.9	223.3 ± 42.3	0.03 ^b
Aortic clamping duration (min)	104.7 ± 26.6	99.2 ± 24.5	0.02 ^b
Circulatory arrest duration (min)	31.1 ± 11.5	30.4 ± 11.7	0.54
Need of extracorporeal support after surgery (%)	16 (6.7)	28 (11.4)	0.07
Including veno-venous extracorporeal support (%)	3 (1.3)	3 (1.2)	0.92
Post-surgical embolization of bronchial artery (%)	10 (4.2)	9 (3.7)	0.78

Data are presented as mean and standard deviation or number and percent, and compared using *t*-test or chi-square test, respectively.

^aIncluding coronary artery bypass graft or aortic valve replacement procedures.

^b*p* < 0.05 (statistically significant).

Table 3 Comparative Characteristics of Patients With CTEPH Subjected to PEA or BPA From 2014 to 2016

	PEA (n = 364)	BPA (n = 177)	p-value
Age (years)	60.4 ± 13.9	63.8 ± 13.9	<0.01 ^a
Female sex (%)	177 (48.6)	80 (45.2)	0.46
Body mass index (kg/m ²)	26.7 ± 5.5	25.5 ± 5.4	0.05
Body surface area (m ²)	1.85 ± 0.22	1.80 ± 0.24	0.05
History of acute pulmonary embolism or deep venous thrombosis (%)	311 (85.4)	147 (83.1)	0.49
Presence of endovascular device (%)	11 (3.0)	21 (11.9)	<0.01 ^a
Implantable port (%)	10 (2.7)	15 (8.5)	<0.01 ^a
Pacemaker (%)	3 (0.8)	3 (1.7)	0.35
Ventriculoatrial shunt (%)	0 (0)	1 (0.6)	0.14
History of splenectomy (%)	5 (1.4)	17 (9.6)	<0.01 ^a
Thrombophilia or blood disorder (%)	64 (17.6)	19 (10.7)	0.04 ^a
Including antiphospholipids antibodies (%)	13 (3.6)	8 (4.5)	0.61
NYHA Class III or IV (%)	271 (74.5)	116 (65.5)	0.03 ^a
6-minute walk test distance (m)	371 ± 124 (n = 152)	396 ± 115 (n = 125)	0.08
Hemodynamics			
Right atrial pressure (mmHg)	8.8 ± 4.6	8.6 ± 4.1	0.74
Mean PAP (mm Hg)	45.6 ± 11.9	44.7 ± 10.0	0.42
Cardiac index (liters/min/m ²)	2.5 ± 0.6	2.8 ± 0.7	<0.01 ^a
Total pulmonary resistance (WU)	10.9 ± 4.9	9.4 ± 3.1	<0.01 ^a
Total pulmonary resistance index (WU/m ²)	19.8 ± 8.4	16.8 ± 5.1	<0.01 ^a
Biologic data			
CrCl (ml/min)	71.6 ± 21.2	78.6 ± 20.3	<0.01 ^a
Renal failure (CrCl <60 ml/min)	122 (33.4)	43 (24.3)	0.03 ^a
Pulmonary hypertension-specific therapies			
Treatment naive (%)	322 (88.5)	94 (53.1)	<0.01 ^a
Prostanoid therapy (%)	12 (3.3)	10 (2.7)	0.71
Phosphodiesterase inhibitors (%)	19 (5.2)	44 (24.9)	<0.01 ^a
Endothelin receptor blockers (%)	28 (7.7)	58 (32.8)	<0.01 ^a
Riociguat (%)	8 (2.2)	20 (8.2)	<0.01 ^a

Data are presented as mean and standard deviation or number and percentage, and compared using *t*-test or chi-square test respectively. BPA, balloon pulmonary angioplasty; CrCl, creatinine clearance; NYHA, New York Heart Association; PAP, pulmonary arterial pressure; PEA, pulmonary endarterectomy.

^a*p* < 0.05 (statistically significant).

be easily translated to non-invasive pre-operative imaging, such as multiple-detector computed tomography. In 2017, Madani and colleagues proposed a preliminary classification aiming to better define the localization of lesions and identifying the degree of difficulty in surgical resection.⁶ Although the present cohort used the Jamieson classification as initially designed in the registry, we would consider prospectively including the UCSD classification. Finally, despite operating on more patients with distal lesions in the second period, our results show stability in short-term outcomes with PEA.

Another aspect of our study is the comparison of patients who underwent PEA or BPA during the same period. In contrast to results from the CTEPH international registry of 679 patients (published in 2011 before the emergence and spread of BPA) showing similar clinical and hemodynamic severity of operable (62.9% of patients) and non-operable patients,⁸ our cohort identified patients with BPA to be less symptomatic and have lower resistance and better cardiac index than those subjected to surgery. Several possibilities can be cited to explain the finding of better hemodynamics in our BPA cohort than in the contemporary PEA cohort: less severe disease or less vascular occlusion, but also higher prevalence of PH-specific therapy in those subjected to BPA. Indeed, in our study, half of the patients with BPA received at least one PH-specific medical therapy compared with one quarter of those with PEA. Several trials have reported the effect of PH-specific medical therapy in improving pulmonary vascular resistance and cardiac output in patients with inoperable CTEPH.²¹ In 2008, the BENEFIT (Bosentan Effects in iNoperable Forms of chronic Thromboembolic pulmonary hypertension) randomized, placebo-controlled trial showed that bosentan reduced pulmonary vascular resistance by more than 20% at 16 weeks from baseline (-24.1% [-31.5% to -16.0%], $p < 0.001$), improved cardiac index (0.3 [0.14 to 0.46] liters/min, $p < 0.001$), whereas it did not significantly improve mPAP (-2.5 [-5.0 to 0.0] mm Hg, $p = 0.07$).²² More recently, the CHEST-1 (Chronic Thromboembolic Pulmonary Hypertension Soluble Guanylate Cyclase–Stimulator Trial 1) trial reported improvement in the secondary endpoint of pulmonary vascular resistance at 16 weeks in patients who received riociguat (-246 [-303 to -190] dyne/s/cm⁵, $p < 0.001$) as compared with those receiving placebo, which was associated with both an improvement in mPAP (-5 [-7 to -3] mm Hg, $p < 0.001$) and cardiac output (0.9 [0.6 to 1.1] liters/min, $p < 0.001$).²³

Our BPA cohort also confirms differential rates of associated conditions and risk factors in non-surgical vs surgical patients with CTEPH. Consistent with the 2011 registry, associated conditions including thrombophilic disorders were documented in more patients subjected to PEA (17.6% in our cohort) than those subjected to BPA (10.7%). However, this rate remains lower than previously described rates,^{8,24} which may be partially underestimated by the fact that screening for coagulation, autoimmune, and hematologic disorders was left at the discretion of the referring physicians. The higher rate of blood disorder predisposition in patients operated during the BPA era may suggest

increased awareness on those factors and more frequent screening. The high rate of splenectomy in our BPA cohort is also consistent with previous reports that have shown the link between asplenia and increased prevalence of thromboembolic events and PH.^{25,26} Interestingly, a history of splenectomy was 7 times more frequent in patients subjected to BPA (up to 10%) than for PEA, reflecting more distal non-surgical forms as well as potential comorbidities. Investigators have hypothesized that, after splenectomy, impaired erythrocyte metabolism or abnormal platelet activation may trigger the formation of more distal in situ thromboembolic lesions.^{25,26} The higher prevalence of endovascular device use in patients with BPA than in operated patients (such as implantable ports) also suggests a link with more distal lesions, either because of comorbidities such as recent cancer reflecting hypercoagulability state or potential repeated embolization of microthrombi by intravascular material. A recent study has highlighted the potential additional role of Staphylococci infection of those microthrombi promoting misguided thrombus resolution by enhancing fibrotic vascular remodeling after thrombosis.^{26,27}

Clinical implications

The originality of our National Reference Center for PH, reflected by this large study, is our 3-part expertise in CTEPH (i.e., surgical expertise for decades, angioplasty expertise as the larger center performing BPA in our country, within the National Reference Center for PH providing the latest up-to-date medical management). This enables a direct comparison of the profile of a large contemporary population referred for surgery or angioplasty, as well as the study of the evolution of epidemiology over time in the last 5 years (in contrast to most registry studies of CTEPH reflecting the practices of the late 1990s or 2000s). Our findings suggest that development of angioplasty has enabled targeting a distinct slightly older population presenting with distal forms and/or contraindication for surgery. As stated by Jenkins et al in their recent review, the classification of patients as operable or inoperable becomes less relevant in the era of BPA as patients may benefit from the 2 treatment modalities in the course of their disease on top of medical therapy.⁶

Limitations

The first limitation of this study is its monocentric tertiary design; however, the cohort studied is from the National Reference Center for PH representing the totality of patients referred for PEA in France and more than half of the patients who underwent BPA during this period. A second limitation is the absence of consensual criteria to define inoperability (i.e., absence of specific risk scores such as the Euroscore for cardiac surgery, difficulty in assessing patients' frailty, and the potential recovery of the right heart) and to define non-accessible lesions for surgical removal. This highlights the importance of an expert

CTEPH team, including a specialized surgeon and an interventionalist, within a high-volume center to consensually decide for therapeutic indications. Finally, because right heart-targeted echocardiography was not available for all patients, we could not compare the right heart component of the patients' assessment. Until recently, cardiac function was mainly routinely assessed by invasive metrics such as cardiac index, and emerging data show the importance of assessing right heart function and remodeling as prognostic factors in patients with PH.²⁸⁻³¹

In conclusion, this study has shown the influence of the initiation of the BPA program on the PEA program at our National Reference Center. Despite the increased complexity of PEA surgery on the basis of more distally located obstructions, short-term outcomes have remained stable. This snapshot reflects the early stage of BPA implementation in the field of CTEPH and it can be expected that, over time, and with the development of medical therapy (such as riociguat), indications of surgery and/or angioplasty will evolve toward more complementarity. These results further strengthen the need for patients to be referred to centers in which indications are decided by a multidisciplinary team including interventional cardiologists, surgeons, PH experts, and specialized radiologists.

Disclosure statement

The authors have no conflicts of interest to disclose.

The prospective endarterectomy registry was funded by a grant from the Programme Hospitalier de Recherche Clinique National 2009 of the French Ministry of Health (RCB 2009-A0098057). M.A., J.G., J.A., L.L., F.H., O.M., E.F., and P.B. are supported by a public grant overseen by the French National Research Agency as part of the second Investissements d'Avenir program (ANR-15-RHUS-0002).

The authors thank Sylvette Mottet (Marie Lannelongue Hospital) and Laurence Rottat (Kremlin Bicêtre Hospital) for assistance with data collection.

References

- Lang IM, Pesavento R, Bonderman D, Yuan JX-J. Risk factors and basic mechanisms of chronic thromboembolic pulmonary hypertension: a current understanding. *Eur Respir J* 2013;41:462-8.
- Guérin L, Couturaud F, Parent F, et al. Prevalence of chronic thromboembolic pulmonary hypertension after acute pulmonary embolism. Prevalence of CTEPH after pulmonary embolism. *Thromb Haemost* 2014;112:598-605.
- Langer NB, Darteville P, Fadel E. Chronic pulmonary emboli. In: *General thoracic surgery*. Shields, in press.
- Mercier O, Arthur Ataam J, Langer NB, et al. Abnormal pulmonary endothelial cells may underlie the enigmatic pathogenesis of chronic thromboembolic pulmonary hypertension. *J Heart Lung Transplant* 2017;36:305-14.
- Simonneau G, Torbicki A, Dorfmueller P, et al. The pathophysiology of chronic thromboembolic pulmonary hypertension. *Eur Respir Rev*, in press.
- Jenkins D, Madani M, Fadel E, et al. Pulmonary endarterectomy in the management of chronic thromboembolic pulmonary hypertension. *Eur Respir Rev* 2017;26:160111.
- Galiè N, Humbert M, Vachiery J-L, et al. ESC/ERS Guidelines for the diagnosis and treatment of pulmonary hypertension: the Joint Task Force for the Diagnosis and Treatment of Pulmonary Hypertension of the European Society of Cardiology (ESC) and the European Respiratory Society (ERS): endorsed by: Association for European Paediatric and Congenital Cardiology (AEPC), International Society for Heart and Lung Transplantation (ISHLT). *Eur Heart J* 2016;37:67-119.
- Pepke-Zaba J, Delcroix M, Lang I, et al. Chronic thromboembolic pulmonary hypertension (CTEPH): results from an international prospective registry. *Circulation* 2011;124:1973-81.
- Feinstein JA, Goldhaber SZ, Lock JE, et al. Balloon pulmonary angioplasty for treatment of chronic thromboembolic pulmonary hypertension. *Circulation* 2001;103:10-3.
- Inami T, Kataoka M, Shimura N, et al. Pulmonary edema predictive scoring index (PEPSI), a new index to predict risk of reperfusion pulmonary edema and improvement of hemodynamics in percutaneous transluminal pulmonary angioplasty. *JACC Cardiovasc Interv* 2013;6:725-36.
- Mizoguchi H, Ogawa A, Munemasa M, et al. Refined balloon pulmonary angioplasty for inoperable patients with chronic thromboembolic pulmonary hypertension. *Circ Cardiovasc Interv* 2012;5:748-55.
- Sugimura K, Fukumoto Y, Satoh K, et al. Percutaneous transluminal pulmonary angioplasty markedly improves pulmonary hemodynamics and long-term prognosis in patients with chronic thromboembolic pulmonary hypertension. *Circ J* 2012;76:485-8.
- Aoki T, Sugimura K, Tatebe S, et al. Comprehensive evaluation of the effectiveness and safety of balloon pulmonary angioplasty for inoperable chronic thrombo-embolic pulmonary hypertension: long-term effects and procedure-related complications. *Eur Heart J* 2017;38:3152-9.
- Darteville P, Fadel E, Mussot S, et al. Chronic thromboembolic pulmonary hypertension. *Eur Respir J* 2004;23:637-48.
- Wolf M, Boyer-Neumann C, Parent F, et al. *Eur Respir J* 2000;15:395-9.
- Bonderman D, Wilkens H, Wakounig S, et al. Risk factors for chronic thromboembolic pulmonary hypertension. *Eur Respir J* 2009;33:325-31.
- Thistlethwaite PA, Mo M, Madani MM, et al. Operative classification of thromboembolic disease determines outcome after pulmonary endarterectomy. *J Thorac Cardiovasc Surg* 2002;124:1203-11.
- Jamieson SW, Kapelanski DP, Sakakibara N, et al. Pulmonary endarterectomy: experience and lessons learned in 1,500 cases. *Ann Thorac Surg* 2003;76:1457-62.
- Condliffe R, Kiely DG, Gibbs JSR, et al. Improved outcomes in medically and surgically treated chronic thromboembolic pulmonary hypertension. *Am J Respir Crit Care Med* 2008;177:1122-7.
- Madani MM, Auger WR, Pretorius V, et al. Pulmonary endarterectomy: recent changes in a single institution's experience of more than 2,700 patients. *Ann Thorac Surg* 2012;94:97-103.
- Pepke-Zaba J, Ghofrani H-A, Hoeper MM. Medical management of chronic thromboembolic pulmonary hypertension. *Eur Respir Rev* 2017;26.
- Jais X, D'Armini AM, Jansa P, et al. Bosentan for treatment of inoperable chronic thromboembolic pulmonary hypertension: BENEFIT (Bosentan Effects in iNopEtable Forms of chronic Thromboembolic pulmonary hypertension), a randomized, placebo-controlled trial. *J Am Coll Cardiol* 2008;52:2127-34.
- Ghofrani H-A, Galiè N, Grimminger F, et al. Riociguat for the treatment of pulmonary arterial hypertension. *New Engl J Med* 2013;369:330-40.
- Bernard J, Yi ES. Pulmonary thromboendarterectomy: a clinicopathologic study of 200 consecutive pulmonary thromboendarterectomy cases in one institution. *Hum Pathol* 2007;38:871-7.
- Hoeper MM, Niedermeier J, Hoffmeyer F, et al. Pulmonary hypertension after splenectomy? *Ann Intern Med* 1999;130:506-9.
- Jais X, Ioss V, Jardim C, et al. Splenectomy and chronic thromboembolic pulmonary hypertension. *Thorax* 2005;60:1031-4.
- Bonderman D, Jakowitsch J, Redwan B, et al. Role for staphylococci in misguided thrombus resolution of chronic thromboembolic pulmonary hypertension. *Arterioscler Thromb Vasc Biol* 2008;28:678-84.

28. Haddad F, Hunt SA, Rosenthal DN, et al. Right ventricular function in cardiovascular disease, part I: Anatomy, physiology, aging, and functional assessment of the right ventricle. *Circulation* 2008;117:1436-48.
29. Haddad F, Doyle R, Murphy DJ, et al. Right ventricular function in cardiovascular disease, part II: Pathophysiology, clinical importance, and management of right ventricular failure. *Circulation* 2008;117:1717-31.
30. Vonk Noordegraaf A, Haddad F, Bogaard HJ, et al. Noninvasive imaging in the assessment of the cardiopulmonary vascular unit. *Circulation* 2015;131:899-913.
31. Amsallem M, Sweatt AJ, Aymami MC, et al. Right heart end-systolic remodeling index strongly predicts outcomes in pulmonary arterial hypertension: comparison with validated models. *Circ Cardiovasc Imaging* 2017;10:pii:e005771.

Experimental Studies

Early Development of Right Ventricular Ischemic Lesions in a Novel Large Animal Model of Acute Right Heart Failure in Chronic Thromboembolic Pulmonary Hypertension

DAVID BOULATE, MD,¹ JENNIFER ARTHUR ATAAM, PhD,¹ ANDREW J. CONNOLLY, MD,² GENEVIEVE GIRALDEAU, MD,³ MYRIAM AMSALLEM, MD,^{1,2} BENOIT DECANTE, MSc,¹ LILIA LAMRANI, RN,¹ ELIE FADEL, MD, PhD,¹ PETER DORFMULLER, MD,¹ FREDERIC PERROS, PhD,⁴ FRANCOIS HADDAD, MD,^{2,*} AND OLAF MERCIER, MD, PhD^{1,*}

Le Plessis-Robinson, France; Stanford, California; and Montreal, Canada

ABSTRACT

Background: Our aim was to develop a model of acute right heart failure (ARHF) in the setting of pulmonary hypertension and to characterize acute right ventricular lesions that develop early after hemodynamic restoration.

Methods and Results: We used a described piglet model of chronic pulmonary hypertension (cPH) induced by pulmonary artery occlusions. We induced ARHF in animals with cPH (ARHF-cPH group, n = 9) by volume loading and iterative acute pulmonary embolism until hemodynamic compromise followed by dobutamine infusion for hemodynamic restoration before sacrifice for right ventricular tissue evaluation. The median duration of ARHF before sacrifice was 162 (135–189) minutes. Although ventriculoarterial coupling (measured with multibeat pressure-volume loops) and stroke volume decreased after iterative pulmonary embolism and improved with dobutamine, relative pulmonary to systemic pressure increased by 2-fold and remained similarly increased with dobutamine. Circulating high-sensitivity troponin I increased after hemodynamic restoration. We found an increase in right ventricular subendocardial and subepicardial focal ischemic lesions and in expression of autophagy-related protein LC3-II (Western blot) in the ARHF-cPH group compared with the cPH (n = 5) and control (n = 5) groups.

Conclusions: We developed and phenotyped a novel large animal model of ARHF on cPH in which right ventricular ischemic lesions were observed early after hemodynamic restoration. (*J Cardiac Fail* 2017;23:876–886)

Key Words: Right ventricle, pulmonary hypertension, ischemia, autophagy.

Right ventricular (RV) myocardial injury is a prognosis factor in different diseases such as acute pulmonary hypertension (PH) or chronic pulmonary hypertension (cPH).^{1–4} Acute right heart failure (ARHF) in patients with PH is a dis-

tinct clinical entity associated with poor short-term prognosis. Sztrymf et al reported the in-hospital mortality of patients with PH developing ARHF to be 41%.⁵ Similarly, Haddad et al reported a 90-day rate of death or transplantation of 38% and Campo et al a 46% rate of in-hospital mortality when these patients required catecholamine infusion.^{6,7} Myocardial damage in patients with ARHF may be linked with myocardial infarction as observed in acute pulmonary embolism (PE) or to a demand ischemia favored by catecholamine use and increased afterload.⁸ To date, myocardial damage has not been clearly studied in the setting of ARHF occurring in patients with chronic PH (cPH). Furthermore, autophagy may be implicated early in cardiomyocyte damage in ARHF because autophagy was reported to be activated within minutes of myocardial ischemia and after ischemia-reperfusion, which are conditions implicated in the pathophysiology of ARHF in

From the ¹Research and Innovation Unit, Université Paris-Sud, Hôpital Marie Lannelongue, Le Plessis-Robinson, France; ²Cardiovascular Institute, Stanford University, Stanford, California; ³Institut de Cardiologie de Montréal, Montreal, Quebec, Canada and ⁴INSERM U999, Hôpital Marie Lannelongue, Le Plessis-Robinson, France.

Manuscript received March 4, 2017; revised manuscript received June 25, 2017; revised manuscript accepted August 1, 2017.

Reprint requests: David Boulate, MD, Research and Innovation Unit, Hôpital Marie Lannelongue, 133 avenue de la Résistance, 92350 Le Plessis-Robinson, France. Tel: +33 0140942501. E-mail: d.boulate@ccml.fr.

*These authors contributed equally to the work.

1071-9164/\$ - see front matter

© 2017 Elsevier Inc. All rights reserved.

<https://doi.org/10.1016/j.cardfail.2017.08.447>

patients with cPH.^{9,10} Indeed, RV ischemia related lesions can develop because of a decreased RV perfusion pressure and ischemia-reperfusion injury can develop after hemodynamic restoration with inotropes. These damages to the right ventricle may explain the poor short-term prognosis of patients with ARHF on cPH despite initial hemodynamic restoration with inotropes.

To date, few studies have focused on acute RV lesions that may develop in the setting of ARHF in cPH. For this study, we choose to focus on the earliest RV lesions that may develop after hemodynamic restoration (ie, within 2–3 hours). This early period allows focus on ischemia and ischemia-reperfusion-related injuries. We previously developed a model of chronic thromboembolic PH in pigs by ligation of the left main pulmonary artery followed by iterative, progressive right lower lobe artery embolism with biological glue in which chronic RV adaptation was described.^{11,12} For this study we managed to reproduce major pathophysiological features observed in patients with ARHF in cPH, namely a preexistent cPH, an acute volume and pressure overload inducing hemodynamic compromise, and a phase of hemodynamic restoration with dobutamine.

Our first objective was to describe acute longitudinal changes in a new model of ARHF in PH by using echocardiography and invasive hemodynamics including RV pressure-volume loops and circulating biomarkers phenotyping. Our second objective was to describe the earliest RV lesions that may develop within few hours after hemodynamic restoration in the setting of ARHF in cPH. We hypothesized that RV ischemic lesions and signs of autophagy and apoptosis may be observed early after hemodynamic restoration. We compared the cardiac tissues of the ARHF on cPH model (ARHF-cPH) harvested 2–3 hours after hemodynamic restoration with dobutamine with the cardiac tissues of animals with compensated cPH and non-PH controls harvested in resting conditions.

Methods

Animal Model

The study complied with the principles of laboratory animal care according to the National Society for Medical

Research and was approved by the local ethics committee for animal experiments at Hospital Marie Lannelongue.

cPH Model

We induced cPH in 14 piglets (large white pigs, 6 weeks old) by extrapericardial left pulmonary artery ligation at week 0 followed by weekly embolization of the right lower lobe pulmonary artery with embucrylate (Histoacryl, B Braun Medical, France) between week 1 and week 6 and 1 embolization at week 10. This model of cPH corresponds to a model of thromboembolic PH and was previously described by our group.¹² For this study, we induced ARHF with hemodynamic restoration at week 16 in 9 of these animals with cPH (ARHF-cPH group). We sacrificed the 5 animals with cPH only at week 16 for cardiac tissue comparison (see groups for RV tissue comparison described in the following section).

Induction of ARHF

We first induced a volume overload by progressive infusion of 60 mL/kg of saline infusion over 2 hours because volume overload is an important pathophysiological feature of ARHF in cPH. Furthermore, volume loading allowed us to determine the adaptive RV phenotype of the model at rest and after volume challenge. Volume loading was performed under diuresis monitoring with a percutaneous vesical catheter. The volume-loading phase was followed by iterative PE every 2 minutes (0.15 mL embucrylate per bolus) until obtaining preestablished criteria of hemodynamic compromise (ie, left ventricular [LV] systolic pressure <90 mmHg or a ratio of RV systolic pressure over LV systolic pressure >0.9). After induction of hemodynamic compromise, we started dobutamine infusion at a dose of 2.5 $\mu\text{g}/\text{kg}^{-1}/\text{min}^{-1}$ and increased the infusion dose to 7.5 $\mu\text{g}/\text{kg}^{-1}/\text{min}^{-1}$. We evaluated ARHF longitudinally using right heart catheterization, multibeat RV pressure-volume loops with inferior vena cava occlusion, echocardiography, and blood samples harvesting at baseline, after the volume loading phase, after hemodynamic compromise criteria were reached secondary to iterative PE, and after each dose of dobutamine infusion (Fig. 1). Cardiac tissues were harvested for pathology and Western blot analysis at the

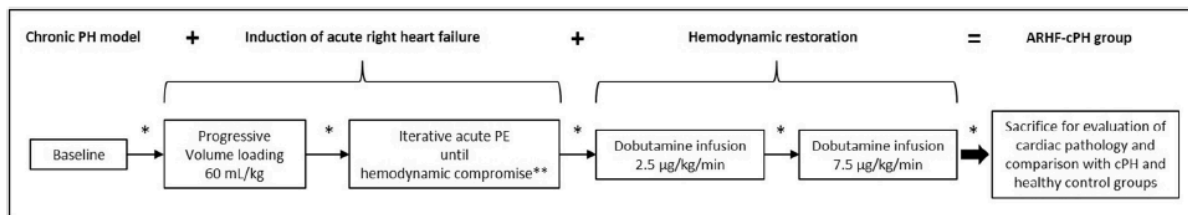


Fig. 1. Protocol for induction of acute right heart failure in chronic pulmonary hypertension followed by hemodynamic restoration. *Evaluation of hemodynamics, right ventricular pressure-volume loops, HS-troponin I, and echocardiography. **0.15 mL of embucrylate per embolus; hemodynamic compromise was defined by a left ventricular systolic pressure <90 mmHg or a systolic right ventricular pressure over systolic left ventricular pressure ratio >0.9. ARHF, acute right heart failure; cPH, chronic pulmonary hypertension; PE, pulmonary embolism.

end of the protocol were undertaken as described in the tissue harvesting method section.

Measurements in Animals

Hemodynamics and RV Pressure—Volume Loops. Animals were anesthetized as previously described.¹³ Right heart catheterization was performed with a Swan-Ganz catheter (thermal dilution catheter; 5 French; Edwards Lifesciences Corporation, Irvine, CA). We measured LV pressures using a fluid-filled catheter positioned in the left ventricle. We acquired the multibeat RV pressure-volume loops with a conductance catheter (Venti-Cath, Millar Instrument, Houston, TX) positioned in the right ventricle (Powerlab 16/35 and LabChart pro software v7.3.7, AD instrument, Bella Vista, Australia) through a jugular vein. Calibrations of pressures and volumes were performed according to the manufacturer's instruction using Millar's MPVS ultra system. External stroke volume (SV) calibration was performed using Swan-Ganz catheter-derived SV. Hemodynamic data were recorded and analyzed secondarily by author D.B. (blinded from pathological and biological findings) to determine the RV end-systolic elastance (Ees), the pulmonary arterial elastance (Ea) and the right ventricle–pulmonary artery coupling (Ees/Ea ratio). The RV Ees was the slope of the linear regression of end-systolic pressure-volume relationship during inferior vena cava (IVC) occlusion; pulmonary artery (PA) Ea was the ratio of RV end-systolic pressure (RVESP) over SV; the RV-PA coupling was the ratio Ees/Ea (Fig. S1). End-systolic pressure-volume relationship regressions were performed by the least squares method using at least 5 manually determined end-systolic (corresponding to T wave) pressure-volume couples during IVC occlusion. Each Ees value was the mean derived from 2 IVC occlusions. For each regression, if R^2 was <0.90 or if the difference between 2 values of the same condition exceeded 10%, a third occlusion was analyzed and the two closest values were used.

Echocardiography. We acquired cardiac images using an echocardiograph Vivid 9 with a 5S probe (GE Healthcare, Fairfield, CT) as previously described.^{13,14} The imaging protocol consisted of parasternal long- and short-axis views and an apical 5-chambers view because the 4-chamber view is not reliably acquired in pigs. Each acquisition was in 2-dimensional and tissue Doppler imaging modes. Transvalvular flows were acquired in continuous and pulsed Doppler modes. Each view was acquired during 3 beats in the end-expiratory period. Images were stored in cine loop format and analyzed offline with a GE EchoPAC workstation by a cardiologist (G.G.), accordingly to the current guidelines, while blinded to other parameters. On the apical view, we quantified the morphologic parameters RV end-systolic and end-diastolic areas and the functional parameters RV fractional area change, tricuspid annular plane systolic excursion, systolic pulsed-wave tissue Doppler pic velocity of the free-wall insertion of the tricuspid valve (S' wave). We quantified the LV functional parameters LV ejection fraction on the apical view, and on the transaortic outflow pulsed

Doppler spectrum, the RV ejection time (RVET) and RVET over RR interval ratio (RVET/RR), which are prognostic indices in patients with ARVF in cPH.¹⁵ We also quantified the indices of interventricular interaction LV end-systolic and end-diastolic eccentricity index that are the ratio of the LV diameters (perpendicular to septum over parallel to septum measured on the parasternal short-axis view).

Circulating Biomarkers. Blood samples (EDTA tubes) were centrifuged at 1500 g for 10 minutes. Plasma samples were stored at -80°C . Plasma levels of circulating biomarkers Hs-troponin I, NT-proBNP, and interleukin-6 (IL-6) were measured using a pig-specific (*sus scrofa*) sandwich enzyme-linked immunosorbent assay according to the manufacturer's instructions (CS-Bio, Menlo Park, CA).

RV Tissue Comparison in Animal Models

Groups for RV Tissue Evaluation. The 5 pigs with cPH without ARHF (cPH group) and 5 other non-PH pigs (control group) matched for age were evaluated at week 16 in baseline conditions with right heart catheterization and then sacrificed for tissue harvesting and pathological evaluation. The 9 pigs in the ARHF-cPH group were sacrificed at the end of the protocol for tissue harvesting (Fig. 1).

Tissue Harvesting and Coloration. Under general anesthesia, a longitudinal sternotomy was performed. RV free wall and LV free wall samples were harvested after a hyperpotassic cardioplegia in all groups; 2 samples (2 cm length) of mid-RV free wall and LV free wall were immediately snap frozen and stored at -80°C or placed into formalin and paraffin embedded. RV samples were stained with hematein-eosin-saffron.

Pathological Analysis of Cardiac Lesions. We first qualitatively identified RV lesions that were present in RV samples stained with HES. We observed 2 kinds of quantifiable lesions: (1) focal ischemic lesions corresponding to clusters of hyper eosinophilic cardiomyocytes with pyknotic nucleus surrounded by cardiomyocytes with intracytoplasmic vacuolization; these lesions were present in subendocardial and subepicardial RV layers; and (2) scattered lesions corresponding to isolated cardiomyocytes with hyper eosinophilia and pyknotic nuclei that were observed in the mid-RV layer. Because these lesions were not present in the LV samples, we did not quantify LV lesions.

RV pathological lesions were quantified in subendocardial, subepicardial, and mid-layers in the 3 animal groups by D.B. while blinded from group, hemodynamic, functional, and biologic data. Ischemic lesions were verified and validated independently by cardiac pathologist A.C. We quantified the pathological lesions of 2 free wall samples per ventricle (in a 2-cm length stained with hematein-eosin-saffron).

Western Blot. Western blots were performed on frozen samples from RV and LV free wall from the 3 animal groups to compare autophagy using antibodies to microtubule-associated protein 1A/1B light chain 3-phosphatidyletanolamine conjugate (LC3-II) and apoptosis using antibodies to cleaved caspase 3. RV and LV biopsies

were lysed and sonicated in RIPA buffer supplemented with protease/phosphatase inhibitor cocktail. Following incubation for 45 minutes on ice, the lysate was obtained by centrifugation at 4000 g for 10 minutes at 4°C. Protein concentration of lysates was determined by BCA protein assay kit (Thermo Scientific, Rockford, IL); 20 µg of total proteins were separated on 4–20% sodium dodecyl sulfate-polyacrylamide gel electrophoresis gels (Criterion, Biorad). Proteins were transferred to polyvinylidene difluoride membranes (Hybond, Amersham) and blocked for 1 hour at room temperature with 5% nonfat dry milk in Tris-buffered saline and 0.5% Tween 20. Incubation with specific primary antibodies: LC3 II (Abcam), cleaved caspase 3 (Abcam), and GAPDH (Fischer Scientific) were performed in blocking buffer overnight at 4°C. Horseradish peroxidase-conjugated anti-IgG was used as secondary antibody. Immunoreactive bands were detected by ECL chemiluminescent substrate (Perkin Elmer). Membrane stripping was done by incubating the membrane in Restore Western blot stripping buffer (Thermo Scientific) according to the manufacturer's instructions.

Statistics

We expressed quantitative data as median and interquartile range except when specified. We compared quantitative data using nonparametric Mann-Whitney rank tests for unpaired data and Wilcoxon matched-pairs signed rank test for paired data. Differences with $P < .05$ were considered significant. Statistics were performed using Graphpad prism 6 (GraphPad software, Inc, San Diego, CA).

Results

Longitudinal Analysis of the ARHF Model

ARHF Model. Volume loading alone did not induce hemodynamic compromise criteria in any of the 9 cPH pigs but rather increased systemic pressure and cardiac output (Fig. 2). Diuresis was preserved in all animals during the volume-loading period (between 0.17 and 0.22 mL/kg⁻¹/min⁻¹). After iterative PE, the hemodynamic compromise criteria were reached in each of the 9 animals. Two animals died immediately after iterative PE and 1 required an epinephrine bolus before dobutamine infusion, precluding imaging and hemodynamic acquisitions in this animal at the hemodynamic compromise time point. The number of iterative acute PE necessary to reach the hemodynamic compromise criteria was 1 in 1 animal that died immediately, 2 in 2 animals, 3 in 5 animals, and 4 in 1 animal that died immediately. The median duration between the last PE and the start of dobutamine infusion was 18^{13,15-23} minutes; the median duration of dobutamine infusion was 144 (120–165) minutes. At the end of the protocol, 7 of 9 animals (78%) had survived. We analyzed the cardiac samples of the 7 animals that fulfilled the protocol; the tissue analysis of 1 of these animals was not feasible because of poor quality. Gross cardiac examination of the 2 dead animals revealed acute thrombosis of the right heart cavities, explaining the irreversible RV failure.

Hemodynamics and RV Pressure Volume Loops.

Longitudinal hemodynamic and invasive RV function evaluations are shown in Fig. 3A. Briefly, volume loading did not modify the mean pulmonary artery pressure (MPAP) over mean arterial pressure (MAP) ratio or the ventriculoarterial coupling (Ees/Ea ratio) compared with baseline (both $P = NS$), whereas the cardiac output increased ($P < .05$). Among survivors, iterative PE more than doubled the MPAP/MAP ratio (220%, $P < .05$), decreased the Ees/Ea ratio by 57%, and decreased the cardiac output by 31% compared with baseline (both $P < .05$). Maximal dose dobutamine did not modify the MPAP/MAP ratio compared with post-PE values (114%; $P = NS$), whereas Ees/Ea more than tripled (314%; $P < .05$), reaching baseline values (125%; $P = NS$). Dobutamine also doubled the cardiac output after PE (207%, $P < .05$).

Echocardiography During ARHF. After dobutamine infusion imaging analysis showed persistent end-systolic and end-diastolic RV dilation as well as persistent flattened interventricular septum (increased eccentricity index) (Table 1 and Fig. 3B), RV functional parameters (RV fractional area change, tricuspid annular plane systolic excursion, and S' wave) were not significantly different from baseline levels (all $P = NS$). LV ejection fraction was preserved and LV ejection time decreased after dobutamine infusion (both $P < .05$).

Circulating Biomarkers. Plasma HS-troponin I significantly increased in ARHF-cPH piglets after volume loading, dobutamine 2.5, and dobutamine 7.5 compared with baseline (all $P = .03$) and significantly increased between volume loading and dobutamine 7.5 ($P = .03$). NT-proBNP did not change significantly, whereas IL-6 significantly increased at the end of the protocol compared with baseline ($P < .05$) (Fig. S2). These results suggest that myocardial damage may be detected at the earliest stage of hemodynamic restoration with infusion of dobutamine without prior increase in NT-proBNP.

RV Lesions Comparison

Group Characteristics. ARHF-cPH and c-PH groups were not different in baseline conditions at week 16 in terms of weight, MPAP, right atrial pressure, and cardiac output (all $P = NS$, Table 1). As expected, ARVF-cPH and cPH groups had increased MPAP and total pulmonary resistances compared with controls (both $P < .05$; Table 2).

RV Histopathology. Ischemic cardiomyocytes were identified by combined nuclear pyknosis and cytoplasmic hyper eosinophilia. Clusters of ischemic cardiomyocytes were usually surrounded by vacuolated cardiomyocytes, as is typical of noncritical ischemia in peri-ischemic zones. We observed a significant increase in subendocardial and subepicardial focal ischemic lesions per 2 cm RV free wall section in the ARHF-cPH group (4.5 [2.75,5.75]) compared with cPH group (1.0 [0.25,1.75]; $P = .014$) and the control group (2.0 [0,2.0], $P = .048$), Fig. 4. The number of scattered isolated ischemic cardiomyocytes in the mid-RV layer

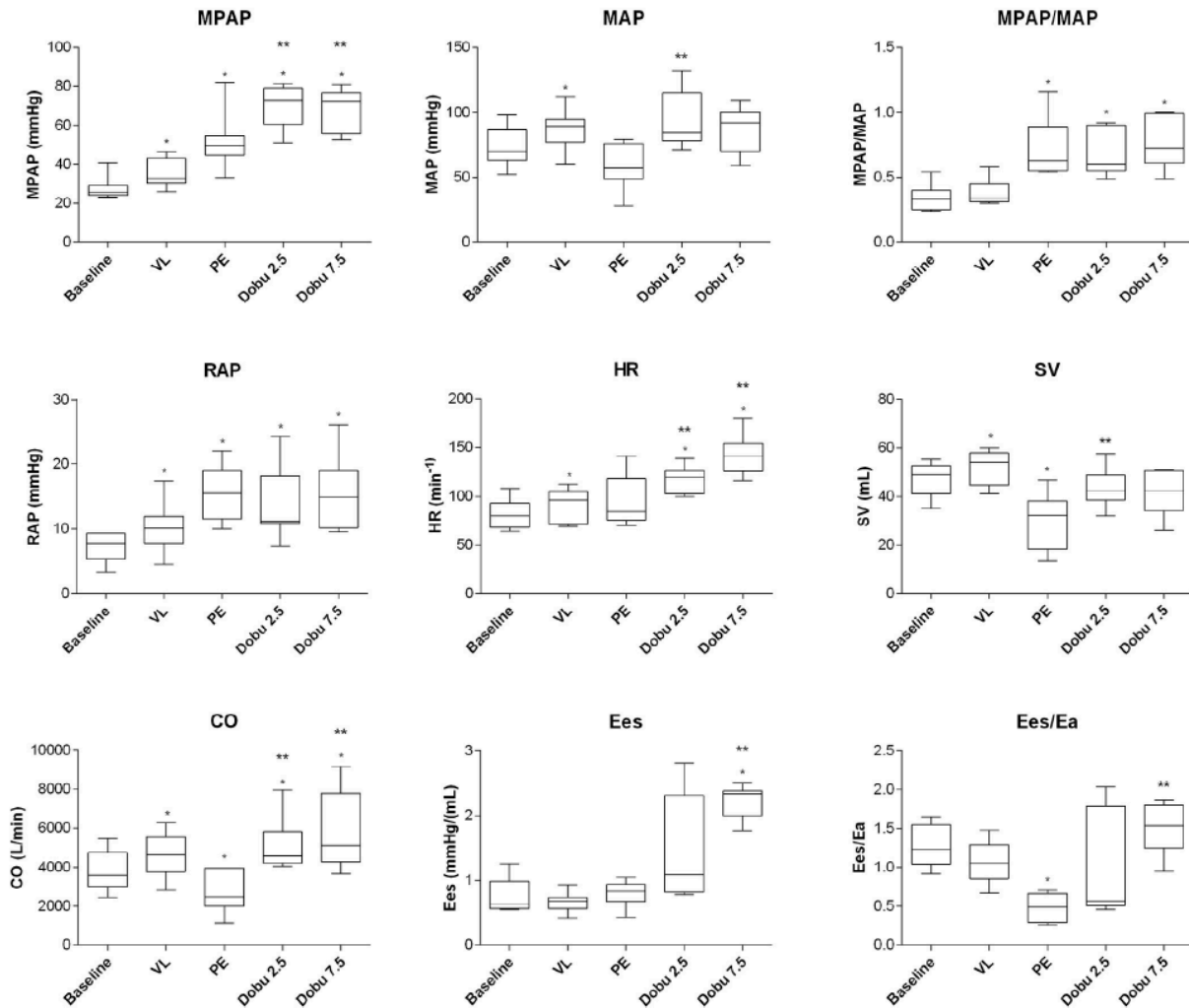


Fig. 2. Hemodynamics and pressure-volume loops derived parameters of the ARHF model. CO, cardiac output; Ea, pulmonary artery elastance; Ees, end-systolic elastance; Ees/Ea, right-ventricular-pulmonary artery coupling; HR, heart rate; MAP, mean blood pressure; MPAP, mean pulmonary artery pressure; RAP, right atrial pressure; SV, stroke volume. Scatter boxes show median, interquartile range, and extreme values. * $P < .05$ compared with baseline value; ** $P < .05$ compared with postpulmonary embolism (PE) value.

was significantly increased in ARHF-cPH (1 [0,2]) compared with control (0 [0,1]; $P = .029$) and cPH groups (1.75 [0.5,1.75]; $P = .62$).

Autophagy and Apoptosis. We completed Western blot analysis of autophagy and apoptosis markers in right and left ventricles in the 3 animal groups (Fig. 5). The marker of autophagy, LC3-II, was significantly increased in right ventricles of ARVF-cPH group compared with control (3.50-fold, $P = .008$) and cPH group (2.63-fold, $P = .003$). The marker of apoptosis, cleaved caspase 3, was significantly increased in the right ventricles of the cPH ($P = .032$) and ARHF-cPH group ($P = .017$) compared with the control group, whereas there was no significant difference in cleaved caspase 3 content between cPH and ARHF-cPH groups ($P = .18$).

Discussion

In this study, we showed the feasibility to induce ARHF in a large animal model with cPH. We described the sequential changes in hemodynamic and functional imaging that occur in this condition including early after hemodynamic restoration with dobutamine that correspond to a particular clinical entity. With a low dose of dobutamine, the increase in cardiac output was due to the increase in stroke volume, whereas for a higher dose of dobutamine, the chronotropic effect was prevalent for the increase in cardiac output. This model was an opportunity to capture the earliest RV lesions that may develop after hemodynamic restoration with dobutamine. We qualitatively described and quantified the subendocardial and subepicardial ischemic lesions that developed during the

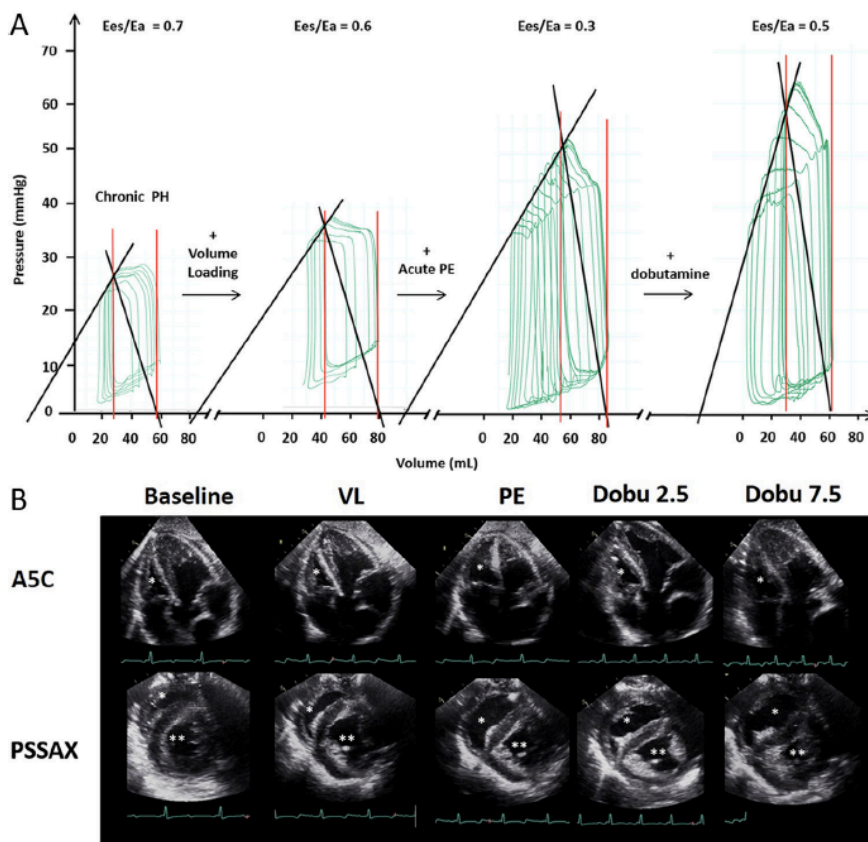


Fig. 3. (A) Example of families of right ventricular pressure-volume loops during inferior vena cava occlusion showing acute changes in ventriculoarterial coupling (Ees/Ea), right ventricular pressures and volumes during the main steps of the protocol reproducing acute right ventricular failure with hemodynamic restoration. Black lines are Ees and Ea; red lines are end-systolic volume and end-diastolic volume. (B) Representative end-systolic echocardiographic features during induction of ARHF and hemodynamic restoration. Upper row: representative apical 5-chamber view (A5C) showing the RV end-systolic enlargement (*) developing between baseline and acute pulmonary embolism (PE) that tends to remain with dobutamine infusion. Lower row: parasternal short axis view (PSSAX) in the same animal showing the enlargement of the right ventricle (*) after PE associated with a D-shaped left ventricle (**) concordant with the increased LV eccentricity index. VL, volume loading.

Table 1. Longitudinal Echocardiographic Values During Induction of Acute Right Heart Failure and Hemodynamic Restoration

	Baseline (n = 9)	Volume Loading (n = 9)	Pulmonary Embolism (n = 6)	Dobutamine 2.5 (n = 7)	Dobutamine 7.5 (n = 7)
Right ventricle					
RVEDA (cm ²)	8.6 (7.7,11.3)	10.9 (9.1,12.9)*	17.2 (14.1,20.2)*	11.2 (9.5,14.8)*	12.6 (9.5,15.1)*
RVESA (cm ²)	5.5 (4.3,6.5)	6.2 (6.0,7.7)*	12.0 (9.7,13.9)*	6.8 (6.0,10.7)*	8.1 (6.2,10.9)*
RVFAC (%)	38 (30,50)	43 (34,46)	29 (27,34)	35 (29,40)	34 (20,39)
TAPSE (mm)	15 (14,18)	20 (19,23)*	12 (6,15)	14 (10,18)	10 (8,18)
S' wave (cm/s)	6.0 (5.0,8.0)	7.0 (7.0,7.0)	4.5 (4.0,5.5)	6.0 (3.5,15.5)	12.5 (5.5,15.8)
Left ventricle					
LVEF (%)	67 (60,74)	61 (59,70)	68 (62,78)	65 (59,73)	75 (68,84)
LVET (ms)	313 (297,348)	347 (334,418)*	295 (226,333)	219 (208,284)*	142 (124,187)*
LVET/RR	0.40 (0.39,0.44)	0.52 (0.50,0.57)*	0.41 (0.39,0.44)	0.45 (0.42,0.47)	0.40 (0.26,0.41)
EIs	1.00 (0.95,1.04)	1.05 (0.99,1.14)	1.59 (1.29,1.83)*	1.55 (1.25,1.93)*	1.81 (1.58,2.82)*
EId	1.00 (0.96,1.03)	1.02 (1.00,1.06)	1.20 (1.20,1.68)*	1.22 (1.06,1.50)	1.22 (1.07,1.56)*

Values are median (interquartile range).

EId, diastolic eccentricity index; EIs, systolic eccentricity index; LVEF, left ventricular ejection fraction; LVET, left ventricular ejection time; LVET/RR, LVET over RR interval ratio; RVEDA, right ventricular end diastolic diameter; RVESA, right ventricular end systolic diameter; RVFAC, right ventricular fractional area change; S' wave, peak velocity of the free wall tricuspid insertion; TAPSE, tricuspid annular plan systolic excursion.

*P < .05 compared with baseline values using Wilcoxon matched-pairs signed rank test.

Table 2. Morphological and Hemodynamic Parameters of the 3 Animal Groups

	Control (N = 5)	cPH (N = 5)	ARHF-cPH	
			Baseline (N = 9)	After Hemodynamic Restoration (End Protocol) (N = 7)
Weight (kg)	32.0 (31.0,36.5)	39.5 (34.5,40.0)	36.5 (33.0,37.0)	—
MPAP (mmHg)	14 (13,15)	25 (24,38)*	26 (24,29)*	72 (56,77) [†]
RAP (mmHg)	6 (4,7)	10 (8,11)	7 (6,8)	15 (10,19) [†]
CO (L/min)	3.5 (3.1,3.9)	4.1 (3.4,5.8)	3.6 (3.0,4.6)	5.1 (4.3,7.8) [†]
TPR (WU)	4.3 (3.6,4.8)	6.5 (5.5,8.2)*	7.4 (6.3,9.6)*	11 (10,17) [†]

Values are median (interquartile range).
 CO, cardiac output; MPAP, mean pulmonary artery pressure; PH, pulmonary hypertension; RAP, mean right atrial pressure; TPR, total pulmonary resistance; WU, Wood unit.
 **P* < .05 compared with control group.
[†]*P* < .05 compared with baseline values of the same group.

earliest phase (a few hours) after hemodynamic restoration, which was confirmed by concomitant troponin elevation. The original contribution of our study is the description of the first model of ARHF in cPH; this model represents an extreme course of acute decompensation of RV function in cPH. Right heart lesions have been previously described in acute PE as well as in cPH conditions; in this study, we charac-

terized RV lesions in the setting of ARHF in patients with PH.¹⁶⁻²⁰

The phenotyping of hemodynamic worsening and restoration provided interesting results for monitoring critical patients with PH. The ARHF on cPH model was characterized by an increased MPAP/MAP ratio that did not change during the restoration of the cardiac output with dobutamine.

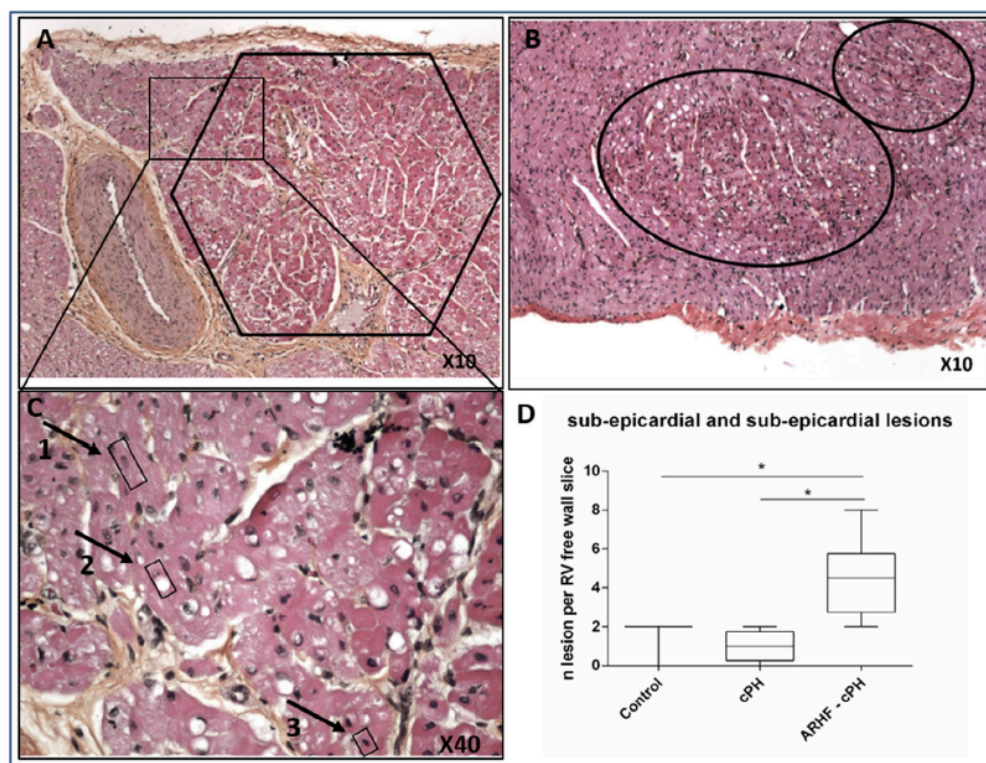


Fig. 4. Example and quantification of right ventricular focal ischemic lesions in subendocardial and subepicardial (hematein-eosin-saffron stain). (A) representative view of a subepicardial focal ischemic lesion (hexagonal area; ×10 magnification). (B) representative view of a subendocardial focal ischemic lesion (oval areas; ×10 magnification). (C) Border of a focal ischemic lesion (magnification ×40) showing 3 concentric layers: (1) normal cardiomyocyte, (2) vacuolated cardiomyocytes in the peri-ischemic zone, (3) ischemic cardiomyocytes with pyknotic nuclei and hyper-eosinophilic cytoplasm. (D) Comparison of the number of right ventricular free wall focal ischemic lesions in the 3 groups. Values expressed as median, interquartile range, and extreme values; **P* < .05.

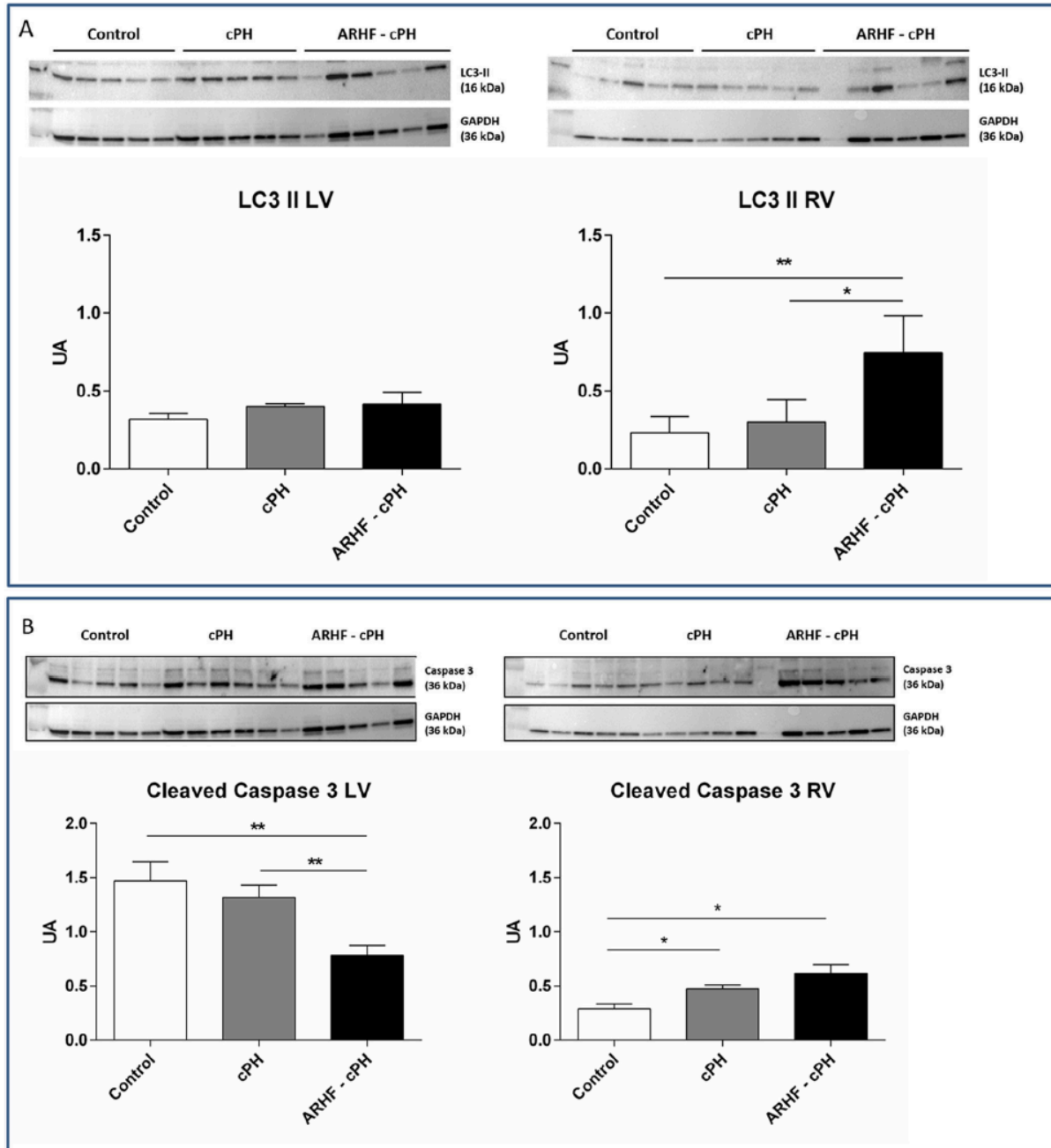


Fig. 5. Quantification of myocardial proteins related to activation of autophagy and apoptosis the 3 groups with western blot. (A) Autophagy activation-related protein LC3 II quantification (mean, standard error of the mean) in right ventricles (RV) and left ventricles (LV) in the 3 groups. (B) Apoptosis activation-related protein quantification cleaved caspase 3 in RV and LV in the 3 groups. Values are mean, standard error of the mean; * $P < .05$.

As a consequence, the pulmonary to systemic pressure ratio and surrogates may be interesting to characterize severity of patients with ARHF in cPH independently from cardiac output. The pulmonary to systemic pressure ratio was previously found to be an independent predictor of outcomes in patients un-

dergoing cardiac surgery.²¹ Conversely, the ventriculoarterial coupling (Ees/Ea) and the cardiac output can change significantly with dobutamine. As a consequence, ventriculoarterial coupling and cardiac output variations may better reflect responsiveness to catecholamine. As noted previously, we

observed an increase in SV only for low-dose dobutamine, whereas the increase in cardiac output for higher doses of dobutamine resulted from the chronotropic effect of dobutamine. This is an important observation because dobutamine may promote inflammation and apoptosis, whereas other methods may be used to increase the heart rate to increase cardiac output.²² As expected, during the ARHF phase, the Ees/Ea ratio, a marker of ventriculoarterial coupling, was decreased, whereas Ees, a marker of ventricular contractility, was conserved. This supports previous findings showing that surrogates of RV pulmonary artery coupling may be a better phenotype of right heart function compared with indices of ventricular contractility.¹³

This model provided the opportunity to describe RV pathological lesions that may develop within the first hours of an ARHF in cPH after hemodynamic restoration, a situation observed in patients with cPH who present with ARHF. We found focal lesions located in the subepicardial and subendocardial layers of the right ventricle that were confirmed by the concomitant increase in circulating HS-troponin I, a marker of myocardial necrosis. The increase in circulating troponin is concordant with pathological lesions and thus improves the internal validation of the pathological findings. Also, the lack of increase in NT-proBNP was concordant with the decrease in RV dilation immediately after dobutamine infusion, which provides further internal validation of the dynamic phenotyping. The late and low increase in the inflammatory marker IL-6 did not permitted us to capture an early inflammatory systemic response in our model. The focal ischemic lesions were characterized by a core of hypereosinophilic cardiomyocytes with pyknotic nuclei, a common early pathologic feature of ischemic cardiomyocytes. These lesions were specifically observed in the right ventricles, which contrasted with the lack of observed ischemic lesions in left ventricles. We did not observe transmural myocardial infarction as described in patients dying from massive acute PE despite normal coronary arteries.^{8,23} Based on our findings, it is not possible to determine whether these RV lesions may play a role in secondary worsening of RV function and hemodynamics because we reported the characteristics of the earliest phase after hemodynamic restoration during which hemodynamics and RV function remained preserved. Future studies should determine whether RV function and hemodynamic worsening would develop later in this model as observed in clinical practice. Also, a prolonged observation of the model could help to determine whether other factors than ischemia may lead to secondary RV function worsening such as inflammation or other types of cardiomyocyte death as apoptosis.

By using Western blot analysis, we observed an early increase in the autophagy-related protein LC3 II in the right ventricle of the ARHF-cPH model, whereas we were not able to observe a simultaneous acute increase in apoptosis using activated caspase 3. Because there was no increase in LC3 II in the left ventricle, we conclude that the increase in LC3 II in the right ventricle was due to the succession of volume and pressure overload—hemodynamic compromise and he-

modynamic restoration—and not to the prolonged fasting for the protocol. Conversely, we were not able to detect an acute increased activity of RV apoptosis by using activated caspase-3 semiquantification with Western blot. Interestingly, activated caspase-3 was increased in both ARHF-cPH and cPH groups compared with healthy controls, suggesting a chronic increase in apoptosis secondary to cPH. The lack of evidence of early increase in apoptosis in our ARHF model should be balanced with the early evaluation of the RV proteins in our protocol. Apoptosis is a transient phenomenon in which cellular vesicles are rapidly cleared; consequently, acute accumulation of apoptotic proteins may require a massive process of apoptosis that may not be the case of our model at the evaluation time. We hypothesize that apoptosis quantification could show increased value at a more delayed timeline after hemodynamic restoration. Autophagy is a cytoplasmic mechanism playing a role in immediate response to energy depletion and oxidative stress such as during early stages of cardiac ischemia and ischemia-reperfusion.^{24,25} Autophagy is a well-preserved intracytoplasmic vesicular process that allows the degradation of intracytoplasmic damaged proteins and organelles within a few minutes in situations of energy depletion or oxidative stress.^{9,26} The autophagic process consists of the formation of a double-membrane vesicle autophagosome that incorporates damaged proteins or organelles. The double-membrane autophagosome fusions with lysosomes, inducing protein degradation and recycling. During the autophagosome formation, the soluble LC3-I proteins turns into the LC3-II by phosphatidylethanolamine conjugation. LC3-II is covalently linked to the autophagosome double membrane and is therefore a marker of autophagy activation.²⁷ The beneficial or detrimental role of autophagy in acute myocardial stress as currently discussed in the literature may be linked either with promotion of cardiomyocyte survival during acute stress or with abnormal long-term remodeling. For instance, Sala-Mercado et al reported that autophagy was activated (increased LC3-II and beclin-1 myocardial content) in myocardium after 45 minutes of coronary artery occlusion followed by 3 hours of reperfusion in swine.²⁸ Furthermore, they showed that promotion of autophagy with chloramphenicol was associated with a reduced infarction size. Our data are consistent with these findings; we found an increase of LC3-II in the right ventricle after mean 20 minutes of hemodynamic compromise with ARVF followed by hemodynamic restoration with inotropes.

The implications of our study are relative to the monitoring of patients with ARHF with preexisting cPH admitted to the intensive care unit. The ratio of pulmonary to systemic pressure may represent an interesting parameter to evaluate the hemodynamic severity of patients because it is not significantly modified by cardiac output changes after dobutamine infusion. Our findings suggest that an early increase in troponin may be a marker of focal ischemic lesions despite hemodynamic restoration achieved with inotropes. This suggests that further increase in troponin may signify an extension of the RV ischemic lesions, particularly in case of persistent pressure overload associated with increased energetic demand

with dobutamine infusion. Recent studies have suggested that mechanical unloading after myocardial infarction reduced infarction size.²⁹ Consequently, increasing mechanical load with dobutamine in case of existing ischemic lesions may lead to more myocardial injury in patients with ARHF with preexisting PH. Finally, autophagy activation seems to be implicated early in the acutely stressed right ventricle. This merits more study to determine the role of autophagy as it may emerge as a prognosis indices or a therapeutic target.

We acknowledge several limits to our study. Our model is a key model of acute PE on compensated chronic thromboembolic PH and not a model of acute decompensation of severe cPH. Our model represents extreme pathophysiological conditions but provided insights into monitoring and specific RV lesions. We acknowledge that autophagy and apoptosis quantification in right ventricles would require further evaluation and are presented in this study as preliminary data.

Conclusion

We describe a new model of ARHF on compensated cPH reproducing the main pathophysiological conditions that are observed in clinical practice. This may help to improve patient monitoring and provides an opportunity to further understand RV dysfunction in patients managed in intensive care unit.

Supplementary Data

Supplementary data related to this article can be found online at doi:10.1016/j.cardfail.2017.08.447.

References

- Torbicki A, Kurzyrna M, Kuca P, Fijalkowska A, Sikora J, Florczyk M, et al. Detectable serum cardiac troponin T as a marker of poor prognosis among patients with chronic precapillary pulmonary hypertension. *Circulation* 2003;108:844–8.
- Pruszczyk P, Bochowicz A, Torbicki A, Szulc M, Kurzyrna M, Fijalkowska A, et al. Cardiac troponin T monitoring identifies high-risk group of normotensive patients with acute pulmonary embolism. *Chest* 2003;123:1947–52.
- Zelniker T, Uhlmann L, Spaich S, Friedrich J, Preusch MR, Meyer FJ, et al. Novel biomarkers for risk stratification in pulmonary arterial hypertension. *ERJ Open Res* 2015;1:00008-2015 [pii].
- Giannitsis E, Muller-Bardorff M, Kurowski V, Weidtmann B, Wiegand U, Kampmann M, et al. Independent prognostic value of cardiac troponin T in patients with confirmed pulmonary embolism. *Circulation* 2000;102:211–7.
- Sztrymf B, Souza R, Bertolotti L, Jais X, Sitbon O, Price LC, et al. Prognostic factors of acute heart failure in patients with pulmonary arterial hypertension. *Eur Respir J* 2010;35:1286–93.
- Haddad F, Peterson T, Fuh E, Kudelko KT, de Jesus Perez V, Skhiri M, et al. Characteristics and outcome after hospitalization for acute right heart failure in patients with pulmonary arterial hypertension. *Circ Heart Fail* 2011;4:692–9.
- Campo A, Mathai SC, Le Pavec J, Zaiman AL, Hummers LK, Boyce D, et al. Outcomes of hospitalisation for right heart failure in pulmonary arterial hypertension. *Eur Respir J* 2011;38:359–67.
- Coma-Canella I, Gamallo C, Martinez Onsurbe P, Lopez-Sendon J. Acute right ventricular infarction secondary to massive pulmonary embolism. *Eur Heart J* 1988;9:534–40.
- Kuma A, Hatano M, Matsui M, Yamamoto A, Nakaya H, Yoshimori T, et al. The role of autophagy during the early neonatal starvation period. *Nature* 2004;432:1032–6.
- Kanamori H, Takemura G, Goto K, Maruyama R, Tsujimoto A, Ogino A, et al. The role of autophagy emerging in postinfarction cardiac remodelling. *Cardiovasc Res* 2011;91:330–9.
- Boulate D, Perros F, Dorfmueller P, Arthur-Ataam J, Guihaire J, Lamrani L, et al. Pulmonary microvascular lesions regress in reperfused chronic thromboembolic pulmonary hypertension. *J Heart Lung Transplant* 2015;34:457–67.
- Guihaire J, Haddad F, Noly PE, Boulate D, Decante B, Dartevielle P, et al. Right ventricular reserve in a piglet model of chronic pulmonary hypertension. *Eur Respir J* 2015;45:709–17.
- Guihaire J, Haddad F, Boulate D, Decante B, Denault AY, Wu J, et al. Non-invasive indices of right ventricular function are markers of ventricular-arterial coupling rather than ventricular contractility: insights from a porcine model of chronic pressure overload. *Eur Heart J Cardiovasc Imaging* 2013;14:1140–9.
- Rudski LG, Lai WW, Afilalo J, Hua L, Handschumacher MD, Chandrasekaran K, et al. Guidelines for the echocardiographic assessment of the right heart in adults: a report from the American Society of Echocardiography endorsed by the European Association of Echocardiography, a registered branch of the European Society of Cardiology, and the Canadian Society of Echocardiography. *J Am Soc Echocardiogr* 2010;23:685–713.
- Sztrymf B, Gunther S, Artaud-Macari E, Savale L, Jais X, Sitbon O, et al. Left ventricular ejection time in acute heart failure complicating precapillary pulmonary hypertension. *Chest* 2013;144:1512–20.
- Zhao LB, Jia ZY, Lu GD, Zhu YS, Jing L, Shi HB. Establishment of a canine model of acute pulmonary embolism with definite right ventricular dysfunction through introduced autologous blood clots. *Thromb Res* 2015;135:727–32.
- Lee JH, Chun YG, Lee IC, Tudor RM, Hong SB, Shim TS, et al. Pathogenic role of endothelin 1 in hemodynamic dysfunction in experimental acute pulmonary thromboembolism. *Am J Respir Crit Care Med* 2001;164:1282–7.
- Kudlicka J, Mlcek M, Hala P, Lacko S, Janak D, Hrachovina M, et al. Pig model of pulmonary embolism: where is the hemodynamic break point? *Physiol Res* 2013;62:S173–9.
- Ryan JJ, Huston J, Kutty S, Hatton ND, Bowman L, Tian L, et al. Right ventricular adaptation and failure in pulmonary arterial hypertension. *Can J Cardiol* 2015;31:391–406.
- Tudor RM, Archer SL, Dorfmueller P, Erzurum SC, Guignabert C, Michelakis E, et al. Relevant issues in the pathology and pathobiology of pulmonary hypertension. *J Am Coll Cardiol* 2013;62(25 Suppl):D4–12.
- Robitaille A, Denault AY, Couture P, Belisle S, Fortier A, Guertin MC, et al. Importance of relative pulmonary hypertension in cardiac surgery: the mean systemic-to-pulmonary artery pressure ratio. *J Cardiothorac Vasc Anesth* 2006;20:331–9.
- Adamopoulos S, Parissis JT, Iliodromitis EK, Paraskevaidis I, Tsiapras D, Farmakis D, et al. Effects of levosimendan versus dobutamine on inflammatory and apoptotic pathways in acutely decompensated chronic heart failure. *Am J Cardiol* 2006;98:102–6.
- Jerjes Sanchez C, Gutierrez-Fajardo P, Ramirez-Rivera A, Garcia-Mollinedo Mde L, Hernandez Chavez G. [Acute infarct of the right ventricle secondary to a massive pulmonary thromboembolism]. *Arch Inst Cardiol Mex* 1995;65:65–73.
- Hamacher-Brady A, Brady NR, Gottlieb RA. Enhancing macroautophagy protects against ischemia/reperfusion injury in cardiac myocytes. *J Biol Chem* 2006;281:29776–87.

25. Matsui Y, Takagi H, Qu X, Abdellatif M, Sakoda H, Asano T, et al. Distinct roles of autophagy in the heart during ischemia and reperfusion: roles of AMP-activated protein kinase and Beclin 1 in mediating autophagy. *Circ Res* 2007;100:914–22.
26. Riehle C, Wende AR, Sena S, Pires KM, Pereira RO, Zhu Y, et al. Insulin receptor substrate signaling suppresses neonatal autophagy in the heart. *J Clin Invest* 2013;123:5319–33.
27. Tanida I, Ueno T, Kominami E. LC3 and autophagy. *Methods Mol Biol* 2008;445:77–88.
28. Sala-Mercado JA, Wider J, Undyala VV, Jahania S, Yoo W, Mentzer RM Jr, et al. Profound cardioprotection with chloramphenicol succinate in the swine model of myocardial ischemia-reperfusion injury. *Circulation* 2010;122(11 Suppl):928242.
29. Saku K, Kakino T, Arimura T, Sakamoto T, Nishikawa T, Sakamoto K, et al. Total mechanical unloading minimizes metabolic demand of left ventricle and dramatically reduces infarct size in myocardial infarction. *PLoS ONE* 2016;11:e0152911.

SUPPLEMENTARY ARTICLE 6

REVIEW



Right heart imaging in patients with heart failure: a tale of two ventricles

Myriam Amsallem^a, Tatiana Kuznetsova^b, Kate Hanneman^c, Andre Denault^d, and François Haddad^a

Purpose of review

The purpose is to describe the recent advances made in imaging of the right heart, including deformation imaging, tissue, and flow characterization by MRI, and molecular imaging.

Recent findings

Recent developments have been made in the field of deformation imaging of the right heart, which may improve risk stratification of patients with heart failure and pulmonary hypertension. In addition, more attention has been given to load adaptability metrics of the right heart; these simplified indices, however, still face challenges from a conceptual point of view. The emergence of novel MRI sequences, such as native T1 mapping, allows better detection and quantification of myocardial fibrosis and could allow better prediction of postsurgical recovery of the right heart. Other advances in MRI include four-dimensional flow imaging, which may be particularly useful in congenital heart disease or for the detection of early stages of pulmonary vascular disease.

Summary

The review will place the recent developments in right heart imaging in the context of clinical care and research.

Keywords

coupling, heart failure, imaging, pulmonary hypertension, right heart

INTRODUCTION

In the past 3 decades, significant progress has been made in the imaging of the right heart. One of the most important changes has been the greater awareness given to right heart function in both clinical and research settings [1]. In this review, we will highlight recent innovations in the field of right heart imaging, including myocardial deformation imaging, three-dimensional and three-dimensional time-resolved flow MRI, as well as molecular imaging. These recent developments will be placed in the context of how right heart imaging can improve the management of heart failure and pulmonary hypertension. The value of right heart imaging in the setting of congenital heart disease or cardiac surgery is beyond the scope of the current review and has recently been reviewed [2^{*,3*}].

RIGHT AND LEFT HEART: IS THERE A REAL DISTINCTION?

Although the separation between the right and left heart has a clear anatomical and embryological

basis, it does not reflect the complexity of the structural and functional relationships and interactions between the heart and the circulation. Anatomically, the right (RV) and left (LV) ventricles are strongly connected through the septum and myofiber architecture [4]. Because of the functional interactions between the ventricles, interpretation of RV performance should always be made in the context of LV function and vice versa. In the absence

^aDivision of Cardiovascular Medicine, Stanford University School of Medicine, Stanford, California, USA, ^bResearch Unit Hypertension and Cardiovascular Epidemiology, Department of Cardiovascular Sciences, University of Leuven, Leuven, Belgium, ^cDepartment of Medical Imaging, Toronto General Hospital, University of Toronto, Toronto, Ontario and ^dDepartment of Anesthesiology and Critical Care Division, Centre hospitalier de l'Université de Montréal and Montreal Heart Institute, Montreal, Quebec, Canada

Correspondence to François Haddad, MD, Division of Cardiovascular Medicine, Stanford University School of Medicine, 300 Pasteur Drive, Stanford, 94305 CA, USA. Tel: +1 415 770 4279; e-mail: fhaddad@stanford.edu

Curr Opin Cardiol 2016, 31:469–482
DOI:10.1097/HCO.0000000000000315

KEY POINTS

- Although having an anatomic and embryological basis, the separation between the right and the left ventricles is in part physiologically artificial.
- Myocardial deformation imaging has gathered strong interest in imaging of the right heart; future studies will need to assess its value compared with end-systolic metrics.
- Load-adaptability metrics can help answer the question of ‘proportionality’ of ventricular adaptation to pulmonary hypertension.
- RV myocardial fibrosis can be detected using MRI LGE and T1 mapping; three-dimensional time-resolved flow MRI is a promising tool for blood flow quantification.
- Molecular imaging, such as PET, provides information on the RV metabolism.

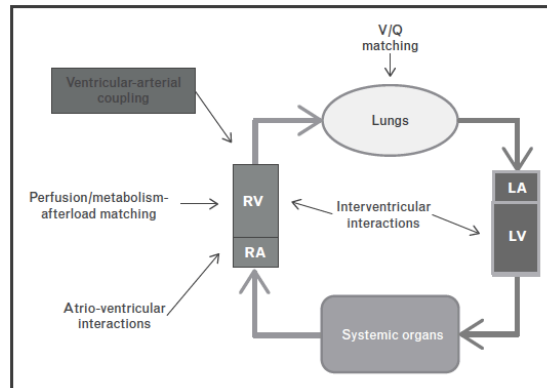


FIGURE 1. Simplified representation of the ‘unfolded circulation’. Reproduced with permission from Laboratory of Surgical Research of the Marie Lannelongue Hospital and Springer International Publishing Switzerland. LA, left atrium; LV left ventricle; RA, right atrium; RV, right ventricle; V/Q: ventilation/perfusion.

of complex congenital heart disease, the effective stroke volume of both ventricles is equal on average. Consequently, RV dysfunction in patients with predominantly ‘left heart failure’ could mainly reflect low stroke volume and not necessarily intrinsic myocardial involvement of the right heart. In addition to systolic interactions, diastolic interactions, neurohormonal factors, and interventricular dyssynchrony blur the lines between the right and left heart [5–7].

THE RIGHT HEART, AS PART OF THE CARDIOPULMONARY UNIT

In addition to interventricular interactions, a comprehensive understanding of RV function should also consider the cardiopulmonary unit [1]. As shown in Fig. 1, this includes a better assessment of ventriculoarterial coupling (matching between RV contractility and afterload), ventilation perfusion matching, and atrioventricular coupling.

RIGHT HEART REFERENCE VALUES: HAVE WE MADE ANY PROGRESS?

Recent efforts have been made to develop reference values for RV structure and function assessment. In 2010, Rudski *et al.* [8] published an American/European consensus document on the evaluation of the right heart, later incorporated in the 2015 American Society of Echocardiography and European Association of Cardiovascular Imaging recommendations on chamber quantification [8,9^{***}]. Table 1 summarizes the different proposed thresholds for enlargement or dysfunction [8–16]; a recent large

community-based study also proposed population-derived values [17]. Some controversies still exist on which threshold to use for RV longitudinal strain (RVLS) and tricuspid annular plane systolic excursion (TAPSE). For example, some authors use slightly higher thresholds than those suggested in the guidelines, such as 25% for RVLS compared with the 20% recommended, or 18 mm used for TAPSE instead of 17 mm [9^{***},12]. Another area of uncertainty comes from the absence of well-established gradation for RV enlargement or dysfunction, in contrast to well-defined left heart metrics, realizing that some of the gradation will be in part arbitrary. RV ejection fraction less than 35% has often been used as a criterion for moderate RV systolic dysfunction, which corresponds to an RV fractional area change (RVFAC) of approximately 25% [18]. Additionally to the normative values, several right heart metrics thresholds have been proposed for risk stratification. Tables 2 and 3 summarize the main prognostic right heart metrics in heart failure and pulmonary hypertension [10,12,19–33].

PITFALLS OF RIGHT HEART IMAGING

Several pitfalls in the assessment of the right heart have been described. First, as the annular motion frequently decreases after cardiac surgery following pericardial opening, it should be kept in mind that annular indices (such as TAPSE or S’ velocity) do not consequently reflect RV systolic function [34,35]. This represents the most common cause of misdiagnosis of RV dysfunction postoperatively. A second important pitfall is to consider the different RV

Table 1. Selection of the most relevant right heart imaging metrics

Metrics	Reference values ^a	Clinical relevance and comments
Dimensional indices		
RV volumes	Sex dependent	Increased RV volumes and decreased LV end-diastolic volume are predictors of poor survival in pulmonary hypertension
RV mass	Indexed on BSA 21 ± 4 g/m ²	Hypertrophy is predictor of poor survival in PAH, but better survival in patients with Eisenmenger Reflects adaptive response, but has to be interpreted with regard to load
RA enlargement	>11.0 cm ² /m ²	>15.4 cm ² /m ² is associated with poor survival in PAH
Systolic functional indices		
RVEF	>50%	<35% by MRI or SPECT often used as threshold to discriminate outcome associated with poor survival in HFrEF and pulmonary hypertension <45% by three-dimensional echocardiography usually reflects abnormal RV systolic function, though laboratories may choose to refer to age and gender-specific values
RVFAC	>35%	<25% denotes moderate-to-severe dysfunction Predictor of poor survival in pulmonary hypertension and heart failure
TAPSE	>17 mm	<14 mm is predictor of poor survival in pulmonary hypertension load dependent Limited value after cardiac surgery
S'peak velocity	>12 cm/s	< 8 cm/s is considered abnormal load dependent
Deformation indices		
Global longitudinal strain	≤20%	Severe often if ≥15% by speckle tracking predictor of survival in pulmonary hypertension [12]
Systolodiastolic functional index		
RVMPI-pulsed tissue	<0.55	>0.88 predicts poor survival in idiopathic PAH Possible pseudonormalized in case of severe RV dysfunction
Diastolic metric		
IVRT (TDI) corrected	<65 ms	> 75 ms (noncorrected) has been associated with RV dysfunction Requires indexation by heart rate (IVRT divided by square root of RR interval)
Pulmonary flow		
Pulmonary acceleration time	>93 ms	Useful to screen for pulmonary hypertension (>105 ms), particularly in case of severe tricuspid regurgitation No evidence of prognosis value, time dependent (adjustment to heart rate in theory)
Ventricular interdependency		
Eccentricity index	No normative value, usually <1	Diastolic eccentricity index predictor of poor survival in pulmonary hypertension (no consensus on the threshold) End-systole eccentricity index reflects pressure overload while end-diastole eccentricity index reflects volume overload
Myocardial fibrosis		
Delayed contrast – enhancement (gadolinium)	Absent	Presence reflects localized fibrosis Strongly correlates with increased RV mass, volumes, and pulmonary pressures
Native T1 mapping	T1 times: RV > LV	Able to detect diffuse fibrosis Correlates with RV–PA coupling, RV performance and pulmonary pressures in a piglet model

Table 1 (Continued)

Metrics	Reference values ^a	Clinical relevance and comments
Nuclear imaging		
18F-fluorodeoxyglucose PET	No uptake by the RV	RV/LV uptake ratio increased in pulmonary hypertension
201-thallium or 99mTc SPECT	Uptake LV > RV	Relative increase in RV perfusion compared with LV with stress may indicate multivessel coronary artery disease [15,16]

BSA, body surface area; HFrEF, left heart failure with reduced ejection fraction; IVRT, isovolumic relaxation time; LV, left ventricle; PA, pulmonary artery; PAH, pulmonary arterial hypertension; PET, positron emission tomography; PH, pulmonary hypertension; RA, right atrium; RV, right ventricle; RVEF, RV ejection fraction; RVFAC, RV fractional area change; RVMPI, RV myocardial performance index; SPECT, single photon emission computed tomography; TAPSE, tricuspid annular plane systolic excursion; TDI, tissue Doppler imaging.

^aNormative values and thresholds are from the following references: [8,9[■],10–14].

indices as equivalent; for example, TAPSE is a less sensitive marker of ventricular dysfunction than RVFAC or RVLS. Third, when analyzing RV size on the apical four-chamber view, careful attention should be given to ensure that the imaging plane reflects the major axis of the right ventricle (i.e., neither off-axis nor foreshortened). These two considerations are especially important for accurate two-dimensional quantification of RV size. A corollary pitfall is to draw conclusions on RV dimensions based on relative RV to LV size, as this leads to underestimation of RV size in patients with dilated LV. Fourth, ventricular dysfunction should not be equated with impaired RV contractility. Evidence has been shown of the potential recovery of the RV, even if severely impaired in the setting of abnormal afterload, as illustrated by the remodeling after lung transplant in patients with pulmonary arterial hypertension (PAH) [36]. Fifth, presence of a severe tricuspid regurgitation should systematically be assessed, as it can lead to overestimation of RV function based on volumetric metrics (such as ejection fraction and RVFAC), TAPSE or RVLS. Lastly, presence of RV artifacts using nuclear imaging, such as PET, can be caused by attenuation or cardiac and respiratory motion.

LATEST DEVELOPMENTS IN ECHOCARDIOGRAPHY

Right ventricular deformation imaging

Myocardial deformation imaging has gathered a lot of attention in recent years, leading to several thousand publications [37]. Myocardial deformation encompasses different concepts, including strain, usually expressed as longitudinal, circumferential, or radial strain; strain rate, which represents the deformation over time; and velocity-based parameters. As summarized in a statement study

by Voigt *et al.* [37], strain may refer to either natural strain or Lagrangian strain. One of the landmark studies in the field is that of Dumesnil *et al.*, which outlines the principles of axial and transverse shortening of the LV [38]. Both reflect deformation of the myocardial wall, but while natural strain is expressed relative to the length at a previous time, Lagrangian strain is expressed relative to the initial length as follows: (end-systolic length–end-diastolic length)/end-diastolic length, and is usually assessed using speckle tracking or by manual tracing (Fig. 2) [39,40]. Both concepts are related to each other mathematically, but are not equivalent. Moreover, studying strain adds value to other volumetric metrics, especially in cases of nondilated ventricles [40]. We recently showed that in ‘left heart failure’, left ventricular ejection fraction (LVEF) and LV strain are more collinearly related to each other in patients with reduced ejection fraction compared with higher ejection fraction.

Primarily developed in the LV, several studies have explored the value of longitudinal shortening of the RV-free wall in patients with advanced heart failure referred for heart transplant [23] and outpatients with heart failure [26]. The software used for speckle tracking has mainly been developed for the LV. Tracking of the RV may be more challenging and is often more reliable in the basal and mid portion. Recently, Ryo *et al.* [41] have developed software evaluating both axial and surface RV strain using three-dimensional methodology. Finally, it should be highlighted that right heart strain derived by MRI often focuses on the circumferential strain, whereas strain derived by echocardiography focuses on the longitudinal strain.

Three-dimensional imaging of the right heart

Three-dimensional echocardiography opens up the possibility of evaluating RV volumes by overcoming

Table 2. Selected studies associating right heart metrics with survival in left heart failure

Study	Population	Number of patients	Outcomes	Afterload metrics ^a	Right ventricular metrics ^a	Comments
Heart failure with reduced ejection fraction (HFrEF)						
Ghio <i>et al.</i> 2000 [19]	Chronic heart failure LVEF <35%	140	Death or urgent transplant during follow-up (2 years)	–	TAPSE ≤14 mm	
Meyer <i>et al.</i> 2010 [20]	Chronic heart failure LVEF ≤35%	2008	Death during follow-up (2 years)	–	RVEF <20%	Large nuclear study
Dupont <i>et al.</i> 2012 [21]	Chronic and acute heart failure LVEF = 19 ± 9%	724	Death or transplant during follow-up (3.2 years)	Capacitance	Visual right ventricular systolic dysfunction cardiac index	First study to demonstrate prognostic value of capacitance in HFrEF
Gulati <i>et al.</i> 2013 [22]	Nonischemic dilated cardiomyopathy	250	Death or transplant during follow-up (6.8 years)	–	RVEF ≤45%	MRI study
Cameli <i>et al.</i> 2013 [23]	Advanced heart failure referred for heart transplant	98	Composite endpoint (death, transplant, hospitalization, and mechanical assistance) during follow-up (1.5 years)	–	Free-wall RV longitudinal strain RV global longitudinal strain RVFAC	First study to report the prognostic value of RV strain in end-stage heart failure
Aronson <i>et al.</i> 2013 [24]	Acute heart failure HFrEF or HFpEF	326	Death during follow-up (1 year)	–	RVFAC <35% in patients with pulmonary hypertension	Rare study on acute failure, irrespective of LVEF
Iacoviello <i>et al.</i> 2016 [26]	Chronic heart failure LVEF <45%	332	Death during follow-up (3 years)	–	Free-wall RV longitudinal strain RV global longitudinal strain	First study to report the prognostic value of RV strain in stable outpatients
Heart failure with preserved ejection fraction (HFpEF)						
Al-Naamani <i>et al.</i> 2015 [25]	LVEF >50% with pulmonary hypertension	73	Death during follow-up (3.6 years)	Capacitance	–	First study to demonstrate prognostic value of capacitance in HFpEF, more studies with multivariate models are needed

LVEF, left ventricular ejection fraction; RV, right ventricle; RVEF, right ventricular ejection fraction; RVFAC, RV fractional area change.

^aIn multivariate analysis.

the limitations of conventional two-dimensional echocardiography RV views with regard to orientation and reference points. A meta-analysis has indeed shown the good correlation between MRI and three-dimensional echocardiography for RV volumes and ejection fraction assessment in patients and healthy study participants, with three-dimensional echocardiography slightly underestimating volumes as compared with MRI [42]. So far, only one multicenter study provides age, body size, and sex-specific reference values of

three-dimensional echocardiography-derived RV volumes and ejection fraction in 507 healthy study participants [43]. Overall, women have smaller indexed RV volumes and higher ejection fraction compared with men, whereas older age is associated with smaller RV volumes [a decrement of 5 ml per decade for end-diastolic volume (EDV) and 3 ml per decade for end-systolic volume] and higher ejection fraction (an increment of 1% per decade) [43]. Lastly, a recent quantitative three-dimensional echocardiography study has explored

Table 3. Selected studies associating right heart metrics with survival in pulmonary hypertension

Study	Population	Number of patients	Outcomes	Afterload metrics ^a	Right ventricular metrics ^a	Comments
NIH registry						
D'Alonzo <i>et al.</i> 1991 [27]	PAH	194	Death or heart–lung transplant during follow-up (2.8 years)	MPAP Mean right atrial pressure	Cardiac index	Does not reflect the current survival rate Only applicable to naïve-treatment patients
Pulmonary Hypertension Connection registry						
Thenappan <i>et al.</i> 2010 [28]	PAH	578	Death during follow-up (3.9 years)	MPAP Mean right atrial pressure	Cardiac index	Does not reflect the recent treatments available
French National registry						
Humbert <i>et al.</i> 2010 [29]	Idiopathic, familial, drug, and toxins-associated PAH	354	Death at 3 years	–	Cardiac index	
REVEAL Registry						
Benza <i>et al.</i> 2010 [30]	Idiopathic, familial, CHD, and CTD-associated PAH	2716	Death at 1 year	Pulmonary vascular resistance (>32 wood units)	Pericardial effusion Mean right atrial pressure (>20 mmHg)	
UK registry						
Lee <i>et al.</i> 2012 [31]	Idiopathic, familial, CHD, and CTD-associated PAH	182	Death at 1 and 2 years	–	Mean right atrial pressure	
Right Heart score						
Haddad <i>et al.</i> 2015 [10]	Idiopathic, familial, drug, and toxins-associated PAH	95 + 87	Death or lung transplant at 5 years	–	RV dysfunction Severe RA enlargement SBP <110 mmHg	Simple echocardiographic score in PAH
Others						
Mahapatra <i>et al.</i> 2006 [32]	Idiopathic PAH	104	Death at 4 years	Capacitance	–	
Haddad <i>et al.</i> 2011 [33]	PAH admitted for acute right heart failure	119	Death or lung transplant at 90 days	–	Tricuspid regurgitation severity per grade	Rare study on acutely deteriorated patients with pulmonary hypertension
Fine <i>et al.</i> 2013 [12]	Group 1, 3 and 4 pulmonary hypertension versus no pulmonary hypertension	406 + 169	Death at 18 months	None retained	Peak RV longitudinal strain Pericardial effusion Log (NT-proBNP)	Large study on prognostic value of RV strain in PAH

CHD, congenital heart disease; CTD, connective tissue disease; MPAP, mean pulmonary arterial hypertension; NT-proBNP, N-terminal pro-brain natriuretic peptide; PAH, pulmonary arterial hypertension; RV, right ventricle. For other abbreviations, see Table 2.
^aIn multivariate analysis.

morphological subsets of RV adaption and remodeling in 92 patients with pulmonary hypertension, and linked them to clinical outcomes [41]. Three-dimensional RV end-systolic volume had indeed significantly better predictive values than EDV or global strain to predict the combined endpoint of hospitalization, death, or lung transplantation.

Right ventricular–pulmonary arterial coupling

The measure of RV function routinely used in clinical practice reflects overall function and not contractility [44]. The concept of ventriculoarterial coupling has been developed to describe matching between RV contractility and afterload; a ventricle

that can increase its contractility in response to the increase in afterload usually stays well compensated. In PAH, for example, RV contractility is increased but insufficient to match the increase in load; thus RV dysfunction ensues [1,45]. This is an important distinction, as RV contractility is not decreased in PAH, as illustrated by the RV recovery postlung transplantation in those patients.

As a related concept, there has been a recent interest in focusing on markers of load adaptability of the RV. This could help addressing two questions. The first is whether RV function is disproportionately reduced considering the ventricular wall stress or load. The second is how to best combine right heart function and load metrics into a simple index, to

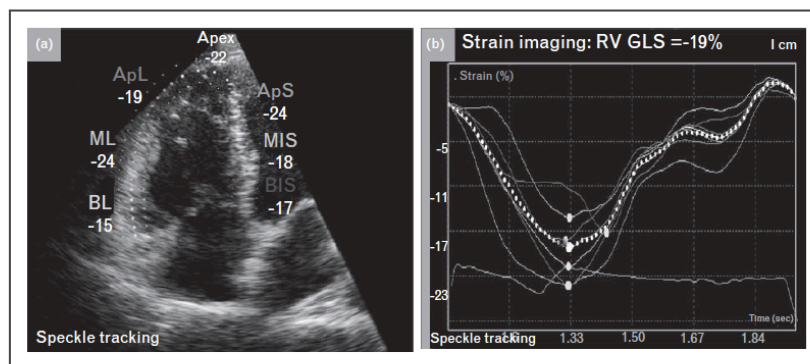


FIGURE 2. Myocardial deformation and velocity imaging of the right heart. (a) Superposed RV speckle tracking tracing with numbers representing segmental peak strain. Example from Philips tracking (developed for LV and applied to RV); specific RV tracking has also been developed by other vendors. (b) Strain-time curve of the different signals. ApL, apex lateral; ApS, apex septum; BIS, basal interventricular septum; BL, basal lateral; GLS, global longitudinal strain; LV, left ventricle; MIS, mid interventricular septum; ML, mid lateral; RV, right ventricle. Adapted from [1].

more accurately assess RV function and pulmonary hypertension. In the present review, we will highlight two examples. The first index, proposed by Guazzi *et al.*, is a simplified index of RV length–force relationship defined by TAPSE/systolic pulmonary arterial pressure (PAP) ratio. A value less than 0.36 mm/mmHg was associated with an increased cardiovascular mortality [hazard ratio of 10.4, (5.4–19.8), $P < 0.001$] in 293 patients with heart failure with reduced or preserved ejection fraction [46]. However, the applicability of this ratio in patients with PAH, who have a wider range of pulmonary pressures, has not been validated yet. In addition, simple ratios may not address the question of dis/proportionality of function, as the relationship between function and afterload follows a nonlinear and often inverse fit [47,48]. Figure 3 schematically represents the curvilinear fit of the relationships between RV function, or end-systolic dimension, and afterload metrics (such as pressure, resistance, capacitance, or estimation of the RV wall stress). Based on the literature, this figure schematically represents the curvilinear fit (usually a logarithmic fit) of the relationships between RV function, or end-systolic dimension, and afterload (such as pressure, resistance, capacitance, or estimation of the RV wall stress). Estimation of the wall stress is more challenging, but better reflects the force opposing ventricular function. The shape of the fit would be reversed if capacitance were used as afterload. Two examples are depicted in this figure (patient 1 and patient 2). Despite similar moderate right ventricular function, patients 1 and 2 differ in terms of RV adaptation. Patient 1 has a disproportional dysfunction, as the function is worse than would be expected for the mild increase in afterload

compared with patient 2. The second load adaptation index, proposed by Dandel *et al.* [49], is defined as $(\Delta P_{RV} - \Delta P_{RA}) / [EDV / L_{ED}]$, estimated by $[VTI_{TR} \times L_{ED}] / A_{ED}$, with L_{ED} the RV length in end-diastole, A_{ED} the RV area in end-diastole, and VTI_{TR} the velocity time integration of the TR signal. The prognostic value of this index was primarily demonstrated for the assessment of RV function recovery in patients with end-stage left heart failure on left ventricular assist device [22]. It was also validated in 79 patients with PAH awaiting lung transplantation, and shown to be associated with the risk of RV failure and transplant-free survival at 1 and 3 years [50]. However, while this index provides complementary information about proportionality of ventricular adaptation, it does not replace remodeling or function parameters.

INNOVATIONS IN MAGNETIC RESONANCE IMAGING

Beyond volumetric and functional analysis, MRI also allows tissue characterization, pulmonary stiffness assessment, and accurate quantification of blood flow. Table S1, <http://links.lww.com/HCO/A34>, compares the advantages and limitations of MRI and other imaging modalities.

Myocardial tissue characterization

Two novelties in myocardium characterization by MRI need to be mentioned. The first one is the noninclusion of RV myocardial fatty infiltration in the recent revised Task Force diagnostic criteria for arrhythmogenic right ventricular cardiomyopathy/dysplasia (ARVC/D) (Table 4) [51]. In fact,

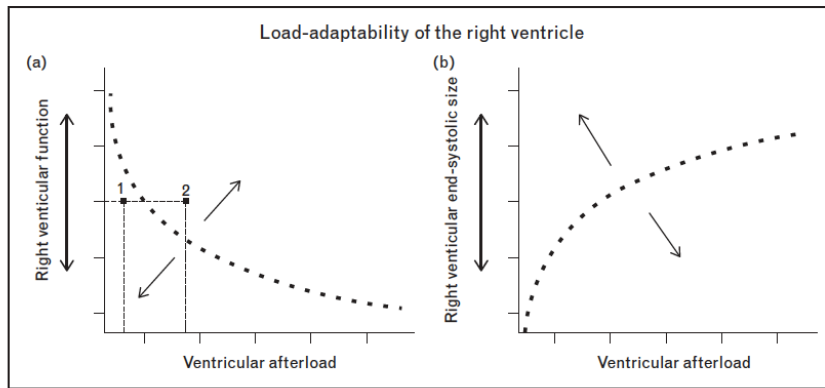


FIGURE 3. Relationships between right ventricular function (a) or end-systolic size (b) and ventricular afterload.

although fatty infiltration had been considered as indicative of ARVC/D for years, recent evidence has questioned its specificity, showing the high rate of physiological fatty infiltration (without concomitant fibrosis) in healthy controls [52]. The presence of regional RV akinesia or dyskinesia remains an important diagnostic criterion of ARVC/D [51]. A specific MRI pattern, described as a focal ‘crinkling’ of the RV outflow tract and subtricuspid regions (accordion sign), has been reported as a promising sign for early diagnosis of ARVC/D, as only found in mutation carriers [53]. The accordion sign is an example of regional RV wall motion abnormalities, similar to the regional contraction abnormalities first described by McConnell *et al.* [54] two decades ago in patients with acute pulmonary embolism, and recently revisited using echocardiographic strain [55].

The second novelty is the assessment of myocardial fibrosis by late gadolinium enhancement (LGE) or more recently T1 mapping. LGE identifies myocardial fibrosis, which has diagnostic [56] and prognostic [57] value. One of the main potential pitfalls of LGE imaging is that it may fail to adequately characterize diffuse interstitial myocardial fibrosis because of reliance on relative signal intensity changes and nulling of normal-appearing myocardium [58]. Quantitative assessment of the myocardial longitudinal relaxation time constant (T1) has in parallel emerged as a promising technique to assess for diffuse myocardial changes. T1 maps can be produced of noncontrast (native) myocardial T1 values (providing information on both the myocyte and the interstitium) or after gadolinium-based contrast administration (enabling quantification of the extracellular space) [59]. In healthy controls, RV noncontrast T1 values have been shown to be higher than LV values, which may be explained by the higher collagen content

of the RV myocardium [60,61]. In the setting of RV dysfunction and pulmonary hypertension, RV and hinge point noncontrast T1 and extracellular volume fraction values are elevated. Postcontrast T1 values are reduced [62,63] and may correlate with pulmonary hemodynamics, RV–PA coupling and RV function [64]. Finally, several advanced techniques have been proposed to improve T1 quantification of thin-walled structures such as the RV, including imaging in systole and higher-resolution sequences [60,61,63,65].

Pulmonary arterial stiffness

Several parameters have been developed to provide information on local, regional, or global stiffness: pulse pressure, elasticity, distensibility, compliance, capacitance, and stiffness index β [66], as detailed in Supplementary Table S2, <http://links.lww.com/HCO/A34>. Among them, capacitance [invasively estimated as the ratio of stroke volume (SV) divided by pulse pressure] has been associated with RV dysfunction, remodeling, and mortality, independently of the level of resistance, in a wide spectrum of diseases (idiopathic and scleroderma-associated PAH, heart failure with reduced ejection fraction, and heart failure with preserved ejection fraction) [21,25,32,47,67,68]. Pulmonary arterial elasticity is measured as [maximal pulmonary artery (PA) area – minimum area]/minimum area, using phase-contrast MRI, on the transverse perpendicular plane. It may be valuable for the detection of exercise-induced pulmonary hypertension or earlier stages of pulmonary vascular disease [69].

Quantification of blood flow

Three-dimensional time-resolved flow MRI is an evolving imaging technique that yields both a

Table 4. 2010 Revised Task Force imaging criteria for diagnosis of arrhythmogenic right ventricular cardiomyopathy/dysplasia

	Major criteria	Minor criteria
Two-dimensional echocardiography	Regional RV akinesia, dyskinesia, or aneurysm and one of the following (end-diastole): PLAX RVOT ≥ 32 mm (corrected for body size PLAX/BSA ≥ 19 mm/m ²) PSAX RVOT ≥ 36 mm (corrected for body size PSAX/BSA ≥ 21 mm/m ²) Or fractional area change $\leq 33\%$	Regional RV akinesia, dyskinesia, or aneurysm and one of the following (end-diastole): PLAX RVOT ≥ 29 to < 32 mm (corrected for body size PLAX/BSA ≥ 16 to < 19 mm/m ²) PSAX RVOT ≥ 32 to < 36 mm (corrected for body size PSAX/BSA ≥ 18 to < 21 mm/m ²) Or fractional area change > 33 to $\leq 40\%$
MRI	Regional RV akinesia or dyskinesia ^a or dyssynchronous RV contraction And one of the following: Ratio of RV end-diastolic volume to BSA ≥ 110 ml/m ² (men) or ≥ 100 ml/m ² (women) Or RV ejection fraction $\leq 40\%$	Regional RV akinesia or dyskinesia ^a or dyssynchronous RV contraction And one of the following: Ratio of RV end-diastolic volume to BSA ≥ 100 to < 110 ml/m ² (men) or ≥ 90 to < 100 ml/m ² (women) Or RV ejection fraction > 40 to $\leq 45\%$
RV angiography	Regional RV akinesia, dyskinesia, or aneurysm	NA

BSA, body surface area; PLAX, parasternal long axis view; PSAX, parasternal short axis view; RVOT, right ventricular outflow tract. Other abbreviations: please refer to Tables 1, 2, 3.

^aInclude the 'accordion sign'.

vector of blood velocity and the magnitude signal intensity over an imaging volume. For each temporal phase of the cardiac cycle, three-dimensional time-resolved flow MRI allows the evaluation of blood flow, including valvular regurgitation (Fig. 4, left panel), quantification of biventricular volumes, function and mass, and visualization of intracardiac and extracardiac structures [71,72]. A recent study demonstrated that RV volume, function, and mass can be quantified with three-dimensional time-resolved flow MRI with precision and interobserver agreement comparable to those of cine steady-state free precession [73]. Whole heart three-dimensional time-resolved flow MRI also enables detection and visualization of both normal and abnormal right heart flow patterns [74]. In patients with pulmonary hypertension, three-dimensional time-resolved flow MRI often demonstrates a vortex pulmonary artery flow pattern (as shown in Fig. 4, right panel [70]); the relative period of existence of the vortex significantly correlates to the mean pulmonary artery pressure [70,75]. Peak systolic velocity, peak flow, stroke volume, and wall shear stress by three-dimensional time-resolved flow MRI are significantly lower in patients with PAH compared with healthy study participants [76,77]. The prognostic value of three-dimensional time-resolved flow MRI still needs to be proven; however, it could offer in the future a noninvasive alternative to catheterization for flow assessment and may help in early detection of RV dysfunction.

WHAT IS NEW IN COMPUTED TOMOGRAPHY IMAGING?

In patients with pulmonary hypertension, computed tomography (CT) angiography is widely used to rule out chronic thromboembolic pulmonary hypertension and underlying lung disease, as well as to characterize precise anatomy in the setting of congenital heart defects [78^{***}]. A recent study evaluated the utility of routinely performed non-ECG chest CT to screen for pulmonary hypertension. Spruitj *et al.* showed that both pulmonary arterial dilation (ratio relative to the ascending aorta diameter ≥ 1) and RV enlargement (ratio relative to the LV diameter ≥ 1.2), measured on the axial view, were incremental for the detection of pulmonary hypertension in 51 patients with advanced precapillary pulmonary hypertension versus 25 non-pulmonary hypertension controls [79]. The application of this screening detection in a large population still remains to be done.

MOLECULAR IMAGING: A DEEPER VIEW INTO THE BIOLOGY OF THE RIGHT HEART

Multiple molecular changes occur in a failing RV exposed to an increased afterload. Four of them represent potential targets for imaging. The first target derives from the RV metabolic shift from lipolysis toward glycolysis, which has been linked to worse ventricular function and poor survival [80]. The increased uptake by the cardiomyocytes of the

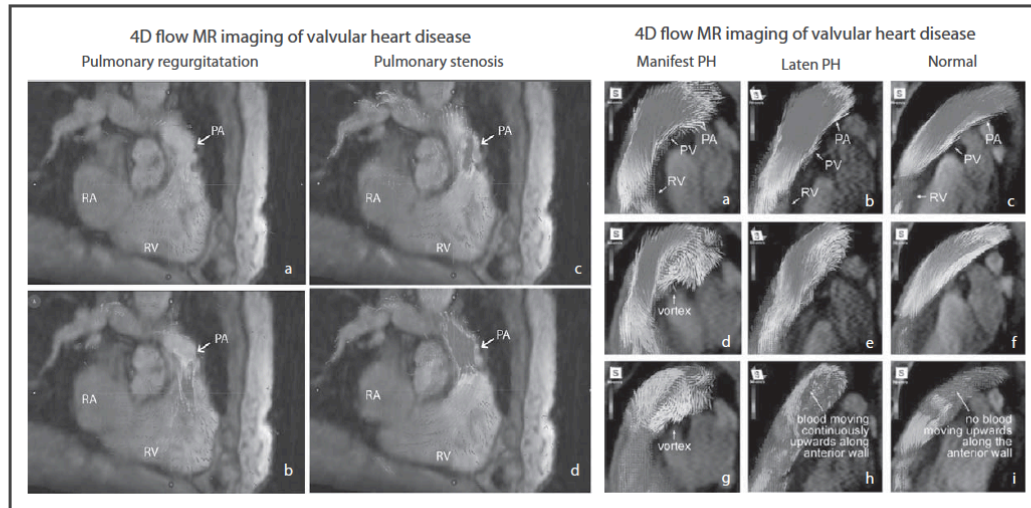


FIGURE 4. Four-dimensional flow MRI of a patient with pulmonary valvular disease (left); patients with pulmonary hypertension compared with a healthy control (right panel). Left panel: Flow pattern of a patient with both pulmonary regurgitation (a and b, acquired during diastole) and pulmonary stenosis (c and d, acquired during systole). Right panel: Typical flow patterns in the RV outflow tract at different cardiac phases for a patient with manifest PH (a, d, and g), a patient with latent PH (b, e, and h), and a normal study participant (c, f, and i). Right panel adapted from [70]. PA, main pulmonary artery; PH, pulmonary hypertension; PV, pulmonary valve; RV, right ventricle.

alternative source of energy (glucose) can be easily quantified using PET¹⁸F-2-deoxy-2-fluoro-D-Glucose. An increase in the RV-to-LV ratio tracer uptake has been reported in patients with PAH [81]. It remains, however, unclear whether this increased ratio is explained by an increased RV glucose uptake [82] or a decreased LV uptake [83]. Moreover, pre-clinical studies have suggested that this metabolic shift may be transient during progression of RV failure [84], which compromises the relevance of RV PET¹⁸F-2-deoxy-2-fluoro-D-Glucose uptake as a routine biomarker in PAH. The second target is the myocardial oxygen consumption, which can be imaged using ¹⁵O-labeled tracer or ¹¹C-acetate tracers. An increased resting oxygen consumption by the RV, and hence a reduced efficiency, has been shown in patients with PAH [85]. Neurohormonal dysregulation is the third target. There has been growing evidence of the importance of upregulated sympathetic nervous system and renin–angiotensin–aldosterone system in the pathophysiology of right heart failure in PAH [86]. Finally, angiogenesis and apoptosis are additional promising targets for detection of maladaptive RV in pulmonary hypertension [87]. Although these processes have been imaged in LV diseases [88] and pulmonary hypertension animal models, their clinical application in PAH is still pending.

NEW INSIGHTS IN RIGHT HEART HEMODYNAMICS

Although the review focuses on right heart imaging, hemodynamics remains one of the most important biomarkers that help guide management in patients with pulmonary hypertension and right-sided disease. In addition to right atrial and pulmonary pressures, three important parameters or ratios may be of clinical utility: RV diastolic pressure waveforms, relative pulmonary hypertension (defined as the mean pulmonary to mean arterial pressure ratio, MPAP/MAP), and indices of load adaptability.

Displaying the right ventricular waveform provides insights for monitoring and management of patients. Using a pulmonary arterial catheter and transducing the RV pacing port (Paceport, Edwards Lifescience, Irvine, California, USA), continuous RV and pulmonary arterial pressure waveforms can be obtained [89]. As RV dysfunction occurs, the shape of the diastolic waveform progressively changes, from horizontal to an oblique aspect, followed by the appearance of a square root sign suggesting progressive loss in RV diastolic compliance (Fig. 5). These modifications observed on the RV pressure waveform can also be diagnosed using careful central venous pressure waveform analysis and Doppler hepatic and portal venous flow interrogation [90]. The second metric is the relative

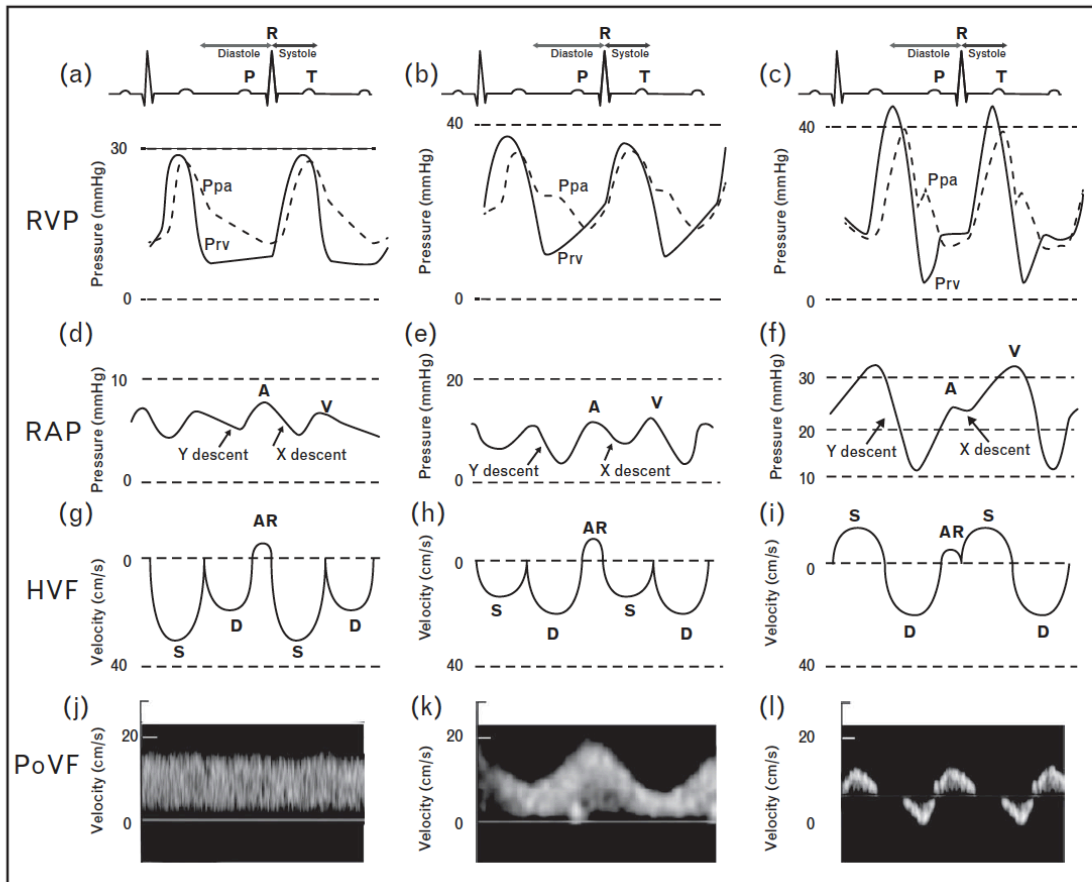


FIGURE 5. Right ventricular pressure, right atrial pressure, hepatic venous flow, and portal venous flow in normal patients (a, d, g, j) and typical patterns commonly observed in patients with mild (b, e, h, k) and severe (c, f, i, l) right ventricular dysfunction. AR, atrial reversal HVF velocity; D, diastolic HVF Doppler velocity; HVF, hepatic venous flow; PPA, pulmonary artery pressure; PoVF, portal venous flow; PRV, right ventricular pressure; RAP, right atrial pressure; RVP, right ventricular pressure; S, systolic HVF velocity. Adapted from [3].

estimation of mean pulmonary arterial pressure (MPAP). In the case of RV failure, MPAP can be underestimated as it can be reduced proportionally to the decrease in systemic pressures, for example, following anesthesia induction. The value of the MPAP/MAP ratio has previously been shown to be the best hemodynamic predictor of postoperative circulatory failure [91]. The ratio is additionally associated with long-term aortic valve survival [92] and correlates with ventricular septal curvature [4]. Finally, there has been a growing interest in proposing invasive load-adaptability indices such as the RV functional index (RFI), measured as the systolic pressure divided by cardiac index [69]. The RFI can be used to evaluate the extent to which elevated pulmonary arterial pressure is associated with preserved RV function. Elevated RFI may result

from increasing pulmonary arterial pressure or decreasing cardiac index, both indicative of RV failure. Increased RFI has been associated with poor survival in 53 patients admitted to the ICU with severe pulmonary hypertension [69] and in 1439 patients undergoing cardiac surgery [91].

CONCLUSION

The recent improvements in right heart imaging bring perspective into the physiology of the right heart, help early detection and prognostic stratification, and slowly bring the field into the new era of imaging biomarker guided management. Table 5 summarizes the six challenging unmet needs in the field of imaging of the right heart that are expected to be resolved in the coming 10 years.

Table 5. A look into the future of imaging the right heart

Unmet needs and future directions	
Echocardiography	Validation of simple diagnostic and prognostic scores Identifying useful load-adaptability indices Compare the value of deformation imaging strain with the value of end-systolic dimension for early detection of dysfunction and risk stratification
MRI	Early detection of myocardial fibrosis and adverse remodeling using native T1 mapping sequences
CT	Validation of quantitative assessment of right ventricular morphology in routine chest CT
PET	Use of metabolic phenotype to tailor clinical care and management in patients with right heart failure

CT, computer tomography.

Acknowledgements

We would like to warmly thank Professor Dominik Fleischmann (from the Division of Radiology, at Stanford University, USA) for his assistance with the review and mentorship, and Professor Marlene Rabinovitch (from the Vera Moulton Wall Center and the Cardiovascular Institute, Stanford School of Medicine, Stanford University, USA) for her mentorship. We would also like to thank Dr Marcus Chen (from the NHLBI – NIH, USA) for his permission to reproduce Table S1, as well as Professor Olaf Mercier and Dr David Boulate (from the Marie Lannelongue Hospitals, Le Plessis Robinson, France) for their authorization to reproduce Fig. 1.

Financial support and sponsorship

This work was supported by the Stanford Cardiovascular Institute, the Vera Moulton Wall Center of Pulmonary Hypertension (Stanford University, Stanford, CA) and a NIH/NHLBI grant 5R01HL07418609. M.A. received a Young Investigator Seed Grant from the Vera Moulton Wall Center of Pulmonary Hypertension at Stanford University.

Conflicts of interest

There are no conflicts of interest.

REFERENCES AND RECOMMENDED READING

Papers of particular interest, published within the annual period of review, have been highlighted as:

- of special interest
- of outstanding interest

1. Vonk Noordegraaf A, Haddad F, Bogaard HJ, Hassoun PM. Noninvasive imaging in the assessment of the cardiopulmonary vascular unit. *Circulation* 2015; 131:899–913.

2. D’Alto M, Dimopoulos K, Budts W, et al. Multimodality imaging in congenital heart disease-related pulmonary arterial hypertension. *Heart* 2016; 102:910–918.

3. Haddad F, Elmi-Sarabi M, Fadel E, et al. Pearls and pitfalls in managing right heart failure in cardiac surgery. *Curr Opin Anaesthesiol* 2016; 29:68–79.

Review on right heart imaging in congenital heart disease.

4. Haddad F, Guilhaire J, Skhiri M, et al. Septal curvature is marker of hemodynamic, anatomical, and electromechanical ventricular interdependence in patients with pulmonary arterial hypertension. *Echocardiography* 2014; 31:699–707.

5. Atherton JJ, Moore TD, Lele SS, et al. Diastolic ventricular interaction in chronic heart failure. *Lancet* 1997; 349:1720–1724.

6. Belenkie I, Smith ER, Tyberg JV. Ventricular interaction: from bench to bedside. *Ann Med* 2001; 33:236–241.

7. Gan C, Lankhaar JW, Marcus JT, et al. Impaired left ventricular filling due to right-to-left ventricular interaction in patients with pulmonary arterial hypertension. *Am J Physiol Heart Circ Physiol* 2006; 290:1528–1533.

8. Rudski LG, Lai WW, Filalo J, et al. Guidelines for the echocardiographic assessment of the right heart in adults: a report from the American Society of Echocardiography endorsed by the European Association of Echocardiography, a registered branch of the European Society of Cardiology, and the Canadian Society of Echocardiography. *J Am Soc Echocardiogr* 2010; 23:685–788.

9. Lang RM, Badano LP, Mor-Avi V, et al. Recommendations for cardiac chamber quantification by echocardiography in adults: an update from the American Society of Echocardiography and the European Association of Cardiovascular Imaging. *J Am Soc Echocardiogr* 2015; 28:1–39.

Latest American and European guidelines on right heart chamber quantification.

10. Haddad F, Spruijt OA, Denault AY, et al. Right heart score for predicting outcome in idiopathic, familial, or drug- and toxin-associated pulmonary arterial hypertension. *JACC Cardiovasc Imaging* 2015; 8:627–638.

11. Ghio S, Klersy C, Magrini G, et al. Prognostic relevance of the echocardiographic assessment of right ventricular function in patients with idiopathic pulmonary arterial hypertension. *Int J Cardiol* 2010; 140:272–278.

12. Fine NM, Chen L, Bastiansen PM, et al. Outcome prediction by quantitative right ventricular function assessment in 575 subjects evaluated for pulmonary hypertension. *Circ Cardiovasc Imaging* 2013; 6:711–721.

13. Tei C, Dujardin KS, Hodge DO, et al. Doppler echocardiographic index for assessment of global right ventricular function. *J Am Soc Echocardiogr* 1996; 9:838–847.

14. Zimbarra Cabrita I, Rulsanchez C, Grapsa J, et al. Validation of the isovolumetric relaxation time for the estimation of pulmonary systolic arterial blood pressure in chronic pulmonary hypertension. *Eur Heart J Cardiovasc Imaging* 2013; 14:51–55.

15. Williams KA, Schneider CM. Increased stress right ventricular activity on dual isotope perfusion SPECT: a sign of multivessel and/or left main coronary artery disease. *J Am Coll Cardiol* 1999; 34:420–427.

16. Mannting F, Zabrodina YV, Dass C. Significance of increased right ventricular uptake on 99mTc-sestamibi SPECT in patients with coronary artery disease. *J Nucl Med* 1999; 40:889–894.

17. Kavut SM, Lima JA, Barr RG, et al. Sex and race differences in right ventricular structure and function: the multi-ethnic study of atherosclerosis-right ventricle study. *Circulation* 2011; 123:2542–2551.

18. Shiran H, Zamanian RT, McConnell MV, et al. Relationship between echocardiographic and magnetic resonance derived measures of right ventricular size and function in patients with pulmonary hypertension. *J Am Soc Echocardiogr* 2014; 27:405–412.

19. Ghio S, Recusani F, Klersy C, et al. Prognostic usefulness of the tricuspid annular plane systolic excursion in patients with congestive heart failure secondary to idiopathic or ischemic dilated cardiomyopathy. *Am J Cardiol* 2000; 85:837–842.

20. Meyer P, Filippatos GS, Ahmed MI, et al. Effects of right ventricular ejection fraction on outcomes in chronic systolic heart failure. *Circulation* 2010; 121:252–258.

21. Dupont M, Mullens W, Skouri HN, et al. Prognostic role of pulmonary arterial capacitance in advanced heart failure. *Circ Heart Fail* 2012; 5:778–785.

22. Gulati A, Ismail TF, Jabbour A, et al. The prevalence and prognostic significance of right ventricular systolic dysfunction in nonischemic dilated cardiomyopathy. *Circulation* 2013; 128:1623–1633.

23. Cameli M, Righini FM, Lisi M, et al. Comparison of right versus left ventricular strain analysis as a predictor of outcome in patients with systolic heart failure referred for heart transplantation. *Am J Cardiol* 2013; 112:1778–1784.

24. Aronson D, Darawsha W, Atamna A, et al. Pulmonary hypertension, right ventricular function, and clinical outcome in acute decompensated heart failure. *J Card Fail* 2013; 19:665–671.

25. Al-Naamani N, Preston IR, Paulus JK, et al. Pulmonary arterial capacitance is an important predictor of mortality in heart failure with a preserved ejection fraction. *JACC Heart Fail* 2015; 3:467–474.

26. Iacoviello M, Citarelli G, Antonceccchi V, et al. Right ventricular longitudinal strain measures independently predict chronic heart failure mortality. *Echocardiography* 2016; 33:992–1000.

27. D'Alonzo GE, Barst RJ, Ayres SM, *et al.* Survival in patients with primary pulmonary hypertension. Results from a national prospective registry. *Ann Intern Med* 1991; 115:343–349.
28. Thenappan T, Shah SJ, Rich S, *et al.* Survival in pulmonary arterial hypertension: a reappraisal of the NIH risk stratification equation. *Eur Respir J* 2010; 35:1079–1087.
29. Humbert M, Sitbon O, Chaouat A, *et al.* Survival in patients with idiopathic, familial, and anorexigen-associated pulmonary arterial hypertension in the modern management era. *Circulation* 2010; 122:156–163.
30. Benza RL, Miller DP, Gomberg-Maitland M, *et al.* Predicting survival in pulmonary arterial hypertension: insights from the Registry to Evaluate Early and Long-Term Pulmonary Arterial Hypertension Disease Management (REVEAL). *Circulation* 2010; 122:164–172.
31. Lee WT, Ling Y, Sheares KK, *et al.* Predicting survival in pulmonary arterial hypertension in the UK. *Eur Respir J* 2012; 40:604–611.
32. Mahapatra S, Nishimura RA, Sorajja P, *et al.* Relationship of pulmonary arterial capacitance and mortality in idiopathic pulmonary arterial hypertension. *J Am Coll Cardiol* 2006; 47:799–803.
33. Haddad F, Peterson T, Fuh E, *et al.* Characteristics and outcome after hospitalization for acute right heart failure in patients with pulmonary arterial hypertension. *Circ Heart Fail* 2011; 4:692–699.
34. Wranne B, Pinto FJ, Hammarström E, *et al.* Abnormal right heart filling after cardiac surgery: time course and mechanisms. *Br Heart J* 1991; 66:435–442.
35. Tamborini G, Muratori M, Brusoni D, *et al.* Is right ventricular systolic function reduced after cardiac surgery? A two- and three-dimensional echocardiographic study. *Eur J Echocardiogr* 2009; 10:630–634.
36. Kusunose K, Tsutsui RS, Bhatt K, *et al.* Prognostic value of RV function before and after lung transplantation. *JACC Cardiovasc Imaging* 2014; 7:1084–1094.
37. Voigt J-U, Pedrizzetti G, Lysyansky P, *et al.* Definitions for a common standard for 2D speckle tracking echocardiography: consensus document of the EACVI/ASE/Industry Task Force to standardize deformation imaging. *Eur Heart J Cardiovasc Imaging* 2015; 16:1–11.
38. Dumesnil JG, Shoucri RM, Laurenceau JL, Turcot J. A mathematical model of the dynamic geometry of the intact left ventricle and its application to clinical data. *Circulation* 1979; 59:1024–1034.
39. Dandel M, Lehmkuhl H, Knosalla C, *et al.* Strain and strain rate imaging by echocardiography: basic concepts and clinical applicability. *Curr Cardiol Rev* 2009; 5:133–148.
40. Kobayashi Y, Ariyama M, Kobayashi Y, *et al.* Comparison of left ventricular manual versus automated derived longitudinal strain: implications for clinical practice and research. *Int J Cardiovasc Imaging* 2016; 32:429–437.
41. Ryo K, Goda A, Onishi T, *et al.* Characterization of right ventricular remodeling in pulmonary hypertension associated with patient outcomes by 3-dimensional wall motion tracking echocardiography. *Circ Cardiovasc Imaging* 2015; 8:e003176.
42. Shimada YJ, Shiota M, Siegel RJ, Shiota T. Accuracy of right ventricular volumes and function determined by three-dimensional echocardiography in comparison with magnetic resonance imaging: a meta-analysis study. *J Am Soc Echocardiogr* 2010; 23:943–953.
43. Maffessanti F, Muraru D, Esposito R, *et al.* Age-, body size-, and sex-specific reference values for right ventricular volumes and ejection fraction by three-dimensional echocardiography: a multicenter echocardiographic study in 507 healthy volunteers. *Circ Cardiovasc Imaging* 2013; 6:700–710.
44. Guihaire J, Haddad F, Boulate D, *et al.* Non-invasive indices of right ventricular function are markers of ventricular-arterial coupling rather than ventricular contractility: insights from a porcine model of chronic pressure overload. *Eur Heart J Cardiovasc Imaging* 2013; 14:1140–1149.
45. Vonk-Noordegraaf A, Haddad F, Chin KM, *et al.* Right heart adaptation to pulmonary arterial hypertension: physiology and pathobiology. *J Am Coll Cardiol* 2013; 62:22–33.
46. Guazzi M, Bandera F, Pellissiero G, *et al.* Tricuspid annular plane systolic excursion and pulmonary arterial systolic pressure relationship in heart failure: an index of right ventricular contractile function and prognosis. *Am J Physiol Heart Circ Physiol* 2013; 305:1373–1381.
47. Stevens GR, Garcia-Alvarez A, Sahni S, *et al.* RV dysfunction in pulmonary hypertension is independently related to pulmonary artery stiffness. *JACC Cardiovasc Imaging* 2012; 5:378–387.
48. Bellofiore A, Chesler NC. Methods for measuring right ventricular function and hemodynamic coupling with the pulmonary vasculature. *Ann Biomed Eng* 2013; 41:1384–1398.
49. Dandel M, Potapov E, Krabatsch T, *et al.* Load dependency of right ventricular performance is a major factor to be considered in decision making before ventricular assist device implantation. *Circulation* 2013; 128:14–23.
50. Dandel M, Knosalla C, Kemper D, *et al.* Assessment of right ventricular adaptability to loading conditions can improve the timing of listing to transplantation in patients with pulmonary arterial hypertension. *J Heart Lung Transplant* 2015; 34:319–328.
51. Marcus FI, McKenna WJ, Sherrill D, *et al.* Diagnosis of arrhythmogenic right ventricular cardiomyopathy/dysplasia: proposed modification of the task force criteria. *Circulation* 2010; 121:1533–1541.
52. Bomma C, Rutberg J, Tandri H, *et al.* Misdiagnosis of arrhythmogenic right ventricular dysplasia/cardiomyopathy. *J Cardiovasc Electrophysiol* 2004; 15:300–306.
53. Dalal D, Tandri H, Judge DP, *et al.* Morphologic variants of familial arrhythmogenic right ventricular dysplasia/cardiomyopathy: a genetics-magnetic resonance imaging correlation study. *J Am Coll Cardiol* 2009; 53:1289–1299.
54. McConnell MV, Solomon SD, Rayan ME, *et al.* Regional right ventricular dysfunction detected by echocardiography in acute pulmonary embolism. *Am J Cardiol* 1996; 78:469–473.
55. Tuzovic M, Adigopula S, Amsallem M, *et al.* Regional right ventricular dysfunction in acute pulmonary embolism: relationship with clot burden and biomarker profile. *Int J Cardiovasc Imaging* 2015; 32:389–398.
56. Swift AJ, Rajaram S, Capener D, *et al.* LGE patterns in pulmonary hypertension do not impact overall mortality. *JACC Cardiovasc Imaging* 2014; 7:1209–1217.
57. Freed BH, Gomberg-Maitland M, Chandra S, *et al.* Late gadolinium enhancement cardiovascular magnetic resonance predicts clinical worsening in patients with pulmonary hypertension. *J Cardiovasc Magn Reson* 2012; 14:11.
58. Azevedo CF, Nigri M, Higuchi ML, *et al.* Prognostic significance of myocardial fibrosis quantification by histopathology and magnetic resonance imaging in patients with severe aortic valve disease. *J Am Coll Cardiol* 2010; 56:278–287.
59. Baksi AJ, Pennell DJ. T1 mapping in heart failure: from technique to prognosis, toward altering outcome. *Circ Cardiovasc Imaging* 2013; 6:861–863.
60. Kawel-Boehm N, Dellas Buser T, Greiser A, *et al.* In-vivo assessment of normal T1 values of the right-ventricular myocardium by cardiac MRI. *Int J Cardiovasc Imaging* 2014; 30:323–328.
61. Mehta BB, Auger DA, Gonzalez JA, *et al.* Detection of elevated right ventricular extracellular volume in pulmonary hypertension using Accelerated and Navigator-Gated Look-Locker Imaging for Cardiac T1 Estimation (ANGIE) cardiovascular magnetic resonance. *J Cardiovasc Magn Reson* 2015; 17:110.
62. Spruijt OA, Vissers L, Bogaard HJ, *et al.* Increased native T1-values at the interventricular insertion regions in precapillary pulmonary hypertension. *Int J Cardiovasc Imaging* 2016; 32:451–459.
63. Bilchick K, Mehta BB, Workman V, *et al.* Right ventricular extracellular volume fraction by magnetic resonance T1 mapping in pulmonary hypertension and heart failure. *Circulation* 2015; 132:A14921.
64. Garcia-Alvarez A, Garcia-Lunar I, Pereda D, *et al.* Association of myocardial T1-mapping CMR with hemodynamics and RV performance in pulmonary hypertension. *JACC Cardiovasc Imaging* 2015; 8:76–82.
- The study shows the association between myocardial T1 mapping signal and pulmonary pressures and RV performance in pulmonary hypertension.
65. Kawel N, Nacif M, Zavodni A, *et al.* T1 mapping of the myocardium: intra-individual assessment of the effect of field strength, cardiac cycle and variation by myocardial region. *J Cardiovasc Magn Reson* 2012; 14:27.
66. Sanz J, Kariisa M, Dellegrottaglie S, *et al.* Evaluation of pulmonary artery stiffness in pulmonary hypertension with cardiac magnetic resonance. *JACC Cardiovasc Imaging* 2009; 2:286–295.
67. Campo A, Mathai SC, Le Pavec J, *et al.* Hemodynamic predictors of survival in scleroderma-related pulmonary arterial hypertension. *Am J Respir Crit Care Med* 2010; 182:252–260.
68. Pellegrini P, Rossi A, Pasotti M, *et al.* Prognostic relevance of pulmonary arterial compliance in patients with chronic heart failure. *Chest* 2014; 145:1064–1070.
69. Saydain G, Awan A, Manickam P, *et al.* Pulmonary hypertension an independent risk factor for death in intensive care unit: correlation of hemodynamic factors with mortality. *Clin Med Insights Circ Respir Pulm Med* 2015; 9:27–33.
70. Reiter G, Reiter U, Kovacs G, *et al.* Magnetic resonance-derived 3-dimensional blood flow patterns in the main pulmonary artery as a marker of pulmonary hypertension and a measure of elevated mean pulmonary arterial pressure. *Circ Cardiovasc Imaging* 2008; 1:23–30.
71. Hsiao A, Lustig M, Alley MT, *et al.* Rapid pediatric cardiac assessment of flow and ventricular volume with compressed sensing parallel imaging volumetric cine phase-contrast MRI. *AJR Am J Roentgenol* 2012; 198:W250–W259.
72. Frydrychowicz A, Wieben O, Niespodzany E, *et al.* Quantification of thoracic blood flow using volumetric magnetic resonance imaging with radial velocity encoding: in vivo validation. *Invest Radiol* 2013; 48:819–825.
73. Hanneman K, Kino A, Cheng JY, *et al.* Assessment of the precision and reproducibility of ventricular volume, function, and mass measurements with ferumoxytol-enhanced 4D flow MRI. *J Magn Reson Imaging* 2016. [Epub ahead of print].
74. François CJ, Srinivasan S, Schiebler ML, *et al.* 4D cardiovascular magnetic resonance velocity mapping of alterations of right heart flow patterns and main pulmonary artery hemodynamics in tetralogy of Fallot. *J Cardiovasc Magn Reson* 2012; 14:16.
75. Reiter U, Reiter G, Kovacs G, *et al.* Evaluation of elevated mean pulmonary arterial pressure based on magnetic resonance 4D velocity mapping: comparison of visualization techniques. *PLoS One* 2013; 8:e82212.
76. Barker AJ, Roldán-Alzate A, Entezari P, *et al.* Four-dimensional flow assessment of pulmonary artery flow and wall shear stress in adult pulmonary arterial hypertension: results from two institutions. *Magn Reson Med* 2015; 73:1904–1913.
- The study demonstrates the feasibility of assessing pulmonary artery flow and wall shear stress in adult pulmonary arterial hypertension using three-dimensional time-resolved flow MRI.

77. Truong U, Fonseca B, Dunning J, *et al*. Wall shear stress measured by phase contrast cardiovascular magnetic resonance in children and adolescents with pulmonary arterial hypertension. *J Cardiovasc Magn Reson* 2013; 15:81.
78. Galié N, Humbert M, Vachiery JL, *et al*. 2015 ESC/ERS Guidelines for the diagnosis and treatment of pulmonary hypertension: the Joint Task Force for the Diagnosis and Treatment of Pulmonary Hypertension of the European Society of Cardiology (ESC) and the European Respiratory Society (ERS); endorsed by: Association for European Paediatric and Congenital Cardiology (AEPC), International Society for Heart and Lung Transplantation (ISHLT). *Eur Heart J* 2016; 37:67–119.
- These are the latest European guidelines on pulmonary hypertension.
79. Spruijt OA, Bogaard HJ, Heijmans MW, *et al*. Predicting pulmonary hypertension with standard computed tomography pulmonary angiography. *Int J Cardiovasc Imaging* 2015; 31:871–879.
80. Nagaya N, Goto Y, Satoh T, *et al*. Impaired regional fatty acid uptake and systolic dysfunction in hypertrophied right ventricle. *J Nucl Med* 1998; 39:1676–1680.
81. Bokhari S, Raina A, Rosenweig EB, *et al*. PET imaging may provide a novel biomarker and understanding of right ventricular dysfunction in patients with idiopathic pulmonary arterial hypertension. *Circ Cardiovasc Imaging* 2011; 4:641–647.
82. Lundgrin EL, Park MM, Sharp J, *et al*. Fasting 2-deoxy-2-[18F]fluoro-D-glucose positron emission tomography to detect metabolic changes in pulmonary arterial hypertension hearts over 1 year. *Ann Am Thorac Soc* 2013; 10:1–9.
83. Kluge R, Barthel H, Pankau H, *et al*. Different mechanisms for changes in glucose uptake of the right and left ventricular myocardium in pulmonary hypertension. *J Nucl Med* 2005; 46:25–31.
84. Sutendra G, Dromparis P, Paulin R, *et al*. A metabolic remodeling in right ventricular hypertrophy is associated with decreased angiogenesis and a transition from a compensated to a decompensated state in pulmonary hypertension. *J Mol Med (Berl)* 2013; 91:1315–1327.
85. Wong YY, Ruiter G, Lubberink M, *et al*. Right ventricular failure in idiopathic pulmonary arterial hypertension is associated with inefficient myocardial oxygen utilization. *Circ Heart Fail* 2011; 4:700–706.
86. de Man FS, Handoko ML, Guignabert C, *et al*. Neurohormonal axis in patients with pulmonary arterial hypertension: friend or foe? *Am J Respir Crit Care Med* 2013; 187:14–19.
87. Paffett ML, Hesterman J, Candelaria G, *et al*. Longitudinal *in vivo* SPECT/CT imaging reveals morphological changes and cardiopulmonary apoptosis in a rodent model of pulmonary arterial hypertension. *PLoS One* 2012; 7:e40910.
88. Amsalleem M, Saito T, Tada Y, *et al*. Magnetic resonance imaging and positron emission tomography approaches to imaging vascular and cardiac inflammation. *Circ J* 2016; 80:1269–1277.
89. Denault A, Lamarche Y, Rochon A, *et al*. Innovative approaches in the perioperative care of the cardiac surgical patient in the operating room and intensive care unit. *Can J Cardiol* 2014; 30:459–477.
90. Laflamme M, Perrault LP, Carrier M, *et al*. Preliminary experience with combined inhaled milrinone and prostacyclin in cardiac surgical patients with pulmonary hypertension. *J Cardiothorac Vasc Anesth* 2015; 29:38–45.
91. Robitaille A, Denault AY, Couture P, *et al*. Importance of relative pulmonary hypertension in cardiac surgery: the mean systemic-to-pulmonary artery pressure ratio. *J Cardiothorac Vasc Anesth* 2006; 20:331–339.
92. Bianco JC, Qizilbash B, Carrier M, *et al*. Is patient-prosthesis mismatch a perioperative predictor of long-term mortality after aortic valve replacement? *J Cardiothorac Vasc Anesth* 2013; 27:647–653.

SUPPLEMENTARY ARTICLE 7

The International Journal of Cardiovascular Imaging
<https://doi.org/10.1007/s10554-018-1356-7>

ORIGINAL PAPER



Optimizing right ventricular focused four-chamber views using three-dimensional imaging, a comparative magnetic resonance based study

Myriam Amsallem^{1,2,3} · HongQuan Lu^{1,2} · Xiu Tang¹ · Nadia L. Do Couto Francisco¹ · Yukari Kobayashi^{1,2} · Kegan Moneghetti^{1,2} · Hadas Shiran¹ · Ian Rogers^{1,2} · Ingela Schnittger^{1,2} · David Liang^{1,2} · François Haddad^{1,2}

Received: 13 February 2018 / Accepted: 11 April 2018
© Springer Science+Business Media B.V., part of Springer Nature 2018

Abstract

Obtaining focused right ventricular (RV) apical view remains challenging using conventional two-dimensional (2D) echocardiography. This study main objective was to determine whether measurements from RV focused views derived from three-dimensional (3D) echocardiography (3D-RV-focused) are closely related to measurements from magnetic resonance (CMR). A first cohort of 47 patients underwent 3D echocardiography and CMR imaging within 2 h of each other. A second cohort of 25 patients had repeat 3D echocardiography to determine the test–retest characteristics; and evaluate the bias associated with unfocused RV views. Tomographic views were extracted from the 3D dataset: RV focused views were obtained using the maximal RV diameter in the transverse plane, and unfocused views from a smaller transverse diameter enabling visualization of the tricuspid valve opening. Measures derived using the 3D-RV-focused view were strongly associated with CMR measurements. Among functional metrics, the strongest association was between RV fractional area change (RVFAC) and ejection fraction (RVEF) ($r=0.92$) while tricuspid annular plane systolic excursion moderately correlated with RVEF ($r=0.47$), all $p < 0.001$. Among RV size measures, the strongest association was found between RV end-systolic area (RVESA) and volume ($r=0.87$, $p < 0.001$). RV unfocused views led on average to 10% underestimation of RVESA. The 3D-RV-focused method had acceptable test–retest characteristics with a coefficient of variation of 10% for RVESA and 11% for RVFAC. Deriving standardized RV focused views using 3D echocardiography strongly relates to CMR-derived measures and may improve reproducibility in RV 2D measurements.

Keywords Right heart imaging · Three-dimensional echocardiography · Cardiac magnetic resonance · Quality control

Myriam Amsallem, HongQuan Lu, David Liang and François Haddad have contributed equally to this work.

Electronic supplementary material The online version of this article (<https://doi.org/10.1007/s10554-018-1356-7>) contains supplementary material, which is available to authorized users.

✉ Myriam Amsallem
mamsalle@stanford.edu

¹ Division of Cardiovascular Medicine, Stanford University School of Medicine, 300 Pasteur Drive, Stanford, CA 94305, USA

² Cardiovascular Institute, Stanford University School of Medicine, Stanford, CA, USA

³ Laboratory of Surgical Research and INSERM U999, University of Paris-Sud, Marie Lannelongue Hospital, Le Plessis Robinson, France

Introduction

In the past 25 years, right ventricular (RV) size and function have emerged as strong predictors of outcome in patients with heart failure, pulmonary hypertension and congenital heart disease [1]. Although two-dimensional (2D) echocardiography is the mainstay in evaluating the right heart in clinical practice, the crescent shape of the right ventricle makes standardization of RV views more challenging. The conventional apical four-chamber view (i.e. focused on the left ventricle) results in considerable variability in the way the right ventricle is sectioned. Consequently, RV linear dimensions and areas may vary widely with relatively minor rotations in transducer position. For these reasons, the American Society of Echocardiography/European Association of Cardiovascular Imaging recommend imaging the right heart using RV focused apical four-chamber view (i.e. four-chamber view passing through the RV maximal transverse diameter) [2].

Published online: 13 April 2018

Springer

Obtaining an RV focused apical four-chamber view may however be challenging without three-dimensional (3D) guidance. Although not done routinely, one could verify that the transverse RV diameter obtained in the apical four-chamber view corresponds to the maximal transverse diameter obtained in the short axis view. An alternate method would be to use 3D echocardiography dataset to identify the maximal RV transverse diameter and extract the optimal tomographic RV focused apical view (3D-RV-focused method).

In this study, we hypothesized that the 3D-RV-focused method would provide clinically valuable and reproducible estimation of RV size and function as compared to the gold standard cardiac magnetic resonance (CMR). We further hypothesized that the test–retest characteristics will be favorable after a learning period.

To test these hypotheses, we analyzed two cohorts. In a first retrospective cohort, patients underwent 3D echocardiography and CMR imaging on the same day allowing evaluation of the association between 3D-RV-focused views and corresponding CMR metrics. In a second prospective cohort, we quantified the analytic error range introduced by unfocused view on RV size and function estimates. We further compared RV measurements derived from 3D-RV-focused and optimized 2D-RV-focused views and analyzed their test–retest characteristics.

Materials and methods

Study design

The first retrospective cohort included 47 patients (among 50, with three having non-interpretable 3D data) who underwent 3D echocardiography and CMR within 2 h from January to September 2012. Indications of imaging were diverse: heart failure ($n=12$), congenital heart disease ($n=9$), pulmonary arterial hypertension ($n=8$), arrhythmogenic RV cardiomyopathy ($n=8$), evaluation for possible ischemia ($n=4$) or other indications such as suspicion of RV enlargement ($n=6$). This first cohort was used to compare the 3D-RV-focused method accuracy compared to corresponding CMR measurements of RV size and function. A second cohort of 25 patients (among 27, with two having non-interpretable 3D data) was prospectively included from January to March 2017, to assess bias introduced by unfocused RV views as well as to compare 3D-RV-focused and optimized 2D-RV-focused views and evaluate their test–retest characteristics. These patients underwent 3D and 2D acquisitions within 5 min of each other. Indications for imaging included pulmonary arterial hypertension ($n=12$), heart failure ($n=6$), congenital heart disease ($n=2$) and patients referred for pre-operative cardiovascular evaluation ($n=5$). Stanford University Institutional Review Board approved the study

conducted in agreement with the Helsinki-II-declaration; all patients gave their informed consent.

Cardiac magnetic resonance imaging

ECG-gated breath-hold CMR imaging was performed using a 1.5 T TwinSpeed scanner (GE Healthcare, USA) and an 8-channel cardiac phased-array receiver surface coil for signal reception by one cardiologist (PK). Short-axis slices spanning the volume of the left and right ventricles were obtained using initial 3-plane-localizer sequences. Standard 2-, 3-, and 4-chamber views as well as RV 2- and 3-chamber views were acquired. RV-focused 4-chamber views were derived from the maximal RV transverse diameter on the localizer short axis plane. The tricuspid annulus was defined on this RV-focused 4-chamber view from the lateral to the septal insertions of the tricuspid valve leaflets. RV end-diastolic (RVEDV) and end-systolic volumes (RVESV) were calculated using manual contour tracing of short-axis slices from the base to the apex including the RV outflow tract and excluding all trabeculations, using RV 3-chamber, 4-chamber views and multi-phase scans in movie play mode for contour tracing guidance. RV ejection fraction (RVEF,%) was defined as $100 \times (RVEDV - RVESV)/RVEDV$ [3]. Measurements were performed offline by an experienced cardiologist (HS) blinded from the echocardiography data on an independent workstation using Medis Medical Imaging software (Medis Medical Imaging Systems Inc., Leiden, The Netherlands). A second cardiologist reanalyzed all CMR for intervariability of RVEF measurements (IR), showing a 7.2% coefficient of variation.

The 3D-RV-focused method

Echocardiograms were acquired using Philips IE33 ultrasound systems in 2012 and EPIQ ultrasounds system in 2017 (Philips, Amsterdam, The Netherlands), using X5-1 matrix transducer. The volume rate median (25th–75th) was similar between the two cohorts: 18.0 (16.0–19.0) in 2012 vs. 18.0 (16.0–20.0) in 2017. Full volume 3D datasets were acquired over four cycles from the four-chamber apical view ensuring inclusion of the entire right ventricle [4]. Harmonic imaging could be used to optimize signal-to-noise ratio and to enhance visualization of the blood-endocardial borders. Images were digitally stored and analyzed offline using Philips QLAB v10.0 software. As illustrated in Fig. 1, RV focused views were derived from the image plane (perpendicular to the interventricular septum plane) that passes through the maximal transverse RV diameter.

The following 2D measures, presented in Fig. 2, were performed on the 3D-RV-focused view: RV end-diastolic and end-systolic areas (RVEDA and RVESA), basal diameter (D1, at 10% of the RV height), mid diameter (D2, at

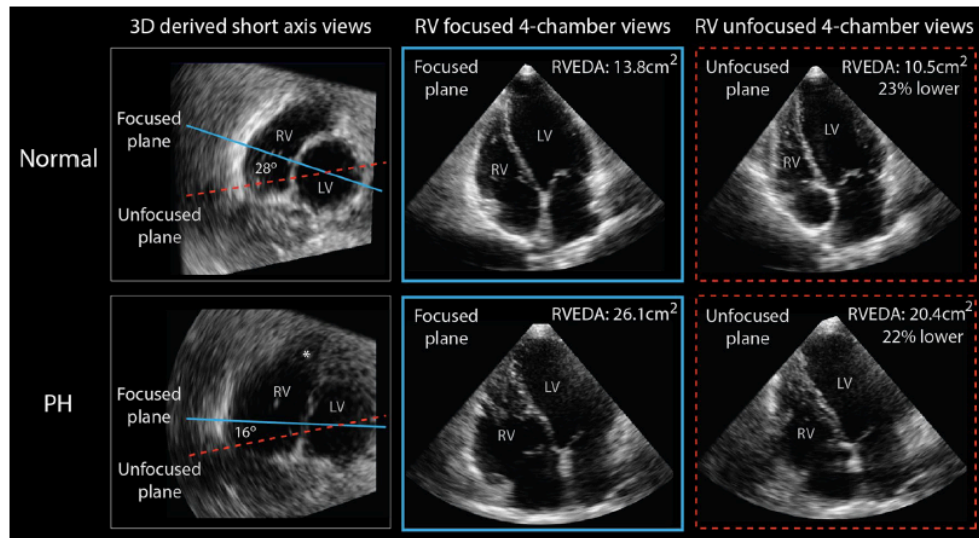
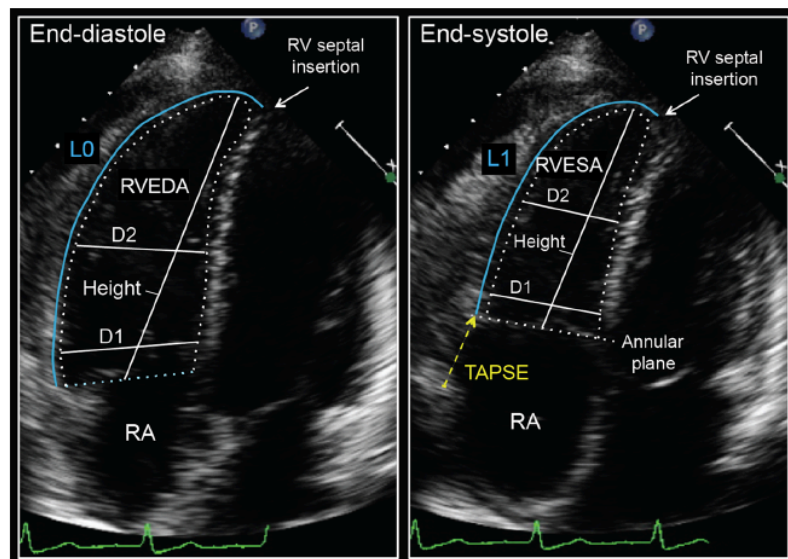


Fig. 1 Example of right ventricular focused and unfocused apical 4-chamber views derived from the 3D dataset, in end-diastole, in a patient with normal right ventricular phenotype and in a patient with mild pulmonary arterial hypertension (PH). Unfocused views

provided 23 and 22% underestimation of RV end-diastolic area (RVEDA) respectively. *Note the drop in spatial resolution of the RV anterior wall, particularly in the patient with PH. LV left ventricle RV right ventricle

Fig. 2 Illustration of measurements of selected right ventricular (RV) metrics in end diastole (left) and end systole (right). D1: basal diameter (at 10% of the RV height); D2: mid diameter (at 50% of the RV height); ventricular height; L0 and L1: lateral wall ventricular length in diastole and systole; RA right atrium, RVEDA RV end-diastolic area, RVESA RV end-systolic area, RVFAC fractional area change and TAPSE tricuspid annular plane systolic excursion



50% of the RV height), ventricular height, lateral wall ventricular length in diastole and systole (L0 and L1) as well as functional measures, i.e. fractional area change (RVFAC, %), basal fractional shortening [FS, defined as (end-diastolic D1 – end-systolic D1)/end-diastolic D1], mid FS [defined as (end-diastolic D2 – end-systolic D2)/end-diastolic D2], height shortening (Height S), tricuspid annular plane systolic

excursion (TAPSE) and free-wall Lagrangian longitudinal strain (RVLS, absolute value %). RVLS was measured from mid-endocardial end-diastolic (L0) and end-systolic (L1) lengths and calculated as $(L1 - L0)/L0$ [2]. Sphericity index was defined as mid RV transverse diameter divided by RV length. The tricuspid annulus was defined on the RV focused view from the lateral and septal insertions of the tricuspid

valve leaflets. All measures were averaged over three cycles and analyzed according to the latest guidelines by level three certified reader experienced in RV analysis (FH), blinded to the CMR values.

Analytic error introduced by an unfocused RV view

The 3D-RV-focused method was used to determine the extent of measures variation introduced by unfocused RV planes. Figure 1 shows an example of measurement of end-diastolic areas from focused and unfocused RV views in a patient with normal RV phenotype and in a patient with mild pulmonary arterial hypertension. Both optimally RV focused views and the smallest RV unfocused view that still allowed visualization of tricuspid valve opening were extracted. Rotating the plane in the transverse view, both clockwise and anticlockwise, identified the smallest RV dimension. The angle between focused and unfocused planes was 18.5° in average, always less than 30°.

Optimized 2D-RV-focused views

All patients from the second cohort underwent 2D echocardiography during which optimized 2D-RV-focused view was obtained by rotation of the transducer as the view with the largest RV basal diameter while avoiding foreshortening. All analyses were made by an attending level 3 cardiologist (FH) and a level 3 reader (HQL) [2, 5].

Test–retest characteristics

In order to assess the variability of 3D and 2D acquisitions of RV-focused views, a test–retest was performed in all patients from the prospective cohort. First, a certified sonographer (XT or NF) performed a complete 2D and 3D echocardiographic study followed by a new acquisition by the cardiologist (FH). The time span between the two acquisitions was less than 5 min.

Learning curve

The influence of training on variability of 2D RV measurements was assessed by the non-expert level reader (HQL) at the beginning of the study (i.e. before training) and after training with the RV expert reader (FH). Phase 1 of training included a 15 min slide presentation of the 3D- and 2D-RV-focused methods, and supervised acquisition and analysis of five cases. The junior cardiologist then performed 20 cases with variable RV dimension and function (i.e. before training cohort). Phase 2 of training consisted of supervised acquisition and reading of > 30 cases with the expert during a 3 month period. Then, the junior cardiologist performed 20 additional cases (i.e. after training cohort). Variability

from the reference RV measures performed by expert reader was assessed.

Statistical analysis

Data are summarized as mean \pm standard deviation (SD) or median and interquartile range (25th–75th) for continuous variables, and number of subjects (%) for categorical variables. Comparisons between groups were performed using two-sided Student *t* tests, Mann–Whitney test, analysis of covariance or Chi square test. Pearson correlation coefficients (*r*) were used to assess correlation between echocardiographic and CMR metrics, and 2D measures obtained from the 3D-RV-focused and optimized 2D-RV-focused views. Change in 2D measurements between focused and unfocused view was expressed as relative change from the 3D-RV-focused view (%). Reproducibility was expressed by coefficient of variation and intraclass correlation coefficient. Results were considered significant when two-sided *p* values were < 0.05. Statistical analysis was performed using SPSS® statistical software (SPSS V.23, Inc, Chicago, IL).

Results

3D-RV-focused method and cardiac magnetic resonance imaging

Forty-seven patients underwent echocardiography and CMR within a median (25th–75th) of 116 (56–150) min of each other (cohort 1) (Table 1). All patients were in sinus rhythm except for one having atrial and ventricular-paced rhythm. Figure 3a displays the correlations between CMR-derived RVEF, RVEDV and RVESV, and 3D-RV-focused measures. The best correlate for RVEF was RVFAC ($r=0.92$), while RV volumes were strongly correlated to their respective areas ($r=0.77$ in end-diastole and 0.87 in end-systole), all $p<0.001$. Figure 3b–e illustrates correlations between CMR and echocardiographic measurements according to etiologies, suggesting better correlation between volume and area in non-dilated RVs. The correlation between functional metrics (RVEF and RVFAC or RVLS) seemed slightly better in patients with pulmonary hypertension ($n=14$) versus in those without pulmonary hypertension ($n=22$) as illustrated in the Online Resource 1, although not reaching statistical significance (all $p>0.21$): $r=0.96$ versus $r=0.90$ for correlation between RVEF and RVFAC, and $r=0.68$ versus $r=0.45$ between RVEF and RVLS. The small number of patients with severe tricuspid regurgitation ($n=5$) precluded any assessment of the influence of tricuspid regurgitation severity.

Table 1 Characteristics of the first cohort used to compare 3D right ventricular focused (3D-RV-focused) measures and cardiac magnetic resonance measures

	n=47
Demographics	
Age	47 ± 15
Male sex	26 (55%)
Comorbidities	
Hypertension	7 (15%)
Diabetes	6 (13%)
Active smoking or < 3 years cessation	12 (26%)
Indication for imaging	
Left heart failure	12 (26%)
Congenital heart disease	9 (19%)
Ebstein's anomaly	1 (2%)
Pulmonary arterial hypertension	8 (17%)
Pulmonary arterial hypertension	8 (17%)
Arrhythmogenic right ventricular dysplasia	8 (17%)
Evaluation for myocardial ischemia	4 (9%)
Others	6 (13%)
3D-RV-focused metrics	
Basal diameter (cm)	4.0 ± 0.8
Mid-diameter (cm)	3.2 ± 1.0
End-diastolic area (cm ²)	24.3 ± 8.1
End-systolic area (cm ²)	16.0 ± 7.2
RV fractional area change (%)	35.9 ± 8.7
RV longitudinal strain (%)	19.4 ± 5.3
Tricuspid annular plane systolic excursion (cm)	2.0 ± 5.0
Basal fractional shortening (%)	20.4 ± 9.9
Mid fractional shortening (%)	23.5 ± 11.6
End-diastolic sphericity	0.40 ± 0.11
End-systolic sphericity	0.37 ± 0.12
Severe tricuspid regurgitation	5 (11%)
RV systolic pressure > 40 mm Hg ^a	14 (39%)
Cardiac magnetic resonance metrics	
RV end-diastolic volume (mL)	191.2 ± 74.9
RV end-systolic volume (mL)	102.0 ± 57.3
RV ejection fraction (%)	48.1 ± 11.4
LV ejection fraction (%)	54.4 ± 11.3

Results are presented as mean ± SD or number (percentage)

LV left ventricle, RV right ventricle

^aRV systolic pressure estimated from the tricuspid regurgitation maximal velocity, available in 77% of patients

Analytic error associated with unfocused RV apical views

The mean age of the second cohort (n = 25) was 56 ± 20 years with 64% of female, 12% had hypertension, 8% diabetes and 4% were smokers. The majority of patients were in sinus rhythm except for one having atrial fibrillation and one having atrial paced rhythm. No patient had

severe tricuspid regurgitation, while 18/25 (72%) patients had RV systolic pressure > 40 mm Hg. As shown in Fig. 4 and Online Resource 2, unfocused views were associated with a greater underestimation of RV areas. Functional metrics were less affected on average than RV dimensions but showed a wide range of variability. When assessing the influence of PH on the effect of unfocused RV views, RVLS was significantly more underestimated in patients with PH than in those without PH [difference in RVLS from focused to unfocused view was - 15.3 (19.9; 11.6) versus 16.5 (- 5.1; 29.0) respectively, p = 0.04]. There was no significant difference in other RV metrics.

Comparison between the 3D- and 2D-RV-focused views

In the second cohort, the use of optimized 2D-RV-focused views provided measurements that were strongly associated with those derived from 3D-RV-focused views (Fig. 5). These associations were stronger for RVEDA (r = 0.96) and RVFAC (r = 0.95) than for RVLS (r = 0.83) or TAPSE (r = 0.84), all p < 0.001.

Reproducibility and learning curve for 3D- and 2D RV-focused views

The second cohort enabled comparison of the reproducibility of the 3D and 2D methods to obtain an RV-focused view. There was small intra- and interobserver variability for 3D-RV-focused and 2D-RV-focused measures (Table 2 and Online Resource 3). The coefficient of variations for test and retest for the 3D-RV-focused method and 2D-RV-focused method were similar, ranging from 5% for RV free-wall length in end-diastole (LO) to 15% for RVLS (Fig. 6a). Training of the non-expert level reader enabled improvement of the variability of 2D measurements from 3D-RV-focused views (Fig. 6b) and from 2D-RV-focused views (Fig. 6c) as detailed in Online Resource 4.

Discussion

The main finding of our study is that 3D echocardiography can help standardize RV focused four-chamber views. Measures based on this methodology are closely associated with corresponding CMR measures in patients with different etiologies of RV enlargement and dysfunction. Although the 3D-RV-focused method measures have good test-retest characteristics, one has to acknowledge the limitation of lower spatial and temporal resolution as well as a longer learning curve when compared to optimized 2D-RV-focused views. Our study further determines the range of variability provided by unfocused views.

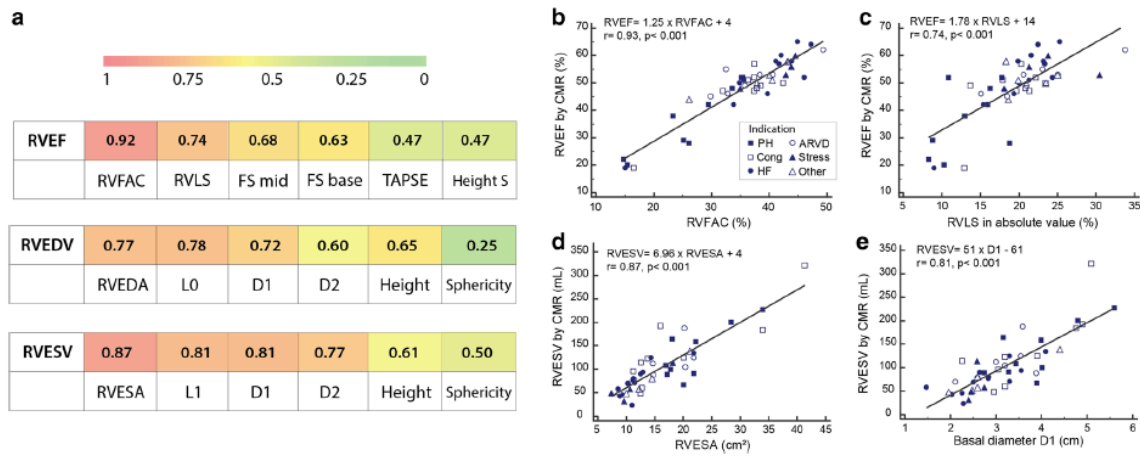


Fig. 3 Pearson correlation (*r*) heatmap between 3D-RV-focused views and CMR metrics of right ventricular size and function (**a**); selected correlations according to etiology (**b–e**). *ARVD* arrhythmogenic right ventricular dysplasia, *Cong* congenital heart disease, *D1* basal diameter, *D2* mid diameter, *FS* fractional shortening, *Height S* height shortening, *HF* heart failure, *L0* end-diastolic free-wall length, *L1*

end-systolic free-wall length, *PH* pulmonary hypertension, *RVFAC* fractional area change, *RVEF* ejection fraction, *RVEDA* end-diastolic area, *RVEDV* end-diastolic volume, *RVESA* end-systolic area, *RVESV* end-systolic volume, *RVLS* free-wall longitudinal strain, *TAPSE* tricuspid annular plane systolic excursion

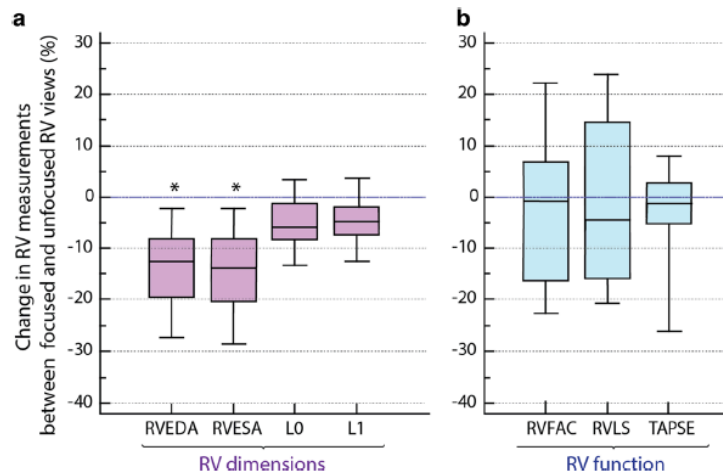


Fig. 4 Change in RV measurements from an RV focused view to an unfocused view extracted from the 3D dataset. *L0* end-diastolic free-wall length, *L1* end-systolic free-wall length, *RVEDA* right ventricular end-diastolic area, *RVESA* end-systolic area, *RVFAC* fractional area change, *RVLS* free-wall longitudinal strain, *TAPSE* tricuspid annular plane systolic excursion. Change was calculated as: $100 \times (RV \text{ meas-}$

urement using focused view – unfocused view)/focused view. Negative values of change denote underestimation of RV metrics using unfocused view as compared to the optimal focused apical 4-chamber view. *Both *p* values of comparison of *RVEDA* and *L0*, and *RVESA* and *L1* using Mann–Whitney test are < 0.05

While 3D imaging is the gold standard for assessing RV volumes and ejection fraction, 3D echocardiography presents some methodological limitations such as lower spatial and temporal resolutions than 2D echocardiography and acoustic dropout of the RV anterior and lateral walls. This favors the use of 2D echocardiography in clinical practice

in which RV focused view plays a central part. Practically, different methods can help obtain a true RV focused view. First, one could verify that transverse diameter in RV four-chamber view corresponds to the maximal transverse diameter of the short axis view. Second and more directly, as in our study, one can use 3D acquisition to standardize the

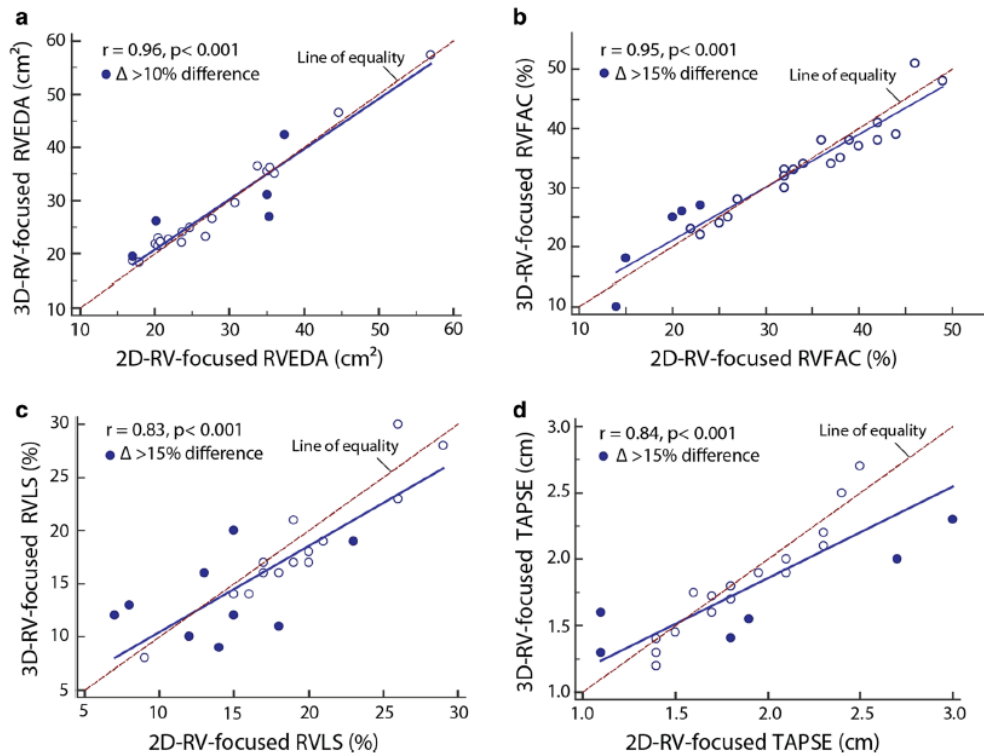


Fig. 5 Comparison between 2D right ventricular (RV) size or function metrics obtained on the 3D-RV-focused and the 2D-RV-focused view. Correlation is expressed by the coefficient r of the regression

line. All p values are significant (< 0.05). *RVEDA* end-diastolic area, *RVFAC* fractional area change, *RVLS* free-wall longitudinal strain, *TAPSE* tricuspid annular plane systolic excursion

Table 2 Reproducibility of 3D right ventricular focused (3D-RV-focused) and optimized 2D-RV-focused metrics

	Intra-observer reproducibility	Inter-observer reproducibility	Test-retest
3D-RV-focused view			
RVEDA	6.0	7.9	10.7
L0	4.5	4.7	6.5
RVFAC	5.3	9.7	11.3
RVLS	11.8	18.2	15.1
TAPSE	5.7	11.4	10.7
2D-RV-focused view			
RVEDA	6.3	8.7	11.8
L0	3.2	3.8	5.1
RVFAC	6.2	9.3	10.2
RVLS	14.0	14.1	14.1
TAPSE	6.3	10.1	10.4

Intra-observer reproducibility represents non-expert reader's reproducibility. For test-retest and inter-reproducibility, expert read presented as the first value. Results are expressed as coefficient of variation. *L0* end-diastolic length of the free-wall, *RVEDA* end-diastolic area, *RVFAC* fractional area change, *RVLS* free-wall longitudinal strain, *TAPSE* tricuspid annular plane systolic excursion

four-chamber view on the maximal transverse diameter on the cross-sectional view.

The first step of our study was to assess whether 2D echocardiographic RV metrics (such as areas or function) measured on an RV focused view derived from 3D acquisition are accurate approximations of gold standard CMR metrics. The association between 2D echocardiographic metrics and CMR volumetric metrics has already been subject of studies but varies in the literature. Among recent studies that included patients with pulmonary hypertension or left heart disease, RVFAC emerged as one the strongest correlate of RVEF with an association (r) ranging from 0.42 to 0.87 (all significant) [6–10]. This variability may be partially explained by the absence of standardization of RV focused views from one study to another. Our 3D-RV-focused method provided even stronger association than previously reported for RVFAC ($r = 0.92$) potentially reflecting the better standardization of RV focused apical views. Consistent with previous studies, TAPSE was not as strongly associated with RVEF as other 2D functional metrics such as RVFAC in our first cohort ($r = 0.47$). RV free-wall strain has been shown in Focardi et al.'s study to be the strongest correlate

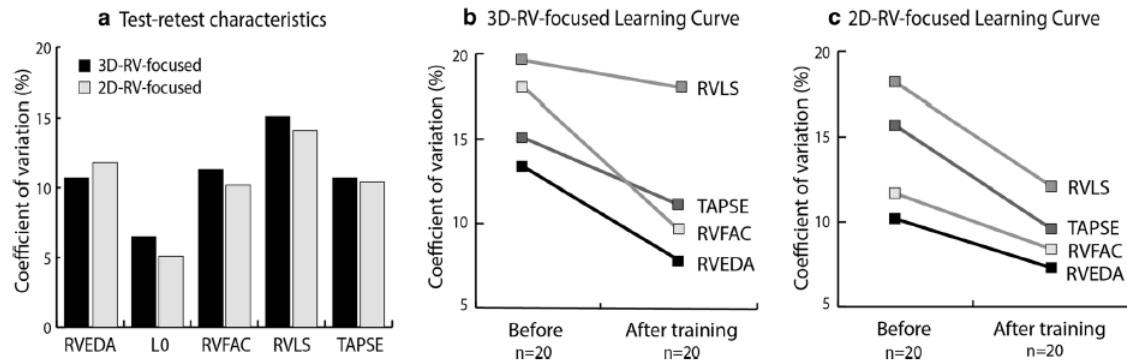


Fig. 6 **a** Test–retest variability for 2D right ventricular (RV) metrics derived from 3D-RV-focused and 2D-RV-focused views. **b–c** Learning curve of the junior reader for the 3D-RV-focused method (**b**) and the 2D-RV-focused method (**c**). Test–retest variability is expressed as coefficient of variation (%). For the learning curve assessment, the junior cardiologist acquired 3D-RV-focused and 2D-RV-focused

views, and performed the following 2D RV measures in two separate groups of 20 cases with diverse etiologies. Variability is expressed as coefficient of variation (%) using the expert cardiologist reading as reference. *L0* end-diastolic length of the free-wall, *RVEDA* end-diastolic area, *RVFAC* fractional area change, *RVLS* free-wall longitudinal strain, *TAPSE* tricuspid annular plane systolic excursion

of RVEF ($r = -0.77$) in 63 patients with suspicion of myocarditis, dilated or hypertrophic cardiomyopathy, arrhythmogenic right ventricular dysplasia or infiltrative cardiomyopathy [10]. Although RVLS was more strongly associated with RVEF than TAPSE or transverse fractional shortening in our cohort, it did not prove to be superior to RVFAC. The excellent association observed between 2D metrics and CMR 3D metrics would likely be weaker in patients with RV segmental disease such as in RV myocardial infarction or acute pulmonary embolism with McConnell's sign [11].

Our study is additionally one of the first to provide insights on the potential systematic error introduced by unfocused RV four-chamber views. The use of an unfocused view can indeed result in 10–15% on average of underestimation of RV areas, which increases the variability in estimating RV size. This further strengthens the need to optimize and standardize 2D acquisitions of RV views. The variance however appeared to be smaller for TAPSE compared to RVFAC or RVLS.

No technique would be acceptable without good test–retest characteristics. 3D-RV-focused measures had excellent reproducibility almost comparable to optimized 2D imaging planes. There was significant variability in RV measures using 3D-RV-focused method between the expert reader and the junior reader, highlighting the importance of proper training. The decreased spatial resolution provided by the 3D method may partially explain the increased variability of RV free-wall metrics such as TAPSE and RVLS. Our second prospective cohort also shows the good correlation between 3D-RV-focused views and optimized 2D-RV-focused views by rotation. As relying on 2D acquisition, the optimized 2D method to obtain an RV-focused view offers a better spatial resolution than the 3D method. However, it

should be kept in mind that our study was conducted in a tertiary echocardiography lab with high-skilled sonographers and expert cardiologists. It can be speculated that optimized 2D-RV focused views would be less accurate in a general echocardiography lab than in the present study.

The main limitation of this methodological study is the use of two separate cohorts. The retrospective cohort of patients with CMR and 3D echocardiography within 2 h (used for comparison of 3D-RV-focused metrics and CMR data) was acquired in 2012. The data was only processed and analyzed in 2017. At that time, the prospective cohort was included to determine the reproducibility of the 3D-RV-focused method. These two cohorts prevented direct comparison of optimized 2D RV-focused measurements and CMR volumes or ejection fraction but enabled comprehensive comparison of test–retest characteristics. Regarding the potential evolution in 3D technology between 2012 and 2017 (despite similar volume rates), it can be speculated that the improvement in spatial resolution may provide even better correlation with CMR, and thus the results provided from the first cohort may be lower than what we could obtain in 2017.

Conclusion

Standardization of RV focused views is needed to improve the evaluation of RV size and function. The 3D based method provides reproducible estimation of RV size and function strongly correlating with gold-standard CMR measurements. This comes however with the trade-off of a steeper learning curve and a lower spatial resolution than optimized 2D-RV-focused views. One potential advantage

of the 3D method that remained to be further explored is its better reproducibility for follow-up than optimized 2D RV-focused views.

Acknowledgements The authors would like to thank Paul Kim and Semhar Sibhatu (Stanford University for their help in data collection, and Allan Paloma (from Stanford Cardiovascular Echocardiography Laboratory) for his technological expertise and knowledge.

Funding This study was funded by the Stanford Cardiovascular Institute and the Vera Moulton Wall Center of Pulmonary Hypertension at Stanford.

Compliance with ethical standards

Conflict of interest MA received a Young Investigator Seed Grant from the Vera Moulton Wall Center. FH received funds from Pai Chan Lee Research fund. The authors declare that they have no conflict of interest.

Ethical approval All procedures performed in studies involving human participants were approved by Stanford University Institutional Review Board in accordance with the ethical standards of the institutional and/or national research committee and with the 1964 Helsinki declaration and its later amendments or comparable ethical standards.

Informed consent Informed consent was obtained from all individual participants included in the study. This article does not contain any studies with animals performed by any of the authors.

References

1. Amsallem M, Kuznetsova T, Hanneman K, Denault A, Haddad F (2016) Right heart imaging in patients with heart failure: a tale of two ventricles. *Curr Opin Cardiol* 31:469–482
2. Lang RM, Badano LP, Mor-Avi V, Afilalo J, Armstrong A, Ernande L et al (2015) Recommendations for cardiac chamber quantification by echocardiography in adults: an update from the American Society of Echocardiography and the European Association of Cardiovascular Imaging. *J Am Soc Echocardiogr* 28:1–39
3. Hendel RC, Patel MR, Kramer CM, Poon M, Hendel RC, Carr JC et al (2006) ACCF/ACR/SCCT/SCMR/ASNC/NASCI/SCAI/SIR appropriateness criteria for cardiac computed tomography and cardiac magnetic resonance imaging: a report of the American College of Cardiology Foundation Quality Strategic Directions Committee Appropriateness Criteria Working Group, American College of Radiology, Society of Cardiovascular Computed Tomography, Society for Cardiovascular Magnetic Resonance, American Society of Nuclear Cardiology, North American Society for Cardiac Imaging, Society for Cardiovascular Angiography and Interventions, and Society of Interventional Radiology. *J Am Coll Cardiol* 2006; 48:1475–1497
4. Lang RM, Badano LP, Tsang W, Adams DH, Agricola E, Buck T et al (2012) EAE/ASE recommendations for image acquisition and display using three-dimensional echocardiography. *J Am Soc Echocardiogr* 25:3–46
5. Rudski LG, Lai WW, Afilalo J, Hua L, Handschumacher MD, Chandrasekaran K et al (2010) Guidelines for the echocardiographic assessment of the right heart in adults: a report from the American Society of Echocardiography endorsed by the European Association of Echocardiography, a registered branch of the European Society of Cardiology, and the Canadian Society of Echocardiography. *J Am Soc Echocardiogr* 23:685–713
6. Yang T, Liang Y, Zhang Y, Gu Q, Chen G, Ni X-H et al (2013) Echocardiographic parameters in patients with pulmonary arterial hypertension: correlations with right ventricular ejection fraction derived from cardiac magnetic resonance and hemodynamics. *PLoS ONE* 8:e71276
7. Wang Z, Yang Z, Wan Z, Yu T, Jia L, Du X et al (2014) Association between echocardiography derived right ventricular function parameters with cardiac magnetic resonance derived right ventricular ejection fraction and 6-minute walk distance in pulmonary hypertension patients. *Zhonghua Xin Xue Guan Bing Za Zhi* 42:748–752
8. Shiran H, Zamanian RT, McConnell MV, Liang DH, Dash R, Heidary S et al (2014) Relationship between echocardiographic and magnetic resonance derived measures of right ventricular size and function in patients with pulmonary hypertension. *J Am Soc Echocardiogr* 27:405–412
9. Li Y, Wang Y, Zhai Z, Guo X, Wu Y, Yang Y et al (2015) Relationship between echocardiographic and cardiac magnetic resonance imaging-derived measures of right ventricular function in patients with chronic thromboembolic pulmonary hypertension. *Thromb Res* 135:602–606
10. Focardi M, Cameli M, Carbone SF, Massoni A, De Vito R, Lisi M et al (2015) Traditional and innovative echocardiographic parameters for the analysis of right ventricular performance in comparison with cardiac magnetic resonance. *Eur Heart J Cardiovasc Imaging* 16:47–52
11. Tuzovic M, Adigopula S, Amsallem M, Kobayashi Y, Kadoch M, Boulate D et al (2015) Regional right ventricular dysfunction in acute pulmonary embolism: relationship with clot burden and biomarker profile. *Int J Cardiovasc Imaging* 32:389–398

FRENCH SUMMARY

FRENCH SUMMARY

L'insuffisance cardiaque droite est la première cause de morbi-mortalité chez les patients atteints d'hypertension pulmonaire, malgré les récents progrès dans la compréhension de l'importance de l'adaptation ventriculaire droite et dans le traitement des patients avec hypertension pulmonaire. La transition entre l'état adapté et l'état maladapté du ventricule droit à l'augmentation de la post-charge du ventricule droit reste un phénomène complexe encore mal compris.

Dans cette thèse, nous avons démontré le rôle de l'imagerie cardiaque non-invasive (échocardiographie) pour identifier le phénotype adaptatif du cœur droit en présence d'hypertension pulmonaire et pour contribuer à identifier les mécanismes moléculaires associés à la défaillance droite.

Le premier chapitre de cette thèse est dédié à l'évaluation et à l'amélioration de la méthode utilisant l'échographie cardiaque trans-thoracique pour dépister l'hypertension pulmonaire au repos dans une population de patients à risque d'hypertension pulmonaire pré-capillaire. Dans la plus large cohorte à ce jour, nous avons d'abord confirmé la relation linéaire qui relie la pression artérielle pulmonaire moyenne et la pression artérielle pulmonaire systolique, mesurées de manière invasive par cathétérisme cardiaque droit. Dans la mesure où la définition de l'hypertension pulmonaire repose sur une valeur de pression artérielle pulmonaire moyenne supérieure à 25 mmHg, nos résultats ont renforcé la pertinence de l'usage de l'estimation de la pression systolique ventriculaire droite en échocardiographie-Doppler pour dépister l'hypertension pulmonaire. Nous avons ensuite proposé une classification simple de la qualité de l'enveloppe du signal Doppler continu d'insuffisance tricuspide afin de limiter le risque de surestimation et de sous-estimation de la pression systolique ventriculaire droite. Les principaux écueils étaient la tendance à rapporter une valeur de pression systolique ventriculaire droite en présence d'une enveloppe Doppler incomplète et la surestimation de la pression systolique ventriculaire droite en présence d'une extra-échogénicité à la pointe de l'enveloppe (souvent appelé «cheveux» de l'enveloppe). Cependant, tout

en appliquant ces conseils méthodologiques pratiques pour améliorer la précision de l'estimation des pressions pulmonaires, notre étude a mis en évidence la variabilité résiduelle de l'échocardiographie pour l'estimation de la pression. Globalement, il convient de garder à l'esprit que l'objectif de cette étude n'était pas de démontrer la supériorité de l'échocardiographie par rapport au cathétérisme cardiaque droit pour l'estimation des pressions pulmonaires, mais d'améliorer la méthodologie d'utilisation de l'échocardiographie pour dépister l'hypertension pulmonaire. Le cathétérisme cardiaque droit restant la méthode de référence pour mesurer les pressions pulmonaires, l'échocardiographie demeure la pierre angulaire du dépistage clinique de l'hypertension pulmonaire, en particulier chez les patients atteints de cardiopathie gauche ou de maladie pulmonaire avancée. Publiée dans le Journal de l'American Society of Echocardiography, notre étude a été choisie dans le cadre du programme de formation médicale continue de l'American Society of Echocardiography. Dans notre établissement (Hôpital Marie Lannelongue), le protocole méthodologique utilisé dans cette étude a été mis en œuvre et adopté aux laboratoires d'échographie clinique et de recherche.

Bien que l'échocardiographie transthoracique soit la technique d'imagerie la plus couramment utilisée pour évaluer la fonction cardiaque gauche, les dimensions des cavités cardiaques et l'estimation des paramètres hémodynamiques, il faut rappeler les limites de l'échographie pour l'estimation des volumes et de la fraction d'éjection du ventricule droit. Notre groupe a démontré que l'utilisation de la vue apicale 4-cavités centrée sur le ventricule droit améliorerait la précision de la mesure des dimensions et de la fonction du ventricule droit. L'imagerie par résonance magnétique (IRM) cardiaque reste la référence en matière d'évaluation des volumes, de la masse ventriculaire et de la fraction d'éjection, malgré son accès limité en routine clinique. Le domaine de recherche sur l'évaluation non invasive du cœur droit va vers l'adoption de nouvelles séquences IRM telles que le 4D blood flow, requérant encore validation chez les patients atteints d'hypertension pulmonaire. Notre équipe mène actuellement une étude visant à valider l'exactitude du débit sanguin 4D pour l'estimation des volumes, de la masse et de la fraction d'éjection dans une cohorte prospective de patients atteints d'hypertension pulmonaire post-embolique bénéficiant d'une endartériectomie pulmonaire et de patients atteints d'hypertension artérielle

pulmonaire bénéficiant d'une transplantation pulmonaire (étude PRINCEPT, ClinicalTrials.gov Identifier : NCT03205085).

Le deuxième chapitre de cette thèse a permis d'identifier, parmi les multiples **indices d'imagerie non invasive du cœur droit**, les indices télé-systoliques de remodelage du ventricule droit comme les biomarqueurs pronostiques les plus forts chez les patients atteints d'hypertension artérielle pulmonaire, et ce quelle qu'en soit l'étiologie. En combinaison à la classe fonctionnelle NYHA et au taux de NT-proBNP, l'indice télé-systolique de remodelage du ventricule droit (ratio de la paroi latérale et de la hauteur septale) prédit la survenue d'évènements (décès, transplantation pulmonaire ou réadmission pour insuffisance cardiaque droite) à long terme au cours du suivi dans une cohorte prospective de 228 patients avec hypertension artérielle pulmonaire, et ce de manière incrémentielle par rapport aux scores de risque existants (tels que le score REVEAL). En plus de sa forte valeur pronostique, notre étude a suggéré que l'indice télé-systolique de remodelage du ventricule droit puisse être utilisé en tant que prédicteur de réponse au traitement, si nos résultats sont validés par d'autres études.

La deuxième partie du chapitre est consacrée à la redéfinition des trois concepts physiologiques sous-jacents au terme «**d'adaptation cardiaque à la post-charge**». Dans deux études menées chez des patients atteints d'hypertension artérielle pulmonaire et de patients atteints de sclérodermie avec hypertension artérielle pulmonaire, les indices complexes d'adaptation cardiaque droite à la post-charge, publiées précédemment, ne fournissaient pas de valeur pronostique supplémentaire au-delà de celle d'indices simples, tels que la surface télé-systolique du ventricule droit. La forte valeur pronostique des indices télé-systolique du ventricule droit en hypertension pulmonaire s'explique par le fait que le stress de paroi est le plus élevé en fin de systole dans les cardiopathies hypertensives. En hypertension pulmonaire, l'évolution du remodelage ventriculaire droit est caractérisée par l'hypertrophie des cardiomyocytes, associée à des altérations de la matrice interstitielle éventuellement associées à une dilatation de la chambre. Par conséquent, il n'est pas surprenant de constater que le remodelage télé-systolique ventriculaire droit est un fort marqueur pronostique.

Le troisième chapitre de cette thèse explore le rôle des **biomarqueurs immunitaires** plasmatiques chez les patients atteints d'hypertension pulmonaire.

La première étude démontre la valeur pronostique de taux plasmatiques pré-opératoires élevés de C-reactive protein (CRP) pour la prédiction de la survenue d'évènements post-opératoires précoces (décès ou transplantation ou besoin d'une ECMO ou d'un support prolongé par inotrope ou vasopresseurs) après endartériectomie pulmonaire chez des patients atteints d'hypertension pulmonaire post-embolique. La présence d'inflammation systémique pré-opératoire (indiquée par un taux de CRP supérieur ou égal à 10mg/dL était associée à une instabilité hémodynamique post-opératoire plus fréquente secondaire à une vasodilatation périphérique. Dans cette étude rétrospective, nous n'avons pu démontrer l'existence d'une corrélation significative entre le taux plasmatique de CRP et l'adaptation du cœur droit à l'hypertension pulmonaire évaluée par échocardiographie dans le sous-groupe de patients ayant bénéficié d'une échocardiographie. Les deux sous-groupes analysés (avec CRP élevée ou basse) avaient des niveaux similaires de résistance pulmonaire, contrairement à la population totale. Le résultat négatif contraste avec les conclusions précédentes du lien entre l'inflammation systémique et la fonction cardiaque droite chez les patients atteints d'hypertension pulmonaire post-embolique, qui avait été démontré en comparant des patients avec ou sans inflammation systémique mais sans ajustant pour le niveau de résistance pulmonaire. Des investigations ultérieures sont nécessaires pour déterminer si, après appariement pour la post-charge, les patients opérables atteints d'hypertension pulmonaire post-embolique avec CRP élevée ont une fonction ventriculaire droite différente de ceux des patients avec une CRP basse.

La deuxième étude fournit un exemple d'application pratique du phénotypage approfondi du cœur droit pour l'identification du **profil protéomique** immunitaire plasmatique associé à la défaillance cardiaque droite chez les patients atteints d'hypertension artérielle pulmonaire. Cette étude protéomique génératrice d'hypothèses a identifié des taux plasmatiques élevés de facteur de croissance hépatique (HGF : hepatic growth factor), de facteur de croissance nerveuse (NGF : nerve growth factor) et de

facteur de croissance de cellules souches bêta (SCGFb : stem cell growth factor bêta) comme étant associés à la défaillance cardiaque droite dans deux cohortes avec hypertension artérielle pulmonaire, et ce au delà du niveau de résistance pulmonaire. Le rôle de ces biomarqueurs dans l'adaptation du ventricule droit à l'hypertension pulmonaire reste à être précisé et une validation expérimentale est en cours.

Titre: Etude du Remodelage du Ventricule Droit dans l'Hypertension Pulmonaire: du Phénotypage Approfondi à l'Etude de la Protéomique

Mots clés: Hypertension Pulmonaire, Imagerie Cardiaque, Immunité, Insuffisance Cardiaque, Protéomique, Ventricule Droit.

Abstract: L'insuffisance cardiaque droite est la première cause de morbi-mortalité chez les patients atteints d'hypertension pulmonaire. Améliorer le phénotypage de l'adaptation du coeur droit en imagerie non-invasive est essentiel afin de mieux comprendre les mécanismes favorisant la transition d'un état adapté à un état maladapté.

Le premier chapitre a démontré la fiabilité de l'échographie cardiaque pour la détection de l'hypertension pulmonaire, fournissant des conseils méthodologiques pratiques.

Le second chapitre a permis d'identifier les indices télé-systoliques de remodelage du ventricule droit comme les plus puissants paramètres pronostiques en imagerie chez les

patients atteints d'hypertension artérielle pulmonaire (HTAP), en association avec la classe NYHA et le taux de NT-proBNP.

Le troisième chapitre est dédié à l'étude des biomarqueurs immunitaires en hypertension pulmonaire, en mettant en utilisant la méthode de phénotypage approfondi du coeur droit pour déterminer le profile circulant protéomique associé à la défaillance droite chez les patients atteints d'HTAP. Cette étude a permis de montrer que des taux élevés plasmatiques d'hépatique growth factor, de nerve growth factor et de stem cell growth factor beta sont associés à la défaillance droite dans deux cohortes d'HTAP. Le rôle direct de ces biomarqueurs dans le ventricule droit reste à être élucidé.

Title: Right Ventricular Remodeling in Pulmonary Hypertension: from Deep Phenotyping to Proteomics Profiling

Keywords: Cardiac Imaging, Heart failure, Immunity, Pulmonary Hypertension, Right Ventricle, Proteomics.

Abstract: Right heart failure is the major cause of morbi-mortality in patients with pulmonary hypertension (PH). Improving right heart adaptive phenotyping using non-invasive imaging is needed in order to better understand the transition from right ventricular (RV) adaptation to maladaptation in PH.

The first chapter of this thesis has been dedicated to demonstrate the reliability of echocardiography to detect PH in patients with group 1 or 3 PH, providing methodology pearls and pitfalls.

The second chapter has enabled to identify, among the multiple right heart non-invasive imaging metrics, RV end-systolic remodeling indices as the strongest prognostic biomarkers

in patients with pulmonary arterial hypertension (PAH), combined with the NYHA class and NT-proBNP levels.

The third chapter has explored the role of immune biomarkers in PH, providing a practical application of right heart deep phenotyping to determine the circulating immune proteomic profile associated with right heart failure in patients with PAH. This screening proteomics study has identified high plasmatic levels of hepatic growth factor, nerve growth factor and stem cell growth factor beta to be associated with right heart maladaptation in two cohorts with PAH. The role of these biomarkers within the right ventricle itself remains to be fully explored.



